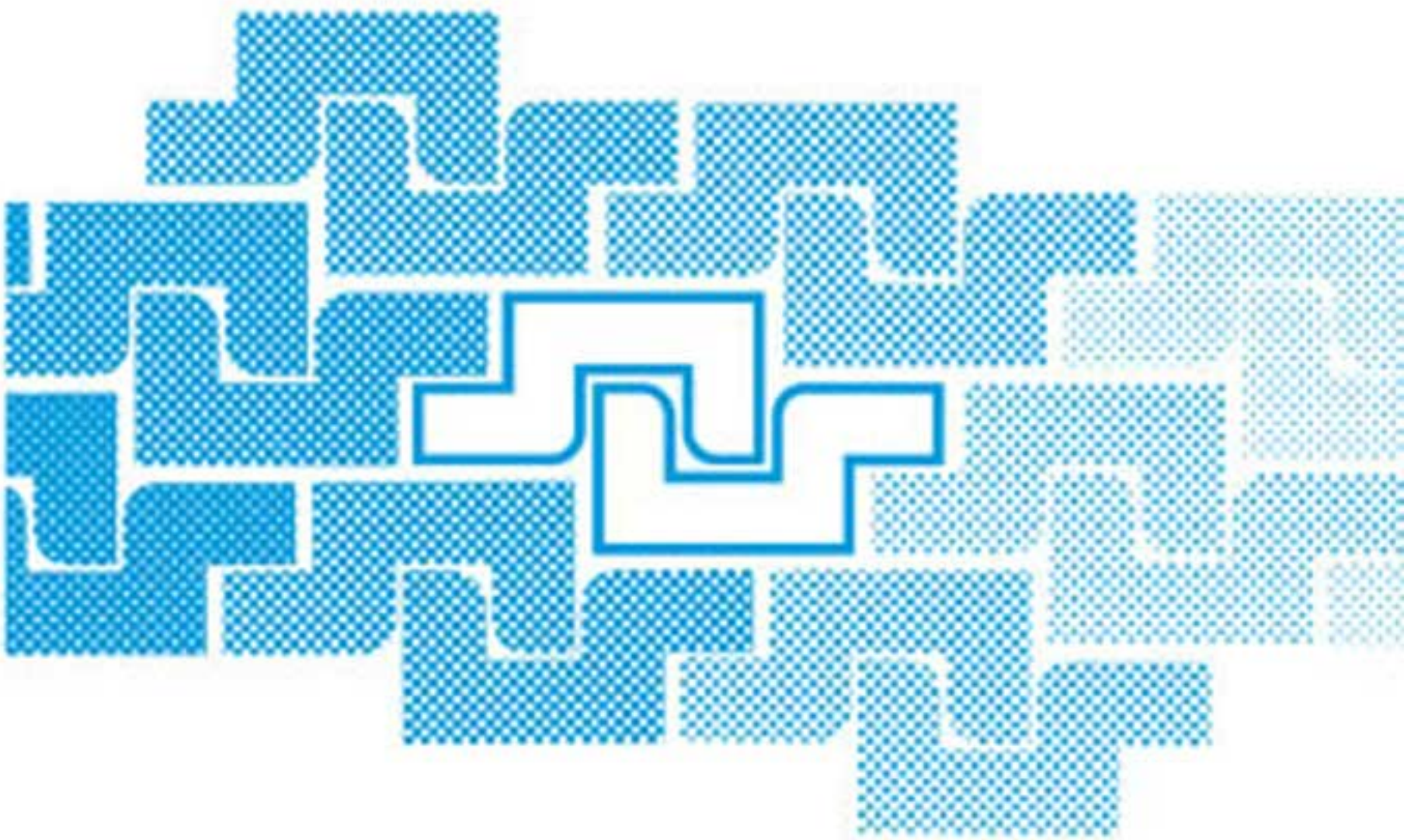

Superdense QCD Matter and Compact Stars

Edited by

David Blaschke and David Sedrakian

NATO Science Series

II. Mathematics, Physics and Chemistry – Vol. 197

Superdense QCD Matter and Compact Stars

NATO Science Series

A Series presenting the results of scientific meetings supported under the NATO Science Programme.

The Series is published by IOS Press, Amsterdam, and Springer (formerly Kluwer Academic Publishers) in conjunction with the NATO Public Diplomacy Division.

Sub-Series

I. Life and Behavioural Sciences	IOS Press
II. Mathematics, Physics and Chemistry	Springer (formerly Kluwer Academic Publishers)
III. Computer and Systems Science	IOS Press
IV. Earth and Environmental Sciences	Springer (formerly Kluwer Academic Publishers)

The NATO Science Series continues the series of books published formerly as the NATO ASI Series.

The NATO Science Programme offers support for collaboration in civil science between scientists of countries of the Euro-Atlantic Partnership Council. The types of scientific meeting generally supported are "Advanced Study Institutes" and "Advanced Research Workshops", and the NATO Science Series collects together the results of these meetings. The meetings are co-organized by scientists from NATO countries and scientists from NATO's Partner countries — countries of the CIS and Central and Eastern Europe.

Advanced Study Institutes are high-level tutorial courses offering in-depth study of latest advances in a field.
Advanced Research Workshops are expert meetings aimed at critical assessment of a field, and identification of directions for future action.

As a consequence of the restructuring of the NATO Science Programme in 1999, the NATO Science Series was re-organized to the four sub-series noted above. Please consult the following web sites for information on previous volumes published in the Series.

http://www.nato.int/science
http://www.springeronline.com
http://www.iospress.nl

Series II: Mathematics, Physics and Chemistry – Vol. 197

Superdense QCD Matter and Compact Stars

edited by

David Blaschke
Rostock University,
Germany and
JINR Dubna,
Russia

and

David Sedrakian
Yerevan State University,
Armenia

Published in cooperation with NATO Public Diplomacy Division

Proceedings of the NATO Advanced Research Workshiop on
Superdense QCD Matter and Compact Stars
Yerevan, Armenia
27 September–4 October 2003

A C.I.P. Catalogue record for this book is available from the Library of Congress.

ISBN-10 1-4020-3429-6 (PB)
ISBN-13 978-1-4020-3429-9 (PB)
ISBN-10 1-4020-3428-8 (HB)
ISBN-10 1-4020-3430-X (e-book)
ISBN-13 978-1-4020-3428-2 (HB)
ISBN-13 978-1-4020-3430-5 (e-book)

Published by Springer,
P.O. Box 17, 3300 AA Dordrecht, The Netherlands.

www.springeronline.com

Printed on acid-free paper

Printed in the Netherlands.

This book is dedicated to the memory of Victor Ambartsumyan and Gurgen Sahakian who pioneered the field of superdense matter and compact stars in Armenia.

Contents

Foreword xv

Acknowledgments xvii

Part I Compact Stars

Dynamic stability of compact stars 3
G. S. Bisnovatyi-Kogan
1 Introduction 3
2 Early development of the theory of compact stars: 1931-1965 4
3 Criteria of hydrodynamic stability 7
4 Energetic method 11
5 Search of quark stars 16
6 Summary 19

Acknowledgments 19

References 20

Constraints on Superdense Matter from X-ray Binaries 23
M. Coleman Miller
1 Introduction and Overview 23
2 Overview of Neutron Star X-ray Binaries 25
3 Radial Velocity Measurements 31
4 Spectral Line Profiles 35
5 Light Curve Profiles 37
6 Orbital Frequencies 37
7 Summary 40

Acknowledgments 41

References 41

Postglitch Relaxations of Angular Velocity of Pulsars 43
David M. Sedrakian and M. V. Hayrapetyan
1 Introduction 43
2 Relaxation solutions 46

3 Discussion 48
References 50

Isolated neutron stars: An astrophysical perspective 53
Sergei Popov, and Roberto Turolla
1 Introduction 53
2 What's new 55
3 Discussion 61
4 Conclusion. What do we – astrophysicists – want from QCD theorists? 68

Acknowledgments 69

References 69

Part II Superdense QCD Matter

Clusters and Condensates in the Nuclear Matter Equation of State 75
Gerd Röpke, Alexander Grigo, Kohsuke Sumiyoshi, and Hong Shen
1 Introduction 75
2 Ideal Mixture of Different Components 77
3 Relativistic mean field theory 80
4 Medium modifications of two-particle correlations 82
5 Medium modification of higher clusters 86
6 Comparison with the concept of excluded volume 88
7 Isospin singlet (pn) and triplet (nn, pp) pairing in nuclear matter 88
8 Alpha cluster condensation in threshold states of self-conjugate $4n$ nuclei 89
9 Conclusions 90

References 91

Nuclear equation of state and the structure of neutron stars 93
A.E.L. Dieperink, D. Van Neck Y. Dewulf, and V. Rodin
1 Introduction 93
2 Equation of state and symmetry energy 94
3 How well do we know the symmetry energy? 96
4 Empirical information on the SE 102
5 Constraints on EoS from neutron stars 109

Acknowledgments 110

References 110

Neutron Star Structure with Hyperons and Quarks 113
M. Baldo, F. Burgio, and H.-J. Schulze
1 Brueckner theory 113
2 Three-body forces 115
3 EOS of nuclear matter from different TBF 118
4 Neutron star structure 120
5 Hyperons in nuclear matter 122

6 Quark matter 127
7 Conclusions 131

References 132

The QCD equation of state and quark star properties 135
A. Peshier, B. Kämpfer, and G. Soff
1 Introduction 135
2 Resummation and quasiparticle models 136
3 Implications for quark stars 143

References 146

Effective Lagrangians for QCD: Duality and Exact Results 147
Francesco Sannino
1 Effective Lagrangians for QCD 147
2 Color Flavor Locked Phase 149
3 Duality made transparent in QCD 150
4 2 SC General Features and Effective Lagrangian 156
5 Non Perturbative Exact Results: Anomaly Matching Conditions 161

Acknowledgments 162

References 162

Color superconductivity and high density effective theory 165
Deog Ki Hong
1 Introduction 165
2 High Density Effective Theory 166
3 More on matching 171
4 Color superconductivity in dense QCD 172
5 Quark matter under stress 175
6 Positivity of HDET 177

References 183

Color superconducting quark matter and the interior of neutron stars 187
Micaela Oertel, and Michael Buballa
1 Introduction 187
2 The scalar color antitriplet condensate 188
3 Spin-1 condensate for a two-flavor system 189
4 Neutral quark matter 194
5 Compact stars with a color superconducting quark matter core 201

Acknowledgments 205

References 205

Superconductivity with deformed Fermi surfaces and compact stars 209
Armen Sedrakian

1 Introduction 209
2 Homogeneous superconducting state 210
3 Superconducting phases with broken space symmetries 213
4 Flavor asymmetric quark condensates 219
5 Concluding remarks 221

Acknowledgments 222

References 223

Neutral Dense Quark Matter 225
Mei Huang and Igor Shovkovy
1 Introduction 225
2 Local charge neutrality: homogeneous phase 226
3 Global charge neutrality: mixed phase 234
4 Conclusion 238

References 238

Possibility of color magnetic superconductivity 241
Toshitaka Tatsumi, Tomoyuki Maruyama, and Eiji Nakano
1 Introduction 241
2 What is ferromagnetism in quark matter? 243
3 Color magnetic superconductivity 248
4 Chiral symmetry and magnetism 253
5 Summary and Concluding remarks 258

Acknowledgments 260

References 260

Magnetic Fields of Compact Stars with Superconducting Quark Cores 263
David M. Sedrakian, David Blaschke, and Karen M. Shahabasyan
1 Introduction 263
2 Free Energy 265
3 Ginzburg-Landau equations 267
4 Vortex Structure 269
5 Solution of Ginzburg-Landau Equations 271
6 The Magnetic Field Components 273
7 Summary 275

Acknowledgments 275

References 275

Thermal Color-superconducting Fluctuations in Dense Quark Matter 277
D.N. Voskresensky
1 Introduction 277
2 Physics of pairing fluctuations 279
3 Thermodynamical potential and its mean field solution 280
4 Fluctuations of gap in self-consistent Hartree approximation 281
5 Contribution of fluctuations of gap to specific heat below T_c 283

6 Ginzburg – Levanyuk criterion and Ginzburg number 286
7 Fluctuations of the gap above T_c 288
8 Assumptions which we have done 289
9 Fluctuations of temperature, density, magnetic susceptibility 289
10 How gap fluctuations may manifest in heavy ion collisions 290
11 Pairing fluctuations in hybrid stars 291
12 Concluding 293

Acknowledgments 294

References 294

The inner structure of hybrid stars 297
Bela Lukacs, Gergely G. Barnafoldi, and Peter Levai
1 Introduction 297
2 The Fifth Dimension 298
3 Field Equations 298
4 A Special Solution of the Field Equations 300
5 On the General Solution of the Field Equations 301
6 Matching Conditions on the Surface 302
7 The External Solution 302
8 Conclusion 303
9 Outlook 304

Acknowledgments 306

References 306

Part III Signals for Superdense QCD Matter in Compact Stars

Gamma-ray Bursts and their Central Engines 309
Stephan Rosswog
1 Introduction 309
2 Observations 309
3 The fireball model 312
4 Models for the Central Engine 313
5 Summary and Prospects 327

Acknowledgments 328

References 328

Superdense stars with a quark core 331
G. B. Alaverdyan, A. R. Harutyunyan, and Yu. L. Vartanyan
1 Introduction 331
2 Equations of state 332
3 Superdense configurations with a strange quark core. Results and Discussion 333
4 Summary 339

Acknowledgments 340

References 340

Diquark condensation effects on hot quark star configurations 341
A. Öztas, D. Blaschke, S. Fredriksson, and H. Grigorian
1 Introduction 341
2 Thermodynamic potential for asymmetric 2SC quark matter 343
3 EoS for 2SC quark matter in β-equilibrium 344
4 EoS of quark matter in 2SC phase for finite temperature 345
5 Configurations of hot quark stars 346
6 Conclusion 349

References 350

Gamma Ray Bursts and delayed Quark-deconfinement 353
Ignazio Bombaci, Irene Parenti, and Isaac Vidaña
1 Introduction 353
2 Quantum nucleation of quark matter in hadronic stars 357
3 Results 361
4 Mass-to-radius ratio and internal constitution of compact stars 368
5 Quark Deconfinement Nova and GRBs 372
6 Summary 373

References 373

Color Superconducting Quark Matter and Compact Star Observables 377
D. N. Aguilera, J. Berdermann, D. B. Blaschke, H. A. Grigorian, A. Khalatyan, G. Poghosyan and D. N. Voskresensky
1 Introduction 378
2 Nonlocal chiral quark model (NCQM) 379
3 EoS for nonstrange compact stars 381
4 Cooling of compact stars 395
5 Protoquark star evolution and Gamma Ray Bursts 397
6 Conclusions 402

Acknowledgments 402

References 402

Looking inside the Earth with solar and supernova neutrinos: An analytic approach 405
A. N. Ioannisian and A. Yu. Smirnov
1 Introduction 405
2 ϵ- perturbation theory and oscillation probabilities 406
3 Effect of averaging over neutrino energy 410
4 Conclusions 411

References 413

Deconfinement Phase Transition in Relativistic Neutron Star Mergers 415
G. Poghosyan, R. Oechslin, K. Uryū, and F. K. Thielemann
1 Introduction 416

2 Equation of State 417
3 Summary 419

Acknowledgments 424

References 424

Index 427

Foreword

In the early thirties of the last century Baade and Zwicky conjectured in their studies of supernova explosions that supernovae represent a transition from ordinary stars to compact objects, whose size is an order of magnitude smaller than the size of a white dwarf. At that time it was already known that the atomic nucleus consists of neutrons and it was clear that the density of the remnant objects must be of the same order as the nuclear density. Baade and Zwicky predicted that a supernova explosions will result in objects composed of closely packed neutrons (neutron stars). Prior to the beginning of the second World War (1939) a number of theoretical works by Landau, Oppenheimer, Volkoff and Snider showed, that indeed objects could exist with sizes about 10 km and masses about a solar mass. The density in these objects is about the nuclear saturation density and they basically consist of neutrons with a small amount of protons and electrons. The studies of neutron stars were subsequently stopped most likely due to the engagement of the nuclear scientists in the development of the nuclear bomb both in the West and the East.

After a 20 year break V. H. Ambartsumyan and G. S. Sahakian initiated an intensive research on compact objects during the 1960s in Armenia. In their pioneering work on compact stars they showed, that with increasing density, hyperons appear in nuclear matter and thus a neutron star at high densities consists predominantly of hyperons. Thus, as the density increases more and more heavy particles become stable. After the discovery of quarks as basic constituents of hadrons (including hyperons) the ideas of compact stars with quark cores or stars entirely composed of quark matter were presented.

Another important result obtained by Armenian physicists during the 1960s, is the observation that the mass of superdense objects is limited and is about several solar masses. This conclusion made in the beginning of the 1960s, actually proved the statement that the stars with masses above several solar masses turn into black holes at the end of their evolution. These works have stimulated intensive studies of black holes which are continued until now.

The problem of rotation of neutron stars in the framework of General Relativity Theory was solved before the discovery of pulsars and the important contribution of the Armenian scientists in this work is well documented. With all

the theoretical work done on compact objects by the late 1960s, the fortuitous discovery of pulsars in 1968 was both gratifying and encouraging, however this was not a surprise to most of the practitioners in this field. The scientists in Armenia continued contributing to the investigations of pulsars and compact objects since then; their work includes studies of the equation of state of matter, strong magnetic fields, superfluid and superconducting properties of neutrons and protons in neutron stars, strange neutron stars, dynamics of pulsar rotation and other phenomena related to superdense objects.

The organization of this conference on superdense QCD matter in compact stars in Yerevan in 2003, the year in which the founders of the Armenian scientific school V. H. Ambartsumyan and G. S. Sahakian would become 95 and 85 years old, was the homage to them and all the Armenian scientists, who have made contributions to the investigation of superdense stellar matter.

This conference which brought together leading experts in the fields of dense matter as well as compact star physics from the Eastern and the Western hemispheres was made possible due to the support by the NATO Science programme which is gratefully acknowledged.

David Sedrakian
Department of Physics
Yerevan State University
Yerevan, January 2004

David Blaschke
Department of Physics
Rostock University
Rostock, December 2003

Acknowledgments

This is to acknowledge the help of the local organizing committee: Edvard Chubarian, Roland Avagyan, Vladimir Papoyan(†), Julieta Drnoyan, Narine Gevorgyan, Avetis Sadoyan, Anna Sargsyan, Armen Yeranyan in the preparation and conduction of the conference. Special thanks go to Armen Sedrakian and Jens Berdermann for their assistance in the process of making of this book.

I

COMPACT STARS

DYNAMIC STABILITY OF COMPACT STARS

G. S. Bisnovatyi-Kogan
Space Research Institute RAN, Moscow, Russia
and Joint Institute for Nuclear Research, Dubna, Russia *
gkogan@mx.iki.rssi.ru

Abstract After some historical remarks we discuss different criteria of dynamical stability of stars and the properties of the critical states where the loss of dynamical stability leads to a collapse with formation of a neutron star or a black hole. At the end some observational and theoretical problems related to quark stars are discussed.

Keywords: stellar stability, white dwarfs, neutron stars, quark stars

1. Introduction

It was first noted by S. Chandrasekhar in 1931 that the mass of a compact star at very large densities, when electrons become relativistically degenerate, cannot exceed a value, which is now called the Chandrasekhar limit for white dwarfs (Chandrasekhar, 1931). After the discovery of the neutron in 1932 the idea of the existence of neutron stars was developed. The matter in these stars is so dense, that neutrons become relativistically degenerate, which again leads to a maximum possible mass of a neutron star. There are two important differences between the white dwarfs and the neutron stars, which are influencing their stability and mass limit. The neutron stars are about 6 orders of magnitude denser than the white dwarfs, which makes it necessary to use the general relativity (GR) in the description of gravitation, instead of Newtonian gravity. In GR the gravitational force is growing faster than $1/r^2$; this reduces the stability and decreases the mass limit. On the other hand, neutron interactions become important at densities exceeding the nuclear one. The repulsion forces between nucleons at large densities lead to additional stabilization against collapse and increase in the limiting mass of a neutron star. The influence of the second factor appears to be more important, so that presently the limiting mass of a neutron star is taken about two times larger than that of the white dwarf.

*Partial funding provided by RFBR grant 02-02-16900.

D. Blaschke and D. Sedrakian (eds.), Superdense QCD Matter and Compact Stars, 3–21.

The discovery of the quark structure of matter led to the suggestion of possible existence of quark stars, which are even more compact than neutron stars. In the presence of indefiniteness concerning the quark structure of matter it is not possible now to make definite statements about the existence or nonexistence of stable quark stars, observational and theoretical investigations on this topic are still in progress.

In this review I first make a historical excursus into the problem, mentioning the results of the key works. Several criteria of stability are discussed, with the main focus on the static criteria, and the energetic method, which permits to obtain conclusions about the stability (sometimes approximate) in a most simple way. Critical states of compact stars at the boundary of the dynamic stability are considered, at which the star is becoming unstable in the process of energy losses, and a collapse begins leading to formation of a neutron star or a black hole. Physical processes leading to a loss of stability are discussed. At the end some observations and theoretical problems connected with quark stars are considered.

2. Early development of the theory of compact stars: 1931-1965

From the theory of polytropic gravitating gas spheres with the equation of state $P = K\rho^\gamma$ it was known (Emden, 1907), that at $\gamma = 4/3$ the equilibrium mass has a unique value

$$M = 4\left(\frac{K\pi}{G}\right)^{3/2} M_3, \tag{1}$$

where $M_3 = 2.01824$ is a non-dimensional mass, corresponding to the polytropic index $n = 3$, $\gamma = 1 + \frac{1}{n}$. Such a star is in a neutral equilibrium at any density. Chandrasekhar (1931) first noticed, that at large densities the electron degeneracy is becoming ultrarelativistic with the equation of state

$$P = \frac{\pi}{4}\left(\frac{3}{\pi}\right)^{1/3} \hbar c n_{\rm e}^{4/3}, \quad n_{\rm e} = \frac{\rho}{\mu m_p}. \tag{2}$$

For some unknown reason Chandrasekhar (1931) took "μ equal to the molecular weight, 2.5, for a fully ionized material", corresponding to $K = 3.619{\cdot}10^{14}$ and obtained the limiting mass from (1) equal to $1.822{\cdot}10^{33}$g$= 0.91\,M_\odot$. Landau (1932) noticed, that for most stable nuclei: He^4, C^{12}, O^{16} etc. the value of μ, which is the number of nucleons to one electron, is equal to 2, and he obtained the realistic value of the limiting mass $M_{lim} = 1.4\,M_\odot$.

Soon after the discovery of the neutron (Chadwick, 24 Feb. 1932, letter to N. Bohr), "Landau improvised the concept of neutron star" in discussion with Bohr (Rosenfeld, 1974). The modern conception of the neutron star origin is

due to Baade and Zwicky (1934), which appeared as a result of their studies of supernova explosions. Their conclusion: "With all reserve we advance the view that supernovae represent the transitions from ordinary stars into *neutron stars*, which in their final stages consist of extremely closely packed neutrons", is an example of classic astrophysical predictions, finally proved only 35 years later after the discovery of the pulsar in the center of the Crab nebula (Lovelace et al., 1968; Comella et al., 1969). Investigations of the properties of matter at nuclear and larger densities expected in neutron stars were started in the papers by Hund (1936), Landau (1938) and Gamow (1938).

The first neutron star model in GR was constructed by Oppenheimer and Volkoff (1939). They derived the equations governing a spherically symmetric stellar equilibrium in GR using a metric of the form

$$ds^2 = -e^{\nu}\,dt^2 + e^{\lambda}\,dr^2 + r^2(d\theta^2 + \sin^2\theta\,d\varphi^2) \tag{3}$$

with equilibrium equations

$$\frac{dP}{dr} = -\frac{G(\rho + P/c^2)(m + 4\pi r^3 P/c^2)}{r^2(1 - 2Gm/rc^2)}, \tag{4}$$

$$\frac{dm}{dr} = 4\pi\rho r^2, \quad \rho = \rho_0\left(1 + \frac{E}{c^2}\right), \;\; \rho(R) = 0, \;\; M = m(R).$$

An ideal degenerate neutron gas at zero temperature was considered with energy E_n, pressure P_n, and rest mass density ρ_0 defined as

$$\begin{aligned} E_n &= \frac{m_n^4 c^5}{24\pi^2\hbar^3\rho} g(y) = \frac{6.860\cdot 10^{35}}{\rho} g(y), \\ P_n &= \frac{m_n^4 c^5}{24\pi^2\hbar^3\rho_0} f(y) = \frac{6.860\cdot 10^{35}}{\rho_0} f(y), \\ \rho_0 &= \frac{m_n^4 c^3}{3\pi^2\hbar^3} y^3 = 6.105\cdot 10^{15} y^3 \end{aligned} \tag{5}$$

where

$$\begin{aligned} f(y) &= y(2y^2 - 3)\sqrt{y^2+1} + 3\sinh^{-1} y, \\ g(y) &= 3y(2y^2 + 1)\sqrt{y^2+1} - 3\sinh^{-1} y, \quad y = \frac{p_{n,Fe}}{m_n c}. \end{aligned} \tag{6}$$

The parameters they obtained for neutron stars of different masses are listed in Table 1. Between white dwarfs and neutron stars there is a neutronization and a transition from normal matter with electrons and nuclei to superdense matter consisting of neutrons and other strongly interacting particles: mesons and hadrons. The continuous curve $M(\rho_c)$ in the whole region from white

Table 1. Total mass of the neutron star model versus its radius calculated by Oppenheimer and Volkoff (1939).

Total mass in Solar units	Radius in km
0.30	21.1
0.60	13.3
0.71	9.5
0.64	6.8
0.34	3.1

dwarfs to neutron stars was first constructed by Wheeler (1958), where only neutrons have been considered in the superdense phase, like in Oppenheimer and Volkoff (1939). The results of Wheeler (1958) are given in Fig. 1. The first neutron star model with a realistic equation of state, including mesons, hyperons and nuclear interaction, was constructed by Cameron (1959). The following equilibrium reactions between strongly interacting particles have been taken into account

$$\begin{gathered} n+n \to n+n+2\pi^0 \to \Lambda^0+\Lambda^0-2(177)\ \mathrm{MeV}, \\ p+p \to p+p+2\pi^0 \to \Sigma^+ + \Sigma^+ - 2(251)\ \mathrm{MeV}, \\ \Lambda^0+\Lambda^0 \to \Lambda^0+\Lambda^0+\pi^0 \to \Sigma^0+\Sigma^0-2(77)\ \mathrm{MeV}, \\ n+n \to n+p+\pi^- \to p+\Sigma^- - 256\ \mathrm{MeV}, \\ n+\Lambda^0 \to p+\pi^-+\Lambda^0 \to p+\Xi^- - 204\ \mathrm{MeV}, \\ \Lambda^0+\Lambda^0 \to \Lambda^0+\Lambda^0+2\pi^0 \to \Xi^0+\Xi^0-2(195)\ \mathrm{MeV}. \end{gathered} \tag{7}$$

The nuclear interaction was considered according to Skryme (1959), see Fig. 2. This equation of state is not perfect, because at large densities it violates the causality principle, according to which the sound speed cannot exceed the light speed (see Zeldovich, 1961). Neutron star models obtained by Cameron (1959) are presented in Fig. 3. The most important result of this work was the indication that for realistic equation of state the limiting mass of a neutron star may exceed the Chandrasekhar mass limit for white dwarfs. Therefore, after the loss of stability a stellar core with mass exceeding the Chandrasekhar mass limit may stop its contraction forming a stable neutron star with enormous energy output, according to Baade and Zwicky (1934). In the model of Oppenheimer and Volkoff (1939) the collapse would not stop, because of the low mass limit of neutron stars. Cameron (1959) obtained that models at high densities have monotonously decreasing mass, which asymptotically tend to a constant value. That was probably the result of crudeness of calculations,

because the behavior of the curve $M(\rho_c)$ at large densities has oscillating, and not monotonous dependence. Such oscillations are present in the calculations of Ambartsumyan and Saakyan (1961), who also improved physical description of superdense matter (Ambartsumyan and Saakyan, 1960). The nature of the high density oscillations of mass in GR equilibrium was explained by Dmitriyev and Kholin (1963) (see also Misner and Zapolsky, 1964). They showed that all models beyond the first neutron star mass maximum on the curve $M(\rho_c)$ are unstable, and after each new extremum the model acquires one new unstable mode. Later this problem was analyzed at length in the book of Harrison et al. (1965). Detailed calculations of neutron star models with a realistic equation of state have been carried out by Saakyan and Vartanyan (1964).

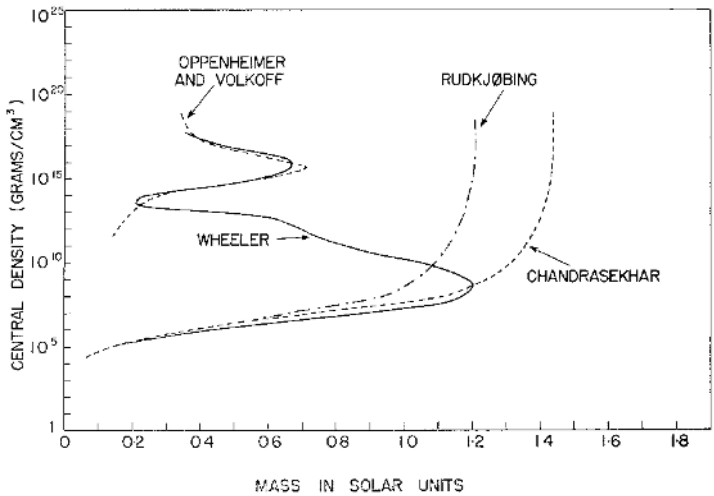

Figure 1. The relation between central density and the mass of various degenerate star models. Chandrasekhar's curve is for white dwarfs with a mean molecular weight 2 of atomic mass units. Rudkjóbing's curve is the same except for inclusion of the relativistic spin-orbit effects Rudkjóbing (1952). The curve labeled "Oppenheimer and Volkoff" is for a set of neutron star models. The solid line marked "Wheeler" is a set of models computed with a generalized equation of state, from Cameron (1959).

.

3. Criteria of hydrodynamic stability

The exact approach to the problem of dynamic (linear) stability is based on the solution of the equations for small perturbations, and finding eigenvalues and eigenfunctions of these equations. In a conservative system a variational principle may be derived, which determines the exact value of eigenfrequency

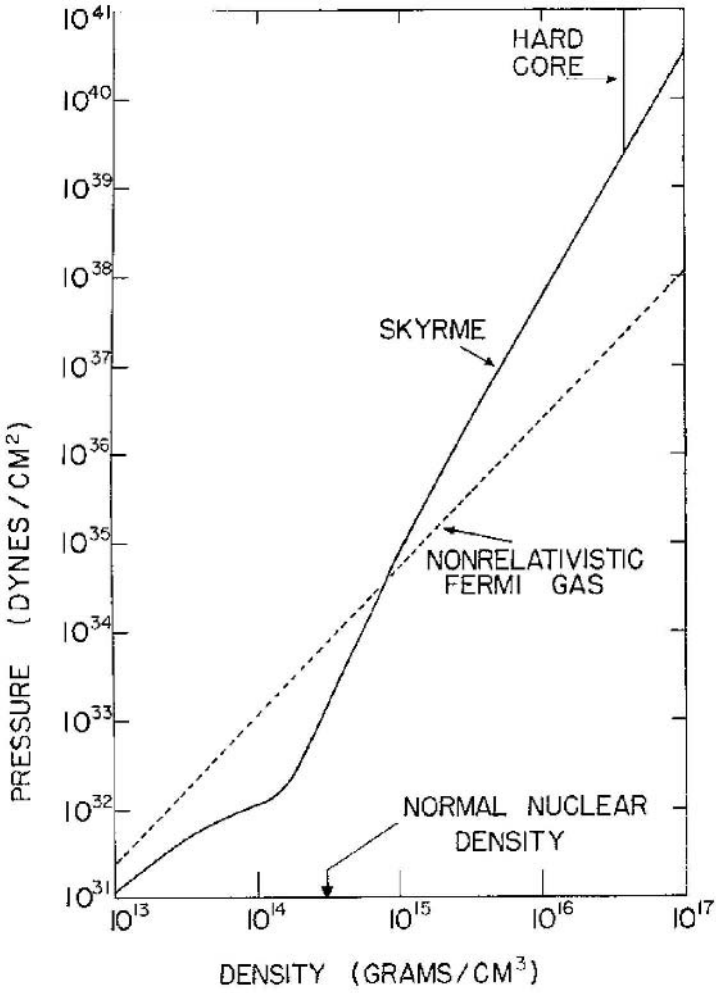

Figure 2. Skryme's equation of state. The hard core modification is shown at the upper right, and the dashed line is the equation of state for a non-relativistic Fermi gas of neutrons, from Cameron (1959).

if the exact eigenfunction is known. In practice, even the use of an approximate linear eigenfunction often defines the eigenfrequency with a good precision. The variational principle for a spherically symmetric star in GR was first derived by Chandrasekhar (1964) from the equations of small perturbations, and later by Harrison et al. (1965) by variation of the potential energy of the star. The exact method for determination of the dynamic stability of a star with respect to adiabatic perturbations based on the sequence of static solutions was formulated by Zeldovich (1963). He had shown, that at the extremum of the

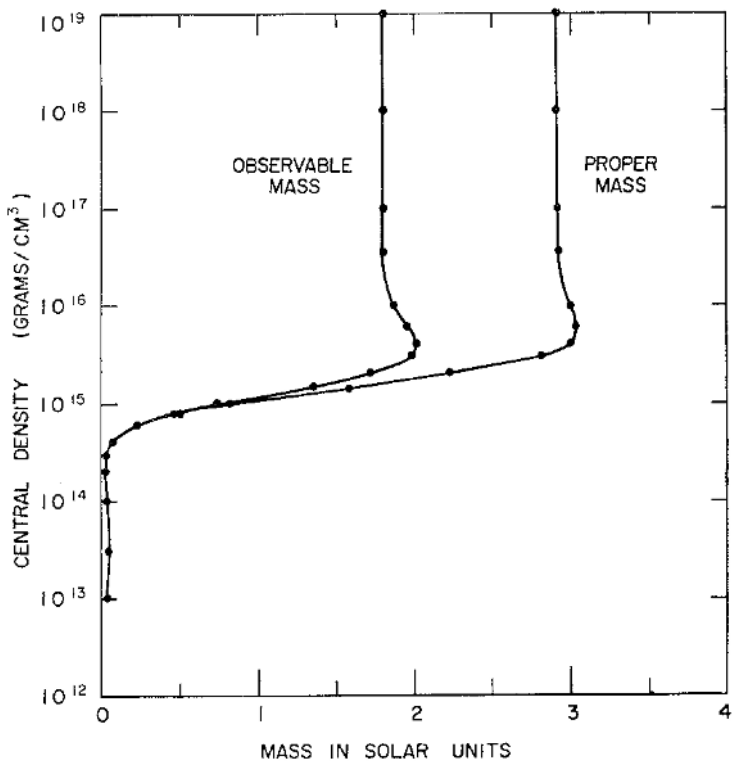

Figure 3. The observable and proper masses of neutron star models with non-ideal matter, from Cameron (1959).

function $M(\rho_c)$, or $M(R)$ along the sequence with a constant entropy S one unstable mode is added or subtracted. On the curve of cold stars in Fig. 1 the stability is lost in the first maximum due to neutronization, or GR effects, but it is restored in the minimum, where a stable neutron star appears. The static criterion of stability was generalized to the case of arbitrary rotating stars with arbitrary distribution of entropy over the star in the paper of Bisnovatyi-Kogan and Blinnikov (1974). It was noted, that in the presence of three quantities conserved during adiabatic oscillations, the critical points are the extrema of three functions $M(\rho_c)|_{s,j}$, $s(\rho_c)|_{M,j}$, $J(\rho_c)|_{M,s}$. Here along the sequences not only the total values of stellar angular momentum J and entropy S should be conserved, but also their distributions over the Lagrangian coordinate N, which is the number of baryons inside the cylindrical radius, $j(N)$ and $s(N)$. Note that in the Newtonian case a Lagrangian coordinate coincides with the Lagrangian mass $m = \rho N = \rho_0 N$, but differs from it in the GR case. Examples of an application of the static criteria by Bisnovatyi-Kogan and Blinnikov (1974) are

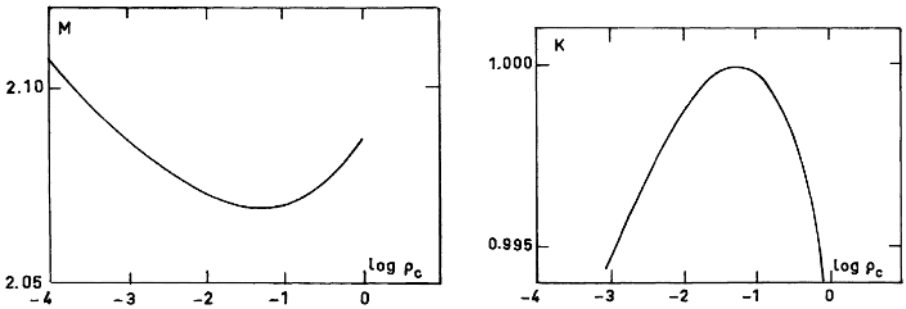

Figure 4. The dependence of the mass M on the central density for fixed entropy and angular momentum, for isentropic models with a polytropic index $n = 3.03$. The angular momentum distribution is given in Eq. (8) (**left**). The dependence of K on central density for fixed angular momentum distribution, corresponding to the minimum of mass in the left figure, for isentropic models with polytropic index $n = 3.03$ (**right**). From Bisnovatyi-Kogan and Blinnikov (1974).

represented in Fig. 4 for polytropic equation of state and angular momentum distribution similar to the rigid rotation

$$P = K\rho^{1+1/n}, \;\; K = \text{const} \cdot e^s, \;\; j(m) = \frac{5}{2}\frac{J}{M}[1-(1-m)^{2/3}] \qquad (8)$$

Let us stress, that along the curve appropriate for a static criterion of stability the rotation does not remain rigid, but only the angular momentum of each Lagrangian loop is conserved. This means that if you have a curve of rigidly rotating stars with a fixed total angular momentum you should construct an adjusted curve from each point of this curve with a constant angular momentum of a Lagrangian loop, the maximum of which indicates loss of stability. The rigidly rotating model is on the border of stability, when its position coincides with the maximum of the adjusted curve. For a cold white dwarf with the equation of state

$$\rho = Ax^3\left(2 + a_1 x + a_2 x^2 + a_3 x^3\right),$$

$$P = B\left[x\left(2x^2-3\right)\left(x^2+1\right)^{1/2} + 3\ln\left(x+\sqrt{1+x^2}\right)\right],$$

$$A = 9.82\times 10^5 \text{ g cm}^{-3}, \quad B = 6.01\times 10^{22} \text{ erg cm}^{-3}, \qquad (9)$$

$$a_1 = 1.255\times 10^{-2}, \quad a_2 = 1.755\times 10^{-5}, \quad a_3 = 1.376\times 10^{-6},$$

the adiabatic index is close to $n = 3$ at the critical point, and the eigenfunction is close the linear one. For a homologous transformation the rigid rotation is preserved, so that the adjusted curve for white dwarfs differs only slightly from the curve of rigidly rotating models, see Fig. 5 (left). For a more complicated

equation of state with highly variable adiabatic index, like in the equation of state

$$\rho(H) = \frac{1}{2}\,\rho_1 \left[\left(\frac{H}{H_1} \right)^{0.3} + \left(\frac{H}{H_1} \right)^{10} \right], \tag{10}$$

$$P(H) = \frac{1}{2}\,\rho_1 H_1 \left[\frac{(H/H_1)^{1.3}}{1.3} + \frac{(H/H_1)^{11}}{11} \right];$$

here H is the enthalpy and the subscript 1 on physical quantities indicates that their values are those for the rigidly rotating configurations; the value $\gamma_1 = \frac{4}{3}$ at $\rho = \rho_1$ and falls off steeply when $\rho > \rho_1$. The results of calculations for a model with solid-body rotation and three associated series of models are given in Fig. 5 (right). The loss of stability occurs at the point of intersection of the associated curve D with the solid-body one, this point coinciding with the maximum on the curve D. It can be seen from Fig. 5 (right) that the point of stability loss differs from the maximum on the solid-body curve by almost 5% with respect to ρ_c. An extension of static criteria to general relativity and toroidal magnetic fields is made in the paper of Bisnovatyi-Kogan and Blinnikov (1974). Static criteria remain valid also in the presence of phase transitions. Variational principles and other methods of investigation of stability in the presence of phase transitions are considered by Bisnovatyi-Kogan, Blinnikov and Shnol (1975). The review of stellar stability methods is given in the book of Bisnovatyi-Kogan (2002).

4. Energetic method

In the case of a complicated equation of state and entropy distribution along the star, the static criteria are hard to apply. In this case it is more convenient to use an approximate energetic method, which follows from the exact variational principle where linear trial function is used for estimation of the eigenfrequency. The energetic method was first applied for investigation of stability of supermassive isentropic stars by Zeldovich and Novikov (1965) where first GR corrections to the energy of such star have been found. This method was generalized for arbitrary stars by Bisnovatyi-Kogan (1966). Equations, giving an approximate description of the equilibrium and determining the critical point where stability is lost have been derived. The first equation represents equilibrium condition, following from the first variation of the total potential energy of star (gravitational plus internal for nonrotating stars) equal to zero. The model with adiabatic index $n = 3$, $\gamma = 4/3$ is in a neutral stability with a linear eigenfunction. In application of the energetic method the density distribution of the model is prescribed by the polytropic $n = 3$ distribution, $\rho = \rho_c \varphi(m/M)$, where m is a Lagrangian mass coordinate, and $\varphi(m/M)$ is connected with the Emden function corresponding to $n = 3$, with

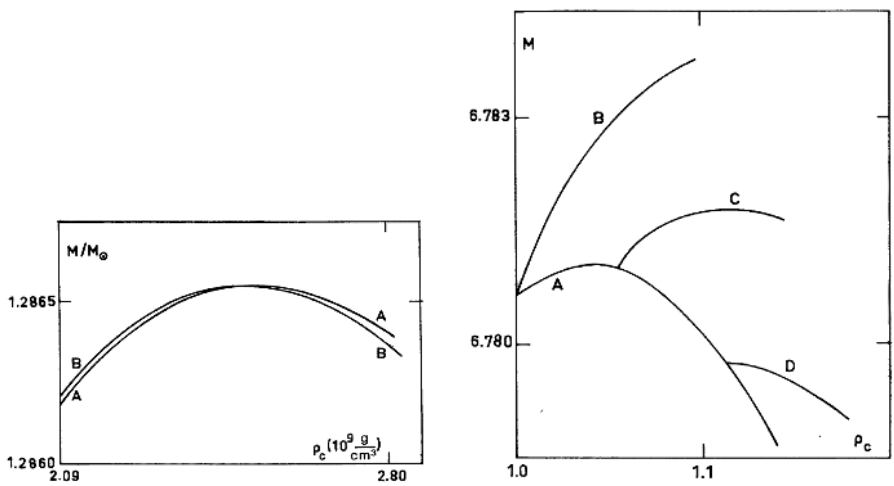

Figure 5. The dependence of the mass M on the central density for rigidly (Curve A) and differentially (Curve B) rotating white dwarfs with the equation of state defined by Eq. (9). The angular momentum distribution of the Curve B is that of the extremal model of Curve A (**left**). The dependence of the mass M on the central density for rigidly (Curve A) and differentially (Curves B,C and D) rotating models with the equation of state defined by Eq. (10). The angular momentum distribution of the Curves B, C and D are those of the rigidly rotating models of the Curve A at the points of its intersection with the Curves B, C and D. The curve C is intersecting the Curve A in its maximum. The maximum of the Curve D coincides with the point of intersection, which is a critical point for rigidly rotating models.(**right**). From Bisnovatyi-Kogan and Blinnikov (1974).

a linear trial function $\delta r = \alpha r$, α=const. The equation of state is arbitrary with the prescribed entropy distribution over the Lagrangian coordinate, and first GR correction to the energy, including all terms $\sim R/R_g$, R is stellar radius, $R_g = 2GM/c^2$ is the gravitational radius, are taken into account. The equilibrium equation in the approximate energetic method is:

$$3\rho_c^{4/3}\int_0^M P\frac{dm}{\varphi\left(\frac{m}{M}\right)} - 0.639\,GM^{5/3} - 1.84\,\frac{G^2M^{7/3}}{c^2}\,\rho_c^{1/3} = 0. \qquad (11)$$

Under the above mentioned conditions the second variation of the energy is also reduced to an integral relation. The zeros of this relation approximately corresponds to the critical state of the loss of stability. We have

$$9\rho_c^{-5/3}\int_0^M \left(\gamma - \frac{4}{3}\right) P\frac{dm}{\varphi(m/M)} - 1.84\,\frac{G^2M^{7/3}}{c^2} = 0. \qquad (12)$$

These equations have been obtained by Bisnovatyi-Kogan (1966), using the expression of the energy with the prescribed distributions of the density (Emden polytrope $n = 3$) and entropy (arbitrary) over the Lagrangian coordinate m/M,

$$\epsilon = \int_0^M E(\rho,T)\,dm - \int_0^M \frac{Gm\,dm}{r} - 5.06\,\frac{G^2M^3}{R^2c^2} \qquad (13)$$

$$= \int_0^M E(\rho,T)\,dm - 0.639\,GM^{5/3}\,\rho_c^{1/3} - 0.918\,\frac{GM^{7/3}}{c^2}\,\rho_c^{2/3},$$

$$dm = 4\pi\rho r^2 dr$$

by differentiation over the central density. The critical parameters of iron isentropic stellar cores for masses between 5 and 1000 $M_\odot$ at the point of the loss of stability have been calculated by Bisnovatyi-Kogan and Kazhdan (1966). The dependence of the critical central density on mass is represented in Fig. 6 (Bisnovatyi-Kogan, 2002) for a wide range of masses. For low masses and high densities the stability in the iron core is lost due to neutronization. For larger masses the temperature in the critical point is increasing, and the stability is lost due to iron disintegration, decreasing the adiabatic power, and making it $\gamma \le 1$. At masses around 1000 $M_\odot$ with decreasing density and temperature, the adiabatic power becomes less than 4/3 mainly due to pair creation, and at further increasing of mass the effects of GR are the main reason of the loss of stability (Zeldovich and Novikov, 1965). For large masses the dependence $\rho_c(M)$ is described by the relation

$$\rho_{c,\mathrm{cr}}(M) = 2.4\times10^{17}\frac{1}{\mu^3}\left(\frac{M_\odot}{M}\right)^{7/2}\ \mathrm{g\ cm^{-3}}, \qquad (14)$$

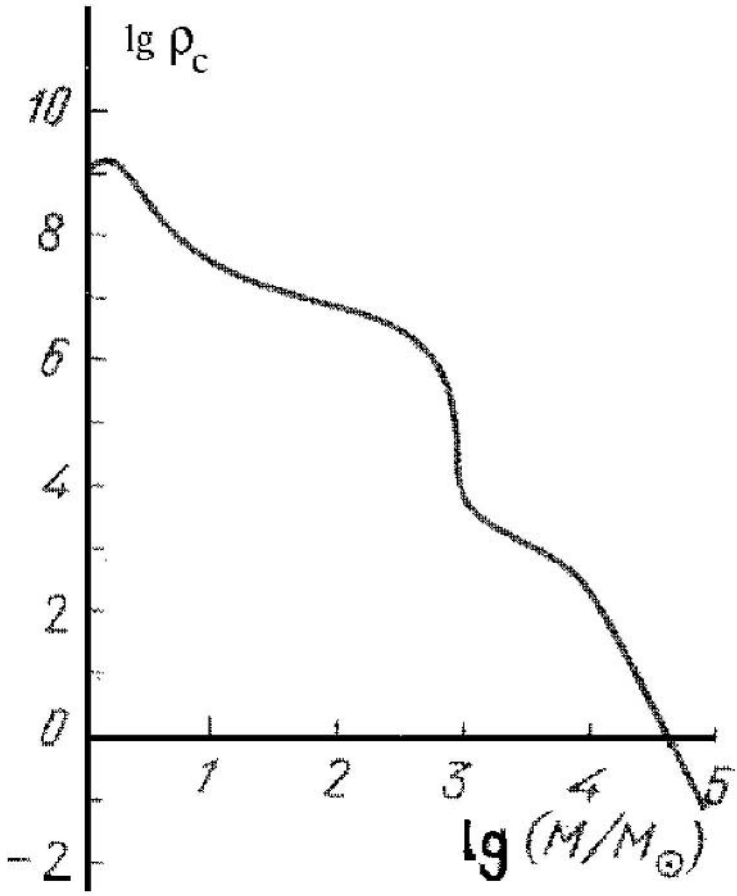

Figure 6. Central density as a function of stellar core mass (in solar mass units) for the critical states, from Bisnovatyi-Kogan (2002).

where μ is the molecular weight.

Models of hot isentropic neutron stars have been calculated by Bisnovatyi-Kogan (1968), where equilibrium between iron, protons and neutrons was calculated, and the ratio of protons and neutrons was taken in the approximation of zero chemical potential of neutrino. The stability was checked using a variational principle in full GR (Chandrasekhar, 1964) with a linear trial function. The results of calculations, showing the stability region of hot "neutron" stars are given in Fig. 7. Such stars may be called "neutron" only by convention, because they consist mainly of nucleons with almost equal number of neutrons and protons. The maximum of the mass is about $70M_{\odot}$, but from comparison of the total energies of hot neutron stars with presupernova cores we may conclude, that only collapsing cores with masses less that $15M_{\odot}$ have

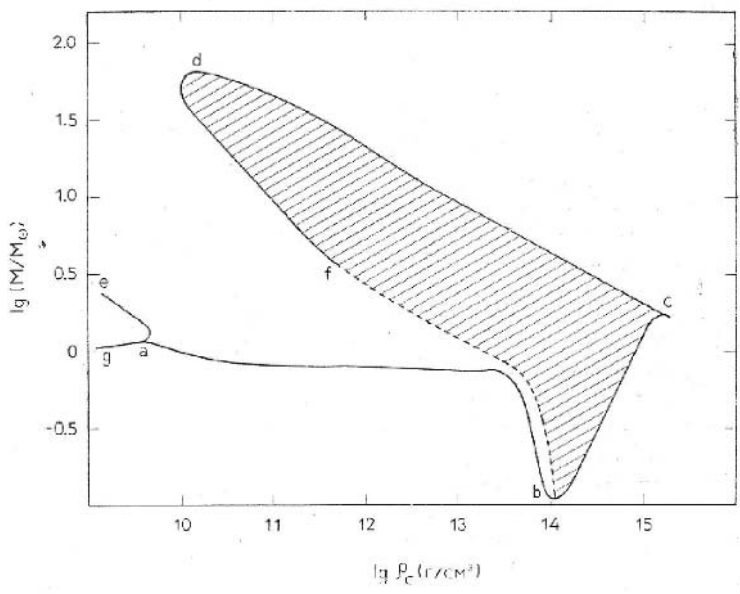

Figure 7. Equilibrium stable configurations on the mass M, central rest-mass density ρ_c diagram for superdense isentropic stars (hatched). The stars become stable at sufficiently large densities because of nucleon pressure, and become unstable again at larger densities due to GR effects, from Bisnovatyi-Kogan (1968).

a chance to stop at the state of a hot neutron star, and larger masses collapse directly to black holes.

The energetic method was generalized for rotating stars in the paper of Bisnovatyi-Kogan, Zeldovich and Novikov (1967), and in a more precise formulation by Bisnovatyi-Kogan and Ruzmaikin (1973). The density distribution remains the same, and the rotational energy term, written as a function of the total angular momentum is added. Rotational energy of the whole star depends on the central density as $\sim R^{-2} \sim \rho^{2/3}$, like the first GR correction term in (13). Therefore next order GR corrections $\sim R^{-3}$, which include also GR corrections to the internal and rotational energies have been taken into account, Calculations of the second GR corrections to the energy of nonrotating stars have been first done by Vartanyan (1972). Energetic method with two GR corrections for rotating stars was applied for an investigation of stability of supermassive stars by Bisnovatyi-Kogan and Ruzmaikin (1973). It was obtained, that for large angular momenta rotation stabilizes the star against a collapse and prevents the formation of a black hole. It is in correspondence with the fact, that the Kerr solution for a rotating black hole exist only for sufficiently small angular momenta, and there are no black holes at larger values. Only radiation with $\gamma = 4/3$ was taken into account in the equation of state, what led

to the absence of equilibrium configurations at low angular momenta j. The curves for equilibrium configurations at different j are represented in Fig. 8 on the plane: equilibrium entropy s_{eq} - $x = R_g/R$. The results are expressed in non-dimensional variables and are valid for an arbitrary mass star with the adiabatic equation of state $P = K\,\rho^{4/3}$. The energetic method gives asymptotically exact results for slowly rotating supermassive stars, but even at large j the results remain correct qualitatively.[1]

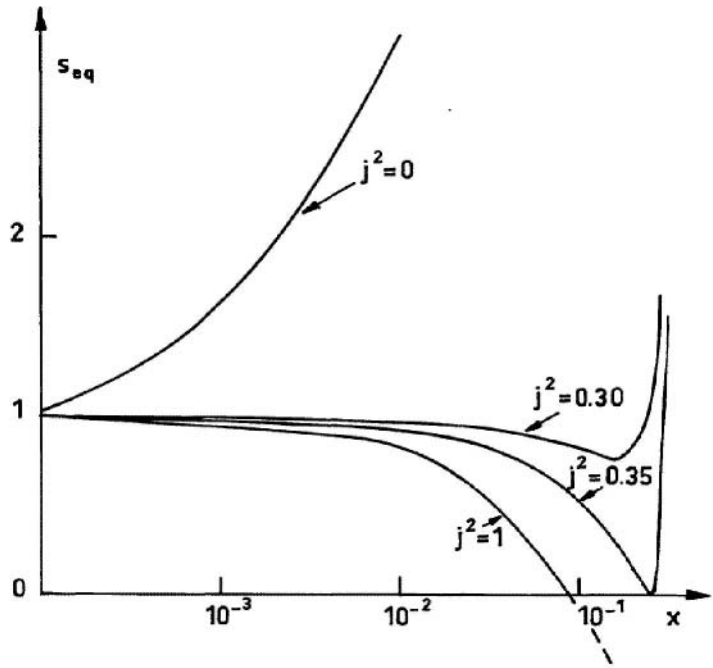

Figure 8. The curves s_{eq} which characterize the equilibrium entropy versus of $x = \frac{R_g}{R}$ for different values of the angular momentum j. The broken part corresponds to nonphysical states $s_{eq} < 0$. The parts of curves to the left of minima correspond to stable states, from Bisnovatyi-Kogan and Ruzmaikin (1973).

5. Search of quark stars

At very high densities the equilibrium lowest energy state corresponds to quarks. However because of large uncertainties in the theory the condition

[1]Because an approximate trial function does not give an absolute minimum of the energy functional, the loss of stability happens, strictly speaking, "before" the point obtained by the energetic method (EM), when going along the sequence of decreasing entropy or angular momentum. It means, that the model is definitely unstable at the EM critical point.

at which the quark state becomes preferable lies in a large density interval. Moreover, the process of transition between nucleon and quark state is also not definite, and even at very large densities the time of this transition may be enormously long. The idea of a possibility of quark stars was first suggested by Ivanenko and Kurdgelaidze (1965). Depending on the theory parameters it is possible to obtain 3 types of quark stars: strange stars (SS), which consists of strange matter which may be stable at nuclear density with a zero pressure; hybrid stars with hadronic envelope, which have a core composed of pure quarks (QC), or have a mixed core of hadrons and quarks (MC). There are different approaches to describe a quark matter, see Aguirre and De Paoli (2002), Andersen and Strickland (2002), Burgio et al. (2002), Sedrakian and Blaschke (2002), Kohri et al. (2003), Lugones and Horvath (2003), Alford (2003), Mishustin et al. (2003). The results of calculation of hadronic (H) and quark stellar models (SS, QC and MC) in Hard-Dense-Loop approach are represented in Fig. 9 from Thoma et al. (2003), where one of the model parameters is changing. The free quarks exist in the state of deconfined quarks, and the density when deconfined quarks become energetically preferable is also rather indefinite (Berezhiani et al., 2003).

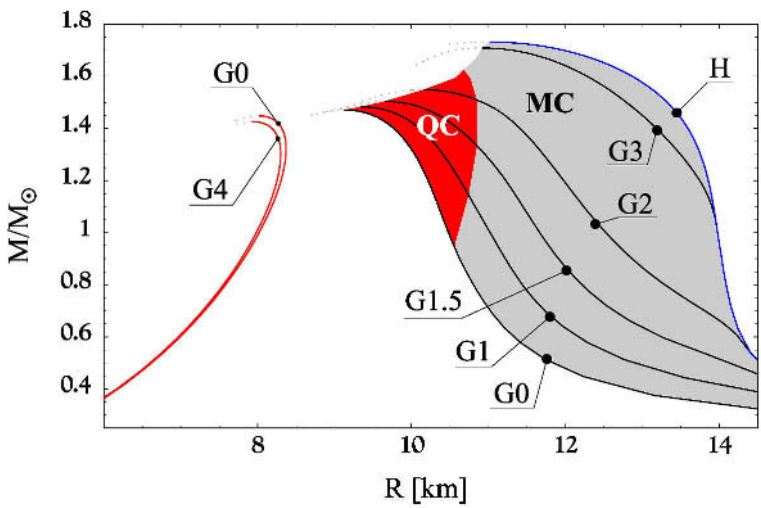

Figure 9. Mass-radius relation for pure strange quark matter stars (left) and hybrid stars (right). G0 - G4 models of hybrid stars corresponding to different parameters of the model. H: pure hadron star, QC: star has a quark core, MC: star has a mixed core, from Thoma et al. (2003).

Larger scattering of the properties of quark stars is obtained by Andersen and Strickland (2002), who used the same Hard-Dense-Loop approach, but with wider variation of parameters. Their models of quark stars are represented in Fig. 10.

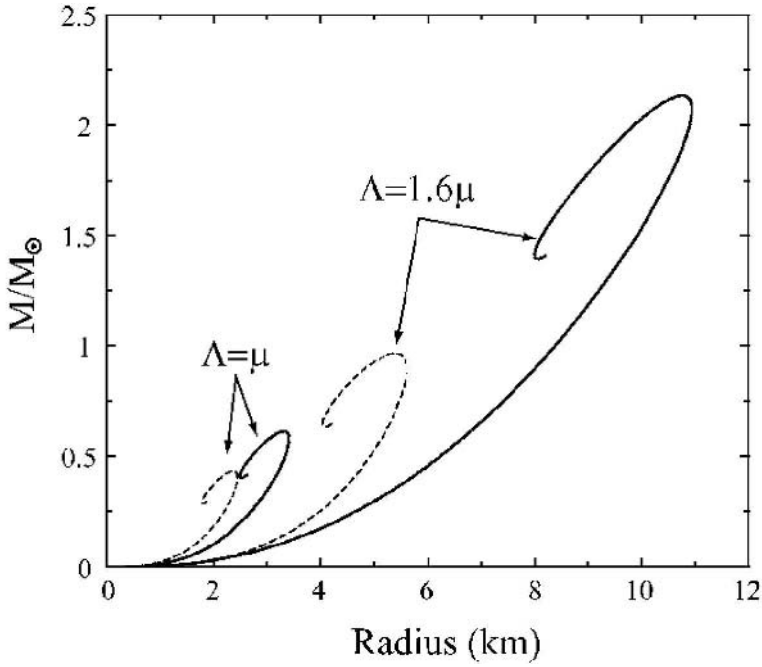

Figure 10. Mass-radius relation for a quark star with $\Lambda/\mu = 1.6$ and $\Lambda/\mu = 1$. The weak-coupling results for the same choice of renormalization scales are shown as dashed lines, from Andersen and Strickland (2002).

In the presence of such problems with theory, only observations could give an answer about the possibility of existence of quark stars. Even in the presence of theoretical indefiniteness, it is impossible to have a neutron (pure hadronic) star with a radius smaller than about 10 kilometers. Observational discovery of a compact star with considerably smaller radius would be an important evidence that this star is not pure hadronic. Such claim was made by Drake et al. (2002) based on the deep Chandra observations of the isolated compact star RX J1856.5-3754. They wrote: "We argue that the derived interstellar medium neutral hydrogen column density of $8 \times 10^{19} \leq N_H \leq 1.1 \times 10^{20}$ cm^{-2} favors the larger distance from two recent HST parallax analyses, placing RX J1856.5-3754 at $\sim$ 140 pc instead of $\sim$ 60 pc. ...' The combined observational evidence – a lack of spectral and temporal features, and an implied radius $R_\infty = 3.8$-8.2 km that is too small for current neutron star models – points to a more compact object, such as allowed for quark matter equations of state." Subsequent analysis of observational data did not confirm this conclusion. Thoma et al. (2003) came to contrary result of an unusually large value of the radius even for a neutron star: "Combining such a X-ray spectrum with the optical spectrum, one finds a black-body radius $R_\infty > 17$ km, indi-

cating a stiff equation of state, which would exclude a strange quark matter star or even hybrid star. This is a rather conservative lower limit for the radius since a black-body emitter is the most efficient radiator." Similar conclusion was made by Turolla et al. (2003): "While a quark star may be a conceivable option, present observations do not necessarily demand this solution and more conventional scenarios involving a neutron star are certainly possible. Neutron star models based on a two-temperature surface distribution can account for both the X-ray and optical emission, giving at the same time acceptable values for the stellar radius." Meanwhile a new candidate for a quark (strange) star in the X-ray source 4U 1728-34 was suggested by Bombaci (2003), and farther discussion about this object is expected.

So far no reliable candidate for a quark (strange) star was found by observations. The theoretical predictions remain uncertain, and could explain either the existence or nonexistence of quark stars. The solution of the intriguing problem of cosmological gamma ray burst (GRB) origin was proposed by Berezhiani et al (2003) basing on energy production during transformation of the neutron star into a stable quark (strange) star. This model could explain the connection of GRB with supernovae explosions with a formation of a neutron star, and subsequent huge energy release during transition to a state of a quark star producing GRB. An attractive feature of this model is a possibility of explanation of any time delay between SN and GRB explosions, which depends on the transition time from hadron to quark state, and is very sensitive to parameters. In this model the time delay may be arbitrary long, so majority of SN explosions in accordance with observations do not produce GRB, because this time exceeds the cosmological Hubble time.

6. Summary

1. The formation of quark (strange) stars does not follow unambiguously from the theory, which may be compatible either with the existence or nonexistence of these objects.

2. There are no firm observational contradictions to the conventional model of the hadronic neutron star.

3. Speculations about connection of the cosmological GRB with transition from the hadronic to quark star seems to be interesting, because they explain connection between GRB and supernovae explosion, with arbitrary time delay between these events, including very large, exceeding the Hubble time.

Acknowledgments

The author wishes to thank D. Sedrakyan, D. Blaschke, G. Hadjan, Yu. Vartanyan, E. Chubaryan and A. Sadoyan for support and hospitality during the conference and I. D. Novikov for useful discussions.

References

Aguirre, R. M., De Paoli, A. L. (2002). Neutron star structure in a quark model with excluded volume correction. *Phys.Rev.C68:055804*.

Alford, M. J. (2003). Dense quark matter in compact stars. *J.Phys.G30:S441-S450*.

Ambartsumyan, V. A., Saakyan, G.S. (1960). On degenerate superdense gas of elementary particles. *Astron. Zh.*, 37: 193–209.

Ambartsumyan, V. A., Saakyan, G.S. (1961). Internal structure of hyperonic configurations of stellar masses. *Astron. Zh.*, 38: 1016–1024.

Andersen, J. O., Strickland, M. (2002) The Equation of State for Dense QCD and Quark Stars. *Phys.Rev.*, D66: 105001-105005.

Baade, W., Zwicky, F. (1934). Supernovae and cosmic rays. *Phys. Rev.*, 45: 138–139.

Berezhiani, Z., Bombaci, I., Drago, A., Frontera, F., Lavagno, A. (2003). Gamma Ray Bursts from delayed collapse of neutron stars to quark matter stars. *Astrophys.J.*, 586: 1250-1253.

Bisnovatyi-Kogan, G. S. (1966). Critical mass of hot isothermal white dwarf with the inclusion of general relativity effects. *Astron. Zh.*, 43: 89–95.

Bisnovatyi-Kogan, G. S. (1968). The mass limit of hot superdense stable configurations. *Astrofizika*, 4: 221–238.

Bisnovatyi-Kogan, G. S. (2002). *Stellar Physics. Vol.2. Stellar evolution and stability.* Berlin Heidelberg: Springer.

Bisnovatyi-Kogan,G.S., Blinnikov,S.I. (1974). Static criteria for stability of arbitrary rotating stars. *Astron. Ap.*, 31: 391–404.

Bisnovatyi-Kogan, G. S., Blinnikov, S. I., Shnol', E. E. (1975). The stability of a star in the presence of a phase transition. *Astron. Zh.*, 52: 920-929.

Bisnovatyi-Kogan, G. S., Kajdan, Ya. M. (1966). Critical parameters of stars. *Astron. Zh.*, 43: 761–771.

Bisnovatyi-Kogan,G.S., Ruzmaikin,A.A. (1973). The stability of rotating supermassive stars. *Astron.Ap.*, 27: 209–221.

Bisnovatyi-Kogan, G. S., Zel'Dovich, Ya. B., Novikov, I. D. (1967). Evolution of supermassive stars stabilized by large-scale motions. *Astron. Zh.*, 44: 525-536.

Bombaci, I. (2003). A possible signature for quark deconfinement in the compact star in 4U 1728-34. *astro-ph/0307522*.

Burgio, G. F., Baldo, M., Schulze, H.-J., Sahu, P. K. (2002). The hadron-quark phase transition in dense matter and neutron stars. *Phys.Rev.*, C66: 025802-025815.

Cameron, A. G. (1959). Neutron star models. *Astrophys. J.*, 130: 884-894.

Chandrasekhar, S. (1931). The maximum mass of ideal white dwarf. *Astrophysical J.*, 74: 81-82.

Chandrasekhar, S. (1964). The dynamical instability of gaseous masses approaching the Schwarzschild limit in general relativity. *Astrophys. J.*, 140: 417–433.

Comella, J. M., Craft, H. D. Jr., Lovelace, R. V. E., Sutton, J.M. and Tyler, G.I. (1969). Crab nebula pulsar NP 0532. *Nature*, 221: 453-454.

Dmitriyev, N. A. and Kholin, S. A. (1963). Features of static solutions of the gravity equations. *Voprosy Kosmogonii*, 9: 254–262.

Drake, J. J., Marshall, H. L.. Dreizler, S., Freeman, P. E., Fruscione, A., Juda, M., Kashyap, V., Nicastro, F., Pease, D. O., Wargelin, B. J., Werner, K. (2002) Is RX J1856.5-3754 a Quark Star? *Astrophys. J.*, 572: 996-1001.

Emden, R. (1907). *Gaskugeln*. Leipzig.

Gamow, G. (1938). Zusammenfassender Bericht. Kernumwandlungen als Energiequelle der Sterne. *Zeitschrift für Astrophysik*, 16: 113-160.

Harrison, B. K., Thorne, K. S., Wakano, M., Wheeler,J.A. (1965). *Gravitational Theory and Gravitational Collapse* Chicago, University of Chicago Press.

Hund, F. (1936). *Ergebn. Exakt. Naturwiss.*, 15: 189-212.
Ivanenko, D.D., Kurdgelaidze, D.F. (1965). *Astrofizika*, 1: 251-253.
Kohri, K., Iida, K., Sato, K. (2003). Upper limit on the mass of RX J1856.5–3754 as a possible quark star. *Prog.Theor.Phys.*, 109: 765-780.
Landau, L. D. (1932). On the theory of stars. *Phys. Zeit. Sov.*, 1: 285-288.
Landau, L. D. (1938). Nature, 141: 333-334.
Lovelace, R. V. E., Sutton, J.M., Craft, H. D. Jr. (1968). Pulsar NP 0532 near Crab nebula. *IAU Circular No. 2113*.
Lugones, G., J.E. Horvath, J.E. (2003). Quark-diquark equation of state and compact star structure. *Int. J. Mod. Phys.*, D12: 495-508.
Mishustin, I.N., Hanauske, M., Bhattacharyya, A., Satarov, L.M., Stoecker, H., Greiner, W. (2003). Ca tastrophic re arrangement of a compact star due to the quark core formation. *Phys.Lett.*, B552: 1-8.
Misner, C. W.; Zapolsky, H. S. (1964). High-Density Behavior and Dynamical Stability of Neutron Star Models. *Phys. Rev. Let.*, 12: 635-637.
Oppenheimer, J. R.; Volkoff, G. M. (1939). On Massive Neutron Cores. *Phys. Rev.*, 55: 374-381.
Rosenfeld, L. (1974). Astrophys. and gravitation. *in Proc. 16 Solvay Conf. on Phys*, Univ. de Bruxells, p. 174.
Rudkjöbing, M. (1952). *Publ. Köbenhavns Obs.*, No.160.
Saakyan, G. S., Vartanyan, Yu. L. (1964). Basic Parameters of Baryon Configurations. *Astron. Zh.*, 41: 193–201.
Sedrakian, D. M., Blaschke, D. (2002). Magnetic field of a neutron star with color superconducting quark matter core. *Astrofiz.*, 45: 203-212.
Skryme, T. H. R. (1959). *Nucl. Phys.*, 9: 615-625.
Thoma, M.H., Trümper, J., Burwitz, V. (2003). Strange Quark Matter in Neutron Stars? - New Results from Chandra and XMM. *J.Phys.G30:S471-S478*.
Turolla, R., Zane, S., Drake, J.J. (2003). Bare Quark Stars or Naked Neutron Stars: The Case of RX J1856.5-3754. *Astrophys.J.603:265-282*.
Vartanyan, Yu. L. (1972). *Doctor. Diss.*, Yerevan.
Wheeler, J.A. (1958). Paper read at 11 Solvay conference, Brussels. Published with Harrison, B.K. and Wakano, M. in *La structure et l'evolution de l'universe*. (Brussels: R. Stoops.)
Zel'dovich,Ya.B. (1961). Equation of state at a superhigh density and relativistic restrictions. *Journ. Exp. Theor. Fiz.* 41: 1609–1615.
Zel'dovich, Ya. B. (1963). Hydrodynamical stability of star. *Voprosy Kosmogonii*, 9: 157–170.
Zel'dovich, Ya. B., Novikov, I. D. (1965). Relativistic astrophysics. II. *Uspekhi. Fiz. Nauk*, 86: 447–536.

CONSTRAINTS ON SUPERDENSE MATTER FROM X-RAY BINARIES

M. Coleman Miller
University of Maryland, College Park, MD, USA
miller@astro.umd.edu

Abstract From the earliest measurements of the masses of binary pulsars, observations of neutron stars have placed interesting constraints on the properties of high-density matter. The last few years have seen a number of observational developments that could place strong new restrictions on the equilibrium state of cold matter at supranuclear densities. We review these astronomical constraints and their context, and speculate on future prospects.

1. Introduction and Overview

Neutron stars are important laboratories for the physics of high-density matter. Unlike particles in relativistic heavy-ion colliders, the matter in the cores of neutron stars has a thermal energy that is much less than its rest-mass energy. Various researchers have speculated whether neutron star cores contain primarily nucleons, or whether degrees of freedom such as hyperons, quark matter, or strange matter are prevalent (see Lattimer & Prakash 2001 for a recent review of high-density equations of state).

However, it is impossible to isolate the matter in the core of a neutron star for detailed study. It is thus necessary to identify observable aspects of neutron stars that can be, in some sense, mapped to the equation of state of high-density material. In this review we discuss various constraints on the equation of state from astronomical observations. We focus on observations of accreting binary systems.

We start by listing a few of the structural aspects of neutron stars that are affected by high-density microphysics and can be observed astronomically. We assume that the neutron star is in dynamical equilibrium. In this list, by "mass" we mean the gravitational mass, rather than the sum of the rest masses of the individual particles.

- Mass M, from binary orbits (extra information is available if the orbits are relativistic; see § 3).

D. Blaschke and D. Sedrakian (eds.), Superdense QCD Matter and Compact Stars, 23–42.

- Radius R, from surface emission, linear surface velocity, or orbital constraints. Estimates of radius have historically been fraught with systematic uncertainties; see § 6.

- Compactness GM/Rc^2, from surface redshifts or general relativistic light deflection; see § 4 and § 5.

- Dimensionless angular momentum cJ/GM^2, which is potentially measurable by its effects on light deflection or characteristic particle frequencies in certain orbits; see § 4 and § 6.

In addition to these, there are some overall theoretical constraints. For example, neutron stars are believed to originate via the collapse of the core of a massive star. The rest mass of the core is close to the Chandrasekhar limit of $1.4\,M_\odot$ at which degeneracy pressure can no longer compete with gravity. Thus a neutron star is constrained by having a rest mass no less than about $1.4\,M_\odot$; for typical equations of state, this translates into a gravitational mass that is greater than about $1.2\,M_\odot$ (for a more detailed model of a protoneutron star, see, e.g., Goussard, Haensel, & Zdunik 1998).

The strength of a particular constraint depends on how precisely one can measure the associated quantity. Lattimer & Prakash (2001) show that if the radius is measured to within ~ 1 km this will distinguish between several competing EOS even if nothing else is known about the star. Mass measurements alone are only constraining if the masses are fairly high. For example, a neutron star with gravitational mass $M = 1.4\,M_\odot$ can be accommodated by any existing EOS, but if $M = 2.2\,M_\odot$ and the spin is less than a few hundred Hz then only the hardest of current EOS would survive. In addition, the indirect nature of most observations means that one must be cautious about interpretation. For example, the radius is not measured directly, but rather is inferred through the filter of some model.

In this review, after describing accreting neutron star binary systems in § 2, we discuss various proposed observational constraints from the least model-dependent to the most speculative. In § 3 we talk about the status of mass measurements from observations of radial velocity curves. In § 4 we discuss an exciting recent observation of a surface redshift as estimated from atomic resonance scattering features, and speculate on the prospects for future line observations and analysis. In § 5 we examine another new development: constraints on neutron star parameters by the detailed profiles of regular pulses from accreting neutron stars. In § 6 we evaluate current constraints on stellar radius, especially from orbital frequencies. We conclude in § 7 with the opinion that, although EOS with just nucleonic degrees of freedom are consistent with all current data, exotic components are not yet excluded.

2. Overview of Neutron Star X-ray Binaries

We now discuss the differences between neutron stars with a low-mass companion (usually $M < 1\,M_\odot$) and neutron stars with a high-mass companion (usually $M \gtrsim 3\,M_\odot$), then show that low-mass X-ray binaries (LMXBs) are likely to provide the most important future constraints on neutron star structure. We begin with an overview of accretion and magnetic fields, because both the field strength and type of accretion are thought to differ between LMXBs and high-mass X-ray binaries (HMXBs). For an excellent general discussion of accretion in binary systems, see Frank, King, & Raine (2002).

Basics of accretion and magnetic fields

Neutron stars in binaries can accrete significant amounts of mass from their companions. This happens primarily via Roche lobe overflow if the companion star is low-mass, but primarily via accretion from a wind if the companion star is high-mass. In either case, most of the energy release is due to accretion. This is because the accretion energy release per mass, which is $\sim GM/R \sim 0.2c^2$, is much larger than the energy release from any competing mechanism (e.g., fusion of hydrogen to helium releases $\sim 0.007c^2$ per mass). Characteristic luminosities of accreting neutron stars span the range of $< 10^{33}$ erg s^{-1} to $> 10^{38}$ erg s^{-1}. If the energy is thermal and emitted over most of the $4\pi R^2 \sim 1000$ km^2 area of a neutron star, then the characteristic energy is $kT \sim 100 - 2000$ eV, in the X-ray range. Various processes such as Compton upscattering in a hot corona can cause the spectrum to deviate from thermal (e.g., Psaltis & Lamb 1997), but nonetheless X-rays contain most of the luminosity of these systems. Given that these systems are primarily accretion-powered, if the accretion and emission are both roughly isotropic then their luminosities are limited by the Eddington luminosity $L_E \equiv 4\pi GMm_pc/\sigma_T \approx 1.3 \times 10^{38}(M/M_\odot)$ erg s^{-1}. Here G is Newton's constant, M is the stellar mass, m_p is the mass of the proton, c is the speed of light, and $\sigma_T = 6.65 \times 10^{-25}$ cm^2 is the Thomson cross section for electron scattering. Above this luminosity, the radial acceleration due to radiation is greater than the gravitational acceleration, halting accretion. This assumes a fully ionized plasma (a good approximation at these temperatures). Strong beaming could in principle violate this constraint (e.g., King et al. 2001).

Observations of neutron stars suggest that they have a wide range of magnetic field strengths, from surface fields of 10^{7-10} G for neutron stars in LMXBs (see below) to 10^{11-15} G for young neutron stars (e.g., Morris et al. 2002 for one recent survey) and 10^{11-13} G for neutron stars in HMXBs (see below). At the high temperatures of accretion disks surrounding the stars, the gas is mostly ionized and therefore couples strongly to the field. The details of this coupling are debated (e.g., Ghosh & Lamb 1979; Shu et al. 1994). However,

one can make simple estimates to show that, generically, one expects that far from the star the stellar magnetic field has little effect on the flow, but near the star the field can be important.

To do this, consider the material stress and the magnetic stress. As an approximation, the magnetic stress in a region with total field strength B is $T_B \sim B^2$. The material stress in a region of matter density ρ and speed v is $T_M \sim \rho v^2$. How do these depend on radius? If the magnetic field is dipolar, then $B \sim r^{-3}$, hence $T_B \sim r^{-6}$. To estimate the material stresses, assume that the matter flows in an accretion disk with a disk half-thickness h that is a constant fraction of r. This implies that at radius r, the cross-sectional area of a cylindrical section of the disk scales as $A \sim r^2$. For a geometrically thin ($h \ll r$), optically thick disk, accretion disk theory (e.g., Shakura & Sunyaev 1973) indicates that in addition to the orbital speed $v_K \sim r^{-1/2}$, there is a sound speed $c_s \sim (h/r)v_K$ and an inward radial speed $v_r \sim \alpha(h/r)^2 v_K$, where $\alpha \sim 0.01 - 1$ is related to the mechanism for transport of angular momentum (Shakura & Sunyaev 1973). For a thin disk, the total velocity is therefore $v_{\rm tot} \approx v_K \sim r^{-1/2}$. In addition, if there is a constant mass flux rate through all radii, mass continuity implies $\rho v_r A = {\rm const}$, hence $\rho \propto r^{-3/2}$ and the material stress is $T_M \sim r^{-5/2}$.

Therefore, the radial dependence of the magnetic stress is much steeper than the radial dependence of the material stress. This implies that at large distances material stress dominates, but that close to the star the magnetic stress can be more important (indeed, it will be for $B \gtrsim 10^8$ G at the surface). In detail, one actually needs to compare specific components of the magnetic and material stresses (primarily the $r\phi$ component; e.g., Ghosh & Lamb 1979), but the large differences in radial dependences means that the overall picture is robust. One implication of this picture is that disks with higher accretion rates are able to push in closer to the star.

This comparison suggests that there will be a transition region between materially-dominated and magnetically-dominated flow. The region inside of which the stellar magnetic field controls the flow is called the *magnetosphere*. To within a factor of 2–3, the radius at which the transition occurs is (e.g., Ghosh & Lamb 1979)

$$r_M \approx 3 \times 10^8 (\dot{M}/10^{17}\ {\rm g\ s^{-1}})^{-2/7} (\mu/10^{30}\ {\rm G\ cm^3})^{4/7}\ {\rm cm}\ . \qquad (1)$$

Here μ is the stellar dipole magnetic moment and $\dot{M}$ is the mass accretion rate through the disk. For this formula we assume a purely dipolar field; higher multipoles weaken the dependence on $\dot{M}$ because the field is effectively stiffer.

If one pictures the transition region as sharp, then in a rough sense one can imagine the ionized gas orbiting in a disk outside the magnetosphere, but flowing along field lines at the stellar angular velocity inside the magnetosphere. Let us denote r_M as the "magnetospheric radius" (understanding that there is

no single such radius, but rather a transition zone). Suppose that the Keplerian orbital angular velocity at this radius is $\omega_K(r_M)$. Suppose also that the stellar angular velocity is ω_s. Consider a particle fixed to a field line at r_M, corotating with the star. If $\omega_s < \omega_K(r_M)$, then the particle falls towards the star and accretes. If instead $\omega_s > \omega_K(r_M)$, then the particle is flung outwards. Another way of phrasing this is that there is some radius $r_{\rm co}$ in the disk, the *corotation radius*, at which the Keplerian angular velocity equals the stellar angular velocity. If $r_M < r_{\rm co}$ then particles in the magnetosphere fall towards the star, and because the matter couples to the star with a higher angular velocity than the current stellar spin rate, the star is spun up over time. If instead $r_M > r_{\rm co}$ then particles tied to field lines that corotate with the star will be pushed outwards, and the stellar spin rate slows down. From equation (1) we see that if the average mass accretion rate is fixed, stars with weaker magnetic fields will be spun up to higher frequencies.

The magnetic torque picture therefore implies the possibility of a centrifugal barrier, or "propeller effect" (Illarionov & Sunyaev 1975). For example, imagine a source that undergoes a large range of mass accretion rates (as is true for transient sources). At a high accretion rate, r_M is small and all the matter accretes. However, at a low accretion rate, r_M is large (by equation [1]), so when the matter couples to the field it is flung out again, preventing accretion. This simple picture may not be correct. The disk-magnetosphere boundary is highly complex and many instabilities may be present (Stella, White, & Rosner 1986). In addition, because the coupling to the field is not perfectly abrupt, matter in the disk is more likely heated than flung out, and if cooling is efficient then there could be a buildup of matter that occasionally dumps onto the star (Maraschi, Traversini, & Treves 1983).

With this general introduction, we now discuss the specifics of systems with low-mass or high-mass companions.

Low-mass X-ray binaries

Consider a neutron star in a binary with a $1\,M_\odot$ companion. The companion star loses very little mass to winds; for example, solar-type stars typically lose only few$\times 10^{-14}\,M_\odot$ yr^{-1} (e.g., Wood et al. 2002), so there is negligible mass transfer via this channel. The only way that significant mass can be transferred to the neutron star is if the separation between the two is small enough that gas on the near side of the companion is more attracted gravitationally to the neutron star than to the companion itself. That is, mass transfer only occurs if the companion fills its Roche lobe. If the companion and neutron star were initially not in Roche contact, then evolutionary processes can drive them into contact. For example, the companion could evolve into a red giant, or orbital angular momentum could be lost (shrinking the orbit). Loss of angular mo-

mentum is thought to occur in two main ways (see Frank et al. 2002). For well-separated systems, the primary mechanism is magnetic braking. A star with a wind of charged particles loses angular momentum to the wind because the particles are forced by the magnetic field of the star to rotate at the stellar angular velocity, hence as they move away they increase their angular momentum per mass. If the companion star is tidally locked to the neutron star, then as the companion slows down in its rotation it extracts angular momentum from the orbit. If the companion gets close enough to the neutron star, then angular momentum can instead be lost to gravitational radiation.

The companions are made primarily of hydrogen (or helium in some cases, if the outer hydrogen envelope has been stripped). As hydrogen and helium flow onto the surface of the neutron star, some of it undergoes thermonuclear fusion. In some cases, however, hydrogen or helium can build up on the surface without being burned completely. As investigated by many researchers, this can lead to an ignition of the layer of fuel under certain circumstances (see Woosley & Taam 1976; Joss 1977, 1978; Lamb & Lamb 1977, 1978; Woosley & Wallace 1982). This ignition is unstable, so once the layer starts burning it is completely consumed within seconds to hours, depending on the details of the burning (see Cumming 2003 for a recent overview including the hours-long "superbursts"). In a number of these so-called thermonuclear bursts, or type 1 bursts, nearly coherent oscillations in the brightness are observed (for a review in the overall context of bursts see, e.g., Strohmayer & Bildsten 2003). These are thought to be caused by rotational modulation of the flux we receive from a "hot spot" on the surface, and imply spin frequencies as seen at infinity of several hundred Hertz. The high spin frequencies are consistent with these objects being the progenitors of millisecond-period rotation-powered pulsars, suggesting that neutron stars are spun up by the accretion.

One would also expect that fast pulsations would be observed during the persistent accretion-powered emission, and this is indeed seen in five transient LMXBs. For a review, see Wijnands (2003). In order of their discovery, the five sources are SAX J1808–3658 (401 Hz; Wijnands & van der Klis 1998; Chakrabarty & Morgan 1998), XTE J1751–305 (435 Hz; Markwardt et al. 2002), XTE J0929–314 (185 Hz; Galloway et al. 2002), XTE J1807–294 (191 Hz; Markwardt, Smith, & Swank 2003b; Markwardt, Juda, & Swank 2003a); and XTE J1814–338 (314 Hz; Markwardt et al. 2003c; Strohmayer et al. 2003). However, the majority of LMXBs do not have detectable pulsations in their persistent emission. The reason for this is debated, but one possibility is that most LMXBs are shrouded by a corona of hot electrons with a large enough optical depth to smear out the beamed pulsations (e.g., Titarchuk, Cui, & Wood 2003). The lack of pulsations in most sources does suggest that their magnetic fields are comparatively weak ($B \lesssim 10^{10}$ G), otherwise the flow would be channeled relatively far from the star and pulsations would be strong.

The weak-field hypothesis is also supported by the high spin frequencies of these sources; from equation (1), if these sources are in magnetic spin equilibrium then their surface magnetic field strengths are $B \sim 10^8$ G (Chakrabarty et al. 2003).

The thermonuclear X-ray bursts observed from LMXBs argue strongly that their crusts down to a density of at least $\sim 10^8$ g cm^{-3} are composed of normal nuclei. The relevant properties are (1) the time-averaged energy released in persistent emission divided by the time-averaged energy released in bursts is typically 20–200, consistent with the ratio of gravitational binding energy per mass to nuclear binding energy per mass; (2) the recurrence time of ∼hours to weeks, which is consistent with the time to build up a new fuel layer that becomes unstable to nuclear burning; and (3) the durations of seconds to hours seen in different types of bursts, which fits well with the expected time to burn the layer and transport the energy from the instability region. For recent detailed reviews, see Cumming (2003) and Strohmayer & Bildsten (2003). The data are well-fit quantitatively in this model. Of course, this does not rigorously exclude any other possible explanations, but it does suggest that a model in which the compact objects are truly bare strange stars (down to zero density) will have a very difficult time explaining these phenomena. Models in which there is a normal crust to densities $\rho \gg 10^8$ g cm^{-3}, then an abrupt transition to strange matter at much higher densities, could be consistent with the data.

High-mass X-ray binaries

Now consider a companion star of mass $10\,M_\odot$. Such a star is more massive than a neutron star, and angular momentum conservation implies that Roche lobe mass transfer is usually unstable in these systems (see Frank et al. 2002). However, even if the companion is out of Roche contact, it can still transfer significant mass via a wind. High-mass main-sequence stars can have winds that lose more than $10^{-6}\,M_\odot$ per year, or $\sim 10^{20}$ g s^{-1}. If just 1% of this falls on the neutron star, the luminosity can be close to the Eddington luminosity. Indeed this happens in many systems, with the key being that gravitational focusing and self-interaction of the plasma give the neutron star an effective cross section to the wind that is many orders of magnitude greater than its geometric cross section.

The short lifetimes of high-mass stars means that HMXBs are not thought to be long-lived, typically only a few million years. As a result, even at an Eddington accretion rate of $\dot{M} = 10^{18}$ g s^{-1}, only a few hundredths of a solar mass is transferred to the neutron star. Therefore, the mass of a neutron star in an HMXB is expected to be close to its birth mass. In contrast, LMXBs can last for tens of millions of years and in principle accrete tenths of a solar mass.

Many neutron stars in HMXBs are pulsars, with periods ranging from seconds to minutes. The slow rotation periods suggest strong magnetic fields, typically $B \sim 10^{12}$ G, from the arguments presented earlier, and this is corroborated by the detection of features identified with electron cyclotron resonance scattering (the first being in Her X-1; Trümper et al. 1978). The strong fields are consistent with spindown measurements of young isolated pulsars. The puzzle, therefore, is why LMXBs have much weaker fields. Various explanations have been suggested. For example, it could be that there is a characteristic rate of decay of neutron star magnetic fields that is independent of external factors such as accretion, and that LMXBs simply live long enough for this decay to be significant (this would suggest that old enough isolated pulsars also experience field decay; see Geppert & Rheinhardt 2002). Alternately, accretion could speed the decay of the field (Ruderman 1995; Konar & Bhattacharya 1999) or even bury the field (for a recent study see Cumming, Zweibel, & Bildsten 2001), although magnetic instabilities may make it difficult to start the burial process.

Unlike neutron stars in LMXBs, neutron stars in HMXBs do not display thermonuclear bursts. This is understood in terms of stable versus unstable burning (see Cumming 2003 for a review). If a neutron star has a strong magnetic field, accreting matter is funneled into a small patch of the star's surface. The effective accretion rate per area is therefore high, and hence so is the temperature. At high temperatures, nuclear fusion proceeds steadily as the matter accretes, not allowing buildup of nuclear fuel for a later flash. The lower accretion rates per area in low-field neutron stars, however, can allow such buildup.

Magnetic fields revisited

For the purposes of constraining neutron star structure and gaining insight into high-density matter, strong magnetic fields complicate analysis. The accretion flow is controlled by the field out to large radii, so emission from the flow does not contain information about orbits near the star, and hence does not inform us about strong gravity effects or constraints on the stellar radius. In addition, for the field strengths inferred from neutron stars in HMXBs, even atomic physics is influenced considerably. This can be seen by comparing the electron cyclotron energy $\hbar\omega_c = \hbar eB/m_e c = 11.6(B/10^{12}\ \mathrm{G})$ keV to atomic binding energies, which are at most a few keV even for heavy elements such as iron. This adds another unknown to the identification of spectral lines and their interpretation. In contrast, $\sim 10^8$ G fields such as those inferred for neutron stars in LMXBs have negligible impact on atomic lines from iron or other heavy elements, so more confident inferences may be made (Cottam et al. 2002; Loeb 2003).

Even for estimates of mass from radial velocities (see § 3), for which magnetic fields are irrelevant, LMXBs have advantages over HMXBs. One important advantage is that because the active lifetimes of LMXBs are larger than those of HMXBs, more mass can be transferred, meaning that the masses of neutron stars in LMXBs could well be larger on average than those in HMXBs by a few tenths of a solar mass. These higher masses are important because many theories predict transitions to new forms of matter in the cores of neutron stars when the mass gets high enough. For all of these reasons, LMXBs are more promising than HMXBs for a variety of constraints on neutron star structure and high density matter.

3. Radial Velocity Measurements

The most rigorous constraints on neutron star structure are derived from mass measurements using binary orbits. Ideally, one would like to measure the full three-dimensional velocity, but this is not possible because accreting binaries are so small that they cannot be spatially resolved, hence motions transverse to the line of sight are undetectable. For example, an LMXB with a few hour orbit has a semimajor axis of $\lesssim 0.01$ AU, meaning that even for a relatively nearby source at 1 kpc the angular separation is $\lesssim 10^{-5}$ arcseconds, far below current instrumental capability. Only the line of sight component of the motion can be observed, using Doppler shifts. These can be measured by periodic shifts of atomic lines (if the star observed is a white dwarf or main sequence star) or of pulse frequency (if the star observed is a pulsar).

To understand this effect more quantitatively, consider an idealized measurement of Doppler shifts from one member of a binary, call it star 1. Assume that both objects are effectively point masses. One can measure the period P of the orbit and the velocity semiamplitude v_1 of star 1 in the direction of the line of sight. If the two stars have masses m_1 and m_2 and are orbiting in a circle with a semimajor axis a and an inclination i (such that $i = 90^\circ$ means an orbit edge-on to our line of sight), then

$$\begin{aligned} P &= 2\pi\sqrt{a^3/G(m_1+m_2)} \\ v_1/\sin i &= [m_2/(m_1+m_2)]\sqrt{G(m_1+m_2)/a}\ . \end{aligned} \tag{2}$$

Combining these, we can define the *mass function* f

$$f \equiv Pv_1^3/(2\pi G) = (m_2 \sin i)^3/(m_1+m_2)^2\ . \tag{3}$$

The mass function, which is a pure combination of observables, is a lower limit to the possible mass of star 2; if the orbit is other than edge-on (that is, if $i < 90^\circ$) or the observed star has $m_1 > 0$, then $m_2 > f$. Thus, observation of one star constrains the mass of the other star. Note, incidentally, that in a neutron star binary system with a high-mass companion ($m_1 \gg m_2$), f is low

and it is difficult to constrain the neutron star mass strongly. If the companion is instead low-mass ($m_1 \ll m_2$), then $f \approx m_2 \sin^3 i$ and the only significant uncertainty is in the inclination. Regardless of the mass of the companion, if Doppler shifts from both stars can be observed then an measurement of the inclination would solve the system completely.

Various methods of estimating the inclination have been suggested in the literature. By far the most robust are applicable when the system contains two neutron stars, one of which is a rotation-powered pulsar. Such systems involve no mass transfer and no tidal effects, and are therefore a perfect theorist's problem with two point masses. The extraordinary intrinsic stability of rotation-powered pulsars means that a number of subtle post-Newtonian effects can be measured (for a review see Taylor 1994), such as orbital decay, precession of the pericenter, and Shapiro delay (the delay in propagation caused by passage through the warped spacetime near a massive object). These effects involve different combinations of the masses and semimajor axis; for example, the angle of precession of the pericenter per orbit is $\Delta\phi \propto G(m_1 + m_2)/a$, and the orbital decay time due to gravitational radiation is $T_{\rm decay} \propto a^4/[m_1 m_2 (m_1 + m_2)](1 - e^2)^{7/2}$ for eccentricity e. These effects therefore break the degeneracies of the system and allow the measurement of the masses of both components to high precision as well as sensitive tests of the predictions of general relativity (see Taylor 1994).

If one of the stars in the binary is not a neutron star, then the tests become less precise. Suppose that one observes the optical light from the companion to a neutron star. In addition to the spectral information that allows measurement of P and v_1, one also has photometric information (e.g., the total optical flux from the companion). The companion is distorted into a pear shape by the gravity of the neutron star, with the point towards the neutron star. Therefore, from the side there is more projected area and hence greater flux than from either end. If the orbit is edge-on ($i = 90^\circ$) then the flux varies maximally; if the orbit is face-on ($i = 0^\circ$) then there is no variation. Therefore, by modeling the system one can estimate the inclination from the flux variations. This is called the method of *ellipsoidal light curves* (Avni & Bahcall 1975).

However, one must be careful because in an LMXB the optical emission from the accretion disk (whether in the outer, cool regions or as reprocessed X-ray emission) can outshine the companion by a large factor. This makes spectral lines difficult to measure and also complicates the ellipsoidal light curve technique. The ideal systems to study are therefore transient systems, which undergo periods of active mass transfer (often for a few weeks to a few months) before lapsing into quiescence, where there is little to no mass transfer. During quiescence, the companion is still distorted by the gravity of the neutron star, hence the flux variations still occur, but without any contamination by the accretion disk. There is a relatively new approach similar to this that

uses flux variations from the disk itself that has good promise for constraining the inclination in many neutron star systems (Juett, Galloway, & Chakrabarty 2003).

Results: neutron star and white dwarf companions

As just described, the most precise measurements of masses come from double neutron star systems. There are currently five such systems known, three of which will coalesce due to gravitational radiation in less than the age of the universe, $\sim 10^{10}$ yr (Taylor 1994). These three systems in particular allow very precise measurements of the masses of the components, which are between $1.33\,M_\odot$ and $1.45\,M_\odot$ (Thorsett & Chakrabarty 1999). The other two double neutron star systems also have component masses consistent with a canonical $\sim 1.4\,M_\odot$. It has been suggested that the tight grouping of masses implies that the maximum mass of a neutron star is $\sim 1.5\,M_\odot$ (Bethe & Brown 1995). However, it is important to remember that double neutron star systems all have the same evolutionary pathway and thus the similar masses may simply be the result of a narrow selection of systems.

Pulsars with white dwarf companions produce the next most robust constraints on mass, because white dwarfs are small enough ($\sim 10^{8-9}$ cm radius compared to 10^{10-12} cm for a main sequence star) that tidal effects are relatively unimportant. Timing of such systems yields masses that are typically consistent with $1.4\,M_\odot$, within broad error bars (Thorsett & Chakrabarty 1999). However, Nice, Splaver, & Stairs (2003) recently reported that the 22 ms pulsar in the 0.26 day binary J0751+1807 may be well above this mass. The mass function is only $10^{-3}\,M_\odot$, suggesting a low-mass white dwarf companion. This system likely underwent significant mass transfer, as its eccentricity is $e = 3 \times 10^{-6}$, which is consistent with circularization due to tidal interactions and accretion. Orbital decay is detected, as is Shapiro delay (marginally), which suggest that $M > 1.6\,M_\odot$ at better than 95% confidence. Further observations have the potential to refine this considerably. If so, this could be the first indisputable case of a mass well above the usual $1.4\,M_\odot$ quoted for neutron stars. A high mass would be consistent with the idea that a few tenths of a solar mass are transferred to a neutron star during the lifetime of an LMXB. If the mass turns out to be large enough, this would place tight constraints on the state of matter at high densities.

Results: Vela X–1

Even stronger constraints are potentially available from the high-mass X-ray binary Vela X–1. This source contains a $\sim 20\,M_\odot$ star, and radial velocity variations from the star have been measured as well as periodic timing variations from X-ray pulses. The orbital period is 8.96 days and the eccentricity of

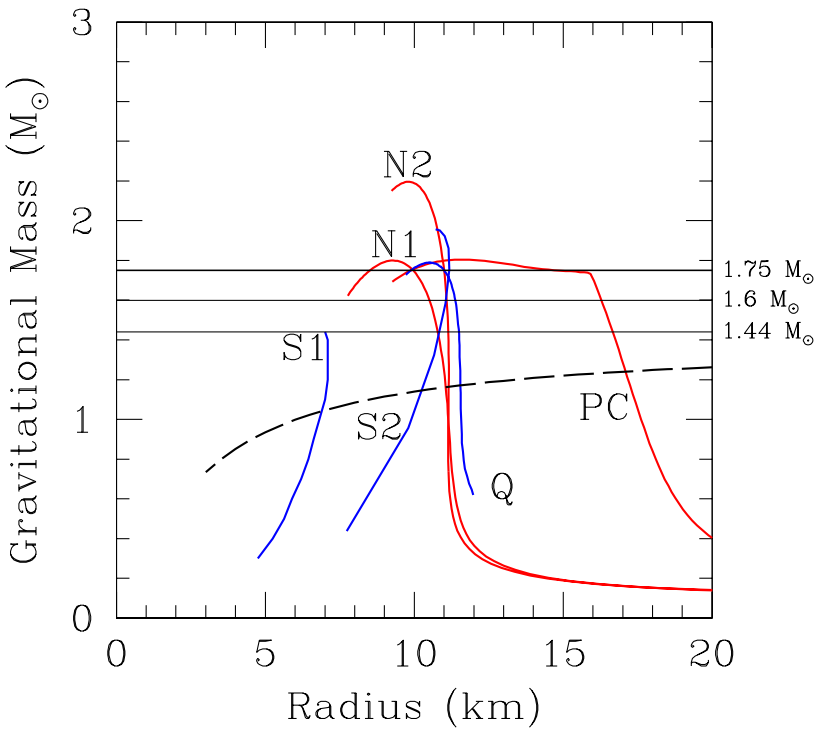

Figure 1. Mass-radius curves for different representative high-density equations of state, compared with gravitational mass estimates for neutron stars in different binary systems. The mass-radius curves are all for equilibrium nonrotating stars; note that rotation only affects these curves to second order and higher. Curves N1 and N2 are for nucleonic equations of state; N1 is relatively soft (Friedman & Pandharipande 1981), whereas N2 includes significant three-body repulsion (Wiringa, Fiks, & Fabrocini 1988). PC has a sharp change to a Bose-Einstein condensate of pions in the core when the mass reaches $\approx 1.8\,M_\odot$ (Pandharipande & Smith 1975). Equations of state N1, N2, and PC are not modern (i.e., not fitted to the most current nuclear scattering data), but are included for easy comparison to previous work on equation of state constraints. Curve S1 is for a compact strange star (Dey et al. 1998), whereas curve S2 is for a more standard strange star equation of state (Zdunik 2000). Curve Q is a quark matter equation of state with a Gaussian form factor and a diquark condensate (kindly provided by David Blaschke and Hovik Gregorian). The horizontal lines are mass constraints from different binaries, ranging from most certain to least certain going upwards. PSR 1913+16 has a measured mass of $1.44\,M_\odot$ (e.g., Taylor 1994), PSR J0751+1807 has a 95% lower limit of $1.6\,M_\odot$ (Nice et al. 2003), and Vela X-1 has a 90% lower limit of $1.75\,M_\odot$ if the measured radial velocities are purely orbital (Quaintrell et al. 2003). The dashed line shows the gravitational mass corresponding to a rest mass of $1.4\,M_\odot$ if the binding energy per mass is uniform throughout a star and equal to its surface value. In practice, this provides a strong lower limit to the gravitational mass (see, e.g., the numerical calculations of Cook, Shapiro, & Teukolsky 1994).

the orbit is $e \sim 0.1$. From the radial velocities measured in the lines and pulses by Quaintrell et al. (2003), the mass ratio is $M_{\rm comp}/M_{\rm NS} = 12.3$. The minimum mass of the neutron star (for an edge-on orbit) is $M_{\rm NS} = 1.88 \pm 0.13$. This is a rather high mass, and is surprising because this is precisely the type of system that could end up as a double neutron star binary, where measured masses are all consistent with $M \sim 1.4\,M_\odot$.

However, Quaintrell et al. (2003) point out a potential complication. The radial velocity measurements of the optical companion show puzzling residuals after the orbital motion is subtracted. Quaintrell et al. (2003) suggest that these could be caused by non-radial oscillations in the companion star induced by tidal forces from the neutron star. If such oscillations are in phase with the orbit then some of the observed radial velocity might not be from the orbit at all. This would decrease the required mass of the neutron star, potentially to the usual $1.4\,M_\odot$. Such high amplitudes of oscillation seem a priori implausible because they would require very high-order modes, but at the moment one cannot rule them out rigorously (C. Hansen, personal communication). A thorough theoretical study of non-radial oscillations in this system would go a long way towards resolving these issues, and if such a study showed that tidally induced oscillations are negligible then the Vela X–1 observations would place the strongest existing constraints on high-density matter.

4. Spectral Line Profiles

Atomic line spectroscopy has provided quantitative insight into countless astronomical objects. However, until recently, such information was unavailable for neutron stars. This could be because in an isolated neutron star the heavy elements (which produce strong lines) settle out quickly, leaving behind only fully ionized light elements. There was hope that accreting neutron stars, which receive continuing supplies of heavy elements, might have observable atomic lines. This hope was realized with the report (Cottam, Paerels, & Méndez 2002) that the LMXB EXO 0748–676 displays iron resonance scattering lines in the summed spectra of 28 thermonuclear X-ray bursts. These lines imply a redshift $z = 0.35$, consistent with an origin at the surface of a nucleonic neutron star in this system but not excluding more exotic components (Miller 2002).

These results have motivated researchers to determine theoretically what information could be extracted from a future high spectral resolution X-ray satellite. For example, Özel & Psaltis (2003) show that if the redshift is estimated from the energy of minimum flux in the line (assuming the line is absorption-like), then substantial systematic errors are possible in the resulting inference of the compactness GM/Rc^2 if the star rotates rapidly. Bhattacharyya, Miller, & Lamb (2003, in preparation) have begun a systematic

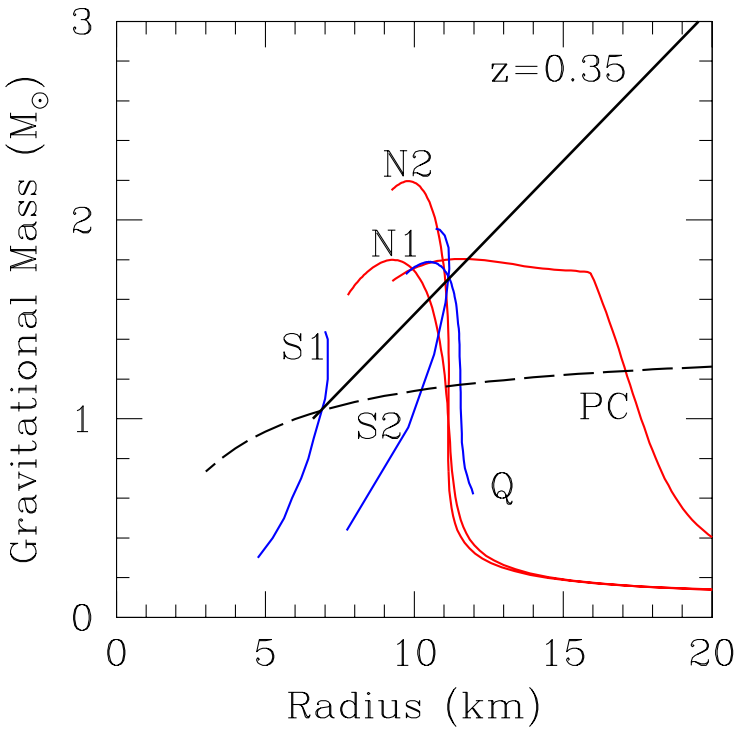

Figure 2. Equation of state constraints based on the surface redshift of $z = 0.35$ measured for EXO 0748–676 by Cottam et al. (1998). Other lines are as in Figure 1.

study of spectral line profiles as influenced by various physical effects. These include Doppler boosts, special relativistic beaming, gravitational redshifts, light-bending, and frame-dragging. They find a robust estimator of the compactness, using the following procedure. Suppose that the energies E_1 and E_2 of the red and blue limits of the line feature are identified. Calculate their geometric mean $E_{\rm gm} = \sqrt{E_1 E_2}$ and use it to define an effective redshift $z_{\rm eff} \equiv (E_{\rm rest}/E_{\rm gm}) - 1$, where $E_{\rm rest}$ is the rest energy of the line. Estimate the compactness using the Schwarzschild formula

$$GM/Rc^2 = \frac{1}{2}\left[1 - 1/(1 + z_{\rm eff})^2\right] \ . \tag{4}$$

The error in this estimate compared to the equatorial value of GM/Rc^2 is always less than 4% for a spin frequency $\nu_* < 600$ Hz (Bhattacharyya et al. 2003). Bhattacharyya et al. (2003) also find that future high-precision measurements could detect a signature of frame-dragging if there are two horns in the line profile. The ratio of the depth of the low energy (red) horn to the depth of the high energy (blue) horn increases quickly with the increase of a/M, but it either decreases or slowly increases with the increase of other parameters. Hence a precise measurement of a line profile could demonstrate the existence of frame-dragging.

5. Light Curve Profiles

Both thermonuclear burst brightness oscillations and pulsations from the persistent accretion-powered emission in LMXBs are caused by rotational modulation of the flux from a hot spot on the star. The light curve produced by this rotation is influenced by effects such as special relativistic aberration and general relativistic light deflection, hence detailed observation of light curves can produce constraints on neutron star structure. However, these effects are imprinted primarily in harmonic ratios, so if only the fundamental of the oscillation is detected (as it is in most burst oscillations), then the information content is minimal (Pechenick, Ftaclas, & Cohen 1983; Strohmayer 1992; Miller & Lamb 1998; Braje, Romani, & Rauch 2000; Psaltis, Özel, & DeDeo 2000; Weinberg, Miller, & Lamb 2001; Muno, Özel, & Chakrabarty 2002; Nath, Strohmayer, & Swank 2002). Therefore, the recent report of significant harmonic content in the millisecond pulsar XTE J1814–338 (Strohmayer et al. 2003) opens up exciting new ways to constrain neutron star structure.

Analysis of the bursts from this source is ongoing (Bhattacharyya, Strohmayer, & Miller 2003, in preparation). As with spectral line analyses (e.g., Bhattacharyya, Miller, & Lamb 2003, in preparation), one calculates model light curves as a function of parameters such as the compactness, stellar spin frequency, and emission parameters related to the hot spot and compares those model curves with the data. Initial analysis of the bolometric light curves of 22 bursts from XTE J1814–338 indicates that, at the 90% confidence level, the compactness GM/Rc^2 is between 0.21 and 0.27. Further analysis, including the energy-dependent light curves, will tighten these constraints.

6. Orbital Frequencies

A more model-dependent way to constrain neutron star structure has to do with measurements of orbital frequencies in the accretion disk near the neutron star. Suppose that the frequency of some observed phenomenon could be identified with an orbital frequency $\nu_{\rm orb}$, and that this phenomenon lasted many cycles. The orbital radius $R_{\rm orb}$ is clearly greater than the stellar radius R. In

addition, the relative stability of the orbit requires that it be outside the region of unstable circular orbits predicted by general relativity. For a nonrotating star, for which the exterior spacetime is described by the Schwarzschild geometry, the radius of the innermost stable circular orbit (ISCO) is $R_{\rm ISCO} = 6GM/c^2$. The constraint $R_{\rm orb} > R$ places a mass-dependent limit on the radius; for example, for a nonrotating star $R < (GM/4\pi^2\nu_{\rm orb}^2)^{1/3}$ (Miller, Lamb, & Psaltis 1998). The additional constraint $R_{\rm orb} > R_{\rm ISCO}$ places a absolute upper limit on the mass and hence on the radius. When one considers frame-dragging effects, then the upper limits on the mass and radius are (Miller, Lamb, & Psaltis 1998)

$$\begin{aligned} M &< 2.2\, M_\odot (1000\ {\rm Hz}/\nu_{\rm orb})(1+0.75j) \\ R &< 19.5\ {\rm km} (1000\ {\rm Hz}/\nu_{\rm orb})(1+0.2j)\ . \end{aligned} \tag{5}$$

Here $j \equiv cJ/GM^2$ is a dimensionless spin parameter, where J is the stellar angular momentum. If in a particular case one believes that the observed frequency is in fact the orbital frequency at the ISCO, then the mass is equal to the upper limit given above.

A strong candidate for the orbital frequency has in fact been observed from more than twenty neutron star LMXBs, using the *Rossi* X-ray Timing Explorer (RXTE). This is the phenomenon of kilohertz quasi-periodic brightness oscillations. The basic phenomenon is that power density spectra of the X-ray countrates from these systems show peaks with frequencies of hundreds of Hertz, often in a pair (for a detailed review, see van der Klis 2000). In the most widely developed models, the higher frequency of the two peaks is identified with the orbital frequency or close to it (e.g., Miller, Lamb, & Psaltis 1998; see van der Klis 2000 for a more general discussion of proposed models). The highest frequency QPO so far detected with confidence has a frequency $\nu_{\rm QPO} = 1330$ Hz (van Straaten et al. 2000), which would imply $M \lesssim 1.8\, M_\odot$ and $R \lesssim 15$ km for a system with spin parameter $j = 0.1$. These constraints essentially rule out the hardest equations of state proposed. Observations of higher frequencies would be more constraining. Projection of the amplitudes of QPOs versus their countrate suggest that a future timing mission with a ~ 10 m^2 area could detect QPOs to a frequency of ~ 1500 Hz or higher (M. van der Klis, personal communication). This would reduce the allowed region in the $M - R$ diagram significantly. It would also have strong prospects for the detection of the signature of the ISCO if $M > 1.6\, M_\odot$ for some of these systems (as suggested by the timing measurements of J0751–1807; Nice et al. 2003). Such a detection would confirm the presence of unstable orbits, a key prediction of strong-gravity general relativity, and allow a direct mass measurement. It is possible that the system 4U 1820–30 has already shown such a signal (Zhang et al. 1998), but there are complications in the spectral behavior that make this uncertain (Méndez et al. 1999).

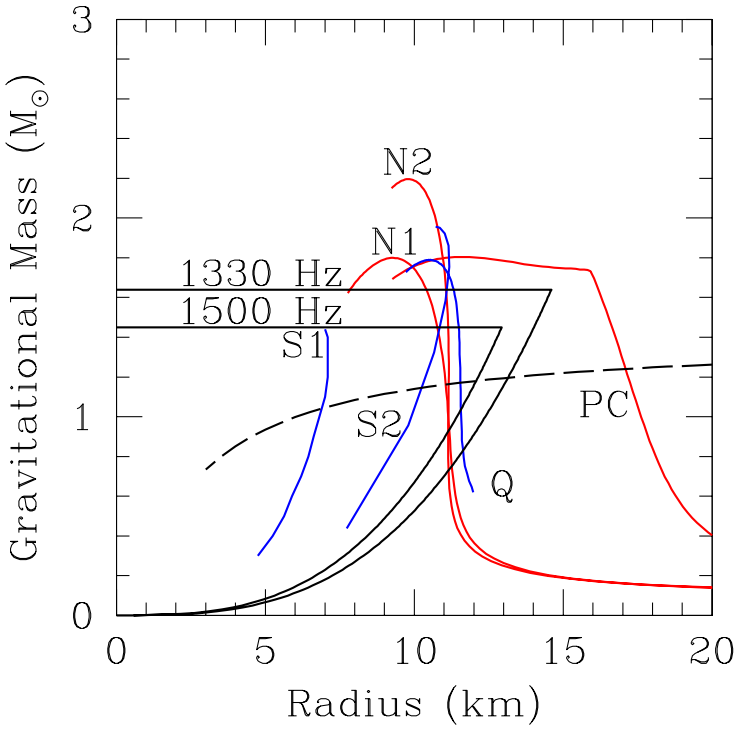

Figure 3. Constraints from orbital frequencies. The 1330 Hz curve is for the highest kilohertz quasi-periodic oscillation frequency yet measured (for 4U 0614+091, by van Straaten et al. 2000). The 1500 Hz curve shows a hypothetical constraint for a higher-frequency source. Other lines are as in Figure 1. All curves are drawn for nonrotating stars; the constraint wedges would be enlarged slightly for a rotating star (see Miller, Lamb, & Psaltis 1998).

More speculative constraints on the radius have been proposed by Li et al. (1999). Observations in 1998 of the accreting millisecond X-ray pulsar SAX J1808–3658 show pulsations at 401 Hz with a relatively steady pulse fraction and energy spectrum even as the flux from this source changed by a factor of $\sim$ 100. Li et al. (1999) then argue as follows. From the spin frequency we know the corotation radius $R_{\rm co}$ for a given mass. If the radius of the magnetosphere R_M is governed by equation (1), then if the mass accretion rate $\dot{M}$ is proportional to the flux and the field is primarily dipolar we

know that $R_M \propto F^{-2/7}$, where F is the observed flux. If we assume further that $R_M > R$ (to allow funneling and pulsations), and $R_M < R_{\rm co}$ (to allow accretion and keep the energy spectrum relatively constant), then we find $R < (F_{\rm min}/F_{\rm max})^{2/7} R_{\rm co}$. The data would then imply $R < 7.5$ km with a very weak dependence on stellar mass (Li et al. 1999).

If the radius is indeed this small then this result is of profound importance because it conflicts with all standard nucleonic or hyperonic equations of state. However, caution is necessary. The constraint $R_M < R_{\rm co}$ comes from the assumption that matter that couples to the magnetic field outside of corotation will be flung away from the star. But as discussed in § 2, this is not necessarily true. Instabilities at the magnetospheric interface, or cooling of matter there, could allow accretion even if $R_M > R_{\rm co}$. Li et al. (1999) argue that this is implausible because of the steadiness of the energy spectrum, but the spectral formation mechanism is not well-established; for example, if it only requires matter to get to the stellar surface, then perhaps it is irrelevant whether all the matter flows to the surface or only a small fraction. In that case, $\dot{M} \not\propto F$ and rigorous constraints on the radius are no longer possible. In particular, when $R_M \gtrsim R_{\rm co}$, the accretion rate on the stellar surface may decrease rapidly as the accretion rate at R_M decreases slightly, hence the flux could change by a large factor even if R_M itself changes little. It may be that as numerical magnetohydrodynamical codes become faster and more efficient, simulations of this system from first principles will eventually become possible and this issue can be resolved.

7. Summary

Equations of state involving only nucleonic matter are consistent with all available data. Some hints of evidence for very compact stars have been proposed (Li et al. 1999), which could indicate strange matter, but these are very model-dependent at the present. Even so, exotic states such as quark matter or strange matter are not excluded.

In just the last year, several observations have allowed new constraints on neutron star structure: (1) a mass of $M > 1.6\,M_\odot$ (at >95% confidence) has been measured for a neutron star (Nice et al. 2003); (2) the first surface redshift, $z = 0.35$, has been detected from a neutron star (Cottam et al. 2002), and (3) the first non-sinusoidal light curve has been measured from an accreting millisecond neutron star (Strohmayer et al 2003). These observations, along with many previously available data, hold out good hope for strong constraints on high-density matter in the next few years.

Acknowledgments

I appreciate many productive discussions with my collaborators Sudip Bhattacharyya, Fred Lamb, and Tod Strohmayer, and with the participants at the NATO ASW meeting in Yerevan. I also am grateful to David Blaschke and David Sedrakian for their superb organization of the conference. This work was supported in part by NSF grant AST 0098436.

References

Avni, Y., & Bahcall, J. N. 1975, ApJ, 197, 675
Bethe, H. A., & Brown, G. E. 1995, ApJ, 445, L129
Braje, T. M., Romani, R. W., & Rauch, K. P. 2000, ApJ, 531, 447
Chakrabarty, D., et al. 2003, Nature, 424, 42
Chakrabarty, D., & Morgan, E. H. 1998, Nature, 394, 346
Cook, G. B., Shapiro, S. L., & Teukolsky, S. A. 1994, ApJ, 424, 823
Cottam, J., Paerels, F., & Méndez, M. 2002, Nature, 420, 51
Cumming, A. 2003, Nucl.Phys.Proc.Suppl.132:435-445
Cumming, A., Zweibel, E., & Bildsten, L. 2001, ApJ, 557, 958
Dey, M., Bombaci, I., Dey, J., Ray, S., & Samanta, B. C. 1998, Phys. Lett. B, 439, 123
Frank, J., King, A. R., & Raine, D. J. 2002, "Accretion Power in Astrophysics", 3rd ed. (Cambridge: Cambridge University Press)
Friedman, B., & Pandharipande, V. R. 1981, Nucl. Phys. A, 361, 501
Galloway, D. K., Chakrabarty, D., Morgan, E. H., & Remillard, R. A. 2002, ApJ, 576, L137
Geppert, U., & Rheinhardt, M. 2002, A&A, 392, 1015
Ghosh, P., & Lamb, F. K. 1979, ApJ, 234, 296
Goussard, J.-O., Haensel, P., & Zdunik, J. L. 1998, A&A, 330, 1005
Illarionov, A. F., & Sunyaev, R. A. 1975, A&A, 39, 185
Joss, P. C. 1977, Nature, 270, 310
Joss, P. C. 1978, ApJ, 225, L123
Juett, A. M., Galloway, D. K., & Chakrabarty, D. 2003, ApJ, 587, 754
King, A. R., Davies, M. B., Ward, M. J., Fabbiano, G., & Elvis, M. 2001, ApJ, 552, L109
Konar, S., & Bhattacharya, D. 1999, MNRAS, 303, 588
Lamb, D. Q., & Lamb, F. K. 1977, in Proceedings 8th Texas Symposium on Relativistic Astrophysics, *Ann. N. Y. Acad. Sci.*, 302, 261
Lamb, D. Q., & Lamb, F. K. 1978, ApJ, 220, 291
Lattimer, J. M., & Prakash, M. 2001, ApJ, 550, 426
Li, X.-D., Bombaci, I., Dey, M., Dey, J., & van den Heuvel, E. P. J. 1999, Phys. Rev. Lett., 83, 3776
Loeb, A. 2003, PRL, 91, 071103
Maraschi, L., Traversini, R., & Treves, A. 1983, MNRAS, 204, 1179
Markwardt, C. B., Juda, M., & Swank, J. H. 2003a, ATel 127
Markwardt, C. B., Smith, E., & Swank, J. H. 2003b, ATel 122
Markwardt, C. B., Strohmayer, T. E., & Swank, J. H. 2003c, ATel 164
Markwardt, C. B., Swank, J. H., Strohmayer, T. E., in 't Zand, J. J. M., & Marshall, F. E. 2002, ApJ, 575, L21
Méndez, M., van der Klis, M., Ford, E. C., Wijnands, R., & van Paradijs, J. 1999, ApJ, 511, L49
Miller, M. C. 2002, *Nature* News and Views, 420, 31
Miller, M. C., & Lamb, F. K. 1998, ApJ, 499, L37

Miller, M. C., Lamb, F. K., & Psaltis, D. 1998, ApJ, 508, 791
Morris, D. J., et al. 2002, MNRAS, 335, 275
Muno, M. P., Özel, F., & Chakrabarty, D. 2002, ApJ, 581, 550
Nath, N. R., Strohmayer, T. E., & Swank, J. H. 2002, ApJ, 564, 353
Nice, D. J., Splaver, E. M., & Stairs, I. H. 2003, astro-ph/0311296
Özel, F., & Psaltis, D. 2003, ApJ, 582, L31
Pandharipande, V. R., & Smith, R. A. 1975, Nucl. Phys., A237, 507
Pechenick, K. R., Ftaclas, C., & Cohen, J. M. 1983, ApJ, 274, 846
Psaltis, D., & Lamb, F. K. 1997, ApJ, 488, 881
Psaltis, D., Özel, F., & DeDeo, S. 2000, ApJ, 544, 390
Quaintrell, H. et al. 2003, A&A, 401, 313
Ruderman, M. 1995, J. Astrophys. Astr., 16, 207
Shakura, N. I., & Sunyaev, R. A. 1973, A&A, 24, 337
Shu, F., Najita, J., Ostriker, E., Wilkin, F., Ruden, S., & Lizano, S. 1994, ApJ, 429, 781
Stella, L., White, N. E., & Rosner, R. 1986, ApJ, 308, 669
Strohmayer, T. E. 1992, ApJ, 388, 138
Strohmayer, T. E., & Bildsten, L. 2003, astro-ph/0301544
Strohmayer, T. E., Markwardt, C. B., Swank, J. H., & in 't Zand, J. J. M. 2003, ApJ, 596, L67
Taylor, J. H. 1994, Rev. Mod. Phys., 66, 711
Thorsett, S. E., & Chakrabarty, D. 1999, ApJ, 512, 288
Titarchuk, L., Cui, W., & Wood, K. 2002, ApJ, 576, L49
Trümper, J. Pietsch, W., Reppin, C., Voges, W., Staubert, R., & Kendziorra, E. 1978, ApJ, 219, L105
van der Klis, M. 2000, ARA&A, 38, 717
van Straaten, S., Ford, E. C., van der Klis, M., Méndez, M., & Kaaret, P. 2000, ApJ, 540, 1049
Weinberg, N., Miller, M. C., & Lamb, D. Q. 2001, ApJ, 546, 1098
Wijnands, R. 2003, Nucl.Phys.Proc.Suppl.132:496-505
Wijnands, R., & van der Klis, M. 1998, Nature, 394, 344
Wiringa, R. B., Fiks, V., & Fabrocini, A. 1988, Phys. Rev., C38, 1010
Wood, B. E., Müller, H.-R., Zank, G. P., & Linsky, J. L. 2002, ApJ, 574, 412
Woosley, S. E., & Taam, R. E. 1976, Nature, 263, 101
Woosley, S. E., & Wallace, R. K. 1982, ApJ, 258, 716
Zdunik, J. L. 2000, A&A, 359, 311
Zhang, W., Smale, A. P., Strohmayer, T. E., & Swank, J. H. 1998, ApJ, 500, L171

POSTGLITCH RELAXATIONS OF ANGULAR VELOCITY OF PULSARS

David M. Sedrakian
Department of Physics, Yerevan State University, 375025 Yerevan, Armenia
dsedrak@www.physdep.r.am

M. V. Hayrapetyan
Department of Physics, Yerevan State University, 375025 Yerevan, Armenia
mhayr@server.physdep.r.am

Abstract We consider the dynamics of rotation of a two-component neutron star with pinning and depinning of neutron vortices in the superfluid core. Solutions are obtained for the spin-down relaxation rate after a sudden glitch in the rotation rate. These solutions are compared with the observational data on the first eight post-glitch relaxations of the Vela pulsar. It is shown that vortex pinning and depinning between glitches and changes of the vortex number density in the superfluid region during a glitch can produce postglitch relaxations with observed parameters and time constants.

1. Introduction

The discovery of pulsars - astronomical compact objects radiating periodic electromagnetic pulses - is one of the most significant achievements of physics and astrophysics of the twentieth century. This discovery strongly stimulated developments of new methods of observation of rotating compact objects in a wide range of the electromagnetic wave spectrum - from low frequency radio waves to γ-radiation. More than 1300 radio-pulsars, i.e. neutron stars radiating in the radio band, have been discovered to date along with a few anomalous X-ray pulsars (AXP) and soft γ -ray repeaters (SGR) which are associated with highly magnetized rotating neutron stars radiating X-rays. All pulsars spin-down, i.e., the derivative of a pulsar's period is positive: $\dot{p} > 0$. The periods of observed pulsars are in the range from $10^{-3}s$ (millisecond pulsars) to about $10s$ (AXP and SGR), and at the same time the values of $\dot{p}$ are in wide interval from $10^{-20}s/s$ (millisecond pulsars) to $10^{-9}s/s$ (AXP and SGR). Several classes of rotational irregularities like glitches (macrojumps)

D. Blaschke and D. Sedrakian (eds.), Superdense QCD Matter and Compact Stars, 43–51.

and timing noise (microjumps) are superimposed on the steady state rotation and spin-down rates of pulsars. The first glitch was observed in the Vela pulsar PSR 0833-45 [1, 2]. The fractional changes of the period during a glitch are about $\Delta p/p \sim 10^{-6} - 10^{-9}$. At each glitch the decrease of pulsar's period is accompanied by an increase of $\dot{p}$ which is of the order $\Delta\ \dot{p}\ /\ \dot{p} \backsim 10^{-2} - 10^{-3}$. Other non-stationary dynamic phenomena observed in pulsars are the post-glitch relaxations. During several months after glitches the period p and $\dot{p}$ recover mostly to their pre-glitch values. The measurements of the discontinuities in pulsar rotation periods and period derivatives is a unique source of information about the interior of these objects, where matter exists in extreme states at densities ($\rho \backsim 10^{14} - 10^{15} g.cm^{-3}$) and in superstrong magnetic fields ($B \backsim 10^{12} Gs$).

The commonly accepted pulsar model is a neutron star of about one solar mass and a radius of the order of ten kilometers. A neutron star consists of a crust, which is about 1 km thick, and a high-density core. In the crust free neutrons and electrons coexist with a lattice of nuclei. The star's core consists mainly of neutrons and a few percents of protons and electrons. The central part of the core may contain some exotic states of matter, such as quark matter or a pion condensate. Inner parts of a neutron star cool up to temperatures $\sim 10^8 K$ in a few days after the star is formed. These temperatures are less than the critical temperatures T_c for the superfluid phase transitions of neutrons and protons. Thus, the neutrons in the star's crust and the core from a superfluid, while the protons in the core form a superconductor. The rotation of a neutron superfluid is achieved by means of an array of quantized vortices, each carrying a quantum of vorticity

$$\chi_0 = \pi\hbar/m_n \tag{1}$$

where $\hbar$ is the Planck constant and m_n is the neutron mass. The vortex array rotates about the spin axis and mimics a rigid-body rotation of the superfluid with angular velocity Ω_s. As the superfluid neutrons are weakly coupled with the charged component (electrons and nuclei), the superfluid component of the star must rotate faster than the normal component. In the case of frictional interaction between these components superfluid decelerates with the secular spin-down of the star's crust (observable part of the pulsar). The neutron vortex density is proportional to the angular velocity of the superfluid component, and therefore the radial outward motion of neutron vortices occurs when the star slows down.

Several theories were proposed in the past to describe the postglitch relaxation of pulsars' angular velocity. Each physical model considers the spin-down of the superfluid in a different way. Alpar et al. [3, 4] suggest that the crustal superfluid is responsible for the glitches and postglitch relaxation; they describe the dynamical properties of the crust superfluid in terms of a thermal

creep of neutron vortex lines. In the steady state thermally activated vortex lines slowly creep through pinning sites; the vortex creep rate is a nonlinear function of the lag between the superfluid angular velocity Ω_s and that of normal component Ω_e. During a glitch all pinned vortices are unpinned, after which superfluid component transfers gradually its angular momentum to the normal component. The postglitch behavior of $\dot{\Omega}_e$ is a result of the reestablishment of the steady state of the vortex creep process.

Contrary to the model above, Jones suggests that the maximum pinning force is small due to the vortex rigidity and a high degree of cancellation of the elementary pinning forces [5–8]. Thus, the neutron vortices in the star's crust move in an approximate corotation with the neutron-drip superfluid and are subject to a resistive force produced by interaction of vortex normal cores with nuclear lattice. Whether the free flow or the creep regimes are realized in the crust depends on a number of factors like the relative orientation of nuclear and neutron vortex lattices, strength of the pinning potential, repinning time scale, etc.

In the above discussed models of neutron star dynamics a general assumption is made that the core superfluid has a negligible role in the dynamical manifestations of pulsars. However, further investigations demonstrated that the superfluid component in the core could be responsible for the postglitch relaxation process. One of the most important features of the neutron-proton superfluid mixture in the core is the effect of mutual entrainment of superfluid components. Within an approach based on the nondissipative three-velocity hydrodynamics adapted for neutron star core superfluid, Sedrakian [9] and Sedrakian et al. [10] showed that due to the generation of strong magnetic fields by the entrainment currents it is energetically favorable to form proton vortex cluster around each neutron vortex. Then, the most effective process that couples the superfluid and normal components is the electron scattering from magnetized vortex clusters which carry a magnetic field of the order of $10^{14}Gs$ [11]. Subsequently Sedrakian and Sedrakian [12] formulated the general equations of dissipative three-velocity superfluid hydrodynamics of a rotating mixture and derived the continuity equation for vorticity, equation of motion of vortices including forces at the boundaries, and the equation of motion of vortex clusters. It was shown in this work that due to the strong density dependence of the free vortex flow viscosity coefficient, the core superfluid has a wide range of dynamical coupling times, which are consistent with the observed postglitch relaxation constants [14]. In Ref. [15] the equations describing the dynamics of motion of superfluid systems with pinning were derived. The solutions of these equations makes it possible to explain the time-dependent behavior of the angular velocity of the Vela pulsar. It has been shown that vortex pinning in between two consecutive jumps in the pulsar angular velocity can redistribute the vortex number density so as to produce both

the glitch and postglitch relaxation of a pulsar. The theory of nonstationary dynamics of neutron star rotation was compared with the observed relaxations after six glitches of the Vela pulsar [13]. It was assumed that the bulk of the superfluid shell may be divided into several distinct superfluid regions that respond to the jump independently. In addition, each superfluid region has been divided into active and passive shells. In the passive shells the condition $\dot{\Omega}_s{=}\dot{\Omega}_e$ has to be fulfilled, therefore these shells will not contribute to the relaxation process. In the active shells the condition $\dot{\Omega}_s{\neq}\dot{\Omega}_e$ is satisfied, which means that the momentum transfers from superfluid component to the normal one becomes possible. However, such a separation of the superfluid region into passive and active shells is rather arbitrary. It is clear that postglitch relaxation of pulsar's angular velocity is the manifestation of the whole superfluid region to the normal component of the star. Hence, fits to the postglitch data using a continuum model is necessary, where the whole spectrum of time scales is present.

In section I we consider the dynamics of rotation of a two-component neutron star and obtain the relaxation solutions for spin-down rate of the star. In section II we compare our solutions for the relaxation process with the observation data from the Vela pulsar.

2. Relaxation solutions

Let us consider the rotational dynamics of a two-component neutron star taking into account the pinning and depinning of neutron vortices. Equations of motion of the superfluid and normal components have the following forms [15, 17]:

$$I_e \frac{d\Omega_e}{dt} + \frac{\partial}{\partial t} \int \Omega_s dI_s = -K_{ext}, \tag{2}$$

$$\frac{\partial \Omega_s}{\partial t} = -\chi_0 [n - n_p] k (\Omega_s - \Omega_e), \tag{3}$$

$$\frac{\partial}{\partial r} \left(r^2 \Omega_s \right) = \chi_0 n r, \tag{4}$$

$$\frac{\partial n_p}{\partial t} = \frac{n - n_p}{\tau_p} - \frac{n_p}{\tau_d} \tag{5}$$

where Ω_e, I_e and Ω_s, I_s are the angular velocities and the moment of inertia of the normal and superfluid components respectively, K_{ext} is the external torque acting on the star, $n(r)$ and $n_p(r)$ are the densities of vortices and pinned vortices at the point r, τ_p and τ_d are the characteristic times of pinning and depinning processes. Here k is defined as [12]:

$$k = \frac{\chi_0 \rho_s / \eta}{1 + \left[\left(\chi_0 \rho_s - \beta \chi_0 \right) / \eta \right]^2}, \tag{6}$$

where ρ_s is the superfluid density, η and β are the longitudinal and tangential friction coefficients between the neutron vortices and the normal component. The star's relaxation time, defined as $\tau = 1/2k\Omega_e(0)$, is a rapidly growing function of density in the core superfluid region [13]. Accordingly, we separate the core into two regions with essentially different relaxation time-scales and refer to them as the active and passive regions. In the active region the dynamical relaxation time τ is less than or of the order of the maximal characteristic time of the relaxation process (for the Vela pulsar $\tau \lesssim 1000d$). We suppose that $\Delta\Omega = \Omega_s - \Omega_e$ changes only in this region, which is responsible for the glitch and relaxation, i.e. we have $\partial\Delta\Omega/\partial t \neq 0$ here. The passive region, where τ is larger than the characteristic relaxation times, can be divided into two subregions. In the first subregion we have $\tau \lesssim \tau_0$, where τ_0 is the spin-down time of pulsar (for Vela $\tau_0 \approx 10^4 yr$). Here a distribution of neutron vortices will be established such that the normal and superfluid components share the external torque and decelerate at the same rate. Therefore we have $\dot{\Omega}_s$=$\dot{\Omega}_e$ and $\partial\Delta\ \dot{\Omega}\ /\partial t = 0$ in this subregion. In the second subregion $\tau \gtrsim \tau_0$ and the vortex distribution does not change during the spin-down time of the star, i.e. $\Omega_s = const$ and $\partial\Delta\Omega/\partial t = -\partial\Omega_e/\partial t$. With above-mentioned conditions, we obtain from Eqs. (2)-(4) the following equations for $\Delta\Omega$ and Ω_e:

$$\Delta\Omega - \Delta\Omega_0 = [\gamma_2\tau\alpha - \Delta\Omega_0]\left(1 - e^{-t/\tau}\right), \tag{7}$$

$$\dot{\Omega}_e\ (t) = -\frac{p_0}{1+\lambda p_0}\int_0^{\mu}[\gamma_2\tau\alpha - \Delta\Omega_0]\,\frac{e^{-t/\tau}}{\tau}dy - \gamma_2, \tag{8}$$

where $\alpha = \tau_d/\tau_p$ and $p_0 = I_s/I_e, \mu p_0, \lambda p_0$ are the relative moments of inertia of the superfluid, the active region and the first passive subregion, respectively. Here $\mu \ll \lambda$ as the observed relaxation times are much smaller than the star's spin-down time. In Eqs. (7) and (8) $\gamma_2 = K_{ext}/I_e(1+\lambda p_0)$.

Now let us find the initial condition $\Delta\Omega_0$. As we can see from Eq. (7)

$$\Delta\Omega\,(r, t_g) = \gamma_2\tau\alpha_1, \tag{9}$$

where t_g is the interglitch time, $\alpha_1(r)$ is the pre-jump value of $\alpha(r)$. Then from the identity

$$\Delta\Omega(r,t_g) - \Delta\Omega_0 = [\Omega_s(r,t_g) - \Omega_s(0)] + [\Omega_e(0) - \Omega_e(t_g)] = -\Delta\Omega_s + \Delta\Omega_e \tag{10}$$

we find that

$$\Delta\Omega_0 = \gamma_2\tau\alpha_1 + \Delta\Omega_s - \Delta\Omega_e, \tag{11}$$

where $\Delta\Omega_s$ and $\Delta\Omega_e$ are the jumps of the angular velocities of the superfluid and normal components respectively. From Eqs. (8) and (10) we obtain the final expression for the deviation of the $\dot{\Omega}_e\ (t)$ from the steady state value:

$$\Delta\ \dot{\Omega}_e\ (t) = -\frac{p_0}{1+\lambda p_0}\int\limits_0^{\mu}(\Delta\Omega_e - \Delta\Omega' - \Delta\Omega_s)\frac{e^{-t/\tau}}{\tau}dy, \qquad (12)$$

where

$$\Delta\Omega' = \gamma_2\tau\left[\alpha_2(r) - \alpha_1(r)\right] = \gamma_2\tau\Delta\alpha, \qquad (13)$$

and α_2 is the postjump value of $\alpha(r)$. In the case of pinning we have for $\Delta\Omega'$ in Eq. (11)

$$\frac{t_g^2}{4\tau\tau_p} = \ln\left(1 + \frac{\Delta\Omega'}{\gamma_2\tau}\right) \qquad (14)$$

as found by Sedrakian and Sedrakian [12].

3. Discussion

Next we compare Eq. (11) with an interpolation formula for the eight glitches of the Vela pulsar [16]:

$$\Delta\dot{\Omega}(t) = -\sum_{j=1}^{3} a_j e^{-t/\tau_j} + At/t_g - A, \qquad (15)$$

where $\tau_1 = 10$ hours, $\tau_2 = 3.2$ days, $\tau_3 = 32.7$ days and the values of the coefficient a_j, A, t_g are presented in Table 1. To make a comparison, we suppose that the terms in Eq. (14) correspond to four shells of the active region of the star's core. In three of them the mean relaxation times are equal to τ_j, while in the fourth the relaxation time is of the order of the interglitch time. To find the relaxation regions, we use a standard model of a neutron star from Ref. [18] with a mass $M = 1.4M_{\odot}$, a radius $R \approx 10.13$ km and moment of inertia $I = 1.156 \cdot 10^{45}$ g cm^2; the corresponding dynamical relaxation times are calculated in the framework of General Relativity [19]. The results of a comparison are presented in Fig. 1, where the dependence of $\Delta\Omega' + \Delta\Omega_s$ on the radius of the star is shown for the first glitch of the Vela pulsar.

Note that similar curves are obtained for the eight glitches of the Vela pulsar. As we see from Fig. 1, the behavior of $\Delta\Omega' + \Delta\Omega_s$ is quite different in different parts of the relaxation region. The first part is the region of exponential relaxation with constants τ_1 and τ_2 and is located within the shell $9.533 \lesssim r \lesssim 9.61$ km. The second part is the region of the exponential relaxation with τ_3 and linear relaxation, located within the shell $9.36 \lesssim r \lesssim 9.533$

Table 1. The relaxation parameters a_i and A for the first eight glitches of the Vela pulsar, $\Delta\Omega_c$ is the jump value, t_g is an interglitch time [16].

	1	*2*	*3*	*4*	*5*	*6*	*7*	*8*
a_1 $10^{-15} r.s^{-2}$	0.1	0.02	0.0	0.04	48	26	89	211
a_2 $10^{-15} r.s^{-2}$	198	613	164	477	392	580	471	680
a_3 $10^{-15} r.s^{-2}$	285	303	202	717	74	617	280	452
A $10^{-24} r.s^{-2}$	4962	5334	7875	5455	11589	4578	7578	3745
$\Delta\Omega_c$ $10^{-6} r.s^{-1}$	166	145	140	216	82	145	92	128
$t_g(days)$	912	1491	1009	1227	272	1067	1261	907

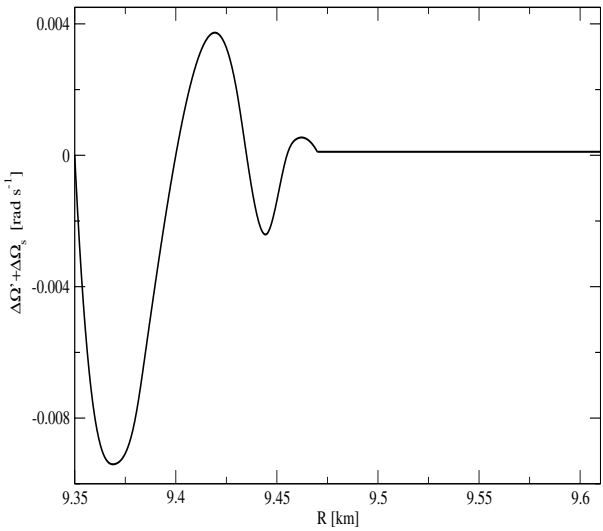

Figure 1. The dependence of $\Delta\Omega' + \Delta\Omega_s$ on the radius of the star for the first glitch of Vela pulsar.

km. In the region $9.533 \lesssim r \lesssim 9.61$ km, $\Delta\Omega' + \Delta\Omega_s$ is positive and is of the same order of magnitude as $\Delta\Omega_e$. The positive value of $\Delta\Omega' + \Delta\Omega_s$ could be the result of a change of the angular velocity of the superfluid component, i.e. an increase of the neutron vortex density in this region. However, this region borders the "glitch region", where the dynamical relaxation time is less than two minutes [15]. In the "glitch region" vortex pinning is essential in order to accumulate sufficient number of vortices, sudden unpinning of which gives an observed jump in the rotation rate of a pulsar. Therefore in the above-mentioned region the changes of vortex distribution are less probable, i.e. $\Delta\Omega_s \approx 0$. Then the condition $\Delta\Omega' > 0$ has to be satisfied which agrees with Eq. (13). However, small changes of $\Delta\Omega' + \Delta\Omega_s$ in this region are affected by random changes of $\Delta\Omega_s$.

Starting from the radius $r \lesssim 9.533$ km the sign of $\Delta\Omega' + \Delta\Omega_s$ becomes variable; its absolute value exceeds the jump value $\Delta\Omega_e$. We could try to explain the above-mentioned behavior of $\Delta\Omega' + \Delta\Omega_s$ only by means of the changes of the angular velocity of superfluid component, choosing $\Delta\Omega' = 0$. This means that during a glitch only some amount of neutron vortices are transfered from one part of the core to another. Then the changes of vortex density are defined from the local conservation condition of total vortex number. As seen in Fig. 1, the absolute magnitude of the negative value of $\Delta\Omega' + \Delta\Omega_s$ can exceeds its positive value by a factor of 2-3. This means that the behavior of $\Delta\Omega' + \Delta\Omega_s$ cannot be explained by the redistribution of vortices, especially in the linear relaxation region, where its changes are most essential. Therefore it is impossible to explain the behavior of $\Delta\Omega' + \Delta\Omega_s$ without depinning. For this reason we will suppose that rare cases of depinning act in such a way that $\alpha \ll 1$ in this region. If we suppose also that α increases after a glitch and the relaxation, then $\Delta\Omega' = \gamma_2 \tau \Delta\alpha$ will be negative, with its modulus increasing with density as a result of the strong density dependence of τ. In this manner we can explain the asymmetry of $\Delta\Omega' + \Delta\Omega_s$ in the region of exponential relaxation with characteristic time τ_3 as well as in the linear relaxation region. In particular, the deep negative minimum of $\Delta\Omega' + \Delta\Omega_s$ in the linear relaxation region can be explained by the increase of $\tau\Delta\alpha$ with increasing density. Once the observational data on further glitches of the Vela pulsar (the total number is 15) will become available, more could be said about the role of the jump in distribution of vortices and the correlation between jump value and relaxation parameters.

This work is supported by CRDF award 12006/NFSAT PH067-02. D.S. acknowledges the ISTC support at Yerevan State University, Grant No. A-353.

References

[1] Radhakrishnan V., Manchester R.N. Nature 222, (228),1969.

[2] Reichly R.E., Downs G.S. (1969), Nature 222, 229.

[3] Alpar M.A., Anderson P.W., Pines D., Shaham J. (1984), ApJ 276, 325.

[4] Alpar M.A., Anderson P.W., Pines D., Shaham J. (1984), ApJ 278, 791.

[5] Jones P.B. (1990), MNRAS 242, 257.

[6] Jones P.B. (1990), MNRAS 246, 315.

[7] Jones P.B. (1993), MNRAS 263, 619.

[8] Jones P.B. (1998), MNRAS 296, 217.

[9] Sedrakian D.M. (1982), Astrofizika 18, 417.

[10] Sedrakian D.M., Shahabassian K.M., Movsissian A.G. (1983), Astrofizika 19, 303.

[11] Sedrakian D.M., Shahabassian K.M., Movsissian A.G. (1985), Astrofizika 22, 137.

[12] Sedrakian A.D., Sedrakian D.M. (1995), ApJ 447, 305.

[13] Sedrakian A.D., Sedrakian D.M., Cordes J., Terzian Y. (1995), ApJ 447, 324.

[14] Cordes J.M., Downs G.S., Krause-Polstorff J. (1988), ApJ 330, 847.

[15] Sedrakian A.D., Sedrakian D.M. (1995), Zh. Eksp. Teor. Fiz. 108, 631.

[16] Alpar M.A., Chau H.F., Cheng K.S., Pines D. (1996), ApJ 459, 706.

[17] Sedrakian D.M., Hayrapetyan M.V. (2002), Astrofizika 45, 575.

[18] Weber F. (1992), "Hadron Physics and Neutron Star Properties", Habilitation Thesis, Univ. Munich.

[19] Sedrakian D.M., Hayrapetyan M.V. (1999), Astrofizika 42, 89.

ISOLATED NEUTRON STARS: AN ASTROPHYSICAL PERSPECTIVE

Sergei Popov,[1,2] and Roberto Turolla[1]

[1] *University of Padova, via Marzolo 8, 35131, Padova, Italy*
turolla@pd.infn.it, popov@pd.infn.it

[2] *Sternberg Astronomical Institute, Universitetski pr. 13, 119992 Moscow, Russia*
polar@sai.msu.ru

Abstract We briefly review selected results in astrophysics of neutron stars (NSs) obtained during the last two years, focusing on isolated radioquiet objects. We discuss in some detail the population synthesis of close-by isolated NSs (INSs), the spectra of INSs, the detection of spectral features in these sources (including cyclotron features), and the recent results on velocity distribution of NSs and accretion onto INSs from the interstellar medium.

Keywords: Anomalous X-ray pulsars, Soft gamma repeaters, radioquiet isolated neutron stars

1. Introduction

Neutron stars (NSs) are perhaps the most interesting astronomical objects from the physical point of view. They are associated with a variety of *extreme* phenomena and matter states; for example, magnetic fields beyond the QED vacuum pair-creation limit, supranuclear densities, superfluidity, superconductivity, exotic condensates and deconfined quark matter, etc.

There are about $10^8 - 10^9$ NSs in the Galaxy and their local density is about 3×10^{-4} pc^{-3} (see Fig. 1). [1] At present only a small fraction (about 2000 sources) of this large population is observed either as isolated objects of different nature or as accreting objects or millisecond radio pulsars in binaries. Young NSs can be observed for several million years dissipating their rotational, thermal or/and magnetic energy. Most of the old NSs are dim objects without significant internal sources of energy. If a NS looses its strong magnetic field on a time scale $< 10^8$–10^9 yrs then it can be resurrected by accretion

[1] Here and below we will not distinguish between NSs, quark stars, hybrid stars etc. unless explicitely stated.

D. Blaschke and D. Sedrakian (eds.), Superdense QCD Matter and Compact Stars, 53–72.

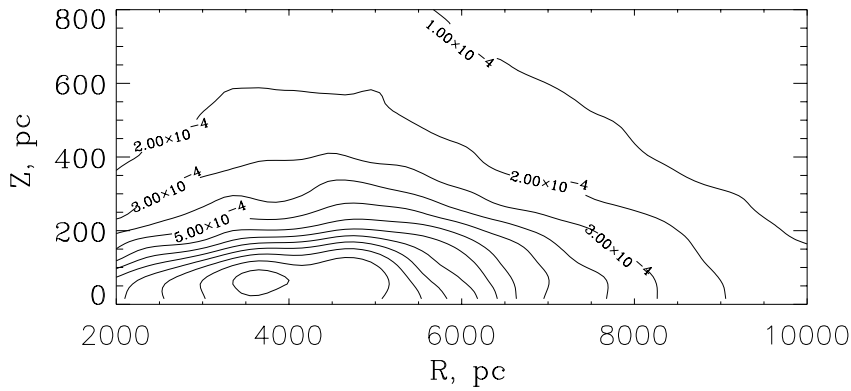

Figure 1. Spatial distribution of NSs in the Galaxy. The data was calculated by a Monte-Carlo simulation. The kick velocity was assumed following Arzoumanian et al. (2002). NSs were born in a thin disk with a semithickness 75 pc. Those NS that were born inside $R = 2$ kpc and outside $R = 16$ kpc were not taken into account. NS formation rate was assumed to be constant in time and proportional to the square of the ISM density at the birthplace. Results were normalized to have in total 5×10^8 NSs born in the described region. Density contours are shown with a step 0.0001 pc^{-3}. At the solar distance from the center close to the galactic plane the NS density is about $2.8 \cdot 10^{-4}$ pc^{-3}. From Popov et al. (2003a).

from the interstellar medium (ISM) or from a binary companion (small number of old NSs can spin-up by disc accretion and emerge as millisecond radio pulsars). However, as we will discuss later on, there is no much hope that a significant number of isolated NSs can be bright accretors, so that most of NSs are unobservable.

The main parameters which determine the astrophysical appearance of NSs are:

- Spin period, p
- Magnetic field, B
- Mass, M
- Spatial velocity, v
- Surface temperature, T
- Angle between spin and magnetic axis, α

The parameters that characterize the surrounding medium (interstellar medium or matter from the binary companion) are also important.

Here we will focus on isolated NSs (INSs). At present the following types of these sources are observed:

1 Radio pulsars (PSRs)

2 Anomalous X-ray pulsars (AXPs)

3 Soft gamma repeaters (SGRs)

4 Compact central objects in supernova remnants (CCOs in SNRs)

5 Geminga and geminga-like object(s)

6 The "Magnificent seven" — seven dim ROSAT sources

INSs may lurk within unidentified EGRET and ROSAT sources and, possibly, among dim X-ray sources observed by XMM-Newton and Chandra in globular cluster (see Pfahl, Rappaport 2001) or in the galactic center (see Muno et al. 2003). Except PSRs all others are more or less radioquiet (which, however, does not mean that they are necessarily radio silent).

Astronomy is the only purely observational natural science. All the information we have comes through the electromagnetic emission from celestial bodies – no direct experiments are possible (of course, except some rare cases in the Solar system). This is why progress in astronomy is necessarily connected with new observational facilities. Astrophysics of NSs is a quickly growing field. New space observatories (especially XMM-Newton and Chandra) give us an opportunity to obtain increadible spatial and spectral resolution in the X-ray band. New radio surveys of PSRs doubled the number of know objects of this type over the last few years. Data from optical and IR telescopes foster new discoveries in NS astrophysics. The huge flow of new observational data stimulated theoretical studies. Here we briefly review some recent results in astrophysics of NSs which can be of interest for the participants of this conference – mainly physicists working on quark stars and related subjects. In the next section we just give a list of these new results (we do not try to summarize those results which are directly connected to quark stars since they are presented in other contributions to this proceedings). Then, in the following sections we comment on some of them in more detail, focusing on INSs and paying more attention to the results related to our own research.

2. What's new

In this section we give a list of the new important discoveries in observational and in theoretical astrophysics of NSs. In the observational part of the list we commonly give the object's name(s), determined parameters and the reference to the original paper. In the theoretical part we occasionally just refer to the topic of research and give references to the original papers or/and reviews on that topic.

Table 1. Local ($D < 1$ kpc) population of young (age < 4.25 Myrs) isolated neutron stars

Source name	Period s	CR[a] cts/s	$\dot{P}$ 10^{-15} s/s	D kpc	Age[b] Myrs	Refs
RINSs						
RX J1856.5-3754	—	3.64	—	0.117[e]	~ 0.5	[1,2]
RX J0720.4-3125	8.39	1.69	$\sim 30 - 60$	—	—	[1,3]
RX J1308.6+2127	10.3	0.29	—	—	—	[1.4]
RX J1605.3+3249	—	0.88	—	—	—	[1]
RX J0806.4-4123	11.37	0.38	—	—	—	[1,5]
RX J0420.0-5022	3.45	0.11	—	—	—	[1,11]
RX J2143.7+0654	—	0.18	—	—	—	[6]
Geminga type						
PSR B0633+17	0.237	0.54[d]	10.97	0.16[e]	0.34	[7]
3EG J1835+5918	—	0.015	—	—	—	[8]
Thermally emitting PSRs						
PSR B0833-45	0.089	3.4[d]	124.88	0.294[e]	0.01	[7,9,10]
PSR B0656+14	0.385	1.92[d]	55.01	0.762[f]	0.11	[7,10]
PSR B1055-52	0.197	0.35[d]	5.83	~ 1[c]	0.54	[7,10]
PSR B1929+10	0.227	0.012[d]	1.16	0.33[e]	3.1	[7,10]
Other PSRs						
PSR J0056+4756	0.472	—	3.57	0.998[f]	2.1	[10]
PSR J0454+5543	0.341	—	2.37	0.793[f]	2.3	[10]
PSR J1918+1541	0.371	—	2.54	0.684[f]	2.3	[10]
PSR J2048-1616	1.962	—	10.96	0.639[f]	2.8	[10]
PSR J1848-1952	4.308	—	23.31	0.956[f]	2.9	[10]
PSR J0837+0610	1.274	—	6.8	0.722[f]	3.0	[10]
PSR J1908+0734	0.212	—	0.82	0.584[f]	4.1	[10]

[a]) ROSAT PSPC count rate; [b]) Ages for pulsars are estimated as $P/(2\dot{P})$,
for RX J1856 the estimate of its age comes from kinematical considerations.
[c]) Distance to PSR B1055-52 is uncertain ($\sim$ 0.9-1.5 kpc)
[d]) Total count rate (blackbody + non-thermal)
[e]) Distances determined through parallactic measurements
[f]) Distances determined with dispersion measure
[1] Treves et al. (2000) ; [2] Kaplan et al. (2002); [3] Zane et al. (2002);
[4] Hambaryan et al. (2001); [5] Haberl, Zavlin (2002); [6] Zampieri et al. (2001);
[7] Becker, Trumper (1997); [8] Mirabal, Halpern (2001); [9] Pavlov et al. 2001;
[10] ATNF Pulsar Catalogue (see Hobbs et al. 2003); [11] Haberl et al. (2004, in prep.)

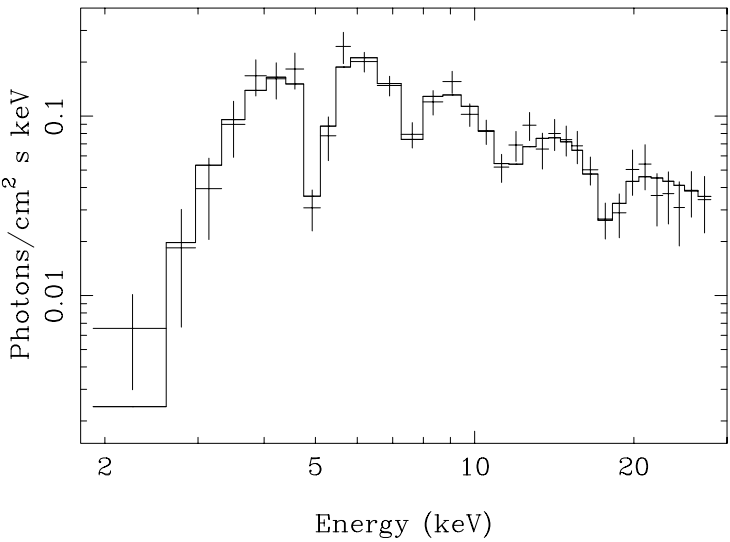

Figure 2. Spectrum of SGR 1806-20. Observed by RXTE. From Ibrahim et al. (2002).

2.1 Observations

1 Magnetic field determination from cyclotron features

- SGR 1806-20. $B \sim 10^{15}$ G (if it is a proton cyclotron resonance feature) (Ibrahim et al. 2002). See Fig. 2.
- AXP 1RXS J170849-400910. $B \sim 9 \cdot 10^{11}$ G (electron resonance) or $1.6 \cdot 10^{15}$ G (proton resonance) (Rea et al. 2003).
- AXP 1E 1048-5937. $B \sim 1.2 \cdot 10^{12}$ G (electron resonance) or $B \sim 2.4 \cdot 10^{15}$ G (proton resonance) (Gavriil et al. 2002, 2003). Not a very strong feature. Not consistent with spin-down.
- 1E 1207.4-5209. CCO in SNR. $B \sim 8{\cdot}10^{10}$ G (electron resonance) or $\sim 1.6 \cdot 10^{14}$ G (proton resonance) (Bignami et al. 2003). From spin-down measurements the field estimate is $B \sim (2-3) \cdot 10^{13}$ G (see Fig. 3).
- RBS 1223. "Magnificent seven". $B \sim (2-6) \cdot 10^{13}$ G (proton resonance) (Haberl et al. 2003).

2 Relations between AXPs and SGRs

Observations of X-ray bursts from AXPs which are very similar to the ones from SGRs.

- AXP 1E1048-5937 (Gavriil et al. 2002, 2003). See Fig. 4.

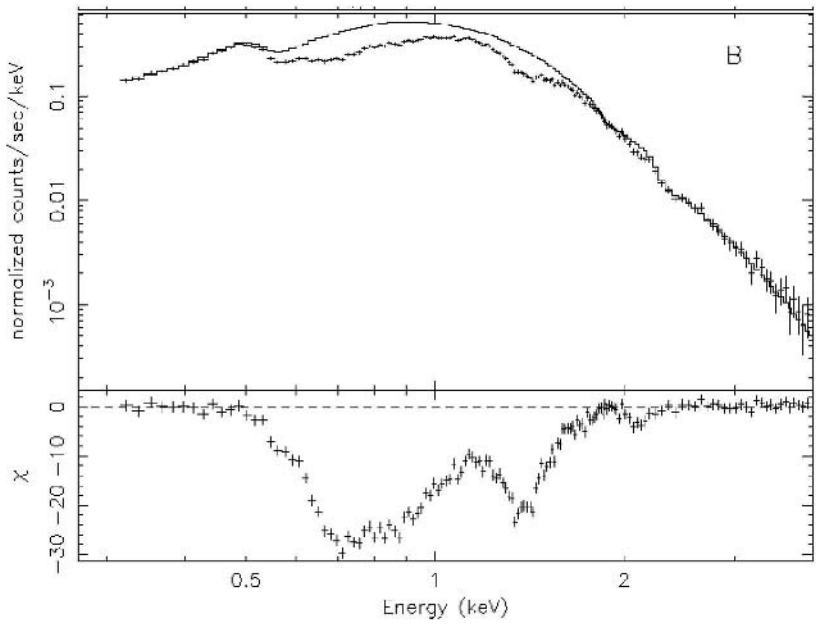

Figure 3. Spectrum of 1E 1207.4-5209 collected by the MOS camera on the EPIC instrument of XMM-Newton. Also the best fit continuum and residuals are shown. From Bignami et al. (2003).

- AXP 1E 2259+586 (Kaspi, Gavriil 2002).

3 More radiopulsars.

- On-line ATNF catalogue. 1300 PSRs (Hobbs et al. 2003).
- Parkes survey. > 800 new PSRs (Kramer et al. 2003, Morris et al. 2002).
- A pulsar with magnetar parameters: $p = 6.7$ s, $B \approx 9.4 \cdot 10^{13}$ G (McLaughlin et al. 2003).
- A new double NS system (Burgay et al. 2003).

4 NS initial velocity distribution

- New PSRs proper motions (Brisken et al. 2003).
- New model for the galactic distribution of free electrons (Cordes, Lazio 2002).
- Bimodal initial velocity distribution with two maxwellian components: σ_1=90 km s^{-1} and σ_2=500 km s^{-1} (Arzoumanian et al. 2002).

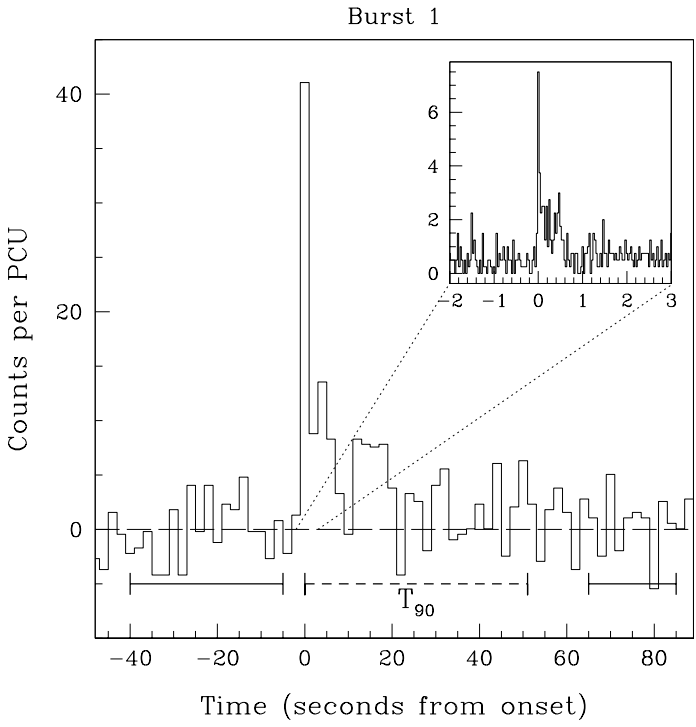

Figure 4. AXP 1E 1048-5937 burst. Observed by RXTE. From Gavriil et al. (2002).

5 Proper motions of radioquiet INSs

- RX 1856.5-3754. $d = 117$ pc, $v_T = 185$ km s^{-1}. Excludes accretion from the ISM (Walter, Lattimer 2002; Kaplan et al. 2002). Distance to this source is still uncertain.
- RX 0720.4-3125. $v_T = 50(d/100\mathrm{pc})$ km s^{-1}. Excludes accretion from the ISM (Motch et al. 2003).

6 Discovery of a new Geminga-like object

- 3EG 1835+5918. EGRET source (Halpern et al. 2002).

7 $\dot{p}$ for radioquiet INS.

- RX 0720.4-3125. $\dot{p} \sim (3-6) \cdot 10^{-14}$ (Zane et al. 2002).
- Kes 75. $p = 0.325$ s, $\dot{p} = 7.1 \cdot 10^{-12}$ (Mereghetti et al. 2002).
- G296.5+10. $p = 0.424$ s, $\dot{p} = (0.7-3) \cdot 10^{-14}$ (Pavlov et al. 2002).

- Non-constant $\dot{p}$ for 1E 1207.d-5209 (Zavlin et al. 2003).

8 IR radiation from AXPs

- 1E 2259+586 (Hulleman et al. 2001).
- 1E 1048.1-5937 (Wang, Chakrabarty 2002).
  Variability (Israel et al. 2002).
- 1RXS J1708.9-400910 (Israel et al. 2003).

9 Pulsars jets and toruses

- Variable jet of the Vela pulsar (Pavlov et al. 2003)
- Alignment between spin axis and spatial velocity for Crab and Vela pulsars (see for example Lai et al. 2001)

10 NS masses

- Vela X-1. $M \approx 2\,M_{\odot}$ (Quaintrell et al. 2003).
- PSR J0751+1807. $M \approx 1.6 - 1.28\,M_{\odot}$ (Nice, Splaver 2003).

11 Gravitationaly redshifted line from an accreting NS

- EXO 0748-676. z=0.35 (Cottam et al. 2002).

2.2 Theory

1 Spectra of strongly magnetized NSs

- Lines for high magnetic field (Zane et al. 2001; Ho, Lai 2001, 2003; Ozel 2001).
- Bare neutron and quark star emission (Turolla et al. 2004).
- Atmospheres and opacities for high magnetic fields (Potekhin, Chabrier et al.).

2 Gould Belt in population synthesis calculations

- Population synthesis of EGRET sources (Grenier 2003).
- Population synthesis of young cooling INS (Popov et al. 2003a).

3 SN explosions (See the contribution by S. Rosswog in this volume for more details.)

- 3-Dimensional core-collapse (Fryer, Warren 2003).
- Nucleosynthesis, collapse dynamics (Woosley et al. 2002).

- Jets, GRB connection, X-ray flashes, HETE-2 data (Lamb et al. 2003).

4 Accretion and spin evolution

- CDAF – convection dominated accretion flows (Igumenschev et al. 2002, 2003)
- Low angular momentum accretion (Proga, Begelman 2003).
- Accretion onto INSs (Toropina et al., Romanova et al. 2003).
- Propeller regime for INSs (Ikhsanov 2003).

5 Cooling curves

- Impact of superfluidity on cooling (Kaminker et al. 2003, Tsuruta et al. 2002).
- Cooling curves for quark stars (see contributions by Grigorian et al. and others in this procedings)

6 Discussion on models of fossil discs around INSs

- Discs can explain AXPs and other types of INS (Alpar 2003).
- Discs can't explain it (Francischelli, Wijers 2002).
- General picture of pulsars with jets and disks (Blackman, Perna 2003).

7 Electrodynamics of magnetars

- SGR phenomena due to magnetospheric activity (Thompson et al. 2002).

3. Discussion

Here we discuss some results in more detail focusing on topics of our personal interest.

3.1 Spectral features and magnetic field determination

Investigations on the emission properties of INSs started quite a long time ago, mainly in connection with the X-ray emission from PSRs. In the seventies it was a common wisdom that the radiation emitted by INSs comes directly from their solid crust and is very close to a blackbody. Lenzen and Trumper (1978) and Brinkmann (1980) were the first to address in detail the issue of the spectral distribution of INS surface emission. Their main result was that

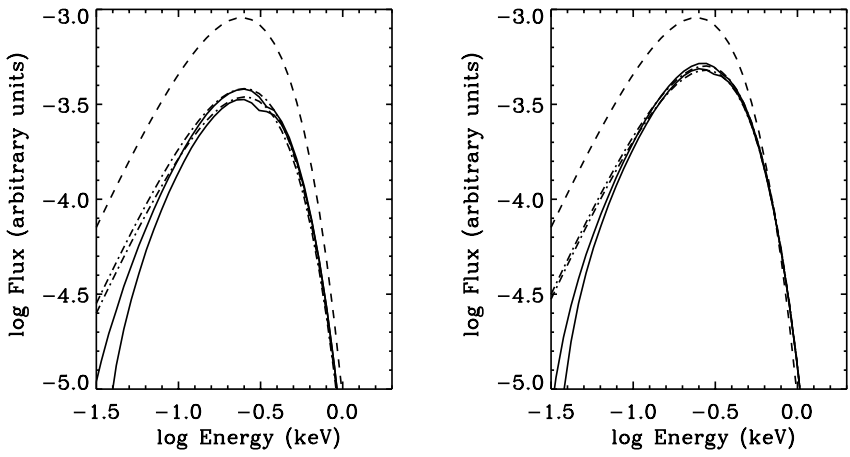

Figure 5. Model spectra of a naked neutron star. The emitted spectrum with electron-phonon damping accounted for and $T_{surf} = 10^6$ K. Left panel: uniform surface temperature; right panel: meridional temperature variation. The dashed line is the blackbody at T_{surf} and the dash-dotted line the blackbody which best-fits the calculated spectrum in the 0.1–2 keV range. The two models shown in each panel are computed for a dipole field $B_p = 5 \times 10^{13}$ G (upper solid curve) and $B_p = 3 \times 10^{13}$ G (lower solid curve). The spectra are at the star surface and no red-shift correction has been applied. From Turolla, Zane and Drake (2004).

the star emissivity is strongly suppressed below the electron plasma frequency which, for the case of X-ray pulsars, is at about 1 keV.

Later on, the role played by the thin atmosphere covering the star crust in shaping the emergent spectrum started to be appreciated. Romani (1987) investigated the properties of fully-ionized, H atmospheres around unmagnetized, cooling NSs and showed that the spectrum is harder than a blackbody at the star effective temperature. The spectra from magnetized NSs were studied, under similar assumptions, by the St. Petersburg group in a series of papers (Shibanov et. al 1992; Pavlov et al. 1994; Zavlin et al. 1995). Because the opacity is higher in the presence of a strong magnetic field ($B \sim 10^{12}$ G or larger), the magnetic spectra tend to be more blackbody-like. In these investigations, the focus was on the middle-aged NSs with $T_{eff} \approx 10^5 - 10^6$ K and typical fields $\approx 10^{12}$–10^{13} G. Under such conditions the bulk of the emission is in the soft X-ray band ($\approx$ 0.1–1 keV) while the electron cyclotron line at $\hbar\omega_{c,e} \sim 11.6(B/10^{12}\,\mathrm{G})$ keV falls in the tens of keVs range. For this reason no detailed modeling of the line was attempted. An (approximate) treatment of the proton cyclotron line was included, although its energy, $\hbar\omega_{c,p} \sim 6.3(B/10^{12}\,\mathrm{G})$ eV, falls in the optical/UV region for pulsar-like fields.

Being related to a resonant behavior of the opacity for the extraordinary mode, the proton cyclotron line appears as an absorption feature in the spectrum. Atmospheres comprised of heavy elements (Fe) were studied by Rajagopal et al. (1997); the emergent spectra exhibit a variety of emission/absorption features produced by atomic transitions. Such models, however, suffer from our lack of knowledge of the ionization states and opacities of metals in a strong magnetic field.

Until quite recently, model atmosphere calculations were restricted to fields not exceeding a few 10^{13} G. Ultra-magnetized NSs has been long suspected to exist in SGRs. It was only in the late nineties that the positive detection of large spin-down rates in SGR 1806-20 and SGR 1900+14 (Kouveliotou et al. 1998; 1999) provided decisive evidence in favor of the magnetar scenario. At about the same time spin-down measurements supported the magnetar nature of the AXPs. In nearly all AXPs and in at least one SGR, a thermal component was clearly detected in the X-ray spectrum. This prompted renewed interest in the study of the thermal emission from NSs with surface fields in the 10^{14}–10^{15} G range. The main goal was to identify possible signatures of the super-strong magnetic field which could provide an unambiguous proof of the existence of magnetars. The proton cyclotron resonance, being in the keV range for a magnetar, is an ideal candidate for this. Zane et al. (2001) were the first to construct model atmospheres for $B \sim 10^{14}$–10^{15} G and luminosities appropriate to SGRs/AXPs. They considered completely ionized, pure H atmospheres in radiative equilibrium and solved the transfer problem in a magnetized medium in the normal modes approximation and planar symmetry. Computed spectra are blackbody-like and show a relatively broad absorption line at $\hbar\omega_{c,p}$ with an equivalent width EW ≈ 100 eV, within the detection capabilities of Chandra and XMM-Newton. This issue was further addressed by Ho and Lai in a recent series of papers (Ho, Lai 2001, 2002; Lai, Ho 2003). Their approach differs from that used by Zane et al. (2001) in the treatment of vacuum polarization and mode conversion. This affects the line properties in a non-negligible way. In the first paper no adiabatic mode conversion was included and the line EW found was larger than that predicted by Zane et al. Accounting for adiabatic mode conversion produces a depression in the continuum at energies close to the cyclotron energy, thus reducing the line EW to values somewhat smaller than those of Zane et al. Spectra from ultra-magnetized NSs were also computed by Ozel (2001) who, however, did not account for the proton contribution.

While a proper solution of the radiative transfer problem in media at $B \gg B_{QED} \simeq 4.4 \times 10^{13}$ G has necessarily to wait for a description in terms of the Stokes parameters, the search for the proton cyclotron feature in the spectra of AXPs and SGRs begun. Up to now no evidence for the proton line has been found in the thermal components of SGRs and AXPs, although these

observations can not be regarded as conclusive yet. Quite recently a cyclotron absorption feature in the spectrum of SGR 1806-20 during an outburst has been reported by Ibrahim et al. (2002) and further confirmed by the same group in several other events from the same source (Ibrahim et al. 2003). The line parameters are similar to those predicted by Zane et al. (2001), even if the line in this case is not superimposed on a thermal continuum and is not expected to originate from the cooling surface of the star. The line energy ($\simeq 5$ keV) implies a field strength $B \sim 10^{15}$ G in excellent agreement with the spin-down measure.

Model spectra from standard cooling NSs proved successful in fitting X-ray data for a number of sources and in some cases solved the apparent discrepancy between the star age as derived from the temperature and from the $\dot{P}/2P$ measure. However, model atmospheres seem to be of no avail in interpreting the multiwavelength spectral energy distribution (SED) of the seven ROSAT INSs. The X-ray spectrum of the most luminous source RX J1856.5-3754 is convincingly featureless and shows, possibly, only slight broadband deviations from a blackbody (Drake et al. 2002; Burwitz et al. 2003). The situation is more uncertain for the fainter sources, and the possible presence of a (phase-dependent) broad feature at 200–300 eV has been reported very recently in RBS 1223 (Haberl et al. 2003). In all the cases in which an optical counterpart has been identified, the optical flux lies a factor $\approx 5 - 10$ above the Rayleigh-Jeans tail of the blackbody which best-fits the X-ray spectrum (Kaplan et al. 2003).

The small radiation radius implied by the distance (~ 120 pc, but this value is still under debate) led to the suggestion that RX J1856.5-3754 may host a quark star (Drake et al. 2002; Xu 2002, 2003). Other, more conventional explanations are well possible. Pons et al. (2002) and Braje and Romani (2002) suggested a scenario in which the X-rays come from a hotter region close to the poles, while the reminder of the star surface is at lower temperature and produces the optical/UV flux. While this picture is appealing and is still consistent with the lack of pulsations (pulsed fraction $< 1.3\%$ see Haberl et al. 2003), no explanation is offered for the formation of a pure blackbody spectrum in an object which should conceivably be covered by an optically thick atmosphere. Very recently Turolla et al. (2004) considered the possibility that RX J1856.5-3754 is a bare NS, that is to say no atmosphere sits on the top of its crust. Lai and Salpeter (1997; see also Lai 2000) have shown that for low surface temperatures and high enough magnetic fields, the gas in the atmosphere undergoes a phase transition which turns it into a solid. While the onset of such a transition appears unlikely for an H atmosphere, it might be possible for a Fe composition for the temperature of RX J1856.5-3754 ($T_{BB} \sim 60$ eV) and $B > 3 - 5 \times 10^{13}$ G. Turolla et al. computed the spectrum emitted by the bare Fe surface including electron-phonon damping in the highly degenerate crust,

and found that it is close to depressed blackbody. If indeed RX J1856.5-3754 is a bare NS, and keeping in mind that their results depend on the assumed properties of the crust-vacuum interface, the optical/UV emission may be due to a thin H layer which covers the star and is optically thick up to energies $\approx 10 - 100$ eV. The Rayleigh-Jeans optical/UV emission is at the star surface temperature, and the optical excess with respect to the X-ray spectrum arises because the latter is depressed.

3.2 Velocity distribution

The number of PSRs with known transverse velocities is continuously growing. New velocity determinations are based on a new model of galactic distribution of free electrons (Cordes, Lazio 2002). Unlike the situation 10 years ago, when updated data on free electrons distribution led to nearly doubling of distances (and, correspondingly, transverse velocities), results of Cordes and Lazio brought serious corrections only for distant PSRs.

In the last two years a new initial velocity distribution of NSs became standard. It is a bimodal distribution with peaks at ~ 130 km s^{-1} and ~ 710 km s^{-1} (Arzoumanian et al. 2002). Contributions from the low and high velocity populations is nearly equal. Brisken et al. (2003) confirm this type of distribution, however they give arguments for smaller fraction of low velocity NSs (about 20%).

The nature of this bimodality is unknown, and recently several papers appeared where authors suggested (or modified) different kick mechanisms. There are three main mechanism for a natal kick (see for example Lai et al. 2001). The first is the hydrodynamical one. In many models of that mechanism NSs do not receive kicks higher than $\sim (100 - 200)$ km s^{-1} due to it (Burrows et al. 2003). The second one is a modification of an electromagnetic rocket mechanism (see Huang et al. 2003). In this scenario velocity is dependent on the initial spin rate ($v \propto p^{-2}$). It can provide high velocities if the initial spin period of a NS is about 1 ms (probably quark stars can spin faster than NSs, so that for them this mechanism can be more effective). The third mechanism is connected with instabilities in a newborn NS which lead to its fragmentation into two stars followed by an explosion of the lightest one (see Colpi, Wasserman 2002). Also one should have in mind disruption of high-mass binaries, so that newformed compact objects receive significant spatial velocity due to orbital motion even without any natal kick (Iben, Tutukov 1996). However, this mechanism can not provide enough number of high velocity NSs to explain the second peak of the distribution.

In connection with quark stars one can speculate, that additional energy due to deconfinement can lead to additional kick, so that among high velocity compact objects the fraction of quark stars can be higher. For example, if the

delayed deconfinement proposed by Berezhiani et al. (2003) is operating (see the contribution by Bombaci in this proceedings), then quark stars can obtain additional (second) kick. Note, that the two most studied NSs – Crab and Vela (which both show spin-velocity alignment, glitches and other particular properties) – belong to the low velocity population. Also most of compact objects in binaries in the scenario with delayed deconfinement should belong to the low velocity normal NSs since otherwise there is a high probability of system disruption.

3.3 Young close-by NSs and the Gould Belt

The Gould Belt is a structure consisting of clusters of massive stars. The Sun is situated not far from the center of that disc-like structure. The Gould Belt radius is about 300 pc. It is inclined at 18° with respect to the galactic plane.

Due to the presence of the Belt the rate of SN around us (say in few hundred parsecs) during the last several tens of million years is higher, than it is in an average place at a solar distance from the galactic center. Because of that there should be a local overabundance of young NSs which can appear as hot cooling objects, as gamma-ray sources etc.

Grenier (2003) estimated the number of possible unidentified EGRET sources originated from the Belt. Popov et al. (2003a) calculated Log N – Log S distribution of cooling NSs in the solar vicinity, which can be observed by ROSAT and other X-ray missions. Results are shown in the Fig. 6.

3.4 Period evolution of INSs and accretion from the ISM

In early 70s it was suggested that INSs can be observed due to accretion of the ISM and that significant part of INSs is at that stage. Actually, for such a prediction it is necessary to make some assumptions about the magnetorotational evolution of NSs. In particular, a combination of spin period, magnetic field, spatial velocity and density of the medium needs to be such that accretion is possible and proceeds nearly at the Bondi rate. Recent data shows that these assumptions were incorrect. ROSAT observations resulted in just a few radioquiet INSs non of which is considered to be a good candidate to be an accreting INSs. There are many reasons for that (see Popov et al. 2003b for discussion).

Recent studies show that it is very difficult for an INS to reach the stage of accretion. There are three main reasons for that:

1 High spatial velocity.

2 Magnetic field decay.

3 Long subsonic propeller stage.

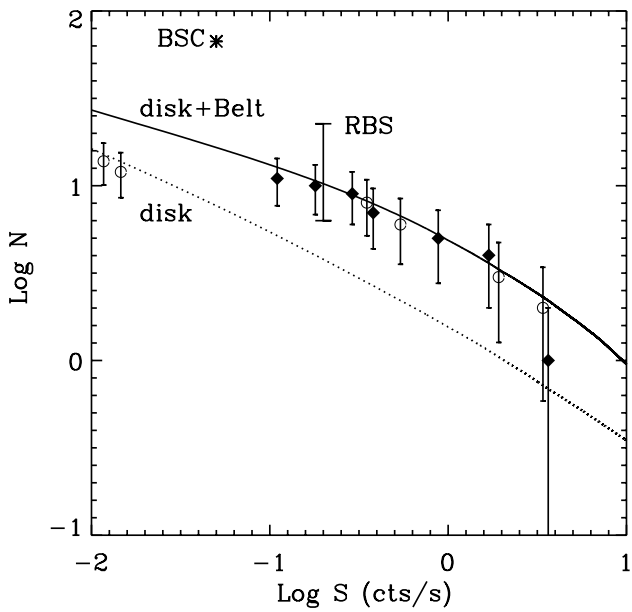

Figure 6. Log N – Log S distribution for close-by cooling INSs. Black symbols are plotted if the dimmest source at specified flux is one of the "Magnificent seven". Otherwise we plot an opaque symbol (see the list of sources in Table 1). Two lines represent results of calculation. Dotted line – only stars from the galactic disc contribute to the Log N – Log S distribution. Solid line – contribution of the Gould Belt is added. "RBS" and "BSC" are two observational limits, obtained from the ROSAT data (RBS: Schwope et al. 1999; BSC: Rutledge et al. 2003). From Popov et al. (2003a).

Subsonic propeller stage was introduced by Davies and Pringle (1981). Recently Ikhsanov (2003) re-investigated this issue in connection with INSs. His main conclusion is that in a realistic situation an INS spends a significant part of its life ($> 10^9$ yrs) in this stage during which only a small amount of matter can diffuse inwards and reach the star surface. If this situation is realized in nature, then many of low-velocity INSs may never become bright accretors. Long subsonic propeller stage also leads to very long spin periods of INSs at the onset of accretion, much longer, than it was suggested for example in Prokhorov et al. (2002), who explored period evolution of INSs in some details.

Even if an INS starts to accrete, then its luminosity can be very low due to:

1 Heating.

2 Magnetospheric effects.

3 Low accretion rate due to turbulence etc.

Heating was discussed in detail by Blaes et al. (1995). During the last two years last two topics attracted much interest. Magnetospheric effects were studied in a series of papers by Romanova, Toropina et al. 2D MHD simulations have shown that accretion onto a rotating dipole is substantially different from that onto an unmagnetized star (Romanova et al. 2003; Toropina et al. 2003). Magnetic effects scale with the magnetic field strength. For lower fields their are less pronounced.

Recent investigations strongly support the idea that the Bondi rate is just an upper limit which is rarely realized in nature (see Popov et al. 2003b and references therein). 2D and 3D simulations of accretion flows show that convection and other effects can reduce the accretion rate by orders of magnitude. In particular Igumenshchev et al. (2002, 2003) explored the so-called convection dominated accretion flows (CDAF). Proga and Begelman (2003) studied accretion with low angular momentum. Both studies were done for black hole accretion and showed very low accretion efficiency. However, these results in principle can be applied to isolated NSs (see Perna et al. 2003).

According to all these studies there is not much hope to observe accreting INSs.

4. Conclusion. What do we – astrophysicists – want from QCD theorists?

Astronomy is in some sense a unique science: we have only emission from objects under investigation. Because of that there is a wide field for speculations. Having a lot of uncertain parameters to explain properties of observed compact objects we have troubles even without quark stars!

What do we want to have from theoretical physicists is an input for astrophysical models of compact objects to produce some output which can then be compared with observations. We want initial parameters of quark stars + evolutionary laws:

- Initial spin period, magnetic field, spatial velocity, mass, radius etc. (plus possible correlations between them).
- "Ejectorability" (the ability to produce relativistic wind, i.e. to produce a radio pulsar).
- Emission properties of the surface of bare strange stars.
- Cooling curves.
- Magnetic field decay.

We hope that this brief review will help to link advanced theoretical research in physics of extremely dense matter with observational properties of compact objects.

Acknowledgments

SP thanks the organizers for hospitality and financial support.

References

Alpar, A. (2003), "Accretion models for young neutron stars", in: "Pulsars, AXPs and SGRs observed with BeppoSAX and other observatories". Edited by G. Cusumano, E. Massaro, T. Mineo. p. 197; [astro-ph/0306179].

Arzoumanian, Z., Chernoff, D.F., Cordes, J.M. (2002), "The velocity distribution of isolated radio pulsars", ApJ 568, 289.

Becker, W., Trumper, J. (1997), "The X-ray luminosity of rotation-powered neutron stars", A&A 326, 682.

Berezhiani, Z., Bombaci, I., Drago, A., Frontera, F., Lavagno, A. (2003), "Gamma-ray bursts from delayed collapse of neutron stars to quark matter stars", ApJ 586, 1250.

Bignami, G.F., Caraveo, P.A., de Luca, A., Mereghetti, S. (2003), "The magnetic field of an isolated neutron star from X-ray cyclotron absorption lines", Nature 423, 725.

Blackman, E.G., Perna, R. (2003), "Pulsars with jets harbor dynamically important accretion disks", ApJ 601, L71.

Blaes, O., Blandford, R.D., Rajagopal, M. (1995), "Accreting isolated neutron stars. III. Preheating of infalling gas and cometary HII regions", ApJ 454, 370.

Braje, T.M., Romani, R.W. (2002), "RX J1856-3754: evidence for a stiff equation of state", ApJ 580, 1043.

Brinkmann, W. (1980), "Thermal radiation from highly magnetized neutron stars" A&A 82, 352.

Brisken, W.F. Fruchter, A.S. Goss, W.M., Herrnstein, R.S. Thorsett, S.E. (2003), "Proper-motion measurements with the VLA. II. Observations of twenty-eight pulsars," astro-ph/0309215.

Burgay, M. et al. (2003), "An increased estimate of the merger rate of double neutron stars from observations of a highly relativistic system", Nature 426:531-533.

Burrows, A., Ott, C.D., Meakin, C. (2003), "Topics in core-collapse supernova theory", astro-ph/0309684.

Burwitz, V. et al. (2003), "The thermal radiation of the isolated neutron star RX J1856.5-3754 observed with Chandra and XMM-Newton", A&A 399, 1109.

Camilo, F. et al. (2002). "Discovery of radio pulsations from the X-ray pulsar J0205+6449 in supernova remnant 3C58 with the Green Bank Telescope" ApJ 571, L71.

Colpi, M., Wasserman, I. (2002), "Formation of an evanescent proto-neutron star binary and the origin of pulsar kicks", ApJ 581, 1271.

Cordes, J.M., Lazio, T.J.W. (2002), "NE2001.I. A new model for the galactic distribution of free electrons and its fluctuations", astro-ph/0207156.

Cottam, J., Paerels, F., Mendez, M. (2002), "Gravitationally redshifted absorption lines in the X-ray burst spectra of a neutron star", Nature 420, 51.

Davies, R.E., Pringle, J.E. (1981), "Spindown of neutron stars in close binary systems - II", MNRAS 196, 209.

Drake, J.J. et al. (2002), "Is RX J1856.5-3754 a quark star ?", ApJ 572, 996.

Francischelli, G.J., Wijers, R.A.M.J. (2002), "On fossil disk models of anomalous X-ray pulsars", astro-ph/0205212.

Fryer, C. L. Warren, M.S. (2003), "3-Dimensional core-collapse", ApJ 601, 391.

Gavriil, F.P., Kaspi, V.M., Woods, P.M. (2002), "Magnetar-like X-ray bursts from an anomalous X-ray pulsar", Nature 419, 142.

Gavriil, F.P., Kaspi, V.M., Woods, P.M. (2003), "Anomalous X-ray pulsars: long-term monitoring and soft-gamma repeater like X-ray bursts", in :"Pulsars, AXPs and SGRs observed with

BeppoSAX and Other Observatories". Edited by G. Cusumano, E. Massaro, T. Mineo. p. 173; [astro-ph/0301092].

Grenier, I.A. (2003), "Unidentified EGRET sources in the Galaxy", astro-ph/0303498.

Haberl, F., Schwope, A.D., Hambaryan, V., Hasinger, G., Motch, C. (2003), "A broad absorption feature in the X-ray spectrum of the isolated neutron star RBS1223 (1RXS J130848.6+212708)", A&A 403, L19.

Haberl F., Zavlin V. (2002), "XMM-Newton observations of the isolated neutron star RX J0806.4-4123 ", A&A 391, 571.

Halpern, J.P., Gotthelf, E.V., Mirabal, N., Camilo, F. (2002), "The next Geminga: deep multi-wavelength observations of a neutron star identified with 3EG J1835+5918", ApJ 573, L41.

Hambaryan, V., Hasinger, G., Schwope, A. D., Schulz, N. S. (2001), "Discovery of 5.16 s pulsations from the isolated neutron star RBS 1223", A&A 381, 98.

Ho, W.C.G., Lai, D. (2001), "Atmospheres and spectra of strongly magnetized neutron stars", MNRAS 327, 1081.

Ho, W.C.G., Lai, D. (2003), "Transfer of polarized radiation in strongly magnetized plasmas and thermal emission from magnetars: effect of vacuum polarization", MNRAS 338, 233.

Hobbs, G. Manchester, R. Teoh, A. Hobbs, M. (2003), "The ATNF Pulsar Catalogue", in: Proc. of IAU Symp. 218: "Young neutron stars and their environment"; [astro-ph/0309219].

Huang, Y. F., Dai, Z.G., Lu, T., Cheng, K.S., Wu, X.F. (2003), "Gamma-ray bursts from neutron star kicks", ApJ 549, 919.

Hulleman, F., Tennant, A.F., van Kerkwijk, M.H., Kulkarni, S.R., Kouveliotou, C., Patel, S.K. (2001), "A possible faint near-infrared counterpart to the AXP 1E 2259+58.6", ApJ 563, L49.

Iben, I., Tutukov, A.V. (1996), "On the origin of the high space velocities of radio pulsars", ApJ 456, 738.

Ibrahim, A.I., Safi-Harb, S., Swank, J.H., Parke, W., Zane, S., Turolla, R. (2002), "Discovery of cyclotron resonance features in the soft gamma repeater SGR 1806-20," ApJ 574, L51.

Ibrahim, A.I., Swank, J.H., Parke, W. (2003), "New evidence of proton-cyclotron resonance in a magnetar strength field from SGR 1806-20", ApJ 584, L17.

Igumenshchev, I.V., Narayan, R. (2002), "Three-dimensional magnetohydrodynamic simulations of spherical accretion", ApJ 566, 137.

Igumenshchev, I.V., Narayan, R., Abramowicz, M.A. (2003), "Three-dimensional magnetohydrodynamic simulations of radiatively inefficient accretion flows", ApJ 592, 1042.

Ikhsanov, N.R. (2003), "On the accretion luminosity of isolated neutron stars", A&A 399, 1147.

Israel, G.L. et al. (2002), "The detection of variability from the candidate IR counterpart to the anomalous X-ray pulsar 1E1048.1-5937", ApJ 580, L143.

Israel, G.L. et al. (2003), "The IR counterpart to the anomalous X-ray pulsar 1RXS J170849-400910", ApJ 589, L93.

Kaminker A.D., Yakovlev, D.G., Gnedin, O.Y. (2002), "Three types of cooling superfluid neutron stars: theory and observations", A&A 383, 1076.

Kaplan, D.L., van Kerkwijk, M.H., Anderson, J. (2002), "The parallax and proper motion of RX J1856.5-3754 revisited", ApJ, 571, 447.

Kaplan, D.L., Kulkarni, S.R., van Kerkwijk, M.H. (2003), "The optical counterpart of the isolated neutron star RX J1605.3+3249", ApJ 588, L33.

Kaspi, V.M., Gavriil, F.P. (2002), "1E 2259+586", IAUC 7924.

Kouveliotou, C. et al. (1998), "An X-ray pulsar with a superstrong magnetic field in the soft gamma-ray repeater SGR 1806-20", Nature 393, 235.

Kouveliotou, C. et al. (1999), "Discovery of a magnetar associated with the soft gamma repeater SGR 1900+14", ApJ 510, L115.

Kramer, M. et al. (2003), "The Parkes multibeam pulsar survey - III. Young pulsars and the discovery and timing of 200 pulsars", MNRAS 342, 1299.

Lai, D. (2001), "Matter in strong magnetic fields", Rev. Mod. Phys. 73, 629.
Lai, D., Salpeter, E.E. (1997), "Hydrogen phases on the surface of a strongly magnetized neutron star", ApJ 491, 270.
Lai, D., Chernoff, D.F. Cordes, J.M. (2001), "Pulsar jets: implications for neutron star kicks and initial spins", ApJ 549, 1111.
Lai, D., Ho, W.C.G. (2002), "Resonant conversion of photon modes due to vacuum polarization in a magnetized plasma: implications for X-ray emission from magnetars", ApJ, 566, 373.
Lamb, D. Q. Donaghy, T.Q. Graziani, G. (2003), "A unified jet model of X-ray flashes and gamma-ray bursts", New Astron.Rev.48:459-464.
Lenzen, R., Trümper, J. (1978), "Reflection of X rays by neutron star surfaces", Nature 271, 216.
McLaughlin, M.A. et al. (2003), "PSR J1847–0130: a radio pulsar with magnetar spin characteristics", ApJ 591, L135.
Mereghetti, S., Bandiera, R., Bocchino, F., Israel, G.L. (2002), "BeppoSAX observations of the young pulsar in the Kes 75 supernova remnant", ApJ 574, 873.
Mirabal, N., Halpern, J.P. (2001), "A neutron star identification for the high-energy gamma-ray source 3EG J1835+5918 detected in the ROSAT All-Sky Survey", ApJ 547, L137.
Morris, D.J., Hobbs, G., Lyne, A.G. et al. (2002), "The Parkes multibeam pulsar survey — II. Discovery and timing of 120 pulsar ", MNRAS 335, 275.
Motch, C. Zavlin, V. Haberl, F. (2003), "The proper motion and energy distribution of the isolated neutron star RX J0720.4-3125", A&A 408, 323.
Muno, M.P. et al. (2003), "A deep Chandra catalog of X-ray point sources toward the galactic center", ApJ 589, 225.
Nice, D.J., Splaver, E.M. (2003), "Heavy neutron stars? A status report on Arecibo timing of four pulsar - white dwarf systems", astro-ph/0311296.
Ozel, F. (2001), "Surface emission properties of strongly magnetic neutron stars", ApJ 563, 276.
Pavlov, G.G. et al. (1994), "Model atmospheres and radiation of magnetic neutron stars: Anisotropic thermal emission", A&A 289, 837.
Pavlov, G.G., Zavlin, V.E., Sanwal, D., Trümper, J. (2002), "1E 1207.4-5209: the puzzling pulsar pulsar at the center of the PKS 1209-51/52 supernova remnant", ApJ 569, L95.
Pavlov, G. et al. (2001), "The X-ray spectrum of the Vela pulsar resolved with the Chandra X-ray observatory", ApJ 552, L129.
Pavlov, G. G., Teter, M. A., Kargaltsev, O., Sanwal, D. (2003), "The variable jet of the Vela pulsar", ApJ 591, 1157.
Perna, R., Narayan, R., Rybicki, G., Stella, L., Treves, A. (2003), "Bondi accretion and the problem of the missing isolated neutron stars", ApJ 594, 936.
Pfahl, Rappaport, S. (2001), "Bondi-Hoyle-Lyttleton accretion model for low-luminosity X-ray sources in globular clusters", ApJ 550, 172.
Pons, J.A. et al. (2001), "Toward a mass and radius determination of the nearby isolated neutron star RX J185635-3754", ApJ, 564, 981.
Popov, S.B., Turolla, R., Prokhorov, M.E., Colpi, M., Treves, A. (2003a), "Young close-by neutron stars: the Gould Belt vs. the galactic disc", astro-ph/0305599.
Popov, S.B., Treves, A., Turolla, R. (2003b). "Radioquiet isolated neutron stars: old and young, nearby and far away, dim and very dim", in: Proc. of the 4th AGILE workshop (in press), [astro-ph/0310416].
Proga, D., Begelman, M.C. (2003), "Accretion of low angular momentum material onto black holes: two-dimensional magnetohydrodynamic case", ApJ 592, 767.
Prokhorov, M.E., Popov, S.B., Khoperskov, A.V. (2002), "Period distribution of old accreting isolated neutron stars", A&A 381, 1000.
Quaintrell, H. et al. (2003), "The mass of the neutron star in Vela X-1 and tidally induced nonradial oscillations in GP Vel", A&A 401, 313.

Rajagopal, M., Romani, R.W., Miller, M.C. (1997), "Magnetized iron atmospheres for neutron stars", ApJ 479, 347.

Rea, N., et al. (2003), "Evidence of a cyclotron feature in the spectrum of the anomalous X-ray pulsar 1RXS J170849-400910", ApJ 586, L65.

Romani, R.W. (1987), "Model atmospheres for cooling neutron stars", ApJ 313, 71.

Romanova, M.M., Toropina, O.D., Toropin, Yu.M., Lovelace, R.V.E. (2003), "Magnetohydrodynamic simulations of accretion onto a star in the "propeller" regime", ApJ 588, 400.

Rutledge, R.E., Fox, D.W., Bogosavljevic, M., Mahabal, A. (2003), "A limit on the number of isolated neutron stars detected in the ROSAT Bright Source Catalogue", ApJ 598, 458.

Schwope, A.D., Hasinger, G., Schwarz, R., Haberl, F., Schmidt, M. (1999), "The isolated neutron star candidate RBS 1223 (1RXS J130848.6+212708)", A&A 341, L51.

Shibanov, Yu.A., Zavlin, V.E., Pavlov, G.G., Ventura, J. (1992), "Model atmospheres and radiation of magnetic neutron stars. I - The fully ionized case", A&A 266, 313.

Thompson, C., Lyutikov, M., Kulkarni, S.R. (2002), "Electrodynamics of magnetars: implications for the persistent X-ray emission and spindown of the soft gamma repeaters and anomalous X-ray pulsars", ApJ 574, 332.

Toropina, O.D., Romanova, M.M., Toropin, Yu.M., Lovelace, R.V.E. (2003), "Magnetic inhibition of accretion and observability of isolated old neutron stars", ApJ 593, 472.

Treves, A., Turolla, R., Zane, S., Colpi, M. (2000), "Isolated neutron stars: accretors and coolers", PASP 112, 297.

Tsuruta, S., Teter, M.A., Takatsuka, T., Tatsumi, T., Tamagaki, R. (2002), "Confronting neutron star cooling theories with new observations", ApJ 571, L143.

Turolla, R., Zane, S., Drake, J.J. (2004), "Bare quark stars or naked neutron stars ? The case of RX J185635-3754", Astrophys.J.603:265-282.

Walter, F.M., Lattimer, J.M. (2002), "A revised parallax and its implications for RX J185635-3754", ApJ 576, L145.

Wang, Z., Chakrabarty, D. (2002), "The likely near-infrared counterpart to the anomalous X-ray pulsar 1E 1048.1-5937", ApJ 579, L33.

Woosley, S.E., Heger, A., Weaver, T.A. (2002), "The evolution and explosion of massive stars", Rev. Mod. Phys, 74, 1015.

Xu, R.X. (2002), "A thermal featureless spectrum: evidence for bare strange stars ?", ApJ 570, L65.

Xu, R.X. (2003), "Solid quark stars ?", ApJ 596, 59.

Zampieri, L. et al. (2001), "1RXS J214303.7+065419/RBS 1774: a new isolated neutron star candidate", A&A 378, L5.

Zane, S. et al. (2001), "Proton cyclotron features in thermal spectra of ultramagnetized neutron stars", ApJ 560, 384.

Zane, S. et al. (2002), "Timing analysis of the isolated neutron star RX J0720.4-3125", MNRAS 334, 345.

Zavlin, V.E., Pavlov, G.G., Shibanov, Y.A., Ventura, J. (1995), "Thermal radiation from rotating neutron star: effect of the magnetic field and surface temperature distribution", A&A 297, 441.

Zavlin, V.E., Pavlov, G.G., Sanwal, D. (2003), "Variations in the spin period of the radio-quiet pulsar 1E 1207.4-5209", ApJ 606, 444.

II

SUPERDENSE QCD MATTER

CLUSTERS AND CONDENSATES IN THE NUCLEAR MATTER EQUATION OF STATE

Gerd Röpke [1], Alexander Grigo [1], Kohsuke Sumiyoshi [2], and Hong Shen [3]

[1] *Fachbereich Physik, Universität Rostock, Universitätsplatz 1, 18051 Rostock, Germany*

[2] *Numazu College of Technology (NCT), Ooka 3600, Numazu, Shizuoka 410-8501, Japan*

[3] *Department of Physics, Nankai University, Tianjin 300071, China*

Abstract The equation of state (EOS) of nuclear matter at finite temperature and density with various proton fractions is considered, in particular the region of medium excitation energy given by the temperature range $T \leq 30$ MeV and the baryon density range $\rho_B \leq 10^{14.2}$ g/cm^3. In this region, in addition to the mean-field effects the formation of few-body correlations, in particular light bound clusters up to the alpha-particle ($1 \leq A \leq 4$) has been taken into account. The calculation is based on the relativistic mean field theory with the parameter set TM1. We show results for different values for the asymmetry parameter, and β equilibrium is considered as a special case.

The medium modification of the light clusters is described by self-energy and Pauli blocking effects, using an effective nucleon-nucleon interaction potential. Furthermore, the formation of quantum condensates is considered, in particular Cooper pairing in different (isospin singlet and triplet) channels as well as alpha-like quartetting. It is shown that the formation of light clusters and quantum condensates is of relevance in calculating thermodynamic properties of nuclear matter at moderate densities and temperatures, e.g., in context with the calculation of compact astrophysical objects.

Keywords: nuclear matter equation of state, cluster formation, supernova simulations, medium effects, relativistic mean field, condensates, pairing, quartetting

1. Introduction

The equation of state (EOS), the composition and the possible occurrence of phase transitions in nuclear matter are widely discussed topics not only in nuclear theory, but are also of great interest in astrophysics and cosmology. Experiments on heavy ion collisions, performed over the last decades, gave new insight into the behavior of nuclear systems in a broad range of densities and temperatures. The observed cluster abundances, their spectral distribution

D. Blaschke and D. Sedrakian (eds.), Superdense QCD Matter and Compact Stars, 75–91.

and correlations in momentum space can deliver informations about the state of dense, highly excited matter. A particular interesting topic is the possible existence of a new state, the quark-gluon phase. Matter under such extreme conditions occurs in compact objects such as neutron stars and in supernova explosions. Furthermore, the EOS of hot and dense matter is needed for cosmological models like the hot big bang as an essential input. References can be found in a recent monograph on the nuclear EOS [1].

We will restrict ourselves to matter in equilibrium at temperatures $T \leq 30$ MeV and baryon number densities $n_B \leq 0.2$ fm^{-3}, where the quark substructure and the excitation of internal degrees of freedom of the nucleons (protons p and neutrons n) are not of relevance and the nucleon-nucleon interaction can be represented by an effective interaction potential. In this region of the temperature-density plane, we will investigate how the quasi-particle picture will be improved if few-body correlations are taken into account, in particular the formation of deuteron (d), triton (t), ^{3}He (h) and ^{4}He (α) clusters. The influence of cluster formation on the EOS is calculated for different situations, and the occurrence of phase instabilities are investigated. Instead of the full spectral function, the concept of composition will be introduced as an approximation to describe correlations in dense systems. Another interesting point is the formation of quantum condensates. Some results for pairing and quartetting are given below.

A quantum statistical approach to the thermodynamic properties of nuclear matter can be given using the method of thermodynamic Green functions [2]. In general, within the grand canonical ensemble, the EOS $n(T, \mu)$ relating the particle number density n to the chemical potential μ is obtained from the single-particle spectral function, which can be expressed in terms of the self-energy. Then, thermodynamic potentials such as the pressure $p(T, \mu) = \int_{-\infty}^{\mu} n(T, \mu')d\mu'$ or the density of free energy $f(T, n) = \int_0^n \mu(T, n')dn'$ are obtained by integrations.

The main quantity to be evaluated is the self-energy. Different approximations can be obtained by partial summations within a diagram representation. The formation of bound states is taken into account considering ladder approximations [3], leading in the low-density limit to the solution of the Schrödinger equation. The effects of the medium can be included in a self-consistent way within the cluster-mean field approximation (see [4] for references), where the influence of the correlated medium on the single particle states as well as on the clusters is considered in first order with respect to the interaction. As a point of significance, the single particle and the bound states are considered on equal footing. Besides single-particle self-energy shifts of the constituents, the bound state energies are also modified by the Pauli blocking due to the correlated medium. An extended discussion of the two-particle problem can be

found in [5]. We will consider also the medium modification of the three and four-particle bound states, see [6].

If a singularity in the medium modified few-body T matrix is obtained, it may be taken to indicate the formation of a quantum condensates. Different kinds of quantum condensates are also considered [7, 8]. They become obvious if the binding energy of nuclei is investigated [9]. Correlated condensates are found to give a reasonable description of near-threshold states of $n\alpha$ nuclei [10]. The contribution of condensation energy to the nuclear matter EOS would be of importance and has to be taken into account not only in mean-field approximation but also considering correlated condensates.

The relativistic EOS of nuclear matter for supernova explosions was investigated recently [11]. To include bound states such as α-particles, medium modifications of the few-body states have to be taken into account. Simple concepts used there such as the excluded volume should be replaced by more rigorous treatments based on a systematic many-particle approach. We will report on results including two-particle correlations into the nuclear matter EOS. New results are presented calculating the effects of three and four-particle correlations.

In [11] the alpha-particles were included into the EOS, and detailed comparisons of the outcome with respect to the alpha-particle contribution has been made. We will elaborate this item further, first by using a systematic quantum statistical treatment instead of the simplifying concept of excluded volume, second by including also other (two- and three-particle) correlations.

2. Ideal Mixture of Different Components

In the simplest approximation we consider an ideal quantum gas of elementary particles such as protons, neutrons, electrons and possibly neutrinos (the quark-gluon substructure will not be considered at densities and temperatures considered). The EOS is found in textbooks and will not be discussed any further here.

Inclusion of strong, weak, electromagnetic and gravitational interaction leads to changes in the relevant degrees of freedom and to modification of the EOS, possibly connected with phase transitions. This way, we first discuss the formation of correlations between the nucleons at given proton fraction. In a next step, β equilibrium is considered, so that only the baryon density as a conserved quantity is prescribed. Electrical charge neutrality then fixes also the electron concentration, but will not be discussed here in detail, as well as equilibrium in the gravitational field.

In the low-density limit, the most important effect of interaction with respect to the nuclear matter EOS is the formation of bound states characterized by the proton content Z_i and the neutron content N_i. We will restrict us to only the

Table 1. Properties of light clusters.

	binding energy	mass	spin	rms–radius
n	0	$939.565\,\mathrm{MeV/c^2}$	1/2	0.34 fm
p	0	$938.783\,\mathrm{MeV/c^2}$	1/2	0.87 fm
d	$-2.225\,\mathrm{MeV}$	$1876.12\,\mathrm{MeV/c^2}$	1	2.17 fm
t	$-8.482\,\mathrm{MeV}$	$2809.43\,\mathrm{MeV/c^2}$	1/2	1.70 fm
h	$-7.718\,\mathrm{MeV}$	$2809.41\,\mathrm{MeV/c^2}$	1/2	1.87 fm
α	$-28.3\,\mathrm{MeV}$	$3728.40\,\mathrm{MeV/c^2}$	0	1.63 fm

light clusters with $A \leq 4$ since the α particle is strongly bound, and the large strongly bound clusters such as iron can be described using other concepts such as the formation of another (liquid) phase in the matter, see, e.g., [11]. The occurrence of large nuclei is of importance in considering the outer crust of neutron stars.

In thermal equilibrium, within a quantum statistical approach a mass action law can be derived, see [12]. The densities of the different components are determined by the chemical potentials μ_p and μ_n and temperature T. The densities of the free protons and neutrons as well as of the bound states follow in the non-relativistic case as

$$n_i = \frac{2\sigma_i+1}{2\,\pi^2}\int_0^\infty dk\,k^2 \times \frac{1}{\exp\left[\left(E_i(k;T,\mu_p,\mu_n) - Z_i\mu_p - N_i\mu_n\right)/T\right] - (-1)^{Z_i+N_i}}\,, \quad (1)$$

where for deuterons $\sigma_d = 1$, for tritons $\sigma_t = 1/2$, for helions $\sigma_h = 1/2$, and for α particles $\sigma_\alpha = 0$. In the low-density limit where the medium effects can be neglected, the energies $E_i(k;T,\mu_p,\mu_n) = m_i + k^2/(2m_i)$ can be used, where $m_i = Z_i m_p + N_i m_n + E_i^b$ and the binding energies E_i^b are given in Tab. 1.

We define the abundances of the different constituents as $X_n = n_n/n_B$, $X_p = n_p/n_B$, $X_d = 2\,n_d/n_B$, $X_t = 3\,n_t/n_B$, $X_h = 3\,n_h/n_B$ and $X_\alpha = 4\,n_\alpha/n_B$, where $n_B = n_n + n_p + 2\,n_d + 3\,n_t + 3\,n_h + 4\,n_\alpha$ is the total baryon density. Furthermore we introduce the total proton fraction as $Y_p^{\rm tot} = (n_p + n_d + n_t + 2\,n_h + 2\,n_\alpha)/n_B$.

Results for the composition of nuclear matter at temperature T = 10 MeV with proton fraction $Y_p^{\rm tot} = 0.2$ are shown in Fig. 1, for symmetric matter $Y_p^{\rm tot} = 0.5$ in Fig. 2. The model of an ideal mixture of free nucleons and clusters applies to the low density limit. At higher baryon density, medium effects are relevant to calculate the composition shown in Figs. 1, 2, which are described in the following sections.

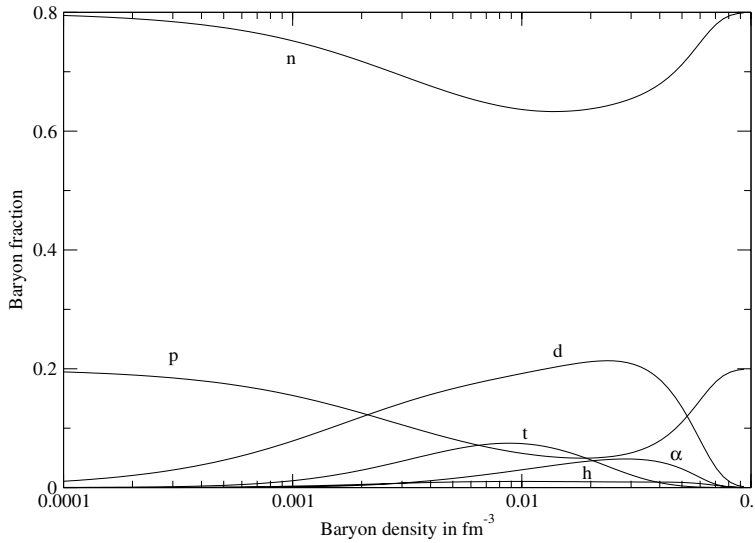

Figure 1. Composition of nuclear matter with proton fraction 0.2 as function of the baryon density, T = 10 MeV.

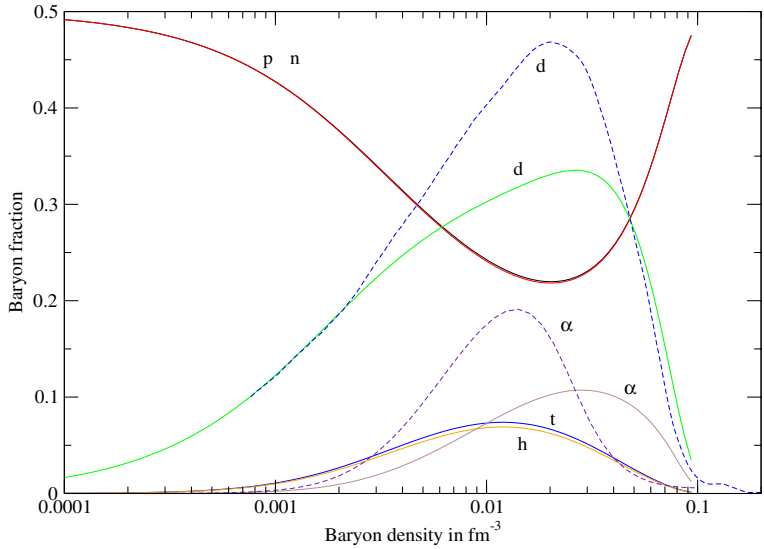

Figure 2. Composition of nuclear matter with proton fraction 0.5 as function of the baryon density, T = 10 MeV.

Up to densities of about $0.001\,\mathrm{fm}^{-3}$ density effects can be neglected. This way we describe an ideal mixture in chemical equilibrium. The composition as well as the thermodynamical functions can be calculated immediately

by solving the equations given above. Also the β-equilibrium can be calculated describing the chemical equilibrium with respect to the weak decay $n \rightleftharpoons p+e+\bar{\nu}_e$, where one usually neglects the chemical potential of the neutrinos. For the electron chemical potential the relativistic ideal fermion gas model is used. The corresponding results for the proton fraction as well as the thermodynamical functions are well known from the literature and are presently used to describe nuclear matter in β–equilibrium to calculate the structure of neutron stars. We have an additional relation between the chemical potentials of the proton, neutron and electron as well as the charge neutrality condition so that $n_e = Y_p^{\rm tot}\, n_B$. Notice that for the present purpose we only use empirical values without specifying the underlying nucleon-nucleon interaction.

3. Relativistic mean field theory

A description of nuclear matter as an ideal mixture of protons and neutrons, possibly in β equilibrium with electrons and neutrinos, is not sufficient to give a realistic description of dense matter. The account of the interaction between the nucleons can be performed in different ways. For instance we have effective nucleon-nucleon interactions, which reproduce empirical two-nucleon data, e.g. the PARIS and the BONN potential. On the other hand we have effective interactions like the Skyrme interaction, which are able to reproduce nuclear data within the mean-field approximation. The most advanced description is given by the Walecka model, which is based on a relativistic Lagrangian and models the nucleon-nucleon interactions by coupling to effective meson fields. Within the relativistic mean-field approximation, quasi-particles are introduced, which can be parameterized by a self-energy shift and an effective mass.

We will use the so called TM1 model which is given by the following Lagrangian, describing coupling of the nucleon field to the non-linear sigma, omega and rho meson fields (index $i = p, n$ denotes protons or neutrons),

$$\begin{aligned}
\mathcal{L} \;=\; & \bar{\psi}_i[i\gamma_\mu\partial^\mu - m_i - g_\sigma\sigma - g_\omega\gamma_\mu\omega^\mu - g_\rho\gamma_\mu\tau_a\rho_a^\mu]\psi_i \\
& + \frac{1}{2}\partial_\mu\sigma\partial^\mu\sigma - \frac{1}{2}m_\sigma^2\sigma^2 - \frac{1}{3}g_2\sigma^3 - \frac{1}{4}g_3\sigma^4 \\
& - \frac{1}{4}W_{\mu\nu}W^{\mu\nu} + \frac{1}{2}m_\omega^2\omega_\mu\omega^\mu + \frac{1}{4}c_3(\omega_\mu\omega^\mu)^2 \\
& - \frac{1}{4}R^a_{\mu\nu}R^{a\mu\nu} + \frac{1}{2}m_\rho^2\rho^a_\mu\rho_a^\mu \;. \qquad (2)
\end{aligned}$$

The TM1 parameterization was given in [11]

For further details with respect to notation and the derivation of the corresponding Euler-Lagrange equations we refer to [11]. By replacing the meson fields by their expectation values one obtains an effective Dirac equation for

Table 2. TM1 parameter values.

Parameter	**Numerical value**	
m_p	938.783	MeV
m_n	939565	MeV
m_σ	511.19777	MeV
m_ω	783.0	MeV
m_ρ	770.0	MeV
g_σ	10.02892	
g_ω	12.61394	
g_ρ	4.63219	
g_2	-7.23247	fm^{-1}
g_3	0.61833	
c_3	71.30747	

the nucleons, which gives

$$\begin{aligned} m_i^* &= m_i + g_\sigma\,\sigma_0\,, \\ E_p(k;T,\mu_p,\mu_n) &= \sqrt{k^2+m_p^{*\,2}} + g_\omega\,\omega_0 + g_\rho\,\rho_0\,, \\ E_n(k;T,\mu_p,\mu_n) &= \sqrt{k^2+m_n^{*\,2}} + g_\omega\,\omega_0 - g_\rho\,\rho_0 \end{aligned} \tag{3}$$

as the expressions for the effective nucleon mass and the corresponding proton and neutron energies, respectively.

For a temperature T and chemical potentials μ_i (relative to the nucleon masses) the nucleon occupation probability reads

$$f_i(k) = \frac{1}{1+\exp\left[\left(E_i(k;T,\mu_p,\mu_n)-\mu_i\right)/T\right]} \tag{4}$$

The antinucleon distribution functions follow by changing the sign of the effective chemical potential [11]. Since we are interested in the low density region the contribution of the antinucleons can be neglected. Then, in mean-field approximation the chemical potential is related to the nucleon number density according to

$$n_i = \frac{1}{\pi^2}\int_0^\infty dk\,k^2\,\frac{1}{\exp\left[\left(E_i(k;T,\mu_p,\mu_n)-\mu_i\right)/T\right]+1}\,. \tag{5}$$

The meson fields σ_0, ω_0 and ρ_0 are found by solving a set of equations self-consistently as shown in [11]. Also expressions for the energy density, pressure and the entropy density can be found there. The empirical values of the binding energy of nuclear matter and nuclear matter density are reproduced using the above mentioned parameterization. The nuclear matter EOS can be found expressing the chemical potentials as functions of temperature, baryon density

and asymmetry. Within this relativistic mean-field approach the chemical potential as a function of density, temperature and the asymmetry parameter can be calculated. In particular, for symmetric matter an instability region is obtained below a critical temperature T_c where a Maxwell construction has to be applied.

4. Medium modifications of two-particle correlations

Expressions for the medium modifications of the cluster distribution functions can be derived in a quantum statistical approach to the few-body states, starting from a Hamiltonian describing the nucleon-nucleon interaction by the potential $V(12,1'2')$ (1 denoting momentum, spin and isospin). We first discuss the two-particle correlations which have been considered extensively in the literature [5, 7]. Results for different quantities such as the spectral function, the deuteron binding energy and wave function as well as the two-nucleon scattering phase shifts in the isospin singlet and triplet channel have been evaluated for different temperatures and densities. The composition as well as the phase instability was calculated.

The account of two-particle correlations in nuclear matter can be performed considering the two-particle Green function in ladder approximation. The solution of the corresponding Bethe–Salpeter equation taking into account mean-field and Pauli blocking terms is equivalent to the solution of the wave equation

$$\begin{aligned}&\left[E^{\rm MF}(1)+E^{\rm MF}(2)-E_{nP}\right]\psi_{nP}(12)\\&+\left[1-f_1(1)-f_1(2)\right]\sum_{1'2'}V(12,1'2')\,\psi_{nP}(1'2')=0\ ,\end{aligned}\qquad(6)$$

$E^{\rm MF}(1)=p_1^2/2m+\sum_2 V(12,12)_{\rm ex}f_1(2)$ are the Hartree-Fock single-particle energies, $f_1(1)=\{\exp[E^{\rm MF}(1)/T-\mu_1/T]+1\}^{-1}$. From the solution of this in-medium two-particle Schrödinger equation or the corresponding T matrix the scattering and possibly bound states are obtained. Due to the self-energy shifts and the Pauli blocking, the binding energy of deuteron $E_d(P,T,\mu_p,\mu_n)$ as well as the scattering phase shifts $\delta_{\tau_2}(E,P,T,\mu_p,\mu_n)$ in the isospin singlet or triplet channel τ_2, respectively, will depend on the temperature and the chemical potentials. For a separable interaction $V(12,1'2')$ like the PEST4 potential [13], an analytical solution of Eq. (5) can be found in the low-density limit, and the results for the shift of the binding energy and the medium modification of the scattering phase shifts are discussed extensively, see [5, 7]. We will discuss the medium shift of the binding energy in perturbation theory.

An important phenomenon is the Mott effect. At given temperature T and total momentum P, the binding energy of the deuteron bound state vanishes at the density $n_d^{\rm Mott}(P,T)$ due to the Pauli blocking. As a consequence, the

virial expansion of the EOS (generalized Beth-Uhlenbeck formula)

$$n_B(T,\mu_p,\mu_n) = n_1(T,\mu_p,\mu_n) + n_2(T,\mu_p,\mu_n) \tag{7}$$

constitutes of the single-particle contributions $n_1 = n_p^f + n_n^f$, where $n_\tau^f(T,\mu_\tau) = 2/(2\pi\hbar)^3 \int d^3p f_\tau(E_\tau(p))$ describes the free quasiparticle contributions of protons ($\tau = p$) or neutrons ($\tau = n$), respectively, and the two-particle contributions $n_2 = n_2^{\rm bound} + n_2^{\rm scat}$ containing the contribution of deuterons (spin factor 3)

$$n_2^{\rm bound}(T,\mu_p,\mu_n) = 3\int_{P>P_{\rm Mott}} \frac{d^3P}{(2\pi\hbar)^3}\; f_d(E_d) \tag{8}$$

with $f_d(E_d) = [e^{E_d(P,T,\mu_p,\mu_n)/T - \mu_p/T - \mu_n/T} - 1]^{-1}$, and scattering states of the isospin singlet and triplet channel τ_2 (degeneration factor γ_{τ_2})

$$\begin{aligned} n_2^{\rm scat}(T,\mu_p,\mu_n) \;&=\; \sum_{\tau_2}\gamma_{\tau_2}\int\frac{d^3P}{(2\pi\hbar)^3}\int_0^\infty\frac{dE}{2\pi} \\ &\quad f_{\tau_2}(\Delta E_d^{\rm SE}(P)+E)\sin^2\delta_{\tau_2}\frac{d}{dE}\delta_{\tau_2}\;, \end{aligned} \tag{9}$$

$\Delta E_d^{\rm SE}(P)$ is the shift of the continuum edge (self-energies at momentum $P/2$).

The EOS (7) shows some interesting features: (i) In the low-density limit, a mass action law is obtained describing an ideal mixture of free nucleons and deuterons. We stress that a quasi-particle picture is not able to reproduce this important limiting case correctly. (ii) With increasing density, the single-particle properties as well as the two-particle properties are simultaneously modified by the medium. In particular, the bound states are dissolved at high densities. (iii) There is also a contribution from scattering states to the two-particle density. As a consequence of the Levinson theorem, the contribution of the disappearing bound states is replaced by a contribution from the scattering states (resonances) at the Mott density so that the total two-particle density n_2 behaves smoothly. (iv) Due to the pole of the Bose distribution function at low temperatures, pairing can occur in n_2. A smooth transition from Bose-Einstein condensation of deuterons at low densities to Cooper pairing at high densities is observed [7].

Calculations of the composition (n_2/n_B) of symmetric nuclear matter ($n_p = n_n$, no Coulomb interaction) are shown in Fig. 3 [7]. At low densities, the contribution of bound states becomes dominant at low temperatures. At fixed temperature, the contribution of the correlated density n_2 is first increasing with increasing density according to the mass action law, but above the Mott line it is sharply decreasing, so that near nuclear matter density ($n_B = n_{\rm tot}$ = 0.17 fm^{-3}) the contribution of the correlated density almost vanishes. Also, the critical temperature for the pairing transition is shown.

For a given temperature $T = 10\,\mathrm{MeV}$ the composition with respect to the two-particle correlation is shown as a function of the baryon density in Fig.2.

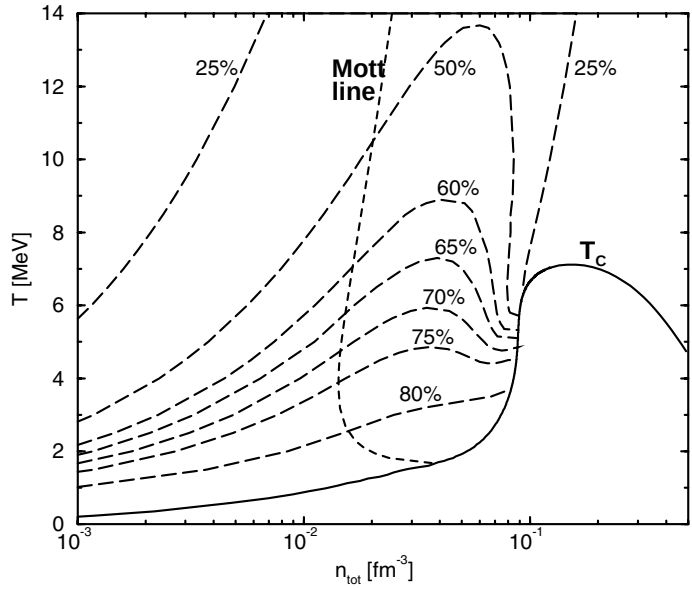

Figure 3. Fraction of correlated density for symmetric nuclear matter, T = 10 MeV. Only two-particle correlations are taken into account.

The values are taken from [7], where it is shown, that the correlated density contains the contribution of bound states as well the contribution of scattering states. Above the so called Mott density, where the bound states begin to disappear, according to the Levinson theorem, the continuous behavior of the correlated density is produced by the scattering states.

Form these considerations we see that at high densities the clusters are dissolved and should be described as weekly interacting quasi-particles. To give an optimal description of the quasi-particle energies, instead of using the Hartree-Fock approximation of the Yamaguchi model we will adopt the well established Walecka model. This way the self-energy effects are consistently described for the free and bound states. Since the Pauli blocking terms cannot be evaluated using the Walecka model, these expressions are computed using the Yamaguchi model. It should be stressed that in the density region where clusters are relevant both interaction models give self-energies and effective masses which are in reasonable agreement. So the mixing of these two interaction models is not contradictory.

This way we take the quasi-particle energies which are described by an effective mass and a self-energy shift and solve the Schrödinger equation for the separable Yamaguchi potential. Separating the center of mass motion, with energy $p^2/2\,M_d^*$ from the relative motion, with reduced mass $M_p^*\,M_n^*/(M_p^* +$

M_n^*) we find the binding energy $E_d^{\rm quasi}$, which is density depended due to the effective masses. The corresponding wave function is used to evaluate the Pauli blocking term

$$\Delta E_d^{\rm Pauli} = \sum_{1\,2\,1'\,2'} \psi(1\,2)\, V(1\,2, 1'\,2')\, [f(1) + f(2)]\, \psi^*(1'\,2') \qquad (10)$$

in first order perturbation theory. The self-energy shift $\Delta E_d^{\rm SE}$ is simply by the sum of the quasi-particle self-energy shift of the proton and neutron, obtained by the Walecka model.

Within our exploratory calculation we will use a simplified description of the contribution of correlated states, considering only the bound state with an effective shift, which reproduces the correlated density. This shift is taken as a quadratic function in the densities, where the linear term is calculated from perturbation theory and the quadratic term is fitted to reproduce the results for the composition as found by the full microscopic calculation including the contribution of scattering states.

To evaluate the linear term of the bound state energy shift within perturbation theory we need the bound state wave function. For this, we have to specify the interaction. We will adopt the following parameterization of the nucleon-nucleon interaction.

With the deuteron wave function, the contribution of the single-particle self-energy shift to the shift of the binding energies of clusters is evaluated using the quasiparticle shifts derived within the Walecka model. This ensures that the nucleons are described consistently also above the Mott density where the bound state merges in the continuum of scattering states. For the Pauli blocking term we evaluate the average over the interaction potential, multiplied with the distribution function.

Since we will perform only an exploratory calculation with respect to the density modification, instead of highly sophisticated parameterization of the interaction such as the PARIS and BONN potential we will use a simple, separable Yamaguchi interaction.

$$\begin{aligned} \langle k, K|V|k', K'\rangle &= V(k,k')\,\delta_{K,K'} && (11)\\ V(k,k') &= \sum_{i=s,t} \lambda_i\, w(k) w(k') && (12)\\ w(k) &= (k^2+\beta^2)^{-1} && (13) \end{aligned}$$

Parameter	Numerical	value
β	1.4488	fm^{-1}
λ_s	4263.05	$\mathrm{MeV\,fm}^{-1}$
λ_t	2550.03	$\mathrm{MeV\,fm}^{-1}$

Table 3. Parameter values for a simple rank 1 separable nucleon-nucleon interaction.

This set of parameters is chosen in order to reproduce the binding energy of the deuteron as well as of the alpha particle. The further properties, as the wave functions are assumed to be reasonable approximations in evaluating the density effects.

In the low-density limit, perturbation theory gives $E_d = E_d^0 + P^2/2M_d + \Delta E_d^{\rm SE} + \Delta E_d^{\rm Pauli}$ with E_d^0 = –2.22 MeV, and

$$\Delta E_d^{\rm Pauli} = \sum_{12,1'2'} \psi_{d,P}(12)[f_1(1) + f_1(2)]V(12,1'2')\psi_{d,P}(1'2') \approx \psi_{d,P}^2(0)(n_p + n_n)(E_d^0 - E_d^{\rm kin}) \ , \quad (14)$$

where $E_d^{\rm kin}$ denotes the mean kinetic energy for the unperturbed deuteron. To reproduce the behavior shown in Fig. 2, we adopt the following parameterization

$$\Delta E_d \approx 340 \ (n_p + n_n) \ \mathrm{MeV\ fm}^3 + 13000 \ (n_p^2 + n_n^2) \ \mathrm{MeV\ fm}^6 \ . \quad (15)$$

The result of this calculation is also seen in Fig. 2, to be compared with the evaluation of the correlated density shown in [5]. Two particle correlations are suppressed for densities higher then the Mott density of about 0.001 fm^{-3}, but will survive to densities of the order of nuclear matter density.

5. Medium modification of higher clusters

The modification of the three and four-particle system due to the medium can be considered in cluster-mean field approximation. Describing the medium in quasi-particle approximation, a medium-modified Faddeev equation can be derived which was already solved for the case of three-particle bound states in [9], as well as for the case of four-particle bound states in [10]. Similar to the two-particle case, due to the Pauli blocking the bound state disappears at a given temperature and total momentum at the corresponding Mott density.

For our exploratory calculation we use Guaussian type wave functions to find optimal bound states in the three and four particle case. Then we are able to calculate the perturbative expression for the shift of the bound states energy

and find

$$\begin{aligned}
\Delta E_t &= 600\ (n_p + 2n_n)\ \mathrm{MeV\ fm^3} + 3300\ (n_p^2 + 2n_n^2)\ \mathrm{MeV\ fm^6}\ , \\
\Delta E_h &= 600\ (2n_p + n_n)\ \mathrm{MeV\ fm^3} + 3300\ (2n_p^2 + n_n^2)\ \mathrm{MeV\ fm^6}\ , \\
\Delta E_\alpha &= 709\ (2n_p + 2n_n)\ \mathrm{MeV\ fm^3} + 6500\ (2n_p^2 + 2n_n^2)\ \mathrm{MeV\ fm^6} \quad (16)
\end{aligned}$$

Now we can calculate the composition replacing the binding energies by the density dependent ones. Results for the composition are shown in Figs.1, 2. It is shown that in particular α-clusters are formed in symmetric nuclear matter but they are destroyed at about nuclear matter density. In the case of asymmetric matter, triton becomes abundant.

We conclude that not only the α-particle but also the other light clusters contribute significantly to the composition. Furthermore they also contribute to the baryon chemical potential and this way the modification of the phase instability region with respect to the temperature, baryon density and asymmetry can be obtained. As an example, for symmetric matter the baryon chemical potential as a function of density for $T = 10\,\mathrm{MeV}$ is shown in Fig.3

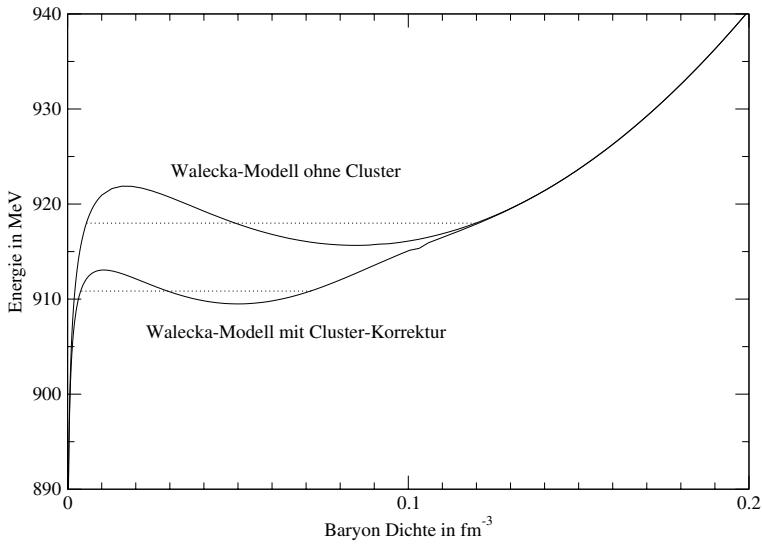

Figure 4. Baryon chemical potential as function of the baryon density for symmetric nuclear matter, T = 10 MeV. Without and including the formation of light clusters.

We see that the instability region is reduced if cluster formation is taken into account.

Within the approach, given here, also the β-equilibrium can be calculated and the influence of the cluster formation on the proton fraction can be considered. The formation of clusters will increase the proton fraction.

6. Comparison with the concept of excluded volume

In order to get the correct physical behavior, medium modifications for the clusters have to be taken into account at high densities. A simple approach is the concept of an excluded volume as used in [11]. Other effects such as the modification of quasi-particles forming a bound state are not considered. For details we refer to [11]. We have also shown in Fig.2 the result for the composition if only α-particle formation is taken into account, using the concept of the excluded volume. The abundance of the α-particle increases up to baryon densities of about a tenth of nuclear matter density and is rapidly decreasing with higher densities. In contrast, the quantum statistical approach shows a more weak decrease of the correlated density with the baryon density. In particular, two-particle correlations are present up to nuclear matter density. Discussing the difference in both approaches, we firstly note that the concept of a hard core which leads to the excluded volume overestimates the Pauli blocking, which makes the interaction potential more softer. Further, in addition to the medium modification due to the Pauli blocking the effect of the quasi-particle self-energy shift has to taken into account.

7. Isospin singlet (pn) and triplet (nn, pp) pairing in nuclear matter

One of the most amazing phenomena in quantum many-particle systems is the formation of quantum condensates. Of particular interest are strongly coupled fermion systems where bound states arise. In the low-density limit, where even-number fermionic bound states can be considered as bosons, Bose-Einstein condensation is expected to occur at low temperatures. The solution of Eq. (6) with $E_{2nP} = 2\mu$ gives the onset of pairing, the solution of Eq. (7) with $E_{4nP} = 4\mu$ the onset of quartetting in (symmetric) nuclear matter. At present, condensates are investigated in systems where the cross-over from Bardeen-Cooper-Schrieffer (BCS) pairing to Bose-Einstein condensation (BEC) can be observed, see [11,12]. In these papers, a two-particle state is treated in an uncorrelated medium. Some attempts have been made to include the interaction between correlated states, see [7,13].

Due to the strong interaction of protons and neutrons in the deuteron channel, isospin singlet pn pairing is favored in symmetric nuclear matter comparing with isospin triplet pp or nn pairing. Considering asymmetric matter, with increasing difference between the chemical potentials of protons and neutrons, isospin triplet pairing will become more favored. As can be shown from the evaluation of condensation energy, coexisting isospin singlet and isospin triplet condensates are not stable in symmetric matter. It is an open question how in the ground state of nuclear matter the transition from isospin singlet pairing to isospin triplet pairing occurs if the asymmetry parameter increases.

In a recent letter [14] it has been shown from the solution of Eqs. (6), (7) that in a certain region of density, pairing has to compete with quartetting. It has been found that in low-density symmetric nuclear matter the transition to triplet pairing, which is stronger than singlet pairing, will not occur because the quartetting transition occurs earlier. The transition temperature to quartetting has been estimated as a function of the chemical potential as well as of the density by using a variational calculation. Quartetting (α -like condensate) beats the transition to triplet pairing (deuteron-like condensate) if the density is smaller than $0.03\mathrm{fm}^{-3}$. A more detailed investigation of the quartetting solution near its break down at about $0.03\mathrm{fm}^{-3}$ is missing up to now.

The consequences of isospin singlet pairing and α -like quartetting on the binding energies of nuclei has been investigated within the local density approach [9]. The Wigner energy in $N = Z$ nuclei was identified with the formation of an isospin singlet condensate, and for nuclei with medium atomic number $A \approx 40$ this additional contribution of nuclear binding energy is decreasing with increasing asymmetry and vanishes at $N - Z \approx 4$. Exploratory calculations for the binding energy of nuclei with $Z = N$ show that the contribution due to quartetting is small but may become large for small A or for nuclear matter at low density.

8. Alpha cluster condensation in threshold states of self-conjugate $4n$ nuclei

A possible application for the formation of α-like condensates are self-conjugate $4n$ nuclei such as ^{8}Be, ^{12}C, ^{16}O, ^{20}Ne, ^{24}Mg, and others. Of course, results obtained for infinite nuclear matter cannot immediately be applied to finite nuclei. However, they are of relevance, e.g., in the local density approximation. We know from the pairing case that the wave function for finite systems can more or less reflect properties of quantum condensates.

It is a well known fact that in light nuclei many states are of the cluster type, see [16]. States close to the threshold energy of break up into constituent clusters are precisely of the cluster type. For example it was found that the calculated second 0^+ state in ^{12}C, which corresponds to the observed second 0^+ state located at 0.39 MeV above the 3α threshold energy, has a structure where individual α-clusters interact predominantly in relative S-waves. Thus it was concluded that the cluster state near $E_{n\alpha}^{\mathrm{thr}} = nE_\alpha$ with $n = 3$ and where E_α is the α-particle binding energy has an α-particle gas-like structure.

In [10] a new type of α-cluster wave function describing an α-particle Bose condensed state was introduced,

$$|\Phi_{n\alpha}\rangle = (C_\alpha^\dagger)^n|\mathrm{vac}\rangle \ , \tag{17}$$

where the α-particle creation operator is given by

$$C_\alpha^\dagger = \int d^3R\, e^{-\mathbf{R}^2/R_0^2} \int d^3r_1 \cdots d^3r_4 \times\varphi_{0s}(\mathbf{r}_1-\mathbf{R})a^\dagger_{\sigma_1\tau_1}(\mathbf{r}_1)\cdots\varphi_{0s}(\mathbf{r}_4-\mathbf{R})a^\dagger_{\sigma_4\tau_4}(\mathbf{r}_4) \quad (18)$$

with $\varphi_{0s}(\mathbf{r}) = (1/(\pi b^2))^{3/4}e^{-\mathbf{r}^2/(2b^2)}$ and $a^\dagger_{\sigma\tau}(\mathbf{r})$ being the creation operator of a nucleon with spin-isospin $\sigma\tau$ at the spatial point $\mathbf{r}$. The total $n\alpha$ wave function therefore can be written as

$$\langle \mathbf{r}_1\sigma_1\tau_1,\cdots \mathbf{r}_{4n}\sigma_{4n}\tau_{4n}|\Phi_{n\alpha}\rangle \propto \mathcal{A}\{e^{-\frac{2}{B^2}(\mathbf{X}_1^2+\cdots+\mathbf{X}_n^2)}\,\phi(\alpha_1)\cdots\phi(\alpha_n)\}, \quad (19)$$

where $B = (b^2+2R_0^2)^{1/2}$ and $\mathbf{X}_i = (1/4)\sum_n \mathbf{r}_{in}$ is the center-of-mass coordinate of the i-th α-cluster α_i. The internal wave function of the α-cluster α_i is $\phi(\alpha_i) \propto \exp[-(1/8b^2)\sum_{m>n}^4(\mathbf{r}_{im}-\mathbf{r}_{in})^2]$. The wave function of Eq.(19) is totally antisymmetrized by the operator $\mathcal{A}$. It is to be noted that the wave function of Eqs.(17),(19) expresses the state where $n\alpha$-clusters occupy the same $0s$ harmonic oscillator orbit $\exp[-\frac{2}{B^2}\mathbf{X}^2]$ with B an independent variational width parameter. For example if B is of the size of the whole nucleus whereas b remains more or less at the free α-particle value, then the wave function (19) describes a $n\alpha$ cluster condensed state in the macroscopic limit $n\to\infty$. Of course the total center-of-mass motion can and must be separated out of the wave function of Eq.(17) for finite systems. In the limit of $R_0 = 0$, i.e. $B = b$, the normalized wave function $|\Phi^{\rm N}_{n\alpha}\rangle = |\Phi_{n\alpha}\rangle\,/\sqrt{\langle\Phi_{n\alpha}|\Phi_{n\alpha}\rangle}$ is identical to a harmonic oscillator shell model wave function with the oscillator parameter b.

The energy surfaces in the two parameter space spanned by (R_0, b), are given by $E_{n\alpha}(R_0,b) = \langle\Phi^{\rm N}_{n\alpha}(R_0,b)|\hat{H}|\Phi^{\rm N}_{n\alpha}(R_0,b)\rangle$, and have been evaluated for n = 3 and 4 in Ref. [10].

9. Conclusions

In certain regions of the density-temperature plane, a significant fraction of nuclear matter is bound into clusters. The EOS and the region of phase instability are modified. In the case of β equilibrium, the proton fraction and the occurrence of inhomogeneous density distribution are influenced in an essential way. Important consequences are also expected for nonequilibrium processes.

The inclusion of both three and four-particle correlations in nuclear matter allows not only to describe the abundances of $t,\ h,\ \alpha$ but also their influence on the equation of state and phase transitions. In contrast to the mean-field treatment of the superfluid phase, also higher-order correlations will arise in the quantum condensate.

Acknowledgment

We acknowledge partial support by the DAAD-HOST programme under grant numbers D/02/46710 and D/03/31497.

References

[1] M. Baldo (Ed.), *Nuclear Methods and the Nuclear Equation of State* (World Scientific, Singapore, 1999).

[2] A. L. Fetter, J. D. Walecka, *Quantum Theory of Many-Particle systems* (McGraw-Hill, New York, 1971); A. A. Abrikosov, L. P. Gorkov, I. E. Dzyaloshinski, *Methods of Quantum field Theory in Statistical Mechanics* (Dover, New York, 1975).

[3] G. Röpke, L. Münchow, and H. Schulz, Nucl. Phys. **A379**, 536 (1982); and **A399**, 587 (1983).

[4] G. Röpke, in: *Aggregation Phenomena in Complex Systems*, edts. J. Schmelzer et al. (Wiley-VCH, Weinheim, New York, 1999), Chpts. 4, 12.

[5] M. Schmidt et al., *Ann. Phys.* **202**, 57 (1990).

[6] M. Beyer, W. Schadow, C. Kuhrts, and G. Röpke, *Phys. Rev.* C **60**, 034004 (1999); M. Beyer, S. A. Sofianos, C. Kuhrts, G. Röpke, and P. Schuck, Phys. Letters **B488**, 247 (2000).

[7] T. Alm et al., *Z. Phys.* A **351**, 295 (1995).

[8] G. Röpke, A. Schnell, P. Schuck, and P. Nozières, *Phys. Rev. Lett.* **80**, 3177 (1998).

[9] G. Röpke, A. Schnell, P. Schuck, and U. Lombardo, Phys. Rev. **C 61**, 024306 (2000).

[10] A. Tohsaki, H. Horiuchi, P. Schuck, G. Röpke, *Phys. Rev. Lett.* **87**, 192501 (2001).

[11] H. Shen, H. Toki, K. Oyamatsu, and K. Sumiyoshi, *Progr. Theor. Phys.* **100**, 1013 (1998).

[12] W. D. Kraeft, D. Kremp, W. Ebeling, and G. Röpke, *Quantum Statistics of Charged Particle Systems* (Plenum, New York, 1986).

[13] J. Haidenbauer and W. Plessas, *Phys. Rev.* C **30**, 1822 (1984); L. Mathelitsch, W. Plessas, and W. Schweiger, *Phys. Rev.* C **36**, 65 (1986).

[14] G. Röpke, *Phys. Lett.* B **185**, 281 (1987).

NUCLEAR EQUATION OF STATE AND THE STRUCTURE OF NEUTRON STARS

A.E.L. Dieperink
Kernfysisch Versneller Instituut, Zernikelaan 25, NL-9747AA Groningen, The Netherlands

D. Van Neck and Y. Dewulf
Laboratory of Theoretical Physics, Ghent University, Proeftuinstraat 86, B-9000 Gent, Belgium

V. Rodin
Institut für Theoretische Physik der Universität Tübingen, D-72076 Tübingen, Germany

Abstract The hadronic equation of state for a neutron star is discussed with a particular emphasis on the symmetry energy. The results of several microscopic approaches are compared and also a new calculation in terms of the self-consistent Green function method is presented. In addition possible constraints on the symmetry energy coming from empirical information on the neutron skin of finite nuclei are considered.

1. Introduction

In describing properties of neutron stars the equation of state (EoS) plays a crucial role as an input. During this workshop the effects of QCD degrees of freedom which become important at higher densities have been discussed in great detail. However, a quantitative understanding of the EoS also at lower densities is a prerequisite for the description of neutron stars properties. Conventional nuclear physics methods (i.e., in terms of hadronic degrees of freedom) are still being improved both conceptually as well as numerically, but all microscopic many-body approaches do require some sort of approximation scheme.

The aim of this contribution is to review the present understanding of the hadronic EoS, and the nuclear symmetry energy (SE) in particular. In the past the latter quantity has been computed mostly in terms of the Brueckner-Hartree-Fock (BHF) approach. In order to get an idea about the accuracy of the BHF result we present a recent calculation [1] in terms of the self-consistent

D. Blaschke and D. Sedrakian (eds.), Superdense QCD Matter and Compact Stars, 93–111.

Green function method, that can be considered as a generalization of the BHF approach. The results are compared with those from various many-body approaches, such as variational and relativistic mean field approaches. In view of the large spread in the theoretical predictions we also examine possible constraints on the nuclear SE that may be obtained from information from finite nuclei (such the neutron skin).

2. Equation of state and symmetry energy

The central quantity which determines neutron star properties is the EoS, at $T = 0$ specified by the energy density $\epsilon(\rho)$. For densities above, say, $\rho = 0.1$ fm^{-3} one assumes a charge neutral uniform matter consisting of protons, neutrons, electrons and muons; the conditions imposed are charge neutrality, $\rho_p = \rho_e + \rho_\mu$, and beta equilibrium, $\mu_n = \mu_p + \mu_e$ with $\mu_e = \mu_\mu$.
Given the energy density $\epsilon = \epsilon_N + \epsilon_e + \epsilon_\mu$ the total pressure, $P = P_N + P_e + P_\mu$, is obtained as $P = P(\epsilon/c^2) = \sum \rho_i \mu_i - \epsilon$, with the chemical potentials given by $\mu_i = \frac{\partial \epsilon}{\partial \rho_i}$.

To illustrate the present status of the situation in Fig. 1 a compilation made by the Stony Brook group [2] of the relation between the pressure and density for a wide variety of EoSs (but still a tiny fraction of all available calculations) is shown. This figure shows that there is an appreciable spreading in the calculations of the pressure. Qualitatively one can distinguish three different classes. First the EoSs that correspond to self-bound systems (such as "strange quark matter") have the property that the pressure does not vanish at zero density. Then there are two globally parallel bands. It appears that most conventional non-relativistic approaches fall in the lower (softer) band and the covariant results in the upper (more rigid) band. It is worth noting that even at densities around and below saturation, $\rho_0 \sim 0.17$ fm^{-3}, the predictions vary appreciably (about a factor 4). At higher densities some models show a sudden change in the slope of the pressure. This behavior can be ascribed to the onset of new degrees of freedom, e.g., the appearance of hyperons, kaons and/or quarks which lead to a softening.

It is well known that at lower densities the properties of the EoS are primarily determined by the SE [2]. The latter is defined in terms of a Taylor series expansion of the energy per particle for nuclear matter in terms of the asymmetry parameter $\alpha = (N - Z)/A$ (or equivalently the proton fraction $x = Z/A$),

$$E(\rho, \alpha) = texE(\rho, 0) + S_2(\rho)\alpha^2 + S_4(\rho)\alpha^4 + \ldots, \qquad (1)$$

where S_2 is the quadratic SE. It has been shown [3, 4] that the deviation from the parabolic law in Eq. (1), i.e., the term corresponding to S_4, is quite small.

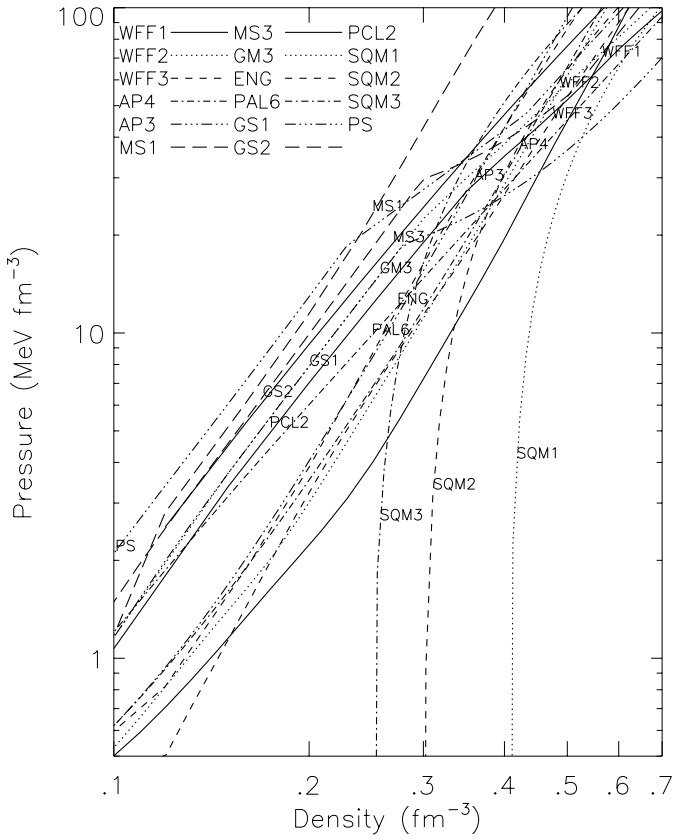

Figure 1. Pressure versus density for a variety of EoS; taken from [2] where explanation of symbols is given.

Near the saturation density ρ_0 the quadratic SE is expanded as

$$S_2(\rho) = \frac{1}{2}\frac{\partial^2 E(\rho,\alpha)}{\partial\alpha^2}|_{\alpha=0} = a_4 + \frac{p_0}{\rho_0^2}(\rho-\rho_0) + \frac{\Delta K}{18\rho_0^2}(\rho-\rho_0)^2 + \ldots. \quad (2)$$

The quantity a_4 corresponds to the SE at equilibrium density and the slope parameter p_0 governs the density dependence.

As a result the pressure can be written as

$$P(\rho,x) = \rho^2\frac{\partial E(\rho,x)}{\partial\rho} = \rho^2[E'(\rho,1/2) + S_2'(\rho)(1-2x)^2 + \ldots]. \quad (3)$$

By using beta equilibrium in a neutron star, $\mu_e = \mu_n - \mu_p = -\frac{\partial E(\rho,x)}{\partial x} \sim S_2(\rho)(1-2x)$, and the result for the electron chemical potential, $\mu_e =$

$3/4\hbar cx(3\pi^2\rho x)^{1/3}$, one finds the proton fraction at saturation density, to be quite small, $x_0 \sim 0.04$. Hence the pressure at saturation density can in good approximation be expressed in terms of (the density dependence of) the SE

$$P(\rho_0) = \rho_0(1-2x_0)(\rho_0 S_2'(\rho_0)(1-2x_0) + S_2(\rho_0)x_0) \sim \rho_0^2 S_2'(\rho_0). \quad (4)$$

3. How well do we know the symmetry energy?

In the following the present status of calculations of the SE is reviewed; first the ones in which a microscopic nucleon-nucleon (NN) interaction is used, followed by the phenomenological mean field approaches. In section 4 we discuss possible constraints that can be obtained from empirical information.

3.1 The SE in the BHF scheme

In the Brueckner-Hartree-Fock (BHF) approximation, the Brueckner-Bethe-Goldstone (BBG) hole-line expansion is truncated at the two-hole-line level [5]. The short-range NN repulsion is treated by a resummation of the particle-particle ladder diagrams into an effective interaction or G-matrix. Self-consistency is required at the level of the BHF single-particle spectrum $\epsilon^{BHF}(k)$,

$$\epsilon^{BHF}(k) = \frac{k^2}{2m} + \sum_{k'<k_F} \mathrm{Re} < kk'|G(\omega = \epsilon^{BHF}(k) + \epsilon^{BHF}(k'))|kk' > . \quad (5)$$

In the standard choice BHF the self-consistency requirement (5) is restricted to hole states ($k < k_F$, the Fermi momentum) only, while the free spectrum is kept for particle states $k > k_F$. The resulting gap in the s.p. spectrum at $k = k_F$ is avoided in the continuous-choice BHF (ccBHF), where Eq. (5) is used for both hole and particle states. The continuous choice for the s.p. spectrum is closer in spirit to many-body Green's function perturbation theory (see below). Moreover, recent results indicate [6, 7] that the contribution of higher-order terms in the hole-line expansion is considerably smaller if the continuous choice is used.

Although the BHF approach has several shortcomings it provides a numerically simple and convenient scheme to provide insight in some aspects of the symmetry energy.

Decomposition of SE. Some insight into the microscopic origin of the SE can be obtained by examining the separate contributions to the kinetic and potential energy [3].

The results of a ccBHF calculation [1] with the Reid93 interaction, including partial waves with $J < 4$ in the calculation of the G-matrix are presented in Fig. 2, where the SE is decomposed into various contributions shown as a function of the density ρ. The kinetic energy contribution, $S_{\rm kin}$, to the SE in

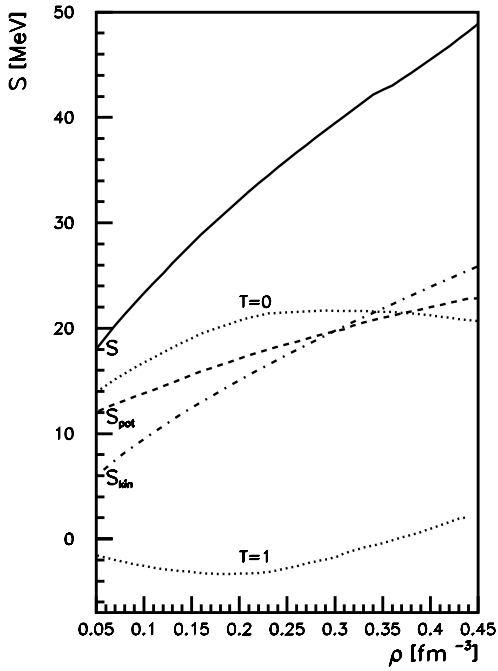

Figure 2 The SE S_2 (full line) and the contributions to S_2 from the kinetic (dash-dotted line) and potential energy (dashed line), calculated within a ccBHF scheme and using the Reid93 interaction. Also shown (dotted lines) are the $T = 0$ and $T = 1$ components of the potential energy contribution.

BHF is given by the free Fermi-gas expression (it differs from the standard one, which is based upon the derivative rather than the finite difference)

$$S_{\rm kin} = E_{\rm kin,PNM} - E_{\rm kin,SNM} = \frac{3}{10m}(3\pi^2)^{\frac{2}{3}}\rho^{\frac{2}{3}}\left(1 - 2^{-\frac{2}{3}}\right), \qquad (6)$$

and it determines to a large extent the density dependence of the SE. In Fig. 2 we also show the symmetry potential $S_{\rm pot} = S_2 - S_{\rm kin}$, which is much flatter, and the contributions to $S_{\rm pot}$ from both the isoscalar ($T = 0$) and isovector ($T = 1$) components of the interaction. Over the considered density range $S_{\rm pot}$ is dominated by the positive $T = 0$ part. The $T = 0$ partial waves, containing the tensor force in the ${}^3S_1$-${}^3D_1$ channel which gives a major contribution to the potential energy in SNM, do not contribute to the PNM energy. The $T = 0$ contribution peaks at $\rho \approx 0.3$ fm^{-3}. The decrease of this contribution at higher densities is compensated by the increase of the $T = 1$ potential energy, with as a net result a much weaker density-dependence of the total potential energy.

Dependence of the SE on NN interaction. Engvik et al. [8] have performed lowest-order BHF calculations in SNM and PNM for all "modern" potentials (CD-Bonn, Argonne v18, Reid93, Nijmegen I and II), which fit the Nijmegen NN scattering database with high accuracy. They concluded that

for small and normal densities the SE is largely independent of the interaction used, e.g. at ρ_0 the value of a_4 varies around an average value of a_4=29.8 MeV by about 1 MeV. At larger densities the spread becomes larger; however, the SE keeps increasing with density, in contrast to some of the older potentials like Argonne v14 and the original Reid interaction (Reid68) for which $S(\rho)$ tends to saturate at densities larger than $\rho = 0.4$ fm^{-3}.

3.2 Variational approach

Detailed studies for SNM and PNM using variational chain summation (VCS) techniques were performed by Wiringa et al. [9] for the Argonne Av14 NN interaction in combination with the Urbana UVIII three-nucleon interaction (3NI), and by Akmal et al. [10] for the modern Av18 NN potential in combination with the UIX-3NI.

It should be noted that the results of VCS and BHF calculations using the same NN interaction disagree in several aspects. For instance for SNM the VCS and BHF calculations saturate at different values of density [5]. As for the SE using only two-body interactions the VCS approach yields a smaller value for a_4 than BHF (see Table 1), and as a function of density in VCS the SE levels off at $\rho \sim 0.6$ fm^{-3}, whereas the BHF result continues to increase. Therefore it seems natural to ask whether the inclusion of more correlations by extending the BHF method (which is basically a mean field approximation) will lead to results closer to those of VCS.

3.3 Self-consistent Green function method

As noted above BHF has several deficiencies: it does not saturate at the empirical density, and it violates the Hugenholz-van Hove theorem.

In recent years several groups have considered the replacement of the BBG hole-line expansion with self-consistent Green's function (SCGF) theory [11–13]. In ref.[13, 14] the binding energy for SNM was calculated within the SCGF framework using the Reid93 potential. In ref.[1] we have extended these calculations to PNM and considered the corresponding SE.

The SCGF approach differs in two important ways from the BHF scheme. Firstly, within SCGF particles and holes are treated on an equal footing, whereas in BHF only intermediate particle ($k > k_F$) states are included in the ladder diagrams. This aspect ensures thermodynamic consistency, e.g. the Fermi energy or chemical potential of the nucleons equals the binding energy at saturation (i.e. it fulfills the Hugenholz-van Hove theorem). In the low-density limit BHF and SCGF coincide. As the density increases the phase space for hole-hole propagation is no longer negligible, and this leads to an important repulsive effect on the total energy. Second, the SCGF generates realistic spectral functions, which are used to evaluate the effective interaction and the corre-

sponding nucleon self-energy. The spectral functions exhibits a depletion of the quasi-particle peak and the appearance of single-particle strength at large values of energy and momentum, in agreement with experimental information from $(e, e'p)$ reactions. This is in contrast with the BHF approach where all s.p. strength is concentrated at the BHF-energy as determined from Eq. (5).

In the SCGF approach the particle states ($k > k_F$), which are absent in the BHF energy sum rule do contribute according to the energy sum rule ($d = 1(2)$ for PNM(SNM))

$$\frac{E}{A} = \frac{d}{\rho} \int \frac{d^3k}{(2\pi)^3} \int_{-\infty}^{\varepsilon_F} d\omega \left(\frac{k^2}{2m} + \omega \right) S_h(k, \omega), \tag{7}$$

expressed in terms of the nucleon spectral function $S_h(k, \omega)$.

To illustrate the difference between the ccBHF and SCGF approaches the results for both SNM and PNM are compared in the left and central panels of Fig. 3 for the Reid93 interaction. One sees that the inclusion of high-momentum nucleons leads roughly to a doubling of the kinetic and potential energy in SNM, as compared to BHF. The net effect for the total energy of SNM is a repulsion, increasing with density [13]. This leads to a stiffer equation of state, and a shift of the SNM saturation density towards lower densities. The above effects which are dominated by the tensor force (the isoscalar $^3S_1$-$^3D_1$ partial wave) are much smaller in PNM.

The corresponding SE, shown in the right panel of Fig. 3, is dominated by the shift in the total energy for SNM, and lies below the ccBHF symmetry energy in the entire density-range. At $\rho_0 = 0.16$ fm^{-3} the parameter a_4 is reduced from 28.9 MeV to 24.9 MeV, while the slope p_0 remains almost the same (2.0 MeV fm^{-3} compared to 1.9 MeV fm^{-3} in BHF).

3.4 Three-body force in microscopic approaches

As noted above at higher densities the EoS is sensitive to 3NF contributions. Whereas the 3NF for low densities seems now well understood its contribution to nuclear matter densities remains unsettled. In practice in calculations of the symmetry energy in the BHF approach two types of 3NF have been used in calculations; in ref.[4] the microscopic 3NF based upon meson exchange by Grangé et al. was used, and in ref.[15] as well in most VCS calculations the Urbana interaction. The latter has in addition to an attractive microscopic two-pion exchange part a repulsive phenomenological part constructed in such a way that the empirical saturation point for SNM is reproduced. Also in practice in the BHF approach to simplify the computational efforts the 3NF is reduced to a density dependent two-body force by averaging over the position of the third particle.

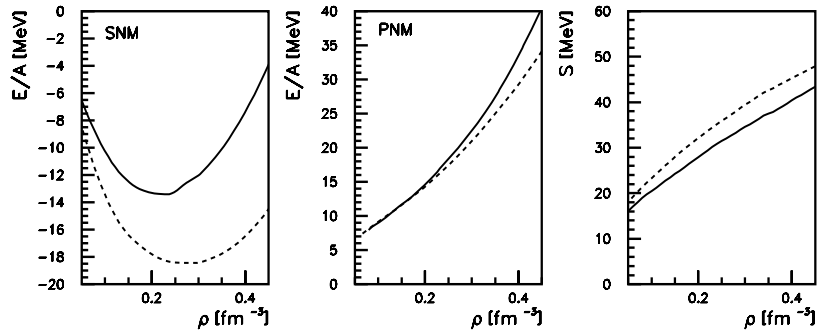

Figure 3. The energy per particle for symmetric nuclear matter (left panel) and pure neutron matter (central panel) for the Reid93 interaction. The dashed line refers to a ccBHF calculation, the full line to a SCGF calculation. The right panel displays the SE in these two approaches.

In general inclusion of the 3NF stiffens the SE for $\rho > \rho_0$. For example, with the Av18+UIX interaction a_4 increases from 27 to 30 MeV and p_0 from 2 to 3 MeV fm^{-3} (see Table 1).

In view of the important contribution from the 3NF to the SE at higher densities there seems a clear need to get a more quantitative understanding of the repulsive part of the 3NF in PNM.

3.5 Dirac-Brueckner-Hartree-Fock

The SE has also been computed in the Dirac-Brueckner-Hartree-Fock (DBHF) approach [16, 17]. Although some of the shortcomings of BHF (mean field treatment of the Pauli operator and violation of Hugenholz-van Hove theorem) persist in the DBHF method it appears that in the latter approach one is able to reproduce the saturation properties of SNM without the inclusion of a three-body interaction. A general feature of relativistic methods is that the SE increases almost linearly with density, and more rapidly than in the non-relativistic case. This difference can be attributed to two effects. First the covariant kinetic energy which is inversely proportional to $\sqrt{k_F^2 + m^{*2}}$ is larger because of the decreasing Dirac mass, m^*, with increasing density. Secondly the contribution from rho-exchange appears to be larger than in the non-relativistic case [16].

3.6 Relativistic mean-field approach

Relativistic mean field (RMF) models have been applied successfully to describe properties of finite nuclei. In general ground state energies, spin-orbit splittings, etc. can be described well in terms of a few parameters ref.[18]. Recently it has lead to the suggestion that the bulk SE is strongly correlated with the neutron skin [19, 20] (see below). In essence the method is based upon the use of energy-density functional (EDF) theory.

In practice covariant approaches are formulated either in terms of a covariant Lagrangian with σ, ω and ρ exchange (and possibly other mesons) [18, 21], or in terms of contact interactions [20], solved as an EDF in the Hartree-Fock approximation. Sets of model parameters are determined by fitting bound state properties of nuclei. Specifically the isovector degree of freedom is governed by the exchange of isovector mesons; in case of ρ-meson exchange the (positive definite) contribution to the SE is given by

$$a_4 = \frac{k_F^2}{6\sqrt{m^{*2}+k_F^2}} + \frac{g_\rho^2}{8m_\rho^2}\rho_0, \tag{8}$$

and its potential energy contribution to p_0, which scales with that for a_4, is $\frac{g_\rho^2}{8m_\rho^2}$ [20]. Typical values obtained for p_0 are around 4-6 MeV fm^{-3}, and $a_4 \sim$ 30-36 MeV, i.e., considerably larger than in non-relativistic approaches (a large part of the enhancement can be ascribed to the fact that the kinetic contribution is larger, because $m^* < m$).

Recently this approach was extended by inclusion of the isovector-scalar partner, the δ-meson, of the isoscalar scalar σ-meson [22]. Unfortunately the value of the coupling for the δ-meson cannot be determined well by fitting properties of stable nuclei. Also in its simplest, density independent form, the inclusion of the δ-meson leads to an even larger net value for p_0. This happens because of the presence of the Lorentz factor m^*/E in the scalar potential contribution, $\sim -\frac{g_\delta^2}{8m_\delta^2}\frac{m^*}{E}$, which decreases with increasing density.

3.7 Effective field theory

Recently the density dependence of the symmetry energy has been computed in chiral perturbation effective field theory, described by pions plus one cutoff parameter, Λ, to simulate the short distance behavior [23]. The nuclear matter calculations have been performed up to three-loop order; the density dependence comes from the replacement of the free nucleon propagator by the in-medium one, specified by the Fermi momentum k_F

$$(\not{p} + M)\left(\frac{i}{p^2 - M^2 + i\epsilon} - 2\pi\delta(p^2 - M^2)\theta(p_0)\theta(k_F - p)\right).$$

Table 1. Results for the symmetry energy parameters a_4 (in MeV) and p_0 (in MeV fm^{-3})

	BHF	BHF+3NF[5]	VCS[10]	VCS+3NF[10]	SCGF[1]	DBHF[16]	RMF[20]
a_4	28.9	30	27	30	24.9	31	30-36
p_0	1.9	2.9	2.0	3.1	2.0	3.0	4-6

The resulting EoS is expressed as an expansion in powers of k_F and the value of $\Lambda \approx 0.65$ GeV is adjusted to the empirical binding energy per nucleon. In its present form the validity of this approach is clearly confined to relatively small values of the Fermi momentum, i.e. rather low densities. Remarkably for SNM the calculation appears to be able to reproduce the microscopic EoS up to $\rho \sim 0.5$ fm^{-3}. As for the SE the value obtained in this approach for $a_4 = 33$ MeV is in reasonable agreement with the empirical one; however, at higher densities ($\rho > 0.2$ fm^{-3}) a downward bending is predicted (see Fig. 4) which is not present in other approaches.

3.8 Comparison of results

To summarize the present situation in Fig. 4 the resulting density dependence of the SE for the approaches discussed above are compared (excluding the 3NF contribution). One sees that the covariant models predict a much larger increase of the SE with the density than the non-relativistic approaches. The lowest-order BHF method predicts a somewhat higher value for a_4 than both the VCS and SCGF methods, which lead to very similar results; whether that can be ascribed to a consistent treatment of correlations in these methods, or is fortuitous, is not clear.

Clearly at least part of the differences should be attributed to the different selection of the mesonic degrees of freedom in the various models. In the microscopic approaches the tensor force mediated by π and ρ exchange seems to play the dominant role. On the other hand in the mean field approach explicit pion exchange is usually not included and hence there the isovector effect solely comes from the shorter range ρ-exchange. In fact it has been argued that in contrast to isoscalar properties the long-range pion exchange should play an essential role in determining the isovector properties [20].

4. Empirical information on the SE

In view of the existing uncertainties in the calculation of the SE one may ask whether from finite nuclei one can obtain experimental constraints on the symmetry energy as a function of density. In this section some recent activities pertaining to this issue are reviewed.

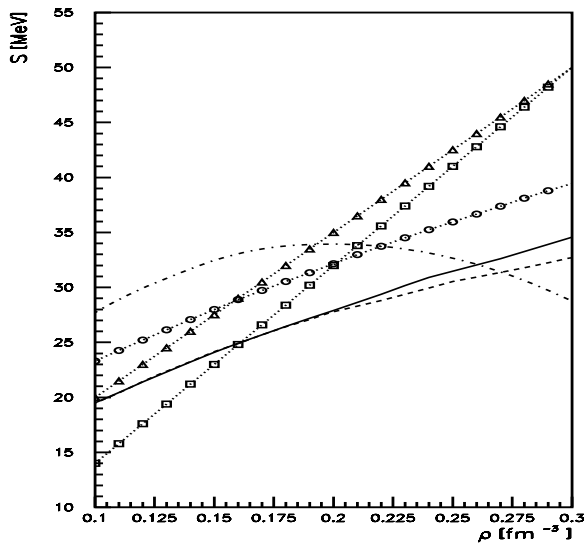

Figure 4. Overview of several theoretical predictions for the SE: Brueckner-Hartree-Fock (continuous choice) with Reid93 potential (circles), self-consistent Green function theory with Reid93 potential (full line), variational calculation from [9] with Argonne Av14 potential (dashed line), DBHF calculation from [16] (triangles), relativistic mean-field model from [22] (squares), effective field theory from [23] (dash-dotted line).

4.1 Relation between SE and neutron skin

Recently in applying the non-relativistic Skyrme Hartree-Fock (SHF) model Brown [19] noted that certain combinations of parameters in the SHF are not well determined by a fit to ground state binding energies alone; as a result a wide range of predictions for the EoS for PNM can be obtained. At the same time he found a correlation between the derivative of the neutron star EoS (i.e., basically the symmetry pressure p_0) and the neutron skin in ^{208}Pb.

Subsequently Furnstahl [20] in a more extensive study pointed out that within the framework of mean field models (both non-relativistic Skyrme as well as relativistic models) there exists an almost linear empirical correlation between theoretical predictions for both a_4 and its density dependence, p_0, and the neutron skin, $\Delta R = R_n - R_p$, in heavy nuclei. This is illustrated for ^{208}Pb in Fig. 5 (from ref.[20]; a similar correlation is found between ΔR and p_0). Note that whereas the Skyrme results cover a wide range of ΔR values the RMF predictions in general lead to $\Delta R > 0.20$ fm.

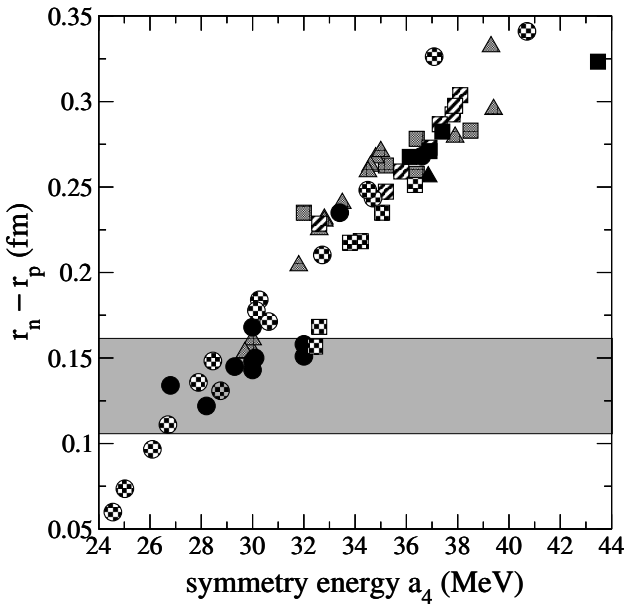

Figure 5. Neutron skin thickness versus a_4 for ^{208}Pb for a variety of mean field models (from [20]). The circles correspond to results for the Skyrme force, the squares to RMF models with mesons, and the triangles to RMF with point couplings; the shaded area indicates the range of ΔR values consistent with the present empirical information for ^{208}Pb.

The interpretation of the nuclear matter results in part depends on the question whether there is a surface contribution to the SE in finite nuclei. In ref. [24] it was found that for heavy nuclei the latter is of minor importance, which has also been confirmed in ref.[20].

4.2 Insight in the correlation of ΔR and a_4

The above observation suggests an intriguing relationship between a bulk property of infinite nuclear matter and a surface property of finite systems. Here we want to point out that this correlation can be understood naturally in terms of the Landau-Migdal approach. To this end we consider a simple mean-field model (see, e.g., ref.[16]) with the Hamiltonian consisting of the single-particle mean field part $\hat{H}_0$ and the residual particle-hole interaction $\hat{H}_{ph}$:

$$\hat{H} = \sum_a (T_a + U_0(x_a) + U_1(x_a) + U_C(x_a)) + \hat{H}_{ph}, \tag{9}$$

where $(x = (r, \sigma, \tau))$

$$U_0(x) = U_0(r) + U_{so}(x);\; U_1(x) = \frac{1}{2} S_{\rm pot}(r)\tau^{(3)};\; U_C(x) = \frac{1}{2} U_C(r)(1-\tau^{(3)}). \tag{10}$$

Here, the mean field potential includes the phenomenological isoscalar part $U_0(x)$ along with the isovector $U_1(x)$ and the Coulomb $U_C(x)$ parts calculated consistently in the Hartree approximation; $U_0(r)$ and $U_{so}(x) = U_{so}(r)\vec{\sigma}\cdot\vec{l}$ are the central and spin-orbit parts of the isoscalar mean field, respectively, and $S_{\rm pot}(r)$ is the potential part of the symmetry energy.
In the Landau-Migdal approach the effective isovector particle-hole interaction $\hat{H}_{ph}$ is given by

$$\hat{H}_{ph} = \sum_{a>b}(F' + G'\vec{\sigma}_a\vec{\sigma}_b)\vec{\tau}_a\vec{\tau}_b\delta(\vec{r}_a - \vec{r}_b), \tag{11}$$

where F' and G' are the phenomenological Landau-Migdal parameters.

The model Hamiltonian $\hat{H}$ in Eq.(9) preserves isospin symmetry if the condition

$$[\hat{H}, \hat{T}^{(-)}] = \hat{U}_C^{(-)}, \tag{12}$$

is fulfilled, where $\hat{T}^{(-)} = \sum_a \tau_a^{(-)}$, $\hat{U}_C^{(-)} = \sum_a U_C(r_a)\tau_a^{(-)}$. With the use of Eqs. (9),(11) the condition eq. (12) in the random phase approximation (RPA) formalism leads to a self-consistency relation between the symmetry potential and the Landau parameter F' [26]:

$$S_{\rm pot}(r) = 2F'n^{(-)}(r), \tag{13}$$

where $n^{(-)}(r) = n^n(r) - n^p(r)$ is the neutron excess density. Thus, in this model the depth of the symmetry potential is controlled by the Landau-Migdal parameter F' (analogously to the role played by the parameter g_ρ^2 in relativistic mean field models).

$S_{\rm pot}(r)$ is obtained from Eq. (13) by an iterative procedure; the resulting dependence of ΔR on the dimensionless parameter $f' = F'/(300\ \text{MeV fm}^3)$ shown in fig. 6 indeed illustrates that ΔR depends almost linearly on f'. Then with the use of the Migdal relation [27] which relates the SE and f',

$$a_4 = \frac{\epsilon_F}{3}(1 + 2f'), \tag{14}$$

an almost linear correlation between the symmetry energy, a_4, and the neutron skin is found.

To get more insight in the role of f' we consider small variations $\delta F'$. Neglecting the variation of $n^{(-)}(r)$ with respect to $\delta F'$ one has a linear variation of the symmetry potential: $\delta S_{pot}(r) = 2\delta F' n^{(-)}(r)$. Then in first order perturbation theory, such a variation of S_{pot} causes the following variation of the ground-state wave function

$$|\delta 0\rangle = \delta F' \sum_s \frac{\langle s|\hat{N}^{(-)}|0\rangle}{E_0 - E_s}|s\rangle, \tag{15}$$

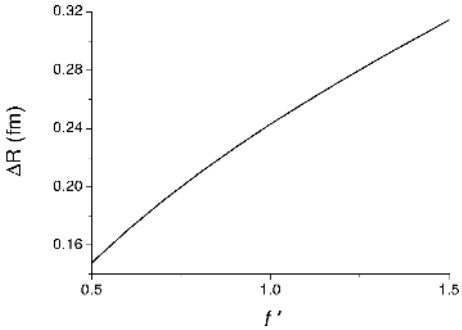

Figure 6. Neutron skin in ^{208}Pb vs. the Landau-Migdal parameter f'.

with s labeling the eigenstates of the nuclear Hamiltonian and a single-particle operator $\hat{N}^{(-)} = \sum_a n^{(-)}(r_a)\tau_a^{(3)}$. Consequently the variation of the expectation value of the single-particle operator $\hat{V}^{(-)} = \sum_a r_a^2\tau_a^{(3)}$ with $\langle 0|\hat{V}^{(-)}|0\rangle = NR_n^2 - ZR_p^2$ can be written as

$$R_p\delta(\Delta R) = \delta F' \frac{2}{A}\sum_s \frac{\mathrm{Re}\langle 0|\hat{N}^{(-)}|s\rangle\langle s|\hat{V}^{(-)}|0\rangle}{E_0 - E_s}. \qquad (16)$$

In practice the sum in Eq. (16) is exhausted mainly by the isovector monopole resonance of which the high excitation energy (about 24 MeV in ^{208}Pb) justifies the perturbative consideration. We checked that Eq. (16) is able to reproduce directly calculated $\delta(\Delta R)$ shown in fig. 6 with the accuracy of about 10%.

As for the correlation between ΔR and p_0 one would need information on the density dependence of F'. Sofar as we know it has not been extracted from data on stable nuclei. In the approximation that F' is density independent one naturally finds the p_0 is proportional to a_4.

4.3 Experimental information on ΔR for ^{208}Pb

What are the experimental constraints on the neutron skin? A variety of experimental approaches have been explored in the past to obtain information on ΔR. To a certain extent all analysis contain a certain model dependence, which is difficult to estimate quantitatively. It is not our intention to present a full overview of existing methods for the special case of ^{208}Pb. In particular the results obtained in the past from the analysis of elastic scattering of protons and neutrons have varied depending upon specifics of the analysis employed. At present the most accurate value for ΔR comes from a recent detailed analysis of the elastic proton scattering reaction at $E = 0.5 - 1$ GeV [28], and of

neutron and proton scattering at $E = 40 - 100$ MeV [29]. For details we refer to these papers. Here we restrict ourselves to a discussion of the some less well known methods that have the potential to provide more accurate information on the neutron skin in the future.

Anti-protonic atoms. Recently neutron density distributions in a series of nuclei were deduced from anti-protonic atoms [30]. The basic method determines the ratio of neutron and proton distributions at large differences by means of a measurement of the annihilation products which indicates whether the antiproton was captured on a neutron or a proton. In the analysis two assumptions are made. First a best fit value for the ratio R_I of the imaginary parts of the free space $\bar{p}p$ and $\bar{p}n$ scattering lengths equal to unity is adopted. Secondly in order to reduce the density ratio at the annihilation side to a a ratio of rms radii a two-parameter Fermi distribution is assumed. The model dependence introduced by these assumptions is difficult to judge. Since a large number of nuclei have been measured one may argue that the value of R_I is fixed empirically.

Parity violating electron scattering. Recently it has been proposed to use the (parity violating) weak interaction to probe the neutron distribution. This is probably the least model dependent approach [31]. The weak potential between electron and a nucleus

$$\tilde{V}(r) = V(r) + \gamma_5 A(r), \tag{17}$$

where the axial potential $A(r) = \frac{G_F}{2^{3/2}} \rho_W(r)$. The weak charge is mainly determined by neutrons

$$\rho_W(r) = (1 - 4\sin^2\theta_W)\rho_p(r) - \rho_n(r), \tag{18}$$

with $\sin^2\theta_W \approx 0.23$. In a scattering experiment using polarized electrons one can determine the cross section asymmetry [31] which comes from the interference between the A and V contributions. Using the measured neutron form factor at small finite value of Q^2 and the existing information on the charge distribution one can uniquely extract the neutron skin. Some slight model dependence comes from the need to assume a certain radial dependence for the neutron density, to extract R_n from a finite Q^2 form factor.

Giant dipole resonance. Isovector giant resonances contain information about the SE through the restoring force. In particular the excitation of the isovector giant dipole resonance (GDR) with isoscalar probes has been used to extract $\Delta R/R$ [32]. In the distorted wave Born approximation optical model analysis of the cross section the neutron and proton transition densities are needed as an input. For example, in the Goldhaber-Teller picture these are

expressed as

$$g_i(r) = -\kappa \frac{2N_i}{A} \frac{d\rho_i}{dr} \tag{19}$$

with κ the oscillation amplitude and $(i = p, n)$; one assumes ground state neutron and proton distributions of the form $(x = (N - Z)/A)$

$$\rho_i(r) = \frac{1}{2}(1 \pm x \mp \gamma x)\rho(r - c(1 \pm \gamma x/3)), \tag{20}$$

where γ is related to the neutron skin ΔR, $\gamma = \frac{3A}{2(N-Z)} \Delta R/R_0$. Then for $N > Z$ the isovector transition density takes on the form

$$\Delta g(r) = \kappa\gamma \frac{N - Z}{A} (\frac{d\rho}{dr} + \frac{c}{3} \frac{d^2\rho}{dr^2}),$$

In practice one studies the excitation of the GDR by alpha particle scattering (isoscalar probe). By comparing the experimental cross section with the theoretical one (calculated as a function of the ratio $\Delta R/R$) the value of ΔR can be deduced [32].

It is difficult to make a quantitative estimate of the uncertainty in the result coming from the model dependence of the approach. In the analysis several assumptions must be made, such as the radial shape of the density oscillations and the actual values of the optical model parameters.

We note that also other types of isovector giant resonances have been suggested as a source of information on the neutron skin, such as the spin-dipole giant resonance [33] and the isobaric analog state [34]. At present studies of these reactions have not led to quantitative constraints for the neutron skin of ^{208}Pb.

Results for ΔR. In table 2 we present a summary of some recent results on ΔR in ^{208}Pb. One sees that the recent results are consistent with ΔR values in the range 0.10-0.16 fm. It appears from Fig. 5 that this range is consistent with the conventional Skyrme model approach but tends to disagree with the results of the RMF models considered in [20]. Also from the correlation plot between ΔR and p_0 shown in Fig. 11 in ref.[20] one may conclude that a small value for $p_0 \sim 2.0$ MeV fm^{-3} is favoured over the larger values from covariant models.

4.4 Information on the SE from heavy-ion reactions

In principle the density dependence of the SE at higher densities (and further away from $N = Z$) can be probed by means of heavy-ion reactions using neutron rich radioactive beams. In ref.[35] possible observable effects from the isovector field are considered in terms of the RMF model. Of particular

Table 2. Summary of recent results for ΔR in ^{208}Pb

method	ΔR [fm]	error [fm]	ref
$(\vec{p}, p')$ at 0.5-1.04 GeV	0.097	0.014	[28]
nucleon scattering (40-200 MeV)	0.17		[29]
anti-protonic atoms	0.15	0.02	[30]
giant dipole resonance excitation	0.19	0.09	[32]
parity violating electron scattering	planned	1%	[31]

interest seems the study of the ratio of π^+/π^- cross sections and its energy dependence which appears sensitive to details of the SE [36].

5. Constraints on EoS from neutron stars

Given the EoS as a function of density the mass versus radius relation of a neutron star can be obtained in the standard way with the use of the Tolman-Oppenheimer-Volkov equation. Do we need the EoS up to all densities or can we already draw some conclusions from the lower densities? In [2] it was argued that there exists a quantitative correlation between the neutron star radius and the pressure which does not depend strongly on the EoS at the highest densities. Generally speaking a stiff (soft) EoS implies a large (small) radius.

Clearly a simultaneous measurement of the radius and the mass of the *same* star would discriminate between various EoS. The presently available observations do not yet offer strong constraints. For example, most observed star masses fall in the range of 1.3-1.5 $M_\odot$. These values seem to rule out the very soft EoSs predicted with hyperons present, which yield $M_{max} \sim 1.3 M_\odot$ [5]. This may suggest that either the NY and YY interactions used as an input must be reexamined, or that the use of the BHF approach at high densities is not reliable.

Other constraints come from recent observations from X-ray satellites. Most robust seem the data from the low mass X-ray binary EXO 0478-676 obtained by Cottam et al. [37]. From the redshifted absorption lines from ionized Fe and O a gravitational redshift $z = 0.23$ was deduced; this gives rise to a mass-to-radius relation

$$M/M_\odot = (1 - \frac{1}{(1+z)^2}) R/R_{g\odot} \tag{21}$$

with $R_{g\odot} = 2.95$ km. As discussed in detail in various contributions in this workshop at present this constraint appears fully consistent not only with conventional EoSs, but also with most more exotic ones.

Acknowledgments

This work is part of the research program of the "Stichting voor Fundamenteel Onderzoek der Materie" (FOM) with financial support from the "Nederlandse Organisatie voor Wetenschappelijk Onderzoek" (NWO). Y. Dewulf acknowledges support from FWO-Vlaanderen.

References

[1] A.E.L. Dieperink et al., to appear in Phys. Rev. C

[2] J.M. Lattimer and M.Prakash, Astrophys. J. **550** 426 (2001)

[3] W. Zuo, I. Bombaci and U. Lombardo, Phys.Rev.C**60** 024605 (1999)

[4] W. Zuo et al. Eur. Phys. J. **A14** 469 (2002)

[5] M. Baldo anf F. Burgio, Lect. Notes Phys. **578** 1 (2001)

[6] M. Baldo, G. Giansiracusa, U. Lombardo and H.Q. Song, Phys. Lett. B**473**, 1 (2000)

[7] M. Baldo, A. Fiasconaro, H.Q. Song, G. Giansiracusa and U. Lombardo, Phys.Rev.C**65**, 017303 (2001)

[8] L. Engvik, M. Hjorth-Jensen, R. Machleidt, H. Müther and A. Polls, Nucl.Phys.A**627** 85 (1997)

[9] R.B. Wiringa, V. Fiks and A. Fabrocini, Phys.Rev.C**38**,1010 (1988)

[10] A. Akmal, V.R. Pandharipande, D.G. Ravenhall, Phys.Rev.C**58**1804(1998)

[11] P. Bozek, Phys. Rev. C**65**, 054306 (2002); Eur. Phys. J. A**15**, 325 (2002); P. Bozek and P. Czerski, Eur. Phys. J. A**11**, 271 (2001)

[12] Y. Dewulf, D. Van Neck and M. Waroquier, Phys. Lett. B**510**, 89 (2001)

[13] Y. Dewulf, D. Van Neck and M. Waroquier, Phys. Rev. C**65**, 054316 (2002)

[14] Y. Dewulf, W.H. Dickhoff, D. Van Neck , E.R. Stoddard and M. Waroquier, Phys. Rev. Lett. **90** 152501 (2003)

[15] M. Baldo, I Bombaci, and G.F. Burgio, Astron. and Astrophys. **328**, 274 (1997)

[16] C.-H. Lee, T.T.S. Kuo, G.Q. Li and G.E. Brown, Phys. Rev. C**57** 3488(1998)

[17] K. Sumiyoshi, K. Oyamatsu, and H. Toki, Nucl.Phys. A**595** 327(1995)

[18] P. Ring, Progr. Part. Nucl. Phys. **37** 193 (1996), and refs therein

[19] B.A. Brown, Phys. Rev. Lett. **85** 5296 (2000)

[20] R.J. Furnstahl, Nucl. Phys. A**706** 85 (2002); and Lect.Notes Phys.641:1-29 (2003)

[21] C.J. Horowitz and J. Piekarewicz, Phys. Rev. C**66** 055803(2002)

[22] B. Liu et al., Phys. Rev. C**65** 045201 (2002)

[23] N. Kaiser, S. Fritsch, and W. Weise, Nucl. Phys. A**697** 255 (2002)

[24] K. Oyamatsu et al., Nucl. Phys. A**634** 3 (19980

[25] M.L. Gorelik, S. Shlomo and M.H. Urin, Phys. Rev. C **62**, 044301 (2000).

[26] B.L. Birbrair and V.A. Sadovnikova, Sov. J. Nucl. Phys. **20**, 347 (1975); O.A. Rumyantsev and M.H. Urin, Phys. Rev. C49, 537 (1994).

[27] A.B. Migdal, Theory of Finite Fermi Systems and Applications to Atomic Nuclei (Interscience, London, 1967)

[28] B.C. Clark, L.J.Kerr and S. Hama, Phys. Rev. C**67** 054605 (2003)

[29] S. Karataglidis, K. Amos, B.A. Brown and P.K. Deb, Phys. Rev. C**65** 044306 (2002)

[30] A. Trzcinska et al., Phys. Rev. Lett. **87** 082501(2001)

[31] C. Horowitz et al., Phys. Rev. C**63** 025501 (2001)

[32] A. Krasznahorkay et al., Nucl. Phys. A**567** 521 (1994)

[33] A. Krasznahorkay et al., Phys. Rev. Lett. **82** 3216 (1999)

[34] N. Auerbach, J. Huefner, A.K. Kerman, C.M. Shakin, Revs. Mod. Phys. **44** 48(1972)

[35] T. Gaitanos et al., Nucl.Phys.A732:24-48, (2003)

[36] Bao-An Li, Phys. Rev. C**67** 017601 (2003) and refs. therein

[37] J. Cottam, F. Paerels and M. Mendez, Nature **420** 51 (2002)

NEUTRON STAR STRUCTURE WITH HYPERONS AND QUARKS

M. Baldo, F. Burgio, H.-J. Schulze
INFN Sezione di Catania, Via S. Sofia 64, I-95123 Catania, Italy

Abstract We discuss the high-density nuclear equation of state within the Brueckner-Hartree-Fock approach. Particular attention is paid to the effects of nucleonic three-body forces, the presence of hyperons, and the joining with an eventual quark matter phase. The resulting properties of neutron stars, in particular the mass-radius relation, are determined. It turns out that stars heavier than 1.3 solar masses contain necessarily quark matter.

Keywords: Neutron Star, Brueckner-Hartree-Fock, Three-Body Force, Hyperons, Quark Matter

1. Brueckner theory

Over the last two decades the increasing interest for the equation of state (EOS) of nuclear matter has stimulated a great deal of theoretical activity. Phenomenological and microscopic models of the EOS have been developed along parallel lines with complementary roles. The former models include nonrelativistic mean field theory based on Skyrme interactions [1] and relativistic mean field theory based on meson-exchange interactions (Walecka model) [2]. Both of them fit the parameters of the interaction in order to reproduce the empirical saturation properties of nuclear matter extracted from the nuclear mass table. The latter ones include nonrelativistic Brueckner-Hartree-Fock (BHF) theory [3] and its relativistic counterpart, the Dirac-Brueckner (DB) theory [4], the nonrelativistic variational approach also corrected by relativistic effects [5], and more recently the chiral perturbation theory [6]. In these approaches the parameters of the interaction are fixed by the experimental nucleon-nucleon and/or nucleon-meson scattering data.

For states of nuclear matter with high density and high isospin asymmetry the experimental constraints on the EOS are rather scarce and indirect. Different approaches lead to different or even contradictory theoretical predictions for the nuclear matter properties. The interest for these properties lies, to a large extent, in the study of astrophysical objects, i.e., supernovae and neu-

D. Blaschke and D. Sedrakian (eds.), Superdense QCD Matter and Compact Stars, 113–134.

tron stars. In particular, the structure of a neutron star is very sensitive to the compressibility and the symmetry energy. The neutron star mass, measured in binary systems, has been proposed as a constraint for the EOS of nuclear matter [7].

One of the most advanced microscopic approaches to the EOS of nuclear matter is the Brueckner theory. In the recent years, it has made a rapid progress in several aspects: (i) The convergence of the Brueckner-Bethe-Goldstone (BBG) expansion has been firmly established [8, 9]. (ii) Important relativistic effects have been incorporated by including into the interaction the virtual nucleon-antinucleon excitations, and the relationship with the DB approach has been numerically clarified [10]. (iii) The addition of microscopic three-body forces (TBF) based on nucleon excitations via pion and heavy meson exchanges, permitted to improve to a large extent the agreement with the empirical saturation properties [10–12]. (iv) Finally, the BHF approach has been extended in a fully microscopic and self-consistent way to describe nuclear matter containing also hyperons [13], opening new fields of applications such as hypernuclei [14] and a more realistic modeling of neutron stars [15, 16].

In the present article we review these issues and present our results for neutron star structure based on the resulting EOS of dense hadronic matter.

Convergence of the hole-line expansion. The nonrelativistic BBG expansion of the nuclear matter correlation energy E/A can be cast as a power series in terms of the number of hole lines contained in the corresponding diagrams, which amounts to a density power expansion [3]. The two hole-line truncation is named the Brueckner-Hartree-Fock (BHF) approximation. At this order the energy D_2 is very much affected by the choice of the auxiliary potential, as shown in Fig. 1 (solid lines), where the numerical results obtained with the gap and the continuous choice are compared for symmetric nuclear matter as well as neutron matter. But, as also shown in the same figure [8, 9], adding the three-hole line contributions D_3, the resulting EOS is almost insensitive to the choice of the auxiliary potential, and very close to the result D_2 with the continuous choice.

In spite of the satisfactory convergence, the saturation density misses the empirical value $\rho_0 = 0.17\ \mathrm{fm}^{-3}$ extracted from the nuclear mass tables. This confirms the belief that the concept of a many nucleon system interacting with only a two-body force is not adequate to describe nuclear matter, especially at high density.

Relativistic corrections. Before the possible effects of TBF are examined, one should introduce relativistic corrections in the preceding nonrelativistic BHF predictions. This is done in the Dirac-Brueckner approach [4], where the nucleons, instead of propagating as plane waves, propagate as spinors in

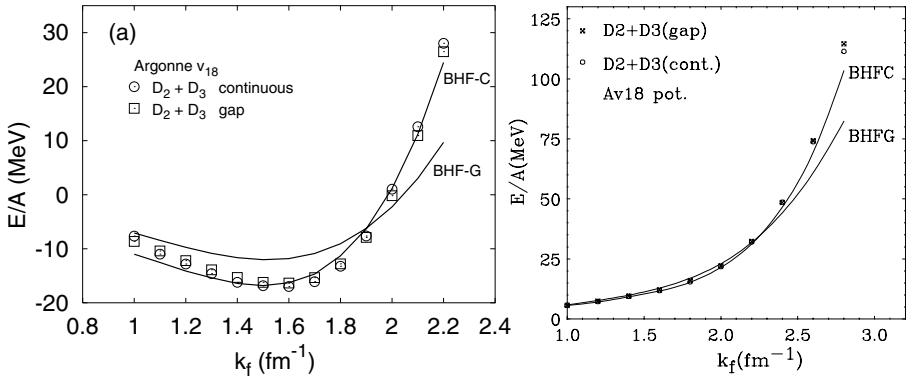

Figure 1. Comparison of BHF two hole-line (lines) and three hole-line (markers) results for symmetric nuclear matter (left plot) and pure neutron matter (right plot), using continuous and gap choice for the single-particle potentials.

a mean field with a scalar component U_S and a vector component U_V, self-consistently determined together with the G-matrix. The nucleon self-energy can be expanded in terms of the scalar field,

$$\Sigma(\mathbf{p}) = \sqrt{(M+U_S)^2+\mathbf{p}^2}+U_V \approx p_0+U_V+\frac{M}{p_0}U_S+\frac{\mathbf{p}^2}{2p_0^3}U_S^2+\ldots . \quad (1)$$

The second-order term can be interpreted as due to the interaction between two nucleons with the virtual excitation of a nucleon-antinucleon pair [17]. This interaction is a TBF with the exchange of a scalar (σ) meson, as illustrated by the diagram (d) of Fig. 2. Actually this diagram represents a class of TBF with the exchange of light (π, ρ) and heavy (σ, ω) mesons. There are, however, several other diagrams representing TBF, Fig. 2(a-c), which should be evaluated as well in a consistent treatment of TBF.

2. Three-body forces

Since long it is well known that two-body forces are not enough to explain some nuclear properties, and TBF have to be introduced. Typical examples are: the binding energy of light nuclei, the spin dynamics of nucleon-deuteron scattering, and the saturation point of nuclear matter. Phenomenological and microscopic TBF have been widely used to describe the above mentioned properties.

In the framework of the Brueckner theory a rigorous treatment of TBF would require the solution of the Bethe-Faddeev equation, describing the dynamics of three bodies embedded in the nuclear matter. In practice a much simpler approach is employed, namely the TBF is reduced to an effective, density dependent, two-body force by averaging over the third nucleon in the medium,

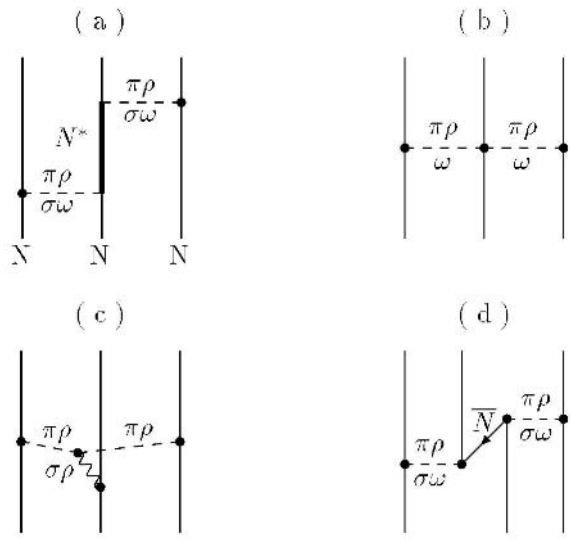

Figure 2. Various diagrams contributing to the microscopic TBF.

taking account of the nucleon-nucleon correlations by means of the BHF defect function g_{ij},

$$\left\langle 12|V(\rho)|1'2'\right\rangle = \sum_{33'} \Psi^*_{123} \left\langle 123|V|1'2'3'\right\rangle \Psi_{1'2'3'} \,. \tag{2}$$

Here $\Psi_{123} = \phi_3(1-g_{13})(1-g_{23})$ and ϕ_3 is the free wave function of the third particle. This effective two-body force is added to the bare two-body force and recalculated at each step of the iterative procedure.

Microscopic TBF. The microscopic TBF of Refs. [10–12] is based on meson-exchange mechanisms accompanied by the excitation of nucleonic resonances, as represented by the diagrams plotted in Fig. 2. Besides the TBF arising from the excitation of a $N\bar{N}$ pair [diagram (d)], already discussed in the preceding section, another important class of TBF [diagram (a)] is due to the excitation of the isobar $\Delta(1232)$ resonance via the exchange of light (π, ρ) mesons, or the lowest non-isobar nucleon excitation $N^*(1440)$ excited by heavy meson (σ and ω) exchanges. Diagrams (b) and (c) are included only for completeness and play a minor role [10].

The combined effect of these TBF is a remarkable improvement of the saturation properties of nuclear matter [12]. Compared to the BHF prediction with only two-body forces, the saturation energy is shifted from -18 to -15 MeV, the saturation density from 0.26 to 0.19 fm^{-3}, and the compression modulus from 230 to 210 MeV. The spin and isospin properties with TBF exhibit also quite satisfactory behavior [18].

Phenomenological TBF. A second class of TBF that are widely used in the literature, in particular for variational calculations of finite nuclei and nuclear matter [5], are the phenomenological Urbana TBF [19]. We remind that the Urbana IX TBF model contains a two-pion exchange potential $V_{ijk}^{2\pi}$ supplemented by a phenomenological repulsive term V_{ijk}^{R},

$$V_{ijk} = V_{ijk}^{2\pi} + V_{ijk}^{R} \,, \tag{3}$$

where

$$V_{ijk}^{2\pi} = A \sum_{\rm cyc} \Big[\{X_{ij}, X_{jk}\} \, \{\boldsymbol{\tau}_i \cdot \boldsymbol{\tau}_j, \boldsymbol{\tau}_j \cdot \boldsymbol{\tau}_k\} + \frac{1}{4} \, [X_{ij}, X_{jk}] \, [\boldsymbol{\tau}_i \cdot \boldsymbol{\tau}_j, \boldsymbol{\tau}_j \cdot \boldsymbol{\tau}_k] \Big], \tag{4}$$

$$V_{ijk}^{R} = U \sum_{\rm cyc} T^2(m_\pi r_{ij}) T^2(m_\pi r_{jk}) \,. \tag{5}$$

The two-pion exchange operator X_{ij} is given by

$$X_{ij} = Y(m_\pi r_{ij}) \boldsymbol{\sigma}_i \cdot \boldsymbol{\sigma}_j + T(m_\pi r_{ij}) S_{ij} \,, \tag{6}$$

where $S_{ij} = 3(\boldsymbol{\sigma}_i \cdot \hat{\mathbf{r}}_{ij})(\boldsymbol{\sigma}_j \cdot \hat{\mathbf{r}}_{ij}) - \boldsymbol{\sigma}_i \cdot \boldsymbol{\sigma}_j$ is the tensor operator and $\boldsymbol{\sigma}$ and $\boldsymbol{\tau}$ are the Pauli spin and isospin operators. Y and T are the Yukawa and tensor functions, respectively, associated to the one-pion exchange [19].

After reducing this TBF to an effective, density dependent, two-body force by the averaging procedure described earlier, the resulting effective two-nucleon potential assumes a simple structure,

$$\overline{V}_{ij}^{\rm pheno}(\mathbf{r}) = (\boldsymbol{\tau}_i \cdot \boldsymbol{\tau}_j) \Big[(\boldsymbol{\sigma}_i \cdot \boldsymbol{\sigma}_j) V_C^{2\pi}(r) + S_{ij}(\hat{\mathbf{r}}) V_T^{2\pi}(r) \Big] + V^R(r) \,, \tag{7}$$

containing central and tensor two-pion exchange components as well as a central repulsive contribution. For comparison, the averaged microscopic TBF [10] involves five different components:

$$\begin{aligned} \overline{V}_{ij}^{\rm micro}(\mathbf{r}) \;\; = \;\; & (\boldsymbol{\tau}_i \cdot \boldsymbol{\tau}_j)(\boldsymbol{\sigma}_i \cdot \boldsymbol{\sigma}_j) V_C^{\tau\sigma}(r) + (\boldsymbol{\sigma}_i \cdot \boldsymbol{\sigma}_j) V_C^{\sigma}(r) + V_C(r) \\ & + S_{ij}(\hat{\mathbf{r}}) \Big[(\boldsymbol{\tau}_i \cdot \boldsymbol{\tau}_j) V_T^{\tau}(r) + V_T(r) \Big] \,. \end{aligned} \tag{8}$$

In the variational approach the two parameters A and U are determined by fitting the triton binding energy together with the saturation density of nuclear matter (yielding however too little attraction, $E/A \approx -12$ MeV, in the latter case [5]). In the BHF calculations they are instead chosen to reproduce the empirical saturation density together with the binding energy of nuclear matter. The resulting parameter values are $A = -0.0293$ MeV and $U = 0.0048$ MeV in the variational Urbana IX model, whereas for the optimal BHF+TBF calculations we require $A = -0.0333$ MeV and $U = 0.00038$ MeV, yielding a

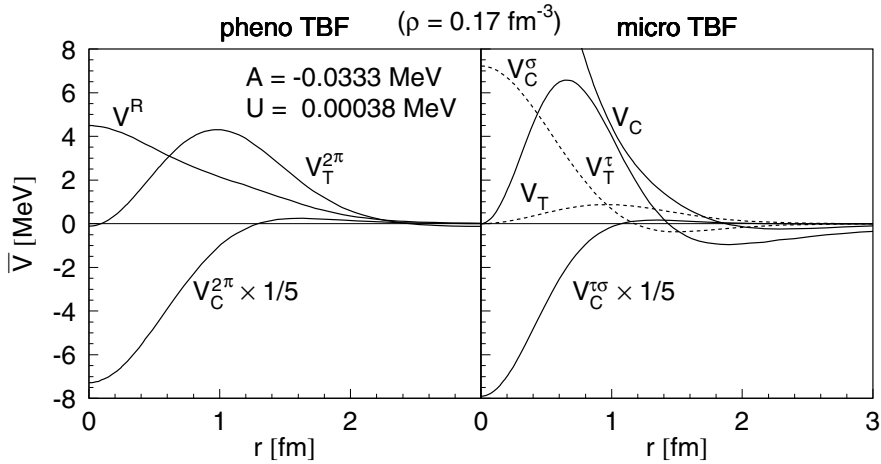

Figure 3. Comparison of the different components of averaged phenomenological and microscopic TBF, Eqs. (7) and (8).

saturation point at $k_F \approx 1.36$ fm^{-1}, $E/A \approx -15.5$ MeV, and an incompressibility $K \approx 210$ MeV.

These values of A and U have been obtained by using the Argonne v_{18} two-body force [20] both in the BHF and in the variational many-body theories. However, the required repulsive component ($\sim U$) is much weaker in the BHF approach, consistent with the observation that in the variational calculations usually heavier nuclei as well as nuclear matter are underbound. Indeed, less repulsive TBF became available recently [21] in order to address this problem.

3. EOS of nuclear matter from different TBF

In Fig. 3 we compare the different components $V_C^{2\pi}, V_T^{2\pi}, V^R$, Eq. (7), and $V_C^{\tau\sigma}, V_C^{\sigma}, V_C, V_T^{\tau}, V_T$, Eq. (8), of the averaged phenomenological and microscopic TBF potentials in symmetric matter at normal density. One notes that the attractive components $V_C^{2\pi}, V_T^{2\pi}$ and $V_C^{\tau\sigma}, V_T^{\tau}$ roughly correspond to each other, whereas the repulsive part (V^R vs. V_C) is much larger for the microscopic TBF. With the choice of parameters A and U given above, one would therefore expect a more repulsive behaviour of the microscopic TBF, which is indeed confirmed in the following.

Let us now confront the EOS predicted by the phenomenological TBF and the microscopic one. In both cases the BHF approximation has been adopted with same two-body force (Argonne v_{18}). In the left panel of Fig. 4 we display the equation of state both for symmetric matter (lower curves) and pure neutron matter (upper curves). We show results obtained for several cases, i.e., i) only two-body forces are included (dotted lines), ii) TBF implemented within the phenomenological Urbana IX model (dashed lines), and iii) TBF treated within

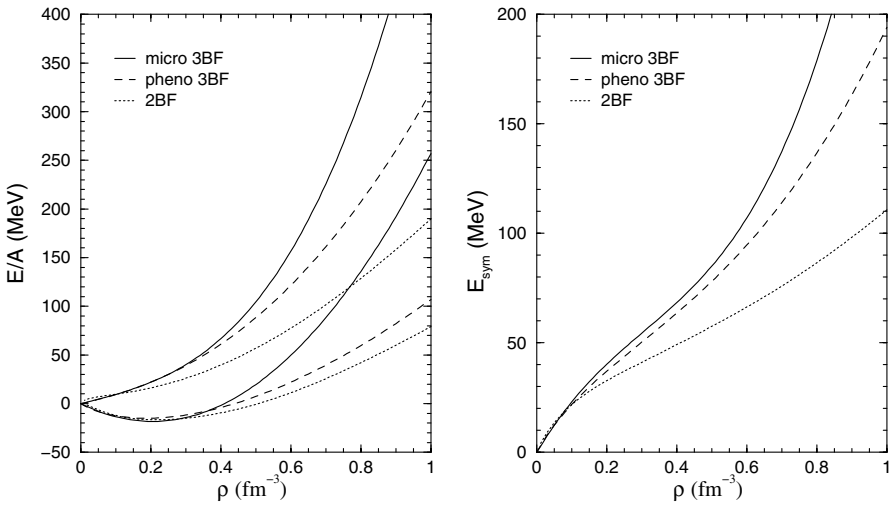

Figure 4. Left plot: Binding energy per nucleon of symmetric nuclear matter (lower curves using a given linestyle) and pure neutron matter (upper curves), employing different TBF. Right plot: Corresponding symmetry energy of nuclear matter.

the microscopic meson-exchange approach (solid lines). We notice that the EOS for symmetric matter with TBF reproduces the correct nuclear matter saturation point. Moreover, the incompressibility turns out to be compatible with the values extracted from phenomenology, i.e., $K \approx 210$ MeV. Up to a density of $\rho \approx 0.4$ fm^{-3} the microscopic and phenomenological TBF are in fair agreement, whereas at higher density the microscopic TBF turn out to be more repulsive.

Within the BHF approach, it has been verified [15, 22] that a parabolic approximation for the binding energy of nuclear matter with arbitrary proton fraction x is well fulfilled,

$$\frac{E}{A}(\rho, x) \approx \frac{E}{A}(\rho, x = 0.5) + (1 - 2x)^2 E_{\rm sym}(\rho) \,, \tag{9}$$

where the symmetry energy $E_{\rm sym}$ can be expressed in terms of the difference of the energy per particle between pure neutron ($x = 0$) and symmetric ($x = 0.5$) matter:

$$E_{\rm sym}(\rho) = -\frac{1}{4}\frac{\partial(E/A)}{\partial x}(\rho, 0) \approx \frac{E}{A}(\rho, 0) - \frac{E}{A}(\rho, 0.5) \,. \tag{10}$$

In the right panel of Fig. 4 we display the symmetry energy as a function of the nucleon density ρ for different choices of the TBF. We observe results in agreement with the characteristics of the EOS shown in the left panel. Namely, the stiffest equation of state, i.e., the one calculated with the microscopic TBF,

yields larger symmetry energies compared to the ones obtained with the Urbana phenomenological TBF. Moreover, the symmetry energy calculated (with or without TBF) at the saturation point yields a value $E_{\rm sym} \approx 30$ MeV, compatible with nuclear phenomenology.

4. Neutron star structure

In order to study the effects of different TBF on neutron star structure, we have to calculate the composition and the EOS of cold, catalyzed matter. We require that the neutron star contains charge neutral matter consisting of neutrons, protons, and leptons (e^-, μ^-) in beta equilibrium. Using the various TBF discussed above, we compute the proton fraction and the EOS for charge neutral and beta-stable matter in the following standard way [23, 24]: The Brueckner calculation yields the energy density of lepton/baryon matter as a function of the different partial densities,

$$\begin{aligned}\epsilon(\rho_n,\rho_p,\rho_e,\rho_\mu) &= (\rho_n m_n + \rho_p m_p) + (\rho_n+\rho_p)\frac{E}{A}(\rho_n,\rho_p) \\ &\quad +\rho_\mu m_\mu + \frac{1}{2m_\mu}\frac{(3\pi^2\rho_\mu)^{5/3}}{5\pi^2} \\ &\quad +\frac{(3\pi^2\rho_e)^{4/3}}{4\pi^2}\,, \end{aligned} \tag{11}$$

where we have used ultrarelativistic and nonrelativistic approximations for the energy densities of electrons and muons, respectively. The various chemical potentials (of the species $i = n,p,e,\mu$) can then be computed straightforwardly,

$$\mu_i = \frac{\partial\epsilon}{\partial\rho_i}\,, \tag{12}$$

and the equations for beta-equilibrium,

$$\mu_i = b_i\mu_n - q_i\mu_e\,, \tag{13}$$

(b_i and q_i denoting baryon number and charge of species i) and charge neutrality,

$$\sum_i \rho_i q_i = 0\,, \tag{14}$$

allow to determine the equilibrium composition $\rho_i(\rho)$ at given baryon density $\rho = \rho_n + \rho_p$ and finally the EOS,

$$p(\rho) = \rho^2\frac{d}{d\rho}\frac{\epsilon(\rho_i(\rho))}{\rho} = \rho\frac{d\epsilon}{d\rho} - \epsilon = \rho\mu_n - \epsilon\,. \tag{15}$$

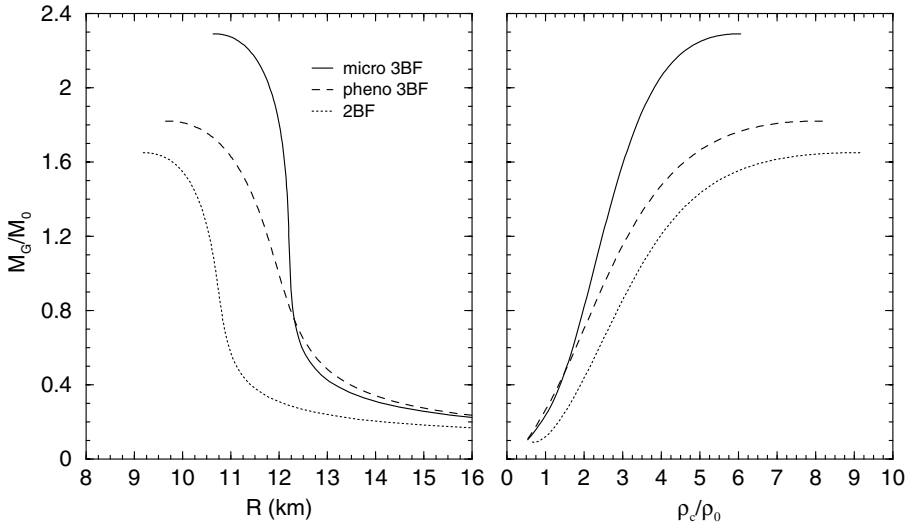

Figure 5. The neutron star gravitational mass (in units of solar mass $M_\odot$) is displayed vs. the radius (left panel) and the normalized central baryon density ρ_c ($\rho_0 = 0.17$ fm^{-3}) (right panel).

In order to calculate the mass-radius relation, one has then to solve the well-known Tolman-Oppenheimer-Volkov equations [23],

$$\frac{dp}{dr} = -\frac{Gm}{r^2}\,\frac{(\epsilon+p)(1+4\pi r^3 p/m)}{1-2Gm/r}\,, \tag{16}$$

$$\frac{dm}{dr} = 4\pi r^2 \epsilon\,, \tag{17}$$

with the newly constructed EOS for the charge neutral and beta-stable case as input (supplemented by the EOS of Feynman-Metropolis-Teller [25], Baym-Pethick-Sutherland [26], and Negele-Vautherin [27] for the outer part of the neutron star, $\rho \lesssim 0.08$ fm^{-3}). The solutions provide information on the interior structure of a star, $\rho(r)$, as well as the mass-radius relation, $M(R)$.

The results are shown in Fig. 5. We notice that the EOS calculated with the microscopic TBF produces the largest gravitational masses, with the maximum mass of the order of 2.3 $\mathrm{M}_\odot$, whereas the phenomenological TBF yields a maximum mass of about 1.8 $\mathrm{M}_\odot$. In the latter case, neutron stars are characterized by smaller radii and larger central densities, i.e., the Urbana TBF produce more compact stellar objects. For completeness, we also show a sequence of stellar configurations obtained using only two-body forces. In this case the maximum mass is slightly above 1.6 $M_\odot$, with a radius of 9 km and a central density equal to 9 times the saturation value.

However, these results should be considered as only provisory, since it is well known that the inclusion of hyperons [15, 16] or quark matter [28] may

strongly affect the structure of the star, in particular reducing substantially the maximum mass. We discuss this point now in detail.

5. Hyperons in nuclear matter

While at moderate densities $\rho \approx \rho_0$ the matter inside a neutron star consists only of nucleons and leptons, at higher densities several other species of particles may appear due to the fast rise of the baryon chemical potentials with density. Among these new particles are strange baryons, namely, the Λ, Σ, and Ξ hyperons. Due to its negative charge, the Σ^- hyperon is the first strange baryon expected to appear with increasing density in the reaction $n + n \rightarrow p + \Sigma^-$, in spite of its substantially larger mass compared to the neutral Λ hyperon ($M_{\Sigma^-} = 1197$ MeV, $M_\Lambda = 1116$ MeV). Other species might appear in stellar matter, like Δ isobars along with pion and kaon condensates. It is therefore mandatory to generalize the study of the nuclear EOS with the inclusion of the possible hadrons, other than nucleons, which can spontaneously appear in the inner part of a neutron star, just because their appearance is able to lower the ground state energy of the nuclear matter dense phase. In the following we will concentrate on the production of strange baryons and assume that a baryonic description of nuclear matter holds up to densities as those encountered in the core of neutron stars.

As we have seen in the previous sections, the nuclear EOS can be calculated with good accuracy in the Brueckner two hole-line approximation with the continuous choice for the single-particle potential, since the results in this scheme are quite close to the full convergent calculations which include also the three hole-line contribution. It is then natural to include the hyperon degrees of freedom within the same approximation to calculate the nuclear EOS needed to describe the neutron star interior. To this purpose, one requires in principle nucleon-hyperon (NY) and hyperon-hyperon (YY) potentials. In our work we use the Nijmegen soft-core NY potential [29] that is well adapted to the available experimental NY scattering data. Unfortunately, up to date no YY scattering data and therefore no reliable YY potentials are available. We therefore neglect these interactions in our calculations, which is supposedly justified, as long as the hyperonic partial densities remain limited. Also, for the following calculations the v_{18} NN potential together with the phenomenological TBF introduced previously, are used.

With the NN and NY potentials, the various G matrices are evaluated by solving numerically the Brueckner equation, which can be written in operatorial form as [13, 15]

$$G_{ab}[W] = V_{ab} + \sum_c \sum_{p,p'} V_{ac} \Big| pp' \Big\rangle \frac{Q_c}{W - E_c + i\epsilon} \Big\langle pp' \Big| G_{cb}[W] \,, \qquad (18)$$

where the indices a, b, c indicate pairs of baryons and the Pauli operator Q and energy E determine the propagation of intermediate baryon pairs. In a given nucleon-hyperon channels $c = (NY)$ one has, for example,

$$E_{(NY)} = m_N + m_Y + \frac{k_N^2}{2m_N} + \frac{k_Y^2}{2m_Y} + U_N(k_N) + U_Y(k_Y)\,. \tag{19}$$

The hyperon single-particle potentials within the continuous choice are given by

$$U_Y(k) = \mathrm{Re} \sum_{N=n,p} \sum_{k'<k_F^{(N)}} \left\langle kk' \middle| G_{(NY)(NY)}\left[E_{(NY)}(k,k')\right] \middle| kk' \right\rangle \tag{20}$$

and similar expressions of the form

$$U_N(k) = \sum_{N'=n,p} U_N^{(N')}(k) + \sum_{Y=\Sigma^-,\Lambda} U_N^{(Y)}(k) \tag{21}$$

apply to the nucleon single-particle potentials. The nucleons feel therefore direct effects of the other nucleons as well as of the hyperons in the environment, whereas for the hyperons there are only nucleonic contributions, because of the missing hyperon-hyperon potentials. The equations (18–21) define the BHF scheme with the continuous choice of the single-particle energies. Due to the occurrence of U_N and U_Y in Eq. (19) they constitute a coupled system that has to be solved in a self-consistent manner. In contrast to the standard purely nucleonic calculation there is now an additional coupled channel structure, which renders a self-consistent calculation quite time-consuming.

Once the different single-particle potentials are known, the total nonrelativistic baryonic energy density, ϵ, can be evaluated:

$$\epsilon = \sum_{i=n,p,\Sigma^-,\Lambda} \int_0^{k_F^{(i)}} \frac{dk\,k^2}{\pi^2} \left[m_i + \frac{k^2}{2m_i} + \frac{1}{2} U_i(k) \right] \tag{22}$$

$$= \epsilon_{NN} + \sum_{Y=\Sigma^-,\Lambda} \int_0^{k_F^{(Y)}} \frac{dk\,k^2}{\pi^2} \left[m_Y + \frac{k^2}{2m_Y} + U_Y^{(n)}(k) + U_Y^{(p)}(k) \right] , \tag{23}$$

where ϵ_{NN} is the nucleonic part of the energy density, Eq. (11). Using for example an effective mass approximation for the hyperon single-particle potentials, one could write the last term due to the nucleon-hyperon interaction as

$$\epsilon_{NY} = \sum_{Y=\Sigma^-,\Lambda} \left(\rho_Y \left[m_Y + U_Y(0) \right] + \frac{1}{2m_Y^*} \frac{(3\pi^2\rho_Y)^{5/3}}{5\pi^2} \right) , \tag{24}$$

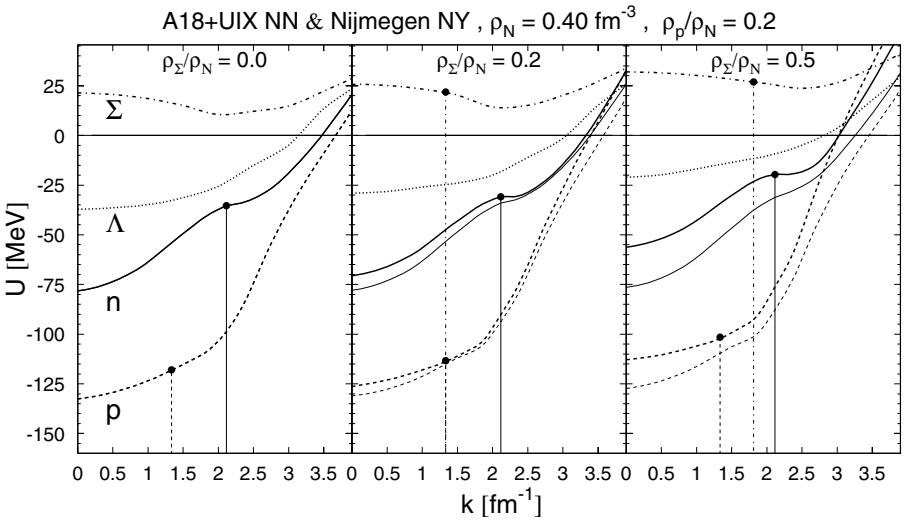

Figure 6. The single-particle potentials of nucleons n, p and hyperons Σ^-, Λ in baryonic matter of fixed nucleonic density $\rho_N = 0.4\,\mathrm{fm}^{-3}$, proton density $\rho_p/\rho_N = 0.2$, and varying Σ^- density $\rho_\Sigma/\rho_N = 0.0, 0.2, 0.5$. The vertical lines represent the corresponding Fermi momenta of n, p, and Σ^-. For the nucleonic curves, the thick lines represent the complete single-particle potentials U_N, whereas the thin lines show the values excluding the Σ^- contribution, i.e., $U_N^{(n)} + U_N^{(p)}$.

which should be added to Eq. (11).

The different single-particle potentials involved in the previous equations are illustrated in Fig. 6, where neutron and proton densities are fixed, given by $\rho_N = 0.4\,\mathrm{fm}^{-3}$ and $\rho_p/\rho_N = 0.2$, and the Σ^- density is varied. Under these conditions the Σ^- single-particle potential is sizeably repulsive, while U_Λ is still attractive (see also Ref. [15]) and the nucleons are both strongly bound. The Σ^- single-particle potential has a particular shape with an effective mass m^*/m close to 1, whereas the
$Lambda$ effective mass is typically about 0.8 and the nucleon effective masses are much smaller.

The knowledge of the energy density allows then to compute EOS and neutron star structure as described before, now making allowance for the species $i = n, p, \Sigma^-,$
$Lambda, e^-, \mu^-$. The main physical features of the nuclear EOS which determine the resulting compositions are essentially the symmetry energy of the nucleon part of the EOS and the hyperon single-particle potentials inside nuclear matter. Since at low enough density the nucleon matter is quite asymmetric,

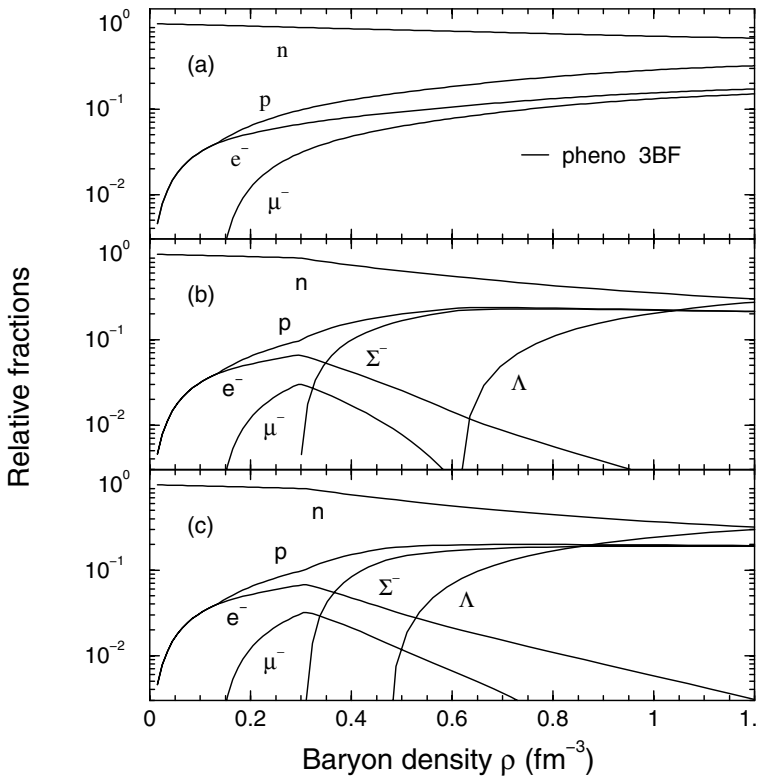

Figure 7. The equilibrium composition of asymmetric and β-stable nuclear matter comprising (a) only nucleons, (b) noninteracting hyperons, (c) interacting hyperons.

the small percentage of protons feel a deep single-particle potential, and therefore it is energetically convenient to create a Σ^- hyperon, since then a neutron can be converted into a proton. The depth of the proton potential is mainly determined by the nuclear matter symmetry energy. Furthermore, the potentials felt by the hyperons can shift substantially the threshold density at which each hyperon sets in.

In Fig. 7 we show the chemical composition of the resulting β-stable and asymmetric nuclear matter containing hyperons. We observe rather low hyperon onset densities of about 2-3 times normal nuclear matter density for the appearance of the Σ^- and
$Lambda$ hyperons. (Other hyperons do not appear in the matter). Moreover, an almost equal percentage of nucleons and hyperons are present in the stellar core at high densities. A strong deleptonization of matter takes place, since it is energetically convenient to maintain charge neutrality through hyperon formation rather than β-decay. This can have far reaching consequences for the onset of kaon condensation.

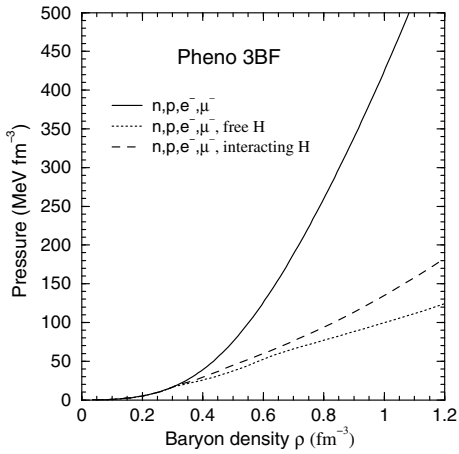

Figure 8. The EOS for hyperon-free (solid line) and hyperon-rich (dashed lines) matter.

The resulting EOS is displayed in Fig. 8. The upper curves show the EOS when stellar matter is composed only of nucleons and leptons. The inclusion of hyperons (lower curves) produces a much softer EOS, which turns out to be very similar to the one obtained without TBF. This is quite astonishing because, in the pure nucleon case, the repulsive character of TBF at high density increases the stiffness of the EOS, thus changing dramatically the equation of state. However, when hyperons are included, the presence of TBF among nucleons enhances the population of Σ^- and Λ because of the increased nucleon chemical potentials with respect to the case without TBF, thus decreasing the nucleon population. Of course, this scenario could partly change if hyperon-hyperon interactions were known or if TBF would be included also for hyperons, but this is beyond our current knowledge of the strong interaction.

The consequences for the structure of the neutron stars are illustrated in Fig. 9, where we display the resulting neutron star mass-radius curves, comparing now results obtained with different nucleonic TBF, in analogy to Fig. 5. One notes that while in Fig. 5 the different TBF still yield quite different maximum masses, the presence of hyperons equalizes the results, leading now to a maximum mass of less than 1.3 solar masses for all the nuclear TBF.

This surprising result is due to the strong softening of the baryonic EOS when including hyperons as additional degrees of freedom, and we do not expect substantial changes when introducing refinements of the theoretical framework, such as hyperon-hyperon potentials, hyperonic TBF, relativistic corrections, etc. The only remaining possibility in order to reach larger maximum masses appears the transition to another phase of dense (quark) matter inside the star. This will be discussed in the following.

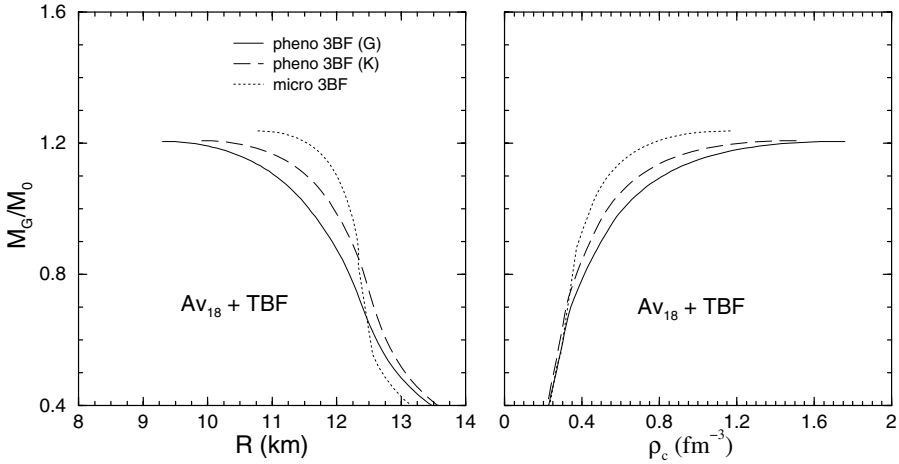

Figure 9. Neutron star gravitational mass vs. radius (left panel) and the central baryon density ρ_c (right panel). Calculations involving different nucleonic TBF are compared.

6. Quark matter

The results obtained with a purely baryonic EOS call for an estimate of the effects due to the hypothetical presence of quark matter in the interior of the neutron star. Unfortunately, the current theoretical description of quark matter is burdened with large uncertainties, seriously limiting the predictive power of any theoretical approach at high baryonic density. For the time being we can therefore only resort to phenomenological models for the quark matter EOS and try to constrain them as well as possible by the few experimental information on high density baryonic matter.

One important condition is constituted by the fact that certainly in symmetric nuclear matter no phase transition is observed below $\approx 3\rho_0$. In fact some theoretical interpretation of the heavy ion experiments performed at the CERN SPS [30] points to a possible phase transition at a critical density $\rho_c \approx 6\rho_0 \approx 1/\mathrm{fm}^3$. We will in the following take this value for granted and use an extended MIT bag model [31] (requiring a density dependent bag "constant") that is compatible with this condition.

We first review briefly the description of the bulk properties of uniform quark matter, deconfined from the β-stable hadronic matter mentioned in the previous section, by using the MIT bag model [31]. The thermodynamic potential of $f = u, d, s$ quarks can be expressed as a sum of the kinetic term and the one-gluon-exchange term [32, 33] proportional to the QCD fine structure

constant α_s,

$$\begin{aligned}\Omega_f(\mu_f) &= -\frac{3m_f^4}{8\pi^2}\left[\frac{y_f x_f}{3}\left(2x_f^2-3\right)+\ln(x_f+y_f)\right] \\ &\quad +\alpha_s\frac{3m_f^4}{2\pi^3}\left\{\left[y_f x_f-\ln(x_f+y_f)\right]^2-\frac{2}{3}x_f^4+\ln(y_f)\right. \\ &\quad \left.+2\ln\left(\frac{\sigma_{\rm ren}}{m_f y_f}\right)\left[y_f x_f-\ln(x_f+y_f)\right]\right\}, \qquad (25)\end{aligned}$$

where m_f and μ_f are the f current quark mass and chemical potential, respectively, $y_f = \mu_f/m_f$, $x_f = \sqrt{y_f^2-1}$, and $\sigma_{\rm ren}$ = 313 MeV is the renormalization point. The number density ρ_f of f quarks is related to Ω_f via

$$\rho_f = -\frac{\partial\Omega_f}{\partial\mu_f}\,, \qquad (26)$$

and the total energy density for the quark system is written as

$$\epsilon_Q(\rho_u,\rho_d,\rho_s) = \sum_f\left(\Omega_f+\mu_f\rho_f\right)+B\,, \qquad (27)$$

where B is the energy density difference between the perturbative vacuum and the true vacuum, i.e., the bag "constant."

In the original MIT bag model the bag constant $B \approx 55\ \mathrm{MeV\,fm^{-3}}$ is used, while values $B \approx 210\ \mathrm{MeV\,fm^{-3}}$ are estimated from lattice calculations [34]. In this sense B can be considered as a free parameter. We found, however, that a bag model involving a constant (density independent) bag parameter B, combined with our BHF hadronic EOS, will not yield the required phase transition in symmetric matter at $\rho_c \approx 6\rho_0 \approx 1/\mathrm{fm}^3$ [28]. This can only be accomplished by introducing a density dependence of the bag parameter. (The dependence on asymmetry is neglected at the current level of investigation). In practice we use a Gaussian parameterization,

$$B(\rho) = B_\infty + (B_0 - B_\infty)\exp\left[-\beta\Big(\frac{\rho}{\rho_0}\Big)^2\right] \qquad (28)$$

with $B_\infty = 50\ \mathrm{MeV\,fm^{-3}}$, $B_0 = 400\ \mathrm{MeV\,fm^{-3}}$, and $\beta = 0.17$, displayed in Fig. 10(a).

For the description of a pure quark phase inside the neutron star, as for neutrino-free baryonic matter, the equilibrium equations for the chemical potentials,

$$\mu_d = \mu_s = \mu_u + \mu_e\,, \qquad (29)$$

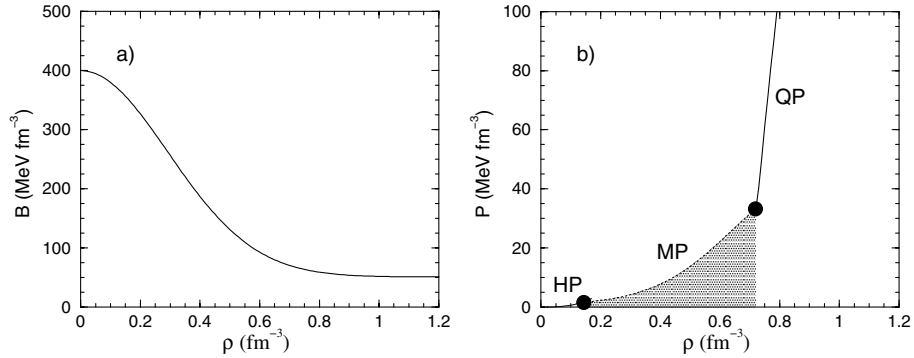

Figure 10. (a) Bag constant B versus baryon number density. (b) EOS including both hadronic and quark components. The shaded region, bordered by two dots, indicates the mixed phase (MP) of quarks and hadrons, while HP and QP label the pure hadron and quark phases.

must be supplemented with the charge neutrality condition and the total baryon number conservation,

$$0 = \frac{1}{3}(2\rho_u - \rho_d - \rho_s) - \rho_e \,, \tag{30}$$

$$\rho = \frac{1}{3}(\rho_u + \rho_d + \rho_s) \,, \tag{31}$$

in order to determine the composition $\rho_f(\rho)$ and the pressure of the quark phase,

$$P_Q(\rho) = \rho \frac{d\epsilon_Q}{d\rho} - \epsilon_Q \,. \tag{32}$$

However, a more realistic model for the phase transition between baryonic and quark phase inside the star is the Glendenning construction [16], which determines the range of baryon density where both phases coexist. The essential point of this procedure is that both the hadron and the quark phase are allowed to be separately charged, still preserving the total charge neutrality. This implies that neutron star matter can be treated as a two-component system, and therefore can be parametrized by two chemical potentials like electron and baryon chemical potentials μ_e and μ_n. The pressure is the same in the two phases to ensure mechanical stability, while the chemical potentials of the different species are related to each other satisfying chemical and beta stability. The Gibbs condition for mechanical and chemical equilibrium at zero temperature between both phases reads

$$p_H(\mu_e, \mu_n) = p_Q(\mu_e, \mu_n) = p_M(\mu_n) \,. \tag{33}$$

From the intersection of the two surfaces representing the hadron and the quark phase one can calculate the equilibrium chemical potentials of the mixed phase,

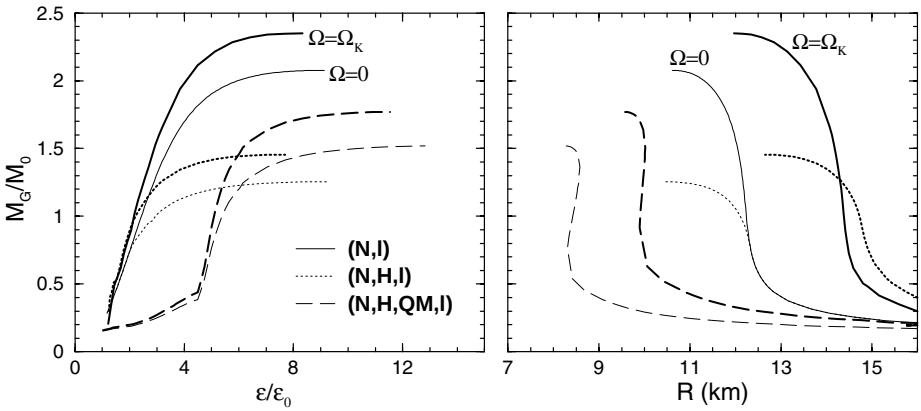

Figure 11. The gravitational mass (in units of the solar mass $M_\odot$) versus the normalized central energy density ($\epsilon_0 = 156$ MeV fm^{-3}) (left panel) and versus the equatorial radius (right panel). The thin lines represent static equilibrium configurations, whereas the thick lines display configurations rotating at their respective Kepler frequencies. Several different stellar matter compositions are considered (see text for details).

as well as the charge densities ρ_c^H and ρ_c^Q and therefore the volume fraction χ occupied by quark matter in the mixed phase,

$$\chi = \frac{\rho_c^H}{\rho_c^H - \rho_c^Q} \,. \tag{34}$$

From this, the baryon density ρ_M and the energy density ϵ_M of the mixed phase can be calculated as

$$\rho_M = \chi\rho_Q + (1-\chi)\rho_H \,, \tag{35}$$

$$\epsilon_M = \chi\epsilon_Q + (1-\chi)\epsilon_H \,. \tag{36}$$

The EOS resulting from this procedure is shown in Fig. 10(b), where the pure hadron, mixed, and pure quark matter portions are indicated. The mixed phase begins actually at a quite low density around ρ_0. Clearly the outcome of the mixed phase construction might be substantially changed, if surface and Coulomb energies were taken into account [36]. For the time being these are, however, unknown and have been neglected.

The final result for the structure of hybrid neutron stars is shown in Fig. 11, displaying mass-radius and mass-central density relations. It is evident that the most striking effect of the inclusion of quark matter is the increase of the maximum mass, now reaching about $1.5\ M_\odot$. At the same time, the typical neutron star radius is reduced by about 3 km to typically 9 km. Hybrid neutron stars are thus more compact than purely hadronic ones and their central energy density is larger. For completeness, the figure shows besides static neutron star

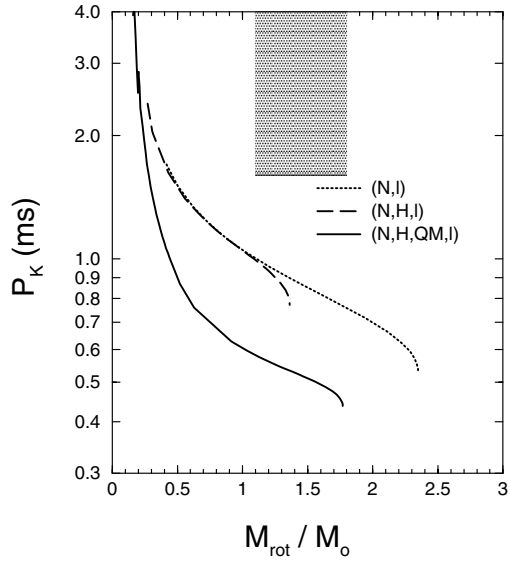

Figure 12. Kepler period versus the rotational mass for purely hadronic stars as well as hybrid stars. The following core compositions are considered: i) nucleons and leptons (dotted line); ii) nucleons, hyperons, and leptons (dashed line); iii) hadrons, quarks, and leptons (solid line). The shaded area represents the current range of observed data.

configurations also those rotating at the maximum (Kepler) frequency [37]. In that case one observes a further enhancement of the maximum mass to about $1.8\ M_\odot$, and an increase of the typical equatorial radius by about 1 km.

Finally, in Fig. 12 we display the Kepler periods P_K ($= 2\pi/\Omega_K$) versus the rotational star mass for several different stellar sequences based on different EOS. Purely hadronic stars, shown by the dotted and long-dashed lines respectively, show instability against mass shedding first, because of their relatively large equatorial radii. Their limiting mass configurations are characterized by values of the Kepler period larger than half a millisecond, in agreement with results usually found in the literature [38]. In contrast, hybrid stars can reach stable periods smaller than half a millisecond.

7. Conclusions

In this contribution we reported the theoretical description of nuclear matter in the BHF approach and its various refinements, with the application to neutron star structure calculation. We pointed out the important role of TBF at high density, which is, however, strongly compensated by the inclusion of hyperons. The resulting hadronic neutron star configurations have maximum masses of only about $1.3\,M_\odot$, and the presence of quark matter inside the star is required in order to reach larger values.

Concerning the quark matter EOS, we found that a density dependent bag parameter $B(\rho)$ is necessary in order to be compatible with the CERN-SPS findings on the phase transition from hadronic to quark matter. Joining the corresponding EOS with the baryonic one, maximum masses of about $1.6\ M_\odot$ are reached, in line with other recent calculations of neutron star properties employing various phenomenological RMF nuclear EOS together with either effective mass bag model [39] or Nambu-Jona-Lasinio model [40] EOS for quark matter.

The value of the maximum mass of neutron stars obtained according to our analysis appears rather robust with respect to the uncertainties of the nuclear and the quark matter EOS. Therefore, the experimental observation of a very heavy ($M \gtrsim 1.6 M_\odot$) neutron star, as claimed recently by some groups [41] ($M \approx 2.2\ M_\odot$), if confirmed, would suggest that either serious problems are present for the current theoretical modelling of the high-density phase of nuclear matter, or that the assumptions about the phase transition between hadron and quark phase are substantially wrong. In both cases, one can expect a well defined hint on the high density nuclear matter EOS.

We would like to thank our collaborators J. Cugnon, A. Lejeune, U. Lombardo, F. Mathiot, P.K. Sahu, F. Weber, X.R. Zhou, and W. Zuo.

References

[1] P. Bonche, E. Chabanat, P. Haensel, J. Meyer, and R. Schaeffer, Nucl. Phys. **A643**, 441 (1998).

[2] B. D. Serot and J. D. Walecka, Adv. Nucl. Phys. **16**, 1 (1986).

[3] M. Baldo, *The many body theory of the nuclear equation of state* in Nuclear Methods and the Nuclear Equation of State, 1999, Ed. M. Baldo, World Scientific, Singapore.

[4] R. Machleidt, Adv. Nucl. Phys. **19**, 189 (1989) and references quoted therein; G. Q. Li, R. Machleidt, and R. Brockmann, Phys. Rev. **C45**, 2782 (1992).

[5] A. Akmal and V. R. Pandharipande, Phys. Rev. **C56**, 2261 (1997); A. Akmal, V. R. Pandharipande, and D. G. Ravenhall, Phys. Rev. **C58**, 1804 (1998); J. Morales, V. R. Pandharipande, and D. G. Ravenhall, Phys. Rev. **C66**, 054308 (2002).

[6] N. Kaiser, S. Fritsch, and W. Weise, Nucl. Phys. **A697**, 255 (2002).

[7] N. K. Glendenning, Nucl. Phys. **A493**, 521 (1989); *Compact Stars, Nuclear Physics, Particle Physics, and General Relativity*, 2nd ed., 2000, Springer-Verlag, New York.

[8] H. Q. Song, M. Baldo, G. Giansiracusa, and U. Lombardo, Phys. Rev. Lett. **81**, 1584 (1998).

[9] M. Baldo, A. Fiasconaro, H. Q. Song, G. Giansiracusa, and U. Lombardo, Phys. Rev. **C65**, 017303 (2002).

[10] P. Grangé, A. Lejeune, M. Martzolff, and J.-F. Mathiot, Phys. Rev. **C40**, 1040 (1989).

[11] S. A. Coon, M. D. Scadron, P. C. McNamee, B. R. Barrett, D. W. E. Blatt, and B. H. J. McKellar, Nucl. Phys. **A317**, 242 (1979).

[12] A. Lejeune, U. Lombardo, and W. Zuo, Phys. Lett. **B477**, 45 (2000); W. Zuo, A. Lejeune, U. Lombardo, and J.-F. Mathiot, Nucl. Phys. **A706**, 418 (2002); Eur. Phys. Journ. **A14**, 469 (2002).

[13] H.-J. Schulze, A. Lejeune, J. Cugnon, M. Baldo, and U. Lombardo, Phys. Lett. **B355**, 21 (1995); Phys. Rev. **C57**, 704 (1998).

[14] J. Cugnon, A. Lejeune, and H.-J. Schulze, Phys. Rev. **C62**, 064308 (2000); I. Vidaña, A. Polls, A. Ramos, and H.-J. Schulze, Phys. Rev. **C64**, 044301 (2001).

[15] M. Baldo, G. F. Burgio, and H.-J. Schulze, Phys. Rev. **C58**, 3688 (1998); Phys. Rev. **C61**, 055801 (2000).

[16] I. Vidaña, A. Polls, A. Ramos, L. Engvik, and M. Hjorth-Jensen, Phys. Rev. **C62**, 035801 (2000).

[17] G. E. Brown et al., Comm. Nucl. Part. Phys. **17**, 39 (1987).

[18] W. Zuo, Caiwan Shen, and U. Lombardo, Phys. Rev. **C67**, 037301 (2003).

[19] B. S. Pudliner, V. R. Pandharipande, J. Carlson, and R. B. Wiringa, Phys. Rev. Lett. **74**, 4396 (1995).

[20] R. B. Wiringa, V. G. J. Stoks, and R. Schiavilla, Phys. Rev. **C51**, 38 (1995).

[21] S. C. Pieper, V. R. Pandharipande, R. B. Wiringa, and J. Carlson, Phys. Rev. **C64**, 014001 (2001).

[22] A. Lejeune, P. Grangé, M. Martzolff, and J. Cugnon, Nucl. Phys. **A453**, 189 (1986); I. Bombaci and U. Lombardo, Phys. Rev. **C44**, 1892 (1991); W. Zuo, I. Bombaci, and U. Lombardo, Phys. Rev. **C60**, 024605 (1999).

[23] S. Shapiro and S. A. Teukolsky, *Black Holes, White Dwarfs, and Neutron Stars*, 1983, ed. John Wiley & Sons, New York.

[24] M. Baldo, I. Bombaci, and G. F. Burgio, Astron. Astroph. **328**, 274 (1997).

[25] R. Feynman, F. Metropolis, and E. Teller, Phys. Rev. **C75**, 1561 (1949).

[26] G. Baym, C. Pethick, and D. Sutherland, Astrophys. J. **170**, 299 (1971).

[27] J. W. Negele and D. Vautherin, Nucl. Phys. **A207**, 298 (1973).

[28] G. F. Burgio, M. Baldo, P. K. Sahu, A. B. Santra, and H.-J. Schulze, Phys. Lett. **B526**, 19 (2002); G. F. Burgio, M. Baldo, P. K. Sahu, and H.-J. Schulze, Phys. Rev. **C66**, 025802 (2002); M. Baldo, M. Buballa, G. F. Burgio, F. Neumann, M. Oertel, and H.-J. Schulze, Phys. Lett. **B562**, 153 (2003).

[29] P. Maessen, Th. Rijken, and J. de Swart, Phys. Rev. **C40**, 2226 (1989).

[30] U. Heinz and M. Jacobs, nucl-th/0002042; U. Heinz, Nucl. Phys. **A685**, 414 (2001).

[31] A. Chodos, R. L. Jaffe, K. Johnson, C. B. Thorn, and V. F. Weisskopf, Phys. Rev. **D9**, 3471 (1974).

[32] E. Witten, Phys. Rev. **D30**, 272 (1984); G. Baym, E. W. Kolb, L. McLerran, T. P. Walker, and R. L. Jaffe, Phys. Lett. **B160**, 181 (1985); N. K. Glendenning, Mod. Phys. Lett. **A5**, 2197 (1990).

[33] E. Fahri and R. L. Jaffe, Phys. Rev. **D30**, 2379 (1984).

[34] H. Satz, Phys. Rep. **89**, 349 (1982).

[35] N. K. Glendenning, Phys. Rev. **D46**, 1274 (1992).

[36] T. Tatsumi, M. Yasuhira, and D. N. Voskresensky, Nucl. Phys. **A718**, 359 (2003); **A723**, 291 (2003); D. N. Voskresensky, these proceedings.

[37] G. F. Burgio, H.-J. Schulze, and F. Weber, Astron. Astrophys. **408**, 675 (2003).

[38] F. Weber, *Pulsars as Astrophysical Laboratories for Nuclear and Particle Physics*, Institute of Physics Publishing, Bristol and Philadelphia (1999); F. Weber, J. Phys. G: Nucl. Part. Phys. **25**, R195 (1999).

[39] K. Schertler, C. Greiner, P. K. Sahu and M. H. Thoma, Nucl. Phys. **A637**, 451 (1998); K. Schertler, C. Greiner, J. Schaffner-Bielich, and M. H. Thoma, Nucl. Phys. **A677**, 463 (2000).

[40] K. Schertler, S. Leupold, and J. Schaffner-Bielich, Phys. Rev. **C60**, 025801 (1999).

[41] P. Kaaret, E. Ford, and K. Chen, Astrophys. J. Lett. **480**, L27 (1997); W. Zhang, A. P. Smale, T. E. Strohmayer, and J. H. Swank, Astrophys. J. Lett. **500**, L171 (1998).

THE QCD EQUATION OF STATE AND QUARK STAR PROPERTIES

A. Peshier*
Institut für Theoretische Physik, University Giessen, 35392 Giessen, Germany
Andre.Peshier@theo.physik.uni-giessen.de

B. Kämpfer
Forschungszentrum Rossendorf, PF 510119, 01314 Dresden, Germany
B.Kaempfer@fz-rossendorf.de

G. Soff
Institut für Theoretische Physik, TU Dresden, 01062 Dresden, Germany
soff@physik.tu-dresden.de

Abstract We review our quasiparticle model for the thermodynamics of strongly interacting matter at high temperature, and its extrapolation to non-zero chemical potential. Some implications of the resulting soft equation of state of quark matter at low temperatures are pointed out.

Keywords: QCD equation of state, quasiparticles, quark stars

1. Introduction

The question for the equation of state of strongly interacting matter is a link between many-particle physics and astrophysics/cosmology. Calculated by means of statistical quantum field theory, it serves as a necessary input, e. g., in models of the early universe, or in the context considered here, it determines the structure of stars.

Astrophysical observations, such as the mass and the radius of dense stars, may in turn also impose constraints on the equation of state of deconfined quark matter.

*Talk given at *Superdense QCD Matter and Compact Stars*, 27 September - 4 October 2003, Yerevan, Armenia

D. Blaschke and D. Sedrakian (eds.), Superdense QCD Matter and Compact Stars, 135–146.

We will focus on static spherically symmetric stars which are described by the Tolman-Oppenheimer-Volkov equations. At low densities, up to a few times nuclear density n_0, matter consists of interacting hadrons. Theoretical models for this state have to start from various assumptions, as for the included states and their interactions. Naturally, the results for the hadronic equation of state become notably model dependent at densities exceeding approximately $2n_0$. This is reflected in uncertainties of the predictions for the shell structure of neutron stars, cf. [18].

At some higher energy density, hadronic matter undergoes a phase transition or a crossover to a quark-gluon plasma (at high temperatures), or a color-superconducting state (at low temperatures). Then the system can be described directly in terms of the fundamental degrees of freedom – quarks and gluons. Notwithstanding, the coupling strength is still large in the regime of physical interest, and perturbative QCD is not reliable or, at least, the calculations have to be interpreted very carefully. Calculations based on various effective theories, on the other hand, rest again on assumptions which seem hard to control a priori.

Non-perturbative results have been obtained from first principles by lattice QCD computations at zero chemical potential and temperatures up to a few times the transition temperature T_c.

At low temperatures and for non-zero chemical potential μ, as relevant for dense stars, Monte-Carlo calculations are, however, hampered by the sign problem. Several approaches to cope with it have been proposed only recently.

The available results still have rather large uncertainties, and they do not yet cover the range of temperatures and chemical potential required in the present context.

This makes worthwhile an approach which extrapolates, with as few assumptions as possible, lattice QCD data from zero chemical potential to $\mu > 0$.

In the following we will outline a thermodynamical quasiparticle model, which can be derived in a series of approximations.

2. Resummation and quasiparticle models

2.1 ϕ^4 theory

For the sake of simplicity we consider, for the moment being, a macroscopic system described by a scalar field theory.

Following [2], the thermodynamic potential, $\Omega = -pV$, can be calculated from a functional of the full propagator $\Delta = (\Delta_0^{-1} - \Pi)^{-1}$,

$$\Omega = \tfrac{1}{2} \sum\!\!\!\!\!\!\int \Big(\ln(-\Delta^{-1}) + \Pi\Delta \Big) - \Phi[\Delta]\,, \tag{1}$$

evaluated at the stationary point $\delta\Omega/\delta\Delta = 0$. This corresponds to a self-consistent calculation of the self-energy, $\Pi = 2\delta\Phi/\delta\Delta$, where Φ is the series of 2-particle irreducible diagrams.

In this scheme, thermodynamically self-consistent approximations [3] can be derived by truncating the expansion of Φ, which amounts to a resummation of whole classes of diagrams in perturbation theory.

To leading order, for the massless case and in the $\overline{MS}$ scheme in $4 - 2\epsilon$ dimensions,

Φ = 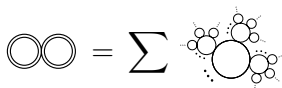 = $\sum$

$$\Pi = \frac{-g_0^2}{4!} \left[\frac{\Pi}{16\pi^2} \left(\frac{1}{\epsilon} + \ln \frac{\bar{\mu}^2}{\Pi} + 1 \right) - \int \frac{d^3k}{(2\pi)^3} \frac{n_b(\omega/T)}{\omega} \right], \tag{2}$$

where $n_b(x) = (e^x - 1)^{-1}$ and $\omega = (k^2 + \Pi)^{1/2}$, the self-energy is simply a mass term.

The non-perturbative gap equation requires the renormalization of the bare coupling g_0. The resummation of the set of 'chain' graphs yields for the coupling at the scale of Mandelstam s

$$g^2(s) = g_0^2 - \frac{g_0^2}{4!} \frac{3}{4\pi^2} \left[\frac{1}{\epsilon} + \ln \frac{\bar{\mu}^2}{-s} + 2 \right] g^2(s)\,. \tag{3}$$

Expressing now g_0 by $g(s)$ leads to the well-defined relation

$$\Pi = \frac{g^2(s)}{2} \left[\frac{\Pi}{16\pi^2} \left(\ln \frac{\Pi}{-s} + 1 \right) + \int_{k^3} \frac{n_b(\omega/T)}{\omega} \right], \tag{4}$$

whose solution is interpreted as a temperature dependent quasiparticle mass squared. The corresponding pressure reads

$$p = -T \int_{k^3} \ln \left(1 - \mathrm{e}^{-\omega/T} \right) + \frac{\Pi}{4} \int_{k^3} \frac{n_b(\omega/T)}{\omega} + \frac{\Pi^2}{128\pi^2}\,. \tag{5}$$

For both calculational details as well as for a discussion of this approximation and its relation to other approaches we refer to [4]; here we only emphasize its structure. The first term on the rhs is simply the pressure of free massive particles. Written in the form $p = p^{\mathrm{id}}(T, m) - B(T)$, the function B is related to $m(T)$ such that the entropy $s = \partial p/\partial T$ reduces, due to the stationarity of Ω, to the entropy $s^{\mathrm{id}}(T, m)$ of an ideal gas.

2.2 QCD at finite temperature

HTL quasiparticle model. In QCD, the truncation of a resummation scheme based on 2-point functions is delicate because of gauge invariance.

However, it can be argued that appropriate approximate solutions of the Schwinger-Dyson equations can yield reasonable approximations for Ω, or the pressure, see the schematic Figure 1.

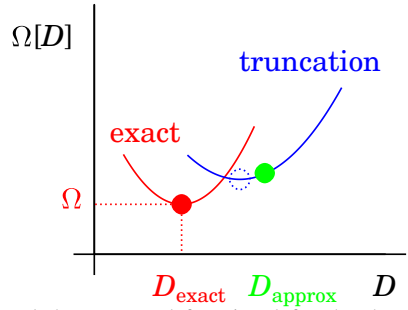

Figure 1. The exact and the truncated functional for the thermodynamic potential. For the latter, a propagator 'near' to the stationary point (which may be unphysical) can give a physically reasonable approximation.

Putting this to a test, we consider the representative case of the pure gauge plasma,

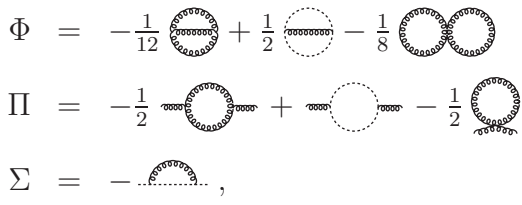

(6)

where the traces are taken over the group indices and the 4-momentum, and $\Sigma = G_0^{-1} - G^{-1}$ is the ghost self-energy. The propagators can be approximated by the hard thermal loop (HTL) contributions, which are gauge invariant and have the correct limit for hard momenta near the light cone. The resulting approximation for the pressure [5], in condensed form

$$p_g^\star = -\tfrac{1}{2}\,\mathrm{Tr}\left[\ln(-D_\star^{-1}) + \tfrac{1}{2}\,D_\star \Pi^\star\right] + \mathrm{Tr}[\ln(-G_0^{-1})]\,, \tag{7}$$

has similar properties as the corresponding expression in the scalar theory. With the standard 2-loop running coupling, it agrees with the lattice data for temperatures down to $3T_c$, see Figure 2,

which is a noteworthy improvement compared to the perturbative results.

Similar results have been obtained by calculating directly the HTL-resumed entropy [7].

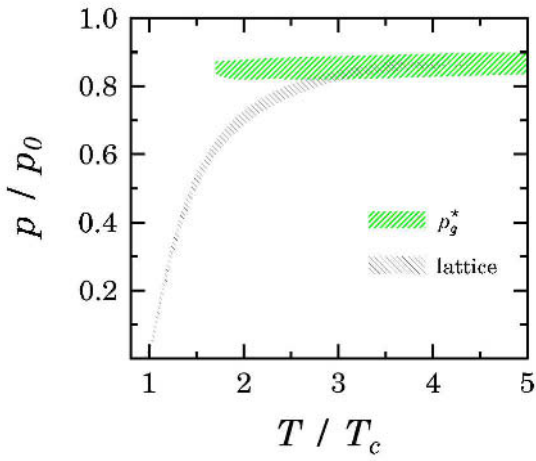

Figure 2. Comparison of the pressure, in units of the free pressure, of the SU(3) plasma from the HTL quasiparticle approximation (7) vs. lattice data [6].

Phenomenological quasiparticle model. Taking into account only the dominant contributions in (7), namely the quasiparticle contributions of the transverse gluons as well as the quark particle-excitations for $N_f \neq 0$, we arrive at the quasiparticle model [8]. The dispersion relations can be even further simplified by their form at hard momenta, $\omega_i^2 = k^2 + m_i^2$, where $m_i \sim gT$ are the asymptotic masses. With this approximation of the self-energies, the pressure reads in analogy to the scalar case

$$p(T) = \sum_i p^{\mathrm{id}}(T, m_i) - B(T)\,. \tag{8}$$

Conceding an enhancement of the running coupling in the infrared, parameterized by $T_s > 0$ in an ansatz compatible with the perturbative limit,

$$g^2(T) = \frac{48\pi^2}{(11N_c - 2\,N_f)\ln\left(\frac{T-T_s}{T_c/\lambda}\right)^2}\,, \tag{9}$$

the thermodynamic lattice data can be quantitatively described even down to T_c, for an example see Figure 3.

The coupling $g(T)$ obtained from available lattice QCD data with a given number of flavors will be an input for the extrapolation to non-zero chemical potential, as outlined in the following.

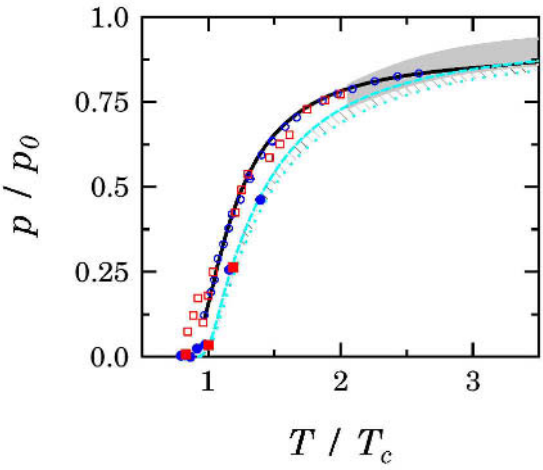

Figure 3. The quasiparticle fit (solid line) of the lattice data [9] (open symbols) for the pressure in QCD with $N_f = 2$ light flavors. The full symbols, representing data with large quark masses, agree with the results for the pure SU(3) plasma (hatched band); for details see [10].

2.3 Non-zero chemical potential

The phenomenological quasiparticle model can be generalized to non-zero chemical potential, where the quasiparticle masses of the gluons and quarks read

$$\begin{aligned} m_g^2 &= \frac{1}{6}\left[\left(N_c + \tfrac{1}{2}\,N_f\right)T^2 + \frac{3}{2\pi^2}\sum_q \mu_q^2\right] g^2 \\ m_q^2 &= \frac{N_c^2-1}{8N_c}\left[T^2 + \frac{\mu_q^2}{\pi^2}\right] g^2\,, \end{aligned} \tag{10}$$

and the pressure, analogous to Equation (8), now depends also on μ.

The predictive power of the approach becomes obvious by noting that the dependence of the coupling on T and μ is completely governed by the requirement of thermodynamic consistency [11]: Maxwell's relation,

$$\frac{\partial s(T,\mu,m_i)}{\partial \mu} = \frac{\partial n(T,\mu,m_i)}{\partial T}\,,$$

where $n = \partial p/\partial\mu$ is the particle density, implies

$$a_\mu(\mu,T,g^2)\frac{\partial g^2}{\partial \mu} + a_T(\mu,T,g^2)\frac{\partial g^2}{\partial T} = b(\mu,T,g^2)\,. \tag{11}$$

While nonlinear in g^2 (the coefficients $a_{\mu,T}$ and b are lengthy integral expressions), the partial differential equation is linear in the derivatives. It can thus be solved by the method of characteristics, with the boundary conditions given by the coupling at $\mu = 0$, as obtained from finite-T lattice QCD.

The resulting elliptic flow shown in Figure 4, which maps the

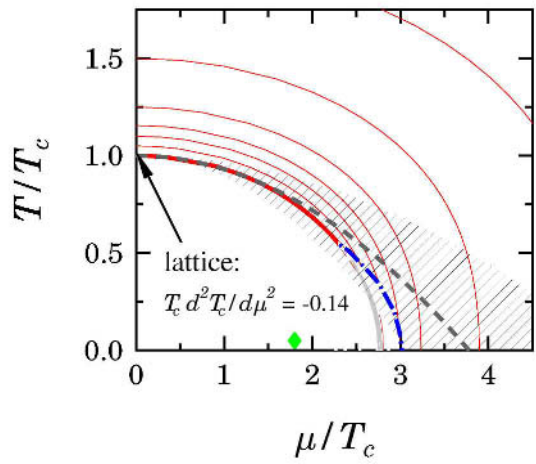

Figure 4. The characteristics of the flow equation (11) for $N_f = 2$ light flavors. The innermost characteristic line coincides with the prediction from lattice QCD [13] for the critical line at small μ, which is represented by the dashed line with the hatched error band.

equation of state from $\mu = 0$ to $\mu > 0$, is plausible from the physical intuition.

In the perturbative limit, $T \to c\mu/\pi$ with $c = (\frac{4N_c+5N_f}{9N_f})^{-1/4} \approx 1$.

It is noteworthy that the correspondence $T \sim \mu/\pi$ holds with a good accuracy even when g is not small. A similar observation was made in the HTL quasiparticle approach [12].

The characteristic line emanating from T_c is naturally related to the critical line $T_c(\mu)$ enclosing the hadronic phase. The comparison, in Figure 4, of our result for the curvature of the critical line at $\mu = 0$, which can be calculated in lattice QCD [13], is a nontrivial and successful test of the extension of the quasiparticle approach to $\mu > 0$.

The quark number susceptibility $\chi(T) = \partial n/\partial\mu|_{\mu=0}$ is another quantity which has been computed on the lattice. As a second derivative of the pressure it is a very sensitive benchmark, and it agrees nicely with our result, see Figure 5.

Finally, as a direct confirmation of our mapping procedure, the quasiparticle model can also successfully describe the available lattice data for $p(\mu, T)$ with

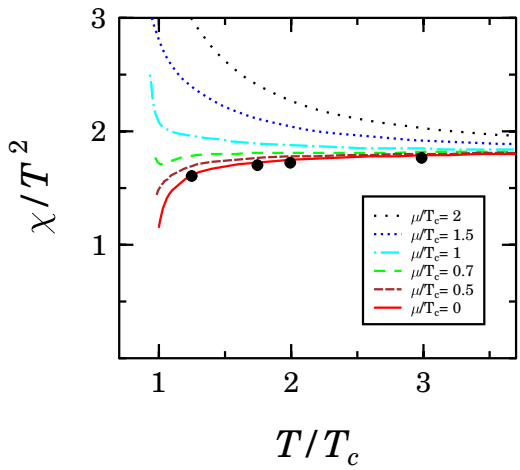

Figure 5. The quark number susceptibility for $N_f = 2$, calculated from the quasiparticle model with the same parameters as in Figs. 3 and 4, for several chemical potentials compared to the lattice data [14] at $\mu = 0$.

$2+1$ flavors [15]. It should be noted, however, that these direct calculations are so far restricted to small lattice sizes, resulting in still rather large uncertainties.

With these supporting arguments we consider our results from the extrapolation of the lattice data at $\mu = 0$ (with controllable small uncertainties) as a realistic estimate for the equation of state at not too small temperatures.

At low temperatures, matter will undergo a transition to a color-superconducting state, with a different quasiparticle structure than presumed in our quasiparticle approach. Nonetheless, pairing affects the thermodynamic bulk properties only at the relative order of $\mathcal{O}(\Delta^2/\mu^2)$, where the estimated gap $\Delta < 100\,\mathrm{MeV}$ is comfortably smaller than the chemical potential. Therefore, our equation of state is a reasonable approximation even at small temperatures (maybe except for the pressure where it becomes very small).

Relevant for the following discussion is the equation of state in the form $e(p)$, at $T \approx 0$. Although both the pressure and the energy density

deviate sizably from their ideal values, cf. Figure 6,

we observe an almost linear relation

$$e(p) = \alpha p + 4\tilde{B}\,, \tag{12}$$

as shown in Figure 7.

The same linear form, with $\alpha = 3$, follows in the familiar MIT-bag approach where $p(x) = cx^4 - B_{\mathrm{MIT}}$ (x is μ or T, and c is some constant). Although this parameterization of the pressure is clearly in contradiction with the ther-

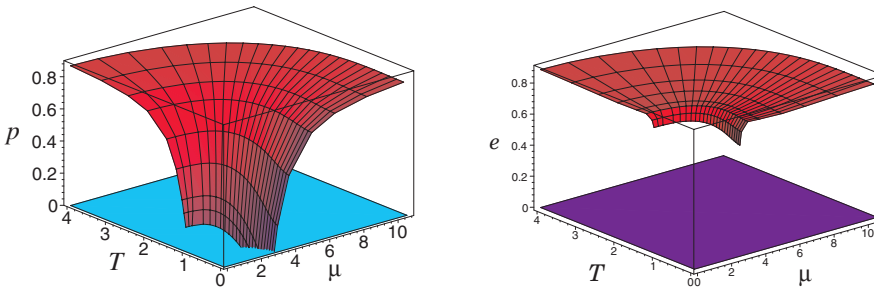

Figure 6. The pressure and the energy density, scaled by the free results, for $N_f = 2$.

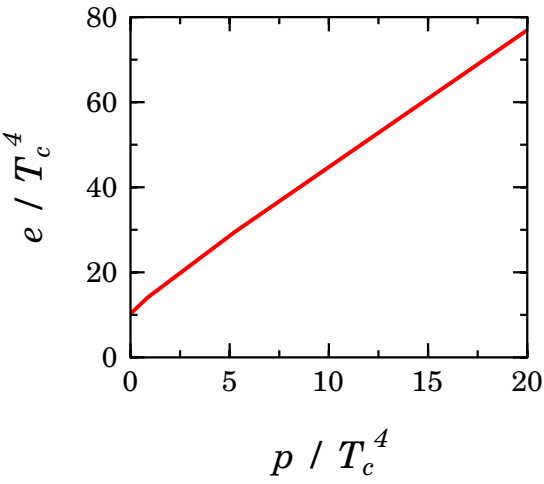

Figure 7. The estimate for the equation of state, for $N_f = 2$, at small temperatures.

modynamic lattice results, the bag model relation for $e(p)$ serves as a standard to compare our results with.

We note in passing that a linear relation between e and p, with a slope $\alpha \approx 3$ is to be expected since both quantities scale with the forth power of either μ or T. Causality requires furthermore $\alpha > 3$.

We find $\alpha \approx 3.2$, as a sign of the seen interaction effects, and $\tilde{B} \approx 3T_c^4$.

3. Implications for quark stars

Although there exist some lattice data for two light and one heavier quark, they still have larger uncertainties than for the case $N_f = 2$ considered so far.

Nevertheless, based on the available data we can point out some interesting implications.

From the universality of the scaled pressure $p/p_0(T/T_c)$ for various numbers of flavors, as observed on the lattice [16], we can expect that also at $\mu > 0$ the results do not change much besides a scaling from the different number of degrees of freedom in the physical case.

On more general grounds we expect an approximately linear relation for $e(p)$ for large ranges of the pressure.

This expectation is confirmed by analyzing the available data, and

approximating the lepton component in β equilibrated matter by an ideal gas.

The results for $e(p) \approx \alpha p + 4\tilde{B}$, in particular, are found to be rather insensitive even under large arbitrary variations of the values λ and T_s which parameterize $g(\mu = 0, T)$.

The slope parameter is found to be constrained by $3 < \alpha < 3.5$.

The value of $\tilde{B}$, on the other hand, is in our approach directly linked to the transition temperature, $B \approx 3T_c^4$. Since $T_c \approx 160\,\mathrm{MeV}$ is measured on the lattice, we have a definite prediction for the absolute scale in the equation of state.

Our estimate, $\tilde{B}^{1/4} \approx 210\,\mathrm{MeV}$, is substantially larger than the typical value of the bag constant obtained from fitting hadron spectra, $B_{\mathrm{MIT}}^{1/4} \approx 150\,\mathrm{MeV}$.

For a linear equation of state, the Tolman-Oppenheimer-Volkov equations imply a scaling property for the total mass and the radius of the star,

$$M, R \sim \tilde{B}^{-1/2}\,. \tag{13}$$

The effects of deviations of α from 3 being small, cf. Figure 8,

we pointed out [11] the possibility of the existence of very dense and compact objects, $M \approx 0.9 M_{\mathrm{sun}}$ and $R \approx 6\,\mathrm{km}$, composed mainly of quark matter.

Similar values for the maximal mass and radius were found in a perturbative approach with a physically motivated choice of the renormalization scale [17]. In a Schwinger-Dyson approach [18], $M \approx 0.7 M_{\mathrm{sun}}$ and $R \approx 9\,\mathrm{km}$ were obtained.

It is interesting to compare these values with the mass and the radius of the object RX J1856: $M \approx 0.9 M_{\mathrm{sun}}$ and $R \approx 6\,\mathrm{km}$ [19], which are not compatible with any hadronic equation of state. The precise values for M and R are, however, still under debate; for a recent discussion, we refer to [20].

Taking into account the effects of the hadronic crust of the star, its properties become sensitive to details of the hadronic equation of state, and of the transition.

For a strong first order transition, as suggested in [21],

a new branch in the mass-radius diagram could exist, see Figure 9.

The observation of so-called twins, as emphasized in [22],

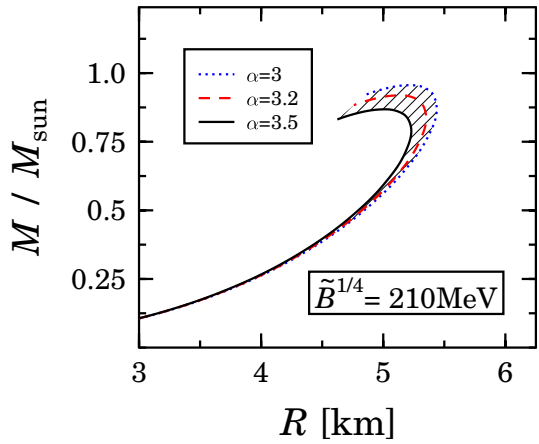

Figure 8. The mass-radius relation, for the linear equation of state (12), of a static quark star.

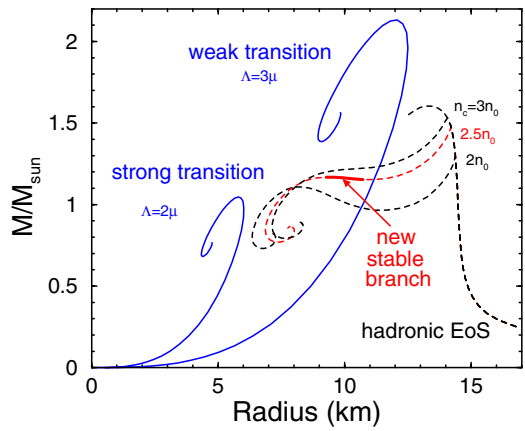

Figure 9. For a strong first order transition, a new stable branch can exist in the mass-radius relation (Figure from [17]).

could be an exciting astrophysical indication of the existence of a non-hadronic phase in the center of neutron stars.

Acknowledgments The work of A. P. is supported by BMBF.

References

[1] F. Weber, J. Phys. G27, 465 (2001).
[2] J. M. Luttinger, J. C. Ward, Phys. Rev. 118, 1417 (1960).
[3] G. Baym, Phys. Rev. 127, 1391 (1962).
[4] A. Peshier, B. Kämpfer, O. P. Pavlenko, G. Soff, Europhys. Lett. 43, 381 (1998).
[5] A. Peshier, Phys. Rev. D63, 105004 (2001).
[6] G. Boyd et al., Nucl. Phys. B469, 419 (1996); M. Okamoto et al., Phys. Rev. D60, 094510 (1999).
[7] J. P. Blaizot, E. Iancu, A. Rebhan, Phys. Rev. D63, 065003 (2001).
[8] A. Peshier, B. Kämpfer, O. P. Pavlenko, G. Soff, Phys. Rev. D54, 2399 (1996).
[9] A. Ali Khan et al., Phys. Rev. D64, 074510 (2001).
[10] A. Peshier, B. Kämpfer, G. Soff, Phys. Rev. D66, 094003 (2002).
[11] A. Peshier, B. Kämpfer, G. Soff, Phys. Rev. C61, 045203 (2000).
[12] P. Romatschke, hep-ph/0210331.
[13] Allton et al., Phys. Rev. D66, 074507 (2002).
[14] R. V. Gavai, S. Gupta, P. Majumdar, Phys. Rev. D65, 054506 (2002).
[15] K. K. Szabo, A. I. Toth, JHEP0306, 008 (2003).
[16] F. Karsch, E. Laermann, A. Peikert, Phys. Lett. B478, 447 (2000).
[17] E. S. Fraga, R. D. Pisarski, J. Schaffner-Bielich, Phys. Rev. D63, 121702 (2001); Nucl. Phys. A702, 217 (2002).
[18] D. Blaschke et al., Phys. Lett. B450, 207 (1999).
[19] J. J. Drake et al., Astrophys. J. 572, 996 (2002).
[20] M. H. Thoma, J. Trümper, V. Burwitz, J.Phys.G30:S471-S478 (2004) .
[21] U.H. Gerlach, Phys. Rev. 172, 1325 (1968); B. Kämpfer, J. Phys. A14, L471 (1981).
[22] K. Schertler, C. Greiner, J. Schaffner-Bielich, M. H. Thoma, Nucl. Phys. A677, 463 (2000).

EFFECTIVE LAGRANGIANS FOR QCD: DUALITY AND EXACT RESULTS

Francesco Sannino
NORDITA, Blegdamsvej 17, Copenhagen, DK-2100, Denmark
francesco.sannino@nbi.dk

Abstract I briefly discuss effective Lagrangians for strong interactions while concentrating on two specific Lagrangians for QCD at large matter density. I then introduce spectral duality in QCD a la Montonen and Olive. The latter is already present in QCD in the hadronic phase. However it becomes transparent at large chemical potential. Finally I show the relevance of having exact non perturbative constraints such as t'Hooft anomaly conditions at zero and nonzero quark chemical potential on the possible phases of strongly interacting matter. An important outcome is that for three massless quarks at any chemical potential the only non trivial solution of the constraints is chiral symmetry breaking. This proves that for three massless flavors at large quark chemical potential CFL is the ground state of matter and is smoothly connected to the ordinary hadronic phase.

1. Effective Lagrangians for QCD

In the non perturbative regime of strongly interacting theories effective Lagrangians play a dominant role since they efficiently describe the non perturbative dynamics in terms of the relevant degrees of freedom. Symmetries, anomalous and exact, are used to constrain the effective Lagrangians. An important point is that the effective Lagrangian approach is applicable to any region of the QCD or QCD-like phase diagram whenever the relevant degrees of freedom and the associated symmetries are defined.

1.1 Zero temperature and quark chemical potential

At zero temperature and quark chemical potential the simplest effective Lagrangian describing a relevant part of the nonperturbative physics of the Yang-Mills (YM) theory is the glueball Lagrangian whose potential is [1–4]:

$$V = \frac{H}{2} \ln \left[\frac{H}{\Lambda^4} \right] \ . \tag{1}$$

D. Blaschke and D. Sedrakian (eds.), Superdense QCD Matter and Compact Stars, 147–164.

The latter is constrained using trace anomaly and $H \sim \mathrm{Tr}\,[G^{\mu\nu}G_{\mu\nu}]$ with $G^{\mu\nu}$ the gluon field stress tensor. It describes the vacuum of a generic Yang-Mills theory. A similar effective Lagrangian (using superconformal anomalies) can be written for the non perturbative super Yang-Mills (SYM) theory. This is the celebrated Veneziano-Yankielowicz [5] Lagrangians. In Yang Mills and super Yang-Mills theories no exact continuous global symmetries are present which can break spontaneously and hence no Goldstones are present. The situation is different when flavors are included in the theory. Here the spontaneous breaking of chiral symmetry leads to a large number of Goldstine's excitations. We note that in [8, 9] we were able, using string techniques, to derive a number of fundamental perturbative and non perturbative properties for supersymmetric QCD such as the beta function, fermion condensate as well as chiral anomalies.

Recently in [6] we constructed effective Lagrangians of the Veneziano-Yankielowicz (VY) type for two non-supersymmetric but strongly interacting theories with a Dirac fermion either in the two index symmetric or two index antisymmetric representation of the gauge group. These theories are planar equivalent, at $N \to \infty$ to SYM [7]. In this limit the non-supersymmetric effective Lagrangians coincide with the bosonic part of the VY Lagrangian.

We departed from the supersymmetric limit in two ways. First, we considered finite values of N. Then $1/N$ effects break supersymmetry. We suggested the simplest modification of the VY Lagrangian which incorporates these $1/N$ effects, leading to a non-vanishing vacuum energy density. We analyzed the spectrum of the finite-N non-supersymmetric daughters. For $N = 3$ the two-index antisymmetric representation (one flavor) *is one-flavor QCD*. We showed that in this case the scalar quark-antiquark state is heavier than the corresponding pseudoscalar state, the η'. Second, we added a small fermion mass term which breaks supersymmetry explicitly. The vacuum degeneracy is lifted, the parity doublets split and we evaluated this splitting. The θ-angle dependence and its implications were also investigated. This new effective Lagrangian provides a number of fundamental results about QCD which can be already tested either experimentally or via lattice simulations.

This new type of expansion in the inverse of number colors in which the quark representation is the two index antisymmetric representation of the gauge group at any given N may very well be more convergent then the ordinary $1/N$ expansion. In the ordinary case one keeps the fermion in the fundamental representation of the gauge group while increasing the number of colors. Indeed recently in [10] we have studied the dependence on the number of colors (while keeping the fermions in the fundamental representation of the gauge group) of the leading pi pi scattering amplitude in chiral dynamics. We have demonstrated the existence of a critical number of colors for and above which the low energy pi pi scattering amplitude computed from the simple sum of the current algebra and vector meson terms is crossing symmetric and unitary at leading

order in a $1/N$ expansion. The critical number of colors turns out to be $N = 6$ and is insensitive to the explicit breaking of chiral symmetry. This means that the ordinary $1/N$ corrections for the real world are large.

1.2 Nonzero temperature and quark chemical potential

At nonzero temperature the center of the $SU(N)$ gauge group becomes a relevant symmetry [11]. However except for mathematically defined objects such as Polyakov loops the physical states of the theory are neutral under the center group symmetry.

A new class of effective Lagrangians have been constructed to show how the information about the center group symmetry is efficiently transferred to the actual physical states of the theory [12–15] and will be reviewed in detail elsewhere. Via these Lagrangians we were also able to have a deeper understanding of the relation between chiral restoration and deconfinement [15] for quarks in the fundamental and in the adjoint representation of the gauge group.

I will focus here on the two basic effective Lagrangians developed for color superconductivity. More specifically the Lagrangian for the color flavor locked phase (CFL) of QCD at high chemical potential and the 2 flavor color superconductive effective Lagrangian.

A color superconducting phase is a reasonable candidate for the state of strongly interacting matter for very large quark chemical potential [16–20]. Many properties of such a state have been investigated for two and three flavor QCD. In some cases these results rely heavily on perturbation theory, which is applicable for very large chemical potentials. Some initial applications to supernovae explosions and gamma ray bursts can be found in [21] and [22] respectively, see also [27]. The interested reader can find a discussion of the effects of color superconductivity on the mass-radius relationship of compact stars in [45]

2. Color Flavor Locked Phase

For $N_f = 3$ light flavors at very high chemical potential dynamical computations suggest that the preferred phase is a superconductive one and the following ansatz for a quark-quark type of condensate is energetically favored:

$$\epsilon^{\alpha\beta} < q_{L\alpha;a,i} q_{L\beta;b,j} > \sim k_1 \delta_{ai}\delta_{bj} + k_2 \delta_{aj}\delta_{bi} \ . \tag{2}$$

A similar expression holds for the right transforming fields. The Greek indices represent spin, a and b denote color while i and j indicate flavor. The condensate breaks the gauge group completely while locking the left/right transformations with color. The final global symmetry group is $SU_{c+L+R}(3)$, and the low energy spectrum consists of 9 Goldstone bosons.

3. Duality made transparent in QCD

Here we seek insight regarding the relevant energy scales of various physical states of the color flavor locked phase (CFL), such as the vector mesons and the solitons [24]. Our results do not support the naive expectation that all massive states are of the order of the color superconductive gap, Δ. Our strategy is based on exploiting the significant information already contained in the low–energy effective theory for the massless states. We transfer this information to the massive states of the theory by making use of the fact that higher derivative operators in the low–energy effective theory for the lightest state can also be induced when integrating out heavy fields. For the vector mesons, this can be seen by considering a generic theory containing vector mesons and Goldstone bosons. After integrating out the vector mesons, the induced local effective Lagrangian terms for the Goldstone bosons must match the local contact terms from operator counting. We find that each derivative in the (CFL) chiral expansion is replaced by a vector field ρ_μ as follows

$$\partial \to \frac{\Delta}{F_\pi}\rho \,. \tag{3}$$

This relation allows us to deduce, among other things, that the energy scale for the vector mesons is

$$m_v \sim \Delta \,, \tag{4}$$

where m_v is the vector meson mass. Our result is in agreement with the findings in [25, 26]. We shall see that this also suggests that the KSRF relation holds in the CFL phase.

In the solitonic sector, the CFL chiral Lagrangian [27, 28] gives us the scaling behavior of the coefficient of the Skyrme term and thus shows that the mass of the soliton is of the order of

$$M_{\rm soliton} \sim \frac{F_\pi^2}{\Delta} \,, \tag{5}$$

which is contrary to naive expectations. This is suggestive of a kind of duality between vector mesons and solitons in the same spirit as the duality advocated some years ago by Montonen and Olive for the $SU(2)$ Georgi-Glashow theory [29]. This duality becomes more apparent when considering the product

$$M_{\rm soliton} m_v \sim F_\pi^2 \,, \tag{6}$$

which is independent of the scale, Δ. In the present case, if the vector meson self-coupling is $\widetilde{g}$, we find that the Skyrme coefficient, $e \sim \Delta/F_\pi$, can be identified with $\widetilde{g}$. Thus, the following relations hold:

$$M_{\rm soliton} \propto \frac{F_\pi}{\widetilde{g}} \quad \text{and} \quad m_v \propto \widetilde{g}\, F_\pi \,. \tag{7}$$

In this notation the electric-magnetic (i.e. vector meson-soliton) duality is transparent. Since the topological Wess-Zumino term in the CFL phase is identical to that in vacuum, we identify the soliton with a physical state having the quantum numbers of the nucleon. We expect that the product of the nucleon and vector meson masses will scale like F_π^2 for any non-zero chemical potential for three flavors. Interestingly, quark-hadron continuity can be related to duality [30]. Testing this relation can also be understood as a quantitative check of quark-hadron continuity. It is important to note that our results are tree level results and that the resulting duality relation can be affected by quantum corrections. Our results have direct phenomenological consequences for the physics of compact stars with a CFL phase. While vector mesons are expected to play a relevant role, solitons can safely be neglected for large values of the quark chemical potential.

3.1 The Lagrangian for CFL Goldstones

When diquarks condense for the three flavor case, we have the following symmetry breaking:

$$[SU_c(3)] \times SU_L(3) \times SU_R(3) \times U_B(1) \to SU_{c+L+R}(3) \, .$$

The gauge group undergoes a dynamical Higgs mechanism, and nine Goldstone bosons emerge. Neglecting the Goldstone mode associated with the baryon number and quark masses (which will not be important for our discussion at lowest order), the derivative expansion of the effective Lagrangian describing the octet of Goldstone bosons is [27, 28]:

$$\mathcal{L} = \frac{F_\pi^2}{8} \mathrm{Tr}\left[\partial_\mu U \partial^\mu U^\dagger\right] \equiv \frac{F_\pi^2}{2} \mathrm{Tr}\left[p_\mu p^\mu\right] \, , \tag{8}$$

with $p_\mu = \frac{i}{2}\left(\xi\partial_\mu\xi^\dagger - \xi^\dagger\partial_\mu\xi\right)$, $U = \xi^2$, $\xi = e^{i\frac{\phi}{F_\pi}}$ and ϕ is the octet of Goldstone bosons. U transforms linearly according to $g_L U g_R^\dagger$ and $g_{L/R} \in SU_{L/R}(3)$ while ξ transforms non-linearly:

$$\xi \to g_L \, \xi \, K^\dagger\left(\phi, g_L, g_R\right) \equiv K\left(\phi, g_L, g_R\right) \, \xi \, g_R^\dagger \, . \tag{9}$$

This constraint implicitly defines the matrix, $K\left(\phi, g_L, g_R\right)$. Here, we wish to examine the CFL spectrum of massive states using the technique of integrating in/out at the level of the effective Lagrangian. F_π is the Goldstone boson decay constant. It is a non-perturbative quantity whose value is determined experimentally or by non-perturbative techniques (e.g. lattice computation). For very large quark chemical potential, F_π can be estimated perturbatively. It is found to be proportional to the Fermi momentum, $p_F \sim \mu$, with μ the quark chemical potential [31]. Since a frame must be fixed in order to introduce a chemical

potential, spatial and temporal components of the effective Lagrangians split. This point, however, is not relevant for the validity of our results.

When going beyond the lowest-order term in derivatives, we need a counting scheme. For theories with only one relevant scale (such as QCD at zero chemical potential), each derivative is suppressed by a factor of F_π. This is not the case for theories with multiple scales. In the CFL phase, we have both F_π and the gap, Δ, and the general form of the chiral expansion is [31]:

$$L \sim F_\pi^2 \Delta^2 \left(\frac{\vec{\partial}}{\Delta}\right)^k \left(\frac{\partial_0}{\Delta}\right)^l U^m U^{\dagger n} \,. \tag{10}$$

Following [31], we distinguish between temporal and spatial derivatives. Chiral loops are suppressed by powers of $p/4\pi F_\pi$, and higher-order contact terms are suppressed by p/Δ where p is the momentum. Thus, chiral loops are parametrically small compared to contact terms when the chemical potential is large.

There is also a topological term which is essential in order to satisfy the t'Hooft anomaly conditions [32–34] at the effective Lagrangian level. It is important to note that respecting the t'Hooft anomaly conditions is more than an academic exercise. In fact, it requires that the form of the Wess-Zumino term is the same in vacuum and at non-zero chemical potential. Its real importance lies in the fact that it forbids a number of otherwise allowed phases which cannot be ruled out given our rudimentary treatment of the non-perturbative physics. As an example, consider a phase with massless protons and neutrons in three-color QCD with three flavors. In this case chiral symmetry does not break. This is a reasonable realization of QCD for any chemical potential. However, it does not satisfy the t'Hooft anomaly conditions and hence cannot be considered. Were it not for the t'Hooft anomaly conditions, such a phase could compete with the CFL phase.

Gauging the Wess-Zumino term with to respect the electromagnetic interactions yields the familiar $\pi^0 \to 2\gamma$ anomalous decay. This term [35] can be written compactly using the language of differential forms. It is useful to introduce the algebra-valued Maurer-Cartan one form $\alpha = \alpha_\mu dx^\mu = (\partial_\mu U)\, U^{-1}\, dx^\mu \equiv (dU)\, U^{-1}$ which transforms only under the left $SU_L(3)$ flavor group. The Wess-Zumino effective action is

$$\Gamma_{WZ}[U] = C \int_{M^5} \mathrm{Tr}\left[\alpha^5\right] \,. \tag{11}$$

The price which must be paid in order to make the action local is that the spatial dimension must be augmented by one. Hence, the integral must be performed over a five-dimensional manifold whose boundary (M^4) is ordinary Minkowski space. In [27, 32, 36] the constant C has been shown to be the

same as that at zero density, i.e.

$$C = -i\frac{N_c}{240\pi^2}\,, \tag{12}$$

where N_c is the number of colors (three in this case). Due to the topological nature of the Wess-Zumino term its coefficient is a pure number.

3.2 The vector mesons

It is well known that massive states are relevant for low energy dynamics. Consider, for example, the role played by vector mesons in pion-pion scattering [10, 37] in saturating the unitarity bounds. More specifically, vector mesons play a relevant role when describing the low energy phenomenology of QCD and may also play a role also in the dynamics of compact stars with a CFL core [38]. In order to investigate the effects of such states, we need to know their in–medium properties including their gaps and the strength of their couplings to the CFL Goldstone bosons. Except for the extra spontaneously broken $U(1)_B$ symmetry, the symmetry properties of the CFL phase have much in common with those of zero density phase of QCD. This fact allows us to make some non perturbative but reasonable estimates of vector mesons properties in medium. We have already presented the general form of the chiral expansion in the CFL phase. As will soon become clear, we are now interested in the four–derivative (non–topological) terms whose coefficients are proportional to

$$\frac{F_\pi^2}{\Delta^2}\,. \tag{13}$$

This must be contrasted with the situation at zero chemical potential, where the coefficient of the four–derivative term is always a pure number before quantum corrections are taken into account. In vacuum, the tree-level Lagrangian which simultaneously describes vector mesons, Goldstone bosons, and their interactions is:

$$\begin{aligned} L &= \frac{F_\pi^2}{2}\mathrm{Tr}\left[p_\mu p^\mu\right] + \frac{m_v^2}{2}\mathrm{Tr}\left[\left(\rho_\mu + \frac{v_\mu}{\widetilde{g}}\right)^2\right] \\ &- \frac{1}{4}\mathrm{Tr}\left[F_{\mu\nu}(\rho)F^{\mu\nu}(\rho)\right]\,, \end{aligned} \tag{14}$$

where $F_\pi \simeq 132$ MeV and v_μ is the one form $v_\mu = \frac{i}{2}\left(\xi\partial_\mu\xi^\dagger + \xi^\dagger\partial_\mu\xi\right)$ with $U = \xi^2$ and $F_{\mu\nu}(\rho) = \partial_\mu\rho_\nu - \partial_\nu\rho_\mu + i\widetilde{g}\left[\rho_\mu, \rho_\nu\right]$. At tree level this Lagrangian agrees with the hidden local symmetry results [39].

When the vector mesons are very heavy with respect to relevant momenta, they can be integrated out. This results in the field constraint:

$$\rho_\mu = -\frac{v_\mu}{\widetilde{g}}\,. \tag{15}$$

Substitution of this relation in the vector meson kinetic term (i.e., the replacement of $F_{\mu\nu}(\rho)$ by $F_{\mu\nu}(v)$) gives the following four derivative operator with two time derivatives and two space derivatives [40]:

$$\frac{1}{64\,\widetilde{g}^2}\mathrm{Tr}\left[[\alpha_\mu,\alpha_\nu]^2\right]\ . \tag{16}$$

The coefficient is proportional to $1/\widetilde{g}^2$. It is also relevant to note that since we are describing physical fields we have considered canonically normalized fields and kinetic terms. This Lagrangian can also be applied to the CFL case. In the vacuum, $\widetilde{g}$ is a number of order one independent of the scale at tree level. This is no longer the case in the CFL phase. Here, by comparing the coefficient of the four–derivative operator in Eq. (16) obtained after having integrated out the vector meson with the coefficient of the same operator in the CFL chiral perturbation theory we determine the following scaling behavior of $\widetilde{g}$:

$$\widetilde{g} \propto \frac{\Delta}{F_\pi}\ . \tag{17}$$

By expanding the effective Lagrangian with the respect to the Goldstone boson fields, one sees that $\widetilde{g}$ is also connected to the vector meson coupling to two pions, $g_{\rho\pi\pi}$, through the relation

$$g_{\rho\pi\pi} = \frac{m_v^2}{\widetilde{g}F_\pi^2}\ . \tag{18}$$

In vacuum $g_{\rho\pi\pi} \simeq 8.56$ and $\widetilde{g} \simeq 3.96$ are quantities of order one. Since v_μ is essentially a single derivative, the scaling behavior of $\widetilde{g}$ allows us to conclude that each derivative term is equivalent to $\widetilde{g}\,\rho_\mu$ with respect to the chiral expansion. For example, dropping the dimensionless field U, the operator with two derivatives becomes a mass operator for the vector meson

$$F_\pi^2\partial_\mu^2 \to F_\pi^2\,\widetilde{g}^2\,\rho_\mu^2 \sim \Delta^2\rho_\mu^2\ . \tag{19}$$

This demonstrates that the vector meson mass gap is proportional to the color superconducting gap. This non-perturbative result is relevant for phenomenological applications. It is interesting to note that our simple counting argument agrees with the underlying QCD perturbative computations of Ref. [25] and also with recent results of Ref. [26]. In [41], at high chemical potential, vector meson dominance is discussed. However, our approach is more general since it does not rely on any underlying perturbation theory. It can be applied to theories with multiple scales for which the counting of the Goldstone modes is known. Since $m_v^2 \sim \Delta^2$, we find that $g_{\rho\pi\pi}$ scales with $\widetilde{g}$ suggesting that the KSRF relation is a good approximation also in the CFL phase of QCD.

3.3 CFL-Solitons

The low energy effective theory supports solitonic excitations which can be identified with the baryonic sector of the theory at non-zero chemical potential. In order to obtain classically stable configurations, it is necessary to include at least a four–derivative term (containing two temporal derivatives) in addition to the usual two–derivative term. Such a term is the Skyrme term:

$$L^{\rm skyrme} = \frac{1}{32\,e^2}{\rm Tr}\left[[\alpha_\mu,\alpha_\nu]^2\right] \ . \tag{20}$$

Since this is a fourth–order term in derivatives not associated with the topological term we have:

$$e \sim \frac{\Delta}{F_\pi} \ . \tag{21}$$

This term is the same as that which emerges after integrating out the vector mesons (see Eq. (16)), and one concludes that $e = \sqrt{2}\,\widetilde{g}$ [40]. The simplest complete action supporting solitonic excitations is:

$$\int d^4x \left[\frac{F_\pi^2}{2}{\rm Tr}\left[p_\mu p^\mu\right] + L^{\rm skyrme}\right] + \Gamma_{WZ} \ . \tag{22}$$

The Wess-Zumino term in Eq. (11) guarantees the correct quantization of the soliton as a spin $1/2$ object. Here we neglect the breaking of Lorentz symmetries, irrelevant to our discussion. The Euler-Lagrangian equations of motion for the classical, time independent, chiral field $U_0(\mathbf{r})$ are highly non-linear partial differential equations. To simplify these equations Skyrme adopted the hedgehog *ansatz* which, suitably generalized for the three flavor case, reads [40]:

$$U_0(\mathbf{r}) = \begin{pmatrix} e^{i\vec{\tau}\cdot\hat{r}F(r)} & 0 \\ 0 & 1 \end{pmatrix} \ , \tag{23}$$

where $\vec{\tau}$ represents the Pauli matrices and the radial function $F(r)$ is called the chiral angle. The *ansatz* is supplemented with the boundary conditions $F(\infty) = 0$ and $F(0) = 0$ which guarantee that the configuration possesses unit baryon number. After substituting the *ansatz* in the action one finds that the classical solitonic mass is, up to a numerical factor:

$$M_{\rm soliton} \propto \frac{F_\pi}{e} \sim \frac{F_\pi^2}{\Delta} \ , \tag{24}$$

and the isoscalar radius, $\langle r^2\rangle_{I=0} \sim 1/(F_\pi^2\,e^2) \sim 1/\Delta^2$. Interestingly, due to the non perturbative nature of the soliton, its mass turns to be dual to the vector

meson mass. It is also clear that although the vector mesons and the solitons have dual masses, they describe two very distinct types of states. The present duality is very similar to the one argued in [29]. Indeed, after introducing the collective coordinate quantization, the soliton (due to the Wess-Zumino term) describes baryonic states of half-integer spin while the vectors are spin one mesons. Here, the dual nature of the soliton with respect to the vector meson is enhanced by the fact that, in the CFL state, $\widetilde{g} \sim \Delta/F_\pi$ is expected to be substantially reduced with respect to its value in vacuum. Once the soliton is identified with the nucleon (whose density–dependent mass is denoted with $M_N(\mu)$) we predict the following relation to be independent of the matter density:

$$\frac{M_N(\mu)\, m_v(\mu)}{(2\pi F_\pi(\mu))^2} = \frac{M_N(0)\, m_v(0)}{(2\pi F_\pi(0))^2} \sim 1.05\ . \tag{25}$$

In this way, we can relate duality to quark-hadron continuity. We considered duality, which is already present at zero chemical potential, between the soliton and the vector mesons a fundamental property of the spectrum of QCD which should persists as we increase the quark chemical potential. Should be noted that differently than in [42] we have not subtracted the energy cost to excite a soliton from the Fermi sea. Since we are already considering the Lagrangian written for the excitations near the Fermi surface we would expect not to consider such a corrections. In any event this is of the order μ [42] and hence negligible with respect to $M_{\rm soliton}$.

We have shown that the vector mesons in the CFL phase have masses of the order of the color superconductive gap, Δ. On the other hand the solitons have masses proportional to F_π^2/Δ and hence should play no role for the physics of the CFL phase at large chemical potential. We have noted that the product of the soliton mass and the vector meson mass is independent of the gap. This behavior reflects a form of electromagnetic duality in the sense of Montonen and Olive [29]. We have predicted that the nucleon mass times the vector meson mass scales as the square of the pion decay constant at any nonzero chemical potential. In the presence of two or more scales provided by the underlying theory the spectrum of massive states shows very different behaviors which cannot be obtained by assuming a naive dimensional analysis.

4. 2 SC General Features and Effective Lagrangian

QCD with 2 massless flavors has gauge symmetry $SU_c(3)$ and global symmetry

$$SU_L(2) \times SU_R(2) \times U_V(1)\ . \tag{26}$$

At very high quark density the ordinary Goldstone phase is no longer favored compared with a superconductive one associated to the following type of diquark condensates:

$$\langle L^{\dagger a}\rangle \sim \langle \epsilon^{abc}\epsilon^{ij} q^{\alpha}_{Lb,i} q_{Lc,j;\alpha}\rangle \,, \qquad \langle R^{\dagger a}\rangle \sim -\langle \epsilon^{abc}\epsilon^{ij} q_{Rb,i;\dot\alpha} q^{\dot\alpha}_{Rc,j}\rangle \,, \quad (27)$$

If parity is not broken spontaneously, we have $\langle L_a\rangle = \langle R_a\rangle = f\delta^3_a$, where we choose the condensate to be in the 3rd direction of color. The order parameters are singlets under the $SU_L(2) \times SU_R(2)$ flavor transformations while possessing baryon charge $\frac{2}{3}$. The vev leaves invariant the following symmetry group:

$$[SU_c(2)] \times SU_L(2) \times SU_R(2) \times \widetilde{U}_V(1) \,, \quad (28)$$

where $[SU_c(2)]$ is the unbroken part of the gauge group. The $\widetilde{U}_V(1)$ generator $\widetilde{B}$ is the following linear combination of the previous $U_V(1)$ generator B and the broken diagonal generator of the $SU_c(3)$ gauge group T^8: $\widetilde{B} = B - \dfrac{2\sqrt{3}}{3} T^8 = \mathrm{diag}(0,0,1)$. The quarks with color 1 and 2 are neutral under $\widetilde{B}$ and consequently so is the condensate.

The spectrum in the 2SC state is made of 5 massive Gluons with a mass of the order of the gap, 3 massless Gluons confined (at zero temperature) into light glueballs and gapless up and down quarks in the direction (say) 3 of color.

4.1 The 5 massive Gluons

The relevant coset space G/H [43, 36] with

$$G = SU_c(3) \times U_V(1) \,, \quad \text{and} \quad H = SU_c(2) \times \widetilde{U}_V(1) \quad (29)$$

is parameterized by:

$$V = \exp(i\xi^i X^i) \,, \quad (30)$$

where $\{X^i\}$ $i = 1, \cdots, 5$ belong to the coset space G/H and are taken to be $X^i = T^{i+3}$ for $i = 1, \cdots, 4$ while

$$X^5 = B + \frac{\sqrt{3}}{3} T^8 = \mathrm{diag}(\frac{1}{2}, \frac{1}{2}, 0) \,. \quad (31)$$

T^a are the standard generators of $SU(3)$. The coordinates

$$\xi^i = \frac{\Pi^i}{f} \quad i = 1,2,3,4 \,, \qquad \xi^5 = \frac{\Pi^5}{\widetilde{f}} \,,$$

via Π describe the Goldstone bosons which will be absorbed in the longitudinal components of the gluons. The vevs f and $\widetilde{f}$ are, at asymptotically high

densities, proportional to μ. V transforms non linearly:

$$V(\xi) \to u_V \, g \, V(\xi) \, h^\dagger(\xi, g, u) \, h^\dagger_{\widetilde{V}}(\xi, g, u) \, , \tag{32}$$

with

$$\begin{aligned} u_V \in U_V(1) \, , \qquad & g \in SU_c(3) \, , \\ h(\xi, g, u) \in SU_c(2) \, , \qquad & h_{\widetilde{V}}(\xi, g, u) \in \widetilde{U}_V(1) \, . \end{aligned} \tag{33}$$

It is convenient to define the following differential form:

$$\omega_\mu = iV^\dagger D_\mu V \quad \text{with} \quad D_\mu V = (\partial_\mu - ig_s G_\mu)V \, , \tag{34}$$

with $G_\mu = G^m_\mu T^m$ the gluon fields while g_s is the strong coupling constant. ω transforms according to:

$$\begin{aligned} \omega_\mu \quad \to \quad & h(\xi, g, u)\omega_\mu h^\dagger(\xi, g, u) + i \, h(\xi, g, u)\partial_\mu h^\dagger(\xi, g, u) \\ + \quad & i \, h_{\widetilde{V}}(\xi, g, u)\partial_\mu h^\dagger_{\widetilde{V}}(\xi, g, u) \, . \end{aligned}$$

We decompose ω_μ into

$$\omega^\parallel_\mu = 2S^a \mathrm{Tr}\left[S^a \omega_\mu\right] \quad \text{and} \quad \omega^\perp_\mu = 2X^i \mathrm{Tr}\left[X^i \omega_\mu\right] \, , \tag{35}$$

S^a are the unbroken generators of H, while $S^{1,2,3} = T^{1,2,3}$ and $S^4 = \widetilde{B}/\sqrt{2}$.

The most generic two derivative kinetic Lagrangian for the Goldstone bosons is:

$$L = f^2 a_1 \mathrm{Tr}\left[\omega^\perp_\mu \omega^{\mu\perp}\right] + f^2 a_2 \mathrm{Tr}\left[\omega^\perp_\mu\right] \mathrm{Tr}\left[\omega^{\mu\perp}\right] \, . \tag{36}$$

The double trace term is due to the absence of the condition for the vanishing of the trace for the broken generator X^5. It emerges naturally in the non linear realization framework at the same order in derivative expansion with respect to the single trace term. In the unitary gauge these two terms correspond to the five gluon masses [43].

4.2 The fermionic sector

For the fermions it is convenient to define the dressed fermion fields

$$\widetilde{\psi} = V^\dagger \psi \, , \tag{37}$$

transforming as $\widetilde{\psi} \to h_{\widetilde{V}}(\xi, g, u) h(\xi, g, u) \, \widetilde{\psi}$. ψ has the ordinary quark transformations (i.e. is a Dirac spinor). Pictorially $\widetilde{\psi}$ can be viewed as a constituent type field or alternatively as the bare quark field ψ immersed in the diquark

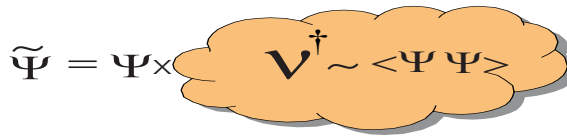

cloud represented by V. The non linearly realized effective Lagrangian describing in medium fermions, gluons and their self interactions, up to two derivatives is:

$$\begin{aligned} L &= f^2 a_1 \mathrm{Tr}\left[\omega_\mu^\perp \omega^{\mu\perp}\right] + f^2 a_2 \mathrm{Tr}\left[\omega_\mu^\perp\right] \mathrm{Tr}\left[\omega^{\mu\perp}\right] \\ &+ b_1 \overline{\widetilde{\psi}} i\gamma^\mu (\partial_\mu - i\omega_\mu^\parallel)\widetilde{\psi} + b_2 \overline{\widetilde{\psi}} \gamma^\mu \omega_\mu^\perp \widetilde{\psi} \\ &+ m_M \overline{\widetilde{\psi}^C}_i \gamma^5 (iT^2) \widetilde{\psi}_j \varepsilon^{ij} + \mathrm{h.c.}\,, \end{aligned} \tag{38}$$

where $\widetilde{\psi}^C = i\gamma^2 \widetilde{\psi}^*$, $i, j = 1, 2$ are flavor indices and

$$T^2 = S^2 = \frac{1}{2}\begin{pmatrix} \sigma^2 & 0 \\ 0 & 0 \end{pmatrix}. \tag{39}$$

Here $a_1,\ a_2,\ b_1$ and b_2 are real coefficients while m_M is complex. From the last two terms, representing a Majorana mass term for the quarks, we see that the massless degrees of freedom are the $\psi_{a=3,i}$. The latter possesses the correct quantum numbers to match the 't Hooft anomaly conditions [32].

4.3 The $SU_c(2)$ Glueball Lagrangian

The $SU_c(2)$ gauge symmetry does not break spontaneously and confines. Calling H a mass dimension four composite field describing the scalar glueball we can construct the following Lagrangian [44]:

$$\begin{aligned} S_{G-ball} &= \int d^4x \left\{ \frac{c}{2}\sqrt{b}\, H^{-\frac{3}{2}} \left[\partial^0 H \partial^0 H - v^2 \partial^i H \partial^i H\right] \right. \\ &- \left. \frac{b}{2} H \log\left[\frac{H}{\hat{\Lambda}^4}\right] \right\}. \end{aligned} \tag{40}$$

This Lagrangian correctly encodes the underlying $SU_c(2)$ trace anomaly. The glueballs move with the same velocity v as the underlying gluons in the 2SC color superconductor. $\hat{\Lambda}$ is related to the intrinsic scale associated with the $SU_c(2)$ theory and can be less than or of the order of few MeVs [46] [1] Once created, the light $SU_c(2)$ glueballs are stable against strong interactions but not

[1] According to the present normalization of the glueball field $\hat{\Lambda}^4$ is $v\,\Lambda^4$ with Λ the intrinsic scale of $SU_c(2)$ after the coordinates have been appropriately rescaled [46, 44] to eliminate the v dependence from the action.

with respect to electromagnetic processes [44]. Indeed, the glueballs couple to two photons via virtual quark loops.

$$\Gamma\left[h \to \gamma\gamma\right] \approx 1.2 \times 10^{-2} \left[\frac{M_h}{1\,\mathrm{MeV}}\right]^5 \mathrm{eV}\,, \tag{41}$$

where $\alpha = e^2/4\pi \simeq 1/137$. For illustration purposes we consider a glueball mass of the order of 1 MeV which leads to a decay time $\tau \sim 5.5 \times 10^{-14} s$. This completes the effective Lagrangian for the 2SC state which corresponds to the Wigner-Weyl phase.

Using this Lagrangian one can estimate the $SU_c(2)$ glueball melting temperature to be [47]:

$$T_c \leq \sqrt[4]{\frac{90 v^3}{2\,e\,\pi^2}}\,\hat{\Lambda} < T_{CSC}\,. \tag{42}$$

Where T_{CSC} is the color superconductive transition temperature. The de-

Figure 1. A zoom of the 2SC phases as function of temperature for fixed quark chemical potential.

confining/confining $SU_c(2)$ phase transition within the color superconductive phase is second order.

5. Non Perturbative Exact Results: Anomaly Matching Conditions

The superconductive phase for $N_f = 2$ possesses the same global symmetry group as the confined Wigner-Weyl phase. The ungapped fermions have the correct global charges to match the t' Hooft anomaly conditions as shown in [32]. Specifically the ${SU(2)_{L/R}}^2 \times U(1)_V$ global anomaly is correctly reproduced in this phase due to the presence of the ungapped fermions. This is so since a quark in the 2SC case is surrounded by a diquark medium (i.e. $q \langle qq \rangle$) and behaves as a baryon.

$$\begin{pmatrix} u \\ d \end{pmatrix}_{color=3} \sim \begin{pmatrix} p \\ n \end{pmatrix} .$$

The validity of the t'Hooft anomaly conditions at high matter density have been investigated in [32, 33]. A delicate part of the proof presented in [33] is linked necessarily to the infrared behavior of the anomalous three point function. In particular one has to show the emergence of a singularity (i.e. a pole structure). This pole is then interpreted as due to a Goldstone boson when chiral symmetry is spontaneously broken.

One might be worried that, since the chemical potential explicitly breaks Lorentz invariance, the gapless (Goldstone) pole may disappear modifying the infrared structure of the three point function. This is not possible. Thanks to the Nielsen and Chadha theorem [48], not used in [33], we know that gapless excitations are always present when some symmetries break spontaneously even in the absence of Lorentz invariance[2]. Since the quark chemical potential is associated with the baryonic generator which commutes with all of the non Abelian global generators the number of Goldstone bosons must be larger or equal to the number of broken generators. Besides all of the Goldstones must have linear dispersion relations (i.e. are type I [48]). This fact not only guarantees the presence of gapless excitations (justifying the analysis made in [33] on the infrared behavior of the form factors) but demonstrates that the pole structure due to the gapless excitations needed to saturate the triangle anomaly is identical to the zero quark chemical potential one in the infrared.

It is also interesting to note that the explicit dependence on the quark chemical potential is communicated to the Goldstone excitations via the coefficients of the effective Lagrangian (see [31] for a review). For example F_π is proportional to μ in the high chemical potential limit and the low energy effective theory is a good expansion in the number of derivatives which allows to consistently incorporate in the theory the Wess-Zumino-Witten term [32] and its corrections.

[2]Under specific assumptions which are met when Lorentz invariance is broken via the chemical potential.

The validity of the anomaly matching conditions have far reaching consequences. Indeed, in the three flavor case, the conditions require the Goldstone phase to be present in the hadronic as well as in the color superconductive phase supporting the quark-hadron continuity scenario [30]. At very high quark chemical potential the effective field theory of low energy modes (not to be confused with the Goldstone excitations) has positive Euclidean path integral measure [6]. In this limit the CFL is also shown to be the preferred phase. Since the fermionic theory has positive measure only at asymptotically high densities one cannot use this fact to show that the CFL is the preferred phase for moderate chemical potentials. This is possible using the anomaly constraints.

While the anomaly matching conditions are still in force at nonzero quark chemical potential [32] the *persistent mass* condition [50] ceases to be valid. Indeed a phase transition, as function of the strange quark mass, between the CFL and the 2SC phases occurs.

We recall that we can saturate the t'Hooft anomaly conditions either with massless fermionic degrees of freedom or with gapless bosonic excitations. However in absence of Lorentz covariance the bosonic excitations are not restricted to be fluctuations related to scalar condensates but may be associated, for example, to vector condensates [51].

Acknowledgments

I thank A.D. Jackson for stimulating collaboration on some of the recent topics presented here and for careful reading of the manuscript. I also thank R. Casalbuoni, Z. Duan, M. Harada, D.K. Hong, S.D. Hsu, R. Marotta, A. Mocsy, F. Pezzella, J. Schechter, M. Shifman and K. Tuominen for their valuable collaboration on some of the topics I presented here. K. Tuominen is thanked also for careful reading of the manuscript.

References

[1] J. Schechter, Phys. Rev. D **21** (1980) 3393.

[2] C. Rosenzweig, J. Schechter and G. Trahern, Phys. Rev. **D21**, 3388 (1980); P. Di Vecchia and G. Veneziano, Nucl. Phys. **B171**, 253 (1980); E. Witten, Ann. of Phys. **128**, 363 (1980); P. Nath and A. Arnowitt, Phys. Rev. **D23**, 473 (1981); A. Aurilia, Y. Takahashi and D. Townsend, Phys. Lett. **95B**, 65 (1980); K. Kawarabayashi and N. Ohta, Nucl. Phys. **B175**, 477 (1980).

[3] A. A. Migdal and M. A. Shifman, Phys. Lett. B **114**, 445 (1982); J. M. Cornwall and A. Soni, Phys. Rev. D **29**, 1424 (1984); Phys. Rev. D **32**, 764 (1985).

[4] A. Salomone, J. Schechter and T. Tudron, Phys. Rev. **D23**, 1143 (1981); J. Ellis and J. Lanik, Phys. Lett. **150B**, 289 (1985); H. Gomm and J. Schechter, Phys. Lett. **158B**, 449 (1985); F. Sannino and J. Schechter, Phys. Rev. D **60**, 056004 (1999) [hep-ph/9903359].

[5] G. Veneziano and S. Yankielowicz, Phys. Lett. B **113**, 231 (1982).

[6] F. Sannino and M. Shifman, "Effective Lagrangians for orientifold theories," Phys.Rev.D69:125004 (2003) [arXiv:hep-th/0309252].

[7] A. Armoni, M. Shifman and G. Veneziano, Nucl. Phys. B **667**, 170 (2003) [arXiv:hep-th/0302163].

[8] R. Marotta, F. Nicodemi, R. Pettorino, F. Pezzella and F. Sannino, JHEP **0209**, 010 (2002) [arXiv:hep-th/0208153].

[9] R. Marotta and F. Sannino, Phys. Lett. B **545**, 162 (2002) [arXiv:hep-th/0207163].

[10] M. Harada, F. Sannino and J. Schechter, "Large N(c) and chiral dynamics," Phys.Rev.D69:034005 (2003) [arXiv:hep-ph/0309206].

[11] B. Svetitsky and L. G. Yaffe, Nucl. Phys. B **210**, 423 (1982).

[12] F. Sannino, Phys. Rev. D **66**, 034013 (2002) [arXiv:hep-ph/0204174].

[13] A. Mocsy, F. Sannino and K. Tuominen, Phys. Rev. Lett. **91**, 092004 (2003) [arXiv:hep-ph/0301229].

[14] A. Mocsy, F. Sannino and K. Tuominen, "Induced universal properties and deconfinement," JHEP 0403:044 (2003) [arXiv:hep-ph/0306069].

[15] A. Mocsy, F. Sannino and K. Tuominen, "Confinement versus chiral symmetry," Phys.Rev.Lett.92:182302 (2003) [arXiv:hep-ph/0308135].

[16] B. C. Barrois, Nucl. Phys. **B129**, 390 (1977).

[17] F. Barrois, Nonperturbative effects in dense quark matter, Ph.D. thesis, Caltech, UMI 79-04847-mc (microfiche).

[18] D. Bailin and A. Love, Phys. Rept. **107**, 325 (1984).

[19] M. Alford, K. Rajagopal and F. Wilczek, Phys. Lett. **B422**, 247 (1998) [hep-ph/9711395].

[20] R. Rapp, T. Schäfer, E. V. Shuryak and M. Velkovsky, Phys. Rev. Lett. **81**, 53 (1998) [hep-ph/9711396].

[21] D. K. Hong, S. D. Hsu and F. Sannino, Phys. Lett. B **516**, 362 (2001), hep-ph/0107017.

[22] R. Ouyed and F. Sannino, Astron. Astrophys. **387**, 725 (2002) [arXiv:astro-ph/0103022].

[23] D. Blaschke, S. Fredriksson, H. Grigorian and A. M. Oztas, Nucl.Phys.A736:203-219 (2003) [arXiv:nucl-th/0301002].

[24] A. D. Jackson and F. Sannino, Phys. Lett. B **578**, 133 (2004) [arXiv:hep-ph/0308182].

[25] R. Casalbuoni, R. Gatto and G. Nardulli, Phys. Lett. B **498**, 179 (2001) [Erratum-ibid. B **517**, 483 (2001)] [arXiv:hep-ph/0010321].

[26] M. Rho, E. V. Shuryak, A. Wirzba and I. Zahed, Nucl. Phys. A **676**, 273 (2000) [arXiv:hep-ph/0001104].

[27] D. K. Hong, M. Rho and I. Zahed, Phys. Lett. B **468**, 261 (1999) [arXiv:hep-ph/9906551].

[28] R. Casalbuoni and R. Gatto, Phys. Lett. B**464**, 11 (1999); Phys. Lett. B**469**, 213 (1999).

[29] C. Montonen and D. I. Olive, Phys. Lett. B **72**, 117 (1977).

[30] T. Schafer and F. Wilczek, Phys. Rev. Lett. **82**, 3956 (1999) [arXiv:hep-ph/9811473].

[31] See T. Schafer, "Quark matter," arXiv:hep-ph/0304281 and references therein for a concise review on the μ dependence of $F_\pi(\mu)$.

[32] F. Sannino, Phys. Lett. B **480**, 280 (2000) [arXiv:hep-ph/0002277].

[33] S. D. Hsu, F. Sannino and M. Schwetz, Mod. Phys. Lett. A **16**, 1871 (2001) [arXiv:hep-ph/0006059].

[34] F. Sannino, "Anomaly matching and low energy theories at high matter density" arXiv:hep-ph/0301035. Proceedings for the review talk at the Electroweak and Strong Matter conference, Heidelberg 2002.

[35] J. Wess and B. Zumino, Phys. Lett. B**37**, 95 (1971).

[36] R. Casalbuoni, Z. Duan and F. Sannino, Phys. Rev. D **63**, 114026 (2001).

[37] F. Sannino and J. Schechter, Phys. Rev. D **52**, 96 (1995). M. Harada, F. Sannino and J. Schechter, Phys. Rev. D **54**, 1991 (1996);*ibid* Phys. Rev. Lett. **78**, 1603 (1997).

[38] C. Vogt, R. Rapp and R. Ouyed, "Photon emission from dense quark matter," Nucl. Phys. **A735**, 543 (2003).

[39] M. Bando, T. Kugo and K. Yamawaki, Phys. Rept. **164**, 217 (1988).

[40] See J. Schechter and H. Weigel, in *Mitra, A.N. (ed.): Quantum field theory* 337-369. [arXiv:hep-ph/9907554] for a recent review on the subject and references therein.

[41] C. Manuel and M. H. Tytgat, Phys. Lett. B **501**, 200 (2001).

[42] D. K. Hong, S. T. Hong and Y. J. Park, Phys. Lett. B **499**, 125 (2001).

[43] R. Casalbuoni, Z. Duan and F. Sannino, Phys. Rev. D **62** (2000) 094004.

[44] R. Ouyed and F. Sannino, Phys. Lett. B **511**, 66 (2001).

[45] See M. Alford, "Dense quark matter in nature," Prog. Theor. Phys. Suppl. **153**, 1 (2003), and references therein.

[46] D. H. Rischke, D. T. Son and M. A. Stephanov, Phys. Rev. Lett. **87**, 062001 (2001).

[47] F. Sannino, N. Marchal and W. Schafer, Phys. Rev. D **66**, 016007 (2002).

[48] H.B. Nielsen and S. Chadha, Nucl. Phys. **B105**, 445 (1976).

[49] D. K. Hong and S. D. H. Hsu, Phys. Rev. D **68**, 034011 (2003).

[50] J. Preskill and S. Weinberg, Phys. Rev. D **24**, 1059 (1981).

[51] F. Sannino, Phys. Rev. D **67**, 054006 (2003). F. Sannino and W. Schäfer, Phys. Lett. B **527**, 142 (2002). F. Sannino and W. Schäfer, hep-ph/0204353. J. T. Lenaghan, F. Sannino and K. Splittorff, Phys. Rev. D **65**, 054002 (2002).

COLOR SUPERCONDUCTIVITY AND HIGH DENSITY EFFECTIVE THEORY

Deog Ki Hong
Department of Physics, Pusan National University
Pusan 609-735, Korea
dkhong@pusan.ac.kr

Abstract We discuss the salient features of the high density effective theory (HDET) of QCD, elaborating more on the matching for vector-vector correlators and axial-vector-vector correlators, which are related to screening mass and axial anomaly, respectively. We then apply HDET to discuss various color-superconducting phases of dense QCD. We also review a recent proposal to solve the sign problem in dense fermionic matter, using the positivity property of HDET. Positivity of HDET allows us to establish rigorous inequalities in QCD at asymptotic density and to show vector symmetry except the fermion number is not spontaneously broken at asymptotic density.

Keywords: effective theory, dense QCD, color superconductivity, sign problem

1. Introduction

As physics advances, its frontier has expanded. One of the frontiers under active exploration is matter at extreme conditions. Recent surprising data, obtained from heavy-ion collisions and compact stars such as neutron stars, and also some theoretical breakthroughs have stimulated active investigation in this field [1].

How does matter behave as we squeeze it extremely hard? This question is directly related to one of the fundamental questions in Nature; what are the fundamental building blocks of matter and how they interact. According to QCD, matter at high density is quark matter, since quarks interact weaker and weaker as they are put closer and closer.

At what temperature and density does the phase transition to quark matter occur? To determine the phase diagram of thermodynamic QCD is an outstanding problem. The phases of matter are being mapped out by colliding heavy-ions and by observing compact stars. Since QCD has only one intrinsic scale, $\Lambda_{\rm QCD}$, the phase transition of QCD matter should occur at that scale as matter is heated up or squeezed down. Indeed, recent lattice QCD calculations

D. Blaschke and D. Sedrakian (eds.), Superdense QCD Matter and Compact Stars, 165–185.

found the phase transition does occur at temperature around 175 MeV [2]. Even though lattice QCD has been quite successful at finite temperature but at zero density, it has not made much progress at finite density due to the notorious sign problem. The lattice calculation is usually done in Euclidean space and Euclidean QCD with a chemical potential has a complex measure, which precludes use of importance samplings, the main technique in the Monte Carlo simulation for lattice calculations.

Lattice QCD at finite density is described by a partition function

$$Z(\mu) = \int \mathrm{d}A \det(M)\, e^{-S(A)}\,, \tag{1}$$

where $M = \gamma_E^\mu D_E^\mu + \mu\gamma_E^4$ is the Dirac operator of Euclidean QCD with a chemical potential μ. The eigenvalues of M are in general complex, since $\gamma_E^\mu D_E^\mu$ is anti-Hermitian while $\mu\gamma_E^4$ is Hermitian. For certain gauge fields such as $A^\mu(-x) = -A^\mu(x)$, M can be mapped into $M^\dagger$ by a similarity transformation and thus its determinant M is nonnegative. However, for generic fields $M \neq P^{-1}M^\dagger P$ and $\det(M)$ is complex.

Recently there have been some progress in lattice simulation at small chemical potential, using a re-weighting method, to find the phase line [3, 4]. Another interesting progress in lattice simulation was made at very high density in [5, 6], where it was shown that for QCD at high density the sign problem is either mild or absent, since the modes, responsible for the complexness of the Dirac determinant, decouple from dynamics or become irrelevant at high baryon density.

2. High Density Effective Theory

At low temperature or energy, most degrees of freedom of quark matter are irrelevant due to Pauli blocking. Only quasi-quarks near the Fermi surface are excited. Therefore, relevant modes for quark matter are quasi-quarks near the Fermi surface and the physical properties of quark matter like the symmetry of the ground state are determined by those modes. High density effective theory (HDET) [7, 8] of QCD is an effective theory for such modes to describe the low-energy dynamics of quark matter.

To find out the modes near the Fermi surface, one needs to know the energy spectrum of QCD, which is very difficult in general since it is equivalent to solving QCD. However, at high density $\mu \gg \Lambda_{\mathrm{QCD}}$, quarks near the Fermi surface carry large momenta and the typical interaction involves a large momentum transfer. Therefore, due to the asymptotic freedom of QCD, the spectrum near the Fermi surface at high density looks very much like that of free fermion: $(\vec{\alpha}\cdot\vec{p} - \mu + \beta\, m)\,\psi_\pm = E_\pm\psi_\pm$, as shown in Fig. 1. We see that at low energy, $E < 2\mu$, the states near the Fermi surface ($|\vec{p}| \simeq p_F$), denoted as

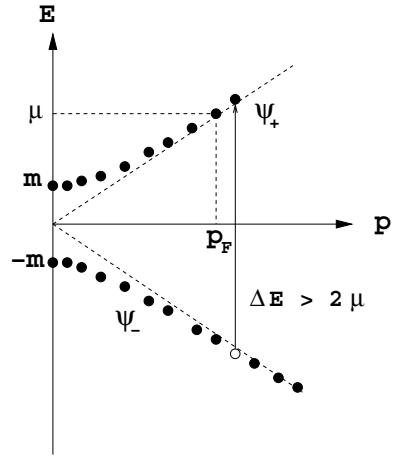

Figure 1. Energy spectrum of quarks at high density

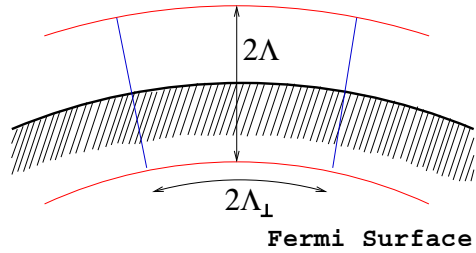

Figure 2. A patch covering the Fermi surface

ψ_+, are easily excited while states deep in the Dirac sea, denoted as ψ_-, are hard to excite.

At low energy, the typical momentum transfer by quarks near the Fermi surface is much smaller than the Fermi momentum. Therefore, similarly to the heavy quark effective theory, we may decompose the momentum of quarks near the Fermi surface as

$$p^\mu = \mu\, v^\mu + l^\mu, \tag{2}$$

where $v^\mu = (0, \vec{v}_F)$ and $\vec{v}_F$ is the Fermi velocity. For quark matter, the typical size of the residual momentum is $|l^\mu| \sim \Lambda_{\rm QCD}$, and the Fermi velocity of the quarks does not change for $\mu \gg \Lambda_{\rm QCD}$, when they are scattered off by soft gluons.

We now introduce patches to cover the Fermi surface, as shown in Fig. 2. The sizes of each patch are 2Λ in vertical direction to the Fermi surface and $2\Lambda_\perp$ in horizontal direction. The quarks in a patch are treated to carry a same Fermi velocity.

The energy of the quarks in the patch is given as

$$E = -\mu + \sqrt{p^2 + m^2} = \vec{l} \cdot \vec{v}_F + \frac{l^2}{2\mu} + O\left(\frac{1}{\mu^2}\right). \tag{3}$$

We see that at the leading order in $1/\mu$ expansion, the energy is independent of the residual momentum, $\vec{l}_\perp$, perpendicular to the Fermi velocity. In HDET, therefore, the perpendicular momentum labels the degeneracy and should satisfy a normalization condition

$$\sum_{\text{patches}} \int_{\Lambda_\perp} \mathrm{d}^2 l_\perp = 4\pi p_F^2. \tag{4}$$

To identify the modes near the Fermi surface, we expand the quark field as

$$\Psi(x) = \sum_{\vec{v}_F} e^{-i\mu \vec{x}\cdot\vec{v}_F} \left[\psi_+(\vec{v}_F, x) + \psi_-(\vec{v}_F, x)\right], \tag{5}$$

where $\psi_\pm(\vec{v}_F, x)$ satisfies respectively

$$\frac{1 \pm \vec{\alpha}\cdot\hat{v}_F}{2}\psi_\pm = \psi_\pm. \tag{6}$$

Note that the projection operator $P_\pm = (1 \pm \vec{\alpha}\cdot\hat{v}_F)/2$ projects out the particle state, ψ_+, and the anti-particle state, ψ_- (or more precisely $\bar{\psi}_-$), from the Dirac spinor field Ψ. The quasi-quarks in a patch carries the residual momentum l^μ and is given as

$$\psi_+(\vec{v}_F, x) = \frac{1 + \vec{\alpha}\cdot\hat{v}_F}{2} e^{-i\mu\vec{v}_F\cdot\vec{x}}\psi(x) \tag{7}$$

The Lagrangian for quark fields becomes

$$\begin{aligned}\mathcal{L} &= \bar{\Psi}\left(i\not{D} + \mu\gamma^0\right)\Psi = \sum_{\vec{v}_F} \bar{\psi}\left(P_+ + P_-\right)\left(\mu\not{V} + \not{D}\right)\left(P_+ + P_-\right)\psi \\ &= \bar{\psi}_+\, i\not{D}_\parallel\, \psi_+ + \bar{\psi}_-(2\mu\gamma^0 + i\not{D}_\parallel)\psi_- + \left[\bar{\psi}_-\, i\not{D}_\perp\, \psi_+ + \text{h.c.}\right], \end{aligned} \tag{8}$$

where we neglected the quark mass term for simplicity and $V^\mu = (1, \vec{v}_F)$. The parallel component of the covariant derivative is $D_\parallel^\mu = V^\mu\, D\cdot V$ and the perpendicular component $D_\perp = D - D_\parallel$. From the quark Lagrangian one can read off the propagators for $\psi_\pm(\vec{v}_F, x)$:

$$S_F^+ = P_+ \frac{i}{\not{l}_\parallel}, \quad S_F^- = P_- \frac{i\gamma^0}{2\mu}\left[1 - \frac{i\gamma^0\not{l}_\parallel}{2\mu} + \cdots\right]. \tag{9}$$

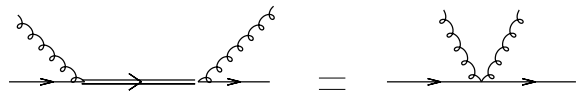

Figure 3. Tree-level matching: The double line denotes ψ_- modes and the single line ψ_+.

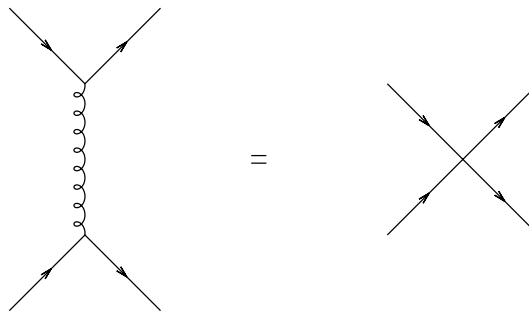

Figure 4. Tree-level matching: Four-Fermi interaction due to hard gluons

We see indeed that in HDET the quarks near the Fermi surface or ψ_+ modes are the propagating modes, while ψ_- are not.

By integrating out ψ_- modes and the hard gluons, one obtains the high density effective theory of QCD. In general the integration results in nonlocal terms in the effective theory and one needs to expand them in powers of $1/\mu$. This is usually done by matching the one-light-particle irreducible amplitudes of the microscopic theory with those of the effective theory. For tree-level amplitudes, this is tantamount to eliminating the irrelevant modes, using the equations of motion.

$$\psi_-(\vec{v}_F, x) = -\frac{i\gamma^0}{2\mu + i\not{D}_\parallel}\not{D}_\perp\psi_+ = -\frac{i\gamma^0}{2\mu}\sum_{n=0}^{\infty}\left(-\frac{i\not{D}_\parallel}{2\mu}\right)^n \not{D}_\perp\psi_+\,. \qquad (10)$$

For instance, a one-light particle irreducible amplitude in QCD of two gluons and two quarks is matched as

$$\bar{\psi}_+ i\not{D}_\perp\psi_-(\vec{v}_F, x)\bar{\psi}_- i\not{D}_\perp\psi_+(\vec{v}_F, y) = \bar{\psi}_+ i\not{D}_\perp\left(-\frac{i\gamma^0}{2\mu}\right) i\not{D}_\perp\psi_+\,, \quad (11)$$

which is shown in Fig. 3. Similarly one can eliminate the hard gluons. Integrating out hard gluons results in four-Fermi interactions of ψ_+ modes. (See Fig. 4.) One continues matching one-loop or higher-loop amplitudes. One interesting feature of HDET is that a new marginal operator arises at the one-loop

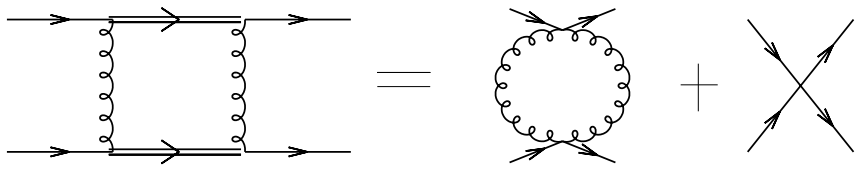

Figure 5. One-loop matching

matching, when incoming quarks are in Cooper-paring kinematics, namely when they have opposite Fermi velocities. As shown in Fig. 5, when the incoming quarks have opposite Fermi velocity, the amplitudes in HDET are ultra-violet divergent while QCD amplitudes are not. Therefore, one needs to introduce a four-Fermi operator as a counter term to remove the UV divergence. If we collect all the terms in the effective theory, it has a systematic expansion in $1/\mu$ and coupling constants α_s as

$$\mathcal{L}_{\rm HDET} = b_1 \bar{\psi}_+ i\gamma_\parallel^\mu D_\mu \psi_+ - \frac{c_1}{2\mu}\bar{\psi}_+\gamma^0(\not{D}_\perp)^2\psi_+ \ + \ \cdots , \tag{12}$$

where $b_1 = 1+O(\alpha_s),\ c_1 = 1+O(\alpha_s), \cdots$. Note that HDET has a reparametrization invariance, similarly to heavy quark effective theory, which is due to the fact that the Fermi velocity of quarks in a patch is not uniquely determined. For a given quark momentum, the corresponding Fermi velocity is determined up to reparametrization; $\vec{v}_F \to \vec{v}_F + \delta\vec{l}_\perp/\mu$ and $\vec{l} \to \vec{l} - \delta\vec{l}$, where $\delta\vec{l}_\perp$ is a residual momentum perpendicular to the Fermi velocity. As in the heavy quark effective theory [9], the renormalization of higher-order operators are restricted due to the reparametrization invariance. For instance, $b_1 = c_1$ at all orders in α_s.

In order for the effective theory to be meaningful, it should have a consistent power-counting. We find the consistent counting in HDET to be for $\Lambda_\perp = \Lambda$

$$\left(\frac{D_\parallel}{\mu}\right)^n \cdot \left(\frac{D_\perp}{\mu}\right)^m \cdot \psi_+^l \sim \left(\frac{\Lambda}{\mu}\right)^{n+m} \Lambda^{3l/2}. \tag{13}$$

To be consistent with the power counting, we impose in loop integration

$$\int_{\Lambda_\perp} \mathrm{d}^2 l_\perp \, l_\perp^n = 0 \quad \text{for} \quad n > 0. \tag{14}$$

So far we have restricted ourselves to operators containing quarks in the same patch. For operators with quarks in different patches, one has to be careful, since the loop integration might jeopardize the power-counting rules. Indeed, consistent counting is to sum up all the hard-loops, as shown by Schäfer [10].

3. More on matching

In HDET, the currents are given in terms of particles and holes but without antiparticles as

$$J^{\mu} = \sum_{\vec{v}_F} \bar{\psi}(\vec{v}_F, x)\gamma_{\parallel}^{\mu}\psi(\vec{v}_F, x) - \frac{1}{2\mu}\psi^{\dagger}\left[\gamma_{\perp}^{\mu},\, i\not{D}_{\perp}\right]\psi + \cdots , \tag{15}$$

where the color indices are suppressed and we have reverted the notation ψ for ψ_+ henceforth. We find that the HDET current is not conserved unless one adds a counter term. Consider the current correlator

$$\langle J^{\mu}(x)J^{\nu}(y)\rangle \;=\; \frac{\delta^2\Gamma_{\rm eff}}{\delta A_{\mu}(x)\delta A_{\nu}(y)} = \int_p e^{-ip\cdot(x-y)}\Pi^{\mu\nu}(p) \tag{16}$$

where the vacuum polarization tensor

$$\Pi_{ab}^{\mu\nu}(p) \;=\; -\frac{iM^2}{2}\delta_{ab}\int\frac{{\rm d}\Omega_{\vec{v}_F}}{4\pi}\left(\frac{-2\vec{p}\cdot\vec{v}_F V^{\mu}V^{\nu}}{p\cdot V + i\epsilon\vec{p}\cdot\vec{v}_F}\right) \tag{17}$$

and $M^2 = N_f g_s^2\mu^2/(2\pi^2)$. We see that the vacuum polarization tensor is not transverse, $p_{\mu}\Pi_{ab}^{\mu\nu}(p) \neq 0$, which means that the current is not conserved. The physical reason for this is that not only modes near the Fermi surface but also modes deep in the Fermi sea respond to external sources collectively. To recover the current conservation in the effective theory, we need to add the DeBye screening mass term due to ψ_- (See Fig. 6):

$$\Gamma^{\rm eff} \mapsto \tilde{\Gamma}^{\rm eff} = \Gamma^{\rm eff} - \int_x \frac{M^2}{2}\sum_{\vec{v}_F} A_{\mu}A_{\nu}g_{\perp}^{\mu\nu}. \tag{18}$$

Then vacuum polarization tensor becomes

$$\Pi^{\mu\nu}(p) \mapsto \tilde{\Pi}^{\mu\nu}(p) = \Pi^{\mu\nu} - \frac{i}{2}\sum_{\vec{v}_F} g_{\perp}^{\mu\nu}M^2\,. \tag{19}$$

The modified polarization tensor is now transverse, $p_{\mu}\tilde{\Pi}^{\mu\nu} = 0$.

Now, let us consider the divergence of axial currents in HDET, which is related to the axial anomaly and also to how the quark matter responds to external axial-current sources like electroweak probes.

It is easy to show that the axial anomaly in dense matter is independent of density or the chemical potential μ [11]. In general one may re-write the divergence of axial currents in dense QCD as follows:

$$\langle\partial_{\mu}J_5^{\mu}\rangle = \frac{g^2}{16\pi^2}\tilde{F}_{\mu\alpha}F^{\mu\alpha} + \Delta^{\alpha\beta}(\mu)A_{\alpha}A_{\beta}\,, \tag{20}$$

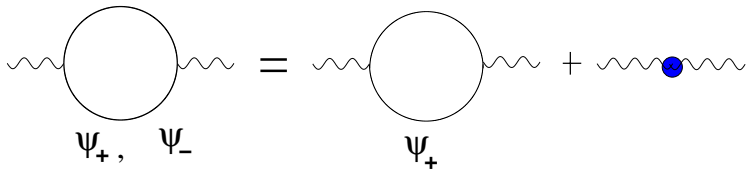

Figure 6. Matching two-point functions

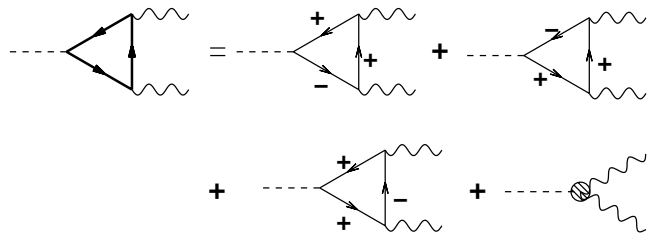

Figure 7. Matching axial anomaly. $+$ denotes ψ_+ and $-$ denotes ψ_-.

where the first term is the usual axial anomaly in vacuum and the second term is due to matter. However, one can explicitly calculate the second term, which is finite, to find $\Delta^{\alpha\beta}(\mu) = 0$. In HDET, the axial anomaly due to modes near the Fermi surface is given as

$$\sum_{\vec{v}_F} \int_{x,y} e^{ik_1\cdot x + ik_2\cdot y} \left\langle \partial_\mu J_5^\mu(\vec{v}_F, 0) J^\alpha(\vec{v}_F, x) J^\beta(\vec{v}_F, y) \right\rangle \equiv \Delta^{\alpha\beta}_{\text{eff}} \qquad (21)$$

By explicit calculation we find

$$\Delta^{0i}_{\text{eff}} = -\frac{g^2}{4\pi^2} \cdot \frac{1}{3} \left(\vec{k}_1 \times \vec{k}_2 \right)^i , \; \Delta^{ij}_{\text{eff}} = \frac{g^2}{4\pi^2} \frac{2}{3} \epsilon^{ijl} \left(k_{10} k_{2l} - k_{1l} k_{20} \right) . \qquad (22)$$

We see that the modes near the Fermi surface contributes only some parts of the axial anomaly. As in the vector current, the rest should come from modes in the deep Fermi sea and from anti-particles. To recover the full axial anomaly we add a counter term (See Fig. 7), which is two thirds of the axial anomaly plus a Chern-Simons term:

$$\tilde{\Delta}^{\alpha\beta}_{\text{eff}} = \Delta^{\alpha\beta}_{\text{eff}} + \frac{g^2}{6\pi^2} \epsilon^{\alpha\beta\rho\sigma} k_{1\rho} k_{2\sigma} + \frac{g^2}{12\pi^2} \epsilon^{\alpha\beta 0 l} \left(k_{10} k_{2l} - k_{1l} k_{20} \right) . \qquad (23)$$

4. Color superconductivity in dense QCD

At high density, quarks in dense matter interact weakly with each other and form a Fermi sea, due to asymptotic freedom. When the energy is much less

than the quark chemical potential ($E \ll \mu$), only the quarks near the Fermi surface are relevant. The dynamics of quarks near the Fermi surface is effectively one-dimensional, since excitations along the Fermi surface do not cost any energy. The momentum perpendicular to the Fermi momentum just labels the degeneracy, similarly to the perpendicular momentum of charged particle under external magnetic field. This dimensional reduction due to the presence of Fermi surface makes possible for quarks to form a Cooper pair for any arbitrary weak attraction, since the critical coupling for the condensation in (1+1) dimensions is zero, known as the Cooper theorem in condensed matter.

While, in the BCS theory, such attractive force for electron Cooper pair is provided by phonons, for dense quark matter, where phonons are absent, the gluon exchange interaction provides the attraction, as one-gluon exchange interaction is attractive in the color anti-triplet channel[1] One therefore expects that color anti-triplet Cooper pairs will form and quark matter is color superconducting, which is indeed shown more than 20 years ago [13, 14].

At intermediate density, quarks and gluons are strongly interacting and gluons are therefore presumably screened. Then, QCD at intermediate density may be modeled by four-Fermi interactions and higher-order terms by massive gluons.

$$\mathcal{L}_{\rm QCD}^{\rm eff} \ni \frac{G}{2}\bar{\psi}\psi\bar{\psi}\psi + \cdots , \tag{24}$$

where the ellipsis denotes higher-order terms induced by massive gluons. When the incoming quarks have opposite momenta, the four-Fermi interaction is marginally relevant, if attractive, and all others are irrelevant. As the renormalization group flows toward the Fermi surface, the attractive four-Fermi interaction is dominant and blows up, resulting in a Landau pole, which can be avoided only when a gap opens at the Fermi surface. This is precisely the Cooper-instability of the Fermi surface. The size of gap can be calculated by solving the gap equation, which is derived by the variational principle that the gap minimizes the vacuum energy:

$$0 = \frac{\partial V_{\rm BCS}(\Delta)}{\partial \Delta} = \frac{\Delta}{G} - i\int \frac{d^4k}{(2\pi)^4}\frac{\Delta}{k_0^2 - (\vec{k}\cdot\vec{v}_F)^2 - \Delta^2}, \tag{25}$$

which gives

$$\Delta = -iG\int \frac{d^4k}{(2\pi)^4}\frac{\Delta}{[(1+i\epsilon)k_0]^2 - (\vec{k}\cdot\vec{v}_F)^2 - \Delta^2}. \tag{26}$$

[1]There is also an attractive force between quarks and holes in the color octet channel: $\langle \bar{\psi}_i(-\vec{p})\psi_j(\vec{p})\rangle \neq 0$, which corresponds to a density wave. However, because of the momentum conservation, the density wave condensate does not enjoy the full Fermi surface degeneracy. Indeed, for QCD, the diquark condensate is energetically preferred to the density wave condensate [12].

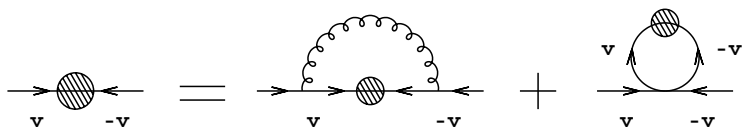

Figure 8. Eliashberg equation at high density.

We note that the integrand in Eq. 40 does not depend on $k_\perp$, whose integration gives the density of states at the Fermi surface, and the $i\epsilon$ prescription is consistent with the Feynman propagator. The pole occurs at

$$k_0 = \pm\sqrt{(\vec{k}\cdot\vec{v}_F)^2 + \Delta^2} \ \mp i\epsilon \tag{27}$$

or in terms of full momentum $p = \mu\, v + k$ it occurs at

$$p_0 = \pm\sqrt{(|\vec{p}| - \mu)^2 + \Delta^2} \ \mp i\epsilon\,. \tag{28}$$

We find the solution to the gap equation

$$\Delta_0 = 2\mu \exp\left(-\frac{\pi^2}{2G\mu^2}\right). \tag{29}$$

For generic parameters of dense QCD, the gap is estimated to be $10 \sim 100\,\mathrm{MeV}$ at the intermediate density. The free energy of the BCS state is given as

$$\begin{aligned} V_{\rm BCS}(\Delta_0) &= \int_0^{\Delta_0} \frac{\partial V_{\rm BCS}}{\partial\Delta}\mathrm{d}\Delta \\ &= \frac{4\mu^2}{G}\int_0^{x_0}\left(x + g^2\ln x\right)dx = -\frac{\mu^2}{4\pi^2}\Delta_0^2, \end{aligned} \tag{30}$$

where $x = \Delta/(2\mu)$ and $g^2 = 2G\mu^2/\pi^2$. At high density magnetic gluons are not screened though electric gluons are screened [15–17]. The long-range pairing force mediated by magnetic gluons leads to the Eliashberg gap equation (See Fig. 8).

$$\Delta(p_0) = \frac{g_s^2}{36\pi^2}\int_{-\mu}^{\mu} dq_0 \frac{\Delta(q_0)}{\sqrt{q_0^2+\Delta^2}} \ln\left(\frac{\bar{\Lambda}}{|p_0 - q_0|}\right), \tag{31}$$

where $\bar{\Lambda} = 4\mu/\pi \cdot (\mu/M)^5 e^{3/2\xi}$ and ξ is a gauge parameter. Due to the unscreened but Landau-damped gluons, there is an extra (infrared) logarithmic divergence in the gap equation, when the incoming quark momentum is collinear with the gluon momentum. The Cooper-pair gap at high density is found to be [17, 18]

$$\Delta_0 = \frac{2^7\pi^4}{N_f^{5/2}} e^{3\xi/2+1} \cdot \frac{\mu}{g_s^5} \exp\left(-\frac{3\pi^2}{\sqrt{2}g_s}\right). \tag{32}$$

The numerical prefactor of the gap is not complete, since the contributions from subleading corrections to the gap equation that lead to logarithmic divergences, such as the wavefunction renormalization and the vertex corrections, are not taken into account. Recently, however, the contributions to the prefactor, coming from the vertex corrections and the wavefunction renormalization for quarks were calculated by finding a (nonlocal) gauge [19], where the quark wavefunction is not renormalized for all momenta, $Z(p) = 1$. At the nonlocal gauge, $\xi \simeq 1/3$. The subleading corrections therefore increase the leading-order gap at the Coulomb gauge by about two thirds.

5. Quark matter under stress

It is quite likely to find dense quark matter inside compact stars like neutron stars. However, when we study the quark matter in compact stars, we need to take into account not only the charge and color neutrality of compact stars and but also the mass of the strange quark, which is not negligible at the intermediate density. By the neutrality condition and the strange quark mass, the quarks with different quantum numbers in general have different chemical potentials and different Fermi momenta. When the difference in the chemical potential becomes too large the Cooper-pairs breaks or other exotic phases like kaon condensation or crystalline phase is more preferred to the BCS phase.

Let us consider for example the pairing between up and strange quarks in chemical equilibrium. The energy spectrum of up quarks is given as

$$E = -\mu \pm |\vec{p}|, \tag{33}$$

while the energy of strange quarks of mass M_s becomes

$$E = -\mu \pm \sqrt{|\vec{p}|^2 + M_s^2}\,. \tag{34}$$

The Fermi sea of up and strange quarks is shown in Fig. 9. Because of the strange quarks mass, they have different Fermi momenta. Note that the Cooper-pairing occurs for quarks with same but opposite momenta. Therefore, at least one of the pairing quarks should be excited away from the Fermi surface, costing some energy. Let us suppose that the Cooper-pair gap opens at $|\vec{p}| = \bar{p}$ between two Fermi surfaces, $p_F^s \le \bar{p} \le p_F^u$.

To describe such pairing, we consider small fluctuations of up and strange quarks near $\bar{p}$. The energy of such fluctuations of up and down quarks is respectively

$$E_u = -\mu + |\bar{p} + \vec{l}\,| \simeq -\delta\mu^u + \vec{v}_u \cdot \vec{l}, \qquad E_s \simeq -\delta\mu^s + \vec{v}_s \cdot \vec{l}, \tag{35}$$

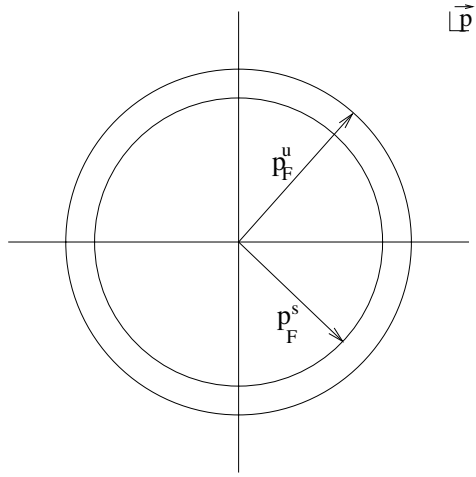

Figure 9. Fermi sea of up and strange quarks.

where $\delta\mu^u = \mu - \bar{p}$ and $\delta\mu^s = \mu - \sqrt{\bar{p}^2 + M_s^2}$. $\vec{v}_u$ and $\vec{v}_s$ are the velocities of up and strange quarks at $|\vec{p}| = \bar{p}$. Let Δ be the BCS gap for the u, s pairing. Then, the Lagrangian for the u, s quarks is given as

$$\mathcal{L} = \bar{u}\left(i\ \partial\!\!\!/ + \mu\gamma^0\right) u + \bar{s}_c\left(i\ \partial\!\!\!/ - \mu\gamma^0 - M_s\right) s_c - \Delta\,\bar{s}_c\, u + \text{h.c.} + \mathcal{L}_{\text{int}}, \quad (36)$$

where s_c is the charge conjugate field of s quark. In HDET, the Lagrangian becomes

$$\mathcal{L}_{\text{HDET}} \ni u^\dagger\left(iV_u \cdot \partial + \delta\mu^u\right) u + s_c^\dagger\left(i\bar{V}_s \cdot \partial - \delta\mu^s\right) s_c - \Delta\bar{s}_c\, u + \text{h.c.}, \quad (37)$$

where $V_u = (1, \vec{v}_u)$ and $\bar{V}_s = (1, -\vec{v}_s)$. The Cooper-pair gap equation is then

$$\Delta(p) = \int_l \frac{i\Delta(l)\, K(p-l)}{\left[(1+i\epsilon)l_0 - \vec{l}\cdot\vec{v}_u + \delta\mu^u\right]\left[(1+i\epsilon)l_0 + \vec{l}\cdot\vec{v}_s - \delta\mu^u\right] - \Delta^2}, \quad (38)$$

where K is the kernel for the gap equation and is a constant for the four-Fermi interaction. By examining the pole structure, we see that the Cooper-pair gap does not exist when

$$-\delta\mu^u\delta\mu^s > \frac{\Delta^2}{4}. \quad (39)$$

Only when $-\delta\mu^u\delta\mu^s < \Delta^2/4$, one can shift $l_0 \to l_0' = l_0 + \delta\mu^u$ or $l_0 \to l_0' = l_0 - \delta\mu^s$ without altering the pole structure. Note that the gap becomes biggest when $\delta\mu^u = -\delta\mu^s (\equiv \delta\mu)$, which determines the pairing momentum to be

$$\bar{p} = \mu - \frac{M_s^2}{4\mu}. \quad (40)$$

If $\delta\mu < \Delta/2$ or $\Delta > M_s^2/(2\mu)$, the solution to the Cooper-pair gap exists. The gap equation then can be written as, shifting l_0, in Euclidean space

$$\Delta(p) = \int \frac{\mathrm{d}^4 l}{(2\pi)^4} \frac{\Delta(l)}{l_\parallel^2 + \Delta^2} K(l-p), \tag{41}$$

where $l_\parallel^2 = l_0^2 + c^2(\vec{l}\cdot\hat{v})^2$ and $c^2 = \bar{p}/\sqrt{\bar{p}^2 + M_s^2}$. In HDET, one can easily see that the Cooper-pair gap closes if the effective chemical potential difference, $2\delta\mu$, due to an external stress, exceeds the Cooper-pair gap when there is no stress. One should note that even before the Cooper-pair gap closes other gap may open as shown by many authors [20, 21]. But, one needs to compare the free energy of each phases to find the true ground state for quark matter under stress.

6. Positivity of HDET

Fermionic dense matter generically suffers from the sign problem, which has thus far precluded lattice simulations [22]. However, the sign problem usually associated with fermions is absent if one considers only low-energy degrees of freedom. The complexness of the measure of fermionic dense matter can be ascribed to modes far from the Fermi surface, which are irrelevant to dynamics at sufficiently high density in most cases, including quark matter [5, 6]. For modes near the Fermi surface, there is a discrete symmetry, relating particles and holes, which pairs the eigenvalues of the Dirac operator to make its determinant real and nonnegative. Especially, the low energy effective theory of dense QCD has positive Euclidean path integral measure, which allows one to establish rigorous inequalities that the color-flavor locked (CFL) phase is the true vacuum of three flavor, massless QCD.

As simple example, let us consider a fermionic matter in 1+1 dimensions, where non-relativistic fermions are interacting with a gauge field A. The action is in general given as

$$S = \int d\tau dx\, \psi^\dagger \left[(-\partial_\tau + i\phi + \epsilon_F) - \epsilon(-i\partial_x + A)\right]\psi, \tag{42}$$

where $\epsilon(p) \simeq p^2/(2m) + \cdots$ is the energy as a function of momentum. Low energy modes have momentum near the Fermi points and have energy, measured from the Fermi points,

$$E(p \pm p_F) \simeq \pm\, v_F p, \quad v_F = \left.\frac{\partial E}{\partial p}\right|_{p_F}. \tag{43}$$

If the gauge fields have small amplitude and are slowly varying relative to scale p_F, the fast modes are decoupled from low energy physics. The low energy

effective theory involving quasi particles and gauge fields has a positive, semi-definite determinant.

To construct the low energy effective theory of the fermionic system, we rewrite the fermion fields as

$$\psi(x,\tau) = \psi_L(x,\tau)e^{+ip_F x} \; + \; \psi_R(x,\tau)e^{-ip_F x}, \tag{44}$$

where $\psi_{L,R}$ describes the small fluctuations of quasiparticles near the Fermi points. Using $e^{\pm ip_F x}\, E(-i\partial_x + A)\, e^{\mp ip_F x}\, \psi(x) \approx \pm\, v_F(-i\partial_x + A)\psi(x)$, we obtain

$$S_{\text{eff}}=\int_{\tau,x}\Big[\psi_L^\dagger(-\partial_\tau + i\phi + i\partial_x - A)\psi_L + \psi_R^\dagger(-\partial_\tau + i\phi - i\partial_x + A)\psi_R\Big]\,. \tag{45}$$

Introducing the Euclidean (1+1) gamma matrices $\gamma_{0,1,2}$ and $\psi_{L,R} = \frac{1}{2}(1 \pm \gamma_2)\psi$, we obtain a positive action:

$$S_{\text{eff}} = \int d\tau\, dx\, \bar\psi\gamma^\mu(\partial_\mu + iA_\mu)\psi \equiv \int d\tau dx\, \bar\psi\, \not{D}\psi. \tag{46}$$

Since $\not{D} = \gamma_2 \not{D}^\dagger \gamma_2$, the determinant of $\not{D}$ is positive, semi-definite.

In this example, we see that near the Fermi surface, modes have low energy, slowly varying, and thus lead to an effective theory without any sign problem what so ever if they couple to slowly varying background fields. QCD at high baryon density falls into this category, since the coupling constant is small at high energy due to asymptotic freedom.

HDET of quark matter is described by

$$\mathcal{L}_{\text{HDET}} = \bar\psi_+ i\gamma_\parallel^\mu D_\mu \psi_+ - \frac{1}{2\mu}\bar\psi_+\gamma^0(\not{D}_\perp)^2\psi_+ \; + \; \cdots\,, \tag{47}$$

where $\gamma_\parallel^\mu = (\gamma^0, \vec v_F \vec v_F\cdot\vec\gamma) = \gamma^\mu - \gamma_\perp^\mu$. We see that the leading term has a positive determinant, since

$$M_{\text{eft}} = \gamma_\parallel^E \cdot D(A) \; = \; \gamma_5 M_{\text{eft}}^\dagger \gamma_5. \tag{48}$$

In order to implement this HDET on lattice, it is convenient to introduce an operator formalism, where the velocity is realized as an operator,

$$\vec v = \frac{-i}{\sqrt{-\nabla^2}}\;\frac{\partial}{\partial \vec x}\;. \tag{49}$$

Then the quasi quarks near the Fermi surface become

$$\psi = \exp\left(+i\mu x\cdot v\right)\frac{1+\alpha\cdot v}{2}\psi_+. \tag{50}$$

Now, neglecting the higher order terms, the Lagrangian becomes with $X = \exp(i\mu x \cdot v)(1 + \alpha \cdot v)/2$,

$$\mathcal{L}_{\rm HDET} = \bar{\psi}_+ \gamma_\parallel^\mu \left(\partial^\mu + iA_+^\mu\right) \psi_+, \tag{51}$$

where $A_+^\mu = X^\dagger A^\mu X$ denotes soft gluons whose momentum $|p_\mu| < \mu$. Since $v \cdot \partial\, v \cdot \gamma = \partial \cdot \gamma$, we get

$$\gamma_\parallel^\mu \partial^\mu = \gamma^\mu \partial^\mu \tag{52}$$

which shows that the operator formalism automatically covers modes near the full Fermi surface.

Integrating out the fast modes, modes far from the Fermi surface and hard gluons, the QCD partition function (1) becomes

$$Z(\mu) = \int \mathrm{d}A_+ \det\left(M_{\rm eff}\right) e^{-S_{\rm eff}(A_+)}, \tag{53}$$

where

$$S_{\rm eff} = \int_{x_E} \left(\frac{1}{4} F_{\mu\nu}^a F_{\mu\nu}^a + \frac{M^2}{16\pi} A_{\perp\mu}^a A_{\perp\mu}^a\right) + \cdots \tag{54}$$

and $A_\perp = A - A_\parallel$, the Debye mass $M = \sqrt{N_f/(2\pi^2)}\, g_s \mu$. At high density the higher order terms ($\sim \Lambda/\mu$) are negligible and the effective action becomes positive, semi-definite. Therefore, though it has non-local operators, HDET in the operator formalism, free from the sign problem, can be used to simulate the Fermi surface physics like superconductivity. Furthermore, being exactly positive at asymptotic density, HDET allows to establish rigorous inequalities relating bound state masses and forbidding the breaking of vector symmetries, except baryon number, in dense QCD [6].

With the help of previous two examples, we propose a new way of simulating dense QCD, which evades the sign problem. Integrating out quarks far from the Fermi surface, which are suppressed by $1/\mu$ at high density, we can expand the determinant of Dirac operator at finite density,

$$\det\left(M\right) = [\text{real}, \text{positive}] \left[1 \;+\; \mathcal{O}\left(\frac{\mathbf{F}}{\mu^2}\right)\right]. \tag{55}$$

As long as the gauge fields are slowly varying, compared to the chemical potential μ, the sign problem can be evaded. As a solution to the sign problem, we propose to use two lattices with different spacings, a finer lattice with a lattice spacing $a_{\rm det} \sim \mu^{-1}$ for fermions and a coarser lattice with a lattice spacing $a_{\rm gauge} \ll \mu^{-1}$ for gauge fields and then compute the determinant on such lattices.

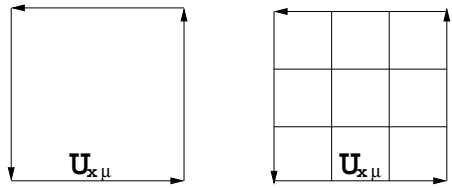

Figure 10. Simulation with two lattices with different lattice spacings

The determinant is a function of plaquettes $\{\mathbf{U}_{\mathbf{x}\mu}\}$ which are obtained by interpolation from the plaquettes on the coarser lattice of lattice spacing $a_{\rm gauge}$. To get the link variables for the finer lattice, we interpolate the link variables $\mathbf{U}_{\mathbf{x}\mu} \in SU(3)$ (see Fig. 10): Connect any two points g_1, g_2 on the group manifold as

$$g(t) = g_1 + t(g_2 - g_1)\ ,\ 0 \le t \le 1\,. \tag{56}$$

For importance sampling in the lattice simulation, one can use the leading part of the determinant, $[\mathrm{real}, \mathrm{positive}]$. This proposal provides a nontrivial check on analytic results at asymptotic density and can be used to extrapolate to intermediate density. Furthermore, it can be applied to condensed matter systems like High-T_c superconductors, which in general suffers from a sign problem.

Positivity of the measure allows for rigorous QCD inequalities at asymptotic density. For example, inequalities among masses of bound states can be obtained using bounds on bare quasiparticle propagators. One subtlety that arises is that a quark mass term does not lead to a quasiparticle gap (the mass term just shifts the Fermi surface). Hence, for technical reasons the proof of nonbreaking of vector symmetries [23] must be modified. (Naive application of the Vafa-Witten theorem would preclude the breaking of baryon number that is observed in the color-flavor-locked (CFL) phase [24]). A quasiparticle gap can be inserted by hand to regulate the bare propagator, but it will explicitly violate baryon number. However, following the logic of the Vafa-Witten proof, any symmetries which are preserved by the regulator gap cannot be broken spontaneously. One can, for example, still conclude that isospin symmetry is never spontaneously broken (although see below for a related subtlety). In the case of three flavors, one can introduce a regulator d with the color and flavor structure of the CFL gap to show rigorously that none of the symmetries of the CFL phase are broken at asymptotic density. On the other hand, by applying anomaly matching conditions [25], we can prove that the $SU(3)_A$ symmetries *are* broken. We therefore conclude that the CFL phase is the true ground state for three light flavors at asymptotic density, a result that was first established by explicit calculation [26, 8, 27].

To examine the long-distance behavior of the vector current, we note that the correlator of the vector current for a given gauge field A can be written as

$$\left\langle J^a_\mu(\vec{v}_F,x)J^b_\nu(\vec{v}_F,y)\right\rangle^A = -\mathrm{Tr}\,\gamma_\mu T^a S^A(x,y;d)\gamma_\nu T^b S^A(y,x;d), \quad (57)$$

where the $SU(N_f)$ flavor current $J^a_\mu(\vec{v}_F,x) = \bar{\psi}_+(\vec{v}_F,x)\gamma_\mu T^a\psi_+(\vec{v}_F,x)$. The propagator with $SU(3)_V$-invariant IR regulator d is given as

$$S^A(x,y;d) = \langle x|\,\frac{1}{M}\,|y\rangle = \int_0^\infty \mathrm{d}\tau\,\langle x|\,e^{-i\tau(-iM)}\,|y\rangle$$

where with $D = \partial + iA$

$$M \;=\; \gamma_0\begin{pmatrix} D\cdot V & d \\ d^\dagger & D\cdot\bar{V}\end{pmatrix} \quad (58)$$

Since the eigenvalues of M are bounded from below by d, we have

$$\left|\langle x|\,\frac{1}{M}\,|y\rangle\right| \le \int_R^\infty \mathrm{d}\tau\, e^{-d\,\tau}\sqrt{\langle x|x\rangle}\sqrt{\langle y|y\rangle} = \frac{e^{-d\,R}}{d}\sqrt{\langle x|x\rangle}\sqrt{\langle y|y\rangle}, \quad (59)$$

where $R \equiv |x-y|$. The current correlators fall off rapidly as $R\to\infty$;

$$\begin{aligned}&\left|\int \mathrm{d}A_+\,\det M_{\rm eff}(A)\;e^{-S_{\rm eff}}\left\langle J^A_\mu(\vec{v}_F,x)J^B_\nu(\vec{v}_F,y)\right\rangle^{A_+}\right| \\ &\le \int_{A_+}\left|\left\langle J^A_\mu(\vec{v}_F,x)J^B_\nu(\vec{v}_F,y)\right\rangle^{A_+}\right| \le \frac{e^{-2d\,R}}{d^2}\int_{A_+}|\langle x|x\rangle|\,|\langle y|y\rangle|\,, \quad (60)\end{aligned}$$

where we used the Schwartz inequality in the first inequality, since the measure of the effective theory is now positive, and equation (59) in the second inequality. The IR regulated vector currents do not create massless modes out of the vacuum or Fermi sea, which implies that there is no Nambu-Goldstone mode in the $SU(3)_V$ channel. Therefore, for three massless flavors $SU(3)_V$ has to be unbroken as in CFL. The rigorous result provides a non-trivial check on explicit calculations, and applies to any system in which the quasiparticle dynamics have positive measure.

It is important to note the order of limits necessary to obtain the above results. Because there are higher-order corrections to the HDET, suppressed by powers of Λ/μ, that spoil its positivity, there may be contributions on the RHS of (60) of the form

$$\mathcal{O}\left(\frac{\Lambda}{\mu}\right)\,f(R)\,, \quad (61)$$

where $f(R)$ falls off more slowly than the exponential in (60). To obtain the desired result, we must first take the limit $\mu\to\infty$ at fixed Λ before taking $R\to\infty$. Therefore, our results only apply in the limit of asymptotic density.

Although our result precludes breaking of vector symmetries at asymptotic density in the case of three *exactly* massless quarks [29], it does not necessarily apply to the case when the quark masses are allowed to be slightly non-zero. In that case the results depend on precisely how the limits of zero quark masses and asymptotic density are taken, as we discuss below.

In [21] the authors investigate the effect of quark masses on the CFL phase. These calculations are done in the asymptotic limit, and are reliable for sufficiently small quark masses. When $m_u = m_d \equiv m << m_s$ (unbroken $SU(2)$ isospin, but explicitly broken $SU(3)$), one finds a kaon condensate. The critical value of m_s at which the condensate forms is $m_s^* \sim m^{1/3}\Delta_0^{2/3}$, where Δ_0 is the CFL gap (see, in particular, equation (8) of the first paper). As kaons transform as a doublet under isospin, the vector $SU(2)$ symmetry is broken in seeming contradiction with our result.

However, a subtle order of limits is at work here. For simplicity, let us set $m = 0$. Note that the CFL regulator d, which was inserted by hand, explicitly breaks $SU(3)_A$ through color-flavor locking, leading to small positive mass squared for the pions and kaons, given as

$$m_{\pi,K}^2 \sim \alpha_s d^2 \, \ln\left(\frac{\mu}{d}\right). \tag{62}$$

The meson mass is not suppressed by $1/\mu$, since, unlike the Dirac mass term, the regulator, being a Majorana mass, does not involve antiquarks [28].

Therefore, even when the light quarks are massless, there is a critical value of m_s necessary to drive negative the mass-squared of kaons and cause condensation:

$$m_s^* \;\sim\; \left[g_s d\mu \, \ln\left(\frac{\mu}{d}\right)\right]^{1/2} \;>\; (d\mu)^{1/2}\,, \tag{63}$$

where g_s is the strong coupling constant. Note the product of g_s with the logarithm grows as μ gets large. To obtain our inequality we must keep the regulator d non-zero until the end of the calculation in order to see the exponential fall off. To find the phase with kaon condensation identified in [21] we must keep m_s larger than m_s^*. (Note $\mu \to \infty$, so to have any chance of finding this phase we must take $d \to 0$ keeping dR large and $d\mu$ small.)

Since the UV cutoff of the HDET must be larger than m_s, we have

$$1 \;>\; \left(\frac{m_s^*}{\Lambda}\right)^2 \;>\; \frac{d}{\Lambda}\,\frac{\mu}{\Lambda}\,, \tag{64}$$

which implies

$$\frac{\Lambda}{\mu}\, f(R) \;>\; \frac{d}{\Lambda}\, f(R)\,. \tag{65}$$

Note the right hand side of this inequality does not necessarily fall off at large R, and also does not go to zero for $\mu \to \infty$ at fixed Λ and d. This is a problem

since to apply our inequality the exponential falloff from (60) must dominate the correction term (61), which is just the left hand side of (65). Combining these equations, we see that the exponential falloff of the correlator is bounded below,

$$\frac{e^{-2d\,R}}{d^2} \;>\; \frac{d}{\Lambda}\, f(R)\,, \tag{66}$$

in the scaling region with a kaon condensate, $m_s > m_s^*$.

Alternatively, if we had taken m_s to be finite for fixed regulator d (so that, as $\mu \to \infty$, eventually $m_s < m_s^*$), the inequality in (60) could be applied to exclude a Nambu-Goldstone boson, but we would find ourselves in the phase without a kaon condensate.

Acknowledgments

The author wishes to thank Mark Alford, Phillipe de Forcrand, Simon Hands, Krishna Rajagopal, Francesco Sannino, Thomas Schäfer for useful discussions. The author is thankful especially to Steve Hsu for the critical discussions and for the collaboration, upon which some of this lecture is based. This work is supported by KOSEF grant number R01-1999-000-00017-0.

References

[1] K. Rajagopal and F. Wilczek, arXiv:hep-ph/0011333; D. K. Hong, Acta Phys. Polon. B **32**, 1253 (2001) [arXiv:hep-ph/0101025]; M. G. Alford, Ann. Rev. Nucl. Part. Sci. **51**, 131 (2001) [arXiv:hep-ph/0102047]; S. D. H. Hsu, arXiv:hep-ph/0003140. T. Schafer, arXiv:hep-ph/0304281. D. H. Rischke, Prog.Part.Nucl.Phys.52:197-296 (2003) [arXiv:nucl-th/0305030].

[2] F. Karsch, E. Laermann and A. Peikert, Nucl. Phys. B **605**, 579 (2001) [arXiv:hep-lat/0012023]; F. Karsch, E. Laermann, A. Peikert, C. Schmidt and S. Stickan, arXiv:hep-lat/0010027; F. Karsch, Nucl. Phys. A **698**, 199 (2002) [arXiv:hep-ph/0103314].

[3] Z. Fodor and S. D. Katz, Phys. Lett. B **534**, 87 (2002) [arXiv:hep-lat/0104001]; JHEP **0203**, 014 (2002) [arXiv:hep-lat/0106002].

[4] C. R. Allton *et al.*, Phys. Rev. D **66**, 074507 (2002) [arXiv:hep-lat/0204010]; P. de Forcrand and O. Philipsen, Nucl.Phys.Proc.Suppl.119:535-537 (2002) [arXiv:hep-lat/0209084]; M. D'Elia and M. P. Lombardo, Phys. Rev. D **67**, 014505 (2003) [arXiv:hep-lat/0209146].

[5] D. K. Hong and S. D. Hsu, Phys. Rev. D **66**, 071501 (2002) [arXiv:hep-ph/0202236].

[6] D. K. Hong and S. D. Hsu, Phys. Rev. D **68**, 034011 (2003) [arXiv:hep-ph/0304156].

[7] D. K. Hong, Phys. Lett. B **473**, 118 (2000) [arXiv:hep-ph/9812510];

[8] D. K. Hong, Nucl. Phys. B **582**, 451 (2000) [arXiv:hep-ph/9905523].

[9] M. Luke and A. V. Manohar, Phys. Lett. B **286** (1992) 348.

[10] T. Schafer, Nucl. Phys. A **728**, 251 (2003) [arXiv:hep-ph/0307074]; T. Schafer, eConf C030614:038 (2003) [arXiv:hep-ph/0310176].

[11] D. K. Hong, B. I. Hur, Y. J. Son and T.-S. park, to appear.

[12] E. Shuster and D. T. Son, Nucl. Phys. B **573**, 434 (2000) [arXiv:hep-ph/9905448]. B. Y. Park, M. Rho, A. Wirzba and I. Zahed, Phys. Rev. D **62**, 034015 (2000) [arXiv:hep-ph/9910347].

[13] F. Barrois, Nucl. Phys. **B129** (1977) 390.

S. C. Frautschi, *Asymptotic freedom and color superconductivity in dense quark matter*, in: Proceedings of the Workshop on Hadronic Matter at Extreme Energy Density, N. Cabibbo, Editor, Erice, Italy (1978).

[14] D. Bailin and A. Love, Phys. Rept. **107** (1984) 325.

[15] G. Baym, H. Monien and C. J. Pethick, In "Hirschegg 1988, Proceedings, Gross properties of nuclei and nuclear excitations" 128-132; C. J. Pethick, G. Baym and H. Monien, Nucl. Phys. A **498**, 313C (1989).

[16] R. D. Pisarski and D. H. Rischke, Phys. Rev. Lett. **83**, 37 (1999) [arXiv:nucl-th/9811104].

[17] D. T. Son, Phys. Rev. D **59**, 094019 (1999) [arXiv:hep-ph/9812287].

[18] D. K. Hong, V. A. Miransky, I. A. Shovkovy and L. C. R. Wijewardhana, Phys. Rev. D **61**, 056001 (2000) [Erratum-ibid. D **62**, 059903 (2000)] [arXiv:hep-ph/9906478]; T. Schafer and F. Wilczek, Phys. Rev. D **60**, 114033 (1999) [arXiv:hep-ph/9906512]; R. D. Pisarski and D. H. Rischke, Phys. Rev. D **61**, 051501 (2000) [arXiv:nucl-th/9907041]; W. E. Brown, J. T. Liu and H. c. Ren, Phys. Rev. D **61**, 114012 (2000) [arXiv:hep-ph/9908248].

[19] D. K. Hong, T. Lee, D. P. Min, D. Seo and C. Song, Phys. Lett. B **565**, 153 (2003) [arXiv:hep-ph/0303181].

[20] M. G. Alford, J. A. Bowers and K. Rajagopal, Phys. Rev. D **63**, 074016 (2001) [arXiv:hep-ph/0008208]; M. Alford, C. Kouvaris and K. Rajagopal, Phys.Rev.Lett.92:222001 (2003) [arXiv:hep-ph/0311286]; R. Casalbuoni, R. Gatto, M. Mannarelli and G. Nardulli, Phys. Lett. B **511**, 218 (2001) [arXiv:hep-ph/0101326].

[21] P. F. Bedaque and T. Schafer, Nucl. Phys. A **697**, 802 (2002) [arXiv:hep-ph/0105150]; D. B. Kaplan and S. Reddy, Phys. Rev. D **65**, 054042 (2002) [arXiv:hep-ph/0107265].

[22] See, for instance, S. Hands, Nucl. Phys. Proc. Suppl. **106**, 142 (2002) [arXiv:hep-lat/0109034]; I. M. Barbour, S. E. Morrison, E. G. Klepfish, J. B. Kogut and M. P. Lombardo, Nucl. Phys. Proc. Suppl. **60A**, 220 (1998) [arXiv:hep-lat/9705042]; M. G. Alford, Nucl. Phys. Proc. Suppl. **73**, 161 (1999) [arXiv:hep-lat/9809166].

[23] C. Vafa and E. Witten, Phys. Rev. Lett. **53**, 535 (1984); Nucl. Phys. B **234**, 173 (1984).

[24] M. G. Alford, K. Rajagopal and F. Wilczek, Nucl. Phys. B **537**, 443 (1999) [arXiv:hep-ph/9804403].

[25] S. D. Hsu, F. Sannino and M. Schwetz, Mod. Phys. Lett. A **16**, 1871 (2001) [arXiv:hep-ph/0006059]; F. Sannino, Phys. Lett. B **480** (2000) 280 [arXiv:hep-ph/0002277]; arXiv:hep-ph/0301035.

[26] N. Evans, J. Hormuzdiar, S. D. Hsu and M. Schwetz, Nucl. Phys. B **581**, 391 (2000) [arXiv:hep-ph/9910313].

[27] T. Schafer, Nucl. Phys. B **575**, 269 (2000) [arXiv:hep-ph/9909574]; I. A. Shovkovy and L. C. Wijewardhana, Phys. Lett. B **470**, 189 (1999) [arXiv:hep-ph/9910225].

[28] D. K. Hong, T. Lee and D. P. Min, Phys. Lett. B **477**, 137 (2000) [arXiv:hep-ph/9912531]; D. K. Hong, Phys. Rev. D **62**, 091501 (2000) [arXiv:hep-ph/0006105].

[29] To investigate spontaneous symmetry breaking, one ordinarily has to start at finite volume and insert a source which explicitly breaks the symmetry. The source is removed only after the infinite volume limit is taken. We stress that the source does not have to be a quark mass (it could be a higher dimension operator), so one can investigate symmetry breaking even when the quark mass is exactly zero throughout the calculation. (To be precise, a quark mass does not explicitly violate vector symmetries, so it cannot play the role of the source in the thermodynamic limit needed here.)

COLOR SUPERCONDUCTING QUARK MATTER AND THE INTERIOR OF NEUTRON STARS

Micaela Oertel
CEA Bruyères-le-Châtel, DPTA/SPN, BP12, F-91680 Bruyères-le-Châtel
oertel@bruyeres.cea.fr

Michael Buballa
Institut für Kernphysik, Schlossgartenstr. 9, D-64289 Darmstadt
michael.buballa@physik.tu-darmstadt.de

Abstract We investigate the phase structure of color superconducting quark matter at intermediate densities for two- and three flavor systems. We thereby focus our attention on the influence of charge neutrality conditions as well as β-equilibrium on the different phases. These constraints are relevant in the context of quark matter at the interior of compact stars. We analyze the implications of color superconductivity on compact star configurations using different hadronic and quark equations of state.

Keywords: Quark matter, color superconductivity, neutron stars

1. Introduction

The structure of the QCD phase diagram is one of the most exciting topics in the field of strong interactions (for reviews see, e.g. [1–3]). For a long time the discussion was restricted to two phases: the hadronic phase and the quark-gluon plasma (QGP). The former contains "our" world, where quarks and gluons are confined to color-neutral hadrons and chiral symmetry is spontaneously broken due to the presence of a non-vanishing quark condensate $\langle\bar{\psi}\psi\rangle$. In the QGP quarks and gluons are deconfined and chiral symmetry is (almost) restored, $\langle\bar{\psi}\psi\rangle \simeq 0$.

Although color superconducting phases were discussed already in the '70s [4–6] and '80s [7], until quite recently not much attention was payed to this possibility. This changed dramatically after it was discovered that due to non-perturbative effects, the gaps which are related to these phases could be of the order of $\Delta \sim 100$ MeV [8, 9], much larger than expected from the early perturbative estimates. Since in standard weak-coupling BCS theory the critical

D. Blaschke and D. Sedrakian (eds.), Superdense QCD Matter and Compact Stars, 187–207.

temperature is given by $T_c \simeq 0.57\,\Delta(T=0)$, this also implies a sizable extension of the color superconducting phases into the temperature direction [10]. It was concluded that color superconducting phases could be relevant for compact stars [11, 12] and – in very optimistic cases – even for heavy-ion collisions [13].

Rather soon after the beginning of this new era, it was noticed that there is probably more than one color superconducting phase in the QCD phase diagram. Due to the large number of quark degrees of freedom –color, flavor, and spin– there are many channels where diquark condensation is neither forbidden by Pauli principle nor by symmetries. Thus the interactions have to decide about the actual condensation pattern realized at a given density or a given chemical potential and temperature. The intention of this talk will not be to discuss all of them, not even all possibilities which have already been discussed in literature, but we will focus on several examples in order to discuss the main concepts of color superconductivity for two- and three-flavor systems, respectively. In the last part of the talk we will discuss some results concerning the question of stable compact star configurations with a color superconducting quark matter core.

2. The scalar color antitriplet condensate

Most interactions favor a condensation in the scalar color antitriplet channel. There are two different condensation patterns in this channel, depending on whether or not the strange quarks, which are more massive than the light up and down quarks, participate in forming a condensate,

$$s_{AA'} \;=\; \langle \psi^T\, C\gamma_5\, \tau_A\, \lambda_{A'}\, \psi \rangle \;. \tag{1}$$

Here both, τ_A and $\lambda_{A'}$ are the antisymmetric generators of $SU(3)$, i.e., the antisymmetric Gell-Mann matrices ($A, A' \;\in\; \{2,5,7\}$), acting in flavor and color space, respectively. In the two-flavor color superconducting phase (2SC) where only the light quarks are involved in the condensation, the flavor index in Eq. (1) is restricted to $A = 2$. In this case it is always possible, without loss of generality, to perform a color rotation such that the 2SC phase is described by $s_{22} \neq 0$ and $s_{AA'} = 0$ if $(A, A') \neq (2, 2)$.

In a first step we will analyze the dominant condensation pattern in the scalar color antitriplet channel for a two-flavor system, i.e., we will consider the limit $M_s \to \infty$. Looking at the transformation properties of the condensate s_{22} we can classify the symmetries of the 2SC phase. It is invariant under a global $U(1)$-symmetry generated by

$$\tilde{B} = B - \sqrt{3}\lambda_8 \;,$$

where $B = \mathbb{1}$ is the generator of baryon number. This global $U(1)$ symmetry can be related to a "rotated" baryon number. In the same way it can be shown

that there exists a linear combination

$$\tilde{Q} = Q - \frac{1}{2\sqrt{3}}\lambda_8 \,,$$

which is related to a conserved local $U(1)$ symmetry, a "rotated" electromagnetism. Q thereby corresponds to the generator of electric charge. It is obvious from Eq. (1) that s_{22} only involves quarks of two colors, e.g., red and green quarks. The quarks of the third color, in our example blue quarks, are left unpaired. This means that color symmetry is broken down to an $SU(2)$-symmetry. This symmetry breaking is –via the Meissner effect– at the origin of five massive gluons which appear in the spectrum [14]. Flavor symmetry is conserved by s_{22}. That means in particular that in the chiral limit, i.e., if we deal with massless current quarks, chiral symmetry is preserved.

Note that this phase breaks no global symmetry at all. This is an important point in connection with the identification of the lowest lying excitation modes which in turn strongly influence the thermodynamic properties of the system. In the 2SC phase we do not find, even in the chiral limit, any real Goldstone bosons, although there are some low-lying (pseudo)-Goldstones related to the axial $U_A(1)$ [15].

The dispersion law of the four (two flavors, two colors) "gapped" quarks gets modified by the condensate,

$$E_1^{\pm}(\vec{p}) = E_2^{\pm}(\vec{p}) \equiv E^{\pm}(\vec{p}) = \sqrt{(\epsilon_p \pm \mu)^2 + |\Delta|^2} \,, \tag{2}$$

where $\epsilon_p = \sqrt{\vec{p}^2 + M^2}$ is the dispersion law of a noninteracting particle with mass M. Often M is an effective Dirac mass, related to the chiral condensate $\langle\bar{\psi}\psi\rangle$ via a selfconsistency equation [16], see below. The energy gap Δ is related to the condensate s_{22} and can be obtained as solution of a selfconsistent gap equation. In general it can also depend on the absolute value of the momentum. It is found to be typically of the order ~ 100 MeV in model calculations [8, 9, 16].

3. Spin-1 condensate for a two-flavor system

Those color or flavor degrees of freedom which do not participate in the dominant condensate s_{22}, i.e., strange quarks and quarks of the third color, could pair in different channels, thus forming additional phases [17–20]. For compact star phenomenology these phases can be interesting because of their thermodynamic properties. For instance, if all quarks are gapped, the specific heat of a potential quark core of a compact star (and hence the cooling of the star) is governed by the size of the *smallest* gap [2]. The same is true for other transport properties, like neutrino emissivity or viscosity. We will discuss here

only one particular example, a more complete discussion of different possibilities can be found in Refs. [20, 21].

Our example deals with quarks of the third color in a phase composed only of up and down quarks. As only quarks of a single color are involved, the pairing must take place in a channel which is symmetric in color. Assuming s-wave condensation in an isospin-singlet channel, a possible candidate is a spin-1 condensate [8]. We consider the condensate

$$\delta' \;=\; \langle \psi^T \, C \, \sigma^{03} \, \tau_2 \, \hat{P}_3^{(c)} \, \psi \rangle \;, \tag{3}$$

where $\sigma^{\mu\nu} \;=\; i/2\,[\gamma^\mu, \gamma^\nu]$ and $\hat{P}_3^{(c)} \;=\; 1/3 \,-\, 1/\sqrt{3}\,\lambda_8$ is the projector on color 3. δ' is a ground-state expectation value of a complex vector order parameter $\phi^{0n} \equiv \phi_n$ describing spin-1 and breaking spontaneously the rotational invariance of the system. There are well-known examples for spin-1 pairing in condensed matter physics, e.g., superfluid ^{3}He, where some phases are also anisotropic [22]. In relativistic systems this is certainly not a very frequent phenomenon. It is possible only at finite chemical potential, which itself breaks Lorentz invariance explicitly. (Relativistic Cooper pairing into spin-1 with nonzero angular momentum was considered elsewhere, e.g., [7, 23].)

Since rotational invariance is a global symmetry of the primary Lagrangian, an arbitrarily small gap of the anisotropic phase implies specific gapless collective excitations with certain Landau critical velocity crucial for the superfluid behavior of the system. We will briefly discuss this at the end of this section. It is also interesting to note that δ' is not neutral with respect to the "rotated" electric charge $\tilde{Q}$ and there is no generalized electric charge for which both, $s_{22} \equiv \delta$ and δ' are neutral. This means, if both, δ and δ', were present in a compact star, there would be an electromagnetic Meissner effect, which would strongly influence the magnetic field. Recently, similar effects have been discussed in Ref. [24]. A detailed evaluation of the Meissner masses and Debye masses can be found in Ref. [25].

For the quantitative analysis we have to specify the interaction. At asymptotically high densities, where the QCD coupling constant becomes small, this can be analyzed starting from first principles [10, 13, 26], whereas at more moderate densities, present (presumably) in the interiors of neutron stars, these methods are no longer justified. In this region the low-energy dynamics of deconfined quark matter is often studied employing effective Lagrangians $\mathcal{L}_{\mathit{eff}}$ which contain local or non-local four-fermion interactions, most importantly interactions derived from instantons or on a more phenomenological basis [8, 9, 16]. The non-confining gluon $SU(3)_c$ gauge fields are then treated as weak external perturbations, and neglected in lowest approximation. We will apply here a phenomenological model with a NJL-type Lagrangian consisting of a free (Dirac) part,

$$\mathcal{L}_{\mathit{free}} \;=\; \bar{\psi}(i\partial\!\!\!/ - \hat{m})\psi \tag{4}$$

and a quark-quark as well as quark-antiquark interaction part. Guided by the structure of instanton-induced interactions (see, e.g., [9]) we consider a quark-antiquark term of the form

$$\mathcal{L}_{q\bar{q}} = G\Big\{(\bar{\psi}\psi)^2 - (\bar{\psi}\vec{\tau}\psi)^2 - (\bar{\psi}i\gamma_5\psi)^2 + (\bar{\psi}i\gamma_5\vec{\tau}\psi)^2\Big\} \tag{5}$$

and a quark-quark term

$$\begin{aligned}\mathcal{L}_{qq} &= -H_s \sum_{\mathcal{O}=\gamma_5,1} (\bar{\psi}\mathcal{O}C\tau_2\lambda_A\bar{\psi}^T)(\psi^T C\mathcal{O}\tau_2\lambda_A\psi^T) \\ &\quad -H_t(\bar{\psi}\sigma^{\mu\nu}C\tau_2\lambda_S\bar{\psi}^T)(\psi^T C\sigma_{\mu\nu}\tau_2\lambda_S\psi^T)\,,\end{aligned} \tag{6}$$

where λ_A and λ_S are the antisymmetric and symmetric color generators, respectively. ψ here denotes a quark field with two flavors and three colors. The mass matrix $\hat{m}$ has the form $\hat{m} = diag(m_u, m_d)$ in flavor space. Throughout this talk we will assume $m_u = m_d$,

For instanton induced interactions the coupling constants fulfill the relation $G : H_s : H_t = 1 : \frac{3}{4} : \frac{3}{16}$, but for the moment we will treat them as arbitrary parameters. As long as they stay positive, the interaction is attractive in the channels giving rise to the diquark condensates δ and δ' as well as to the chiral condensate $\langle\bar{\psi}\psi\rangle$. It is straight forward to calculate the mean-field thermodynamic potential $\Omega(T,\mu)$ in the presence of these condensates:

$$\begin{aligned}\Omega(T,\mu) &= -4\sum_{i=1}^{3}\sum_{+-}\int\frac{d^3p}{(2\pi)^3}\Big[\frac{E_i^{\pm}}{2} + T\ln\Big(1+e^{-E_i^{\pm}/T}\Big)\Big] \\ &\quad +\frac{1}{4G}(M-m)^2 + \frac{1}{4H_s}|\Delta|^2 + \frac{1}{16H_t}|\Delta'|^2\,,\end{aligned} \tag{7}$$

where $m = m_u = m_d$ is the current mass of light quarks, $M = m - 2G\langle\bar{\psi}\psi\rangle$, $\Delta = -2H_s\delta$, and $\Delta' = 4H_t\delta'$. The dispersion law for quarks of color 3 reads

$$E_3^{\mp}(\vec{p}) = \sqrt{(\sqrt{M_{\mathit{eff}}^2 + \vec{p}^{\,2}} \mp \mu_{\mathit{eff}})^2 + |\Delta'_{\mathit{eff}}|^2}\,, \tag{8}$$

where $\mu_{\mathit{eff}}^2 = \mu^2 + |\Delta'|^2\sin^2\theta$, $M_{\mathit{eff}} = M\mu/\mu_{\mathit{eff}}$, and $|\Delta'_{\mathit{eff}}|^2 = |\Delta'|^2\,(\cos^2\theta + M^2/\mu_{\mathit{eff}}^2\,\sin^2\theta)$. Here $\cos\theta = p_3/|\vec{p}|$. Thus, as expected, for $\Delta' \neq 0$, $E_3^{\pm}(\vec{p})$ is an anisotropic function of $\vec{p}$, clearly exhibiting the spontaneous breakdown of rotational invariance. For $M = 0$, the gap Δ'_{eff} vanishes at $\theta = \pi/2$. In general its minimal value is given by $\Delta'_0 = M|\Delta'|/\sqrt{\mu^2 + |\Delta'|^2}$. Expanding E_3^- around its minimum the low-lying quasiparticle spectrum takes the form

$$E_3^-(p_\perp, p_3) \approx \sqrt{\Delta_0'^2 + v_\perp^2(p_\perp - p_0)^2 + v_3^2 p_3^2}\,, \tag{9}$$

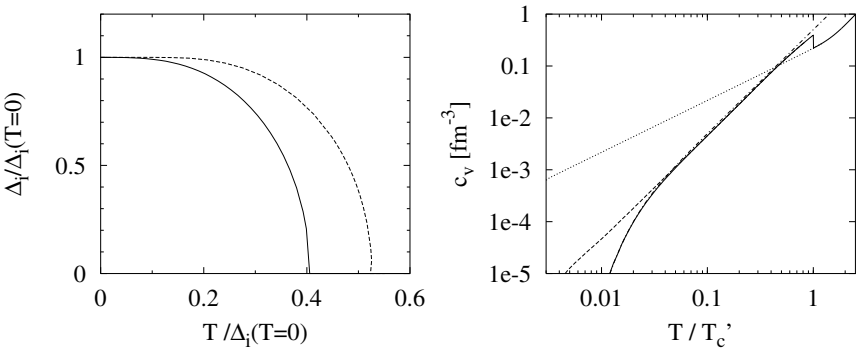

Figure 1. Left: $\Delta_i/\Delta_i(T{=}0)$ as function of $T/\Delta_i(T{=}0)$. Dashed: $\Delta_i = \Delta$, solid: $\Delta_i = \Delta'$. Right: Specific heat as function of T/T_c'. Solid: full calculation, dashed: result for $M = 0$, dotted: without spin-1 condensate. The dash-dotted line indicates the result of Eq. (14).

where $v_\perp = (1 - (\mu\Delta_0'^2/(M\Delta'^2))^2)^{1/2}$, $v_3 = \frac{\Delta_0'}{M}$, $p_0 = \frac{v_\perp}{v_3}|\Delta'|$, and $p_\perp^2 = p_1^2 + p_2^2$. This leads to a density of states linear in energy:

$$N(E) = \frac{1}{2\pi}\frac{\mu^2 + |\Delta'|^2}{|\Delta'|}\, E\, \theta(E - \Delta_0') \,. \tag{10}$$

The actual values for Δ, Δ' and M follow from the condition that the stable solutions correspond to the absolute minimum of Ω with respect to these quantities. Imposing $\partial\Omega/\partial\Delta'^* = 0$ we obtain the following gap equation for Δ':

$$\Delta' = 16 H_t \Delta' \sum_{+-} \int \frac{d^3p}{(2\pi)^3}\,(1 \pm \frac{\vec{p}_\perp^{\,2}}{s})\frac{1}{E_3^\pm}\tanh\frac{E_3^\pm}{2T} \,, \tag{11}$$

where $s = \mu_{\mathit{eff}}(\vec{p}^{\,2} + M_{\mathit{eff}}^2)^{1/2}$. Similarly one can derive gap equations for Δ and M by the requirements $\partial\Omega/\partial\Delta^* = 0$ and $\partial\Omega/\partial M = 0$, respectively. Together with Eq. (11), they form a set of three coupled equations, which have to be solved simultaneously. However, the equations for Δ and Δ' are not directly coupled, but only through their dependence on M.

The values we obtain for Δ' strongly depend on μ, the value of H_t and, as a consequence of the factor $(1 - \vec{p}_\perp^{\,2}/s)$ in the gap equation (11), on value and form of the cutoff. Using values of the parameters leading to reasonable vacuum properties and a sharp 3-momentum cutoff, we find Δ' of the order of 1 MeV with the instanton value for H_t and $\Delta' \approx 10$ MeV with twice this value for H_t. Both results are in agreement with earlier expectations [8] that Δ' is small compared with Δ.

In spite of these uncertainties we can derive some more general results from the above gap equations. With increasing temperature both condensates, δ and δ', are reduced and eventually vanish in second-order phase transitions at

critical temperatures T_c and T_c', respectively. It has been shown [10, 13] that T_c is approximately given by the well-known BCS relation $T_c \simeq 0.57\Delta(T{=}0)$. In order to derive a similar relation for T_c' we inspect the gap equation (11) at $T = 0$ and in the limit $T \to T_c'$. Neglecting M (since $M \ll \mu$ this is valid up to higher orders in M^2/μ^2) and antiparticle contributions one gets

$$\int \frac{d^3p}{(2\pi)^3} \Big\{ \Big[(1-\frac{\vec{p}_\perp^{\,2}}{s}) \frac{1}{E_3^-(\vec{p})} \Big]_{\Delta'(T=0)} - (1-\frac{\vec{p}_\perp^{\,2}}{\mu\,|\vec{p}|}) \frac{1}{|\mu-|\vec{p}||} \tanh \frac{|\mu-|\vec{p}||}{2T_c'} \Big\} \approx 0\,. \tag{12}$$

Since the integrand is strongly peaked near the Fermi surface, the $|\vec{p}|$-integrand must approximately vanish at $|\vec{p}| = \mu$, after the angular integration has been performed. From this condition one finds to lowest order in Δ'/μ:

$$T_c' \;\approx\; \frac{1}{3}\,\Delta'(T=0)\,. \tag{13}$$

The analogous steps would lead to $T_c/\Delta(T{=}0) \approx \frac{1}{2}$ instead of the textbook value of 0.57. This gives a rough idea about the quality of the approximation.

Numerical results for $\Delta(T)$ and $\Delta'(T)$ are shown on the left panel of Fig. 1. The quantities have been rescaled in order to facilitate a comparison with the above relations for T_c and T_c'. Our results are in reasonable agreement with our estimates. These findings turn out to be insensitive to the actual choice of parameters.

The specific heat is given by $c_v = -T\partial^2\Omega/\partial T^2$ [1]. For $T \ll T_c$ it is completely dominated by quarks of color 3, since the contribution of the first two colors is suppressed by a factor $\mathrm{e}^{-\Delta/\mathrm{T}}$. Neglecting the T-dependence of M and Δ', and employing Eq. (10), one finds

$$c_v \;\approx\; \frac{12}{\pi} \frac{\mu^2+|\Delta'|^2}{|\Delta'|}\, T^2\, e^{-\frac{\Delta_0'}{T}} \sum_{n=0}^{3} \frac{1}{n!} \left(\frac{\Delta_0'}{T}\right)^n \,, \tag{14}$$

which should be valid for $T \ll T_c'$. In this regime c_v depends quadratically on T for $T \gtrsim \Delta_0'$, and is exponentially suppressed at lower temperatures.

To test this relation we evaluate $c_v(T)$ explicitly using Eq. (7). The results for fixed μ =450 MeV are displayed on the right panel of Fig. 1. The critical temperature is $T_c' \simeq 0.40\ \Delta'(T{=}0)$. For the energy gap we find $\Delta_0' = 0.074\ T_c'$. It turns out that Eq. (14), evaluated with constant values of Δ' and M, (dashed-dotted) is in almost perfect agreement with the numerical result (solid) up to $T \approx T_c'/2$. The phase transition, causing the discontinuity of c_v at $T = T_c'$, is of course outside the range of validity of Eq. (14). We also display c_v for $M = 0$ (dashed). Since Δ_0' vanishes in this case there is no exponential suppression,

[1] Strictly, $c_v = T/V\partial S/\partial T|_{V,N}$, but the correction term is small [27].

and c_v is proportional to T^2 down to arbitrarily low temperatures. However, even when M is included, the exponential suppression is partially canceled by the extra-terms in the sum of Eq. (14). For comparison we also show c_v for a system with $\Delta' = 0$, which exhibits a linear T dependence at low temperatures (dotted).

Because of the spontaneously broken $U(1) \times O(3)$ symmetry in Eq. (3), for $\Delta' \neq 0$ there should be collective Nambu-Goldstone excitations in the spectrum. However, due to the Lorentz non-invariance of the system there can be subtleties [19, 28–30]. The NG spectrum can be analyzed within an underlying effective Higgs potential

$$V(\phi) = -a^2 \phi_n^\dagger \phi_n + \frac{1}{2}\lambda_1 (\phi_n^\dagger \phi_n)^2 + \frac{1}{2}\lambda_2 \phi_n^\dagger \phi_n^\dagger \phi_m \phi_m, \qquad (15)$$

for the complex order parameter ϕ_n [21, 29], with $\lambda_1 + \lambda_2 > 0$ for stability. For $\lambda_2 < 0$ the ground state is characterized by $\phi_{vac}^{(1)} = (\frac{a^2}{\lambda_1})^{1/2}(0,0,1)$ which corresponds to our ansatz Eq. (3) for the BCS-type diquark condensate δ'. This solution has the property $\langle \vec{S} \rangle^2 = (\phi_{vac}^{(1)\dagger} \vec{S} \phi_{vac}^{(1)})^2 = 0$. The spectrum of small oscillations above $\phi_{vac}^{(1)}$ consists of 1+2 NG bosons, all with linear dispersion law: one zero-sound phonon and two spin waves [29]. Implying a finite Landau critical velocity, this fact is crucial for a macroscopic superfluid behavior of the system [30].

Other pairing configurations than the standard BCS-type pairing discussed so far have been suggested more recently, like for instance crystalline phases [31], deformed Fermi surfaces [32] or the so called gapless 2SC phase [33]. These phases come into play whenever there exists a large mismatch between the Fermi surfaces of the different quark species. Partially they have been covered by other talks during this workshop [34, 35].

4. Neutral quark matter

Let us now come back to pairing in the dominant scalar color antitriplet channel, see Eq. (1), involving this time strange quarks. In that case we can no longer restrict the condensation to s_{22}, but in general (although they are not all independent) all nine condensates $s_{AA'}$ can be nonzero. By symmetry considerations it can be shown that the most favored pattern is the so-called color-flavor-locked (CFL) phase [36] which is characterized by non-vanishing condensates s_{22}, s_{55}, and s_{55}, i.e., it contains ud as well as us and ds pairs. In the limiting case of equal masses and chemical potentials for all quarks these three condensates are equal, whereas in general they can be different from each

other. In contrast to the 2SC phase in the CFL phase quarks of all flavors and colors participate in diquark condensates.

A similar analysis as in the two-flavor-case shows that in the CFL phase we can again define a "rotated" electromagnetism, thus we find a conserved local $U(1)$. This is not true for baryon number. In color and flavor space we find that $SU(3)_c \times SU(3)_L \times SU(3)_R$ is broken to a diagonal subgroup $SU(3)_{c+V}$, i.e., chiral symmetry is broken in the CFL phase. This leads to the existence of eight (pseudo-) Goldstone bosons [37, 38] and all eight gluons become massive [14, 38–40].

Before we can come to a more quantitative discussion we have to specify the interaction. Similarly to the previous section we consider an NJL-type interaction with a free part, a quark-quark interaction part given by

$$\mathcal{L}_{qq} \;=\; H \sum_{A=2,5,7} \sum_{A'=2,5,7} (\bar{\psi}\, i\gamma_5 \tau_A \lambda_{A'}\, C\bar{\psi}^T)(\psi^T C\, i\gamma_5 \tau_A \lambda_{A'}\, \psi)\,. \qquad (16)$$

and a quark-antiquark part by

$$\begin{aligned} \mathcal{L}_{q\bar{q}} \;\;=\;\; & G \sum_{a=0}^{8} \Big[(\bar{\psi}\tau_a \psi)^2 \;+\; (\bar{\psi} i\gamma_5 \tau_a \psi)^2 \Big] \\ & - K \Big[\det{}_f \Big(\bar{\psi}(1+\gamma_5)\psi \Big) \;+\; \det{}_f \Big(\bar{\psi}(1-\gamma_5)\psi \Big) \Big]\,. \end{aligned} \qquad (17)$$

Here $\tau_0 = \sqrt{\frac{2}{3}}\, \mathbb{1}_f$ is proportional to the unit matrix in flavor space. The quark field ψ now contains a third component in flavor space, the strange quark, and consequently the mass matrix $\hat{m}$, see Eq. (4), is equally enlarged by the current strange quark mass, m_s, which can in general be different from up and down quark masses. This interaction consists of a $U(3)_L \times U(3)_R$-symmetric 4-point interaction and a 't Hooft-type 6-point interaction which breaks the $U_A(1)$ symmetry.

For later convenience we introduce the diquark gaps

$$\Delta_A = -2H\, s_{AA}\,, \qquad A = 2, 5, 7, \qquad (18)$$

and the constituent quark masses

$$M_i \;=\; m_i \;-\; 4G\phi_i \;+\; 2K\phi_j\phi_k\,, \quad (i,j,k) = \text{any perm. of } (u,d,s)\,, \qquad (19)$$

where $\phi_f = \langle \bar{f} f \rangle$, $f = u, d, s$, are the quark-antiquark condensates. These quantities will be determined selfconsistently within mean-field approximation.

One of our main interests is to describe quark matter at the interior of a compact star since this is one of the possibilities to find color superconducting matter in nature. It is therefore important to consider electrically and color neutral[2] matter in β-equilibrium. In addition to the quarks we also allow for the presence of leptons, especially electrons muons. As we consider stars older than a few minutes, when neutrinos can freely leave the system, lepton number is not conserved. The conditions for charge neutrality read

$$n_Q = \frac{2}{3}n_u - \frac{1}{3}n_d - \frac{1}{3}n_s - n_e - n_\mu \equiv 0 \tag{20}$$

with n_e and n_μ being number densities of electrons and muons, respectively. For color neutrality we have to require $n_r = n_g = n_b$ or, equivalently,

$$n = n_r{+}n_g{+}n_b\,, \qquad n_3 = n_r{-}n_g \equiv 0\,, \qquad n_8 = \frac{1}{\sqrt{3}}(n_r{+}n_g{-}2n_b) \equiv 0\,. \tag{21}$$

Here n corresponds to the total quark number density, while n_3 and n_8 describe color asymmetries. Note that $n/3$ also describes the conserved baryon number. The charges are related to four chemical potentials, μ, μ_3, μ_8, and μ_Q, and the chemical potentials of all particles in the system can be expressed through these four chemical potentials. This implies β-equilibrium,

$$\mu_{d,c} = \mu_{s,c} = \mu_{u,c} + \mu_e \quad \text{for all colors } c\,. \tag{22}$$

Thus, in the presence of electrons the chemical potentials for up and down quarks become unequal, rendering ud BCS-pairing difficult. The presence of negatively charged strange quarks therefore is likely to favor pairing even if the strange quark mass is considerably larger. Alford and Rajagopal tackled that problem, performing an expansion in terms of the strange quark mass. They found that, whenever the 2SC phase is more favored than no pairing at all, the CFL phase is even more favored [42].

The analysis of Ref. [42] as well as the NJL-type model investigation of Ref. [43] are based on a comparison of homogeneous phases. The neutrality conditions can, however, also be fulfilled giving up the requirement of separately neutral phases and to consider mixed phases in chemical equilibrium which are only neutral in total. This procedure has been pushed forward by Glendenning in the context of the quark-hadron phase transition in neutron stars where a similar problem related to electrical neutrality occurs [44]. For the case of electrically and color neutral quark matter the phase boundaries are

[2]Strictly speaking, color neutrality is not sufficient, but color singletness has to be imposed. This does, however, not induce a large cost in energy [41], such that we can consider matter which is only color neutral.

three-dimensional hypersurfaces in the four-dimensional space spanned by μ, μ_Q, μ_3 and μ_8. The regions where electrically and color neutral mixed phases are possible correspond to one-dimensional lines on these hypersurfaces.

For illustrational purposes we show in Fig. 2 the phase diagram in the $\mu - \mu_Q$-plane for $\mu_8 = \mu_3 = 0$. We thereby used the values of the model parameters obtained by the authors of Ref. [45] by fitting masses and decay constants of pseudoscalar mesons and $H = G$. Since we are interested in neutralizing the electrically positive 2SC phase, we choose μ_Q to be negative. As long as this is not too large, we find a normal phase at lower values of μ, the 2SC phase in the intermediate region and the CFL phase for large μ. This changes dramatically around $\mu_Q \simeq 180$ MeV where both, the 2SC phase and the CFL phase disappear and a new phase emerges. This phase is analogous to the 2SC phase but with ds pairing, instead of ud pairing ("2SC$_{ds}$"). In a small intermediate regime there is even another phase which contains us and ds but no ud pairs ("SC$_{us+ds}$").

Qualitatively, the existence of these phases is quite plausible: At low values of $|\mu_Q|$ the Fermi momenta of the up and down quarks are relatively similar to each other, whereas the strange quarks are suppressed because of their larger mass. With increasing negative μ_Q, however, the up quarks become more and more disfavored and eventually the Fermi momenta are ordered as $p_F^u < p_F^s < p_F^d$. It is then easy to imagine that only ds pairing or – in some intermediate regime – us and ds pairing is possible.

In the phase diagram, Fig. 2, we also indicated the sign of the electric charge density for the various regions, and the line of electrically neutral matter in the CFL phase (dotted line). Note that there is no other electrically neutral regime in this diagram (apart from the vacuum at small μ and $\mu_Q = 0$). In the normal phase, there are no quarks below the dashed line, corresponding to the line $\mu - 1/3\mu_Q = M_d$. This region is nevertheless negatively charged due to the leptons which are present for any $\mu_Q < 0$. Above the dashed line there are also d quarks rendering the matter even more negative.

The "new" phases, 2SC$_{ds}$ and SC$_{us+ds}$, are also negatively charged. On the contrary, the entire 2SC phase is positively charged, even at the largest values of $|\mu_Q|$. The difficulty to obtain electrically neutral 2SC matter can be traced back to the fact that the sum of red and green u quarks is equal to the

Table 1. Color superconducting phases and corresponding non-vanishing diquark gaps. The normal phase ("N") is characterized by the fact that there is no nonzero diquark gap.

phase	2SC	2SC$_{us}$	2SC$_{ds}$	SC$_{ud+us}$	SC$_{ud+ds}$	SC$_{us+ds}$	CFL
diquark gaps	Δ_2	Δ_5	Δ_7	Δ_2, Δ_5	Δ_2, Δ_7	Δ_5, Δ_7	Δ_2, Δ_5, Δ_7

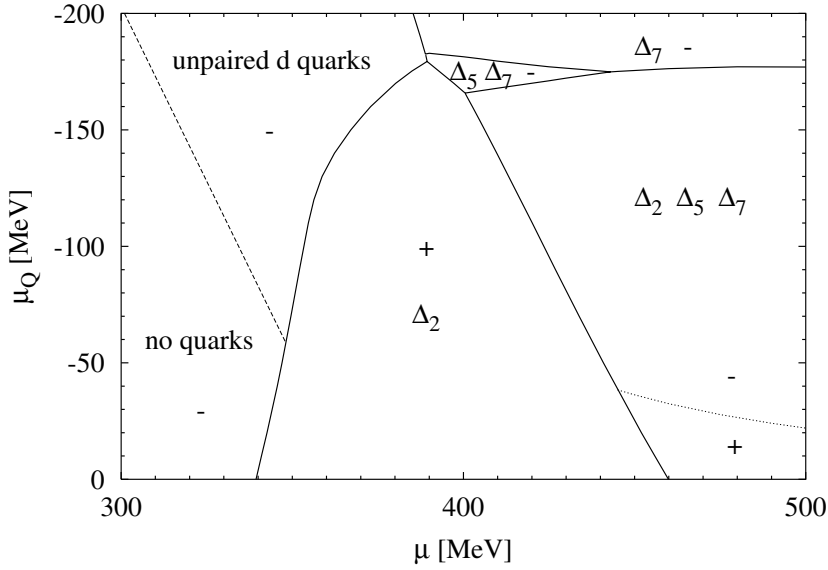

Figure 2. Phase diagram in the $\mu - \mu_Q$ plane for $T = \mu_3 = \mu_8 = 0$. The various phases separated by the solid lines are characterized by different non-vanishing diquark gaps Δ_i as indicated in the figure. In the non-superconducting phase quarks are present only above the dashed line. The "+" and "-" signs indicate the sign of the electric charge density in the corresponding region. The dotted line corresponds to electrically neutral matter in the CFL phase.

sum of red and green d quarks. As long as no strange quarks are present, the related positive net charge can only be compensated by the blue quarks and the leptons, which would require a very large negative μ_Q. However, before this point is reached it becomes more favored to form a different phase with a relatively large fraction of strange quarks which then also participate in a diquark condensate. The selfconsistent treatment, which leads to a sudden drop of the strange quark mass and hence to a sudden increase of the strange Fermi momentum, is crucial in this context.

Although it is interesting to examine the different phase structures as functions of the different chemical potentials (for a more detailed analysis see Ref. [46]), our main intention is to construct color and electrically neutral (mixed) phases. At large μ a homogeneous neutral CFL phase exists. Our starting point for the construction of mixed phases is therefore $\mu = 465.7$ MeV, $\mu_8 = -32.5$ MeV, and $\mu_3 = \mu_Q = 0$ where the line of neutral CFL matter meets the boundary to the 2SC phase. At lower values of μ, mixed phases become possible and are energetically favored as long as Coulomb and surface effects are neglected. In the present example, we find nine regimes characterized by different compositions of coexisting phases (see Table 2). In Table 2 we also list the corresponding minimal and maximal baryon densities, averaged over the components of the respective mixed phase.

In Fig. 3 the volume fractions $x_i = n_i/n$ of the various components of the mixed phases are plotted as functions of μ. Whereas the 2SC-CFL-mixed phase between $\mu = 430.6$ and 465.7 MeV is completely dominated by the CFL component, at lower μ the CFL fraction becomes quickly smaller with decreasing μ, while in particular the 2SC component, becomes more and more important. At $\mu = 407.7$ MeV the CFL component disappears completely.

Table 2. Composition of electrically and color neutral mixed phases, corresponding quark number chemical potentials and average baryon number densities $\rho_B = n/3$ in unities of nuclear matter saturation density $\rho_0 = 0.17/\mathrm{fm}^3$. The various components are defined in Tab. 1.

components	μ [MeV]	ρ_B/ρ_0
N, 2SC	340.9 - 388.6	0.00 - 2.94
N, 2SC, SC_{us+ds}	388.6 - 388.7	2.94 - 2.94
N, 2SC, SC_{us+ds}, $2\mathrm{SC}_{us}$	388.7 - 388.8	2.94 - 3.06
2SC, SC_{us+ds}, $2\mathrm{SC}_{us}$	388.8 - 395.4	3.06 - 3.40
2SC, SC_{us+ds}	395.4 - 407.7	3.40 - 3.86
2SC, SC_{us+ds}, CFL	407.7 - 426.5	3.86 - 5.69
2SC, SC_{us+ds}, CFL, $2\mathrm{SC}_{us}$	426.5 - 427.1	5.69 - 5.75
2SC, CFL, $2\mathrm{SC}_{us}$	427.1 - 430.6	5.75 - 6.10
2SC, CFL	430.6 - 465.7	6.10 - 7.69

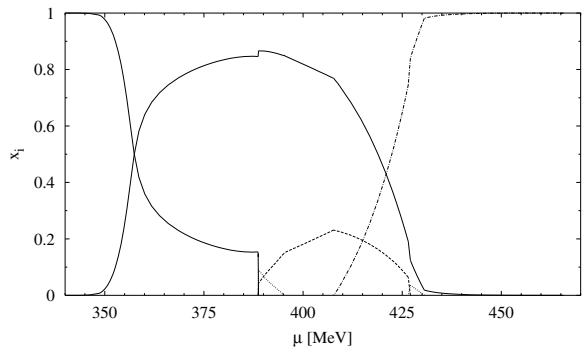

Figure 3. Volume fractions x_i of the various components in the mixed phase region as functions of μ: normal (thin solid), 2SC (thick solid), CFL (dashed-dotted), SC$_{us+ds}$ (dashed), 2SC$_{us}$ (dotted).

An admixture of normal quark matter is found below $\mu = 388.8$ MeV. The fractions of the superconducting phases other than the 2SC phase then rapidly become smaller and vanish at $\mu = 388.6$ MeV, while the fraction of normal matter strongly increases. Nevertheless the 2SC phase stays the dominant component for $\mu \gtrsim 360$ MeV. At $\mu = 340.9$ MeV we finally reach the vacuum.

Qualitatively our results are in agreement with those obtained in Ref. [43], where no mixed phase was admitted. The regions which are dominated by the CFL phase and the 2SC phase, respectively, correspond roughly to those values of the chemical potential where the authors of Ref. [43] find that the CFL or the 2SC phase, respectively, is favored. Of course, since we started from the same Lagrangian, these homogeneous neutral solutions also exist in our model. We find, for instance, below $\mu = 465.7$ MeV a color and electrically neutral CFL phase which is, however, less favored than the 2SC-CFL mixed phase (see Fig 4). At this point we should recall that in our calculations we have neglected the surface energy and the energies of the electric and color-electric fields. Clearly the mixed phases are only stable if the gain in bulk free energy is larger than these so-far neglected contributions.

For the two-component mixed phases the surface and Coulomb contributions can be estimated along the lines of the analysis performed in Ref. [47] for the interface between nuclear and CFL matter. We find a gain in bulk energy of at most 6 MeV/fm^3 which is already weight out by Coulomb and surface energy for relatively small values of the surface tension $\sigma \approx 10$ MeV/fm^2. Note that the true value of σ is an unknown quantity which does not follow from our model. However, as argued in Ref. [47] it is likely to be much larger than the above value. For mixed phases with three or four components the situation is obviously more complicated. It seems, however, rather unlikely that an admix-

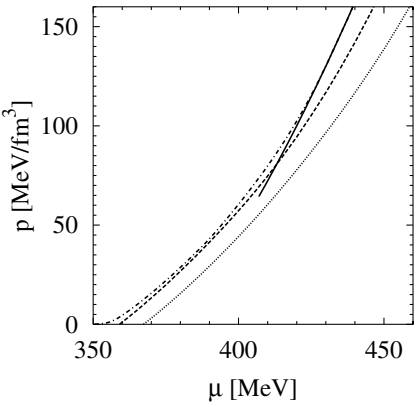

Figure 4. Pressure as a function of μ for homogeneous neutral quark matter in the CFL phase (solid), 2SC (dashed), and the normal quark matter phase (dotted). Also shown is the pressure of the mixed phase solution (dash-dotted).

ture of more than two components can be favored if the surface and Coloumb energy already inhibits the existence of a phase with two components.

5. Compact stars with a color superconducting quark matter core

This section will be devoted to the study of the composition of a compact star including the possibility of a color superconducting quark matter core. Recently this question has been addressed by several authors using a bag-model description of the quark phase [48] or an NJL-type model [49–52]. In the following, we will discuss the results of Refs. [49, 52] where –in contrast to Refs. [50, 51]– strange quarks have been taken into account.

From the above estimations we conclude that is it at least a good approximation to consider only homogeneous phases to describe the quark matter phase. In Fig. 4 we display the pressure as a function of μ for neutral homogeneous quark matter phases. We see that at small μ the 2SC phase (dashed line) is favored whereas at large μ we find a CFL phase (solid line). Normal quark matter (dotted line) turns out to be never favored. This will be our input for the description of the quark matter phase. Of course, in order to construct a compact star, we also have to take into account the possibility of a hadronic component in the equation of state (EOS). To this end, we take a given hadronic EOS and construct a phase transition to quark matter from the requirement of maximal pressure. This is shown in the left panel of Fig. 5 for an example hadronic EOS [53]. At the transition point to the quark-matter phase we directly enter the CFL phase and normal or 2SC quark matter is completely irrelevant in this

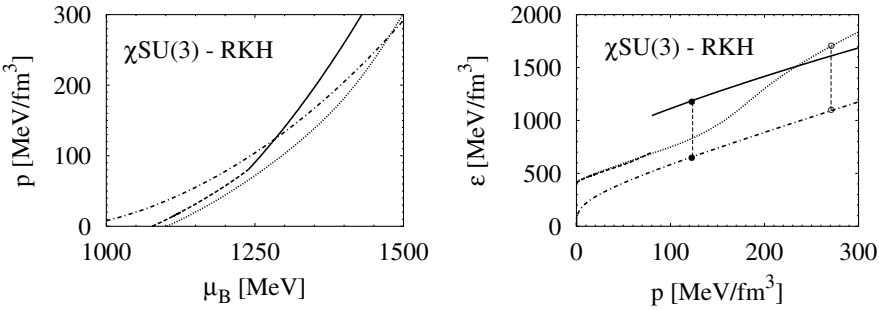

Figure 5. Left: Pressure as a function of μ_B for a hadronic EOS [53] (dash-dotted line) and homogeneous quark matter in the normal phase (dotted line), the 2SC phase (dashed line) and the CFL phase (solid line). Right: Corresponding energy densities as a function of pressure. The closed (open) circles connected by thin dashed lines indicate the discontinuities at the transition points from hadronic to CFL (normal) quark matter.

case. In the right panel we display the corresponding EOS. Note the strong discontinuity of the energy density at the critical chemical potential for the transition to the quark-matter phase. For comparison, we have also marked the phase transition to normal quark matter.

We will not examine a mixed phase of hadronic and quark matter. Following the arguments of Ref. [47] such a mixed phase is unlikely to exist even for rather small values of the surface tension. In any case, as we will argue below this assumption does not considerably change our conclusions. This "hybrid" EOS will then be used as input to integrate the Tolman-Oppenheimer-Volkoff (TOV) equation describing configurations of static compact stars [54].

Neither the quark matter EOS nor the hadronic EOS are very well known quantitatively at the densities relevant for compact objects. In order to get an idea on the uncertainties of our analysis we will consider four different hadronic EOS and two different parameter sets for the NJL description of quark matter. The hadronic EOS are:

- Microscopic Brueckner-Hartree-Fock (BHF) calculation without hyperons [55] ("BHF(N,l)")
- BHF calculation with hyperons [56] ("BHF(N,H,l)")
- Relativistic mean-field calculation as tabulated in Ref. [57] for a compression modulus $K = 240$ MeV ("RMF240")
- Relativistic mean-field model based on $SU(3)$ chiral symmetry [53] ("χSU(3)"), see Fig. 5

The NJL-model parameters are taken from two fits to the masses and decay constants of pseudoscalar mesons in the vacuum, performed by Rehberg et

al. [45] (RKH) –these are the parameters we have used in all the calculations presented so far– and by Hatsuda and Kunihiro [58] (HK). For the coupling constant in the diquark channel, we take $H = G$ in both cases. The main difference between the two parameter sets is the treatment of the η' which lies above the $q\bar{q}$ threshold within the model and thus its mass is not well defined. This results in a smaller constituent mass for the light quarks in vacuum for parameter set HK.

In Fig. 6 we display the mass-radius relation for different compact star configurations obtained by integrating the TOV equation for the different hadronic and quark matter EOS as explained above. We do not show the results for the BHF calculation with hyperons since we do not find a transition to a quark phase in this case [49]. But, as mentioned during this conference [59] this particular hadronic EOS produces too small maximum masses because of its soft character and can therefore perhaps not be trusted up to the densities present at the interior of a compact star. The dash-dotted lines represent purely hadronic configurations, the dotted lines configurations with a normal quark-matter core (shown for comparison) and the solid ones configurations with color superconducting quark-matter cores in the CFL phase. In the lower right panel we also find configurations with a 2SC quark matter core (dashed line). This part of the figure is again shown in more detail on the left hand side of Fig. 7. It is the only example where we find a transition from the hadronic phase to the 2SC phase instead of directly entering the CFL phase. In fact, whereas in all other cases the star becomes unstable at the hadron-quark phase transition, this is the only example where we find stable star configurations with a quark matter core. Note, however, that in this case the star becomes unstable at the 2SC-CFL phase transition.

To interpret this result let us have a closer look at the corresponding EOS shown on the right hand side of Fig.7. We already noted that the transition from the hadronic phase to the CFL phase is accompanied by a strong discontinuity in the energy density. The same is true for the 2SC-CFL phase transition in Fig.7, but not for the hadron-2SC phase transition. This can be attributed to the relatively large mass of the strange quarks which are very rare in the 2SC phase but represent 1/3 of the total density in the CFL phase, and thus contribute considerably to its energy density. Thus, in contrast to Alford and Rajagopal [42] we are tempted to conclude that no CFL phase, but perhaps a 2SC phase could exist at the interior of neutron stars.

Our analysis is, however, not complete in any respect. For instance, as the large difference in Fermi momenta renders the BCS-type condensation in the "classical" 2SC phase difficult, it seems to be worthwhile to consider other possibilities. Among others we thereby think of a crystalline phase, deformed Fermi surfaces [32, 35], spin-1 pairing [20] or the "gapless" 2SC [33, 34] or CFL phase [60]. We conclude that whether quark matter exists in hybrid or

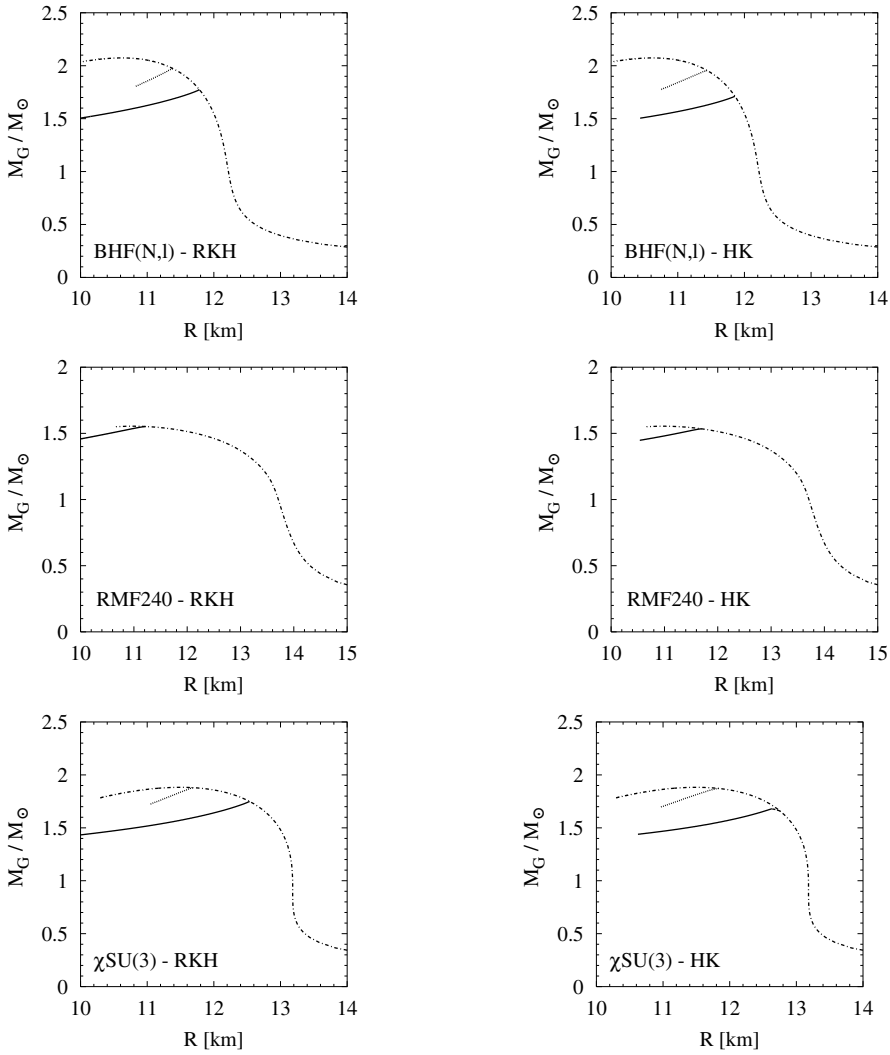

Figure 6. Mass-radius relation of different compact star configurations. The left panels correspond to calculations with parameter set RKH for the quark matter phase and the right panels to parameter set HK, respectively. From the upper panel downwards the hadronic phase is described by a BHF calculation without hyperons [55], a relativistic mean field calculation [57] and a chiral $SU(3)$ model [53].

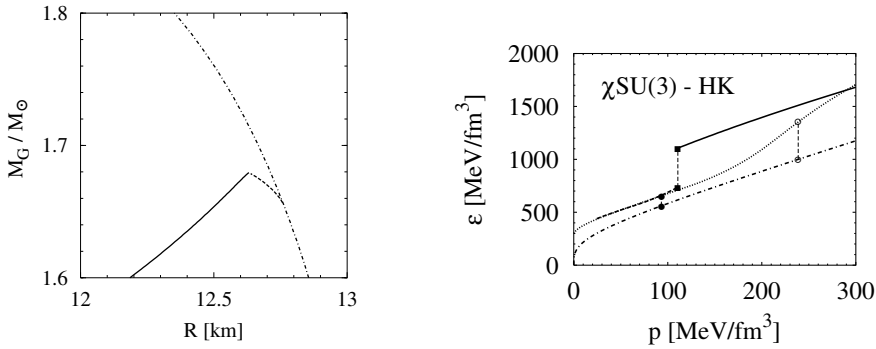

Figure 7. Left: Detail of Fig. 6, lower right. Right: Corresponding EOS. The hadron-normal, hadron-2SC, and 2SC-CFL transitions are marked by open circles, full circles, and boxes, resp..

even quark stars remains an interesting question which demands still a lot of work before a definite answer can be given.

Acknowledgments

This talk was partially based on collaborations with M. Baldo, G.F. Burgio, J. Hošek, F. Neumann, H.-J. Schulze, and I. Shovkovy, which are gratefully acknowledged. We also thank M. Hanauske and D. Zschiesche for supplying us with their hadronic EOS. We thank M. Urban for critically reading the manuscript. M. O. thanks the organizers for invitation and financial support.

References

[1] M.A. Halasz, A.D. Jackson, R.E. Shrock, M.A. Stephanov, and J.J.M. Verbaarschot, Phys. Rev. D 58 (1998) 096007.

[2] K. Rajagopal and F. Wilczek, hep-ph/0011333, and references therein

[3] M. Alford, Ann. Rev. Nucl. Part. Sci. 51 (2001) 131; F. Sannino, hep-ph/0205007; T. Schäfer, hep-ph/0304281; D.H. Rischke, JHEP 0306:032 (2003) hep-ph/0305030.

[4] J.C. Collins and M.J. Perry, Phys. Rev. Lett. 34 (1975) 1353.

[5] B. Barrois, Nucl. Phys. B 129 (1977) 390.

[6] S.C. Frautschi, Asymptotic freedom and color superconductivity in dense quark matter, in: Proc. of the Workshop on Hadronic Matter at Extreme Energy Density, N. Cabibbo (ed.), Erice 1978.

[7] D. Bailin and A. Love, Phys. Rep. 107 (1984) 325.

[8] M. Alford, K. Rajagopal, and F. Wilczek, Phys. Lett. B 422 (1998) 247.

[9] R. Rapp, T. Schäfer, E.V. Shuryak, and M. Velkovsky, Phys. Rev. Lett. 81 (1998) 53.

[10] R.D. Pisarski and D.H. Rischke, Phys. Rev. D 60 (1999) 094013.

[11] F. Weber, Acta Phys. Polon. B30 (1999) 3149.

[12] "Physics of Neutron Star Interiors", D. Blaschke, N.K. Glendenning, and A. Sedrakian (eds.), Springer, in press.

[13] R.D. Pisarski and D.H. Rischke, Phys. Rev. D 61 (2000) 051501; *ibid* 074017.

[14] D. Rischke, Phys. Rev. D 62 (2000) 034007; G.W. Carter and D. Diakonov, Nucl.Phys. B 582 (2000) 571.

[15] V.A. Miransky, I.A. Shovkovy, and L.C.R. Wijewardhana, Phys. Rev. D 64 (2001) 096002.

[16] J. Berges and K. Rajagopal, Nucl. Phys. B 538 (1999) 215; G.W. Carter and D. Diakonov, Phys. Rev. D 60 (1999) 016004; T.M. Schwarz, S.P. Klevansky, and G. Papp, Phys. Rev. C 60 (1999) 055205.

[17] T. Schäfer, Nucl.Phys. B 575 (2000) 269.

[18] M. Buballa, J. Hošek, and M. Oertel, Phys. Rev. Lett. 90 (2003) 182002.

[19] F. Sannino and W. Schäfer, Phys. Lett. B 527 (2002) 142.

[20] M. Alford, J.A. Bowers, J.M. Cheyne, G.A. Cowan, Phys. Rev. D 67 (2003) 054018.

[21] F. Sannino, Phys. Rev. D 67 (2003) 054006.

[22] A.J. Leggett, Rev. Mod. Phys. 47 (1975) 331.

[23] T. Schäfer, Phys. Rev. D 62 (2000) 094007.

[24] A. Schmitt, Q. Wang, D.H. Rischke, Phys.Rev.Lett.91:242301 (2003) nucl-th/0301090.

[25] A. Schmitt, Q. Wang, D.H. Rischke, Phys.Rev.D69:094017 (2003) nucl-th/0311006.

[26] D.T. Son, Phys. Rev. D 59 (1999) 094019; T. Schäfer and F. Wilczek, *ibid* D 60 (1999) 114033; D.K. Hong, V.A. Miransky, I.A. Shovkovy, and L.C.R. Wijewardhana, *ibid* D 61 (2000) 056001, *err.* D 62 (2000) 059903.

[27] A.L. Fetter and J.D. Walecka, Quantum theory of many-particle systems, Mc Graw-Hill, New York (1971).

[28] H. Nielsen and S. Chadha, Nucl. Phys. B 105 (1976) 445; H. Leutwyler, Phys. Rev. D 49 (1994) 3033; T. Schäfer, D.T. Son, M.A. Stephanov, D. Toublan, and J.J. Verbaarschot, Phys. Lett. B 522 (2001) 67;

[29] T.-L. Ho, Phys. Rev. Lett. 81 (1998) 742; T. Ohmi and K. Machida, J. Phys. Soc. Jpn. 67 (1998) 1822.

[30] V.A. Miransky and I.A. Shovkovy, Phys. Rev. Lett. 88 (2002) 111601.

[31] M. Alford, J. Bowers, and K. Rajagopal, Phys. Rev. D 63 (2001) 074016; R. Rapp, E. Shuryak, and I. Zahed, Phys. Rev. D 63 (2001) 034008; J. Bowers and K. Rajagopal, Phys. Rev. D 66 (2002) 065002.

[32] H. Müther and A. Sedrakian, Phys. Rev. D 67 (2003) 085024.

[33] I. Shovkovy and M. Huang, Phys. Lett. B 564 (2003) 205; M. Huang and I. Shovkovy, hep-ph/0307273.

[34] M. Huang, these proceedings.

[35] A. Sedrakian, these proceedings.

[36] M. Alford, K. Rajagopal, and F. Wilczek, Nucl. Phys. B 537 (1999) 443.

[37] R. Casalbuoni and R. Gatto, Phys. Lett. B 464 (1999) 111.

[38] D.T. Son and M. Stephanov, Phys. Rev. D 61 (2000) 074012.

[39] D.H. Rischke, Phys. Rev. D 62 (2000) 054017.

[40] R. Casalbuoni, C. Gatto, and G. Nardulli, Phys. Lett. B 498 (2001) 179; *err.* B 517 (2001) 483.

[41] P. Amore, M.C. Birse, J.A. McGovern, and N. R. Walet, Phys. Rev. D 65 (2002) 074005.

[42] M. Alford and K. Rajagopal, JHEP 0206 (2002) 031.

[43] A. Steiner, S. Reddy, and M. Prakash, Phys. Rev. D 66 (2002) 094007.

[44] N.K. Glendenning, Phys. Rev. D 46 (1992) 1274.

[45] P. Rehberg, S.P. Klevansky, and J. Hüfner, Phys. Rev. C 53 (1996) 410.

[46] F. Neumann, M. Buballa, and M. Oertel, Nucl. Phys. A 714 (2003) 481.

[47] M. Alford, K. Rajagopal, S. Reddy, and F. Wilczek, Phys. Rev. D 64 (2001) 074017.

[48] M. Alford and S. Reddy, Phys. Rev. D 67 (2003) 074024.

[49] M. Baldo, M. Buballa, F. Burgio, F. Neumann, M. Oertel, and H.-J. Schulze, Phys. Lett. B 562 (2003) 153.

[50] I. Shovkovy, M. Hanauske, and M. Huang, Phys. Rev. D 67 (2003) 103004.

[51] D. Blaschke, H. Grigorian, D.N. Aguilera, S. Yasui, and H. Toki, AIP Conf. Proc. 660 (2003) 209.

[52] M. Buballa, F. Neumann, M. Oertel, I. Shovkovy, in preparation.

[53] P. Papazoglou, S. Schramm, J. Schaffner-Bielich, H. Stöcker, and W. Greiner, Phys. Rev. C 57 (1998) 2576; P. Papazoglou, D. Zschiesche, S. Schramm, J. Schaffner-Bielich, H. Stöcker, and W. Greiner, Phys. Rev. C 59 (1999) 411; M. Hanauske, D. Zschiesche, S. Pal, S. Schramm, H. Stöcker, and W. Greiner, Astrophys. J. 537 (2000) 50329.

[54] R.C. Tolman, Phys. Rev. 55 (1939) 364; J.R. Oppenheimer and G. Volkoff, Phys. Rev. 55 (1939) 374.

[55] M. Baldo, I. Bombaci, and G.F. Burgio, Astron. Astrophys. 328 (1997) 274.

[56] M. Baldo, G.F. Burgio, and H.-J. Schulze, Phys. Rev. C 58 (1998) 3688;
Phys. Rev. C 61 (2000) 055801.

[57] N.K. Glendenning, Compact Stars (Springer, New York, 1996).

[58] T. Hatsuda and T. Kunihiro, Phys. Rep. 247 (1994) 221.

[59] H.-J. Schulze, these proceedings.

[60] M. Alford, C. Kouvaris, and K. Rajagopal, Phys.Rev.Lett.92:222001 (2003) hep-ph/0311286.

SUPERCONDUCTIVITY WITH DEFORMED FERMI SURFACES AND COMPACT STARS

Armen Sedrakian
Institute for Theoretical Physics, Tübingen University, D-72076 Tübingen, Germany
sedrakia@tphys.physik.uni-tuebingen.de

Abstract I discuss the deformed Fermi surface superconductivity (DFS) and some of its alternatives in the context of nucleonic superfluids and two flavor color superconductors that may exist in the densest regions of compact stellar objects.

1. Introduction

The astrophysical motivation to study the superconducting phases of dense matter arises from the importance of pair correlations in the observational manifestations of dense matter in compact stars. If the densest regions of compact stars contain deconfined quark matter it must be charge neutral and in β equilibrium with respect to the Urca processes $d \to u + e + \bar{\nu}$ and $u + e \to d + \nu$, where e, ν, and $\bar{\nu}$ refer to electron, electron neutrino, and antineutrino. The u and d quarks in deconfined matter fill two different Fermi spheres which are separated by a gap of the order of electron chemical potential. At high enough densities (where the typical chemical potentials become of the order of the rest mass of a s quark), strangeness nucleation changes the equilibrium composition of the matter via the reactions $s \to u + e + \bar{\nu}$ and $u + e \to s + \nu$. Although the strangeness content of matter affects its u-d flavor asymmetry, the separation of the Fermi energies remains a generic feature. The dense quark matter is expected to be a color superconductor (the early work is in Refs. [1]; recent developments are summarized in the reviews [2]).

Accurate description of the matter in this regime requires, first, tools to treat the Lagrangian of QCD in the nonperturbative regime and, second, an understanding of the superconductivity under asymmetry in the population of fermions that pair. The first principle lattice QCD calculations are currently not feasible for the purpose of understanding the physics of compact stars; the effective models, on the other hand, rarely incorporate all aspects of the known phenomenology like deconfinement and chiral restoration. Despite of the limitations of current models, a lot can be learned about generic features of

D. Blaschke and D. Sedrakian (eds.), Superdense QCD Matter and Compact Stars, 209–224.

possible phases of dense matter at densities where the perturbation theory fails. This mini-review concentrates on the second issue - the BCS superconductors under asymmetric conditions. Since the subject is of importance in a broader context of metallic superconductors, nucleonic superfluids, and dilute atomic gases, and much of our current understanding comes from the research in these fields, I will describe the relevant physics of non-relativistic superconductors first (Sections 2 and 3). Section 4 discusses the flavor asymmetric condensates in the context of QCD within the effective Nambu-Jona-Lasinio model; the emphasis is on the color superconducting state with deformed Fermi surfaces, but the discussion is sufficiently general to be applied to other non-BCS phases.

A comprehensive coverage of the recent developments is not possible in the present format; the choice of the topics will be thus personal and the list of the references necessarily incomplete.

2. Homogeneous superconducting state

Historically, asymmetric superconductors were studied in the early sixties (shortly after the advent of the Bardeen-Cooper-Schrieffer (BCS) theory of superconductivity) in the context of metallic superconductors with paramagnetic impurities [3–5, 16]. There is no bulk magnetic field in these systems due to the Meissner effect, however the paramagnetic impurities flip the spins of electrons in the collisions thereby inducing an asymmetry in the populations of spin-up and down fermions (which are assumed to pair in a state of total spin zero). The effect of impurities can be modeled by an average spin-polarizing field which gives rise to a separation of the Fermi levels of the spin-up and down electrons. Weak coupling analysis of the BCS equations revealed a double valued character of the gap as a function of the difference in chemical potentials $\delta\mu \equiv (\mu_\uparrow - \mu_\downarrow)/2$, where $\mu_{\uparrow\downarrow}$ are the chemical potentials of the spin up/down electrons. The first branch corresponds to a constant value $\Delta(\delta\mu) = \Delta(0)$ over the asymmetry range $0 \leq \delta\mu \leq \Delta(0)$ and vanishes beyond the point $\delta\mu = \Delta(0)$; the second branch exists in the range $\Delta(0)/2 \leq \delta\mu \leq \Delta(0)$ and increases from zero at the lower limit to $\Delta(0)$ at the upper limit. Only the $\delta\mu \leq \Delta(0)/\sqrt{2}$ portion of the upper branch is stable (that is, only in this range of asymmetries the superconducting state lowers the grand thermodynamic potential of the normal state). Thus, the dependence of the superconducting state on the shift in the Fermi surfaces is characterized by a constant value of the gap which vanishes at the Chandrasekhar-Clogston limit $\delta\mu_1 = \Delta(0)/\sqrt{2}$ [3, 4]. The picture above, while formally correct, is physically irrelevant to many systems as it does not conserve the number of particles.

Consider a BCS superconductor under the action of an external field that produces an asymmetry in the population of the fermions; the effect of such

field is to transform the symmetric Hamiltonian $\mathcal{H} \to \mathcal{H} - \sigma_z I a^\dagger a$, where $a^\dagger$ and a are the creation and destruction operators (in the second quantized form), σ_z is the z component of the vector of Pauli matrices, I is the magnitude of the asymmetry (for example, for fermions in a magnetic field $I = \mu_B H$, where μ_B is the Bohr magneton and H is the field intensity). In a non-relativistic set-up the gap and the densities of spin-up and spin-down species are determined by the equations [7–9]

$$\Delta_k = -\sum_{k'} V_{k,k'} \frac{\Delta_{k'}}{2E_{k'}} \left[1 - f(E^{\uparrow}_{k'}) - f(E^{\downarrow}_{k'})\right], \quad (1)$$

$$\rho_{\downarrow(\uparrow)} = \frac{1}{2}\sum_k \left[\left(1 + \frac{\xi_k}{E_k}\right) f(E^{\uparrow(\downarrow)}_k) + \left(1 - \frac{\xi_k}{E_k}\right) f(-E^{\downarrow(\uparrow)}_k)\right], \quad (2)$$

where $V_{k,k'}$ is the pairing interaction, $f(E)$ is the Fermi distribution function, $E_k = \sqrt{\xi_k^2 + \Delta_k^2}$, $E^{\uparrow\downarrow}_k = E_k \pm \delta\varepsilon_k$, and the symmetric and anti-symmetric combinations of the single-particle spectra are defined as

$$\xi_k = \frac{1}{2}\left(\varepsilon_{k\uparrow} + \varepsilon_{k\downarrow}\right), \quad \delta\varepsilon_k = \frac{1}{2}\left(\varepsilon_{k\uparrow} - \varepsilon_{k\downarrow}\right). \quad (3)$$

In the zero temperature limit the Fermi distribution function $f(E)$ reduces to a step function $\theta(-E)$. The single particle spectra $\varepsilon_{k\uparrow(\downarrow)}$ are completely general and may include the differences in the (effective) masses and/or self-energies of the two species. Eqs. (1) and (2) should be solved self-consistently. In the research on metallic superconductors these equations were decoupled and Eq. (1) was solved by parametrizing the asymmetry in terms of the difference in the chemical potentials, with the understanding that once the gap equation is solved the densities of the constituents can be computed *a posteriori*. However, as the value of $\delta\mu$ is changed so does the density of the system, i.e. such a scheme (while being correct) does not incorporate the particle number conservation. If the particle number conservation is implemented explicitely (by solving Eqs. (1) and (2) selfconsistently) the gap becomes a single-valued function of the particle number asymmetry $\alpha = (\rho_\uparrow - \rho_\downarrow)/(\rho_\uparrow + \rho_\downarrow)$ [7–9].

Minimizing the free-energy of a asymmetric superconductor at fixed density and temperature leads to stable solutions for the entire region of density asymmetries where non-trivial solutions of the gap equation exist [8]. This can be seen in Figs. 1 and 2 where the temperature and asymmetry dependence of the pairing gap and the free-energy of a homogenous asymmetric superconductor are shown (the examples here and in Figs. 3-8 below are taken from the studies of the tensor S-wave pairing in isospin asymmetric nuclear matter, but the overall picture is generic to all asymmetric superconductors). In particular, we see that for a fixed temperature the gap and the free-energy are single

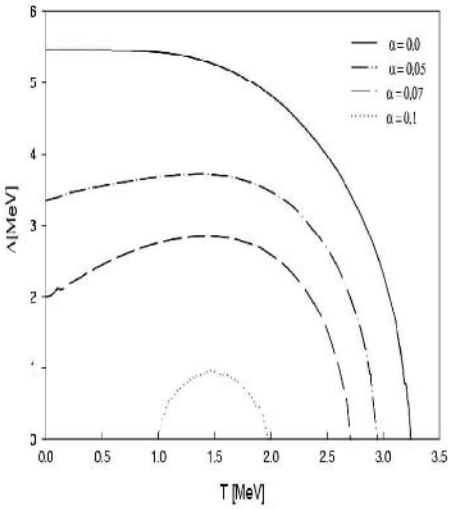

Figure 1. The temperature dependence of the pairing gap for density asymmetries $\alpha = 0.0$ (solid) 0.05 (dashed-doted) 0.07 (dashed) and 0.1 (dotted) [8].

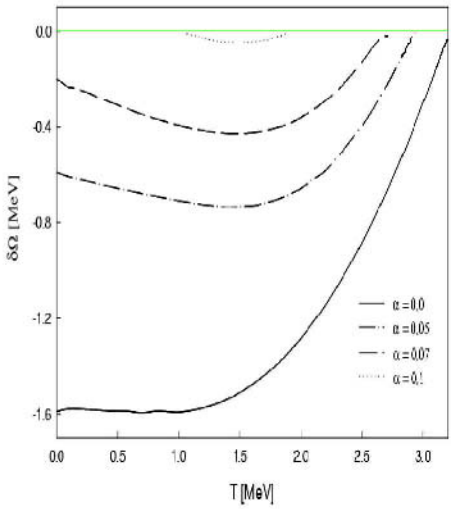

Figure 2. The temperature dependence of the free energy. The labeling of asymmetries is as in Fig. 1 [8].

valued functions of the density asymmetry α in a particle number conserving scheme (contrary to the nonconserving scheme, where double valued solutions appear).

For large asymmetries the dependence of the gap on the temperature shows the re-entrance phenomenon - the pairing correlations are restored (e. g. for $\alpha = 0.1$ in Fig. 1) as the temperature is increased and a second (lower) critical temperature appears. The re-entrance in the superconducting state with increasing temperature can be attributed to the smearing of the Fermi surfaces which increases the phase-space overlap between the quasi-particles that pair. Increasing the temperature further suppresses the pairing gap due to the thermal excitation of the system very much the same way as in the symmetric superconductors. Clearly, the pairing gap has a maximum at some intermediate temperature. The values of the two critical temperatures are controlled by different mechanisms: the superconductivity is destroyed with decreasing temperature at a lower critical temperature when the smearing of the Fermi surfaces becomes insufficient to maintain the phase space coherence. The upper critical temperature is the analog of the BCS critical temperature and corresponds to a transition to the normal state because of the thermal excitation of the system. At low temperatures the transition from the normal to the superconducting state is of the first order, while at the temperatures near the critical temperature - of the second order. The order of the phase transition changes from the first to the second as the temperature is increased. Another aspect of

the asymmetric superconducting state is the gapless nature of the excitations; in analogy to the non-ideal Bose gas where only part of the particles are in the zero-momentum ground state, in the asymmetric superconductors not all the pairs are gapped (see e.g. [9]). The presence of gapless excitations affects the dynamical properties of superconductors - the heat capacity, thermal conductivity, photon and sound absorption, etc.

3. Superconducting phases with broken space symmetries

3.1 LOFF phase

Larkin and Ovchinnikov [10] and, independently, Fulde and Ferrell [11] (LOFF) discovered in 1964 that the superconducting state can sustain asymmetries beyond the Chandrasekhar-Clogston limit if one pairs electrons with nonzero center-of-mass momentum. The weak coupling result for the critical shift in the Fermi surfaces for LOFF phase is $\delta\mu_2 = 0.755\Delta(0)$ [$> \delta\mu_1 = 0.707\Delta(0)$]. Since the condensate wave-function depends on the center-of-mass momentum of the pair its Fourier transform will vary in the configuration space giving rise to a lattice structure with finite share modulus. This spatial variation of the order parameter in the configuration space implies that the condensate breaks both the rotational and translational symmetries. There are thus additional massless Goldstone collective excitations associated with the broken global symmetries (in excess of other collective excitations that are present in the symmetric phase).

Consider again non-relativistic fermions. Their BCS spectrum (for homogeneous systems) is isotropic; when the polarizing field drives apart the Fermi surfaces of spin-up and down fermions the phase space overlap is lost, the pair correlations are suppressed, and eventually disappear at the Chandrasekhar-Clogston limit. The LOFF phase allows for a finite center-of-mass momentum of Cooper pairs $\vec{Q}$ and the quasiparticle spectrum is of the form

$$\varepsilon^0_{\uparrow\downarrow}(\vec{Q},\vec{q}) = \frac{1}{2m}\left(\frac{\vec{Q}}{2} \pm \vec{q}\right)^2 - \mu_{\uparrow\downarrow} + \text{ selfenergy terms.} \tag{4}$$

Thus, the LOFF phase requires a positive $\propto Q^2$ increase in the kinetic energy of the quasiparticles which makes it less favorable than the BCS state. However, the anisotropic term $\propto \vec{Q}\cdot\vec{q}$ (which can be interpreted as a dipole deformation of the isotropic spectrum) modifies the phase space overlap of the fermions and promotes pairing. The LOFF phase becomes stable when the loss in the kinetic energy that is needed to move the condensate is smaller than the gain in the potential pairing energy due to an increase in the phase-space overlap. The magnitude of the total momentum is a (variational) parameter for a minimization of the ground state energy of the system. The dependence

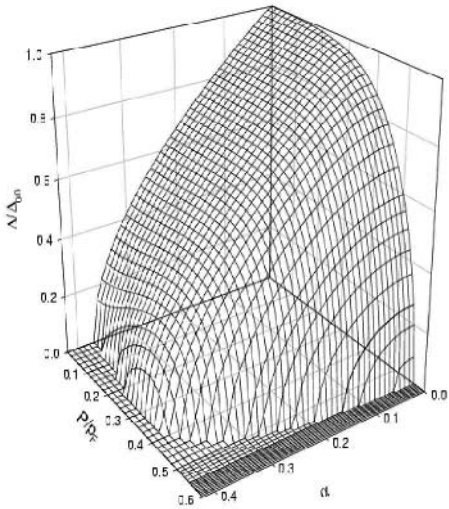

Figure 3. The dependence of the pairing gap in the LOFF phase on the density asymmetry and the total momentum of the condensate [12].

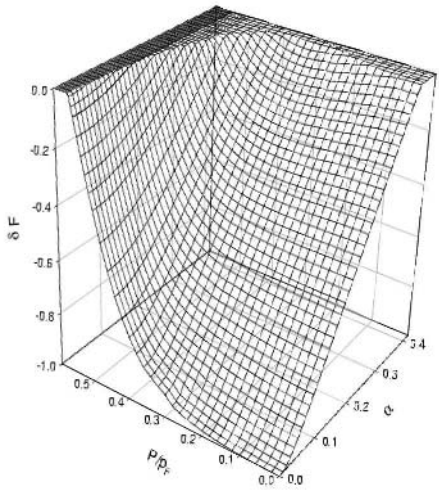

Figure 4. The dependence of the free energy of the LOFF phase on the same parameters as in Fig. 3 [12].

of the pairing gap and the free-energy of a LOFF superconductor on the total momentum of the condensate and the density asymmetry is shown in Figs. 3 and 4 [12]. The self-consistent solution of Eqs. (1) and (2) leads to a single valued pairing gap and stable superconducting state for arbitrary finite momentum of the condensate (below the critical one at which the superconductivity vanishes); in particular $Q \to 0$ limit is consistent with the earlier discussion of homogeneous asymmetric BCS condensates. For large enough asymmetries the minimum of the free-energy moves from the $Q = 0$ line to intermediate values of Q, i.e., the ground state of the system corresponds to a condensate with nonzero center-of-mass momentum of Cooper pairs. Note that for the near critical range of asymmetries the condensate exists only in the LOFF state and its dependence on the total momentum shows the re-entrance behavior seen in the temperature dependence of the homogeneous superconductors. Clearly, a single wave-vector condensate is an approximation; in general the LOFF phase can acquire a complicated lattice structure. A large number of lattice structures were studied in Refs. [13, 14] in the Ginzburg Landau regime, were it was found that the face-centered cubic lattice has the lowest energy. The LOFF phase obtains additional collective excitations (Goldstone modes) due to the breaking of the rotational and translational continuous space symmetries [15]. Identifying the order of the phase transition from the LOFF to the normal state is a complex problem and depends, among other things, on the preferred lattice structure (see Ref. [16] and references therein).

3.2 DFS phase

To motivate our next step recall that the LOFF spectrum can be view as a dipole [$\propto P_1(x)$] perturbation of the spherically symmetrical BCS spectrum, where $P_l(x)$ are the Legendre polynomials, and x is the cosine of the angle between the particle momentum and the total momentum of the Cooper pair. The $l = 1$ term in the expansion about the spherically symmetric form of Fermi surface corresponds to a translation of the whole system, therefore it preserves the spherical shapes of the Fermi surfaces. We now relax the assumption that the Fermi surfaces are spherical and describe their deformations by expanding the spectrum in spherical harmonics [17, 18]

$$\varepsilon_{\uparrow(\downarrow)}(\vec{Q},\vec{q}) = \varepsilon^0_{\uparrow(\downarrow)}(\vec{Q},\vec{q}) + \sum_l \epsilon_{l,\uparrow(\downarrow)} P_l(x), \tag{5}$$

where the coefficients ϵ_l for $l \geq 2$ describe the deformation of the Fermi surfaces which break the rotational O(3) symmetry down to O(2). The O(2) symmetry axis is chosen spontaneously and clearly need not coincide with the direction of the total momentum (this subsection assumes $Q = 0$). A single-component and spatially homogeneous system of non-interacting particles fills the states within its Fermi sphere homogeneously. In Fermi liquids the homogeneous filling prescription is extrapolated to (arbitrarily strongly) interacting quasiparticles. It is by no means obvious that such a prescription should re-

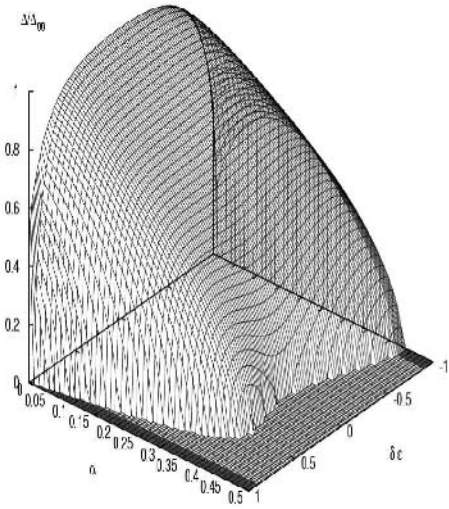

Figure 5. The dependence of the pairing gap in the DFS phase on the density asymmetry and the total momentum of the condensate [17].

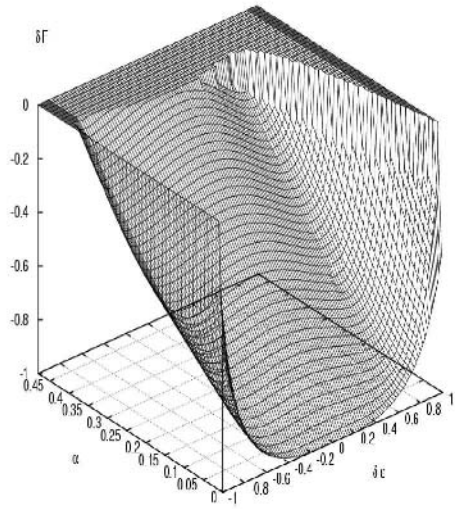

Figure 6. The dependence of the free energy of the DFS phase on the same parameters as in Fig. 5 [17].

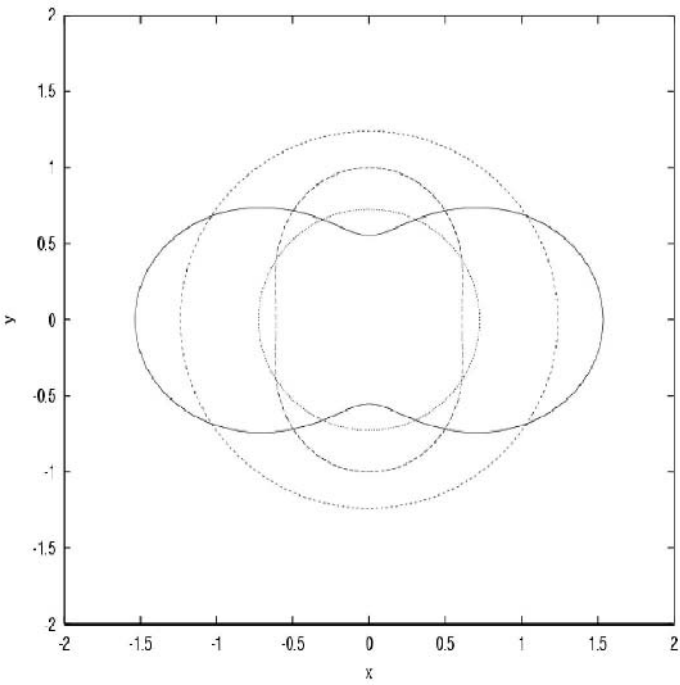

Figure 7. A projection of the Fermi surfaces on a plane parallel to the axis of the symmetry breaking. The concentric circles correspond to the two populations of spin/isospin-up and down fermions in spherically symmetric state ($\delta\epsilon = 0$), while the deformed figures correspond to the state with relative deformation $\delta\epsilon = 0.64$. The density asymmetry is $\alpha = 0.35$.

main valid for two or multi-component systems which interact, for example, by pairing forces. The expansion (5) is an example of a non-Fermi-liquid prescription for filling the particle states within a volume bounded by a (deformed) Fermi surface; the deformations are stable if they lower the ground state energy of the system with respect to the undeformed state. Note that in solids the Fermi surfaces are rarely spherical while their topology is dictated by the form of and interactions with the ion lattice. Note also that one should distinguish between the spontaneous deformation of Fermi-surfaces and explicit breaking of rotational symmetry by external fields. In the latter case the initial Lagrangian contains term(s) that explicitely break the symmetry and the resulting anisotropy of the self-energies can be interpreted as a deformation of the Fermi surfaces [19]. These type of deformations are interaction induced and are unrelated to the spontaneous deformations that appear even if the interaction is O(3) symmetric.

In practice, the deformation parameters ϵ_l ($l \geq 2$) are determined from the minimization of the free-energy of the system in full analogy to the total momentum Q of a Cooper pair. And they can be determined in a volume conserv-

ing manner by solving Eqs. (1) and (2) simultaneously (the resulting phase is abbreviated as the DFS phase). It is convenient to work with dimensionless deformation parameters corresponding to relative and conformal deformations defined as $\delta\epsilon = (\epsilon_{2,\uparrow} - \epsilon_{2,\downarrow})/2\mu$ and $\epsilon = (\epsilon_{2,\uparrow} + \epsilon_{2,\downarrow})/2\mu$, where μ is the chemical potential in the symmetric phase. The dependence of the pairing gap and the free-energy of the DFS phase on asymmetry and the relative deformation (at zero conformal deformation) is shown in Fig. 5 and 6, respectively. Although the density asymmetry (α) changes in the interval $[-1; 1]$ in general, the symmetry of the equations with respect to the indices labeling the species reduces the range of α to $[0; 1]$. The relative deformation is not bounded and can assume both positive and negative values. Fig. 7 shows a typical configuration of deformed Fermi surface which lowers the ground state energy below the non-deformed state. For $\alpha = 0$ Eqs. (1), (2) and (3) are symmetrical under interchange of the sign of $\delta\epsilon$ and the critical deformation for which the pairing vanishes is the same for prolate/oblate deformations. For finite α and the positive range of $\delta\epsilon$, the maximum value of the gap is attained at constant $\delta\epsilon$; for negative $\delta\epsilon$ the maximum increases as a function of the deformation and saturates around $\delta\epsilon \simeq 1$. As for the LOFF phase, the re-entrance phenomenon sets in for large asymmetries as $\delta\epsilon$ is increased from zero to finite values. And the mechanism by which the superconductivity is revived is based on the same phase-space argument, but involves a deformation of the Fermi surfaces rather than a motion of the condensate. Unlike the LOFF phase, the DFS phases does not break the translational symmetry of a superconductor (there are still additional collective excitations generated by the broken continuous rotational symmetry).

3.3 DFS vs LOFF

Which patterns of symmetry breaking are the most favorable if the Cooper pairs move with a finite center-of-mass momentum and the Fermi surfaces are allowed to be deformed? To answer this question we use the set-up of the previous sections and choose to work with the spectrum (5) at finite values of Q and $\delta\epsilon$ [18]. Figure 8 displays the difference between the free energies of the superconducting and normal states $\delta\mathcal{F}$ normalized to its value in the asymmetric BCS state $\delta\mathcal{F}_{00} = \delta\mathcal{F}(Q = 0, \delta\epsilon = 0)$. Since the energy of the pair interactions scales as the square of the pairing gap, the shape of the $\delta\mathcal{F}$ surface closely resembles that of the pairing gap (see for details Ref. [18]). The asymmetric BCS state is the stable ground state of the system ($\delta\mathcal{F} < 0$), however it corresponds to a saddle point - perturbations for finite $\delta\epsilon$ and Q are unstable towards evolution to lower energy states. For the pure LOFF phase ($\delta\epsilon = 0$) the ground state corresponds to finite momentum $Q \sim 0.5$ (in units of Fermi-momentum p_F). For the pure DFS phase ($Q = 0$) there are two

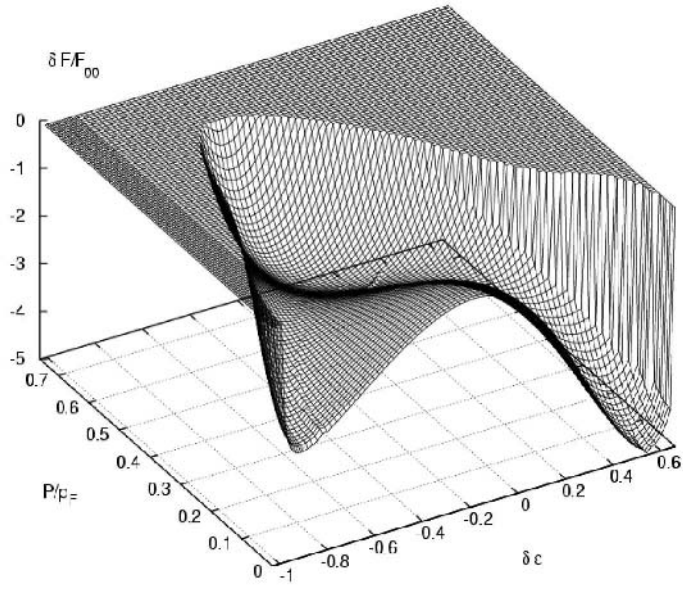

Figure 8. The dependence of the free energy of the combined DFS and LOFF phases on the center-of-mass momentum of the pairs Q (in units of Fermi momentum p_F) and the relative deformations $\delta\epsilon$ for a fixed density asymmetry [18].

minima corresponding to $\delta\epsilon \simeq -0.8$ and $\delta\epsilon \simeq 0.55$, i.e., prolate and oblate deformations of the majority Fermi sphere, respectively. In general the position of the minimum of $\delta\mathcal{F}$ in the $\delta\epsilon$-Q plane (passing through the minima of the limiting cases) prefers either large deformations or large finite momenta. The absolute minimum energy state corresponds to $\delta\epsilon \simeq 0.55$ *and* $Q = 0$; that is, while the LOFF phase is a local minimum state, it is unstable towards evolution to a pure DFS phase with oblate and prolate deformations of the majority and minority Fermi spheres. Further work will be needed to clarify how universal are these features. In particular, the assumption of a single wave-vector LOFF phase should be relaxed.

3.4 Alternatives

To complete our discussion of non-relativistic superfluids let us briefly mention some of the alternatives to the LOFF and DFS phases. One possibility is that the system prefers a phase separation of the superconducting and normal phases in real space, such that the superconducting phase contains particles with the same chemical potentials, i.e. is symmetric, while the normal phase remains asymmetric [20, 21].

Equal spin (isospin, flavor) pairing is another option, if the interaction between the same spin particles is attractive [22–24]. Since the separation of the

Fermi surfaces does not affect the spin-1 pairing on each Fermi surface, an asymmetric superconductor evolves into a spin-1 superconducting state (rather than a non-superconducting state) as the asymmetry is increased. Therefore, the spin-1 pairing is the limiting state for very large asymmetries. If the states corresponding to different Fermi surfaces are characterized by spin (as is the case in the metallic superconductors) the pairing interaction in a spin-1 state should be P wave and the transition is from the S to the P wave pairing. For larger number of discrete quantum numbers that characterize the fermions (say spin and isospin) the transition may occur between different S wave phases (e.g. from isospin singlet to the isospin triplet state in nuclear matter).

4. Flavor asymmetric quark condensates

This section deals with the color superconductors and describes a straightforward formalism for extending the discussion of the previous sections to relativistic systems. Below it will be assumed that the superconducting phase is chirally symmetric and particles are interacting only via a pairing force (self-energy and vertex renormalization are ignored). The flavor asymmetric color superconducting quark matter appears in the context of the two-flavor pairing (2SC-phase) described by the order parameter [1, 2]

$$\Delta \propto \langle \psi^T(x) C\gamma_5\tau_2\lambda_2\psi(x)\rangle, \tag{6}$$

where $C = i\gamma^2\gamma^0$ is the charge conjugation operator, τ_2 is the second component of the Pauli matrix acting in the $\mathrm{SU}(2)_f$ flavor space, λ_A is the antisymmetric Gell-Mann matrix acting in the $\mathrm{SU}(3)_c$ color space. The Ansatz for the order parameter implies that the color $\mathrm{SU}(3)_c$ symmetry is reduced to $\mathrm{SU}(2)_c$ since only two of the quark colors are involved in the pairing while the third color remains unpaired. The effective Lagrangian density of the Nambu-Jona-Lasinio model that describes our system is of the form

$$\begin{aligned} \mathcal{L}_{\text{eff}} &= \bar{\psi}(x)(i\gamma^\mu\partial_\mu)\psi(x) \\ &+ G_1(\psi^T C\gamma_5\tau_2\lambda_A\psi(x))^\dagger(\psi^T C\gamma_5\tau_2\lambda_A\psi(x)). \end{aligned} \tag{7}$$

The partial densities and the gap equation for the up and down paired quarks can be found from the fixed points of the thermodynamic potential density Ω

$$\frac{\partial\Omega}{\partial\Delta} = 0, \quad -\frac{\partial\Omega}{\partial\mu_f} = \rho_f; \tag{8}$$

the flavor index $f = u, d$ refers to up (u) and down (d) quarks. For the Lagrangian density defined by Eq. (6) and the pairing channel Ansatz (6), the finite temperature thermodynamical potential Ω per unit volume is

$$\Omega = -2\sum_{p,ij}\left\{2p + \frac{1}{\beta}\log\left[f(\xi_{ij})\right]^{-1} + E_{ij} + \frac{2}{\beta}\log\left[f(s_{ij}E_{ij})\right]^{-1}\right\} + \frac{\Delta^2}{4G_1}, \tag{9}$$

where the indeces $i,j=(+,-)$ sum over the four branches of the paired and unpaired quasiparticle spectra defined, respectively, as $\xi_{\pm\pm}=(p\pm\mu)\pm\delta\mu$ and $E_{\pm\pm}=\sqrt{(p\pm\mu)^2+|\Delta|^2}\pm\delta\mu$, where $\delta\mu=(\mu_u-\mu_d)/2$ and $\mu=(\mu_u+\mu_d)/2$ with μ_u and μ_d being the chemical potentials of the up and down quarks; $s_{+j}=1$ and $s_{-j}=\mathrm{sgn}(p-\mu)$ and $f(\xi_{ij})$ are the Fermi distribution functions. The variations of the thermodynamic potential (9) provide the gap equation

$$\Delta = 8G_1\sum_p\left\{\frac{\Delta}{E_{+-}+E_{++}}\left[\tanh\left(\frac{\beta E_{++}}{2}\right)+\tanh\left(\frac{\beta E_{+-}}{2}\right)\right]+\mathrm{ex}\right\}, \tag{10}$$

where ex abbreviates a second term which follows from the first one via a simultaneous interchange of the signs; the partial densities of the up/down quarks are

$$\rho_{u/d} = \sum_{\vec{p},j=\pm}\left[2f(\xi_{-\mp})-2f(\xi_{+\pm})\mp\left(1\pm\frac{\xi_{j-}+\xi_{j+}}{E_{j-}+E_{j+}}\right)\tanh\left(\frac{\beta E_{j-}}{2}\right)\right.$$
$$\left.\pm\left(1\mp\frac{\xi_{j-}+\xi_{j+}}{E_{--}+E_{j+}}\right)\tanh\left(\frac{\beta E_{j+}}{2}\right)\right], \tag{11}$$

where and the upper/lower sign corresponds to the u/d-quarks. The free energy F is related to the thermodynamic potential Ω by the relation $F=\Omega+\mu_u\rho_u+\mu_d\rho_d$ and, as already discussed for non-relativistic superconductors, the energy should be minimized at constant temperature and density of the matter at various flavor asymmetries defined as $\alpha\equiv(\rho_d-\rho_u)/(\rho_d+\rho_u)$ [25]. Eqs. (9) and (10) are the (ultra)relativistic counterparts of Eqs. (1) and (2) which, apart from the relativistic form of the spectrum, include the contribution of anti-particles.

To obtain the selfconsistent solutions we employ a three-dimensional momentum space cut-off $|\mathbf{p}|<\Lambda$ to regularize the divergent integrals. The phenomenological value of the coupling constant G_1 in the $\langle qq\rangle$ Cooper channel is related to the coupling constant in the $\langle q\bar{q}\rangle$ diquark channel by the relation $G_1=N_c/(2N_c-2)G$; the latter coupling constant and the cut-off are fixed by adjusting the model to the vacuum properties of the system [26, 27]. Figure 9 summarizes the main features of the color superconducting DFS phase [25]. The physically relevant regime of flavor asymmetries which is likely to occur in the charge-neutral matter under β equilibrium is $0.1\leq\alpha\leq0.3$ [28, 18, 14, 31]. The dependence of the color superconducting gap (left panel) and the free energy difference between the superconducting state and normal state

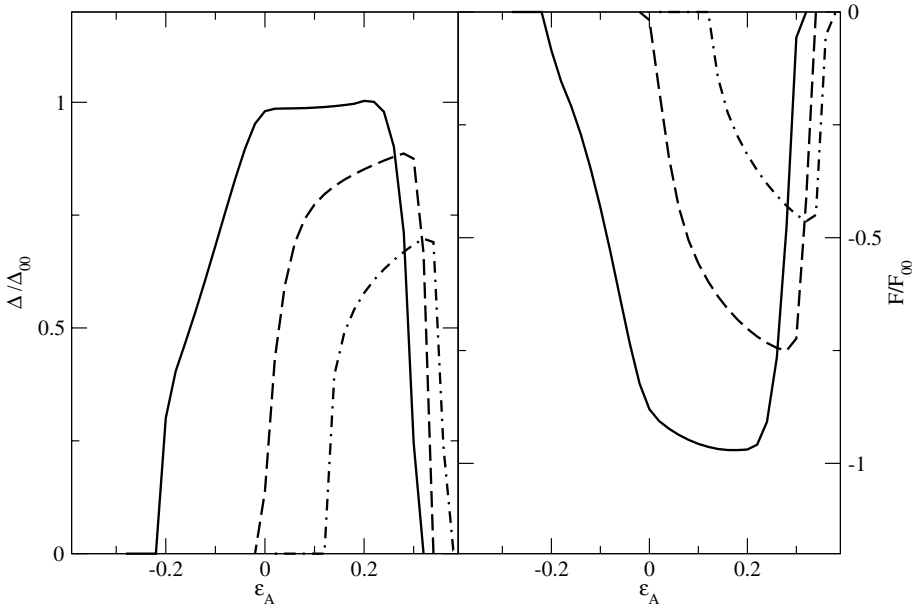

Figure 9. The color superconducting gap (left panel) and the free energy (right panel) as a function of relative deformation parameter ε_A for the values of the flavor asymmetry $\alpha = 0$ (solid lines), 0.1 (dashed lines), 0.2 (short dashed lines) and 0.3 (dashed dotted lines) at density $\rho_B = 0.31$ fm^{-3} and temperature $T = 2$ MeV [25].

(right panel) are shown as a function of deformation parameter ε_A for several flavor asymmetries at the baryonic density $\rho_B = 0.31$ fm^{-3} and temperature $T = 2$ MeV (the conformal deformation $\varepsilon_S = 0$). The β equilibrated quark matter requires an excess of the d over u quarks, therefore the range of the flavor asymmetry is restricted to the positive values. The deformation parameter ε_A assumes both positive and negative values. The main features seen in Fig. 9 are consistent with the results obtained for the non-relativistic superconductors: for a fixed $\alpha \neq 0$ and $\varepsilon_A > 0$, the gap is larger in the DFS state than in the ordinary BCS state ($\varepsilon_A = 0$), i.e., the 2SC phase is unstable towards deformation of the Fermi surfaces. Accordingly, the minimum of the free energy corresponds to the DFS state with $\varepsilon_A \simeq 0.25$ and its position weakly depends on the magnitude of the asymmetry α.

5. Concluding remarks

The properties of the asymmetric superconductors have been an exciting subject since the advent of the BCS theory of superconductivity more than four decades ago. While the early studies were motivated by the effects of the para-

magnetic impurities on the superconducting state and the possible coexistence of the ferromagnetic and superconducting phases in metallic superconductors, the recent work on this subject has been motivated by the need to understand the nucleonic superfluids, the colored quark superconductors and the dilute trapped atomic gases.

This mini-review focused on several non-BCS phases that may be featured by the asymmetric superconductors. The main points are summarized below:

- For small asymmetries, the superconducting state is homogeneous and the order parameter preserves the space symmetries. For most of the systems of interest the number conservation should be implemented by solving equations for the gap function and the densities of species self-consistently. In such a scheme the physical quantities are single valued functions of the asymmetry and temperature, contrary to the double valued results obtained in the non-conserving schemes.

- For large enough asymmetries the homogeneous state becomes unstable towards formation of either the LOFF phase - a superconducting state with nonzero center-of-mass momentum of the Cooper pairs, or the DFS phase - a superconducting state which requires a quadrapole deformation of Fermi surfaces. A combined treatment of these phases in non-relativistic systems shows that while the LOFF phase corresponds to a local minimum, the DFS phase has energy lower that the LOFF phase. These phases break either the rotational, the translational or both symmetries.

- The temperature dependence of the pairing gap for the homogeneous, LOFF and DFS superconducting phases shows the phenomenon of reentrance: the superconducting state is revived at finite temperatures. There exist two critical temperatures corresponding to phase transitions from the normal to the superconducting state and back as the temperature is increased from zero to finite values.

- The color superconducting DFS-phase, which is treated in a four-fermion contact interaction model, is preferred to the homogeneous 2SC state for asymmetries that are typical to matter under β-equilibrium.

Acknowledgments

I would like to thank Umberto Lombardo, Herbert Müther, Philippe Nozieres, Peter Schuck, and Hans Schulze for their contribution to the research reported here. This work was supported by a grant provided by the SFB 382 of the DFG.

References

[1] B. C. Barrois, Nucl. Phys. **B129**, 390 (1977); S. C. Frautschi, in "Hadronic matter at extreme energy density", edited by N. Cabibbo and L. Sertorio (Plenum Press, 1980); D. Bailin and A. Love, Phys. Rep. **107**, 325 (1984) and references therein.

[2] K. Rajagopal and F. Wilczek, hep-ph/0011333; M. G. Alford, Ann. Rev. Nucl. Part. Sci. **51**, 131 (2001);
T. Schaefer, hep-ph/0304281; D. H. Rischke, Prog. Part. Nucl. Phys. **52**, 197 (2003); C. D. Roberts and S. M. Schmidt, Prog. Part. Nucl. Phys. **45**, S1 (2000); R. Casalbuoni and G. Nardulli, Rev. Mod. Phys. **76**, 263 (2003).

[3] A. M. Clogston, Phys. Rev. Lett. **9**, 266 (1962).

[4] B. S. Chandrasekhar, Appl. Phys. Lett. **1**, 7 (1962).

[5] G. Sarma, Phys. Chem. Solids **24**, 1029 (1963).

[6] L. P. Gor'kov and A. I. Rusinov, Zh. Eksp. Teor. Fiz. **46**, 1363 (1964) [Sov. Phys. JETP **19**, 922 (1964)].

[7] A. Sedrakian, T. Alm, and U. Lombardo, Phys. Rev. C **55**, R582 (1996).

[8] A. Sedrakian and U. Lombardo, Phys. Rev. Lett. **84**, 602 (2000).

[9] U. Lombardo, P. Nozieres, P. Schuck, H.-J. Schulze and A. Sedrakian, Phys. Rev. C **64**, 064314 (2001).

[10] A. I. Larkin and Yu. N. Ovchinnikov, Zh. Eksp. Teor. Fiz. **47**, 1136 (1964) [Sov. Phys. JETP **20**, 762 (1965)].

[11] P. Fulde and R. A. Ferrell, Phys. Rev. **135**, A550 (1964).

[12] A. Sedrakian, Phys. Rev. C **63**, 025801 (2001) .

[13] J. A. Bowers and K. Rajagopal, Phys. Rev. D **66**, 065002 (2002).

[14] J. A. Bowers, Ph. D. thesis, hep-ph/0305301.

[15] R. Casalbuoni, R. Gatto, M. Mannarelli and G. Nardulli, Phys. Rev. D **66**, 014006 (2002).

[16] R. Casalbuoni and G. Tonini, Phys. Rev. B **69**, 104505 (2003).

[17] H. Müther and A. Sedrakian, Phys. Rev. Lett. **88**, 252503 (2002).

[18] H. Müther and A. Sedrakian, Phys. Rev. C **67**, 015802 (2003).

[19] E. Nakano, T. Maruyama and T. Tatsumi, Phys. Rev. D **68**, 105001 (2003).

[20] P. F. Bedaque, Nucl. Phys. A **697**, 569 (2002).

[21] P. F. Bedaque, H. Caldas, G. Rupak, Phys.Rev.Lett. **91**, 247002 (2003).

[22] T. Schäfer, Phys. Rev. D **62**, 094007 (2002).

[23] M. Buballa, J. Hosek and M. Oertel, Phys. Rev. Lett. **90**, 182002 (2003).

[24] M. Alford, J. Bowers, J. Cheyne and G. Cowan, Phys. Rev. D **67**, 054018 (2003).

[25] H. Müther and A. Sedrakian, Phys. Rev. D **67**, 085024 (2003).

[26] T. M. Schwarz, S. P. Klevansky and G. Papp, Phys. Rev. C **60**, 055205 (1999).

[27] M. Buballa, J. Hosek and M. Oertel, Phys. Rev. D **65**, 014018 (2002).

[28] K. Iida and G. Baym, Phys. Rev. D **63**, 074018 (2001).

[29] A. W. Steiner, S. Reddy and M. Prakash, Phys. Rev. D **66**, 094007 (2002).

[30] D. Blaschke, S. Fredriksson, H. Grigorian and A. M. Oztas, Nucl. Phys. **A736**, 203 (2003).

[31] M. Huang and I. Shovkovy, Nucl. Phys. **A729**, 835 (2003).

NEUTRAL DENSE QUARK MATTER

Mei Huang
Institut für Theoretische Physik, J.W. Goethe-Universitaet, Germany
huang@th.physik.uni-frankfurt.de

Igor Shovkovy
Institut für Theoretische Physik, J.W. Goethe-Universitaet, Germany
shovkovy@th.physik.uni-frankfurt.de

Abstract The ground state of dense up and down quark matter under local and global charge neutrality conditions with β-equilibrium has at least four possibilities: normal, regular 2SC, gapless 2SC phases, and mixed phase composed of 2SC phase and normal components. The discussion is focused on the unusual properties of gapless 2SC phase at zero as well as at finite temperature.

Keywords: Local and global charge neutrality conditions, mixed phase, gapless color superconductivity

1. Introduction

Currently, our knowledge of sufficiently cold and dense matter is very limited. There are neither experimental data nor lattice data in this region. From the BCS theorem, it is speculated that if the matter is dense enough, the ground state of the deconfined quark matter at low temperature will be a color superconductor [1]. Recent studies show that dense quark matter has a rich phase structure, see Ref. [2] for reviews. At asymptotically high baryon densities, this phenomenon can be studied from first principles [3]. If all three colors of the three light quarks participate in the Cooper pairing, the ground state will be in the color-flavor-locking (CFL) phase [4].

In reality, we are more interested in the intermediate density region, where the color superconducting phase may exist in the interior of neutron stars or may be created in heavy ion collisions. Unfortunately, we have little knowledge about this region: we are not sure how the deconfinement and the chiral restoration phase transitions happen, how the QCD coupling constant evolves and how the strange quark behaves in dense matter, etc. Primarily, our current

D. Blaschke and D. Sedrakian (eds.), Superdense QCD Matter and Compact Stars, 225–239.

understanding of the QCD phase structure in this region is based on assumptions.

In the framework of the bag model [5], or, in general, under the assumption that the strange quark mass is small [6], one can exclude the 2SC phase in the interior of compact stars when charge neutrality is considered.

However, there is another possibility, if the strange quark becomes light at a larger chemical potential than the u, d quarks, there will be a density region where only u, d quarks exist. Here, we focus on the dense quark matter composed of only u and d quarks, assuming that the strange quark is too heavy to involve in the system. If bulk u, d quark matter exists in the interior of compact stars, it should be neutral with respect to electrical as well as color charges [6–13]. Also, such matter should remain in β-equilibrium, i.e., the chemical potential for each flavor and color should satisfy the relationship $\mu_{ij,\alpha\beta} = (\mu\delta_{ij} - \mu_e Q_{ij})\delta_{\alpha\beta} + 2/\sqrt{3}\mu_8\delta_{ij}(T_8)_{\alpha\beta}$, where Q and T_8 are generators of U(1)$_{em}$ of electromagnetism and the U(1)$_8$ subgroup of the color gauge group. Satisfying these requirements imposes nontrivial relations between the chemical potentials of different quarks. We will see that these requirements play very important role in determining the ground state of dense u, d quark matter.

The charge neutrality condition can be satisfied locally [6–11] or globally [12, 13]. In the following, we will firstly discuss the homogeneous phase when the charge neutrality is satisfied locally, then discuss the mixed phase when the charge neutrality condition is satisfied globally.

2. Local charge neutrality: homogeneous phase

2.1 Correct way to find the neutral ground state

To neutralize the electrical charge in the homogeneous dense u, d quark matter, roughly speaking, twice as many d quarks as u quarks are needed, i.e., $n_d \simeq 2n_u$, where $n_{u,d}$ are the number densities for u and d quarks. This induces a mismatch between the Fermi surfaces of pairing quarks, i.e., $\mu_d - \mu_u = \mu_e = 2\delta\mu$, where μ_e is the electron chemical potential.

To get the ground state of the system, we need to know the thermodynamical potential. For simplicity, we use Nambu–Jona-Lasinio (NJL) model [14] to describe 2-flavor quark matter,

$$\begin{aligned} \mathcal{L} &= \bar{q}i\gamma^\mu\partial_\mu q + G_S\left[(\bar{q}q)^2 + (\bar{q}i\gamma_5\tilde{\tau}q)^2\right] \\ &\quad + G_D\left[(i\bar{q}^C\varepsilon\epsilon^b\gamma_5 q)(i\bar{q}\varepsilon\epsilon^b\gamma_5 q^C)\right], \end{aligned} \tag{1}$$

where $q^C = C\bar{q}^T$ is the charge-conjugate spinor and $C = i\gamma^2\gamma^0$ is the charge conjugation matrix. The quark field $q \equiv q_{i\alpha}$ is a four-component Dirac spinor

that carries flavor ($i = 1, 2$) and color ($\alpha = 1, 2, 3$) indices. The Pauli matrices are denoted by $\vec{\tau} = (\tau^1, \tau^2, \tau^3)$, while $(\varepsilon)^{ik} \equiv \varepsilon^{ik}$ and $(\epsilon^b)^{\alpha\beta} \equiv \epsilon^{\alpha\beta b}$ are the antisymmetric tensors in the flavor and color spaces, respectively. We also introduce a momentum cutoff Λ, and two independent coupling constants in the scalar quark-antiquark and scalar diquark channels, G_S and G_D. We define $\eta = G_D/G_S$, and $\eta = 0.75$ is the value from the Fierz transformation, but in principle, η is a free parameter.

In the mean-field approximation, the thermodynamical potential for u, d quarks in β-equilibrium with electrons takes the form [7, 9]:

$$\begin{aligned}\Omega_{u,d,e} &= \Omega_0 - \frac{1}{12\pi^2}\left(\mu_e^4 + 2\pi^2 T^2 \mu_e^2 + \frac{7\pi^4}{15} T^4\right) + \frac{m^2}{4G_S} \\ &+ \frac{\Delta^2}{4G_D} - \sum_a \int \frac{d^3p}{(2\pi)^3}\left[E_a + 2T \ln\left(1 + e^{-E_a/T}\right)\right], \qquad (2)\end{aligned}$$

where Ω_0 is a constant added to make the pressure of the vacuum zero, and the electron mass was taken to be zero, which is sufficient for the purposes of the current study. The sum in the second line of Eq. (2) runs over all (6 quark and 6 antiquark) quasi-particles. The explicit dispersion relations and the degeneracy factors of the quasi-particles read

$$E_{ub}^{\pm} = E(p) \pm \mu_{ub}, \qquad [\times 1] \qquad (3)$$

$$E_{db}^{\pm} = E(p) \pm \mu_{db}, \qquad [\times 1] \qquad (4)$$

$$E_{\Delta^\pm}^{\pm} = E_\Delta^{\pm}(p) \pm \delta\mu. \qquad [\times 2] \qquad (5)$$

Here we introduced the following shorthand notation: $E(p) = \sqrt{\mathbf{p}^2 + m^2}$ and $E_\Delta^{\pm}(p) = \sqrt{[E(p) \pm \bar{\mu}]^2 + \Delta^2}$ with $\bar{\mu} \equiv \mu - \mu_e/6 + \mu_8/3$.

If a macroscopic chunk of quark matter is created in heavy ion collisions or exists inside the compact stars, it must be in color singlet. So in the following discussions, color charge neutrality condition is always satisfied.

Now, we discuss the role of electrical charge neutrality condition. If a macroscopic chunk of quark matter has nonzero net electrical charge density n_Q, the total thermodynamical potential for the system should be given by

$$\Omega = \Omega_{Coulomb} + \Omega_{u,d,e}, \qquad (6)$$

where $\Omega_{Coulomb} \sim n_Q^2 V^{2/3}$ (V is the volume of the system) is induced by the repulsive Coulomb interaction. The energy density grows with increasing the volume of the system, as a result, it is almost impossible for matter inside stars to remain charged over macroscopic distances. So the bulk quark matter should also satisfy electrical neutrality condition, thus $\Omega_{Coulomb}|_{n_Q=0} = 0$,

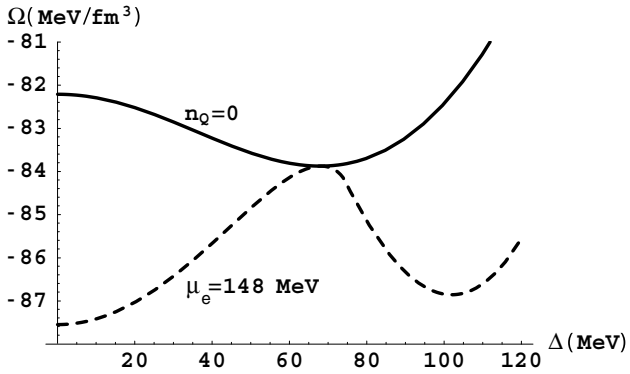

Figure 1. The effective potential as a function of the diquark gap Δ calculated at a fixed value of the electrical chemical potential $\mu_e = 148$ MeV (dashed line), and the effective potential defined along the neutrality line (solid line). The results are plotted for $\mu = 400$ MeV with $\eta = 0.75$.

and $\Omega_{u,d,e}|_{n_Q=0}$ is on the neutrality line. Under the charge neutrality condition, the total thermodynamical potential of the system is $\Omega|_{n_Q=0} = \Omega_{u,d,e}|_{n_Q=0}$.

Here, we want to emphasize that: *The correct way to find the ground state of the homogeneous neutral u, d quark matter is to minimize the thermodynamical potential along the neutrality line $\Omega|_{n_Q=0} = \Omega_{u,d,e}|_{n_Q=0}$, not like in the flavor asymmetric quark system, where β-equilibrium is required but μ_e is a free parameter, and the ground state is determined by minimizing the thermodynamical potential $\Omega_{u,d,e}$.*

From Figure 1, we can see the difference in determining the ground state for a charge neutral system and for a flavor asymmetric system. In Figure 1, at a given chemical potential $\mu = 400$ MeV and $\eta = 0.75$, the thermodynamical potential along the charge neutrality line $\Omega|_{n_Q=0}$ as a function of the diquark gap Δ is shown by the solid line. The minimum gives the ground state of the neutral system, and the corresponding values of the chemical potential and the diquark gap are $\mu_e = 148$ MeV and $\Delta = 68$ MeV, respectively. If we switch off the charge neutrality conditions, and consider the flavor asymmetric u, d quark matter in $\beta-$ equilibrium [15], the electrical chemical potential μ_e becomes a free parameter. At a fixed $\mu_e = 148$ MeV and with color charge neutrality, the thermodynamical potential is shown as a function of the diquark gap by the dashed line in Figure 1. The minimum gives the ground state of the flavor asymmetric system, and the corresponding diquark gap is $\Delta = 104$ MeV, but this state has positive electrical charge density, and cannot exist in the interior of compact stars.

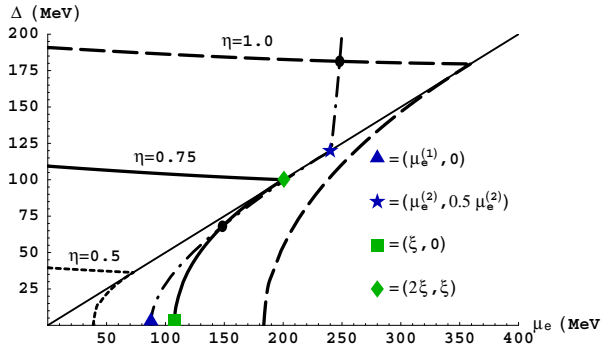

Figure 2. The graphical representation of the solution to the charge neutrality conditions (thick dash-dotted line) and the solution to the gap equation for three different values of the diquark coupling constant (thick solid and dashed lines). The intersection points represent the solutions to both. The thin solid line divides two qualitatively different regions, $\Delta < \delta\mu$ and $\Delta > \delta\mu$. The results are plotted for $\mu = 400$ MeV and three values of diquark coupling constant $G_D = \eta G_S$ with $\eta = 0.5$, $\eta = 0.75$, and $\eta = 1.0$.

2.2 η dependent solutions

In the last subsection, by looking for the minimum of the thermodynamic potential along the charge neutrality line, we found the ground state for the charge neutral u, d quark system.

Equivalently, the neutral ground state can also be determined by solving the diquark gap equation together with the charge neutrality conditions. We visualize this method in Figure 2, with color neutrality always satisfied, at a given chemical potential $\mu = 400\,\mathrm{MeV}$. The nontrivial solutions to the diquark gap equation as functions of the electrical chemical potential μ_e are shown by a thick-solid line ($\eta = 0.75$), a long-dashed line ($\eta = 1.0$), and a short-dashed line ($\eta = 0.5$). It is found that for each η, the solution is divided into two branches by the thin-solid line $\Delta = \delta\mu$, and the solution is very sensitive to η. Also, there is always a trivial solution to the diquark gap equation, i.e., $\Delta = 0$. The solution of the charge neutrality conditions is shown by a thick dash-dotted line, which is also divided into two branches by the thin-solid line $\Delta = \delta\mu$, but the solution of the charge neutrality is independent of η.

The cross-point of the solutions to the charge neutrality conditions and the diquark gap gives the solution of the system. We find that the neutral ground state is sensitive to the coupling constant $G_D = \eta G_S$ in the diquark channel. In the case of a very strong coupling (e.g., $\eta = 1.0$ case), the charge neutrality line crosses the upper branch of the solution to the diquark gap, the ground state is a charge neutral regular 2SC phase with $\Delta > \delta\mu$. In the case of weak coupling (e.g., $\eta = 0.5$), the charge neutrality line crosses the trivial solution

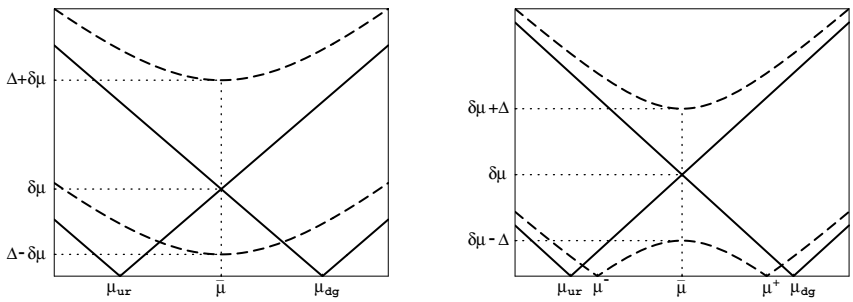

Figure 3. The quasi-particle dispersion relations at low energies in the 2SC phase (left panel) and in the g2SC phase (right panel).

of the diquark gap, i.e., the ground state is a charge neutral normal quark matter with $\Delta = 0$. The regime of intermediate coupling (see, e.g., $\eta = 0.75$ case) is most interesting, the charge neutrality line crosses the lower branch of the solution of the diquark gap. We will see that this phase is a gapless 2SC (g2SC) phase with $\Delta < \delta\mu$, which is different from the regular 2SC phase, and has some unusual properties.

2.3 g2SC phase

In this subsection, we will explain why we call the color superconducting phase with $\Delta < \delta\mu$ the g2SC phase, and we will show some special properties of this phase.

Quasi-particle spectrum

It is instructive to start with the excitation spectrum in the case of the ordinary 2SC phase when $\delta\mu = 0$. With the conventional choice of the gap pointing in the anti-blue direction in color space, the blue quarks are not affected by the pairing dynamics, and the other four quasi-particle excitations are linear superpositions of $u_{r,g}$ and $d_{r,g}$ quarks and holes. The quasi-particle is nearly identical with a quark at large momenta and with a hole at small momenta. We represent the quasi-particle in the form of $Q(quark, hole)$, then the four quasi-particles can be represented explicitly as $Q(u_r, d_g)$, $Q(u_g, d_r)$, $Q(d_r, u_g)$ and $Q(d_g, u_r)$. When $\delta\mu = 0$, the four quasi-particles are degenerate, and have a common gap Δ.

If there is a small mismatch ($\delta\mu < \Delta$) between the Fermi surfaces of the pairing u and d quarks, the excitation spectrum will change. For example, we show the excitation spectrum of $Q(u_r, d_g)$ and $Q(d_g, u_r)$ in the left panel of Figure 3. We can see that $\delta\mu$ induces two different dispersion relations, the quasi-particle $Q(d_g, u_r)$ has a smaller gap $\Delta - \mu$, and the quasi-particle $Q(u_r, d_g)$ has a larger gap $\Delta + \mu$. This is similar to the case when the mismatch is induced by the mass difference of the pairing quarks [16].

If the mismatch $\delta\mu$ is larger than the gap parameter Δ, the lower dispersion relation for the quasi-particle $Q(d_g, u_r)$ will cross the zero-energy axis, as shown in the right panel of Figure 3. The energy of the quasi-particle $Q(d_g, u_r)$ vanishes at two values of momenta $p = \mu^-$ and $p = \mu^+$ where $\mu^\pm \equiv \bar{\mu} \pm \sqrt{(\delta\mu)^2 - \Delta^2}$. This is why we call this phase gapless 2SC (g2SC) phase. An unstable gapless CFL phase has been found in Ref. [16], and a similar stable gapless color superconductivity could also appear in a cold atomic gas or in u, s or d, s quark matter when the number densities are kept fixed [17].

As one would expect, far outside the pairing region, $p \simeq \bar{\mu}$, the quasi-particle dispersion relations are similar to those in the 2SC phase. Also, around $p \simeq \bar{\mu}$, the quasi-particle $Q(u_r, d_g)$ resembles the dispersion relations with that in the regular 2SC phase. The most remarkable property of the quasi-particle spectra in the g2SC phase is that the low energy excitations ($E \ll \delta\mu - \Delta$) are very similar to those in the normal phase represented by solid lines. The only difference is that the values of the chemical potentials of the up and down quarks $\mu_{ur} = \mu_{ug}$ and $\mu_{dg} = \mu_{dr}$ are replaced by the values μ^- and μ^+, respectively. This observation suggests, in particular, that the low energy (large distance scale) properties of the g2SC phase should look similar to those in the normal phase.

Finite temperature properties

In a superconducting system, when one increases the temperature at a given chemical potential, thermal motion will eventually break up the quark Cooper pairs. In the weakly interacting Bardeen-Copper-Schrieffer (BCS) theory, the transition between the superconducting and normal phases is usually of second order. The ratio of the critical temperature $T_c^{\rm BCS}$ to the zero temperature value of the gap $\Delta_0^{\rm BCS}$ is a universal value [18]

$$r_{\rm BCS} = \frac{T_c^{\rm BCS}}{\Delta_0^{\rm BCS}} = \frac{{\rm e}^{\gamma_E}}{\pi} \approx 0.567, \tag{7}$$

where $\gamma_E \approx 0.577$ is the Euler constant. In the conventional 2SC phase of quark matter with equal densities of the up and down quarks, the ratio of the critical temperature to the zero temperature value of the gap is also the same as in the BCS theory [19]. In the spin-0 color flavor locked phase as well as in

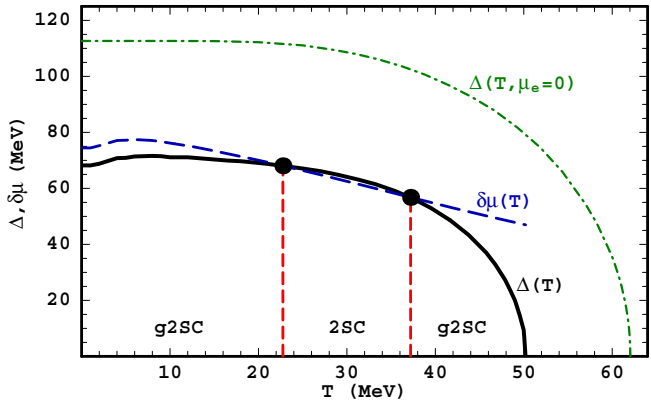

Figure 4. The temperature dependence of the diquark gap (solid line) and the value of $\delta\mu \equiv \mu_e/2$ (dashed line) in neutral quark matter. For comparison, the diquark gap in the model with $\mu_e = 0$ and $\mu_8 = 0$ is also shown (dash-dotted line). The results are plotted for $\mu = 400$ MeV and $\eta = 0.75$.

the spin-1 color spin locked phase, on the other hand, this ratio is larger than the BCS ratio by the factors $2^{1/3}$ and $2^{2/3}$, respectively. These deviations are related directly to the presence of two different types of quasi-particles with nonequal gaps [20].

For the g2SC phase, the typical results for the default choice of parameters $\mu = 400$ MeV and $\eta = 0.75$ are shown in Figure 4. Both the values of the diquark gap (solid line) and the mismatch parameter $\delta\mu = \mu_e/2$ (dashed line) are plotted. One very unusual property of the shown temperature dependence of the gap is a nonmonotonic behavior. Only at sufficiently high temperatures, the gap is a decreasing function. In the low temperature region, $T \leq 10$ MeV, however, it increases with temperature. For comparison, in the same figure, the diquark gap in the model with $\mu_e = 0$ and $\mu_8 = 0$ is also shown (dash-dotted line). This latter has the standard BCS shape.

Another interesting thing regarding the temperature dependences in Figure 4 appears in the intermediate temperature region, $22.5 \leq T \leq 37$ MeV. By comparing the values of $\Delta(T)$ and $\delta\mu$ in this region, we see that the g2SC phase is replaced by a "transitional" 2SC phase there. Indeed, the energy spectrum of the quasi-particles even at finite temperature is determined by the same relations in Eqs. (3) and (5) that we used at zero temperature. When $\Delta > \delta\mu$, the modes determined by Eq. (5) are gapped. Then, according to our standard classification, the ground state is the 2SC phase.

It is fair to say, of course, that the qualitative difference of the g2SC and 2SC phases is not so striking at finite temperature as it is at zero temperature. This difference is particularly negligible in the region of interest where temperatures $22.5 \leq T \leq 37$ MeV are considerably larger than the actual value of the

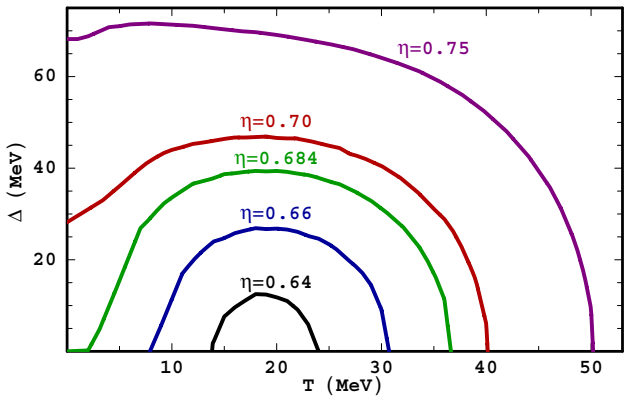

Figure 5. The temperature dependence of the diquark gap in neutral quark matter calculated for several values of the diquark coupling strength $\eta = G_D/G_S$.

smaller gap, $\Delta - \delta\mu$. However, by increasing the value of the coupling constant slightly, the transitional 2SC phase can be made much stronger and the window of intermediate temperatures can become considerably wider. In either case, we find it rather unusual that the g2SC phase of neutral quark matter is replaced by a transitional 2SC phase at intermediate temperatures which, is replaced by the g2SC phase again at higher temperatures.

It appears that the temperature dependence of the diquark gap is very sensitive to the choice of the diquark coupling strength $\eta = G_D/G_S$ in the model at hand. This is not surprising because the solution to the gap equation is very sensitive to this choice. The resulting interplay of the solution for Δ with the condition of charge neutrality, however, is very interesting. This is demonstrated by the plot of the temperature dependence of the diquark gap calculated for several values of the diquark coupling constant in Figure 5.

The most amazing are the results for weak coupling. It appears that the gap function could have sizable values at finite temperature even if it is exactly zero at zero temperature. This possibility comes about only because of the strong influence of the neutrality condition on the ground state preference in quark matter. Because of the thermal effects, the positive electrical charge of the diquark condensate is easier to accommodate at finite temperature. We should mention that somewhat similar results for the temperature dependence of the gap were also obtained in Ref. [21] in a study of the asymmetric nuclear matter, and in Ref. [22] when number density was fixed.

The numerical results for the ratio of the critical temperature to the zero temperature gap in the g2SC case as a function of the diquark coupling strength $\eta = G_D/G_S$ are plotted in Figure 6. The dependence is shown for the most interesting range of values of $\eta = G_D/G_S$, $0.68 \leq \eta \leq 0.81$, which allows the g2SC stable ground state at zero temperature. When the coupling gets weaker

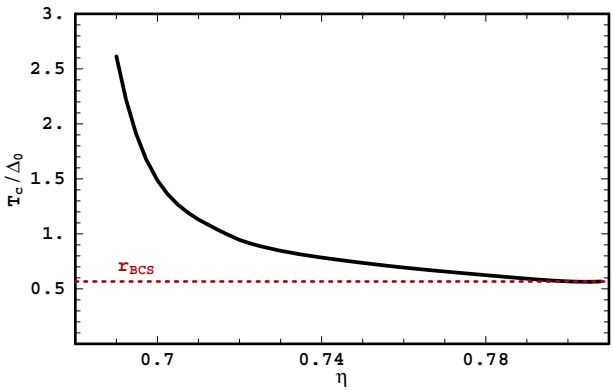

Figure 6. The ratio of the critical temperature to the zero temperature gap in neutral quark matter as a function of the coupling strength $\eta = G_D/G_S$.

in this range, the zero temperature gap vanishes gradually. As we saw from Figure 5, however, this does not mean that the critical temperature vanishes too. Therefore, the ratio of a finite value of T_c to the vanishing value of the gap can become arbitrarily large. In fact, it remains strictly infinite for a range of couplings.

3. Global charge neutrality: mixed phase

We have discussed the homogeneous 2-flavor quark matter when charge neutrality conditions are satisfied locally, and found that the local charge neutrality conditions impose very strong constraints on determining the ground state of the system.

On the other hand, one can construct mixed phase when charge neutrality conditions are satisfied globally. Inside mixed phases, the charge neutrality is satisfied "on average" rather than locally. This means that different components of mixed phases may have non-zero densities of conserved charges, but the total charge of all components still vanishes. In this case, one says that the local charge neutrality condition is replaced by a global one. There are three possible components: (i) normal phase, (ii) 2SC phase, and (iii) g2SC phase.

The pressure of the main three phases of two-flavor quark matter as a function of the baryon and electrical chemical potentials is shown in Figure 7 at $\eta = 0.75$. In this figure, we also show the pressure of the neutral normal quark and gapless 2SC phases (two dark solid lines). The surface of the g2SC phase extends only over a finite range of the values of μ_e. It merges with the pressure surfaces of the normal quark phase (on the left) and with the ordinary 2SC phase (on the right).

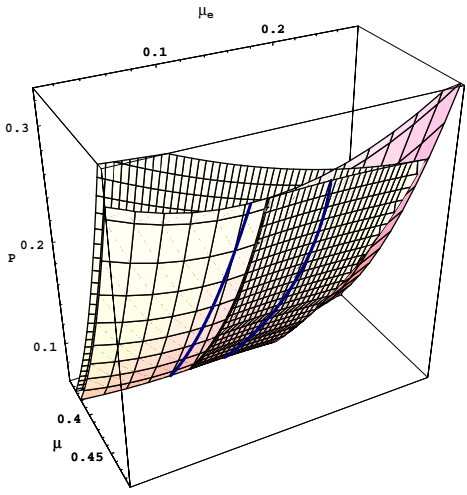

Figure 7. At $\eta = 0.75$, pressure as a function of $\mu \equiv \mu_B/3$ and μ_e for the normal and color superconducting quark phases. The dark solid lines represent two locally neutral phases: (i) the neutral normal quark phase on the left, and (ii) the neutral gapless 2SC phase on the right. The appearance of the swallowtail structure is related to the first order type of the phase transition in quark matter.

It is interesting to notice that the three pressure surfaces in Figure 7 form a characteristic swallowtail structure. As one could see, the appearance of this structure is directly related to the fact that the phase transition between color superconducting and normal quark matter, which is driven by changing parameter μ_e, is of first order. In fact, one should expect the appearance of a similar swallowtail structure also in a self-consistent description of the hadron-quark phase transition. Such a description, however, is not available yet.

From Figure 7, one could see that the surfaces of normal and 2SC quark phases intersect along a common line. This means that the two phases have the same pressure along this line, and therefore could potentially co-exist. Moreover, as is easy to check, normal quark matter is negatively charged, while 2SC quark matter is positively charged on this line. This observation suggests that the appearance of the corresponding mixed phase is almost inevitable.

Let us start by giving a brief introduction into the general method of constructing mixed phases by imposing the Gibbs conditions of equilibrium [23, 18]. From the physical point of view, the Gibbs conditions enforce the mechanical as well as chemical equilibrium between different components of a mixed phase. This is achieved by requiring that the pressure of different components inside the mixed phase are equal, and that the chemical potentials (μ and μ_e) are the same across the whole mixed phase. For example, in relation

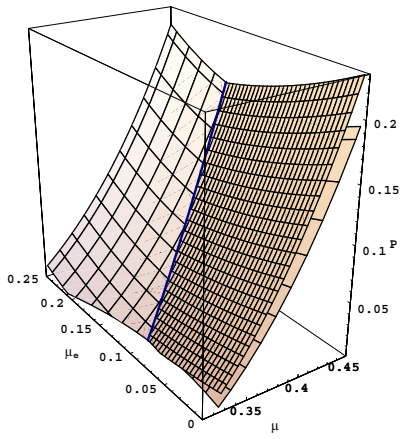

Figure 8. At $\eta = 0.75$, pressure as a function of $\mu \equiv \mu_B/3$ and μ_e for the normal and color superconducting quark phases (the same as in Figure 7, but from a different viewpoint). The dark solid line represents the mixed phase of negatively charged normal quark matter and positively charged 2SC matter.

to the mixed phase of normal and 2SC quark matter, these conditions read

$$P^{(NQ)}(\mu, \mu_e) = P^{(2SC)}(\mu, \mu_e), \tag{8}$$

$$\mu = \mu^{(NQ)} = \mu^{(2SC)}, \tag{9}$$

$$\mu_e = \mu_e^{(NQ)} = \mu_e^{(2SC)}. \tag{10}$$

It is easy to visualize these conditions by plotting the pressure as a function of chemical potentials (μ and μ_e) for both components of the mixed phase. This is shown in Figure 8. As should be clear, the above Gibbs conditions are automatically satisfied along the intersection line of two pressure surfaces (dark solid line in Figure 8).

Different components of the mixed phase occupy different volumes of space. To describe this quantitatively, we introduce the volume fraction of normal quark matter as follows: $\chi_{2SC}^{NQ} \equiv V_{NQ}/V$ (notation χ_B^A means volume fraction of phase A in a mixture with phase B). Then, the volume fraction of the 2SC phase is given by $\chi_{NQ}^{2SC} = (1 - \chi_{2SC}^{NQ})$. From the definition, it is clear that $0 \leq \chi_{2SC}^{NQ} \leq 1$.

The average electrical charge density of the mixed phase is determined by the charge densities of its components taken in the proportion of the corresponding volume fractions. Thus,

$$n_e^{(MP)} = \chi_{2SC}^{NQ} n_e^{(NQ)}(\mu, \mu_e) + (1 - \chi_{2SC}^{NQ}) n_e^{(2SC)}(\mu, \mu_e). \tag{11}$$

If the charge densities of the two components have opposite signs, one can impose the global charge neutrality condition, $n_e^{(MP)} = 0$. Otherwise, a neutral mixed phase could not exist. In the case of quark matter, the charge density of the normal quark phase is negative, while the charge density of the 2SC phase is positive along the line of the Gibbs construction (dark solid line in Figure 8). Therefore, a neutral mixed phase exists. The volume fractions of its components are

$$\chi_{2SC}^{NQ} = \frac{n_e^{(2SC)}}{n_e^{(2SC)} - n_e^{(NQ)}}, \tag{12}$$

$$\chi_{NQ}^{2SC} \equiv 1 - \chi_{2SC}^{NQ} = \frac{n_e^{(NQ)}}{n_e^{(NQ)} - n_e^{(2SC)}}. \tag{13}$$

After the volume fractions have been determined from the condition of the global charge neutrality, we could also calculate the energy density of the corresponding mixed phase,

$$\varepsilon^{(MP)} = \chi_{2SC}^{NQ}\varepsilon^{(NQ)}(\mu, \mu_e) + (1 - \chi_{2SC}^{NQ})\varepsilon^{(2SC)}(\mu, \mu_e). \tag{14}$$

This is essentially all that we need in order to construct the equation of state of the mixed phase.

So far, we were neglecting the effects of the Coulomb forces and the surface tension between different components of the mixed phase. In a real system, however, these are important. In particular, the balance between the Coulomb forces and the surface tension determines the size and geometry of different components inside the mixed phase.

In our case, nearly equal volume fractions of the two quark phases are likely to form alternating layers (slabs) of matter. The energy cost per unit volume to produce such layers scales as $\sigma^{2/3}(n_e^{(2SC)} - n_e^{(NQ)})^{2/3}$ where σ is the surface tension [25]. Therefore, the quark mixed phase is a favorable phase of matter only if the surface tension is not too large. Our simple estimates show that $\sigma_{max} \leq 20$ MeV/fm^2. However, even for slightly larger values, $20 \leq \sigma \leq 50$ MeV/fm^2, the mixed phase is still possible, but its first appearance would occur at larger densities, $3\rho_0 \leq \rho_B \leq 5\rho_0$. The value of the maximum surface tension obtained here is comparable to the estimate in the case of the hadronic-CFL mixed phase obtained in Ref. [26]. The thickness of the layers scales as $\sigma^{1/3}(n_e^{(2SC)} - n_e^{(NQ)})^{-2/3}$ [25], and its typical value is of order 10 fm in the quark mixed phase. This is similar to the estimates in various hadron-quark and hadron-hadron mixed phases [25, 26]. While the actual value of the surface tension in quark matter is not known, in this study we assume that it is

not very large. Otherwise, the homogeneous gapless 2SC phase should be the most favorable phase of nonstrange quark matter [9].

Under the assumptions that the effect of Coulomb forces and the surface tension is small, the mixed phase of normal and 2SC quark matter is the most favorable neutral phase of matter in the model at hand with $\eta = 0.75$. This should be clear from observing the pressure surfaces in Figs. 7 and 8. For a given value of the baryon chemical potential $\mu = \mu_B/3$, the mixed phase is more favorable than the gapless 2SC phase, while the gapless 2SC phase is more favorable than the neutral normal quark phase.

4. Conclusion

Dense u, d quark matter under local and global charge neutrality conditions in β-equilibrium has been discussed.

Under local charge neutrality condition, the homogeneous neutral ground state is sensitive to the coupling constant in the diquark channel, it will be in the regular 2SC phase when the coupling is strong, in the normal phase when the coupling is weak, and in the g2SC phase in the case of intermediate coupling. The low energy quasi-particle spectrum in g2SC phase contains four gapless and only two gapped modes, and this phase has rather unusual properties at zero as well as at finite temperature.

Under global charge neutrality condition, assuming that the effect of Coulomb forces and the surface tension is small, one can construct a mixed phase composed of positive charged 2SC phase and negative charged normal quark matter.

Acknowledgments

M. H would like to thank the organizers of the workshop for invitation and offering a financial support. The work of M. H. was supported by the Alexander von Humboldt-Foundation, and the NSFC under Grant Nos. 10105005, 10135030. The work of I.A.S. was supported by Gesellschaft für Schwerionenforschung (GSI) and by Bundesministerium für Bildung und Forschung (BMBF).

References

[1] B. C. Barrois, Nucl. Phys. **B129**, 390 (1977); S. C. Frautschi, in "Hadronic matter at extreme energy density", edited by N. Cabibbo and L. Sertorio (Plenum Press, 1980); D. Bailin and A. Love, Phys. Rep. **107**, 325 (1984). M. Alford, K. Rajagopal, and

F. Wilczek, Phys. Lett. B **422**, 247 (1998); R. Rapp, T. Schäfer, E. V. Shuryak and M. Velkovsky, Phys. Rev. Lett. **81**, 53 (1998).

[2] K. Rajagopal and F. Wilczek, hep-ph/001133; M. G. Alford, Ann. Rev. Nucl. Part. Sci. bf 51, 131(2001); T. Schafer, hep-ph/0304281; D. H. Rischke, Prog.Part.Nucl.Phys.52:197-296 (2003).

[3] D. T. Son, Phys. Rev. D **59**, 094019 (1999); T. Schäfer and F. Wilczek, Phys. Rev. D **60**, 114033 (1999); D. K. Hong, V. A. Miransky, I. A. Shovkovy, and L. C. R. Wijewardhana, Phys. Rev. D **61**, 056001 (2000); S. D. H. Hsu and M. Schwetz, Nucl. Phys. **B572**, 211 (2000); W. E. Brown, J. T. Liu, and H.-C. Ren, Phys. Rev. D **61**, 114012 (2000).

[4] M. G. Alford, K. Rajagopal and F. Wilczek, Nucl. Phys. **B537**, 443 (1999).

[5] G. Lugones and J. E. Horvath, Phys. Rev. D **66**, 074017 (2002); G. Lugones and J. E. Horvath, Astron. Astrophys. **403**, 173 (2003); M. Alford and S. Reddy, Phys. Rev. D **67**, 074024 (2003)

[6] M. Alford and K. Rajagopal, JHEP **0206**, 031 (2002); A. W. Steiner, S. Reddy and M. Prakash, Phys. Rev. D **66**, 094007 (2002).

[7] M. Huang, P. F. Zhuang and W. Q. Chao, Phys. Rev. D **67**, 065015 (2003).

[8] D. Blaschke, S. Fredriksson, H. Grigorian and A. M. Oztas, Nucl.Phys.A736:203-219 (2003); D. N. Aguilera, D. Blaschke and H. Grigorian, Astron.Astrophys.416:991-996 (2002).

[9] I. Shovkovy and M. Huang, Phys. Lett. B **564**, 205 (2003); M. Huang and I. Shovkovy, Nucl. Phys. **A 729** (2004) 835, hep-ph/0307273.

[10] A. Mishra and H. Mishra, Phys.Rev.D69:014014 (2003).

[11] S. B. Ruster and D. H. Rischke, Phys.Rev.D69:045011 (2003).

[12] F. Neumann, M. Buballa, and M. Oertel, Nucl. Phys. A **714**, 481 (2003).

[13] I. Shovkovy, M. Hanauske and M. Huang, Phys. Rev. D **67**, 103004 (2003).

[14] T. M. Schwarz, S. P. Klevansky and G. Papp, Phys. Rev. C **60**, 055205 (1999).

[15] P. F. Bedaque, Nucl. Phys. A **697**, 569 (2002); O. Kiriyama, S. Yasui and H. Toki, Int. J. Mod. Phys. E **10**, 501 (2001).

[16] M. G. Alford, J. Berges and K. Rajagopal, Phys. Rev. Lett. **84**, 598 (2000).

[17] W. V. Liu and F. Wilczek, Phys. Rev. Lett. **90**, 047002 (2003); E. Gubankova, W. V. Liu and F. Wilczek, Phys. Rev. Lett. **91**, 032001 (2003).

[18] J. R. Schrieffer, *Theory of Superconductivity* (Benjamin, New York, 1964).

[19] R.D. Pisarski and D.H. Rischke, Phys. Rev. D **61**, 051501 (2000).

[20] A. Schmitt, Q. Wang and D. H. Rischke, Phys. Rev. D **66**, 114010 (2002).

[21] A. Sedrakian and U. Lombardo, Phys. Rev. Lett. **84**, 602 (2000).

[22] J. F. Liao and P. F. Zhuang, Phys.Rev.D68:114016 (2003).

[23] N. K. Glendenning, Phys. Rev. D **46**, 1274 (1992).

[24] F. Weber, *Pulsars as Astrophysical Laboratories for Nuclear and Particle Physics* (Institute of Physics, Bristol, 1999).

[25] H. Heiselberg, C. J. Pethick and E. F. Staubo, Phys. Rev. Lett. **70**, 1355 (1993); N. K. Glendenning and S. Pei, Phys. Rev. C **52**, 2250 (1995); N. K. Glendenning and J. Schaffner-Bielich, Phys. Rev. Lett. **81**, 4564 (1998).

[26] M. G. Alford, K. Rajagopal, S. Reddy and F. Wilczek, Phys. Rev. D **64**, 074017 (2001).

POSSIBILITY OF COLOR MAGNETIC SUPERCONDUCTIVITY

Toshitaka Tatsumi
Department of Physics, Kyoto University, Kyoto 606-8502, Japan
tatsumi@ruby.scphys.kyoto-u.ac.jp

Tomoyuki Maruyama
College of Bioresouce Sciences, Nihon University, Fujisawa, 252-8510, Japan
tomo@brs.nihon-u.ac.jp

Eiji Nakano
Department of Physics, Tokyo Metropolitan University, 1-1 Minami-Ohsawa, Hachioji, Tokyo 192-0397, Japan
enakano@comp.metro-u.ac.jp

Abstract Two aspects of quark matter at high density are addressed: one is color superconductivity and the other is ferromagnetism. We are mainly concerned with the latter and its relation to color superconductivity, which we call *color magnetic superconductivity*. The relation of ferromagnetism and chiral symmetry restoration is also discussed.

1. Introduction

Nowadays it is widely accepted that there should be realized various phases of QCD in temperature (T) - density (ρ_B) plane. When we emphasize the low T and high ρ_B region, the subjects are sometimes called physics of high-density QCD. The main purposes in this field should be to figure out the properties of phase transitions and new phases, and to extract their symmetry breaking pattern and low-energy excitation modes there on the basis of QCD. On the other hand, these studies have phenomenological implications on relativistic heavy-ion collisions and compact stars like neutron stars or quark stars.

In this talk we'd like to address magnetic properties of quark matter at low temperature. We first discuss the ferromagnetic phase transition and then a pos-

D. Blaschke and D. Sedrakian (eds.), Superdense QCD Matter and Compact Stars, 241–261.

sibility of the coexistence of ferromagnetism (FM) and color superconductivity (CSC). We also present an idea about how FM is related to chiral symmetry.

CSC should be very popular and many people believe that it is robust due to the Cooper instability even for small attractive quark-quark interaction in color $\bar{3}$ channel [1]. On the contrary, we are afraid that FM has not been so familiar yet. So, we'd like to begin with a brief introduction about our motivation for the study of FM.

Phenomenologically the concept of magnetism should be directly related to the origin of strong magnetic field observed in compact stars [2]; e.g., it amounts to $O(10^{12}\mathrm{G})$ at the surface of radio pulsars. Recently a new class of pulsars called magnetars has been discovered with super strong magnetic field, $B_s \sim 10^{14-15}\mathrm{G}$, estimated from the $P - \dot{P}$ curve [3, 4]. First observations are indirect evidences for super strong magnetic field, but discoveries of some absorption lines stemming from the cyclotron frequency of protons have been currently reported [5].

The origin of the strong magnetic field has been a long standing problem since the first pulsar was discovered [2]. A naive working hypothesis is the conservation of the magnetic flux and its squeezing during the evolution from a main-sequence progenitor star to a compact star, $B_s \propto R^{-2}$ with R being the radius [6].

Table 1. Surface magnetic field and the radius of stars by the conservation of the magnetic flux.

	$B_S[\mathrm{G}]$	$R[\mathrm{cm}]$
Sun (obs.)	10^3	10^{10}
Neutron star	10^{11}	10^6
Magnetar	10^{15}	10^4

The relation of the radius and the expected strength of the magnetic field is listed by the use of the hypothesis in Table. 1. Then, it looks to work well for explaining the strength of the magnetic field observed for radio pulsars. However, it does not work for magnetars; considering the Schwarzschild radius,

$$R_{\mathrm{Sch}} = 2GM/c^2 = 4 \times 10^5[\mathrm{cm}] \gg 10^4[\mathrm{cm}], \tag{1}$$

for the canonical mass of $M = 1.4M_\odot$, we are immediately led to a contradiction.

Since there should be developed hadronic matter inside compact stars, it would be reasonable to consider a microscopic origin of such strong magnetic field: ferromagnetism or spin polarization is one of the candidates to explain it. To grasp a rough idea about how hadronic matter can give such a super strong magnetic field rather easily, it should be interesting to compare typical

energy scales in some systems (see Table 2): the magnetic interaction energy is estimated as $E_{\rm mag} = \mu_i B$ with the magnetic moment, $\mu_i = e_i/(2m_i)$. Thus

Table 2. Magnetic interaction energies $E_{\rm mag}$ for 10^{15}G and the typical energy scales $E_{\rm typ}$ in electron, nucleon and quark systems.

	electron	proton	quark
m_i[MeV]	0.5	10^3	1- 100
$E_{\rm mag}$[MeV]	5 - 6	2.5×10^{-3}	$2.5 \times 10^{-2} - 2.5$
$E_{\rm typ}$	KeV	MeV	MeV

we can see $E_{\rm typ} \ll E_{\rm mag}$ for electrons, while $E_{\rm typ} > E_{\rm mag}$ for nucleons or quarks. This simple consideration may imply that strong interaction gives a feasible origin for the strong magnetic field. The possibility of ferromagnetism in nuclear matter has been elaborately studied when the pulsars were observed, but negative results have been reported so far [7]. Here we consider its possibility in quark matter from a different point of view [8].

2. What is ferromagnetism in quark matter?

Quark matter bears some resemblance to electron gas interacting with the Coulomb potential; the gluon exchange interaction in QCD is similar to the electromagnetic interaction in QED and color neutrality of quark matter corresponds to charge neutrality of electron gas under the background of positively charged ions. It was Bloch who first suggested a mechanism leading to ferromagnetism of itinerant electrons [9, 10]. The mechanism is very simple but largely reflects the Fermion nature of electrons. Since there works no direct interaction between electrons as a whole, the Fock exchange interaction gives a leading contribution; it can be represented as

$$V_{\rm Fock} = -e^2 \frac{1 + \boldsymbol{\zeta} \cdot \boldsymbol{\zeta}'}{|\mathbf{k} - \mathbf{q}|^2}, \tag{2}$$

between two electrons with momenta, $\mathbf{k}$ and $\mathbf{q}$, and spin polarizations, $\boldsymbol{\zeta}$ and $\boldsymbol{\zeta}'$, where the vector $\boldsymbol{\zeta}$ specifies the definite spin polarized state, e.g. $\boldsymbol{\zeta} = (0, 0, \pm 1)$ for spin up and down state. Then it is immediately conceivable that a most attractive channel is the parallel spin pair, whereas electrons with opposite polarizations gives null contribution. This is nothing but a consequence of the Pauli exclusion principle: electrons with the same spin polarization cannot closely approach to each other, which effectively avoid the Coulomb repulsion. On the other hand a polarized state should give a larger kinetic energy by rearranging the two Fermi spheres. Thus there is a trade-off between kinetic and interaction energies, which leads to a *spontaneous spin polarization (SSP)* or

FM at some density [1] . One of the essential points we learned here is that we need no spin-dependent interaction at the original Lagrangian to see SSP. We can see a similar phenomenon in dealing with nuclear matter within the relativistic mean-field theory, where the Fock interaction can be extracted by way of the Fierz transformation from the original Lagrangian [11].

Then it might be natural to ask how about in QCD. We list here some features of QCD related to this subject. (1) the quark-gluon interaction in QCD is rather simple, compared with the nuclear force; it is a gauge interaction like in QED. (2) quark matter should be a color neutral system and only the $exchange$ interaction is relevant like in the electron system. (3) there is an additional flavor degree of freedom in quark matter; gluon exchange never change flavor but it comes in through the generalized Pauli principle. (4) quarks should be treated relativistically, different from the electron system.

The last feature requires a new definition and formulation of SSP or FM in relativistic systems since"spin" is no more a good quantum number in relativistic theories; spin couples with momentum and its direction changes during the motion. It is well known that the Pauli-Lubanski vector W^μ is the four vector to represent the spin degree of freedom in a covariant form,

$$W^\mu = -\frac{1}{4}\epsilon_{\mu\nu\rho\sigma}k^\nu\sigma^{\rho\sigma}. \tag{3}$$

In the rest frame,

$$W^0 = 0, \qquad \frac{\mathbf{W}}{m} = \frac{1}{2}\gamma^5\gamma^0\boldsymbol{\gamma} = \frac{1}{2}\boldsymbol{\Sigma}, \tag{4}$$

where $\boldsymbol{\Sigma} = \begin{pmatrix} \boldsymbol{\sigma} & 0 \\ 0 & \boldsymbol{\sigma} \end{pmatrix}$ in the usual basis. For any space-like four vector a orthogonal to k, $a^\mu k_\mu = 0$, we then have a property,

$$W \cdot a = -\frac{1}{2}\gamma_5 \not{a} \not{k}. \tag{5}$$

By taking a 4-pseudovector a^μ s.t.

$$\mathbf{a} = \boldsymbol{\zeta} + \frac{\mathbf{k}(\boldsymbol{\zeta}\cdot\mathbf{k})}{m(E_k+m)},\ a^0 = \frac{\mathbf{k}\cdot\boldsymbol{\zeta}}{m} \tag{6}$$

with the axial vector $\boldsymbol{\zeta}$, we can see the operator

$$P(a) = \frac{1}{2}(1+\gamma_5\not{a}) \tag{7}$$

[1] FM does not necessarily accompany SSP in some cases with internal degrees of freedom, as is seen in section 4.

is the projection operator for the definite spin-polarized states; actually a^μ is reduced to a three vector $(0, \boldsymbol{\zeta})$ in the rest frame and we can allocate $\boldsymbol{\zeta} = (0, 0, \pm 1)$ to spin "up" and "down" states. Thus we can still use $\boldsymbol{\zeta}$ to specify the two intrinsic polarized states even in the general Lorentz frame.

We briefly present a heuristic argument how quark matter becomes ferromagnetic by the use of above definition [8]. The Fock exchange interaction, $f_{\mathbf{k}\zeta,\mathbf{q}\zeta'}$, between two quarks is defined by

$$f_{\mathbf{k}\zeta,\mathbf{q}\zeta'} = \frac{m}{E_k}\frac{m}{E_q}\mathcal{M}_{\mathbf{k}\zeta,\mathbf{q}\zeta'}. \tag{8}$$

$\mathcal{M}_{\mathbf{k}\zeta,\mathbf{q}\zeta'}$ is the usual Lorentz invariant matrix element and can be written in the lowest order as

$$\mathcal{M}_{\mathbf{k}\zeta,\mathbf{q}\zeta'} = g^2\frac{2}{9m^2}[2m^2 - k\cdot q - m^2 a\cdot b]\frac{1}{(k-q)^2}, \tag{9}$$

where the spin dependent term renders

$$\begin{aligned} a\cdot b &= -\frac{1}{m_q^2}\left[-(\mathbf{k}\cdot\boldsymbol{\zeta})(\mathbf{q}\cdot\boldsymbol{\zeta}') + m^2\boldsymbol{\zeta}\cdot\boldsymbol{\zeta}'\right. \\ &+ \left\{m(E_k+m)(\boldsymbol{\zeta}\cdot\mathbf{q})(\boldsymbol{\zeta}'\cdot\mathbf{q}) + m(E_q+m)(\boldsymbol{\zeta}'\cdot\mathbf{k})(\boldsymbol{\zeta}\cdot\mathbf{k})\right. \\ &+ \left.\left.(\mathbf{k}\cdot\mathbf{q})(\boldsymbol{\zeta}\cdot\mathbf{k})(\boldsymbol{\zeta}'\cdot\mathbf{q})\right\}/(E_k+m)(E_q+m)\right]. \end{aligned} \tag{10}$$

It exhibits a complicated spin-dependent structure arising from the Dirac four spinor, while it is reduced to a simple form,

$$-\frac{2}{9}g^2\frac{1+\boldsymbol{\zeta}\cdot\boldsymbol{\zeta}'}{(\mathbf{k}-\mathbf{q})^2} \tag{11}$$

in the non-relativistic limit as in the electron system. Eq. (11) clearly shows why parallel spin pairs are favored, while we cannot see it clearly in the relativistic expression (10). We have explicitly demonstrated that the ferromagnetic phase should be realized at relatively low density region [8].

Relativistic ferromagnetism

If we understand FM or magnetic properties of quark matter more deeply, we must proceeds to a self-consistent approach, like Hartree-Fock theory, beyond the previous perturbative argument. In ref. [11] we have described how the axial-vector mean field (AV) and the tensor one appear as a consequence of the Fierz transformation within the relativistic mean-field theory for nuclear matter, which is one of the nonperturbative frameworks in many-body theories and corresponds to the Hatree-Fock approximation. We also demonstrated

they are responsible to ferromagnetism of nuclear matter. An important point obtained there is the "condensation" of AV. [2]

When we consider the non-vanishing AV in quark matter,

$$\mathbf{V} = -\gamma_5\gamma_3\mathbf{U}_A,\ \mathbf{U}_A//\hat{z}, \tag{12}$$

we see an interaction between quarks and AV,

$$H_{int} \propto \boldsymbol{\sigma}\cdot\mathbf{U}_A = \sigma_3 U_A, \quad U_A \geq 0, \tag{13}$$

in a similar form to the magnetic interaction in QED. Then the quark propagator in AV renders

$$G_A^{-1}(p) = \not{p} - m - \not{\mathcal{U}} + \gamma_5 \not{U}_A. \tag{14}$$

The poles of $G_A(p)$, $\det G_A^{-1}(p_0{=}\epsilon_n){=}0$, give the single-particle energy spectrum:

$$\epsilon_n = \pm\epsilon_\pm \tag{15}$$

$$\epsilon_\pm = \sqrt{\mathbf{p}^2 + \mathbf{U}_A^2 + m^2 \pm 2\sqrt{m^2\mathbf{U}_A^2 + (\mathbf{p}\cdot\mathbf{U}_A)^2}}, \tag{16}$$

where the subscript $\pm$ in the energy spectrum represents spin degrees of freedom, and the dissolution of the degeneracy corresponds to the *exchange splitting* of different "spin" states [10]. Actually it is reduced to a familiar form, $\epsilon_\pm = m + \frac{p^2}{2m} \pm U_A$, in the non-relativistic limit, while

$$\epsilon_\pm = \sqrt{p_t^2 + (|p_z| \pm U_A)^2} \tag{17}$$

in the extremely relativistic limit, $m \to 0$. Note that U_A only shifts the value of momentum in Eq. (17), so that it should be *redundant* in the massless case.

There are two Fermi seas for a given quark number with different volumes due to the exchange splitting in the energy spectrum. The appearance of the rotation symmetry breaking term, $\propto \mathbf{p}\cdot\mathbf{U}_A$ in the energy spectrum (16) implies deformation of the Fermi sea: so rotation symmetry is violated in the momentum space as well as the coordinate space, $O(3) \to O(2)$. Accordingly the Fermi sea of majority quarks exhibits a prolate shape (F^-), while that of minority quarks an oblate shape (F^+) as seen Fig. 1 [3] .

[2] There appears no tensor mean field in QCD as a result of chiral symmetry. So we, hereafter, only consider AV.

[3] On the contrary, the Fermi sea remains spherical in the non-relativistic case [10]. It would be also interesting to compare our results with those given in the different context [12].

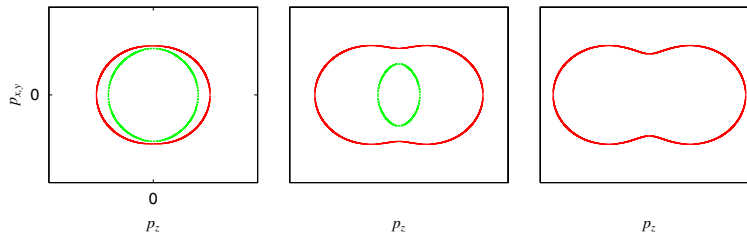

Figure 1. Modification of the Fermi sea as U_A is increased from left to right. The larger Fermi sea (F^-) takes a prolate shape, while the smaller one (F^+) an oblate shape for a given U_A. In the large U_A limit (completely polarized case), F^+ disappears as in the right panel.

The mean spin polarization is then given by

$$\bar{s}_z = \frac{1}{2}\langle\Sigma_z\rangle = -i\int_C \frac{d^4p}{(2\pi)^4}\mathrm{tr}[\gamma_5\gamma_3 G_A(p)] \tag{18}$$

$$= \frac{1}{2}\left[\int_{F^+}\frac{d^3p}{(2\pi)^3}\frac{U_A+\beta}{\epsilon_+} + \int_{F^-}\frac{d^3p}{(2\pi)^3}\frac{U_A-\beta}{\epsilon_-}\right] \tag{19}$$

with $\beta = \sqrt{p_z^2+m^2}$, from which we can immediately see the non-vanishing value of U_A gives rise to spin polarization. Since the spin polarization is not necessarily measurable quantity, we'd better to see another observable, the *magnetization*, which is defined as the magnetic moment per unit volume and the magnetic field directly couples with it. In QED the magnetic field couples with quarks by way of the term, $\mu_q\bar{q}\sigma_{\mu\nu}qF^{\mu\nu}$, with the Dirac magnetic moment $\mu_q = e/(2m)$, and we can easily see that the magnetization $\mathbf{M}$ is directed to the z direction;

$$M_3 = -i\int_C \frac{d^4p}{(2\pi)^4}\mathrm{tr}[\gamma_0\gamma_5\gamma_3 G_A(p)] \tag{20}$$

$$= \frac{1}{2}\left[-\int_{F^+}\frac{d^3p}{(2\pi)^3}\frac{m}{\beta} + \int_{F^-}\frac{d^3p}{(2\pi)^3}\frac{m}{\beta}\right] \tag{21}$$

with $\beta = \sqrt{p_z^2+m^2}$ in the units of the Dirac magnetic moment. Note that the magnetization of each Fermi sea has now the opposite direction and it does not explicitly depend on U_A, but the net magnetization arises by way of the exchange splitting of the Fermi sea. Thus we see the ground state holds ferromagnetism in the presence of U_A.

3. Color magnetic superconductivity

If FM is realized in quark matter, it might be in the CSC phase. In this section we discuss a possibility of the coexistence of FM and CSC, which we call *Color magnetic superconductivity* [13].

In passing, it would be worth mentioning the corresponding situation in condensed matter physics. Magnetism and superconductivity (SC) have been two major concepts in condensed matter physics and their interplay has been repeatedly discussed [14]. Very recently some materials have been observed to exhibit the coexistence phase of FM and SC, which properties have not been fully understood yet; itinerant electrons are responsible to both phenomena in these materials and one of the important features is both phases cease at the same critical pressure [15]. In our case we shall see somewhat different features, but the similar aspects as well.

We begin with an OGE-type action:

$$I_{int} = -g^2 \frac{1}{2} \int \mathrm{d}^4x \int \mathrm{d}^4y \left[\bar{\psi}(x) \gamma^\mu \frac{\lambda_a}{2} \psi(x) \right] D_{\mu\nu}(x,y) \left[\bar{\psi}(y) \gamma^\nu \frac{\lambda_a}{2} \psi(y) \right], \quad (22)$$

where $D^{\mu\nu}$ denotes the gluon propagator. By way of the mean-field approximation, we have

$$I_{MF} = \frac{1}{2} \int \frac{\mathrm{d}^4p}{(2\pi)^4} \begin{pmatrix} \bar{\psi}(p) \\ \bar{\psi}_c(p) \end{pmatrix}^T G^{-1}(p) \begin{pmatrix} \psi(p) \\ \psi_c(p) \end{pmatrix} \quad (23)$$

in the Nambu-Gorkov formalism. The inverse quark Green function $G^{-1}(p)$ involves various self-energy (mean-field) terms, of which we only keep the color singlet particle-hole $V(p)$ and color $\bar{3}$ particle-particle (Δ) mean-fields; the former is responsible to ferromagnetism, while the latter to superconductivity,

$$\begin{aligned} G^{-1}(p) &= \begin{pmatrix} \not{p} - m + \not{\mu} + V(p) & \gamma_0 \Delta^\dagger(p) \gamma_0 \\ \Delta(p) & \not{p} - m - \not{\mu} + \overline{V}(p) \end{pmatrix}, \\ &= \begin{pmatrix} G_{11}(p) & G_{12}(p) \\ G_{21}(p) & G_{22}(p) \end{pmatrix}^{-1} \end{aligned} \quad (24)$$

where

$$\psi_c(k) = C \bar{\psi}^T(-k), \quad \overline{V} \equiv C V^T C^{-1}. \quad (25)$$

Taking into account the lowest diagram, we can then write down the self-consistent equations for the mean-fields, V and Δ:

$$-V(k) = (-ig)^2 \int \frac{\mathrm{d}^4p}{i(2\pi)^4} \{-iD^{\mu\nu}(k-p)\} \gamma_\mu \frac{\lambda_\alpha}{2} \{-iG_{11}(p)\} \gamma_\nu \frac{\lambda_\alpha}{2}. \quad (26)$$

and

$$-\Delta(k) = (-ig)^2 \int \frac{\mathrm{d}^4p}{i(2\pi)^4} \{-iD^{\mu\nu}(k-p)\} \gamma_\mu \frac{-(\lambda_\alpha)^T}{2} \{-iG_{21}(p)\} \gamma_\nu \frac{\lambda_\alpha}{2}. \quad (27)$$

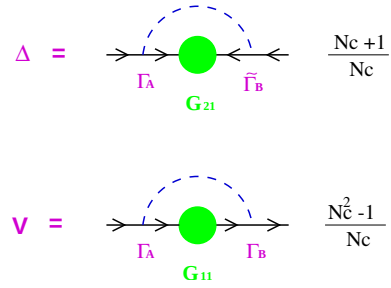

Figure 2. Graphical interpretations of the coupled equations (26) and (27) with coefficients in front of R.H.S. given by N_c.

Applying the Fierz transformation for the Fock exchange energy term (26) we can see that there appear the color-singlet scalar, pseudoscalar, vector and axial-vector self-energies. In general we must take into account these self-energies in V, $V = U_s + \gamma_5 U_{ps} + \gamma_\mu U_v^\mu + \gamma_\mu\gamma_5 U_{av}^\mu$ with the mean-fields U_i. Here we retain only U_s, U_v^0, U_{av}^3 in V and suppose that others to be vanished. We shall see this ansatz gives self-consistent solutions for Eq.(26) because of axial and reflection symmetries of the Fermi seas under the zero-range approximation for the gluon propagator. We furthermore discard the scalar mean-field U_s and the time component of the vector mean-field U_v^0 for simplicity since they are irrelevant for the spin degree of freedom.

According to the above assumptions and considerations the mean-field V in Eq.(24) renders

$$V = \gamma_3\gamma_5 U_A, \quad U_A \equiv U_{av}^3, \tag{28}$$

with VA U_A. Then the diagonal component of the Green function $G_{11}(p)$ is written as

$$G_{11}(p) = \left[G_A^{-1} - \gamma_0\Delta^\dagger\gamma_0\tilde{G}_A\Delta\right]^{-1} \tag{29}$$

with

$$G_A^{-1}(p) = \not{p} - m - \not{\mu} - \gamma_5\gamma_3 U_A, \tag{30}$$

$$\tilde{G}_A^{-1}(p) = \not{p} - m - \not{\mu} - \overline{\gamma_5\gamma_3} U_A, \tag{31}$$

where $\overline{\gamma_5\gamma_3} = \gamma_5\gamma_3$ and $G_A(p)$ is the Green function with U_A which is determined self-consistently by way of Eq. (26).

Before constructing the gap function Δ, we first find the single-particle spectrum and their eigenspinors in the absence of Δ, which is achieved by diagonalization of the operator G_A^{-1}. We have already known four single-particle energies $\epsilon_\pm$ (positive energies) and $-\epsilon_\pm$ (negative energies), which are given

as

$$\epsilon_{\pm}(\boldsymbol{p}) = \sqrt{\boldsymbol{p}^2 + U_A^2 + m^2 \pm 2U_A\sqrt{m^2 + p_z^2}}, \tag{32}$$

and the eigenspinors $\phi_s,\ s = \pm$ should satisfy the equation, $G_A^{-1}(\epsilon_s, \mathbf{p})\phi_s = 0$.

Here we take the following ansatz for Δ:

$$\begin{aligned} \Delta(\boldsymbol{p}) &= \sum_{s=\pm} \tilde{\Delta}_s(\boldsymbol{p}) B_s(\boldsymbol{p}), \\ B_s(\boldsymbol{p}) &= \gamma_0 \phi_{-s}(\boldsymbol{p}) \phi_s^{\dagger}(\boldsymbol{p}). \end{aligned} \tag{33}$$

The structure of the gap function (33) is then inspired by a physical consideration of a quark pair as in the usual BCS theory: we consider here the quark pair on each Fermi surface with opposite momenta, $\mathbf{p}$ and $-\mathbf{p}$ so that they result in a linear combination of $J^{\pi} = 0^-, 1^-$ (see Fig. 3). [4]

$\tilde{\Delta}_s$ is still a matrix in the color-flavor space. Since the antisymmetric nature of the fermion self-energy imposes a constraint on the gap function [1],

$$C\Delta(\boldsymbol{p})C^{-1} = \Delta^T(-\boldsymbol{p}). \tag{34}$$

$\tilde{\Delta}_n(\boldsymbol{p})$ must be a symmetric matrix in the spaces of internal degrees of freedom. Taking into account the property that the most attractive channel of the OGE interaction is the color antisymmetric $\bar{3}$ state, it must be in the flavor singlet state.

Thus we can choose the form of the gap function as

$$\left(\tilde{\Delta}_s\right)_{\alpha\beta;ij} = \epsilon^{\alpha\beta 3}\epsilon^{ij}\Delta_s \tag{35}$$

for the two-flavor case (2SC), where α, β denote the color indices and i, j the flavor indices. Then the quasi-particle spectrum can be obtained by looking for poles of the diagonal Green function, G_{11}:

$$E_s(\boldsymbol{p}) = \begin{cases} \sqrt{(\epsilon_s(\boldsymbol{p}) - \mu)^2 + |\Delta_s(\boldsymbol{p})|^2} & \text{for color 1, 2} \\ \sqrt{(\epsilon_s(\boldsymbol{p}) - \mu)^2} & \text{for color 3} \end{cases} \tag{36}$$

Note that the quasi-particle energy is independent of color and flavor in this case, since we have assumed a singlet pair in flavor and color.

[4] Note that this choice is not unique; actually we are now studying another possibility of quark pair between different Fermi surfaces [16].

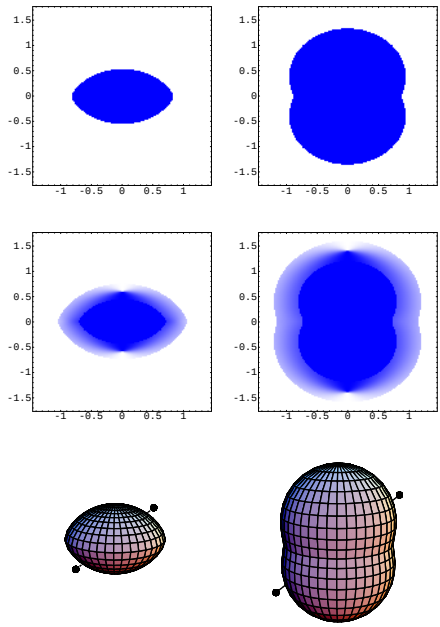

Figure 3. Deformed Fermi seas and the quark pair on each surface. The top figures show those in the absence of $\Delta_\pm$ and the middle figures diffusion of the Fermi surfaces in the presence of $\Delta_\pm$. The bottom ones show the quark pairing on the Fermi surfaces.

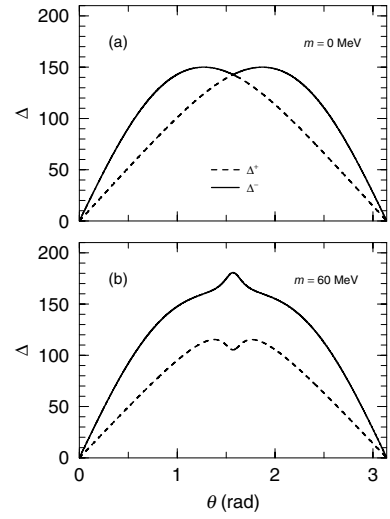

Figure 4. Schematic view of the polar-angle dependence of the gap functions at the Fermi surface, (a) for $m = 0$ and (b) for $m \neq 0$.

Gathering all these stuffs to put them in the self-consistent equations, we have the coupled gap equations for Δ_s,

$$\Delta_{s'}(k,\theta_k) = \frac{N_c+1}{2N_c}\tilde{g}^2 \int \frac{\mathrm{d}p\,\mathrm{d}\theta_p}{(2\pi)^2} p^2 \sin\theta_p \sum_s T_{s's}(k,\theta_k,p,\theta_p) \frac{\Delta_s(p,\theta_p)}{2E_s(p,\theta_p)}, \quad (37)$$

and the equation for U_A,

$$U_A = -\frac{N_c^2-1}{4N_c^2}\tilde{g}^2 \int \frac{\mathrm{d}^3p}{(2\pi)^3} \sum_s \left\{\theta(\mu-\epsilon_s(\boldsymbol{p})) + 2v_s^2(\boldsymbol{p})\right\} \frac{U_A + s\beta_p}{\epsilon_s(\boldsymbol{p})}, \quad (38)$$

within the "contact" interaction, $\tilde{g}^2 \equiv g^2/\Lambda^2$, (see Eq. (40)), where $v_s^2(\boldsymbol{p})$ denotes the momentum distribution of the quasi-particles. We find that the expression for U_A, Eq. (38), is nothing but the simple sum of the expectation

value of the spin operator with the weight of the occupation probability of the quasi-particles v_s^2 for two colors and the step function for remaining one color (cf. (19)).

Carefully analyzing the structure of the function $T_{s's}$ in Eq. (37), we can easily find that the gap function Δ_s should have the polar angle (θ) dependence on the Fermi surface,

$$\Delta_s(p_s^F, \theta) = \frac{p_s^F(\theta)\sin\theta}{\mu}\left(-s\frac{m}{\sqrt{m^2+(p_s^F(\theta)\cos\theta)^2}}R + F\right), \qquad (39)$$

with constants F and R to be determined (see Fig. 4).

As a characteristic feature, both the gap functions have nodes at poles ($\theta = 0, \pi$) and take the maximal values at the vicinity of equator ($\theta = \pi/2$), keeping the relation, $\Delta_- \geq \Delta_+$. This feature is very similar to ${}^3P$ pairing in liquid ^{3}He or nuclear matter [17, 18]; actually we can see our pairing function Eq. (39) to exhibit an effective P wave nature by a genuine relativistic effect by the Dirac spinors. Accordingly the quasi-particle distribution is diffused (see Fig. 3)

Self-consistent solutions

Here we demonstrate some numerical results; we replaced the original OGE by the "contact" interaction with the cutoff around the Fermi surface in the momentum space,

$$D^{\mu\nu} \to -g^{\mu\nu}/\Lambda^2, \quad \Delta_s(\mathbf{p}) \to \Delta_s(\mathbf{p})\theta(\delta - |\epsilon_s - \mu|) \qquad (40)$$

as in the BCS theory in the weak-coupling limit [19].

First we show the magnitude of U_A (Fig. 5). It is seen that the axial-vector mean-field (spin polarization) appears above a critical density and becomes larger as baryon number density gets higher. Moreover, the results for different values of the quark mass show that spin polarization grows more for the larger quark mass. This is because a large quark mass gives rise to much difference in the Fermi seas of two different "spin" states, which leads to growth of the exchange energy in the axial-vector channel. A slight reduction of U_A arises as a result of diffuseness of the Fermi surface due to Δ_s. As seen in Eq. (38), U_A can be obtained as addition and cancellation of the contributions by two different Fermi seas; the latter term is more momentum dependent than the former one and thereby $v_s^2(\mathbf{p})$ enhances the cancellation term (see Fig. 3).

Next we show the gap function as a function of ρ_B (Fig. 6). To see the bulk behavior of the gap function, we use the mean-value with respect to the polar angle on the Fermi surface,

$$\langle\Delta_\pm\rangle \equiv \left(\int_0^\pi \mathrm{d}\theta \frac{\sin\theta}{2}\Delta_\pm^2\right)^{1/2}. \qquad (41)$$

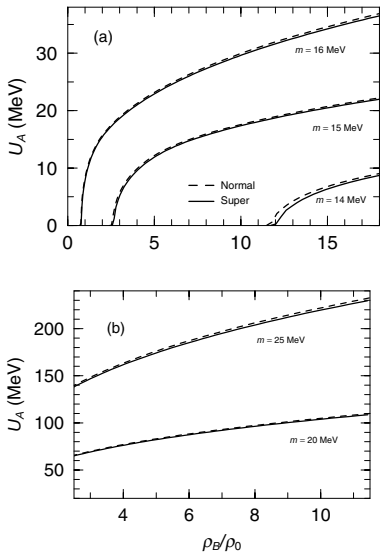

Figure 5. Axial-vector mean-field (VA) as a function of baryon number density $\rho_B(\rho_0 = 0.16\text{fm}^{-3})$. Solid (dashed) lines denote VA in the presence (absence) of CSC.

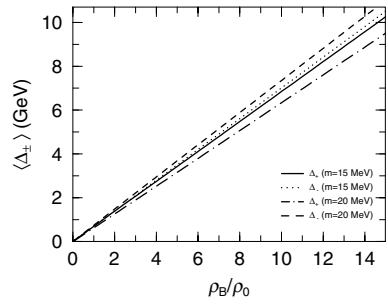

Figure 6. Mean values of the gap functions, $\Delta_\pm$ and their mass dependence.

The mean values $\langle\Delta_\pm\rangle$ begin to split with each other at a density where U_A becomes finite. We'd like to make a comment here. One may be surprised to see their value of $O(\text{GeV})$, coming from our parameter choice. However, what we'd like to reveal here is not their realistic values but a possibility of color magnetic superconductivity and its qualitative features. More realistic study, of course, is needed by carefully checking our approximations, especially the contact interaction and the sharp cutoff at the Fermi surface.

With these figures we can say that FM and CSC barely interfere with each other.

4. Chiral symmetry and magnetism

We have seen that the quark mass dependence of ferromagnetism should be important, while we have treated it as an input parameter. When we consider the realization of chiral symmetry in QCD, the quark mass should be dynamically generated as a result of the vacuum "superconductivity"; $q\bar{q}$ pairs are condensed in the vacuum. We consider here $SU(2)_L \times SU(2)_R$ symmetry. Then Lagrangian should be globally invariant under the operation of any group element with constant parameters, except the symmetry-breaking term

stemming from the small current mass, m_c. Here we'd like to suggest another mechanism leading to FM in quark matter with recourse to chiral symmetry. We shall see that FM may be realized *without accompanying spin polarization*.

Consider the following parameterization for the combination of the quark bilinear fields by introducing the auxiliary fields, ρ and θ_i:

$$\bar{\psi}\psi + i\gamma_5\boldsymbol{\tau}\bar{\psi}i\gamma_5\boldsymbol{\tau}\psi = \rho\exp(i\gamma_5\boldsymbol{\tau}\cdot\boldsymbol{\theta}). \tag{42}$$

Then it resides on the chiral "circle" with "modulus "ρ and " phase"θ_i, any point on which is equivalent with each other in the chiral limit, $m_c = 0$, and moved to another point by a chiral transformation. We conventionally choose a definite point, $\langle \mathrm{vac}|\rho|\mathrm{vac}\rangle = f_\pi$ (f_π: the pion decay constant) and $\langle \mathrm{vac}|\theta_i|\mathrm{vac}\rangle = 0$, for the vacuum, which is flavor singlet and parity eigenstate. In the following we shall see that the phase degree of freedom is related to spin polarization; that is, the "phase condensation" with a non-vanishing value of θ_i leads to FM [20].

Separating the fields ρ and θ_i into the classical ones and fluctuations around them, and discarding any fluctuation the mean-field theory proceeds:

$$\rho \to \langle\rho\rangle[\geq 0], \quad \theta_i \to \langle\theta_i\rangle. \tag{43}$$

Assuming the simplest but nontrivial form of the classical chiral angle such that $\theta_3(\mathbf{r}) = \mathbf{q}\cdot\mathbf{r}, \theta_{1,2} = 0$, we call this set a *dual chiral density wave* (DCDW) [5] :

$$\begin{aligned} \langle\bar{\psi}\psi\rangle &= \Delta\cos\mathbf{q}\cdot\mathbf{r} \\ \langle\bar{\psi}i\gamma_5\tau_3\psi\rangle &= \Delta\sin\mathbf{q}\cdot\mathbf{r}. \end{aligned} \tag{44}$$

It should be obvious that if Δ vanishes, the phase degree of freedom has to become redundant, as seen later. It would be worth mentioning that similar configuration has been studied in other contexts [21–23]. Note that the configuration in (44) breaks rotational invariance as well as translational invariance, but the latter invariance is recovered by an isospin rotation [26].

Taking the Nambu-Jona-Lasinio (NJL) model as a simple but nontrivial model [27], we explicitly demonstrate that quark matter becomes unstable for a formation of DCDW above a critical density; the NJL model has been originally presented to demonstrate a realization of chiral symmetry in the vacuum, while recently it been also used as an effective model embodying spontaneous breaking of chiral symmetry in terms of quark degree of freedom [28] [6]

$$L_{NJL} = \bar{\psi}(i\partial\!\!\!/ - m_c)\psi + G[(\bar{\psi}\psi)^2 + (\bar{\psi}i\gamma_5\boldsymbol{\tau}\psi)^2] \tag{45}$$

[5] Some authors considered similar configuration [24] and called a chiral density wave in analogy with spin density wave (SDW) by Overhauser in condensed-matter physics [25]. However, only the scalar density oscillates with finite wave number and the pseudo-scalar one is discarded in their ansatz.

[6] We can see that the OGE interaction gives the same form after the Fierz transformation in the zero-range limit.

Using the mean-field approximation (MFA) with the DCDW configuration, we introduce a new quark field ψ_W by the Weinberg transformation [29],

$$\psi_W = \exp[i\gamma_5\tau_3\mathbf{q}\cdot\mathbf{r}/2]\psi, \tag{46}$$

to get the transformed Lagrangian,

$$\mathcal{L}_{MF} = \bar{\psi}_W[i\partial\!\!\!/ - M - 1/2\gamma_5\tau_3 q\!\!\!/]\psi_W - G\Delta^2, \tag{47}$$

with the dynamically generated mass, $M \equiv -2G\Delta$ and $q^\mu = (0, \mathbf{q})$. This procedure embodies translational invariance of the ground state, and shows that we essentially consider a "uniform" problem, while we introduced the space-dependent mean-fields at the beginning. We briefly summarize in Table 3 the relation of the transformed frame to the original one. Note that the transformed Lagrangian becomes the same as the familiar form used in discussions of chiral symmetry realization within the NJL model, except the isovector and axial-vector coupling term $\gamma_5\tau_3 q\!\!\!/$. We can see the role of the wave vector $\mathbf{q}$ is the same as AV introduced in the previous sections.

Table 3. Diagram of the Weinberg transformation.

$\langle\bar{\psi}\psi\rangle \neq 0$	$\Longleftrightarrow$	$\langle\bar{\psi}_W\psi_W\rangle = \Delta(\neq 0)$
$\langle\bar{\psi}i\gamma_5\tau_3\psi\rangle \neq 0$		$\langle\bar{\psi}_W i\gamma_5\tau_3\psi_W\rangle = 0$
		$q/2 \propto \nabla\theta$ ("AV")
non-uniform		uniform

The Dirac equation for ψ_W then renders

$$(i\partial\!\!\!/ - M - 1/2\tau_3\gamma_5 q\!\!\!/)\,\psi_W = 0. \tag{48}$$

We can find a spatially uniform solution for the quark wave function, $\psi_W = u_W(p)\exp(i\mathbf{p}\cdot\mathbf{r})$, [7] and the energy eigenvalue is given as

$$E_p^{\pm} = \sqrt{E_p^2 + |\mathbf{q}|^2/4 \pm \sqrt{(\mathbf{p}\cdot\mathbf{q})^2 + M^2|\mathbf{q}|^2}}, \quad E_p = (M^2 + |\mathbf{p}|^2)^{1/2} \tag{49}$$

for positive energy (valence) quarks with different polarizations. For negative energy quarks in the Dirac sea, they have a spectrum symmetric with respect to null line because of charge conjugation symmetry in the Lagrangian (47). The single-particle spectrum (49) shows again an analogous feature to the *exchange splitting* between two eigenenergies with different polarizations in the

[7] This feature is very different from refs.[24], where the wave function is no more plane wave.

presence of $\mathbf{q}$; hereafter, we choose $\mathbf{q}//\hat{z}$, $\mathbf{q} = (0, 0, q),\ q \geq 0$, without loss of generality.

Thus each flavor quark shows the same energy spectrum (49) even in the presence of the isospin dependent AV and its form is the same as in Eq. (14). However, there is one and important difference from the previous sections; we have considered the *flavor singlet AV*, while we are now considering the *isovector AV* here. The eigenspinor $u^{\pm}_{W,i},\ i = u, d$ for each flavor satisfies the same Dirac equation for a given energy eigenvalue, except the different sign in the AV term, so that we have the different form for each flavor; $u^{\pm}_{W,u} = u^{\mp}_{W,d}$. The mean-value of the spin operator $\Sigma_z = \begin{pmatrix} \sigma_3 & 0 \\ 0 & \sigma_3 \end{pmatrix}$ is then given by

$$\bar{s}^{\pm}_{z,u} = \frac{1}{2} u^{\pm\dagger}_{W,u} \Sigma_z u^{\pm}_{W,u} = \frac{1}{2} \frac{q/2 \pm \beta}{E^{\pm}_p}, \tag{50}$$

with $\beta = \sqrt{p_z^2 + M^2}$ for u quarks. The corresponding value for d quarks is also given as $\bar{s}^{\pm}_{z,d} = -\bar{s}^{\pm}_{z,u}$. Thus we can see two flavors are oppositely polarized to each other. Since the integral of $\bar{s}^{\pm}_{z,i}$ over the Fermi seas should be finite for $q \neq 0$ for each flavor, the spin polarization of each flavor is finite but has opposite direction to each other. Consequently the total spin polarization or the *flavor singlet AV* is always vanished in this case. However, note that this result is never conflicted with FM of quark matter by considering the magnetization. As we have already noted, the response of the system to the magnetic field goes through the magnetization. Taking into account the difference of electric charges of two flavors Q_i, $Q_u = +2/3e$ and $Q_d = -1/3e$, we can see that each flavor *coherently* contributes to the magnetization, instead.

Thermodynamic potential

The thermodynamic potential is given as

$$\begin{aligned} \Omega_{\rm total} &= \gamma \sum_{s=\pm} \int \frac{d^3p}{(2\pi)^3} (E^s_p - \mu)\theta_s - \gamma \sum_{s=\pm} \int \frac{d^3p}{(2\pi)^3} E^s_p + M^2/4G \\ &\equiv \Omega_{\rm val} + \Omega_{\rm vac} + M^2/4G. \end{aligned} \tag{51}$$

where $\theta_{\pm} = \theta(\mu - E^{\pm}_p)$, μ the chemical potential and γ is the degeneracy factor $\gamma = N_f N_c$. The first term $\Omega_{\rm val}$ is the contribution by the valence quarks filled up to the chemical potential, while the second term $\Omega_{\rm vac}$ is the vacuum contribution that is formally divergent. We shall see both contributions are *indispensable* in our discussion. Once $\Omega_{\rm total}$ is properly evaluated, the equations to be solved to determine the optimal values of Δ and q are

$$\frac{\partial \Omega_{\rm total}}{\partial \Delta} = \frac{\partial \Omega_{\rm total}}{\partial q} = 0. \tag{52}$$

Since the NJL model is not renormalizable, we need some regularization procedure to get a meaningful finite value for the vacuum contribution. Consider the sum of the negative energy over the Dirac sea,

$$\Omega_{\rm vac} = -\gamma \sum_{s=\pm} \int \frac{d^3p}{(2\pi)^3} E_p^s - \Omega_{\rm ref}, \tag{53}$$

where we subtracted an irrelevant constant $\Omega_{\rm ref} = -2\gamma \int \frac{d^3p}{(2\pi)^3} E_p$ with an arbitrary reference mass $M = M_{\rm ref}$ to make the following procedure mathematically well-defined. Since the energy spectrum is no more rotation symmetric, we cannot apply the usual momentum cut-off regularization (MCOR) scheme to regularize $\Omega_{\rm vac}$. Instead, we adopt the proper-time regularization (PTR) scheme [30]. We think this is a most suitable one for our purpose, since $\Omega_{\rm vac}$ counts the spectrum change under the "external" axial-vector field. It has been shown that the vacuum polarization effect under the external electromagnetic field can be treated in a gauge invariant way, where the energy spectrum is also deformed depending on the field strength [30]. It is also known that the consequences from the NJL model are almost regularization-scheme independent [28], including the PTR scheme.

Introducing the proper-time variable τ, we eventually find

$$\Omega_{\rm vac} = \frac{\gamma}{8\pi^{3/2}} \int_0^\infty \frac{d\tau}{\tau^{5/2}} \int_{-\infty}^\infty \frac{dp_z}{2\pi} \left[e^{-(\sqrt{p_z^2+M^2}+q/2)^2\tau} + e^{-(\sqrt{p_z^2+M^2}-q/2)^2\tau} \right], \tag{54}$$

except an irrelevant constant $\Omega_{\rm ref}$, which is reduced to the standard formula [28] in the limit $q \to 0$.

We can easily see, from Eq. (54), that the q degree of freedom becomes superfluous and theory must become *trivial* in the limit $m \to 0$, which is equivalent to $\Delta \to 0$ in the chiral limit: all the observables must be independent of q. This salient feature is consistent with the form of DCDW. The integral with respect to the proper time τ is not well defined as it is, since it is still divergent due to the $\tau \sim 0$ contribution. Regularization proceeds by replacing the lower bound of the integration range by $1/\Lambda^2$, which corresponds to the momentum cut-off in the MCOR scheme.

For given chemical potential μ, and M and q we can evaluate the valence contribution $\Omega_{\rm val}$ using Eq. (49) and write down the general formula analytically. Then the thermodynamic potential can be expressed as $\Omega_{\rm val} = \epsilon_{\rm val}(q) - \mu\rho_{\rm val}(q)$, where $\epsilon_{\rm val}(q)$ and $\rho_{\rm val}(q)$ are the energy density and the quark-number density, respectively. They consist of two terms corresponding to the two Fermi seas with different polarizations: $\epsilon_{\rm val}(q) = \epsilon^-(q) + \epsilon^+(q)$ and $\rho_{\rm val}(q) = \rho^-_{\rm val}(q) + \rho^+_{\rm val}(q)$. We present some examples about the instability of the usual NJL ground state with respect to spontaneous generation of DCDW. In the present calculation chiral symmetry restoration occurs at the first order in the

case without DCDW. [8] We can see the NJL ground state becomes unstable at the critical chemical potential μ_{c1}, and symmetry restoration is delayed until μ_{c2} by the presence of DCDW. This dragging effect by DCDW is one of the important features.

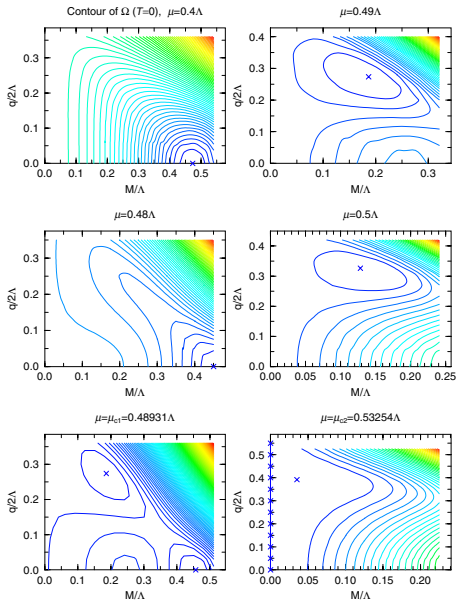

Figure 7. Countour map of the thermodynamic potential in the dynamical mass (M) - wave number (q) plane. The absolute minimum is denoted by the cross for given density. We have the first order phase transitions in this calculation.

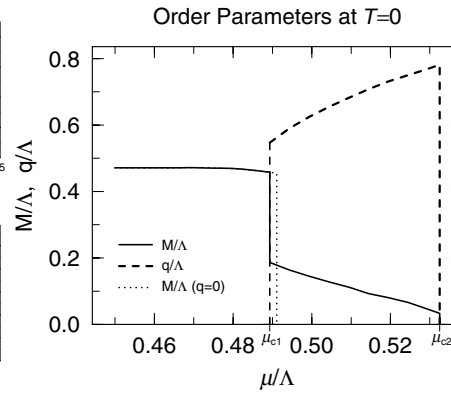

Figure 8. Density dependence of M and q, compared with the usual result with $q = 0$. There appear two critical chemical potentials; the lower one indicates the instability of the ground state for formation of DCDW, while the higher one restoration of chiral symmetry.

5. Summary and Concluding remarks

In this talk we have discussed a magnetic aspect of quark matter based on QCD. First, we have introduced "ferromagnetism" (FM) in QCD, where the Fock exchange interaction plays an important role. Presence of the axial-vector mean-field (AV) after the Fierz transformation is essential to give rise to FM, in the context of self-consistent framework. As one of the features of the relativistic FM, we have seen that the Fermi sea is deformed in the presence of

[8] Note that this is not a unique possibility: we may have the second order phase transitions for other parameter sets [28].

AV; the Fermi sea has a prolate shape for the majority spin particles, while an oblate shape for the minority spin particles.

We have then discussed a possibility of color magnetic superconductivity and seen coexistence of FM and CSC is possible. Our ansatz for quark pairing shows an effective P- wave pair condensation and gives a polar angle dependence of the gap function, which looks similar to liquid ^{3}He A - phase. Note that this ansatz is never unique for color magnetic superconductivity and other types may be also possible [16], where the gap function should show other angle dependence. In this context recent studies about $S = 1$ quark pairing may be interesting [31].

We have briefly discussed a relation of magnetism to chiral symmetry and presented an idea, *dual chiral density wave* (DCDW), which should lead to FM. Using, e.g., the NJL model we have demonstrated under what conditions the ground state becomes unstable for formation of DCDW. We have found the usual ground state becomes surely unstable at the critical density and stays in FM between the first and the second critical densities.

The FM induced by DCDW has many interesting features different from the Bloch mechanism. Unfortunately we have not revealed them yet, but it would be interesting to examine whether DCDW is possible in the CSC phase.

The symmetry breaking pattern is summarized as follows: in the condensation of the flavor singlet AV, it violates rotation symmetry,

$$O(3) \to O(2), \tag{55}$$

while the DCDW state does flavor symmetry as well as rotation symmetry,

$$O(3) \times SU(2)_V \to O(2) \times U_{I_3}(1). \tag{56}$$

The latter situation is similar to the neutral pion condensation in nuclear matter.

It would be important to figure out the low energy excitation modes (Nambu-Goldstone modes) built on the ferromagnetic phase. The spin waves are well known in the Heisenberg model [10]. Then , how about our case [32]?

If quark matter is in the ferromagnetic phase, it may produce the dipolar magnetic field by their magnetic moment. Since the total magnetic dipole moment M_q should be simply given as $M_q = \mu_q \cdot (4\pi/3 \cdot r_q^3) n_q$ for the quark sphere with the quark core radius r_q and the quark number density n_q. Then the dipolar magnetic field at the star surface R takes the maximal strength at the poles,

$$B_{\max} = \frac{8\pi}{3} \left(\frac{r_q}{R}\right)^3 \mu_q n_q = 10^{15}[\mathrm{G}] \left(\frac{r_q}{R}\right)^3 \left(\frac{\mu_q}{\mu_N}\right) \left(\frac{n_q}{0.1\mathrm{fm}^{-3}}\right). \tag{57}$$

We have not considered the electromagnetic interaction between quarks and the induced magnetic field. It would be interesting to see how the situation

changes when we take it into account; symmetry restoration [33] or mixing between magnetic field and gluon field are among them [34].

Finally we'd like to give a comment about fluctuations. In this talk we have completely discarded fluctuations and been only concerned with the mean-field. It would be reasonable to study the phase transition, at least qualitatively. However, we know some fluctuations or correlations between relevant operators should have some effects even before the phase transitions. In particular the axial and magnetic susceptibilities in normal quark matter would be interesting; they might have important consequence,e.g., for quark-quark pairing correlation as in ^{3}He superfluidity [17].

Acknowledgments

The present work of T.T. and T.M. is partially supported by the Japanese Grant-in-Aid for Scientific Research Fund of the Ministry of Education, Culture, Sports, Science and Technology (11640272, 13640282), and by the REIMEI Research Resources of Japan Atomic Energy Research Institute (JAERI).

References

[1] B. C. Barrois, Nucl. Phys. **B129** (1977) 390,
D. Bailin and A. Love, Phys. Rept. **107** (1984) 325.
For recent reviews of CSC, K. Rajagopal and F. Wilczek, hep-ph/0011333; M. Alford, Ann. Rev. Nucl. Part. Sci. 51 (2001) 131, and referenses cited therein.

[2] For a review, G. Chanmugam, Annu. Rev. Astron. Astrophys. **30** (1992) 143.

[3] B. Paczyński, Acta. Astron. **41** (1992) 145; R.C.Duncan and C. Thompson, Astrophys. J. **392** (1992) L19; C. Thompson and R.C.Duncan, Mon. Not. R. Astron. Soc. **275** (1995) 255.

[4] C. Kouveliotou et al., Nature **393** (1998) 235; K. Hurley et al., Astrophys. J. 510 (1999) L111.

[5] S.B. Popov, in this proceedings.

[6] V.L. Ginzburg, Sov. Phys. Dokl. **9** (1964) 329;
L. Woltjer, Ap. J. **140** (1964) 1309.

[7] V.R. Pandharipande, V.K. Garde and J.K. Srivastava, Phys. Lett. **B38** 485.

[8] T. Tatsumi, Phys. Lett. **B489** (2000) 280.

[9] F. Bloch, Z. Phys. **57** (1929) 545.

[10] e.g. K.Yoshida, *Theory of Magnetism* (Springer-Verlag Berlin Heidelberg, 1996).

[11] T. Maruyama and T. Tatsumi, Nucl. Phys. **A693** (2001) 710.

[12] H.Müther and A.Sedrakian, Phys.Rev.Lett. **88** (2002) 252503; Phys.Rev. **D67** (2003) 085024.

[13] E. Nakano, T. Maruyama and T. Tatsumi, Phys. Rev. **D68** (2003) 105001.

[14] L.N. Buaevskii et al., Adv. Phys. **34** (1985) 175.

[15] S.S. Sexena et al., Nature **406** (2000) 587; C.Pfleiderer et al., Nature **412** (2001) 58; N.I.Karchev et al., Phys. Rev. Lett. **86** (2001) 846; K.Machida and T.Ohmi, Phys. Rev. Lett. **86** (2001) 850

[16] K. Nawa, E. Nakano, T. Maruyama and T. Tatsumi, in progress.

[17] A. J. Leggett, Rev. Mod. Phys. 47 (1975) 331.

[18] R. Tamagaki, Prog. Theor. Phys. **44** (1970) 905; M. Hoffberg, A.E. Glassgold, R.W. Richardson and M. Ruderman, Phys. Rev. Lett. **24** (1970) 775.

[19] R.D. Pisarski and D.H. Rischke, Phys. Rev. **D60** (1999) 094013.

[20] T. Tatsumi and E. Nakano, in preparation.

[21] F. Dautry and E.M. Nyman, Nucl. Phys. **319** (1979) 323.

[22] M. Kutschera, W. Broniowski and A. Kotlorz, Nucl. Phys. **A516** (1990) 566.

[23] K. Takahashi and T. Tatsumi, Phys. Rev. **C63** (2000) 015205; Prog. Theor. Phys. **105** (2001) 437.

[24] D.V. Deryagin, D. Yu. Grigoriev and V.A. Rubakov, Int. J. Mod. Phys. **A7** (1992) 659.
B.-Y. Park, M.Rho, A.Wirzba and I.Zahed, Phys. Rev. **D62** (2000) 034015.
R. Rapp, E.Shuryak and I. Zahed, Ohys. Rev. **D63** (2001) 034008.

[25] A.W. Overhauser, Phys. Rev. **128** (1962) 1437.

[26] D.K. Campbell, R.F. Dashen and J.T. Manassah, Phys. Rev. **D12** (1975) 979;1010.

[27] Y. Nambu and G. Jona-Lasinio, Phys. Rev. **122** (1961) 345; **124** (1961) 246.

[28] S.P. Klevansky, Rev. Mod. Phys. **64** (1992) 649.
T. Hatsuda and T. Kunihiro, Phys. Rep. **247** (1994) 221.

[29] S. Weinberg, *The quantum theory of field II*(Cambridge, 1996).

[30] J. Schwinger, Phys. Rev. **92** (1951) 664.

[31] M.G. Alford, J.A. Bowers, J.M. Cheyne and G.A. Cowan, Phys.Rev.D67:054018 (2002).
M. Buballa, J. Hošek and M. Oertel, Phys.Rev.Lett.90:182002 (2002).

[32] F. Sannino, in this proceedings.

[33] S.P. Klevansky and R.H. Lemmer, Phys. Rev. **D39** (1989) 3478.
H. Suganuma and T. Tatsumi, Ann. Phys. **208** (1991) 470.

[34] M. Alford,K. Rajagopal and F. Wilczek, Phys. Lett. **B422** (1998) 247; M. Alford, J. Berges and K. Rajagopal, Nucl. Phys. **B571** (2000) 269.

MAGNETIC FIELDS OF COMPACT STARS WITH SUPERCONDUCTING QUARK CORES

David M. Sedrakian
Department of Physics, Yerevan State University, 375025 Yerevan, Armenia
dsedrak@www.physdep.r.am

David Blaschke
Fachbereich Physik, Universitat Rostock, D-18051 Rostock, Germany
david.blaschke@physik.uni-rostock.de

Karen M. Shahabasyan
Department of Physics, Yerevan State University, 375025 Yerevan, Armenia
kshabas@www.physdep.r.am

Abstract The behavior of the magnetic field of a rotating neutron star with a superconducting color-flavor-locked (CFL) quark matter core is investigated in the framework of the Ginzburg-Landau theory. We take into account the simultaneous coupling of the diquark condensate field to the magnetic and gluomagnetic gauge fields. We solve the Ginzburg-Landau equations by properly taking into account the boundary conditions, in particular the gluon confinement condition. The rotation of the CFL condensate produces neutral vortices with normal cores. We find the distribution of the magnetic field in both the quark and the hadronic phases and show that a magnetic field penetrates into quark phase through normal cores of the rotational vortices. As a result, equivalent "magnetic vortices" are formed due to the induced Meissner currents.

1. Introduction

Recently, the possible formation of diquark condensates in QCD at finite density has been re-investigated in a series of papers following Refs. [1, 2]. It has been shown that in chiral quark models with nonperturbatrive 4-point interaction motivated from instantons [3] or nonperturbative gluon propagators [4, 5], the anomalous quark pair amplitudes can be very large - of the order of 100 MeV. The diquark pairs that are formed as a result of the attractive inter-

D. Blaschke and D. Sedrakian (eds.), Superdense QCD Matter and Compact Stars, 263–276.

action have zero total angular momentum [6, 7]. Because of the large number of the internal degrees of freedom of quarks various types of order parameters can be constructed; two J=0 pairing states with condensates antisymmetric in color and flavor have emerged as the energetically most favorable candidates. One pairing state, known to be favored at low densities, is the two-flavor color antitriplet 2SC state [1–4], in which s-quarks are absent and u- and d-quarks of two of the three colors participate in the pairing. The other pairing state, favored at sufficiently high density, is the color-flavor locked (CFL) state [8–10], where color superconductivity is complete in the sense that diquark condensate produces gap for quarks of all three flavors and colors.

The high-density phases of QCD at low temperatures can be realized in rotating compact stars - pulsars. Therefore, the observational data from pulsars could provide potentially important information on the state of matter at supernuclear densities, in particular the superconducting quark matter.

Bailin and Love [7] investigated the magnetic structure of the 2SC phase. They used a perturbative gluon propagator which yielded a very small pairing gap and concluded that quark matter is a type I superconductor, which expels the magnetic field out of a neutron star within 10^4 years. The authors of Ref. [11] find that within the recent nonperturbative approach for the effective quark interaction the ud-condensate forms a type II superconductor. Using the framework of the Ginzburg-Landau theory they concluded that the magnetic field in the quark core can exist in quantized flux tubes. The simultaneous coupling of the quark fields to gluonic and electromagnetic gauge fields which leads to the "rotated electomagnetism" was ignored in Ref. [11].

The authors of Ref. [12] reconsidered the problem of magnetic field in quark matter taking into account the "rotated electromagnetism". They came to the conclusion that magnetic field can exist in superconducting quark matter in any case, although it does not form a quantized vortex lattice, because it obeys sourceless Maxwell equations and there is no Meissner effect. In our opinion this latter result is incorrect, since the equations for gauge fields were not taken into account and the boundary conditions were not posed correctly.

In Ref. [13] the Ginzburg-Landau equations for 2SC phase were derived taking into account the "rotated electromagnetism". These equations introduce a "new" charge of diquark pair $q_{sc} = \sqrt{e^2 + 3g^2}/3$, where g is the strong coupling constant ($g^2/4\pi = 1$). This "new" charge is much larger than $e/3$ (about 20 times). It changes also the penetration depth λ_q, the quantum of magnetic flux Φ_q, and therefore the lower H_{c1}^q and upper H_{c2}^q critical magnetic fields.

These Ginzburg-Landau equations have been solved in Ref. [14] for the case of a homogeneous external magnetic field for three types of superconducting regions: a) a semi-infinite region with planar boundary, b) a cylindrical region and c) a spherical region. It was shown, that the Meissner effect always exists

inside a color superconductor. The distribution of the magnetic field in the 2SC quark and hadronic phases of a neutron star was found in Ref. [15]. It was shown that the magnetic field penetrates into a quark core in the form of quark vortices due to the Meissner currents.

The Ginzburg-Landau theory for the CFL phase has been derived in Refs. [10, 16–19]. The authors of Ref. [19] have taken into account the "rotated electromagnetism" and the rotation of the star. They conclude that ordinary quantized magnetic vortices are unstable in the CFL phase, but the rotational vortices are topologically stable. They have not considered boundary problems and concluded that the CFL condensate in an external magnetic field behaves like a type I superconductor.

In this paper we study the distribution of the magnetic field of a neutron star with superconducting CFL quark matter core in the framework of the Ginzburg-Landau theory. We solve the Ginzburg-Landau equations with proper boundary conditions.

2. Free Energy

We consider the CFL phase, described by the gapindexGap [10]

$$\Phi_{abij} = k_A(\delta_{ai}\delta_{bj} - \delta_{aj}\delta_{bi}), \tag{1}$$

where a, b and i, j are respectively color and flavor indices. The analysis of the covariant derivative of the Higgs field conducted in [16] has shown that the field

$$\vec{A}_y = \cos\alpha\vec{A} - \sin\alpha\vec{G} \tag{2}$$

is massless in the CFL phase. The orthogonal linear combination

$$\vec{A}_x = \sin\alpha\vec{A} + \cos\alpha\vec{G} \tag{3}$$

is massive. Here $\vec{A}$ is real electromagnetic gauge field.

The linear combination of color gauge fields $\vec{G}$ and the "mixing" angle are defined by

$$\vec{G} = \frac{\sqrt{3}}{2}\vec{A}_3 + \frac{1}{2}\vec{A}_8, \qquad \cos\alpha = \frac{g}{\sqrt{g^2 + \eta^2 e^2}}, \tag{4}$$

where $\eta = 2/\sqrt{3}$. At densities relevant to neutron stars the gluons are strongly coupled while the protons are coupled weakly ($e^2\ /4\pi = 1$), therefore $\alpha = \eta e/g = 1/10$. In order to preserve the normalization we need to introduce the third rotated field

$$\vec{A}_z = -\frac{1}{2}\vec{A}_3 + \frac{\sqrt{3}}{2}\vec{A}_8. \tag{5}$$

In the absence of electromagnetic and gluonic fields the free energy density F of a homogeneous color superconducting phase near T_c is [10, 17]

$$F_h = F_n + \alpha Tr(\Phi^+\Phi) + \lambda_1 \left[Tr(\Phi^+\Phi)\right]^2 + \lambda_2 Tr(\Phi^+\Phi)^2, \qquad (6)$$

where $\alpha = N(\mu/3)\ln(T/T_c)$, $\lambda_2 = 7\zeta(3)N(\mu/3)/16(\pi T_c)^2, \lambda_1 = 0$ in the weak coupling limit. Here $N(\mu/3) = (1/2\pi^2)(\mu/3)^2$ is the ideal gas density of states at the Fermi surface. This structure follows from the invariance of the free energy under special color and flavor rotations. The CFL phase is realized if $\lambda_2 > 0$. It is shown in [18] that in the mean field approximation $\lambda_1 = 0$, $\lambda_2 > 0$. In the inhomogeneous states Φ depends not only on the relative pair momentum k, but also on the center-of-mass coordinate, $\vec{r}$. Such a situation will emerge in an external magnetic field H_{ext} .

We construct the expression for the free energy density of color superconducting state in the external magnetic field by adding to the homogeneous free energy density (6) the kinetic energy density and the energy densities of the electromagnetic and color gauge fields as follows

$$F = F_h + \frac{1}{2}\gamma Tr\left[D_l\Phi(D_l\Phi)^+\right] + \frac{1}{8\pi}(\mathrm{curl}\vec{A})^2 + \frac{1}{8\pi}\sum_{a=1}^{8}(\mathrm{rot}\vec{A}_a)^2, \qquad (7)$$

where $\gamma = 7\zeta(3)n/16\pi^2T_c^2\ \mu$ [7], n is the baryon density, μ - the chemical potential, T_c - the critical temperature. Here the ordinary derivative $\partial_l\Phi$ is replaced by the covariant derivative $D_l\Phi$ [16]

$$D_l\Phi = \partial_l\Phi + \frac{1}{2}ig\left[(\lambda^a)^*\Phi + \Phi\lambda^a\right]A_l^a + ieQ\Phi A_l, \qquad (8)$$

where λ^a are the Gell-Mann matrices, $Q_{abij} = \delta_{ab}(q_i + q_j)$ is the electric charge matrix of the pair. We assume here, that self-couplings of the induced gluon fields are negligible. Note that the term containing γ is the kinetic energy.

In the absence of magnetic and chromomagnetic fields and in the homogeneous limit the free energy density becomes

$$F_h = F_n + 12\alpha\left|k_A\right|^2 + 24\lambda_2\left|k_A\right|^4. \qquad (9)$$

The magnitude of the gap is defined by the following equation

$$\alpha + 4\lambda_2\left|k_A\right|^2 = 0. \qquad (10)$$

This solution motivates the existence of a complete Meissner effect for all gauge fields inside quark superconductor. It corresponds to the absolute minimum value of free energy $F_{\min} = F_n - 3\alpha^2/2\lambda_2$ in the bulk.

We now rewrite the free energy (7) by introducing rotated fields $\vec{A}_x$, $\vec{A}_y$, $\vec{A}_z$ and the "new" charge $q = \sqrt{g^2 + \eta^2 e^2}/\sqrt{6}$ in the following form

$$\begin{aligned} F &= F_h + 6\gamma \left[|\bigtriangledown k_A|^2 + q^2 |k_A|^2 \left(\vec{A}_x\right)^2 \right] + \gamma g^2 |k_A|^2 \left(\vec{A}_z\right)^2 + \\ &+ \gamma g^2 |k_A|^2 \sum_{a=1, a\neq 3}^{7} \left(\vec{A}_a\right)^2 + \frac{1}{8\pi} \left(\mathrm{curl}\vec{A}\right)^2 + \frac{1}{8\pi} \sum_{a=1}^{8} \left(\mathrm{curl}\vec{A}_a\right)^2 . \end{aligned} \tag{11}$$

In the kinetic energy term [the first line of Eq. (11)] q^2 is the actual coupling constant associated with the rotated massive field $\vec{A}_x$, g^2 is the analogous constant associated with the chromomagnetic fields $\vec{A}_a$ and the rotated field $\vec{A}_z$.

3. Ginzburg-Landau equations

To determine the response of the condensate to an external electromagnetic field we derive field equations by minimizing the free energy with respect to the macroscopic fields $\vec{A}_x$, $\vec{A}_y$, $\vec{A}_z$ and $\vec{A}_a$ $(a \neq 3, 8)$. We find

$$\sin\ \alpha\ \mathrm{curl}\ \mathrm{curl}\vec{A} + \cos\alpha\ \mathrm{curl}\ \mathrm{curl}\vec{G} + 48\pi\gamma q^2 \vec{A}_x = 0, \tag{12}$$

$$\cos\alpha\ \mathrm{curl}\ \mathrm{curl}\vec{A} - \sin\ \alpha\ \mathrm{curl}\ \mathrm{curl}\vec{G} = 0, \tag{13}$$

$$\mathrm{curl}\ \mathrm{curl}\vec{A}_z + 8\pi\gamma g^2 |k_A|^2 \vec{A}_z = 0, \tag{14}$$

$$\mathrm{curl}\ \mathrm{curl}\vec{A}_a + 8\pi\gamma g^2 |k_A|^2 \vec{A}_a = 0. \tag{15}$$

Equations (12) and (13) can be written in the following form

$$\lambda_q^2\ \mathrm{curl}\ \mathrm{curl}\vec{A} + \sin\ {}^2\alpha\vec{\mathrm{A}} = -\sin\ \alpha\cos\alpha\vec{G}, \tag{16}$$

$$\lambda_q^2\ \mathrm{curl}\ \mathrm{curl}\vec{G} + \cos^2\alpha\vec{G} = -\sin\ \alpha\cos\alpha\vec{A}, \tag{17}$$

where λ_q is

$$\lambda_q^{-1} = 4\sqrt{3\pi\gamma} q |k_A| . \tag{18}$$

In the case when α =const, Eqs. (12)-(15) will take the form

$$\vec{j}_x = -12\gamma q^2 |k_A|^2 \vec{A}_x , \tag{19}$$

$$\vec{j}_y = 0, \tag{20}$$

$$\vec{j}_z = -2\gamma g^2 |k_A|^2 \vec{A}_z, \tag{21}$$

$$\vec{j}_a = -2\gamma g^2 |k_A|^2 \vec{A}_a , a \neq 3, 8 , \tag{22}$$

where $\vec{j}_i = \mathrm{curl}\ \mathrm{curl}\vec{A}_i/4\pi$, $i = x, y, z, a$. Equations (19), (21) and (22) imply that eight of the nine gauge fields have a magnetic mass, as originally

shown in Ref. [8]. We can divide the field variables in (19) - (22) into two groups, the first group contains $\vec{A}_x$ and $\vec{A}_y$, while the second one includes $\vec{A}_z$ and $\vec{A}_a$ $(a \neq 3, 8)$. The fields $\vec{A}_x$ and $\vec{A}_y$ are coupled to the electromagnetic field, so they will respond to the external electromagnetic field, while the fields $\vec{A}_z$ and $\vec{A}_a$ are decoupled from the electromagnetic field and in the absence of external chromomagnetic fields can be taken equal to zero without loss of generality. Introducing the Abelian field strengths $\vec{B}_x = \mathrm{curl}\vec{A}_x$ and $\vec{B}_y = \mathrm{curl}\vec{A}_y$ we obtain

$$\lambda_q^2 \ \mathrm{curl}\ \mathrm{curl}\vec{B}_x + \vec{B}_x = 0, \tag{23}$$

$$\mathrm{curl}\vec{B}_y = 0; \tag{24}$$

thus the "rotated" field $\vec{B}_x$ is screened by Meissner currents within penetration depth λ_q, see Eq. (18).

In an external magnetic field $\vec{H}_{ext}$ the free energy (11) reduces to

$$F = F_h + 6\gamma \left[|\nabla k_A|^2 + q^2 |k_A|^2 \left(\vec{A}_x \right)^2 \right] + \frac{1}{8\pi}\vec{B}_x + \frac{1}{8\pi}\vec{B}_y \, . \tag{25}$$

We obtain the gap equation by minimizing (25) with respect to k_A^*

$$2\alpha k_A + 8\lambda_2 |k_A|^2 k_A - \gamma\nabla^2 k_A + \gamma q^2 k_A \left(\vec{A}_x \right)^2 = 0 \, . \tag{26}$$

An external magnetic field does not create vortex lines because currents induced by gradients of the phase of k_A are absent [see Eq. (19)]. To determine the response of the CFL condensate to rotation we shall consider its free energy F_r in the frame of reference, rotating with a constant angular velocity $\vec{\omega}$. This energy is defined as follows

$$F_r = F - \vec{\omega}\vec{M}, \tag{27}$$

where M is the angular momentum density [19]

$$\vec{M} = \vec{r} \times 4i\gamma\mu \left(k_A^* \bigtriangledown k_A - k_A \bigtriangledown k_A^* \right) . \tag{28}$$

Here μ is the mass of a baryon, $2\mu/3$ - the mass of a diquark pair. The free energy in the rotating frame now can be written as

$$F_r = F_h + 6\gamma \left[|\bigtriangledown k_A|^2 + q^2 |k_A|^2 \left(\vec{A}_x \right)^2 \right] - 4i\gamma\mu\vec{v}_n \left(k_A^* \bigtriangledown k_A - k_A \bigtriangledown k_A^* \right) , \tag{29}$$

where $\vec{v}_n = \vec{\omega} \times \vec{r}$ is the rigid body rotation velocity. We derive the Ginzburg-Landau equation for the order parameter by minimizing the free energy (29) with respect to k_A^*. In this manner we find

$$6\gamma k_A + 24\lambda_2 |k_A|^2 k_A - 3\gamma \bigtriangledown^2 k_A - 4i\gamma\mu\vec{v}_n \bigtriangledown k_A + 3\gamma q^2 k_A \left(\vec{A}_x \right)^2 = 0. \tag{30}$$

We note that there is a gradient term in Eq. (30), which is independent of the vector potentials; so the rotation of the condensate produces a lattice of neutral vortex lines [12, 19], which simulates the rigid body rotation. We emphasize also that the equations for the current (19) and (20) do not change, because $\vec{j}_x = -\partial F_r/\partial \vec{A}_x$, $\vec{j}_y = -\partial F_r/\partial \vec{A}_y$.

4. Vortex Structure

The superfluid baryon current density is defined by

$$\vec{j}_s = -\frac{1}{\mu}\frac{\partial F_r}{\partial \vec{v}_n} = 4i\gamma\hbar\left(k_A^*\nabla k_A - k_A\nabla k_A^*\right) = n_s\vec{v}_s. \tag{31}$$

The wave function of a singly quantized rotational vortex centered on the cylinder axis is $k_A = |k_A|\exp(-i\varphi)$, where φ is the azimuthal angle around the vortex line. Therefore the superfluid number density n_s and the superfluid velocity $\vec{v}_s$ are

$$n_s = \frac{16\gamma\mu}{3}|k_A|^2, \qquad \vec{v}_s = \frac{3\hbar}{2\mu}\nabla\varphi. \tag{32}$$

The superfluid velocity circulation is

$$\oint \vec{v}_s d\vec{l} = \frac{3\pi\hbar}{\mu}. \tag{33}$$

Thus, the quantum of circulation of an individual quark vortex is $3\pi\hbar/\mu$, and the vortex velocity $v_s = 3\hbar/2\mu r$, where r is the radius of a circular contour. Then we obtain for the energy per unit length of an isolated vortex and for the critical velocity of the vortex appearance the following expressions:

$$E = \frac{9\pi n_s\hbar^2}{4\mu}\ln\frac{R}{\xi}, \qquad \omega_{c1} = \frac{3\hbar}{\mu R^2}\ln\frac{R}{\xi}, \tag{34}$$

where R is the radius of the CFL phase, ξ - the diquark pair's correlation length in the CFL phase or the radius of the vortex normal core.

For the angular velocities $\omega \gg \omega_{c1}$ a triangular lattice of singly quantized vortices with lattice constant $b = \left(2\sqrt{3}\pi\hbar/\mu\omega\right)^{1/2}$ forms in a rotating diquark condensate. The total number of vortices $N_v = 2\mu\omega R^2/3\hbar$ can be determined from the net circulation around a cylinder. For the superfluid velocity we have the following relation

$$\mathrm{curl}\vec{v}_s = \frac{3\pi\hbar\vec{e}_z}{\mu}\sum_i \delta\left(\vec{r} - \vec{r}_i\right), \tag{35}$$

where $\vec{r}_i$ are the two dimensional radius-vectors of the centers of vortex lines, $\vec{e}_z$ - unit vector. We shall assume that a rotating neutron star with a radius

R possesses a spherical core of radius a consisting of quark matter with CFL condensate surrounded by a spherical shell of hadronic matter with thickness $R-a$ containing neutron and proton superfluids. The triangular lattice of singly quantized neutron vortices with quantum of circulation $\pi\hbar/\mu$ forms in response to the rotation. Since the quark vortices carry $3\pi\hbar/\mu$ quantum of circulation, the three singly quantized neutron vortices connect at the spherical interface with one singly quantized quark vortex so that the baryon chemical potential is continuous across the interface [19].

The entrainment of superfluid protons by rotating superfluid neutrons leads to appearance of proton vortices and to generation of a homogeneous mean magnetic field with amplitude $\vec{B}$ and direction parallel to the axis of rotation of the star [20]. This field will penetrate into the quark core through the normal cores of quark vortices.

In the hadronic phase due to the entrainment effect around each neutron vortex appears a cluster of proton vortices which generates mean magnetic field $B=4\cdot 10^{14}G$. The magnetic flux of such a cluster is

$$\Phi_{cl}=B\pi\delta_n^2=1.25\cdot 10^5 G\cdot cm^2, \tag{36}$$

where $\delta_n=10^{-5}cm$ is the radius of the cluster [21]. The magnetic field of three proton clusters penetrates through normal core of a singly quantized quark vortex. Due to the Meissner effect, the screening supercurrents will arise and a neutral vortex will become much alike a magnetic vortex in a type II superconductor. Eqs. (23) and (24) can be rewritten as follows

$$\lambda_q^2\ \mathrm{curl}\ \mathrm{curl}\vec{B}_x+\vec{B}_x = \Phi\vec{e}_z\sum_i\delta\left(\vec{r}-\vec{r}_i\right), \tag{37}$$

$$\mathrm{curl}\vec{B}_y = 0, \tag{38}$$

where $\Phi=3\Phi_{cl}$. The solution of Eq. (37) is well known from the theory of ordinary superconductors:

$$\vec{B}_x\left(\vec{r}\right)=\frac{\Phi\vec{e}_z}{2\pi\lambda_q^2}\sum_i K_0\left(\frac{|\vec{r}-\vec{r}_i|}{\lambda_q}\right). \tag{39}$$

Therefore the triangular lattice of quark "magnetic vortices" is present in the rotating CFL phase. A very crude estimate of the mean magnetic field B^q in the quark core is: $B^q=3\Phi_{cl}N_v/a^2$, where $N_v=10^{13}\omega$. Thus, we find $\mathrm{B}^q=3.75\cdot 10^{10}G$ for $\omega=200s^{-1}$, and $a=10^5cm$.

5. Solution of Ginzburg-Landau Equations

Let us rewrite equations (16) and (17), by taking into account the lattice of "magnetic vortices", in the following form:

$$\lambda_q^2 \text{ curl curl}\vec{A} + \sin\ ^2\alpha\vec{A} = \vec{f}\sin\ \alpha - \sin\ \alpha\cos\alpha\vec{G}, \quad (40)$$

$$\lambda_q^2 \text{ curl curl}\vec{G} + \cos^2\alpha\vec{G} = \vec{f}\cos\alpha - \sin\ \alpha\cos\alpha\vec{A}, \quad (41)$$

where $\vec{f}$ obeys the equation

$$\text{curl curl}\vec{f} = 0. \quad (42)$$

If we introduce

$$\vec{A}' = \vec{A} - \frac{\vec{f}}{\sin\ \alpha}, \qquad \vec{G}' = \vec{G} - \frac{\vec{f}}{2\cos\alpha}, \quad (43)$$

then equations (40) and (41) can be rewritten in the form:

$$\lambda_q^2 \text{ curl curl}\vec{A}' + \sin^2\alpha\vec{A}' = -\sin\ \alpha\cos\alpha\vec{G}', \quad (44)$$

$$\lambda_q^2 \text{ curl curl}\vec{G}' + \cos^2\alpha\vec{G}' = -\sin\ \alpha\cos\alpha\vec{A}'. \quad (45)$$

We can define $\vec{G}'$ from (44) as follows

$$\vec{G}' = -\frac{\lambda_q^2 \text{ curl curl}\vec{A}' + \sin\ ^2\alpha\vec{A}'}{\sin\ \alpha\cos\alpha}. \quad (46)$$

From equations (45) and (46) we obtain the following relation

$$\text{curl curl}\vec{G}' = \cot\alpha \text{ curl curl}\vec{A}. \quad (47)$$

The substitution of $\vec{G}'$ from (46) into (47) in the case of $\alpha = const$ yields

$$\lambda_q^2 \text{ curl curl}\vec{M}' + \vec{M}' = 0, \quad (48)$$

$$\vec{M}' = \text{curl curl}\vec{A}'. \quad (49)$$

Thus the function $\vec{A}'$ can be determined by a simultaneous solution of Eqs. (48) and (49), whereas the electromagnetic potential $\vec{A}$ and the gluonic potential $\vec{G}$ can be found from Eqs. (43) and (46). For the solution of equations (46), (48) and (49) we shall require at the quark-hadronic matter boundary both the continuity of the magnetic field and the vanishing of the gluon potentials ($\vec{G} = 0$, e.g. $\vec{A}_3 = 0, \vec{A}_8 = 0$) due to gluon confinement. Also the potential $\vec{G}$ and the magnetic induction can not be infinite within the region of their existence.

Due to the symmetry of the star the functions $\vec{M}', \vec{A}$ and $\vec{G}$ in the spherical coordinates (r, ϑ, φ) have only $\varphi-$components: $M'_\varphi(r,\vartheta)$, $A_\varphi(r,\vartheta)$ and

$G_\varphi(r,\vartheta)$. For the solution of Eq. (48) we make the ansatz $M'_\varphi(r,\vartheta) = M_\varphi(r)\sin\ \vartheta$. Then Eq. (48) can be written as

$$\frac{d^2M_\varphi(r)}{dr^2}+\frac{2}{r}\frac{dM_\varphi(r)}{dr}-\left(\frac{2}{r^2}+\frac{1}{\lambda_q^2}\right)M_\varphi(r)=0. \tag{50}$$

The solution of Eq. (50) is [14]:

$$M_\varphi(r)=\frac{1}{r^2}\left[c'_1(1-\frac{r}{\lambda_q})\exp(\frac{r}{\lambda_q})+c'_2(1+\frac{r}{\lambda_q})\exp(-\frac{r}{\lambda_q})\right]. \tag{51}$$

The condition that $M_\varphi(r)$ tends to zero at the center of the quark core gives $c'_1=-c'_2$, so that

$$M_\varphi(r)=\frac{c_1}{r^2}\left[\sin\ h\frac{r}{\lambda_q}-\frac{r}{\lambda_q}\cosh\frac{r}{\lambda_q}\right]. \tag{52}$$

Substituting the solution (52) into Eq. (49) for $\vec{A}'$ we obtain the following solution

$$A'_\varphi(r,\vartheta)=M'_\varphi(r,\vartheta)+c'_0r\sin\ \vartheta. \tag{53}$$

Therefore the substitution of Eq. (53) into the definition (43) yields

$$A_\varphi(r,\theta)=M'_\varphi(r,\vartheta)+c'_0r\sin\ \vartheta+\frac{f_\varphi(r,\vartheta)}{2\sin\ \alpha}. \tag{54}$$

We will find the unknown function $f_\varphi(r,\vartheta)$ from the solution of Eq. (42) which gives

$$f_\varphi(r,\vartheta)=c_0r\sin\ \vartheta. \tag{55}$$

Using equations (43) and (46), we find the gluonic potential G_φ in the form

$$G_\varphi(r,\vartheta)=\left[\cot\alpha M_\varphi(r,\vartheta)-\tan\alpha c'_0r+\frac{c_0r}{2\cos\alpha}\right]\sin\ \vartheta. \tag{56}$$

We can define the constant c'_0 using gluon confinement condition on the surface of the quark matter core $G_\varphi(a,\vartheta)=0$. This condition will define c'_0 as

$$c'_0=\cot^2\alpha\frac{M_\varphi(a)}{a}+\frac{c_0}{2\sin\ \alpha}, \tag{57}$$

which is to be substituted into Eqs. (54) and (56). We thus obtain the final expressions for electromagnetic and gluonic potentials

$$A_\varphi(r,\vartheta) = \left[M_\varphi(r)+\frac{r}{a}M_\varphi(a)\cot^2\alpha+\frac{c_0r}{\sin\ \alpha}\right]\sin\ \vartheta, \tag{58}$$

$$G_\varphi(r,\vartheta) = \left[M_\varphi(r)-\frac{r}{a}M_\varphi(a)\right]\cot\alpha\sin\ \vartheta. \tag{59}$$

We note that the expression (58) for the electromagnetic potential in a quark core coincides with the analogous one in the 2SC phase [15], but the expression (59) for the gluonic potential differs from analogous one in Ref [15] by its sign.

To conclude this section we mention that the electromagnetic potential in the hadronic phase of a neutron star can be found from the solution (51) by replacing the penetration depth for quark matter λ_q with that for hadronic matter λ_p.

6. The Magnetic Field Components

The components of the magnetic fields in quark and hadronic matter can be found from those of the vector potentials using the formula $\vec{B} = \mathrm{curl}\vec{A}$. In spherical coordinates we have for the case of quark matter the following expressions (for $r \leq a$)

$$B_r^q = \left[\frac{2M_\varphi(r)}{r} + 2\cot^2\alpha\frac{M_\varphi(a)}{a} + \frac{2c_0}{\sin\ \alpha}\right]\cos\vartheta, \tag{60}$$

$$B_\vartheta^q = -\left[\frac{1}{r}\frac{d}{dr}(rM_\varphi(r)) + 2\cot^2\alpha\frac{M_\varphi(a)}{a} + \frac{2c_0}{\sin\ \alpha}\right]\sin\ \vartheta, \tag{61}$$

where $M_\varphi(r)$ is defined by Eq. (52).

We can find the magnetic field in the hadronic matter phase from the solution (51) by taking into account that proton vortices in this phase generate a homogeneous mean magnetic field with amplitude B and direction parallel to the axis of rotation of the star [22]. For the components of the magnetic field $\vec{B^p}$ in the hadronic phase (for $a \leq r \leq R$) we get the following expressions

$$B_r^p = \left[\frac{2A_\varphi(r)}{r} + B\right]\cos\vartheta, \tag{62}$$

$$B_\vartheta^p = -\left[\frac{1}{r}\frac{d}{dr}\left(rA_\varphi\left(r\right)\right) + B\right]\sin\ \vartheta, \tag{63}$$

where

$$A_\varphi\left(r\right) = \frac{c_2}{r^2}\left(1 - \frac{r}{\lambda_p}\right)\exp\left(\frac{r}{\lambda_p}\right) + \frac{c_3}{r^2}\left(1 + \frac{r}{\lambda_p}\right)\exp\left(-\frac{r}{\lambda_p}\right). \tag{64}$$

The external magnetic field $\vec{B^e}$ in the external region ($r \gg R$) has to be dipolar and their components can be written as

$$B_r^e = \frac{2M}{r^3}\cos\vartheta, \quad B_\vartheta^e = \frac{M}{r^3}\sin\ \vartheta, \tag{65}$$

where M is the full magnetic moment of the star. The unknown constants c_0, c_1, c_2, c_3 and M in equations (52), (58), (64) and (65) have to be defined

from the continuity conditions of the magnetic field components at $r = a$ and $r = R$ and from the condition

$$B^q V_1 + B V_2 = \frac{8\pi}{3} M, \tag{66}$$

where B^q is the z component of the magnetic field in the quark matter region with volume V_1 . V_2 is the volume of the hadronic matter region. Here we suppose that the magnetic field in both regions is mainly constant and parallel to the axis of rotation z .

We shall consider the behavior of the magnetic field at distances r much larger than λ_p and λ_q. Also we take into account that $\lambda_q \leq \lambda_p \leq a$, $\lambda_q \leq \lambda_p \leq R$ and $\lambda_q \leq \lambda_p \leq R - a$. Therefore the components of the magnetic field in the different regions of neutron star are: for $r \leq a$

$$B_r^q = \left[\frac{2D}{ar^2} \frac{\exp -\frac{a-r}{\lambda_q}}{\sin\ ^2\alpha + \frac{\lambda_q}{\lambda_p}} \frac{\lambda_q}{\lambda_p} + 2\cot^2\alpha \frac{M_\varphi(a)}{a} + \frac{2c_0}{\sin\ \alpha} \right] \cos\vartheta, \tag{67}$$

$$B_\vartheta^q = -\left[\frac{D}{ar\lambda_p} \frac{\exp -\frac{a-r}{\lambda_q}}{\sin\ ^2\alpha + \frac{\lambda_q}{\lambda_p}} + 2\cot^2\alpha \frac{M_\varphi(a)}{a} + \frac{c_0}{\sin\ \alpha} \right] \sin\ \vartheta, \tag{68}$$

for $a \leq r \leq R$

$$B_r^p = \left[-\frac{2D}{ar^2} \frac{\exp -\frac{r-a}{\lambda_p}}{\sin\ ^2\alpha + \frac{\lambda_q}{\lambda_p}} \frac{\lambda_q}{\lambda_p} + B \right] \cos\vartheta, \tag{69}$$

$$B_\vartheta^p = -\left[\frac{D}{ar\lambda_p} \frac{\exp -\frac{r-a}{\lambda_p}}{\sin\ ^2\alpha + \frac{\lambda_q}{\lambda_p}} + B \right] \sin\ \vartheta, \tag{70}$$

and for $r \geq R$

$$B_r^e = \frac{BR^3}{r^3} \cos\vartheta, \quad B_\vartheta^e = \frac{BR^3}{2r^3} \sin\ \vartheta, \tag{71}$$

where

$$D = \frac{Ba^3}{2} \sin\ ^2\alpha - c_0 a^3 \sin\ \alpha. \tag{72}$$

As can be seen from obtained solutions, the magnetic field in both quark and hadronic phases depends on r only very close to the phase boundary at $r = a$. So we conclude that in the main part of the volume of the quark and hadron phases the magnetic field is constant and directed parallel to the rotation axis of the star, see the solutions (67) - (70). In this approximation the condition

(66) is satisfied. Therefore inserting in Eq. (66) the relation $M = BR^3/2$, see Eq. (71), we have

$$B^q = 2\cot^2\alpha \frac{M_\varphi(a)}{a} + \frac{2c_0}{\sin\ \alpha} = B. \tag{73}$$

Solving equations (72) and (73) we finally obtain

$$c_0 = \frac{B\sin\ \alpha}{2}, \quad D = 0\,. \tag{74}$$

Thus in this approximation the magnetic field $\vec{B}$ enters from the hadronic phase into the CFL quark phase in the form of quark magnetic vortices. The transition zone is of the order $\lambda_q + \lambda_p$ which entails that quantity D is small, of the order $(\lambda_p + \lambda_q)/a$, so that the condition $D = 0$ is well fulfilled.

7. Summary

We have investigated the behavior of the magnetic field of a rotating neutron star with superconducting CFL quark matter core in the framework of the Ginzburg-Landau theory. We take into account the simultaneous coupling of the CFL diquark condensate field to the usual magnetic and gluomagnetic gauge fields. We have solved the Ginzburg-Landau equations for this problem by properly taking into account the boundary conditions, in particular the gluon confinement condition. The rotation of the CFL condensate produces neutral quantized vortices with normal cores. We have found the distribution of the magnetic field in CFL quark and hadronic phases of a neutron star and have shown that the magnetic field penetrates into the quark core through the normal cores of rotational vortices . Therefore equivalent "magnetic vortices" are formed in the CFL phase due to the presence of Meissner currents. Thus, the CFL diquark condensate in the external magnetic field is like an "equivalent" type II superconductor.

Acknowledgments

D. M. Sedrakian and K. M. Shahabasyan acknowledge the support from CRDF/NFSAT award No. 12006 PH 067-02. D. M. S. also acknowledges the ISTC support at Yerevan State University by ISTC grant A-353.

References

[1] M. Alford, K. Rajagopal, F. Wilczek, Phys. Lett., B 422, 247, 1998.

[2] R. Rapp, T. Schafer, E.V. Shuryak, M. Velkovsky, Phys. Rev. Lett., 81, 53, 1998.

[3] G.W. Carter, D. Diakonov, Phys.Rev. D 60, 010004.

[4] D. Blaschke, C.D. Roberts, Nucl. Phys. A 642, 197, 1998.

[5] J.C.R. Bloch, C.D. Roberts, S.M. Schmidt, Phys.Rev. C 60, 65208, 1999.

[6] B.C. Barrois, Nucl. Phys. B 129, 390, 1977.

[7] D. Bailin, A.Love, Phys. Rep., 107, 325, 1984.

[8] M. Alford, K. Rajagopal, F. Wilczek, Nucl. Phys. B 537, 443, 1999.

[9] T. Schafer, F. Wilczek, Phys. Rev. Lett. 82, 3956, 1999.

[10] T. Schafer, Nucl. Phys. B 575, 269, 2000.

[11] D. Blaschke, D.M. Sedrakian, K.M. Shahabasyan, Astron.& Astrophys. 350, L 47, 1999.

[12] M. Alford, J. Berges, K. Rajagopal, Nucl. Phys. B 571, 269, 2000.

[13] D. Blaschke, D.M. Sedrakian, nucl-th/ 0006038, 2000.

[14] D.M. Sedrakian, D. Blaschke, K.M. Shahabasyan, D.N. Voskresenky, Astrofizika 44, 443, 2001.

[15] D.M. Sedrakian, D. Blaschke. Astrofizika, 45, 203, 2002.

[16] E.V. Gorbar, Phys. Rev. D 62, 014007, 2000.

[17] K. Iida, G. Baym, Phys. Rev. D 63, 074018, 2001.

[18] R.D. Pisarski, D.H. Rischke, Phys. Rev. Lett. 83, 37, 1999.

[19] K. Iida, G. Baym, Phys. Rev. D 66, 0114015, 2002.

[20] D.M Sedrakian, K.M. Shahabasyan, A.G. Movsesyan, Astrofizika 19, 303, 1983.

[21] A.D. Sedrakian, D.M. Sedrakian, Ap. J. 447, 305, 1995.

[22] D.M. Sedrakian, Astrofizika, 43, 377, 2000.

THERMAL COLOR-SUPERCONDUCTING FLUCTUATIONS IN DENSE QUARK MATTER

D.N. Voskresensky
Gesellschaft für Schwerionenforschung mbH, Planckstr. 1, 64291 Darmstadt, Germany; Moscow Institute for Physics and Engineering, Kashirskoe sh. 31, Moscow 115409, Russia
D.Voskresensky@gsi.de

Abstract Thermal fluctuations of the color superconducting order parameter in dense quark matter are investigated in terms of the phenomenological Ginzburg - Landau approach. Our estimates show that fluctuations of the diquark gap may strongly affect some of the thermodynamic quantities even far below and above the critical temperature. If the critical temperature T_c of the diquark phase transition were rather high ($\gtrsim (50 \div 70)$ MeV) one could expect a manifestation of fluctuations of the diquark gap in the course of heavy ion collisions (above T_c). For $T_c \sim 50$ MeV color superconducting fluctuations may also affect an initial stage of the hybrid star evolution.

Keywords: color superconductivity, order parameter, temperature, fluctuations

1. Introduction

The quark-quark interaction in the color antitriplet channel is attractive driving the pairing, cf. [1]. The problem has been re-investigated in a series of papers following Refs. [25, 3], see review [4] and Refs. therein. The attraction comes from the one-gluon exchange, or from a nonperturbative 4-point interaction motivated by instantons [5], or nonperturbative gluon propagators [6]. The zero-temperature pairing gap Δ was predicted to be $\sim (20 \div 200)$ MeV for the quark chemical potentials $\mu_q \sim (300 \div 500)$ MeV. In the standard BCS theory, cf. [4], the critical temperature is estimated as $T_c \simeq 0.57\Delta$.

One expects the diquark condensate to dominate the physics at densities beyond the deconfinement/chiral restoration transition and below the critical temperature. Various phases are possible. E.g., the so called 2-color superconductivity (2SC) phase allows for unpaired quarks of one color. There may also exist a color-flavor locked (CFL) phase [7] for not too large value of the strange quark mass m_s, for $2\Delta > m_s^2/\mu_q$, cf. [8], where the color superconductivity

D. Blaschke and D. Sedrakian (eds.), Superdense QCD Matter and Compact Stars, 277–295.

(CSC) is complete in the sense that the diquark condensation produces a gap for quarks of all three colors and flavors. The values of the gap are of the same order of magnitude for 2SC and CFL phases, whereas relations between critical temperature and the gap might be different, $T_c \simeq 0.57\Delta$ for 2SC and $T_c \simeq 0.7\Delta$ for CFL phase [9]. There are also another possibilities, e.g., of pairing in the spin-one channel, for which the pairing gap proves to be small $\Delta \lesssim 1$ MeV, see [9].

The high-density phases of QCD at low temperatures may exist in the interiors of most massive neutron stars (so called hybrid stars containing a quark core and a hadron shell) affecting the cooling, rotation and magnetic field, cf. [10–12]. It is also possible to ask: Is CSC relevant for terrestrial experiments? To produce color superconducting matter in the laboratory one would need to cook a dense and not too hot baryon enriched matter. The nuclear matter prepared in heavy ion collisions at SIS, AGS, SPS or RHIC in all the cases has presumably not sufficiently high baryon density and, on the other hand, the matter prepared at SPS or RHIC is feasibly too hot in order to expect a manifestation of the CSC. The most relevant is probably the GSI "Compressed baryon matter" future heavy ion collision facility which may cook a sufficiently dense and not too hot state. Baryon densities up to ten normal nuclear matter density ($\lesssim 10\rho_0$) at temperatures $T \lesssim 170$ MeV are expected to be reached at an initial collision stage. It is supposed that the system is in the quark-gluon plasma state at such conditions. Then the system expands and cools down. In this process the temperature decreases down to $T \sim 140$ MeV at still rather high baryon density at an intermediate collision stage. Although the temperatures at relevant densities are most likely larger than the critical temperature T_c of CSC, one may raise the question about possible manifestations of precursor phenomena of the CSC phase transition, if T_c is rather high ($T_c \gtrsim (50 \div 70)$ MeV). Recently, ref. [13] considered such a possibility within the Nambu-Jona-Lasinio model and demonstrated that the fluctuating pair field results in a prominent peak of the spectral function, which survives in the temperature interval $|T - T_c| \lesssim (0.1 \div 0.2)T_c$. Besides, it is interesting to investigate the role of the order parameter fluctuations for $T < T_c$, if T_c is ~ 50 MeV, that still may affect the neutrino radiation of the most massive hot neutron stars (if they indeed have quark cores) and the heat transport at an initial stage of their evolution.

This paper is an extended version of the work [14]. We will study precursor phenomena of the CSC in the framework of the phenomenological Ginzburg - Landau approach. To be specific, we will consider condensates with total angular momentum $J = 0$ that are antisymmetric in color and flavor. Such pairing states can occur in the weak coupling limit because one-gluon exchange is attractive in the color anti-triplet channel. Although for reasonable values of densities and temperatures the conditions of applicability of the weak coupling

limit are hardly fulfilled, in order to get a feeling on possible relevance of fluctuation effects we will still use this limit. At the same time we will by hand vary the relation $\Delta(\mu_q)$, since the corresponding exponential dependence is most sensitive to corrections of the running QCD coupling constant compared to its perturbative value. We will restrict our discussion by the consideration of phases, which feasibly have large gaps, like 2SC and CFL, as the most interesting case for applications.

2. Physics of pairing fluctuations

Like there always exists a vapor under the water, there are excitations on the ground of any condensate. They appear due to quantum and thermal fluctuations. In classical systems and also at not too small temperatures in quantum systems, quantum fluctuations are suppressed compared to thermal fluctuations. Excitations are produced and dissolved with the time passage, although the mean number of them is fixed at given temperature. Pairing fluctuations are associated with formation and breaking of excitations of a particular type, Cooper pairs out of the condensate. Fluctuation theory of phase transitions is a well developed field. In particular, ten thousands of papers in condensed matter physics are devoted to the study of pairing fluctuations. At this instant we refer to an excellent review of Larkin and Varlamov [15].

In some phenomena pairing fluctuations behave similarly to quasiparticles. However there are also differences:

- Typical "binding energy" $E_{\rm bind}$ of pairing fluctuation is of the same order as inverse life-time $\tau_{l.t.}^{-1} \propto 1/|T - T_c|$, whereas for quasiparticles $E \gg \tau_{l.t.}^{-1}$.

- Typical size $l \propto 1/\sqrt{|T - T_c|}$ is large for T near T_c. Quasiparticles have a small typical size.

- Fluctuations near T_c behave as classical fields in sense of Rayleigh-Jeans: 3-momentum distribution is $n(p) \sim T/E(p)$ in the vicinity of T_c.

We will demonstrate below that the Ginzburg number ($Gi = \Delta T/T_c$), which determines the broadness of the energy region near the critical temperature, where fluctuations essentially contribute, is $Gi \sim A(T_c/\mu_q)^4$ with $A \sim 500$ in our case. To compare, for clean metals $A \sim 100$, $\mu_q \to \mu_e$, the latter is the electron chemical potential. Thus $Gi \sim 1$, if T_c is rather high, $T_c \sim (\frac{1}{3} \div \frac{1}{5})\mu_q$, and we expect a broad region of temperatures, where fluctuation effects might be important.

3. Thermodynamical potential and its mean field solution

The Fourier component of the density of the thermodynamic potential (thermodynamic potential per unit volume V) in the superconducting quark matter with the diquark pairing can be written in the following form [12, 16], cf. also [1, 11],

$$\widetilde{\Omega} = \widetilde{\Omega}_n + \sum_{\alpha,i}(-c_0|\partial_\tau d^i_\alpha|^2 + c|\nabla d^i_\alpha|^2) + aD + \frac{b}{2}D^2\,, \qquad (1)$$

$$D = \sum_{\alpha,i}|d^i_\alpha|^2,\ \ \gamma = \frac{1}{D^2}\sum_{\alpha,\beta,i}|d^{i,*}_\alpha \cdot d^i_\beta|^2,\ \ b = b_1 + \gamma b_2\,.$$

The Greek indices $\alpha, \beta = \{R, B, G\}$ count colors, the Latin indices $i = \{u, d, s\}$ count flavors. The expansion is presented up to the fourth order in the diquark field operators (related to the gap) assuming the second order phase transition, although at zero temperature the transition might be of the first order, cf. [17]. $\widetilde{\Omega}_n$ is the density of the thermodynamic potential of the normal state. The order parameter squared is $D = |\vec{d}_{\rm IS}|^2 = |\vec{d}_R|^2 + |\vec{d}_G|^2 + |\vec{d}_B|^2$, $\vec{d}_R \| \vec{d}_G \| \vec{d}_B$ for the isoscalar phase (IS), and $D = 3|\vec{d}_{\rm CFL}|^2$, $|\vec{d}_R|^2 = |\vec{d}_G|^2 = |\vec{d}_B|^2 = |\vec{d}_{\rm CFL}|^2$, $\vec{d}^*_R \cdot \vec{d}_G = \vec{d}^*_G \cdot \vec{d}_B = \vec{d}^*_B \cdot \vec{d}_R = 0$ for the CFL phase, $\vec{d}_\alpha = \{d^u_\alpha, d^d_\alpha, d^s_\alpha\}$. The so called 2SC phase is the IS phase with unpaired quarks of one color (to say R). The interaction of the diquark field with fluctuation gluon fields is usually introduced in the standard way through the corresponding gauge-shifted full covariant derivatives. Recent paper [18] demonstrated that the gluon fluctuations contribute essentially to thermodynamic quantities only at temperatures in a narrow vicinity of the critical temperature, $\Delta T/T_c \lesssim 0.1$ for relevant values of parameters. In this rather small temperature interval, ΔT, gluon field fluctuations change the nature of the phase transition (from the second to the first order). As we will show below, the value ΔT is much less than the temperature region, where fluctuations of the diquark order parameter might be important. Thereby in the latter discussion we suppress the gluon fields as well as the discussion of any peculiarities of this narrow temperature region near T_c.

Near the critical point coefficients of (1) can be expanded in $t = (T - T_c)/T_c$. In the weak coupling limit they render:

$$a = a_0 \ln(T/T_c) \simeq a_0 t,\ \ a_0 = \frac{2\mu_q^2}{\pi^2}, \qquad (2)$$

$$b_1 = b_2 = b/(1+\gamma) = \frac{7\zeta(3)\mu_q^2}{8\pi^4 T_c^2},\ \ c = \frac{b}{3(1+\gamma)},\ \ c_0 = 3c.$$

For the classical (mean) fields $\gamma = 1$ in the IS phase and $\gamma = 1/3$ in the CFL phase, cf. [12], $\mu_q = \mu_B/3$, μ_B is the baryon chemical potential (the contri-

bution of the strange quark mass is neglected), $\zeta(3) = 1.202...$ The critical temperature T_c is the same for the IS and the CFL phases for $m_s \to 0$. For $m_s \neq 0$, T_c would depend on m_s that would result in a smaller T_c for the CFL phase than for the IS phase.

The value of the order parameter follows by solving the equation of motion for the field operators, $\delta\widetilde{\Omega}/\delta d^i_\alpha = 0$:

$$-c_0\partial_\tau^2 d^i_\alpha + c\Delta d^i_\alpha - a d^i_\alpha - bD d^i_\alpha = 0. \tag{3}$$

The stationary, spatially-homogeneous mean field solution of (3) (without taking into account of fluctuations) is

$$D_{\rm MF} = -a\Theta(-t)/b, \;\; \delta\widetilde{\Omega}_{\rm MF} = -\frac{a^2}{2b}\Theta(-t), \tag{4}$$

where the step function $\Theta(-t) = 1$ for $t < 0$ and $\Theta(-t) = 0$ for $t > 0$.

To be specific, discussing $T < T_c$ we further consider the CFL case. For the finite system of a large spherical size $R \gg \xi$, with ξ having the meaning of the coherence length, we obtain

$$d^i_{\alpha,{\rm MF}} = \pm\frac{\delta^i_\alpha}{(N_cN_f)^{1/4}}\sqrt{D_{\rm MF}}\,\Theta(-t)\,{\rm th}\left[\frac{(R-r)}{\sqrt{2}\,\xi}\right], \;\; \xi = \sqrt{\frac{c}{|a|}}, \tag{5}$$

where $N_c = 3$ is the number of colors, $N_f = 3$ is the number of flavors and to be specific we assumed the simplest structure $d^i_{\alpha,{\rm MF}} \propto \delta^i_\alpha$.

4. Fluctuations of gap in self-consistent Hartree approximation

Now we will consider fluctuations. Below T_c we present d^i_α, as $d^i_\alpha = d^i_{\alpha,c} + d^{i,\prime}_\alpha$, and above T_c, as $d^i_\alpha = d^{i,\prime}_\alpha$, where index "c" labels the classical solution.

Since $\delta\widetilde{F}(V,T) = \delta\widetilde{\Omega}(\mu,T)$, cf. [19], the density of the free energy of the CFL phase expanded in $(d^{i,\prime}_\alpha)^2$ terms renders

$$\begin{aligned}
\delta\widetilde{F} &= \delta\widetilde{F}_c + \delta\widetilde{F}' = \sum_{\alpha,i}(-c_0|\partial_\tau d^i_{\alpha,\,c}|^2 + c|\nabla d^i_{\alpha,\,c}|^2) + aD_c \\
&+ \frac{b_1+b_2/3}{2}D_c^2 + \frac{5}{3}(b_1+b_2/3)D_cN_cN_f\sum_k|\phi'_k|^2 \\
&+ N_cN_f\sum_k\left(-c_0\omega^2 + c\vec{k}^{\,2} + a\right)|\phi'_k|^2 \\
&+ \nu_H\frac{b_1+b_2}{2}[N_cN_f\sum_k|\phi'_k|^2]^2.
\end{aligned} \tag{6}$$

The last term is introduced within the self-consistent Hartree approximation (within the Φ functional up to one vertex), $\nu_H = 10/9$ accounts different coefficients in Φ functional for the self-interaction terms (d^4 - for the given field d and $(d^i_\alpha)^2(d^j_\beta)^2$ terms), cf [20]. We presented $d^{i,\prime}_\alpha = \sum_k d^{i,\prime}_{\alpha,k} e^{-ik^\mu x_\mu}$, $k^\mu = (\omega, \vec{k})$, $x_\mu = (\tau, -\vec{r})$, and introduced the notation

$$\sum_{i,\alpha,k} |d^{i,\prime}_{\alpha,k}|^2 = \sum_k |\phi'_k|^2 = i \int \frac{d^4k}{(2\pi)^4} \frac{1}{c_0\omega^2 - c\vec{k}^{\,2} - m^2}. \tag{7}$$

In Matsubara technique the temperature dependence is introduced by the replacements: $\omega \to \omega_n = 2\pi i n T$, $-i\int \frac{d^4k}{(2\pi)^4} \to T\sum_{n=-\infty}^{n=\infty} \int \frac{d^3k}{(2\pi)^3}$. We restricted ourselves by the self-consistent Hartree approximation. Effects of the damping of fluctuations, being produced by the two- and more vertex diagrams of Φ, are beyond the scope of this simple approximation. As we argue below, the main effects we discuss in this paper are not essentially affected by the width terms.

Variation of Eq. (5) over ϕ'_k yields the spectrum of fluctuations

$$c_0\omega^2 - c\vec{k}^{\,2} - m^2 = 0, \tag{8}$$

with the squared mass parameter

$$m^2 = \eta|a| = \frac{5}{3}(b_1 + b_2/3)D_c + a + \nu_H(b_1 + b_2)N_cN_f \sum_k |\phi'_k|^2 . \tag{9}$$

Notice that the real physical meaning of the effective mass has the quantity $m/\sqrt{c_0}$ rather than m, as follows from (8).

Solution of the equation for the fluctuating field presented in the coordinate space is characterized by the length scale $l = \xi/\sqrt{\eta}$ and by the time scale $\widetilde{\tau} = \xi c_0^{1/2}(c\eta)^{-1/2}$. Above the critical point $D_c = 0$, $m^2 = a + O(\sum_k |\phi'_k|^2) > 0$, and neglecting $|\phi'_k|^2$ terms one gets the parameter $\eta \simeq 1$.

Variation of (5) over $d^{i,*}_{\alpha,c}$ yields the equation of motion for the classical field

$$-c_0\partial^2_\tau d^i_{\alpha,c} + c\Delta d^i_{\alpha,c} - \left(a + \frac{5}{3}(b_1 + b_2/3)N_cN_f \sum_k |\phi'_k|^2\right) d^i_{\alpha,c}$$
$$-(b_1 + b_2/3)D_c d^i_{\alpha,c} = 0. \tag{10}$$

Only dropping the term responsible for fluctuations we find $D_c = D_{\rm MF}$, $d^i_{\alpha,\,c} = d^i_{\alpha,\,\rm MF}$, $m^2 = m^2_{\rm MF} = \eta_{\rm MF}|a|$ for $T < T_c$, cf. (4), (9), and we obtain $\eta_{\rm MF} = 2/3$. In reality fluctuations affect the classical solution and renormalize the critical temperature of the phase transition T_c yielding $T_c^{\rm ren} < T_c$. More

generally

$$m^2 = m^2_{\rm MF} + \delta m^2, \quad \delta m^2 = -\frac{5}{3}(b_1 - b_2/9)N_c N_f \sum_k |\phi'_k|^2, \tag{11}$$

for $T < T_c^{\rm ren}$. From (9), (11) one finds $D_c(m^2 = 0) = 0$, as the consequence of the self-consistency of our approximation scheme. As we have mentioned, we neglected fluctuations of the gluon fields, which change the nature of the phase transition but yield only a small jump of the order parameter.

5. Contribution of fluctuations of gap to specific heat below T_c

In order to demonstrate how fluctuations of the order parameter may affect thermodynamic quantities let us calculate the contribution of fluctuations to the specific heat density $\widetilde{C}_V = -T\left(\frac{\partial^2 \delta \widetilde{F}}{(\partial T)^2}\right)_V$, cf. [19]. The mean field contribution is

$$\widetilde{C}_V^{\rm MF} = T\frac{a_0^2}{bT_c^2}\Theta(-t), \tag{12}$$

as it follows from (1), (2) and (4). Here and below we use an approximate expression $a \simeq a_0 t$ valid at T near T_c, see (2). The contribution to the specific heat from the normal quark excitations is suppressed as $\propto T^{-3/2}e^{-\Delta(0)/T}$ for $T \ll T_c$, cf. [21]. We may reproduce correct low temperature behavior multiplying (12) by a formfactor $f \simeq 2e^{-\Delta(0)/T}(T_c/T)^{5/2}(1 - \frac{2T}{3T_c})^{-1}$.

The fluctuation contribution $\widetilde{F}'$ can be determined with the help of the functional integration

$$\exp(-\delta W) = \int D\phi' \exp(-\delta W[\phi']), \tag{13}$$

where δW is an effective potential. Using (13), (5) we obtain

$$\delta \widetilde{F}' = -iN_c N_f \int \frac{d^4k}{(2\pi)^4} \ln[c_0\omega^2 - c\vec{k}^2 - m^2]. \tag{14}$$

Again within the Matsubara technique one still should do the replacement $\omega \to \omega_n = 2\pi i n T$, $-i\int \frac{d^4k}{(2\pi)^4} \to T\sum_{n=-\infty}^{n=\infty} \int \frac{d^3k}{(2\pi)^3}$. We dropped an infinite constant term in (14). However expression (14) still contains a divergent contribution. To remove the regular term that does not depend on the closeness to the critical point we find the temperature derivative of (14) (entropy per unit volume):

$$\delta \widetilde{S}' = \frac{\partial \delta \widetilde{F}'}{\partial T} = \frac{\partial m^2}{\partial T} N_c N_f \sum_k |\phi'_k|^2. \tag{15}$$

The contribution of fluctuations to the specific heat density is then given by

$$\begin{aligned}\widetilde{C}'_V &= -T\frac{\partial m^2}{\partial T}N_cN_f\frac{\partial\sum_k|\phi'_k|^2}{\partial T} - T\frac{\partial^2 m^2}{\partial T^2}N_cN_f\sum_k|\phi'_k|^2 \\ &\simeq -T\frac{\partial m^2_{\rm MF}}{\partial T}N_cN_f\frac{\partial\sum_k|\phi'_k|^2}{\partial T},\ \ \frac{\partial m^2_{\rm MF}}{\partial T}\simeq-\eta_{\rm MF}a_0/T_c. \quad (16)\end{aligned}$$

In the second line (15) we remained only the terms quadratic in fluctuation fields, i.e. we assumed $|\frac{\partial m^2_{\rm MF}}{\partial T}|\gg|\frac{\partial\delta m^2}{\partial T}|$.

Knowing the contribution of fluctuations to the entropy and specific heat we may recover their contribution to the free energy and energy densities

$$\delta\widetilde{F}'=\int_0^T\widetilde{S}'|_{\rho_q}dT,\quad \delta\widetilde{E}'=\int_0^T\widetilde{C}'_V|_{\rho_q}dT. \quad (17)$$

With (15) – (17) one may recover fluctuation contribution to all thermodynamic quantities.

Now we are able to calculate the quantity $iG^{--}(X=0)=\sum_k|\phi'_k|^2$ and its temperature derivative, where $iG^{--}(X)$ is the time-ordered Green function. Using the Matsubara replacement $\omega\to\omega_n=2\pi inT$ and the relation $\sum_n(y^2+n^2)^{-1}=\frac{\pi}{y}{\rm cth}(\pi y)$, or the corresponding relation between the non-equilibrium Green functions $iG^{--}(X)$ and ${\rm Im}G^{ret}$ at finite temperature, we arrive at the expression

$$\sum_k|\phi'_k|^2=\frac{1}{2\sqrt{c_0}}\int\frac{d^3k}{(2\pi)^3}\frac{1}{\sqrt{c\vec{k}^{\,2}+m^2}}{\rm cth}\left(\frac{\sqrt{c\vec{k}^{\,2}+m^2}}{2T\sqrt{c_0}}\right). \quad (18)$$

Using that ${\rm cth}(y/2)=2n_B(y)+1$, where $n_B(y)=(e^y-1)^{-1}$ are Bose occupations, and dropping the regular contribution of quantum fluctuations we obtain

$$\sum_k|\phi'_k|^2_T=\frac{1}{\sqrt{c_0}}\int\frac{d^3k}{(2\pi)^3}\frac{1}{\sqrt{c\vec{k}^{\,2}+m^2}}n_B\left(\frac{\sqrt{c\vec{k}^{\,2}+m^2}}{T\sqrt{c_0}}\right). \quad (19)$$

By index "T" we indicate the thermal contribution.

The integration is performed analytically in the limiting cases. Let $m\gg T\sqrt{c_0}$. Then $n_B(y)\simeq e^{-y}$. In the very same approximation one has $c\vec{k}^2\ll m^2$ for typical momenta. Then

$$\sum_k|\phi'_k|^2_T=\frac{c_0^{1/4}}{8m}\left(\frac{2mT}{\pi c}\right)^{3/2}\exp\left(-\frac{m}{T\sqrt{c_0}}\right),\ \ m\gg2T\sqrt{c_0}\,. \quad (20)$$

In the opposite limiting case, $m\ll2T\sqrt{c_0}$, there are two contributions to the integral (19), from the region of typical momenta $c\vec{k}^{\,2}\sim m^2$ and from the

region $c\vec{k}^2 \gg m^2$. They can be easily separated, if one calculates the auxiliary quantity $\frac{\partial \sum_k |\phi_k'|^2}{\partial T}$. In the region $c\vec{k}^2 \sim m^2$ one may use an approximation $n_B(y) \simeq 1/y$ and

$$\frac{\partial \sum_k |\phi_k'|^2}{\partial T}[c\vec{k}^2 \sim m^2] \simeq -(4\pi c^{3/2})^{-1} T \frac{\partial m}{\partial T}. \tag{21}$$

The region $c\vec{k}^2 \gg m^2$ yields a regular term

$$\sum_k |\phi_k'|^2 [c\vec{k}^2 \gg m^2] \simeq \frac{T^2}{12}\sqrt{\frac{c_0}{c^3}}, \quad \frac{\partial \sum_k |\phi_k'|^2}{\partial T}[c\vec{k}^2 \gg m^2] \simeq \frac{T}{6}\sqrt{\frac{c_0}{c^3}}\,. \tag{22}$$

General expression for the fluctuation contribution to the specific heat is given by the first line (15) and can be resolved with the help of the self-consistent solution of (11), (19) (or (20), (21), (22) in the limiting cases). Assuming for rough estimates that fluctuations can be described perturbatively and putting $m^2 \simeq m_{\rm MF}^2 = \eta_{\rm MF}|a|$, from the second line of (15) we find for $T \ll \frac{m_{\rm MF}}{\sqrt{c_0}}$:

$$\begin{aligned} \widetilde{C}_V' &\simeq \frac{N_c N_f \eta_{\rm MF}^{7/4}\, c^{1/4}\, T^{3/2}}{4\,\pi^{3/2}\sqrt{2}\, c_0^{1/4}\, |t|^{1/4} T_c^2} \\ &\times \left(\frac{a_0}{c}\right)^{7/4} \left(1 + \frac{2|t|T_c}{T}\right) \exp\left(-\frac{\sqrt{\eta_{\rm MF} a_0 |t|}}{T\sqrt{c_0}}\right) \end{aligned} \tag{23}$$

and for $T \gg \frac{m_{\rm MF}}{\sqrt{c_0}}$:

$$\widetilde{C}_V' \simeq \frac{N_c N_f \eta_{\rm MF}^{3/2}\, T^2}{8\pi T_c^2 |t|^{1/2}} \left(\frac{a_0}{c}\right)^{3/2} + \frac{N_c N_f \eta_{\rm MF} T^2}{6 T_c} \frac{a_0}{c} \left(\frac{c_0}{c}\right)^{1/2}. \tag{24}$$

In the weak coupling limit for the CFL phase $a_0/c = 6\pi^2 T_c^2/(7\zeta(3)/8)$, $c_0 = 3c$, $\eta_{\rm MF} = 2/3$. Eq. (22) holds in the low temperature limit $T \ll \pi(|t|/3)^{1/2}\, T_c$, whereas Eq. (24) is valid in the opposite limit. The first term in (24) dominates over the second one for $|t| < 0.7$, i.e., in the whole region of validity of (24) the main term is the first one. Its singular behavior, $\sim 1/\sqrt{|t|}$, is typical for the specific heat in the vicinity of the critical point of the second order phase transition, as in metallic superconductors.

Also in the CFL phase ($T < T_c$) there is a contribution to the specific heat of Goldstone-like excitations, cf. phonons in the ordinary condensed matter. For $T \gg m_{p.G}$, where $m_{p.G}$ is the mass of the pseudo-Goldstone excitation, we get

$$\widetilde{C}_V^{p.G.\prime} = \frac{N_G 3^{3/2} \pi^2 T^3}{30}, \tag{25}$$

where N_G is the number of pseudo-Goldstone modes. One can see that the contribution (25) is numerically small compared to those terms (cf. (22), (24)) we have evaluated for temperatures within the fluctuation region.

Now we are able to discuss the validity of the self-consistent Hartree approximation in our problem. Adding the contribution to Φ functional with two vertices produces the sun-set diagram in the diquark self-energy. In such a way beyond the Hartree approximation there appears the width term in the self-energy (behaving as $-i\gamma\omega$ for small ω). Such a term governs the slow relaxation of the order parameter in the phase transition phenomena outside the equilibrium. In our case (thermal equilibrium) this term can be dropped compared to the $c_0\omega^2$ term, which we have in the thermodynamic potential (1) from the very beginning, at least in both the low and high temperature limits. Indeed, in the low temperature limit three Green functions entering the sun-set diagram produce an extra exponentially small particle occupation factor compared to that governs the Hartree term (20). Near T_c, i.e. in the high temperature limit, we may remain only $n = 0$ term in the Matsubara sum over frequencies, as we have argued, thus suppressing both the linear and the quadratic terms in ω.

6. Ginzburg – Levanyuk criterion and Ginzburg number

Comparing the mean field (12) and the fluctuation (15) contributions to the specific heat (in the low and high temperature limiting cases one may use Eqs. (22), (24)) we may estimate the fluctuation temperature $T^C_{\rm fl,<} < T_c$, at which the contribution of fluctuations of the order parameter becomes to be as important as the mean field one (so called Ginzburg - Levanyuk criterion),

$$\widetilde{C}'_V \simeq \widetilde{C}^{\rm MF}_V, \ \text{ for } \ T < T_c. \tag{26}$$

Fluctuations dominate for $T > T^C_{\rm fl,<}$. For typical values $\mu_q \sim (350 \div 500)$ MeV and for $T_c \gtrsim (50 \div 70)$ MeV in the weak coupling limit from (26), (22) we estimate $T^C_{\rm fl,<} \simeq (0.6 \div 0.8)T_c$. If we took into account the suppression factor f of the mean field term $\propto e^{-\Delta(0)/T}$, a decrease of the mass m due to the fluctuation contribution (cf. (11)), and the pseudo-Goldstone contribution (25), we would get still smaller value of $T^C_{\rm fl,<}$ ($\lesssim 0.5T_c$). We see that fluctuations start to contribute at temperatures when one can still use approximate expressions (22), (20) valid in the low temperature limit. Thus the time (frequency) dependence of the fluctuating fields is important in case of CSC.

In the condensed matter physics one usually performs calculations in the high temperature limit. In this limit one neglects the time (frequency) dependent terms considering quasi-static thermal fluctuations of the order parameter. Then the fluctuation contribution is determined with the help of the functional

integration

$$\exp(-\delta F'/T) = \int Dd' \exp(-\delta F'[d']/T), \quad (27)$$
$$\delta F'[d'] = \sum_{i,\alpha,\vec{k}} (c\vec{k}^{\,2} + \eta|a|)(d^{i,\,\prime}_{\alpha,\,\vec{k}})^2.$$

The integration yields

$$\delta\widetilde{F}' = TN_fN_c \int \frac{d^3k}{(2\pi)^3} \ln[c\vec{k}^{\,2} + \eta|a|]. \quad (28)$$

Comparison of Eqs. (28) and (14) shows that the high temperature expression (28) is recovered, if one drops all the terms except $n = 0$ in the corresponding Matsubara sum over $\omega_n = 2\pi inT$ in Eq. (14). The contribution of $n \neq 0$ terms to the $\sum_k |\phi'_k|^2$ is suppressed in the limit $c_0 4\pi^2 T^2 \gg m^2$. Then one immediately arrives at the specific heat given by the first term of (24). Thus in our case one may suppress the frequency dependence of fluctuations only for $|t| \ll 1$.

Simplifying, the energy width of the fluctuation region, where the fluctuation effects prevail over the mean field ones, is usually estimated following the Ginzburg criterion. The probability of the fluctuation in the volume $V_{\rm fl}$ is given by $W \sim \exp(-\delta\Omega(V_{\rm fl})/T)$. It is ~ 1 for $\delta\Omega(V_{\rm fl}) \sim T$, where $\delta\Omega(V_{\rm fl})$ (the contribution to the thermodynamic potential in the corresponding variables) is the work necessary to prepare the fluctuation within the volume $V_{\rm fl}$. The minimal size of the fluctuation region characterized by an order parameter $d \sim \sqrt{D_{\rm MF}}$ is $\xi(T)\sqrt{2/\eta}$, cf. (5), (8). Thus, taking $\delta\Omega(V_{\rm fl}) = \delta\Omega_{\rm MF}(V_{\rm fl}) = T_{\rm fl}^{\rm G}$ for the typical temperature $T_{\rm fl}^{\rm G}$, when fluctuations start to dominate, we obtain

$$T_{\rm fl}^{\rm G} \simeq \frac{a^2}{2b} \frac{4\pi(\sqrt{2/\eta}\,\xi(T_{\rm fl}^{\rm G}))^3}{3} \simeq \frac{4\pi a_0^{1/2} c^{3/2} |t(T_{\rm fl}^{\rm G})|^{1/2}}{\eta^{3/2} b} \frac{\sqrt{2}}{3}. \quad (29)$$

Although the above estimate is very rough we took care of all the numerical factors. This allows us to notice that the value $T_{\rm fl,<}^{C}$ estimated from (26), if one uses Eq. (24) for $\widetilde{C}'_V$ remaining there only the first term, is $T_{\rm fl,<}^{C} \simeq 0.5|t(T_{\rm fl,<}^{C})/t(T_{\rm fl}^{\rm G})|^{1/2} T_{\rm fl}^{\rm G}$ for $N_c = N_f = 3$. All the dependencies on the parameters in expressions for $T_{\rm fl,<}^{C}$ and $T_{\rm fl}^{\rm G}$ were proven to be essentially the same.

Fluctuation region is determined by the Ginzburg number $Gi = |T_c - T_{\rm fl}^{\rm C}|/T_c$. The larger the value Gi is the broader is the fluctuation region. For clean conventional superconductors [15] $Gi \simeq A(T_c/\mu)^4 \sim 10^{-12} \div 10^{-14}$, $A \sim 80$, whereas for superfluid He^4 and in our case $Gi \sim 1$ (since $A \sim 500$

and T/μ_q can be as large as $\frac{1}{3} \div \frac{1}{5}$ in favorable cases). The role of fluctuations increases in cases, when the effective dimensionality of the droplet decreases or/and when the quark mean free path decreases. Both possibilities result in a significant increase of the Gi-number. In the case of quark droplets of the typical size $L \ll \xi$ one deals with the zero-dimensional system, $Gi \propto \xi^3/L^3$ and the fluctuation contribution to the specific heat behaves as $\widetilde{C}'_V \sim 1/t^2$, for $Gi \ll |t| \ll 1$. For dirty superconductors Gi increases $\propto 1/(p_{Fe} l_e)$, where p_{Fe} is the electron Fermi momentum and l_e is the electron mean free path. A significant decrease of the quark mean free path is expected due to the presence of the hadron impurities inside the quark droplet. Thus, there is still a variety of possibilities for a further enhancement of superconducting fluctuations.

7. Fluctuations of the gap above T_c

All above expressions for fluctuating quantities (except the vanishing of the pseudo-Goldstone contribution above T_c and the appearance of an extra diquark decay contribution to the width) are also valid for $T > T_c$, if one puts $D_c = 0$ in general expressions or $m^2_{\rm MF} = a > 0$, $D_c = 0$, $\eta = \eta_{\rm MF} = 1$ in the corresponding approximate expressions. Above T_c we should compare the fluctuation contribution to a thermodynamic quantity with the quark and gluon contributions of the normal state of the quark-gluon plasma. In the weak coupling limit for the specific heat density of the quark-gluon plasma one has, cf. [22],

$$\widetilde{C}^{qg}_V \simeq 6\mu_q^2 T + \frac{42\pi^2 T^3}{15} + \frac{32\pi^2 T^3}{15}. \tag{30}$$

The first two terms are quark contributions and the third term is the gluon contribution. We omitted a contribution of strange quarks which is rather small for $T < m_s$ and we neglected the temperature dependent effective gluon mass. We also disregarded the α_s corrections to the quark and gluon terms since such corrections were not taken into account for condensate quantities. If we included the quark-gluon masses that appear in the framework of the approach [23] matching the quasiparticle quark-gluon description and the lattice results, we would get even smaller contribution of $\widetilde{C}^{qg}_V$, that is in favor of fluctuation effects.

Above T_c, Eqs. (22) and (24) yield rather smooth functions of T except the region $t \ll 1$. The fluctuation region is rather wide since $\widetilde{C}'_V \sim \widetilde{C}^{qg}_V$ even at T essentially larger then T_c. The appearance of an extra channel of the diquark decay width, $2\gamma_{\rm dec}\omega$, beyond the Hartree approximation does not qualitatively change the situation since $\gamma_{\rm dec}$ is a regular function of T, $\gamma_{\rm dec} \propto T - T_c$, and vanishes in the critical point. Thus the applicability of the high temperature limit (one can put $\omega_n = 0$ in the Matsubara sum) is preserved in a wide temperature region, $T \sim T_c$, [15]. Only far above T_c situation might be

changed. The main uncertainty comes from the values of coefficients (2) which were derived for T rather near T_c and in the weak coupling limit. Bearing all this in mind we estimate the value of the fluctuation temperature $T^C_{\rm fl,>} \sim 2T_c$ for typical value $T_c/\mu_q \sim 0.1 \div 0.3$. The higher this ratio is, the stronger is the contribution of fluctuations at the given ratio T/T_c. Note that a decrease of μ_q with increase of the temperature results in an increase of the ratio $T_c/\mu_q(T)$. On the other hand μ_q should be at least larger than zero temperature gap in order one could speak of any pairing fluctuations at given temperature..

Thus we see that *fluctuations of the diquark gap may essentially contribute to the thermodynamic quantities even well below T_c and above T_c.*

8. Assumptions which we have done

Note that several simplifying assumptions were done. The coefficients (2) were derived for $|t| \ll 1$ in the weak coupling limit neglecting the strange quark mass, but applied in a wider temperature region for may be not sufficiently large μ_q. Only Gaussian fluctuations were taken into account within the self-consistent Hartree approximation. Thus, diquark width effects were assumed to be suppressed. We used the expansion of the thermodynamic potential up to the fourth order terms in the mean field neglecting a small jump in the order parameter due to gluon fluctuations. We incorporated in the thermodynamic quantities only the terms which have a tendency to an irregular behavior near T_c, whereas above T_c the short range correlations begin to be more and more important with the increase of the temperature. Therefore one certainly should be cautious applying above rough estimates outside the region of their quantitative validity. However, as we know from the experience of the condensate matter physics, see [15], such extrapolation equations work usually not too bad even for temperatures well below and above T_c.

9. Fluctuations of temperature, density, magnetic susceptibility

So far we have discussed the specific behavior of fluctuations of the order parameter at fixed temperature and density. There are also fluctuations of the temperature and the local quark density. They are statistically independent quantities [19], $< \delta T \delta\rho_q >= 0$, and their mean squares are

$$< (\delta T)^2 >= \frac{T^2}{V_{\rm fl}\widetilde{C}_V}, \;\; < (\delta\rho_q)^2 >= \frac{T\rho_q}{V_{\rm fl}} \left(\frac{\partial\rho_q}{\partial P}\right)_T . \qquad (31)$$

The averaging is done over the volume, P is the pressure, $V_{\rm fl}$ is as above the volume related to the fluctuation. In the limiting case $\widetilde{C}'_V \ll \widetilde{C}^{qg}_V$, we obtain $< (\delta T)^2 > /T^2 \simeq \rho_q/(N^{\rm fl}_q \widetilde{C}^{qg}_V)$, where $N^{\rm fl}_q$ is the number of quarks involved in the volume $V_{\rm fl}$. Thus, far from the critical point the contribution

of fluctuations is suppressed as $\sqrt{<(\delta T)^2>/T^2} \propto 1/\sqrt{N_q^{\rm fl}}$. This standard fluctuation behavior is essentially changed for $\widetilde{C}_V' \gtrsim \widetilde{C}_V^{qg}$. Then we get even larger suppression of the temperature fluctuations. For $|t| \ll 1$ in the high temperature limit we obtain $\sqrt{<(\delta T)^2>/T_c^2} \sim |t| \to 0$ for $|t| \to 0$, where we assumed that fluctuations are most probable within the typical fluctuation volume $V_{\rm fl} = 4\pi\xi^3/3$ and $\xi \propto 1/\sqrt{|t|}$ for $t \to 0$. Thus, if the system is at the temperature T in a narrow vicinity of T_c, fluctuations of the temperature are significantly suppressed. Being formed at $0 < -t \ll 1$ the condensate region evolves very slowly, since the heat transport is then delayed (the typical evolution time is roughly $\tau \propto 1/\sqrt{|t|}$). At temperatures T outside a narrow vicinity of T_c, fluctuations of the temperature resulting in a significant decrease of the temperature in the volume $V_{\rm fl}$ are rather probable, $\sqrt{<(\delta T)^2>/T_c^2} \sim 1$. This is the consequence of a very short coherence length and, thus, not too large number of quarks contained in the volume $V_{\rm fl}$, $\xi \simeq 0.13/(T_c\sqrt{|t|})$ being $\simeq 0.5$ fm for $T_c \simeq 50$ MeV and for $|t| \sim 1$. Fluctuations of the quark density are also large for typical $|t| \sim 1$, due to the smallness of $V_{\rm fl}$. Thereby, we argue that the system may produce the diquark condensate regions of the typical size ξ, thus feeling the possibility of the phase transition even if its temperature and density are in average rather far from the critical values.

Other quantities associated with second derivatives of the thermodynamic potential are also enhanced near the critical point demonstrating typical $1/\sqrt{|t|}$ behavior, cf. [21]. However numerical coefficients depend strongly on what quantity is studied. E.g. fluctuation contributions above T_c to the color diamagnetic susceptibilities

$$\chi_\alpha = -\left(\partial^2 \delta F/\partial \vec{\mathcal{H}}_\alpha^2\right)_{\vec{\mathcal{H}}_\alpha=0}, \quad \vec{\mathcal{H}}_\alpha = {\rm curl}\vec{\mathcal{A}}_\alpha\,, \tag{32}$$

are proven to be $\ll 1$ everywhere except very narrow vicinity of the critical point. In spite of a smallness, as we know, in metals the fluctuation diamagnetism turns out to be of the order of the Pauli paramagnetism even far from the transition. Also for $T \gg T_c$ contribution of fluctuations to the magnetoconductivity of 2D electron systems is experimentally distinguishable, [15].

10. How gap fluctuations may manifest in heavy ion collisions

Anomalous behavior of fluctuations might manifest itself in the event-by-event analysis of the heavy ion collision data. In small (L) size systems, $L < \xi$, (zero dimension case would be $L \ll \xi$) the contribution of fluctuations of the order parameter to the specific heat is still increased, as we have mentioned, see [15]. The anomalous behavior of the specific heat may affect the heat transport. Also kinetic coefficients are substantially affected by fluctuations due to the shortening of the particle mean free paths, as the consequence of

their rescatterings on diquark fluctuations. If thermalization happened at an initial heavy ion collision stage, and a large size system expands rather slowly, its evolution is governed by the approximately constant value of the entropy. Due to a large contribution to the specific heat (and to the entropy) of diquark fluctuations, an extra decrease of the temperature may occur resulting in an essential slowing of the fireball expansion process (due to smaller pressure). Having the diquark quantum numbers, fluctuations of the gap may affect the dilepton production rate from the quark-gluon plasma, as it has been noted in [13]. Another question is how one can distinguish diquark fluctuations related to the CSC from the quark fluctuations, which may relate to the deconfinement transition? Theoretically, since T_c is, in general, different from the deconfinement transition temperature T_{dec}, in assumption that $T_c > T_{dec}$ there might be two anomalous fluctuation peaks related to two distinct collision energies. E.g., if the observed peak [25] in the K^+/π^+ ratio at $\sim (30 \div 40)$ GeV/A is, indeed, associated with the deconfinement transition [26], it would be worth to search a possibility of another peak at a somewhat higher collision energy than the first one, related to the CSC phase transition, and vice versa, if the observed peak relates to the CSC, another peak at a somewhat lower energy could relate to the deconfinement. However it remains unclear is it possible to distinguish these peaks experimentally, if T_c and T_{dec} are rather close to each other. One needs a careful measurement of K^+/π^+ ratio in the whole collision energy interval.

11. Pairing fluctuations in hybrid stars

Besides the crust and the hadron shell, the hybrid star contains also a quark core. Both the nucleon shell and the quark core can be in superconducting phases, in dependence on the value of the temperature. Fluctuations affect transport coefficients, specific heat, emissivity, masses of low-lying excitations and respectively electromagnetic properties of the star, like electroconductivity and magnetic field structure, e.g., renormalizing critical values of the magnetic field (H_{c1}, H_c, H_{c2}).

The effect of thermal pion fluctuations on the specific heat and the neutrino emissivity of neutron stars was discussed in [27, 28] together with other in-medium effects, see also reviews [29, 30]. Neutron pair breaking and formation (PBF) neutrino process on the neutral current was studied in [31, 32] for the hadron matter. Also ref. [32] added the proton PBF process in the hadron matter and correlation processes, and ref. [33] included quark PBF processes in quark matter. PBF processes were studied by two different methods; with the help of Bogolubov transformation for the fermion wave function [31, 33] and within Schwinger-Kadanoff-Baym-Keldysh formalism for non-equilibrium normal and anomalous fermion Green functions [32, 28, 29].

As was observed in [32, 28], analogously to the Direct Urca (DU) process $n \to pe\bar{\nu}$, these processes ($n \to n\nu\bar{\nu}$ and $p \to p\nu\bar{\nu}$) have a large (one-nucleon) phase space volume, if the pairing gap is $\Delta \gtrsim 1$ MeV in some density interval (in addition to that DU and PBF emissivities have similar exponential suppression factors $\propto e^{-\Delta/T}$). Moreover, these processes are affected by nucleon-nucleon [32] and electron-electron [34, 35, 30] correlations in such a way that the emissivity of the process $n \to n\nu\bar{\nu}$ is not significantly changed but the emissivity of the process $p \to p\nu\bar{\nu}$ increases up to ten – hundred times. This enhancement is due to the fact that the square of the bare vertex for the $p \to p\nu\bar{\nu}$ reaction contains a very small $\sim c_v^2 \simeq 0.006$ factor compared to the corresponding factor ~ 1 for the $n \to n\nu\bar{\nu}$ reaction channel. However the proton may produce the neutron-neutron hole by the strong interaction and the electron-electron hole by the electromagnetic interaction, which then may couple to the weak current. This circumstance is still ignored in a number of works, which rediscovered this process with vacuum vertices and used it within the cooling code, e.g., see [36]. It seems that an artificial a ten – hundred times suppression of the relevant process may affect their conclusions. Numerical simulation of the neutron star cooling that incorporated PBF processes with inclusion of correlation effects, as well as other relevant in-medium effects of the nucleon-nucleon and nucleon-pion interaction, like softening of pion modes, was performed in [37]. The PBF processes in the quark matter are also affected by correlation effects but, as for the case of the reaction $n \to n\nu\bar{\nu}$, in the given case the correlation effects are expected to be not so significant.

Order parameter fluctuations allow for extra neutrino processes having no exponential suppression in a broad region of temperatures near T_c.

Contribution of pairing fluctuations to the specific heat in the hadron shell is minor for the case of the neutron pairing due to a small value of $T_c \lesssim 1$MeV compared to the value of the neutron chemical potential ($\mu_n \gtrsim 50$ MeV). Therefore in the neutron channel fluctuations of the gap are relevant only in a very narrow vicinity of the critical point. However this effect might be not so small for protons, for which the chemical potential is of the order of several MeV, whereas the gap is of the order of one MeV. Therefore it seems that fluctuations may smear the phase transition in a rather broad vicinity of the critical point of the proton superconductivity.

Pairing fluctuation effects in the quark matter are especially important, if the critical temperature of the CSC phase transition is rather high ($T_c \gtrsim 50$ MeV), as is estimated for 2SC and CFL cases. Temperatures $\sim 10 \div 50$ MeV may indeed arise at an initial stage of the hybrid star cooling. The fluctuation contribution to the total specific heat for $T \lesssim T_c$ is evaluated in a line with that we have done above. As noted in ref. [15], the Aslomasov - Larkin contribution to the electro-conductivity proves to be the dominant term in the vicinity of T_c. Analogously, one may expect a significant increase of the heat conductiv-

ity and viscosity that would result in a delay of the heat transport at the initial stage of the hybrid star cooling. Moreover, neutrino may efficiently rescatter on fluctuations that governs their drift to the hadron shell at $T \lesssim T_c$. These effects may be especially important for the CFL phase, since in that case all other mechanisms of the heat transport are suppressed at $T < T_c$. Estimation of all these effects needs however a separate study.

12. Concluding remarks

We would like once more to emphasize that the coefficients of the thermodynamic potential (1) obtained in the weak coupling limit might be essentially modified, in case if we applied the results to the fireball produced in a heavy ion collision or to hybrid stars, somehow changing our conclusions. E.g., the quark chemical potential decreases with the temperature. It results in an additional increase of the contribution of fluctuations, cf. dependences of the coefficients (2) on μ_q. Thus we may need to analyze the strong coupling limit instead of the weak coupling limit we discussed. There exist arguments that the strange quark mass m_s is very large and due to that the phase transition in the CFL phase does not occur up to very high baryon densities [38]. If μ_q becomes smaller than the strange quark mass we come from the possible 3SC phases to the 2SC phases. A more general discussion of modifications beyond the framework of the weak coupling limit can be found in [24]. A discussion how the coefficients (1) may in general vary within the Ginzburg - Landau approach is given in [12]. Our above arguments are admittedly speculative, and mean only to demonstrate a qualitative possibility of their application to heavy ion collisions and to an initial stage evolution of the hybrid star. A more detailed treatment of the problem definitely needs a further work.

Concluding, within the Ginzburg - Landau approach we estimated the fluctuation energy region at the CSC phase transition. The quantitative estimates are based on the values of parameters derived in the weak coupling limit for fluctuations of the CFL order parameter. Qualitative results survive also for fluctuations of other possible phases. We found that the frequency dependence of fluctuations is important for CSC in a wide temperature region. Fluctuations may contribute essentially to the specific heat even at T rather far below and above T_c. We estimated $T_{\mathrm{fl},<} \lesssim 0.5T_c$ and $T_{\mathrm{fl},>} \sim 2T_c$. Our rough estimates show that the high temperature CSC could manifest itself through fluctuations of the diquark gap in the course of the heavy ion collisions at SIS300, if the critical temperature of the phase transition is indeed rather high, $T_c \gtrsim (50 \div 70)$ MeV. The CSC fluctuations are also relevant for an initial stage of the hybrid star evolution, if T_c is ~ 50 MeV. However quantitative results depend on the values of several not sufficiently known parameters and further studies are still needed to arrive at definite conclusions.

Acknowledgments

The author thanks D. Blaschke, T. Kunihiro and M.F.M. Lutz for the discussions. He acknowledges the hospitality and support of GSI Darmstadt. The work has been supported in part by DFG (project 436 Rus 113/558/0-2), and by RFBR grant NNIO-03-02-04008. The author also acknowledges NATO Scientific Program for the support of his participation in Advanced Research Workshop in Erevan, Sept. 2003.

References

[1] D. Bailin, and A. Love, Phys. Rep. **107**, 325 (1984).

[2] M. Alford, K. Rajagopal, and F. Wilczek, Phys. Lett. **B 422**, 247 (1998).

[3] R. Rapp, T. Schäfer, E.V. Shuryak, and M. Velkovsky, Phys. Rev. Lett. **81**, 53 (1998).

[4] K. Rajagopal, and F. Wilczek, hep-ph/0011333.

[5] D. Diakonov, H. Forkel, and M. Lutz, Phys. Let. **B 373**, 147 (1996); G.W. Carter, and D. Diakonov, Phys. Rev. **D 60**, 016004 (1999); R. Rapp, E. Shuryak, and I. Zahed, Phys. Rev. **D 63**, 034008 (2001).

[6] D. Blaschke, and C.D. Roberts, Nucl. Phys. **A 642**, 197 (1998); J.C.R. Bloch, C.D. Roberts, and S.M. Schmidt, Phys. Rev. **C 60**, 65208 (1999).

[7] M. Alford, K. Rajagopal, and F. Wilczek, Nucl. Phys. **B 357**, 443 (1999); T. Schäfer, and F. Wilczek, Phys. Rev. Lett. **82**, 3956 (1999).

[8] M. Alford, J. Berges, and K. Rajagopal, Nucl. Phys. **B 558**, 219 (1999).

[9] A. Schmitt, Q. Wang, and D. H. Rischke, Phys. Rev., **D 66**, 114010 (2002).

[10] D. Page, M. Prakash, J.M. Lattimer and A. Steiner, Phys. Rev. Lett., **85** 2048 (2000); D. Blaschke, H. Grigorian, and D.N. Voskresensky. Astron.Astrophys. **368**, 561 (2001).

[11] D. Blaschke, D. M. Sedrakian, and K. M. Shahabasian, Astron. & Astrophys. **350**, L47 (1999); D. Blaschke, T. Klähn, and D.N. Voskresensky, Ap. J. **533**, 406 (2000); D.M. Sedrakian, D. Blaschke, K.M. Shahabasyan, and D.N. Voskresensky, Astrofizika **44**, 443 (2001).

[12] K. Iida, and G. Baym, Phys. Rev. **D 63**, 074018 (2001); Phys. Rev. **D 65**, 014022 (2002); Phys. Rev. **D 66**, 014015 (2002).

[13] M. Kitazawa, K. Koide, T. Kunihiro, and Y. Nemoto, Phys. Rev. **D 65**, 091504 (2002); hep-ph/0309026.

[14] D.Voskresensky, nucl-th/0306077.

[15] A. Larkin, and A. Varlamov, cond-mat/0109177.

[16] I. Giannakis, and H.-c. Ren, Phys. Rev. **D 65**, 054017 (2002).

[17] R. Pisarski, and D. Rischke, Phys. Rev. **D 60**, 094013 (1999).

[18] I. Giannakis, and H.-c. Ren, Nucl.Phys.B669:462-478 (2003).

[19] L.D. Landau, and E.M. Lifshiz, Statistical Physics, part I, Pergamon press 1958.

[20] Yu.B. Ivanov, J. Knoll, and D.N. Voskresensky, Nucl. Phys. **A657**, 413 (1999).

[21] E.M. Lifshiz, and L.P. Pitaevsky, Statistical Physics, part II, Pergamon press 1980.

[22] B. Müller, hep-th/9211010, Ann. Rev. Nucl. Part. Sci. **46**, 71 (1996).

[23] B. Kampfer, A. Peshier, and G. Soff, hep-ph/0212179.

[24] R. Pisarski, Phys. Rev. **C 62**, 035202 (2002).

[25] S.V. Afanasiev et al., NA49 Collab., Phys. Rev. **C66**, 054902 (2002); C. Alt et al., J.Phys.G30:S119-S128 (2003).

[26] M. Gazdzicki, and M.I. Gorenstein, Acta Phys. Polon., **B30**, 2705 (1999).

[27] D.N. Voskresensky, and A.V. Senatorov, JETP **63**, 885 (1986).

[28] A.V. Senatorov, and D.N. Voskresensky, Phys. Lett. **B184**, 119 (1987).

[29] A.B. Migdal, E.E. Saperstein, M.A. Troitsky, and D.N. Voskresensky, Phys. Rep. **192**, 179 (1990).

[30] D.N. Voskresensky, in "Physics of neutron star interiors", eds. D. Blaschke, N.K. Glendenning, A. Sedrakian, Springer, Heidelberg, 2001, p. 467; astro-ph/0101514.

[31] E.G. Flowers, M. Ruderman, and P.G. Sutherland, Astroph. J. **205**, 541 (1976).

[32] D.N. Voskresensky, and A.V. Senatorov, Sov. J. Nucl. Phys. **45**, 411 (1987).

[33] P. Jaikumar, and M. Prakash, Phys. Lett. **B516,** 345 (2001).

[34] D.N. Voskresensky, E.E. Kolomeitsev, B. Kampfer, JETP **87**, 211 (1998).

[35] L.B. Leinson, Phys. Lett. **B473**, 318 (2000).

[36] D.G. Yakovlev, A.D. Kaminker, O.Y. Gnedin, and P. Haensel, Phys. Rep. **354**, 1 (2001); D.G. Yakovlev, O.Y. Gnedin, A.D. Kaminker, K.P. Levenfish, and A.Y. Potekhin, Adv.Space Res.33:523-530 (2003).

[37] C. Schaab, D. Voskresensky, A.D. Sedrakian, F. Weber, and M.K. Weigel, Astron. Astrophys., **321**, 591 (1997), astro-ph/9605188.

[38] C. Gocke, D. Blaschke, A. Khalatyan, and H. Grigorian, hep-ph/0104183.

THE INNER STRUCTURE OF HYBRID STARS

Bela Lukacs, Gergely G. Barnafoldi, and Peter Levai
RMKI Research Institute for Particle and Nuclear Physics
POB. 49, Budapest, Hungary, H-1525
lukacs@rmki.kfki.hu, bgergely@rmki.kfki.hu, plevai@rmki.kfki.hu

Abstract Hybrid stars with extremely high central energy density in their core are natural laboratories to investigate the appearance and the properties of compactified extra dimensions with small compactification radius – if these extra dimensions exist at all. We introduce the necessary formalism to describe quantitatively these objects and the properties of the formed hydrostatic equilibrium. Different scenarios of the extra dimensions are discussed and the characteristic features of these hybrid stars are calculated.

Keywords: Neutron stars, quark stars, compactified extra dimensions.

1. Introduction

Neutron and quark stars are natural laboratories to investigate the interplay of strong, electro-weak and gravitational interaction. Many theoretically determined properties of these astrophysical objects were tested by the observed properties of pulsars, and detailed calculations exist for these stars[1–4].

However, if new perspectives appear in the description and understanding of the gravitational interaction or in the unification of the above interactions, then revisiting of the models becomes necessary. Such a reinvestigation was triggered by the refreshed attention on compactified extra dimensions[5]. Extra dimensions inside neutron stars were investigated earlier[6], but the Kaluza-Klein (K-K) excitation modes were not considered in the equation of state (EoS). These modes are important constituents of the recent gravitation theories. Introducing the K-K modes into the EoS of fermion stars at their central core, new features and properties emerged [7].

Here we display a few of our ideas about these extra dimensions, their possible connection to particle physics and their appearance in the core of hybrid stars. We summarize our numerical results and discuss the observability of extra dimensions in these objects.

D. Blaschke and D. Sedrakian (eds.), Superdense QCD Matter and Compact Stars, 297–306.

2. The Fifth Dimension

The introduction of the 5th dimension into the real World has a long history. We do not have any direct information about the extra dimensions, so we have an alternative. Either x^5 does not exist, or, it is microscopically small and compact. Obviously in the present paper we take the second horn of the alternative, for details see Refs. [8, 9].

Quantization puts a serious constraint on five-dimensional motion. If there is an independence on x^5, then the particle is freely moving in x^5. However, being that dimension compactified leads to an uncertainty in the position with the size of $2\pi R_c$, where R_c is the compactification radius. Thus a Bohr-type quantum condition appears formally:

$$p^5 = \frac{n\hbar}{R_c} \ . \tag{1}$$

Because of the extra motion into the fifth dimension, an extra mass term appears in 4D descriptions. Considering compactified radius $R_c \sim 10^{-12}-10^{-13}$ cm this extra "mass" is $\widehat{m} \sim 100$ MeV; similar values appear in Ref. [5]. A quite recent approach of hadron spectra by Arkhipov [11] is also worthwhile to consult with.

An interesting consequence of the existence of 5th dimension is that in the "4 dimensional" observations an apparent violation of the equivalence principle must appear as one can show it by writing the geodesic equation in 5 dimensions and then projecting it into 4 dimensions. Without going into details, the $\pm$ sign of p^5 causes the appearance of a "pseudo-charge" $\widehat{q}$ in the 4 dimensional formalism,

$$\widehat{q} = n \cdot \frac{2\hbar\sqrt{G}}{c\ R_c} \ , \tag{2}$$

which acts in a vector-scalar interaction. We can directly see that $\widehat{q}$ is *not* the electric charge. Indeed $\widehat{q}^2 < 16\pi G m_0^2$, where G is the gravitational constant and m_0 is the rest mass [10]. This is either some familiar quantum number (e.g. strangeness, S), or some other not yet observed charge.

3. Field Equations

We are interested in final states of stellar evolution. Therefore we can restrict ourselves to static configurations. Also, fluid-like behavior seems appropriate *in the microscopical dimensions*. Therefore we are looking for *static* configurations. Also, some fluid-like behavior is expected in the sense that stresses in the *macroscopical* directions freely equilibrate. Then in 3 spatial directions *isotropy* is expected and thence *spherical symmetry*. Finally, in the lack of any information so far, we may assume symmetry in the extra dimension. Then in

proper GR language we are looking for solutions with 5 Killing vectors

$$K_{Ai;k} + K_{Ak;i} = 0$$

$A = 0, 1, 2, 3, 5$, with the commutation relations

$$[K_0, K_B] = 0, \quad [K_5, K_B] = 0, \quad [K_\alpha, K_\beta] = \epsilon_{\alpha\beta\gamma} K_\gamma \tag{3}$$

so that the subgroup $1, 2, 3$ acts with 2 dimensional transitivity. Hence the metric has the unique form

$$\mathrm{d}s^2 \;=\; e^{2\nu}\,\mathrm{d}t^2 - e^{2\lambda}\,\mathrm{d}r^2 - r^2\mathrm{d}\Omega^2 - e^{2\Phi}(\mathrm{d}x^5)^2 \;\;, \tag{4}$$

where the quantities ν , λ and Φ depend only on r. As for the energy-momentum tensor we get

$$T^{ik} \;=\; \mathrm{diag}\,(\varepsilon\, e^{2\nu},\; P\, e^{2\lambda},\; P\, r^2,\; P\, r^2 \sin^2\theta,\; P_5\, e^{2\Phi})\,. \tag{5}$$

Total spatial equipartition of particle momenta is not expected (so $P \neq P_5$); indeed we shall see that it does not happen generally.

The Einstein equations are read as

$$-\gamma\,\varepsilon \;=\; e^{-2\lambda}\left[\Phi'' + \Phi'^2 - \lambda'\Phi' + \frac{2\Phi'}{r} - \frac{2\lambda'}{r} + \frac{1}{r^2}\right] - \frac{1}{r^2} \tag{6}$$

$$-\gamma\,P \;=\; e^{-2\lambda}\left[-\nu'\Phi' - \frac{2\Phi'}{r} - \frac{2\nu'}{r} - \frac{1}{r^2}\right] + \frac{1}{r^2} \tag{7}$$

$$-\gamma\,P \;=\; e^{-2\lambda}\left[-\nu'' - \nu'^2 + \nu'\lambda' - \Phi'' - \Phi'^2 - \nu'\Phi' + \lambda'\Phi' - \right.$$
$$\left. - \frac{2\Phi'}{r} - \frac{\nu'}{r} + \frac{2\lambda'}{r}\right] \tag{8}$$

$$-\gamma\,P_5 \;=\; e^{-2\lambda}\left[-\nu'' - \nu'^2 + \nu'\lambda' - \frac{2\nu'}{r} + \frac{2\lambda'}{r} - \frac{1}{r^2}\right] + \frac{1}{r^2} \tag{9}$$

where $\gamma = 8\pi G/c^4$ and all quantities can depend only on the radius r.

For final states ($T = 0$) all local material characteristics of the fluid are expected to depend on one thermodynamic quantity, say on particle density n. The material equations,

$$\varepsilon = \varepsilon(n);\; P = P(n);\; P_5 = P_5(n)\;, \tag{10}$$

and the Einstein equations in Eqs. (6)-(9) are all independent equations, all further equations are consequences. (Indeed there are some thermodynamical constraints between ε, P and P_5.) Considering the appropriate Bianchi identity, one obtains

$$T^{ir}{}_{;r} = 0 \;\;\longrightarrow\;\; P' = -\nu'(\varepsilon + P) + (P_5 - P)\Phi'\;. \tag{11}$$

This equation clearly demonstrates the influence of the extra dimensional behavior on the normal pressure, $P = P_1 = P_2 = P_3$.

The Einstein equations Eqs. (6)-(9) contain two extra variables compared to the more familiar 4 dimensional case, namely P_5 and Φ. However, $P_5(n)$ is a known function of the particle number density and specified by the actual interaction in the matter. Thus $\Phi(r)$ is the only new degree of freedom determined by the extra equation.

4. A Special Solution of the Field Equations

For specially chosen pressure P_5 there is a unique solution of the Einstein equations in Eqs. (6)-(9), namely $\Phi' = 0$. In this case Eqs. (6)-(8) can be solved separately with $\Phi = 0$ and then the last Eq. (9) gives P_5. Although these solutions do not differ formally from the 4 dimensional neutron star solution (except for P_5), but the extra dimension will have its influence on $\varepsilon(n)$ and $P(n)$ [7].

Let us start with a single massive fermion ("neutron", N). Since the minimal nonzero fifth momentum component is $|p^5| = \hbar/R_c$, then the extra direction of the phase space is not populated until the Fermi-momentum $p_F < \hbar/R_c$. However, at the threshold both $p^5 = \pm\hbar/R_c$ states appear. They mimic another ("excited") particle with mass $m_X = \sqrt{m_N^2 + (\hbar/R_c)^2}$ (with a nonelectric "charge" $\widehat{q} = \pm\frac{2\hbar\sqrt{G}}{cR_c}$ as well). The equations obtain a form as if this second particle also appeared in complete thermodynamical equilibrium with the neutron: $\mu_X = \mu_N$. This phenomena is repeated in any case, when p exceeds a threshold $n\hbar/R_c$.

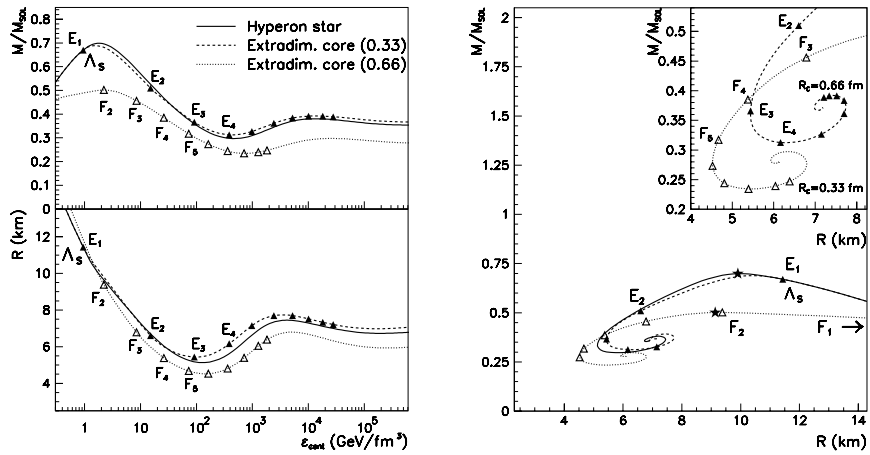

Figure 1. The mass and the radius of heavy hadron stars in 4 dimensions and neutron stars including extradimensional K-K modes into the core (from Ref. [9]).

Fig. 1. compares two calculations. The solid line is 4 dimensional calculation with neutrons and Λ hyperons, the lightest neutral strange baryon. (Ambartsumyan and Saakyan calculated such hybrid compact stars as far back as in 1960 [12].) The dashed and dotted lines come from 5-dimensional calculations with only neutrons, but moving in the extra dimension, too. The higher excitations are started from the triangles and they are named as E_1, E_2, ..., at compactified radius $R_c = 0.33$ fm. In this case the 5 dimensional neutron star is almost indistinguishable from a neutron star with Λ core. However, choosing another compactification radius (e.g. $R_c = 0.66$ fm) one obtains reasonable differences, which can be seen on Fig. 1. The F_2, F_3, ..., indicate the appearance of the excited modes in the latter case (F_1 was left outside of the figure).

5. On the General Solution of the Field Equations

In the most generic case it is true that the derivative $\Phi' \neq 0$. The interior solution of Eqs. (6)-(9) can be obtained only numerically. In principle there is no problem to evaluate these equations, but the structure of them must be understood.

First, there are constraints among the material quantities, which are rather straightforward for ideal quantum fluids. In case of interacting matter one can recall the self-consistent description of the interacting fermions in the 4 dimensional analogy [13]. Second, the particle number density in the center, $n(r = 0)$, is a free initial condition, as it was in the 4 dimensional case. Instead of density, we may use energy density, $\varepsilon(r = 0) \equiv \varepsilon_0$, as well.

Third, the metric tensor is determined by the variables Φ, ν, λ. On the other hand Φ and ν never appear in Eqs.(6)-(9) (reflecting the fact that x^0 and x^5 constant dilatations are always possible without harming the commutator relations for the Killing motions), so these equations are of first order on Φ', ν' and λ. However, the equations can be rearranged resulting in the following symbolic structure:

$$\Phi' = \Phi'(\lambda', \lambda, n) \tag{12}$$

$$\nu' = \nu'(\lambda', \lambda, n) \tag{13}$$

$$\lambda'' = \lambda''(\lambda', \lambda, n) \tag{14}$$

The Eqs. (12)-(13) are algebraic equations for Φ' and ν', but Eq. (14) is a differential equation of second order and it should be reorganized formally into 2 equations of first order.

Fourth, initial conditions are needed for Φ, ν, λ and λ'. For the first two they are free additive constants and for λ and λ' we can proceed as in 4 dimensions. Anyway, it is clear that even if we choose such initial conditions that $\Phi'(r = 0) = 0$, then it does not remain zero out of the center.

6. Matching Conditions on the Surface

The integration must go until the fluid-vacuum interface at r_s, where an exterior vacuum solution continues the interior one. The details of matching conditions can be found in Ref. [14]. Applying them on the present problem we get the continuity of certain derivatives of the metric tensor, and those for the energy-momentum tensor result in the single equation,

$$P(r_s) = 0\,. \tag{15}$$

Observe that no constraint is obtained either for ε or P_5.

Although P_5 might be anything at r_s from the matching conditions, it will be zero for all general (not very exotic) systems. Namely, $P = 0$ is expected at some *low* particle number density n_s on the surface, which is generally much below $p_5 = \hbar/R_c$. So motions in the 5^{th} dimension cease already somewhere in the interior of the star.

Henceforth vacuum solutions of Eqs. (6)-(9) are valid until infinity, and $\Phi(r_s)$, $\nu(r_s)$, $\lambda(r_s)$, and $\lambda'(r_s)$ give initial conditions for the external solution. Interestingly enough, the external solutions can be obtained in analytical (albeit partly implicit) forms.

7. The External Solution

The external solution of the Einstein equations can be obtained in analytic form. Equaling the matter contribution with zero on the left hand sides and using the new variables α and β as

$$\nu' \equiv \alpha + \beta \tag{16}$$

$$\Phi' \equiv \alpha - \beta\,, \tag{17}$$

the 4 Einstein equations results in 3 differential equations,

$$\lambda' = \frac{1}{r}(1 - e^{2\lambda}) + 2\alpha \tag{18}$$

$$\psi' = -\frac{\psi}{r^2}(1 + e^{2\lambda})\,, \tag{19}$$

(where $\psi \equiv \alpha, \beta$), and one more equation becomes an identity. Eqs. (18)-(19) can be integrated as

$$\alpha = \frac{A}{r}e^{-Y} \tag{20}$$

$$\beta = \frac{B}{r}e^{-Y} \tag{21}$$

with two constants A, B. For variable Y Eq.(18) yields the following:

$$Y' = \frac{1}{r}\left[(A^2 + B^2)e^{-2Y} + 4Ae^{-Y} + 1\right] \tag{22}$$

This last equation can be solved in an implicit form. There are three solutions according to the sign of the determinant. Here we give the one for positive determinant:

$$\ln\left[\frac{r}{r_0}\right] = \ln\left[\left(\frac{y-y_+}{y_0-y_+}\right)^u\left(\frac{y-y_-}{y_0-y_-}\right)^v\right] \tag{23}$$

where r_0 and y_0 are constants of integration. Furthermore,

$$D = \sqrt{3A^2-B^2} \tag{24}$$
$$y_\pm = -2A \pm D \tag{25}$$
$$u = \frac{-2A+D}{2D} \tag{26}$$
$$v = \frac{+2A+D}{2D} \tag{27}$$

and then

$$Y = \ln y \tag{28}$$
$$e^{2\lambda} = (A^2+B^2)e^{-2Y} + 4Ae^{-Y} + 1 \tag{29}$$

Of course, this solution goes to flat space-time as $r \longrightarrow \infty$.

The $\Phi' = 0$ special solution belongs to $A = B$. However, as we claimed earlier, $\Phi'(r_s) \neq 0$.

8. Conclusion

We do not know compact stars close to Sun, so the observations are rather hazy for details. However some data exist for masses and radii. In the previous Chapters we showed that the calculations are as straightforward in 5 dimensions as in 4. While some problems must be relegated to the next, last Chapter, in principle one could compare observations with 4- and 5-dimensional calculations, and try to decide if space is 3 dimensional or 4. The difference comes from two reasons.

1) At some Fermi momentum the phase space opens up in the 5^{th} direction. Henceforth p_F increases slower, which will be reflected by the M(R) relation. However note that 5^{th} dimensional effects can mimic particle excitations.

2) Quite new effects can, in principle, be observed around compact stars. Of course, they may be moderate and the present observational techniques are probably insufficient. However, consider 2 situations:

You can perform light deflection experiments. Trajectories differ in 4 and 5 dimensions.

You may perform "free fall" experiments in vacuum but not very far from the star. Then 1) particles moving also into the extra direction would fall

"anomalously", but this is a simple Eotvos-type experiment and can be done in lab too. However 2) $\Phi' \neq 0$, so also a "scalar force" appears for particles moving in the extra dimension, although we are outside of the exotic interior of the star. This means that accelerator experiments not too far from compact stars would show up surprising results *if* 5$^{\text{th}}$ Dimension exists. So not only the dense source would be different. Gravity is a phenomenon of Space-time and 5-dimensional Space-Time differs from the 4-dimensional one.

Before truly realistic 5-dimensional calculations some problems must be fully clarified. They are listed in the last Chapter.

9. Outlook

While we can calculate 5-dimensional compact stars in this moment, the results still depend on parameters to be fixed in the future, We, somewhat arbitrarily, classify problems into 3 groups: factual, technical and fundamental.

1) Factual problems:

The value of the compactification radius, R_c: In the present approach this radius was a free parameter. For demonstration we chose the radius $R_c = 0.33 \cdot 10^{-13}$ cm, when the strange Λ baryon could behave as the first excitation of a neutron. Such an extradimensional object can mimics a compact star with neutrons in the mantle and Λ's in the core. With smaller R_c the "exotic" component appears at larger densities – we may run into the unstable region of the hybrid star and the extra dimension remains undetectable. However, with larger R_c the mass gap becomes smaller and the "transition" happens at "familiar" neutron star densities. In this way, reliable observations could lead to an upper bound on R_c.

The quantum number connected with motion in x^5: We saw that a neutron, starting to move in the 5$^{\text{th}}$ direction, appears in macroscopic 4-dimensional description as if a neutral baryon, but with a higher mass. Particle tables mention such particles in abundance. But we also mentioned that 5 dimensional GR gives that the 4 dimensional projection of the geodesics of such particles would exhibit a really weak apparent violation of the equivalence principle, via a vector-scalar force. In first approximation this would mimic a Coulomb-*like* force, but approximately 10^{-39} times weaker. Now, there was one serious attempt to see the violation of the equivalence principle (in the Eotvos experiment [15]); there it seemed that the strength was in this range. The tentative idea was that the violation might be connected with hypercharge $Y = B + S$, and there was also a discussion [16] whether the mass difference of K^0 and anti-K^0 came from the interaction of Earth's particles with the kaon in lab. Now, in some sense the "first excitation" of n in Y is Λ. It would be a nice minimal theory if Fifth Dimension would explain the CP-violation of weak interaction as well, but of course we cannot expect this.

The way of compactification: Here we chose the simplest compactification: $x^5 \equiv x^5 + 2\pi R_c$. This is a cylindrical compactification. However more complicated cases are also possible, albeit not arbitrary ones. A branch of GR lists all the cases; now we mention only the 2-dimensional example that from a plane by cut and sew you can produce of course a compact cylinder, but the mantle of a cone as well.

The number of the extra dimensions: The present example was the simplest nontrivial case. However maybe particle physicists would prefer 6 extra dimensions appearing with the same length scale in some group structure. The "extra forces" appearing from Fifth Dimension are gravitational, the extra quantum number appearing here cannot be the source of QCD forces [10]. In Ref. [9] we discussed *two* extra dimensions with different scales.

2) Technical problems:

Initial conditions: We mentioned that we need to fix 3 initial conditions in the center: one for the central density of matter ($n(0) = n_0$ or $\epsilon(0) = \epsilon_0$), and two for the metric, either for $\lambda(0)$ and $\lambda'(0)$, or, equivalently, for $\lambda(0)$ and $\Phi'(0)$. But we cannot properly impose these conditions in $r = 0$, and these conditions are somehow not independent. However the technical problem is well known already in 4 dimensions [1] . First, the proper way is to approximate the innermost core of radius δ with a homogeneous sphere of density n_0, where the exact value of δ is irrelevant if small enough. Then $n = n_0$ at $r = \delta$, and $e^{2\lambda} = 1 - 8\pi\delta^3\epsilon_0/3c^2$ there.

Interactions: $N - N$ interaction can be taken into account the same way as in Ref.[13]. Neutrons moving into the extra dimension may interact differently because of an extra momentum dependence. Such momentum dependence appears e.g. in Walecka-type [17, 18] construction.

3) Theory:

A consequent 5-dimensional treatment would require Unified Theory of Quantum Mechanics and General Relativity. This unified theory is not available now, and we know evidences that present QM is incompatible with present GR. The well-known demonstrative examples are generally between QFT and GR (e.g. the notion of Quantum Field Theory vacua is only Lorentz-invariant and hence come ambiguities about the existence of cosmological Hawking radiations [19]). But also, it is a fundamental problem that the lhs of Einstein equation is c-number, while the rhs should be a quantum object.

In the present case QM and GR have to be used in a compatible way for the proper "Bohr-type" quantization of p^5. Our chosen way was intuitive. Sure, it is correct for $\Phi' = 0$. Then one can always introduce such a coordinate system where $\Phi = 0$ and then the circumference is the usual $2\pi R_c$. But in the general case one might use $2\pi R_c$ in the condition as well as $2\pi e^{\Phi} R_c$. All suggestions up to now (as. e.g. Ref. [20]) are restricted to the simpler case.

This paper has displayed the introduction of 5^{th} dimension into astrophysical description in the framework of GR. The new degrees of freedom may solve old problems, but open new questions, as well. We think that this attempt is worthwhile.

Acknowledgments

One of the authors(B.L.) would like to thank for the organizers of this conference for their warm hospitality. This work was supported by the MTA-JINR Grant and OTKA T043455.

References

[1] B.K. Harrison, K.S. Thorne, M. Wakano, and J.A. Wheeler. *"Gravitation theory and gravitational collapse"*, University of Chicago Press, 1965.

[2] N.K. Glendenning. *"Compact Stars"*, Springer, 1997; and references therein.

[3] F. Weber. *"Astrophysical Laboratories for Nuclear and Particle Physics"*, IOP Publishing, Bristol, 1999.

[4] D. Blaschke, N.K. Glendenning, and A. Sedrakian (Eds.), *"Physics of neutron star interiors"*, Springer, Heidelberg, 2001.

[5] L. Randall and R. Sudrum. *Phys. Rev. Lett.* **83**, 3370 (1999); *ibid.* 4690.

[6] A.R. Liddle et al.. *Class. Quantum Grav.* **7**, 1009 (1990).

[7] N. Kan and K. Shiraishi, *Phys. Rev.* **D66**, 105014 (2002).

[8] B. Lukacs, *"May Kaluza ride again?"*, in Relativity Today, eds. C. Hoenselaers, Z. Perjes, Akademiai Kiado, Budapest, 2000, p.161.

[9] G.G. Barnafoldi, P. Levai, and B. Lukacs, *"Heavy quarks or compactified extra dimensions in the core of hybrid stars"*, in Proceedings of the 4th Int. Workshop on New Worlds in Astroparticle Physics, Faro, Portugal, Worlds Scientific, Singapore, 2003. (astro-ph/0312330).

[10] B. Lukacs and T. Pacher, *Phys. Lett.* **A113**, 200 (1985).

[11] A.A. Arkhipov, *"Hadronic Spectra and Kaluza-Klein picture of the World"* AIP Conf.Proc.717:680-684 (2003) and references therein.

[12] V.A. Ambartsumyan, G.S. Saakyan, *Astron. Zh.* **37**, 193 (1960).

[13] J. Zimanyi, B. Lukacs, P. Levai, et al. *Nucl. Phys.* **A484**, 647 (1988).

[14] A. Lichnerowicz, *"Theories relativistes de la gravitation at d'electromagnetisme"*, Masson, Paris, 1955.

[15] E. Fischbach et al., *Phys. Rev. Lett.* **56**, 3 (1986).

[16] S.H. Aronson et al., *Phy. Rev. Lett.* **56**, 1342 (1986).

[17] J.D. Walecka, *Ann. Phys.* **83**, 491 (1974).

[18] J. Zimanyi and S.A. Moszkowski, *Phys. Rev.* **C42**, 1416 (1990).

[19] G.W. Gibbons and S. Hawking, *Phys. Rev.* **D15**, 2738 (1977).

[20] J.-M. Souriau, *Nuovo Cim.* **30**, 565 (1963).

III

SIGNALS FOR SUPERDENSE QCD MATTER IN COMPACT STARS

GAMMA-RAY BURSTS AND THEIR CENTRAL ENGINES

Stephan Rosswog
School of Engineering and Science
International University Bremen
Germany
s.rosswog@iu-bremen.de

Abstract Gamma-ray bursts are the most luminous and probably the most relativistic events in the universe. The last few years have seen a tremendous increase in our knowledge of these events, but the source of the bursts still remains elusive. I will summarize recent progress in this field with special emphasis on our understanding of the possible progenitor systems.

Keywords: gamma rays: bursts; supernovae; stars: neutron; radiation processes: non-thermal; dense matter; hydrodynamics; neutrinos; magnetic fields

1. Introduction

Like some other spectacular discoveries such as the cosmic microwave background, gamma-ray bursts (GRBs) were discovered by accident. Meant to monitor the "outer space treaty", the American VELA satellites detected in July 1967 an intense flash of gamma-rays of unknown origin. It took until 1973 before the first detected GRBs were published for the scientific community (Klebesadel et al. 1973).
This caused furious research activity and a flurry of often very exotic theoretical models. At the Texas conference in 1974, only one year after the first scientific publication, Malvin Ruderman summarised the situation: "The only feature that all but one (and perhaps all) of the very many proposed models have in common is that they will not be the explanation of GRBs. Unfortunately, limitations of time prevent me from telling you which model is the exception....". But his favorite model, accretion onto a black hole, is still a promising horse in today's race.

2. Observations

GRBs are short flashes of gamma-rays that outshine for short moment the whole rest of the gamma-ray sky. The BATSE instruments on board the Comp-

D. Blaschke and D. Sedrakian (eds.), Superdense QCD Matter and Compact Stars, 309–329.

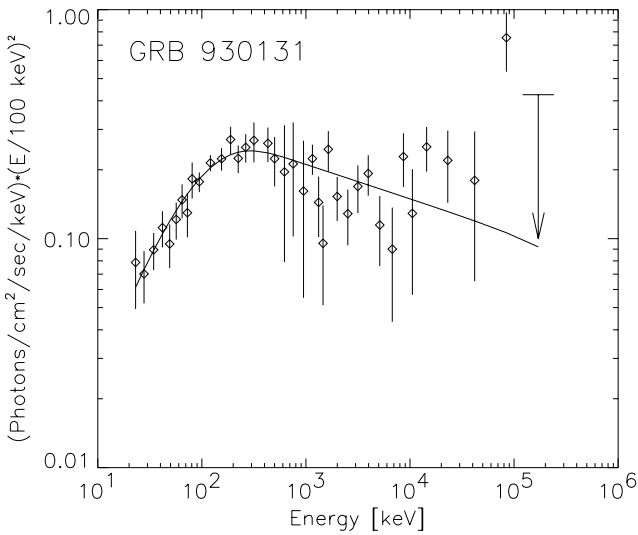

Figure 1. Spectrum of GRB930131 together with a synchrotron model fit (Bromm & Schaefer 1999).

ton Gamma-Ray Observatory observed bursts at a rate of around one event per day (Paciesas et al. 1999). Opposite to initial expectations BATSE detected an inhomogeneous, but highly isotropic distribution of burst sources. GRB lightcurves exhibit a tremendous variety ranging from single featureless spikes, over "FREDS" (fast rise exponential decay) to completely erratic sequences of pulses. The lightcurves vary on millisecond time scales, the shortest variability time scale so far being 0.22 ms for GRB920229 (Schaefer and Walker 1999). The spectra of GRBs are non-thermal (see Figure 1) with high-energy tails extending up to several GeV. The spectra can be accurately fitted with an exponentially smoothed, broken powerlaw, the so-called "Band-function" (Band et al. 1993). The "knee" where both powerlaws are joined is referred to as the break energy. Typically break energies lie around several hundred keV. Generally, the lower spectral energy index is compatible with a synchrotron origin of the radiation (Cohen et al. 1997), there are however some bursts with a lower energy slope steeper than predicted by the synchrotron model (Preece et al. 1998). The duration distribution of GRBs is bimodal with a first peak at ~ 0.2 s and a second one at ~ 30 s. Bursts below (above) 2 s are referred to as "short (long) bursts" (Kouveliotou et al. 1993). Bursts of the short category exhibit predominately harder spectra than their long-duration cousins. The hardness is usually measured via the "hardness ratio", the ratio of photon counts in a high and a low energy channel of BATSE.

The discovery of the first redshifts (Costa et al. 1997) in GRB afterglows settled a long debate about whether they occur at cosmological distances or not. By now, the cosmological origin of long GRBs is a well-established fact. Searches for the host galaxies found long bursts occurring predominantly in galaxies with active star formation (Bloom et al. 2002), pointing to a rather short-lived progenitor system, possibly related to the death of massive stars that die close to their birth-places. A GRB supernova connection had been suspected when in the localization error box of the BeppoSAX wide field camera of GRB980425 a supernova of type Ib/c was found. By now, "bumps" have been detected in the optical afterglow lightcurves of several long GRBs (e.g. Bloom et al. 1999). These bumps were interpreted as the lightcurves from an underlying supernova that occurred roughly at the same time as the GRB. The idea of a long GRB supernova connection has convincingly been corroborated by the detection of a very energetic supernova that occurred temporally and spatially coincident with GRB030329 (Hjorth et al. 2003, Stanek et al. 2003). Thus (at least some of the) long bursts seem to go along directly with a core-collapse supernova.

Short GRBs are usually assumed to be cosmological as well, but we are currently still lacking direct evidence in the form of afterglow observations. There are indications that the observed short GRBs occurred possibly at somewhat shorter distances (Mao et al. 1994). This would be consistent with compact binary sources that merge relatively late in the age of the universe due to their long inspiral time (Fryer et al. 1999).

The fluences of typically 10^{-5} to 10^{-7} erg/cm^2 and cosmological redshifts observed so far imply isotropic burst energies of up to $\sim 4 \cdot 10^{54}$ ergs for GRB990123, corresponding to twice rest mass energy of the sun in gamma-rays alone. This "energy crisis" pointed to beamed emission. By now, in several GRBs achromatic breaks have been identified from which (under certain assumptions) jet opening angles of $\sim 5^o$ have been derived (Frail et al. 2001). Taking beaming angle corrections into account, the energy requirements are alleviated, the initially huge range of isotropic energies ranging from a few times 10^{51} to $4 \cdot 10^{54}$ ergs collapses to a narrow distribution around $\sim 5 \cdot 10^{50}$ erg. If true, this allows the use of GRBs as standard candles to infer, for example, star formation in the high redshift universe (e.g. Lloyd-Ronning et al. 2002).

We briefly want to mention two exciting, but currently still controversial topics: x-ray emission lines and polarization of the prompt GRB-emission. X-ray emission features have been reported for several x-ray afterglows (e.g. Piro et al. 2000). The confidence level for these detections, however, is rather low. The energy contained in these lines is very large, $\sim 10^{49}$ erg. Since the efficiency to produce an x-ray emission line cannot exceed 1 $\%$ the burst would have to have $\sim 10^{51}$ ergs in x-rays (Ghisellini et al. 2002), which sets a strict lower limit on the burst energy that is hard to reconcile with the results of Frail et al. (2001).

Using RHESSI results Coburn and Boggs (2003) reported on a high linear polarisation of the prompt emission of GRB021206, $\Pi = 0.8 \pm 0.2$. This could point to the interesting possibility of magnetic fields being advected from the central source rather than being generated in shocks. A re-analysis of the same data, however, found a no indication of for polarization of GRB021206 (Rutledge and Fox, 2003).

3. The fireball model

The above listed observational facts impose constraints on the progenitor system(s) responsible for gamma-ray bursts.

The first one, often referred to as the "compactness-problem" comes from the non-thermal GRB spectra and was originally used as an argument against a possible cosmological origin of GRBs (Ruderman 1975, Schmidt 1978). The millisecond variability of the lightcurves points to a compact source for the GRB, as from simple causality arguments the dimension of the system should be $D < c \cdot \delta t \approx 300$ km. But if an energy of $\sim 10^{51}$ erg in ~ 1 MeV photons is released in such a small volume the optical depth to pair creation must be huge: $\tau \sim 10^{13}$ and therefore one would expect a thermal spectrum, in blatant contrast to the observations. The way out of this dilemma is relativistic motion (Paczynski 1986, Goodman 1986). If the emission is coming from material moving with Lorentz factor Γ towards the observer, the source can be increased by a factor of Γ^2. Moreover the photons in the local frame are softer by a factor of Γ. A detailed analysis (Lithwick and Sari 2001) shows that the optical depth can be reduced by effects of relativistic motion by a factor $\sim \Gamma^{6.5}$ where the exact value of the exponent depends on the GRB spectrum. The analysis of Lithwick and Sari yields lower limits on GRB Lorentz factors of several hundreds, the highest Lorentz factors in the universe.

A second hard constraint is the so-called "baryon loading problem". The attainable bulk Lorentz factor is determined by the ratio of available energy and rest mass energy. If an energy of 10^{51} erg is available the fireball cannot contain more than 10^{-5} $M_\odot$in baryonic material, otherwise the required Lorentz-factors will not be reached. This poses a hard problem for central engine models: how can a stellar mass object pump so much energy into a region that is essentially devoid of baryons?

The above reasoning has led to the "fireball" internal-external shocks model. This model is rather independent of the nature of the central engine. The latter one is just required to produce highly relativistic outflow, either in the form of kinetic energy or as Poynting flux. The radiation is produced in (collisionless) shocks. These can either occur due to interaction of the outflow with the circumstellar material ("external shocks") or due to interactions of different portions of the outflow with different Lorentz-factors, so-called "internal shocks".

According to the fireball model the GRB is produced via synchrotron radiation (at least in the most simple model version) in internal shocks. The efficiency of internal shocks depends on the variability within the outflow (Kobayashi et al. 1997). A lot of energy remains as kinetic energy in the ejecta and can later be dissipated via external shocks to produce the much longer lasting multi-wavelength afterglow. Afterglow had been predicted before its observation by several researchers (Paczynski and Rhoads (1993), Meszaros and Rees (1993, 1997), Vietri (1997)). The simplest afterglow model with an adiabatic, relativistic blast wave (Blandford and McKee 1976) and synchrotron radiation, seems to fit the bulk of afterglow observations reasonably well (for a detailed discussion see Piran (1999) and Meszaros (2002)).
Detailed investigations of Kobayashi et al. (1997) showed that the GRB lightcurve reflects essentially the activity of the inner engine that produces the relativistic outflow. That means that the engine itself has to produce an erratic sequence of pulses and, whatever the progenitor is, it should be able to produce, depending on its specific system parameters a large variety of different outcomes. This result seems to rule out "one-bang" models, e.g. simple phase transitions in neutron stars.

For an alternative to the fireball model see Dar and De Rujula (2003).

4. Models for the Central Engine

Many many GRB models have been suggested over the years and it is impossible to do justice to all of them here. I will therefore just pick out a few that I consider to be particularly interesting.
When discussing the central engine it is worth keeping in mind that the overall burst duration, τ, is -both for long and for short bursts- *very long* in comparison to the variability time scale, δt, on which the energy output changes substantially, $\delta t/\tau \ll 1$. This requires the engine to provide (at least) these two different time scales. One (but not the only) reasonable possibility is that the central engine consists of a new-born, stellar mass black hole surrounded by an accretion disk. In this view the dynamical time scale close to the hole sets the variability while the viscous accretion time scale sets the overall burst duration. The hole/disk masses then distinguishes between long and short duration bursts. While this is certainly plausible, I want to stress here that plausible models do not necessarily have to involve a black hole, examples of such alternative models are Usov's (1992) highly magnetized pulsar formed in an accretion induced collapse or the temporarily stabilized central object resulting in a neutron star coalescence, see below.
One important question is whether there is a single progenitor that produces (depending on say its initial conditions like the rotation rate) either a short or a long GRAB or whether the two burst classes result form two different progen-

itor systems. An example of a model that produces both long and short Grabs from one progenitor has been suggested by Yo and Blackman (1998). In their model the GRAB is driven by dissipation of Pointing flux extracted from a young, highly magnetized millisecond pulsar formed in an accretion-induced collapse of a white dwarf. If the initial rotation is above a critical rotation rate, the spin-down time scale is determined by gravitational wave emission leading to sub-second spin-down, otherwise its is governed by electromagnetic dipole emission and leads to a much longer duration ($\gg 1$ s).
There are, however, reasons to assume that the two GRB classes are caused by different progenitor systems since there are, apart from the duration further substantial differences. First, as mentioned above, short GRBs seem to be systematically harder than their long-duration cousins. Moreover their lightcurves exhibit fewer sub-pulses and they show a different temporal spectral evolution (Norris et al. 2000). Apart from that the spectral break energies of short bursts seem to be larger than for long bursts (Paciesas et al. 2000). As the spectral break energy is sensitive to the cosmological redshift and the Lorentz-factor of the ejecta producing the burst, the higher spectral break energies could mean that either short GRBs have higher Lorentz-factors or/and that their population is closer, i.e. they have, on average, a lower redshift. Both of these possibilities are compatible with compact binary mergers: due to their inspiral time they could occur relatively late in the age of the universe and therefore be at lower redshifts than long GRBs. Moreover, they are not engulfed in a stellar mantle like in the case of a stellar collapse and the high rotation velocities that naturally occur will centrifugally evacuate the region around the binary rotation axis. This fact will make it easier to obtain higher Lorentz-factors without being slowed down by a stellar mantle that has to be penetrated first. Moreover, the two classes seem to be differently distributed in space (Cohen, Kolatt and Piran 1994), consistent with short GRBs being closer than their long-duration cousins. All this hints to two different progenitor systems.

4.1 Long-soft Bursts

Around 70 $\%$ of the observed GRBs are the long-soft type. They typically occur at cosmological redshifts of $z \sim 1$ and are believed to be beamed with half-opening angles of $\sim 5^o$. Thus, we see on average one burst per 300 beamed GRBs with random jet orientations, i.e. the true rate of long GRBs is around 1000 per day in the universe.

Collapsars. The probably most popular GRB-model is the "Collapsar/failed supernova" model (Woosley 1993, MacFadyen and Woosley 1999), sometimes also referred to as "hypernova" (Paczynski 1998).
The exact supernova mechanism is despite intense research not known with certainty, but the general believe is that the huge neutrino luminosities from

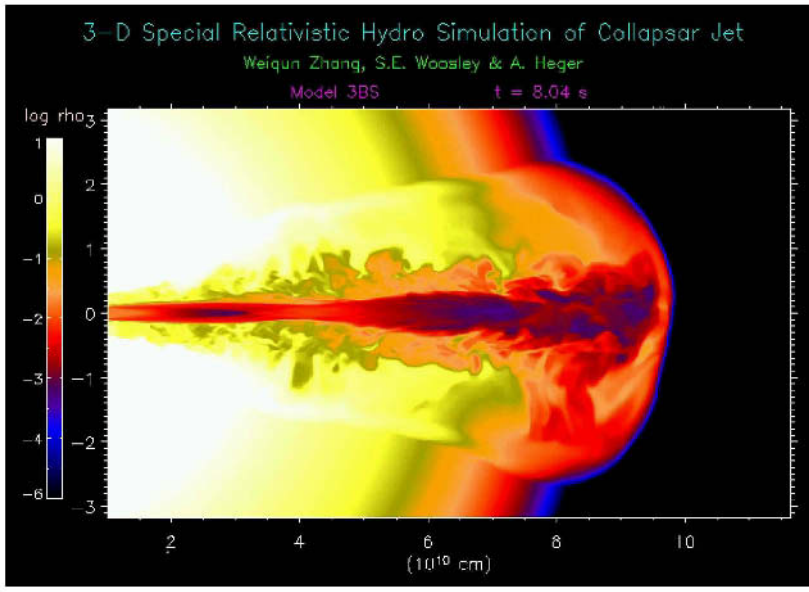

Figure 2. Density distribution of a collapsar jet breaking through the stellar surface. From Zhang, Woosley and Heger 2003.

the newborn proto-neutron star will revive the shock that got stalled in the stellar mantle and will drive the explosion. If, however, a black hole rather than a neutron star is formed early on the neutrino source is essentially shut off and the supernova might "fail". For a non-/slowly rotating star the stellar matter can essentially unhindered disappear in the event horizon of the newborn black hole. If the angular momentum of the star is too high, a disk will form at too large distances to be hot enough for efficient neutrino emission. For intermediate values of angular momentum, however, a more compact, hot accretion disk may form close to the hole. In this case an accretion- rather than neutrino-driven supernova explosion might occur. Although there is no generally accepted mechanism for its explanation there seems to be a general accretion disk-jet connection. Like in many other astrophysical environments such as active galactic nuclei and young stellar objects the formation of a jet is plausible in the collapsar case. It might be powered by energy pumped into the polar region above the hole either via the annihilation of neutrinos emitted from the inner, hot parts of the accretion disk or via MHD mechanisms. Initially the density along the original rotation axis is too high for any plausible jet to overcome the ram pressure of the infalling material. But after a few seconds a channel along the rotation axis opens up allowing later on for jet propagation through the star. This channel is expected to collimate the escaping jet. If the hole, however, has received too large a kick at birth the energy deposition will

not be along the evacuated channel and the jet may be spoilt.
Apart from having the right amount of angular momentum the progenitor star is required to have lost its envelope, since a jet powered for the typical duration of a long burst, $\sim$ 20 s, could not penetrate a giant star, it would rather dissipate its energy in the stellar envelope. To penetrate say a red supergiant it would take around 1000 s and it is hard to see why the burst after having been on for so long should then suddenly shut down within 20 s after breaking through the stellar surface. Therefore, the progenitor stars is expected to have lost its envelope and the GRB is expected to go along with a supernova of type I (i.e. core-collapse but no hydrogen lines). Resulting from very massive stars, collapsars would occur naturally in star forming regions and, as observed, to be associated with a core-collapse supernova of type Ib/c.

The first simulations of the collapsar scenario have been performed using 2D Newtonian, hydrodynamics (MacFadyen & Woosley 1999) exploring the collapse of helium cores of more than 10 $\mathrm{M}_{\odot}$. In their 2D simulation MacFadyen & Woosley found the jet to be collimated by the stellar material into opening angles of a few degrees and to transverse the star within $\sim$ 10 s. The accretion process was estimated to occur for a few tens of seconds. In such a model variability in the lightcurve could result for example from (magneto-) hydrodynamic instabilities in the accretion disk that would translate into a modulation of the neutrino emission/annihilation processes or via Kelvin-Helmholtz instabilities at the interface between the jet and the stellar mantle.
These initial, Newtonian simulations were plagued by highly superluminal motions. Aloy et al. (2000) have improved on this problem using a special relativistic hydrodynamics code to follow jet propagation through a progenitor star. Recently Zhang et al. (2003) have simulated the propagation and breakout of a jet through a Wolf-Rayet star using a 3D, special relativistic grid code. They particularly addressed the question of jet stability going from 2D to 3D and found the gross jet features to be robust against this change. Moreover, they found that even a slowly precessing jet (say a degree per second) is able to penetrate the star and emerge relativistically at its surface. If the jet precesses faster, it is dissipated inside the stellar envelope. At outbreak the jet is surrounded by a mildly relativistic cocoon that will give rise to a transient signal. If the outbreak is seem at a larger angle with the jet axis it may be seen as a so-called "X-ray flash" (Heise 2003)

Despite its obvious success there remain several open questions. First and most important is the progenitor question. Do stars with the right amount of angular momentum at collapse exist at all? If state of the art progenitor models in which angular momentum loss through magnetic torques and wind losses are accounted for (Heger and Woosley 2003) are taken at face value, then the collapse will not result in a sufficiently massive disk to produce a collapsar. However, as the progenitor uncertainties are substantial that does

not necessarily mean a killer argument for collapsars. Another essentially unsolved problem is the question how the jet is launched. In current numerical models the jet *formation* is not modeled, jets are put in by hand and then their propagation through the star is followed. Further uncertainties come from the numerical resolution. As short-wavelength perturbations grow fastest in a Kelvin-Helmholtz instability the question remains whether current models can already resolve the smallest physically important scales. But this will certainly be addressed in future work. As in many current astrophysical simulations the first collapsar models ignored the influence of magnetic fields. Currently a lot of effort is put into MHD-simulations of this event (see e.g. Proga et al. 2003).

Supranova. Stella and Vietri (1998) have suggested a two stage process to create a GRB ("supranova"). The massive star collapses in a "traditional" supernova to form a rotationally supported neutron star that is beyond its non-rotating upper mass limit. They assume the star to spin down via magnetic dipole radiation. Using a "standard" magnetic field of 10^{12} G they estimate a time scale of several years before the "supra-massive" configuration collapses into a black hole. The supernova is expected to leave a $\sim 0.1\ \mathrm{M}_{\odot}$accretion disk in orbit around the neutron star and, once the neutron star collapses to form a black hole, the disk might help to extract the rotational energy of the new-born black hole and to launch the GRB.
The strengths of the model are its natural connection to supernovae and star formation and that the supernova remnant would have enough time to form iron via the decay of nickel and cobalt to possibly produce the claimed iron lines. Moreover, it is expected to be a baryon-clean environment. The model is, however, very sensitive to the fine tuning of parameters. Moreover, GRB030329 places a rather strict limit of a few hours on the delay between the SN and the GRB and thus rules out the supranova model for at least this particular burst.

Fragmenting Core-collapse. Another two stage process, the fragmentation of a core collapse supernova has been suggested recently by Davies et al. (2002). The main idea is that, analogous to the fragmentation of a collapsing molecular cloud into several stars, a sufficiently rapidly rotating progenitor star might undergo fragmentation and form several "lumps" rather than a clean and more or less spherically symmetric neutron star. The various fragments would then be driven towards coalescence via gravitational wave emission and would emit a characteristic chirp signal during inspiral. Once coalesced they will form a "standard GRB central engine", a new-born black hole and an accretion disk. Generally the black hole will receive a kick at birth, a successful GRB-jet can only be launched if the received kick velocity is small. For plausible system parameters a delay of several hours between supernova and GRB can be obtained. This is well within the current limits set by GRB030329. This

model shares with the two previously discussed models its connection with star formation regions and core-collapse supernovae. The exact conditions under which such fragmentation can occur and the corresponding fraction of progenitor systems remains to be explored in future work.

4.2 Short-hard Bursts

As outlined above, the class of short-hard GRBs probably results from a different central engine than long bursts. Compact binaries, either two neutron stars **?** or a neutron star and a low mass black hole **?**, are the most promising candidates for the progenitor of this class. Their gravitational binding energy of a few times 10^{53} erg is expected to easily satisfy the energy requirements of a short GRB (the exact energy in the burst is at present not known since so far no redshift has been detected). As the neutron star dynamical time scale is $\tau_{dyn} = (G\bar{\rho})^{-\frac{1}{2}} \sim 3 \cdot 10^{-4}$ s there should be no problem in providing even the shortest time scales observed in bursts. Moreover, the merger remnants are attractive GRB central engines as the black hole (either preexisting or forming after a neutron star binary coalescence) is guaranteed to be rapidly rotating, either from the angular momentum that has been fed into the hole in the form of neutron star debris or from the orbital motion of a neutron star binary. A soft equation of state leads to more compact neutron stars, therefore a neutron star binary system will have higher orbital velocities at contact and thus a more rapidly rotating black hole will form. The energy stored in the black hole rotation can then possibly be extracted, e.g. via the Blandford-Znajek mechanism (1977).

With the recent discovery of another highly relativistic binary pulsar (Burgay et al. 2003) the estimates for neutron star merger rates have, once again, been increased. With the most likely rates estimated to be as high as $\sim 2 \cdot 10^{-4}$ per year and galaxy (Kalogera et al. 2003), neutron star binary mergers will have no problem to account for all short GRBs, even if substantial beaming is involved.

Neutron star black hole mergers are most often considered to be just a variant of the binary neutron star theme in the sense that they will also produce a black hole plus torus system. It is worth pointing out, however, that the dynamics of this merger process is much more complex than in the neutron star merger case as it is governed by the interplay of gravitational radiation (trying to *decrease* the orbital separation), mass transfer (trying to *increase* the orbital separation) and the reaction of the stellar radius to mass loss. The dynamics of this process is very sensitive to the mass ratio of the binary components which is much less constrained than in the binary neutron star case.

Neutron Star Binary Mergers. Neutron star binaries have for a long time been *the* model for the central engine of GRBs (Goodman et al. 1987, Eichler et al. 1989, Narayan et al. 1992). With the connection of long GRBs with supernovae being well established by now, compact binary mergers are these days not usually considered to be responsible for long duration GRBs, but they are still the leading model for short GRBs.

The coalescence is an intrinsically three-dimensional phenomenon and therefore analytical guidance is rare (although very welcome) and one has to resort to large scale numerical computations. Additional complications arise from the fact that there is almost no field of astrophysics that does not enter at some stage during the coalescence process: the last stages and the merger are certainly dominated by strong-field general relativistic gravity, the neutron star material follows the laws of hydrodynamics, particle physics enters via possible condensates of "exotic" matter in the high-density interiors of the neutron stars and the copiously produced neutrinos in the hot and dense neutron star debris, questions concerning element formation require detailed information on nuclear structure and reactions (often far from stability) to be included and also magnetic fields might play a decisive role since they may, via transport of angular momentum, determine whether and/or when the central, coalesced object collapses into a black hole. Moreover, they are expected to be amplified in the complex fluid motions following the merger to field strengths where they become dynamically important.

Due to this complexity current investigations follow one of two "orthogonal" lines: either ignoring microphysics, resorting to the simplest equations of state (EOS), polytropes, and thereby focusing on solving the complicated set of general relativistic fluid dynamics equations (or some approximation to it; e.g. Shibata and Uryu 2000, Oechslin et al. 2001) or, along the other line, using accurately treatably (Newtonian) self-gravity of the fluid and investigating the influences of detailed microphysics and relating the merger event to astrophysical phenomena (e.g. Ruffert et al. 2001, Rosswog et al. 2002).

How can the available energy now be transformed into outflowing relativistic plasma after such a coalescence event? A fraction of the energy released as neutrinos is expected to be converted, via collisions, into electron-positron pairs and photons. Neutrinos can give rise to a relativistic, pair-dominated wind if they are converted into pairs in a region of low baryon density. Alternatively, strong magnetic fields anchored in the dense matter could convert the available energy of the system into a Poynting-dominated outflow.

Neutrino annihilation

The merger remnant emits neutrinos in copious amounts. The total neutrino luminosities are typically around $2 \cdot 10^{53}$ ergs/s with electron-type antineutrinos carrying away the bulk of the energy. Typical neutrino energies

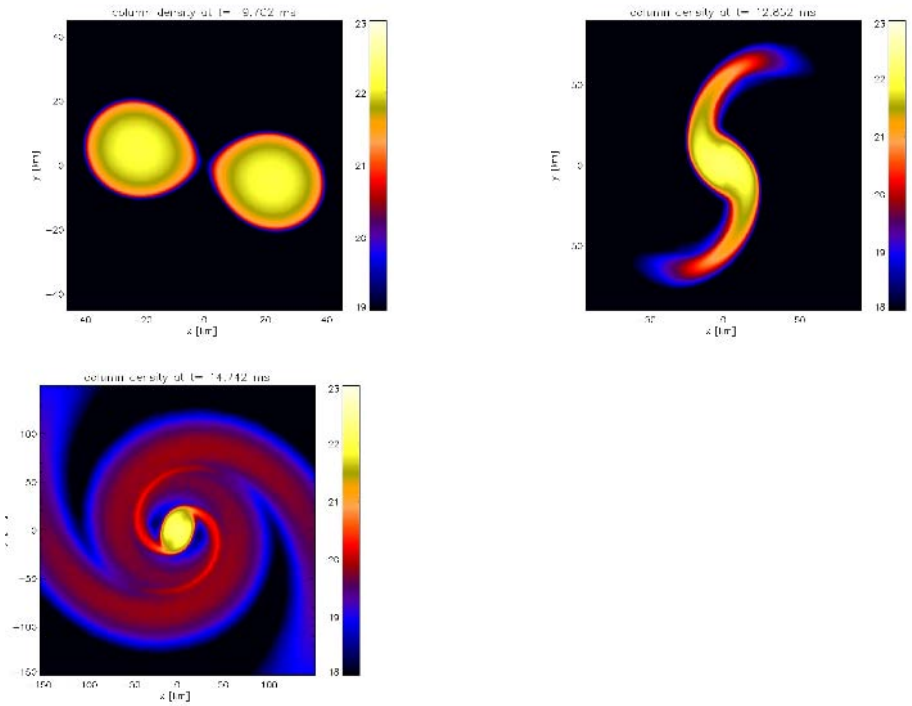

Figure 3. Coalescence of a corotating neutron star binary system (1.4 $M_{\odot}$ each star). Color-coded is the column density, the axes are in kilometers. The simulations are described in detail in Rosswog et al. 2002.

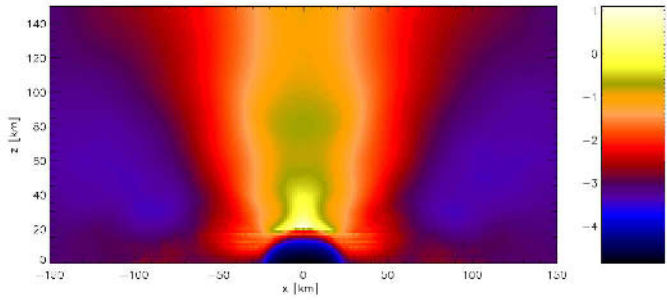

Figure 4. The annihilation of neutrino-antineutrino pairs above the remnant of a neutron star merger drives relativistic jets along the original binary rotation axis (only upper half-plane is shown). The x-axis lies in the original binary orbital plane, the dark oval around the origin is the newly formed, probably unstable, supermassive neutron star formed in the coalescence. Color-coded is the asymptotic Lorentz-factor. Details can be found in Rosswog et al. 2003.

are not too different from those of type II supernovae, electron neutrinos are around 8 MeV, their anti-particles around 15 and the heavy lepton (anti-)neutrinos have energies around 22 MeV (Rosswog and Liebendoerfer 2003).

Neutrino annihilation is an attractive process to launch a fireball as neutrinos can leave the hot remnant easily and can deposit their energy possibly in a region devoid of baryons to avoid prohibitive baryon loading. The centrifugally evacuated funnel region above the remnant is an ideal place for this deposition to occur because it is close to the central energy source (the energy deposition rate scales roughly with the inverse fourth power of the distance) but contains only a small number of baryons (e.g. Ruffert et al. 1997, Rosswog and Davies 2002). Here the $\nu\bar{\nu}$ energy flux can be transformed into a radiation-dominated fluid with a high entropy per baryon. The thick disk geometry of the remnant with its steep density gradients in the radial direction does not allow for lateral expansion. The only escape route is along the initial binary rotation axis. The disk geometry is therefore responsible for channeling the relativistic outflow into a pair of anti-parallel jets. This mechanism is similar to that envisaged by MacFadyen & Woosley (1999) for the collapsar scenario, but offers the advantage that the jets in our case do not have to pierce through a surrounding stellar mantle.

Neutrino annihilation from full merger simulations has been calculated by

Ruffert et al. (1997) and Rosswog et al. (2003), Popham et al.(1999) have studied the annihilation for the case of steady state accretion disks. The resulting bulk Lorentz-factor is determined by the annihilation energy deposited per rest mass energy. This quantity is displayed in Figure 4 (for details see Rosswog et al. 2003). The encountered Lorentz-factors range from around 10 (this is a lower limit as finite numerical resolution leads us to overestimate the funnel density and therefore to underestimate the Lorentz-factor) to a few times 10^4 for extreme cases (see Rosswog et al. 2003 for details), so Lorentz factors of several hundred should not pose any problem for this mechanism.
The total energy in the relativistic outflow, however, is only of order 10^{48} ergs and therefore moderate by GRB standards. Ruffert et al. (1997) find somewhat higher values, but agree that neutrino annihilation can only power a relatively weak burst. To account for the observed luminosities of a short GRB, the relativistic outflow has to remain well-collimated. One such collimation mechanism (Levinson and Eichler 2000) relies on the beaming of the relatively weak, relativistic jet by the ram-pressure of the non-relativistic, but powerful baryonic wind that is blown off the merger remnant via neutrinos (this is very similar to the neutrino-driven wind of a new-born proto-neutron star). Using a theoretical neutron star mass distribution Rosswog and Ramirez-Ruiz (2003) have calculated the resulting beaming angle and the apparent luminosity distribution. They find a broad distribution of apparent luminosities (typical values for isotropized luminosities of $\sim 5 \cdot 10^{50}$ erg/s) with average jet opening angles of $\sim 5^o$. These results are compatible with both the observed fluences for short GRBs and with the estimated neutron star merger rates.

Magnetic mechanisms

Neutron stars are endowed by strong magnetic fields, typically of order 10^{12} G. Even the sun with its comparatively moderate magnetic fields and fluid motions produces a large spectrum of different magnetic activities with sometimes violent outbreaks. Thus it is natural to expect scaled up versions such activity in an event as vigorous as a neutron star merger. Several magnetic GRB scenarios have been discussed over the years, e.g. by Usov (1992, 1994), Narayan et al. (1992), Duncan and Thompson (1992), Thompson and Duncan (1994), Meszaros and Rees (1997), Katz (1997), Kluzniak and Ruderman (1998) and Rosswog et al. (2003).
I want to mention here three different possibilities: first, that the central object formed in the coalescence remains stable for (at least) a short time of the order a second before collapsing to black hole. During this time the seed magnetic fields can be amplified drastically and the central object can, as some kind of a "superpulsar", launch a short lived relativistic wind. Second, similar field amplification processes are expected to occur in the accretion torus around the central object. Finally, if the central object should collapse immediately into a

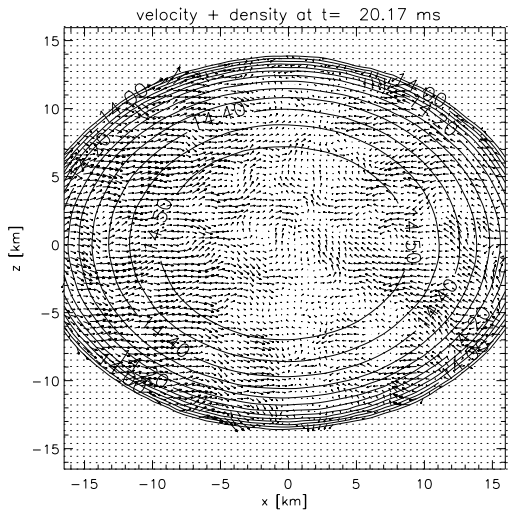

Figure 5. Velocity field (space-fixed frame) inside the central object of the remnant of a neutron star coalescence. The labels at the contour lines refer to $\log(\rho)$, typical fluid velocities are $\sim 10^8$ cm/s.

black hole (i.e. before its rotational energy can be extracted by the superpulsar mechanism) its rotational energy can be extracted via a magnetic coupling to the accretion torus. The latter two processes have been discussed in the literature (e.g. Blandford and Znajek 1977, Narayan et al. 1992, Rosswog et al. 2003). We will therefore draw attention to the first possibility.

The central object of the remnant is rapidly differentially rotating (see Rosswog and Davies 2002 for rotation curves) with rotational periods ranging from ~ 0.4 to ~ 2 ms. Differential rotation is known to be very efficient in stabilizing stars that are substantially more massive than their non-rotating maximum mass. For example, Ostriker and Bodenheimer (1968) constructed differentially rotating white dwarfs of 4.1 $\mathrm{M}_\odot$. A recent investigation analyzing differentially rotating polytropic neutron stars (Lyford et al. 2002) finds it possible to stabilize systems even beyond twice the typical neutron star mass of 2.8 $\mathrm{M}_\odot$. The exact time scale of this stabilization is difficult to determine, as all the poorly known high-density nuclear physics could influence the results, but for this process to work, only a time scale of about a second is needed (some authors have estimated time scales of up to years **?**).

It is worth pointing out that the fluid flow in our calculations of the merger (Rosswog et al. 2003) never becomes axisymmetric during the simulation and therefore Cowlings anti-dynamo theorem does not apply here. When the surfaces of the neutron stars come into contact, a vortex sheet forms between them

across which the tangential velocities exhibit a discontinuity. This vortex sheet is Kelvin-Helmholtz-unstable with the shortest modes growing fastest. These fluid instabilities lead complex flow patterns inside the central object of the merger remnant. In the orbital plane they manifest themselves as strings of vortex rolls that may merge (see Fig. 8 in Rosswog and Davies 2002). An example of the flow pattern perpendicular to the orbital plane is shown in Fig. 5. This pattern caused by fluid instabilities exhibits "cells" of size $l_c \sim 1$ km and velocities of $v_c \sim 10^8$ cm/s. Moreover, we expect neutrino emission to drive convection as in the case of proto-neutron stars. The neutrino optical depth within the remnant drops very steeply from $\sim 10^4$ at the center to the edge of the central object (see Fig. 11 in Rosswog and Liebendoerfer 2003). For this reason the outer layers loose neutrino energy, entropy and lepton number at a much higher rate than the interior, this leads to a gradual build-up of a negative entropy and lepton number gradient which will drive vigorous convection (e.g. Epstein 1979). We expect this to set in after a substantial fraction of the neutrino cooling time (i.e. on time scales longer than our simulated time) when a lot of the thermal energy of the remnant has been radiated away. With neutrinos as dominant viscosity source we find viscous damping time scales of several tens of seconds, i.e. much longer than the processes we are interested in (see below).

We expect an efficient $\alpha-\Omega$-dynamo to be at work in the merger remnant. The differential rotation will wind up initial poloidal into a strong toroidal field ("Ω-effect"), the fluid instabilities/convection will transform toroidal fields into poloidal ones and vice versa ("$\alpha-$effect"). Usually, the Rossby number, $Ro \equiv \frac{\tau_{\rm rot}}{\tau_{\rm conv}}$ is adopted as a measure of the efficiency of dynamo action in a star. In the central object we find Rossby numbers well below unity, ~ 0.4, and therefore expect an efficient amplification of initial seed magnetic fields. A convective dynamo amplifies initial fields exponentially with an e-folding time given approximately by the convective overturn time, $\tau_c \approx 3$ ms; the saturation field strength is thereby independent of the initial seed field (Nordlund et al. 1992).

Adopting the kinematic dynamo approximation we find that, if we start with a typical neutron star magnetic field, $B_0 = 10^{12}$ G, as seed, equipartition field strength in the central object will be reached (provided enough kinetic energy is available, see below) in only ≈ 40 ms. The equipartition field strengths in the remnant are a few times 10^{17} G for the central object and around $\sim 10^{15}$ G for the surrounding torus (see Fig. 8 in Rosswog et al. 2003). To estimate the maximum obtainable magnetic field strength (averaged over the central object) we assume that all of the available kinetic energy can be transformed into magnetic field energy. Using the kinetic energy stored in the rotation of the central object, $E_{\rm kin} = 8 \cdot 10^{52}$ erg for our generic simulation, we find $\langle B_{co} \rangle = (3 \cdot E_{\rm kin}/R_{co}^3)^{1/2} \approx 3 \cdot 10^{17}$ G, where R_{co} is the radius of the central

object (note that if only a fraction of 0.1 of the equipartition pressure should be reached this would still correspond to $\sim 10^{17}$ G).
There are various ways how this huge field strength could be used to produce a GRB. The fields in the vortex rolls (see Fig. 8 in Rosswog and Davies 2002) will wind up the magnetic field fastest. Once the field reaches a strength close to the local equipartition value it will become buoyant, float up, break through the surface and possibly reconnect in an ultra-relativistic blast (Kluzniak and Ruderman 1998). The time structure imprinted on the sequence of such blasts would then reflect the activity of the fluid instabilities inside the central object. The expected lightcurve of the GRB would therefore be an erratic sequence of sub-bursts with variations on millisecond time scales.

Simultaneously such an object can act as a scaled-up "super-pulsar" and drive out an ultra-relativistic wind. A similar configuration, a millisecond pulsar with a magnetic field of a few times 10^{15} G, formed for example in an accretion-induced collapse, has been suggested as a GRB-model by Usov (1992, 1994). The kinetic energy from the braking of the central object is mainly transformed into magnetic field energy that is frozen in the outflowing plasma. At some stage the plasma becomes transparent to its own photons producing a blackbody component. Further out from the remnant the MHD-approximation breaks down and intense electromagnetic waves of the rotation frequency of the central engine are produced. These will transfer their energy partly into accelerating outflowing particles to Lorentz-factors in excess of 10^6 that can produce an afterglow via interaction with the external medium. The other part goes into non-thermal synchro-Compton radiation with typical energies of ~ 1 MeV (Usov 1994).

Neutron Star Black Hole Mergers. Neutron star black hole mergers have been estimated to occur at a rate of 10^{-4} (year Galaxy)$^{-1}$ **?**, i.e. an event rate comparable to that of neutron star binaries is expected. Moreover, their gravitational wave signal is stronger and therefore they could possibly dominate the first detectable signals from inspirals of compact binaries.
Simulations of this scenario have been performed by Lee (Lee 2001 and references therein) using Newtonian gravity and polytropic equations of state of varying stiffness. Ruffert, Janka and Eberl performed similar simulations but with a detailed microphysics input (nuclear equation of state and neutrino leakage **?**). In our own simulations of NS-BH mergers we used a relativistic mean field equation of state **?** together with three-dimensional smoothed particle hydrodynamics and a detailed, multiflavour neutrino treatment.
The interaction of mass transfer, gravitational wave backreaction and the reaction of the neutron star radius to the mass loss leads to a very complicated accretion dynamics in a neutron star black hole system. We find in all of our simulations (apart from an extreme test case with mass ratio $q = 0.93$, i.e. a

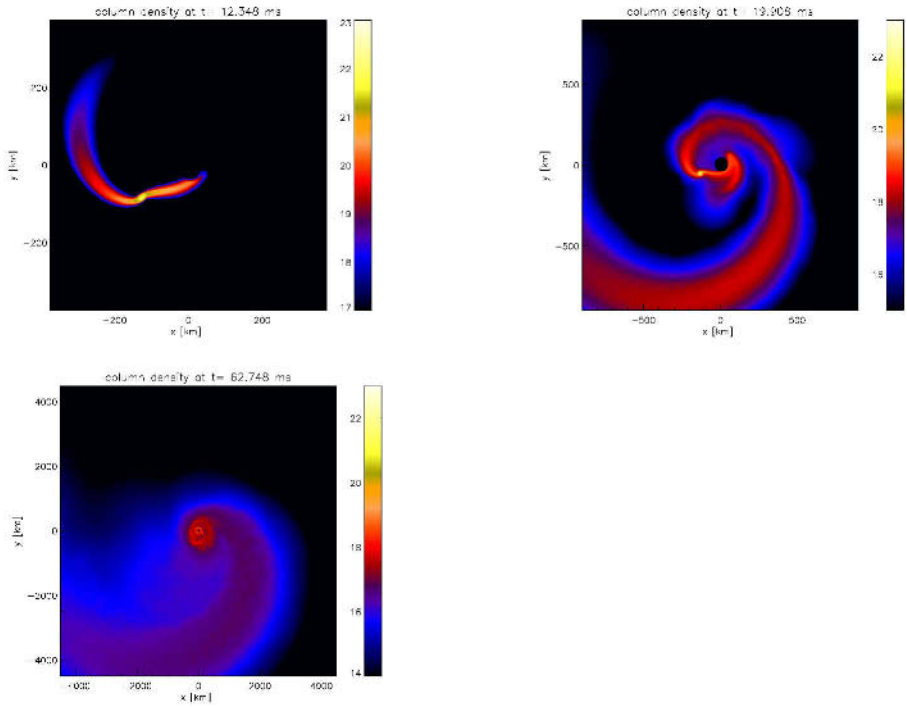

Figure 6. Tidal disruption of 1.4 $M_\odot$ neutron star by a 14 $M_\odot$ black hole. Color-coded is the logarithm of the column density (g/cm^2). Note the change in the scales (km) of the different panels. From Rosswog et al. 2004.

black hole of 1.5 $M_\odot$and a neutron star of 1.4 $M_\odot$) that a "mini-neutron star" survives. A specific example, a black hole with 14 $M_\odot$, an initially tidally locked neutron star of 1.4 $M_\odot$modeled using Newtonian gravity plus gravitational wave backreaction forces is shown in Figure 6. We find initial peak mass transfer rates of $\sim 500\ M_\odot$/s (at about the time shown in the first panel of Figure 6). After that phase the orbit widens, and we find a long sequence of mass transfer episodes, always transferring mass into an accretion disk around the hole, moving out, spiraling in again and so on. At the end of the simulation (after around 64 ms and seven mass transfer phases) the neutron star still has around 0.2 $M_\odot$and shows no sign of being disrupted soon (the later mass transfer rates reduce its mass mass only by small amounts). The accretion disk that forms around the hole is very low in mass ($> 10^{-2}\ M_\odot$) and relatively moderate in temperature ($T \sim 2$ MeV). Under these circumstances the neutrino luminosity is around an order of magnitude smaller than in the binary neutron star merger case and therefore not very encouraging to power a GRB. Systems without initial neutron star spins yield somewhat more promising accretion disks, but details remain to be explored further. These results are sensitive to the stiffness of the equation of state, a softening of the EOS at higher densities (e.g. due to the presence of hyperons) could possibly substantially alter the results.

5. Summary and Prospects

In the last few years the GRB field has seen tremendous progress. The cosmological distance scale is now well-established. Moreover, since GRB030329 the connection of (long) GRBs with supernovae, suspected already in the very first paper on GRBs by Klebesadel et al. (1973), has been put to a firm footing. This lends further strength to the collapsar model of the long burst category.
But there are still myriards of open questions both related to the astrophysical events/central engines as well as related to the fundamental physics involved. For example, is our picture of stellar evolution wrong if state of the art progenitor models cannot produce progenitors of sufficient angular momentum for a collapsar? If collapsars result from Wolf-Rayet stars then why does the expected ambient matter density distribution resulting from a stellar wind ($\rho \propto r^{-2}$) not give better results in interpreting observations than a constant ambient matter density? What is the connection between GRBs and X-ray flashes? Is it the same event seen from different angles? Do short GRBs have afterglows? Why are their spectra harder? Do they also occur close to star forming regions?
Or from the physics side: by which physical mechanisms are jets launched from accretion disks? How are the ejecta accelerated to Lorentz factors beyond 100? How are the magnetic fields at the emission site created? Are they

advected from the central engine or are they produced by in shocks?
Hopefully, at least some of the above questions can be answered in the near future by missions such as SWIFT.

Acknowledgments

The simulations of the compact binary mergers were performed using both the UK Astrophysical Fluids Facility (UKAFF) and the University of Leicester Mathematical Modeling Centre's supercomputer. S.R. gratefully acknowledges a PPARC Advanced Fellowship.

References

Band, D. et al., ApJ, 413, 281 (1993)
Bethe, H.A. and Brown, G.E., ApJ, 506, 780 (1998)
Blandford, R. and McKee,C.F. Physics of Fluids, 19, 1130 (1976)
Blandford, R. and Znajek, MNRAS, 179, 433 (1977)
Bloom, J.S. et al., Nature, 401, 453 (1999)
Bloom, J.S., Kulkarni, S.R. and Djorgovski, S.G., AJ, 123, 1111 (2002)
Burgay, M. et al., Nature, 426, 531 (2003)
Coburn, W. and Boggs, S.E., Nature, 423, 415 (2003)
Cohen, E., Kolatt,T., Piran, T.,astro-ph/9406012 (1994)
Cohen, E. et al., ApJ, 480, 330 (1997)
Costa, E., Nature, 372, 652 (1997)
Davies, M.B., King, A.R., Rosswog, S. and Wynn, G., ApJ, 579, 63 (2002)
Dar, A. and De Rujula, A., astro-ph/0308248 (2003)
Duncan, R.C. & Thompson, C., ApJ, 392, L9 (1992)
Epstein, R.I., MNRAS, 188, 305 (1979)
Ghisellini et al. A&A, 389, L33 (2002)
Eichler,D. et al., Nature, 340, 126 (1989)
Frail D. et al., ApJ, 526, 152 (1999)
Fryer, C.L., Woosely, S.E. and Hartmann, D.H., ApJ, 526, 152 (1999)
Goodman, J., ApJ, 308, L46 (1986)
Goodman, J., Dar, A. and Nussinov, S., ApJ, 314, L7 (1987)
Heger, A. and Woosley, S.E., GRBs in the Afterglow Era, ESO Astrophysics Symposia (2001), AIP Conference Proceedings, Volume 662, p. 214 (2003)
Heise, J., GRBs in the Afterglow Era, ESO Astrophysics Symposia (2001), AIP Conference Proceedings, Volume 662, p. 229 (2003)
Hjorth, J. et al, Nature, 423, 847 (2003)
Janka, H.T. et al. (1999), ApJ, 527, 39 (1999)
Kalogera, V. et al., submitted to ApJL, Astrophys.J.601:L179-L182 (2003)
Klebesadel, R.W., Strong, I.B. and Olson, R.A., ApJ, 182, L85 (1973)
Kobayashi, S., Piran, T. and Sari, R., ApJ, 490, 92 (1997)
Kouveliotou, C., et al., ApJ, 413, L101 (1993)
Lee, W.H., MNRAS, 328, 583 (2001)
Lloyd-Ronning, N.M., Fryer, C.L. and Ramirez-Ruiz, E., ApJ, 574, 554 (2002)
MacFadyen, A.I. and Woosley, S.E., ApJ, 524, 262 (1999)
MacFadyen, A.I., Woosley, S.E. and Heger, A., ApJ, 550, 410 (2001)
Mao, S., Narayan, R. and Piran, T., ApJ, 420, 171, (1994)

Mészáros, P. & Rees, M. J., ApJ, 418, L5 (1993)
Mészáros, P. & Rees, M. J., ApJ, 476, 232 (1997)
Mészáros, P. & Rees, M. J., ApJ, 482, L29 (1997)
Mészáros, P., Ann. Rev. of A & A, 40, 137 (2002)
Narayan, R., Pazcynski, B. and Piran, T., ApJ, 395, L83 (1992)
Norris, J.P., Marani, G.F. and Bonnell, J.T., ApJ, 534, 248 (2000)
Oechslin, R., Rosswog, S. and Thielemann, F.-K., Phys. Rev. D, 65, 103005 (2002)
Paciesas, W.S. et al., ApJS, 122, 465 (1999)
Paciesas, W.S. et al., Gamma-ray Bursts in the Afterglow Era, Proceedings of the International GRB conference in Rome; Berlin Heidelberg, Springer, 2001
Paczynski, B., ApJ, 308, L43 (1986)
Paczynski, B., Acta Astronomica, 41, 257, (1992)
Paczynski, B. and Rhoads, J.E., ApJ, 418, L5 (1993)
Piran, T., Phys. Rep. 314, 575 (1999)
Piro, L., Science, 290, 955 (2000)
Popham, R., Woosley, S.E., Fryer, C., 518,356 (1999)
Preece, R.D. et al., ApJ, 506, 23 (1998)
Proga, D. et al., ApJ, 599, L5 (2003)
Rasio F., Shapiro S., 1992, ApJ, 401, 226
Rasio F., Shapiro S., 1994, ApJ, 432, 242
Rasio F., Shapiro S., 1995, ApJ, 438, 887
Rosswog, S., Liebendoerfer, M., Thielemann, F.-K., Davies, M. B., Benz, W. & Piran, T., A&A, 341, 499
Rosswog S., Davies M. B., Thielemann F.-K., Piran T., 2000, A & A, 360, 171
Rosswog S., Davies M. B., 2002, MNRAS, 334, 481
Rosswog S., Ramirez-Ruiz E., 2002, MNRAS, 336, L7
Rosswog, S. & Liebendoerfer, 2003, MNRAS, 342, 673 (2003)
Rosswog, S. & Ramirez-Ruiz E., 2003, MNRAS, 343, L36 (2003)
Rosswog, S., Ramirez-Ruiz E. & Davies, M.B., 2003, MNRAS, 345, 1077 (2003)
Rosswog, S. et al., in preparation (2004)
Ruffert M., Janka H.-T., Schäfer G., 1996, A & A, 311, 532
Ruffert M., Janka H.-T., Takahashi K., Schäfer G., 1997, A & A, 319, 122
Ruffert M., Janka H.-T., 1999, A & A, 344, 573
Ruffert M., Janka H.-T., 2001, A & A, 380, 544
Ruderman, M, Ann. N.Y. Acad. Sci., 262, 164
Rutledge, R.E. and Fox, D.B., Mon.Not.Roy.Astron.Soc.350:1272 (2003)
Schaefer, B.E. and Walker, K.C., ApJ, 511, L89 (1999)
Schmidt, W.K.H., Nature, 271, 525 (1978)
Shen H., Toki H., Oyamatsu K., Sumiyoshi K., 1998a, Nuclear Physics A, 637, 435
Shibata, M. Phys. Rev. D, 60, 104052 (1999)
Shibata, M. and Uryu, K., Phys. Rev. D, 61, 064001 (2000)
Stanek, K.Z. et al., ApJ, 591, L17 (2003)
Thompson, C. & Duncan, R.C., 1993, ApJ, 408, 194
Usov, V.V., Nature, 357, 472 (1992)
Vietri, M., ApJ, 478, L9 (1997)
Woosely, S.E., ApJ, 405, 273 (1993)
Yi, I. and Blackman, E.G., ApJ, 494, L163 (1998)
Zhang, W., Woosley, S.E. & MacFadyen, ApJ, 586, 356 (2003)

SUPERDENSE STARS WITH A QUARK CORE

G. B. Alaverdyan
Yerevan State University, Alex Manookian 1, Yerevan 375025 , Armenia
galaverdyan@ysu.am

A. R. Harutyunyan
Yerevan State University, Alex Manookian 1, Yerevan 375025 , Armenia
anharutr@ysu.am

Yu. L. Vartanyan
Yerevan State University, Alex Manookian 1, Yerevan 375025 , Armenia
yuvartanyan@ysu.am

Abstract Series of neutron star models with strange quark cores are constructed on the basis of an extensive set of calculated realistic equations of state of superdense matter with quark-hadron phase transition. For some models a new local maximum on the stable branch of the star mass -central pressure diagram is revealed. This maximum arises along with the appearance of a sharp fracture on the core, which is characteristic for models of layered stars with $\lambda > 3/2$ (λ is the relativistic parameter of the density jump) and corresponds to the beginning of formation of a new phase. Such a new local maximum is discovered in the mass range of about $M \sim 0.08 M_\odot$ in some models, as well as at $M \sim 0.82 M_\odot$ in others. Stable equilibrium layered neutron stars, located in these ranges, are characterized also by unusually large values of the stellar radius (from $R \sim 1300$ km to $R \sim 2700$ km for different equations of state). For such equations of state accretion onto a neutron star will lead to two successive jumplike transitions to a quark-core neutron star; as a result, there will be two successive energy releases.

Keywords: Neutron stars, strange quark core, quark phase transition, new branch of stability, accretion

1. Introduction

At superhigh densities a phase transition is possible from the state in which quarks are confined within the baryons, to a continuum quark plasma [1]. At

D. Blaschke and D. Sedrakian (eds.), Superdense QCD Matter and Compact Stars, 331–340.

present an exact theoretical description of matter both in baryon and quark-gluon density ranges is not possible. This makes it very important to study the dependence of parameters of superdense stellar objects on the variants of equation of state (EoS). In many studies models of strange stars were comprehensively analyzed. However, much fewer studies are devoted to configurations with a density jump [2, 4–9]. The most complete calculations of models with a mixed phase are in Refs. [11, 13, 12, 10, 14], which contain various quark configurations in the form of droplet, rodlike, and platelike structures; these models assume continuous energy and density variations in the quark-phase formation region [15]. The results of these authors show that the formation of the mixed phase of quark and nuclear matter may be energetically more or less favorable than an ordinary first-order nucleon-to-quark phase transition, depending on the local surface and Coulomb energies associated with the formation of mixed-phase quark and nuclear structures [11, 13]. Because of uncertainty in the interface tension of strange quark matter, we presently cannot unambiguously establish which of the above alternatives is actually realized [10, 16]. Below, we consider the case that assumes an interface tension that leads to a first-order phase transition with the possible coexistence of the two phases. In the present work, we study the functional dependence of integral parameters and structural characteristics of layered neutron stars with a strange quark core on the form of EoS of superdense matter with first order phase transition to strange quark state. Series of models of neutron stars with strange quark cores are constructed, based on an extensive set of calculated realistic equations of state. The parameters of some characteristic configurations of the calculated series are also presented, and their thorough investigation is carried out. For some models of EoS the possibility of a new additional range of stability for neutron stars with strange quark cores is revealed.

2. Equations of state

In the present work we carry out a thorough study of layered configurations with a density jump, containing strange quark core. By combination of the three EoS of neutron matter with different variants of strange quark-electron plasma calculated within the framework of MIT quark "bag" model [17], we constructed an extensive set of realistic EoS with a quark phase transition. Table 1 gives the variants of the EoS used for the quark component, as well as the values of the energy per baryon ε_{min} and the baryon density n_{min} at the minimum point. If the energy per baryon ε in strange quark phase has a positive minimum ε_{min}, a thermodynamic equilibrium between the quark matter and the baryon component may take place that is realized in neutron stars with a quark core. At subnuclear and supranuclear densities, we used relativistic EoS for neutron matter that were calculated and tabulated by Weber, Glen-

Table 1. The variants of quark-electron plasma

	m_s MeV	B MeV/fm^3	α_c	$\varepsilon_{\min}$ MeV	$n_{\min}$ fm^{-3}
a	175	55	0.5	10.44	0.258
b	200	55	0.5	20.71	0.263
c	175	55	0.6	28.61	0.258
d	175	60	0.5	28.97	0.276
e	200	55	0.6	38.24	0.259
f	200	60	0.5	39.12	0.282
g	175	60	0.6	47.44	0.275
h	200	60	0.6	56.90	0.277

denning and Weigel [18], based on the "HEA" and "$Bonn$" meson-exchange potentials [19–21], by taking into account two-particle correlations in the λ^{00}-approximation [22, 23] ($3.56 \cdot 10^{13}$g/cm^3 $< \rho <$ $4.81 \cdot 10^{14}$g/cm^3). These EoS and the corresponding EoS for nucleon component of layered neutron star matter are labeled by "HEA" and "$Bonn$". These are joined with the EoS of neutron star matter for lower density ranges [24]. As an example of a more stiff EoS (compared with the above mentioned HEA and $Bonn$ EoS) the "$BJ-V$" EoS [25] was used in the same density range.

Note that the conditions for the phase transition to a quark phase and thermodynamic equilibrium with the nucleon component, as it is seen from our analysis, are realized only for eleven EoS from the considered twenty four ones. Furthermore, for all the three used models of neutron matter the equilibrium and simultaneous coexistence with the quark EoS variants e, g and h having high values of ε_{min}, is impossible.

3. Superdense configurations with a strange quark core. Results and Discussion

The integral and structural parameters for models of calculated series of superdense layered stellar configurations are presented in this section, and their thorough investigation for some characteristic configurations is carried out. Among the basic parameters are the calculated stellar radius R, gravitational mass M, rest mass M_0, proper mass M_p, the mass and radius of the strange quark core M_{core} and R_{core}, respectively, relativistic moment of inertia I and gravitational redshift on the surface of the star Z_s. Also given here is the accumulated mass M_{Aen} and the radial coordinate R_{Aen}, corresponding to the threshold for evaporation of neutrons from nuclei ($\rho_{nd} = 4.3 \cdot 10^{11}$g/cm^3). In models of EoS with $\lambda < 3/2$ (in our work seven) a kink (fracture) on the $M(P_c)$ curve without a change of derivative sign appears at the beginning of formation of quark-phase core at the center of the star (the transition to a quark

phase does not cause instability). In the opposite case ($\lambda > 3/2$) at the threshold of formation of quark-phase core a descending branch on the $M(P_c)$ curve occurs; the configurations on this branch are unstable (the so-called instability of configurations with small-mass cores); thus, the local toothlike maximum (kink) arises on the $M(P_c)$ curve. Table 2 gives the basic integral parameters for the four characteristic configurations A, B, F and G obtained using the seven EoS with $\lambda < 3/2$. It also gives the parameters of the first-order phase transition – the values of transition pressure P_0 and energy densities ρ_N and ρ_Q at the transition point in the nucleon and quark phases, respectively. The EoS with phase transition are labeled as follows: the numbers refer to the nuclear EoS with 1 corresponding to HEA, 2 – to $Bonn$, 3 – to $BJ - V$; the letters refer to the corresponding quark model (see Table 1). The relativistic parameter of density jump $\lambda = \rho_Q/(\rho_N + P_0/c^2)$ is given as well; its value determines the stability ranges of layered models on the curve of the dependence of star mass M on the central pressure P_c [26, 28]. The configuration A corresponds to a point of loss of stability in the low-mass range on the $M(P_c)$ curve. These configurations have no quark core. The bulk of their mass is concentrated in "Aen" plasma (which consists of degenerated neutrons and electrons, and neutron-rich atomic nuclei). The radius of this range is of the order of $10 - 11$ km. However the whole radius of these configurations, which varies from 200 km to 250 km, is mainly determined by the so-called "Ae" - matter (matter composed of atomic nuclei and electrons), and the packing factor $\alpha = (M_0 - M)/M_0$ is within the interval $(3 \div 6) \cdot 10^{-3}$, i.e. of the same order of magnitude as for white dwarfs. Configurations B label the models of neutron stars with the central pressure corresponding to the threshold for formation of a quark core. For these models the values of the packing factor α are within $(1.8 \div 7.5) \cdot 10^{-2}$, and the gravitational redshift from the star surface varies in the interval $(3.3 \div 13) \cdot 10^{-2}$. Configurations F represent the models of layered neutron stars with the observationally inferred mass $1.44\ M_\odot$ [27]. Configurations G represent layered neutron stars with a maximal possible mass, i.e. the mass beyond which the stability loss occurs. The values of the maximal mass M_{max} are within $(1.69 \div 1.83)\ M_\odot$. For all the four calculated EoS with $\lambda > 3/2$ whose critical configurations are given in the Table 3, the transition pressure is much less than in models considered above. The toothlike kink characteristic for models with $\lambda > 3/2$ on the $M(P_c)$ curve is well seen for all these EoS, however it is located in the low-mass range for models $1a$, $2a$ and $3b$. Apart from this feature, we found that for the three EoS ($1a$, $2a$ and $3a$) a new additional local maximum is formed on the $M(P_c)$ curve after the characteristic kink.

Such models were obtained and calculated for the first time in Refs. [**?**, **?**]. The appearance of the second local maximum implies the existence of a new family of stable equilibrium stellar configurations - the neutron stars with a

	P_c MeV/fm^3	$\rho_c 10^{-14}$ g/cm^3	R_{core} km	M_{core} $M_\odot$	R_{Aen} km	m_{Aen} $M_\odot$	R km	M $M_\odot$	M_0 $M_\odot$	I $M_\odot km^2$	z_s
EoS 1b	$P_0 = 5.98 MeV/fm^3$,	$\rho_N = 3.49 \cdot 10^{14} g/cm^3$,	$\rho_Q = 4.86 \cdot 10^{14} g/cm^3$,	$\lambda = 1.35$							
A	0.74	2.05	0	0	11.35	0.076	245.01	0.0806	0.0811	9.439	$4.9 \cdot 10^{-4}$
B	5.98	4.86	0	0	9.91	0.318	12.22	0.3184	0.3273	8.776	$4.1 \cdot 10^{-2}$
F	77.53	9.07	9.751	1.209	11.34	1.441	11.73	1.4411	1.6245	74.628	$2.5 \cdot 10^{-1}$
G	321.97	22.80	9.775	1.707	10.67	1.831	10.88	1.8315	2.1431	90.304	$4.1 \cdot 10^{-1}$
EoS 2b	$P_0 = 5.67 MeV/fm^3$,	$\rho_N = 3.52 \cdot 10^{14} g/cm^3$,	$\rho_Q = 4.84 \cdot 10^{14} g/cm^3$,	$\lambda = 1.34$							
A	0.74	2.01	0	0	11.26	0.075	259.07	0.0798	0.0803	10.351	$4.5 \cdot 10^{-4}$
B	5.67	4.84	0	0	9.93	0.305	12.40	0.3048	0.3129	8.317	$3.8 \cdot 10^{-2}$
F	77.53	9.07	9.786	1.219	11.34	1.440	11.73	1.4400	1.6230	74.466	$2.5 \cdot 10^{-1}$
G	322.57	22.83	9.793	1.713	10.66	1.831	10.87	1.8311	2.1425	90.213	$4.1 \cdot 10^{-1}$
EoS 2c	$P_0 = 14.11 MeV/fm^3$,	$\rho_N = 4.13 \cdot 10^{14} g/cm^3$,	$\rho_Q = 5.26 \cdot 10^{14} g/cm^3$,	$\lambda = 1.20$							
A	0.74	2.01	0	0	11.26	0.075	259.07	0.0798	0.0803	10.351	$4.5 \cdot 10^{-4}$
B	14.11	4.13	0	0	11.13	0.686	12.22	0.6864	0.7252	28.894	$9.5 \cdot 10^{-2}$
F	67.28	8.31	8.723	0.879	11.84	1.440	12.27	1.4400	1.6119	79.270	$2.4 \cdot 10^{-1}$
G	170.52	14.07	9.611	1.438	11.58	1.820	11.85	1.8200	2.1075	103.110	$3.5 \cdot 10^{-1}$
EoS 3c	$P_0 = 6.01 MeV/fm^3$,	$\rho_N = 4.08 \cdot 10^{14} g/cm^3$,	$\rho_Q = 4.79 \cdot 10^{14} g/cm^3$,	$\lambda = 1.14$							
A	0.49	1.50	0	0	12.87	0.088	197.84	0.0931	0.0934	9.379	$6.9 \cdot 10^{-4}$
B	6.01	4.79	0	0	10.46	0.307	13.21	0.3072	0.3133	8.676	$3.6 \cdot 10^{-2}$
F	73.09	8.63	9.818	1.200	11.54	1.442	11.94	1.4419	1.6106	76.082	$2.5 \cdot 10^{-1}$
G	170.52	14.07	10.225	1.629	11.38	1.799	11.65	1.7989	2.0760	99.515	$3.5 \cdot 10^{-1}$
EoS 2d	$P_0 = 11.22 MeV/fm^3$,	$\rho_N = 3.97 \cdot 10^{14} g/cm^3$,	$\rho_Q = 5.46 \cdot 10^{14} g/cm^3$,	$\lambda = 1.31$							
A	0.74	2.01	0	0	11.26	0.080	257.43	0.0798	0.0803	10.211	$4.6 \cdot 10^{-4}$
B	11.22	3.97	0	0	10.76	0.561	12.07	0.5612	0.5875	21.040	$7.7 \cdot 10^{-2}$
F	82.86	9.57	9.004	1.044	11.39	1.440	11.78	1.4400	1.6181	73.480	$2.5 \cdot 10^{-1}$
G	335.80	23.59	9.281	1.594	10.60	1.806	10.81	1.8059	2.1029	86.368	$4.0 \cdot 10^{-1}$
EoS 3d	$P_0 = 5.29 MeV/fm^3$,	$\rho_N = 3.87 \cdot 10^{14} g/cm^3$,	$\rho_Q = 5.12 \cdot 10^{14} g/cm^3$,	$\lambda = 1.29$							
A	0.49	1.50	0	0	12.87	0.088	197.84	0.0931	0.0934	9.379	$6.9 \cdot 10^{-4}$
B	5.29	5.12	0	0	10.47	0.285	13.54	0.2852	0.2903	7.937	$3.3 \cdot 10^{-2}$
F	87.70	9.84	9.667	1.254	11.14	1.440	11.51	1.4402	1.6158	71.301	$2.6 \cdot 10^{-1}$
G	345.68	24.13	9.592	1.695	10.44	1.796	10.64	1.7960	2.0873	84.363	$4.1 \cdot 10^{-1}$
EoS 2f	$P_0 = 20.27 MeV/fm^3$,	$\rho_N = 4.48 \cdot 10^{14} g/cm^3$,	$\rho_Q = 6.10 \cdot 10^{14} g/cm^3$,	$\lambda = 1.26$							
A	0.74	2.01	0	0	11.26	0.075	259.07	0.0798	0.0803	10.351	$4.5 \cdot 10^{-4}$
B	20.27	6.10	0	0	11.75	0.925	12.57	0.9256	0.9947	46.547	$1.3 \cdot 10^{-2}$
F	76.89	9.41	7.854	0.737	11.76	1.440	12.18	1.4401	1.6101	77.138	$2.4 \cdot 10^{-1}$
G	148.15	13.46	8.708	1.155	11.47	1.687	11.77	1.6871	1.9289	90.158	$3.2 \cdot 10^{-1}$

Table 2: The basic integral and structural parameters of characteristic configurations for equations of state with $\lambda < 3/2$.

	P_c MeV/fm^3	$\rho_c 10^{-14}$ g/cm^3	R_{core} km	M_{core} $M_\odot$	R_{Aen} km	m_{Aen} $M_\odot$	R km	M $M_\odot$	M_0 $M_\odot$	I $M_\odot km^2$	Z_s
	EoS 1a	$P_0 = 0.761 MeV/fm^3$,	$\rho_N = 2.08 \cdot 10^{14} g/cm^3$,	$\rho_Q = 4.47 \cdot 10^{14} g/cm^3$,	$\lambda = 2.13$						
A	0.741	2.060	0	0	11.35	0.076	248.33	0.0806	0.0811	9.70	$4.8{\cdot}10^{-4}$
B	0.761	4.467	0	0	11.29	0.077	197.21	0.0807	00812	6.25	$6.0{\cdot}10^{-4}$
C	1.086	4.487	1.355	0.002	11.25	0.073	515.51	0.0798	0.0803	58.50	$2.3{\cdot}10^{-4}$
D	1.195	4.493	1.562	0.004	11.17	0.072	702.63	0.0799	0.0804	145.04	$1.7{\cdot}10^{-4}$
E	1.975	4.539	2.582	0.016	10.02	0.070	131.06	0.0723	0.0727	2.37	$8.1{\cdot}10^{-4}$
F	74.469	8.719	10.494	1.408	11.41	1.439	11.05	1.4392	1.6359	74.79	$2.6{\cdot}10^{-1}$
G	296.296	21.054	10.332	1.845	10.85	1.863	10.65	1.8626	2.2039	95.49	$4.2{\cdot}10^{-1}$
	EoS 2a	$P_0 = 0.758 MeV/fm^3$,	$\rho_N = 2.03 \cdot 10^{14} g/cm^3$,	$\rho_Q = 4.47 \cdot 10^{14} g/cm^3$,	$\lambda = 2.19$						
A	0.741	2.014	0	0	11.26	0.075	259.07	0.0798	0.0803	10.35	$4.5{\cdot}10^{-4}$
B	0.758	4466	0	0	11.21	0.076	207.21	0.0799	0.0807	6.65	$5.7{\cdot}10^{-4}$
C	0.939	4.478	1.012	0.003	11.25	0.074	386.02	0.0795	0.0802	26.41	$3.0{\cdot}10^{-4}$
D	1.294	4.498	1.734	0.005	10.99	0.070	1304.5	0.0820	0.0827	1062.00	$9.3{\cdot}10^{-5}$
E	1.975	4.539	2.586	0.016	9.95	0.069	133.88	0.0717	0.0724	2.38	$7.9{\cdot}10^{-4}$
F	74.568	8.724	10.496	1.409	11.05	1.440	11.41	1.4400	1.6369	74.85	$2.6{\cdot}10^{-1}$
G	320.988	22.410	10.264	1.847	10.57	1.863	10.77	1.8635	2.2052	94.12	$4.3{\cdot}10^{-1}$
	EoS 3a	$P_0 = 0.199 MeV/fm^3$,	$\rho_N = 0.86 \cdot 10^{14} g/cm^3$,	$\rho_Q = 4.43 \cdot 10^{14} g/cm^3$,	$\lambda = 5.11$						
A	0.035	0.277	0	0	18.17	0.052	893.6	0.6101	0.6157	$2.4{\cdot}10^{4}$	$1.0{\cdot}10^{-3}$
B	0.199	4.433	0	0	14.58	0.072	2214.6	0.6386	06444	$2.4{\cdot}10^{4}$	$4.3{\cdot}10^{-4}$
C	0.395	4.445	1.07	0.001	14.90	0.066	1708.3	0.6360	0.6418	$1.2{\cdot}10^{5}$	$5.5{\cdot}10^{-4}$
D	2.123	4.547	3.25	0.032	8.29	0.046	2696.5	0.8200	0.8277	$6.3{\cdot}10^{4}$	$4.5{\cdot}10^{-4}$
E	2.395	4.563	3.46	0.039	7.75	0.051	361.7	0.0534	0.0535	9.20	$2.2{\cdot}10^{-4}$
F	74.568	8.724	10.57	1.431	10.93	1.439	11.29	1.4390	1.6356	74.71	$2.7{\cdot}10^{-1}$
G	316.049	22.139	10.32	1.900	10.53	1.863	10.72	1.863	2.2047	94.35	$4.3{\cdot}10^{-1}$
	EoS 3b	$P_0 = 0.796 MeV/fm^3$,	$\rho_N = 1.73 \cdot 10^{14} g/cm^3$,	$\rho_Q = 4.54 \cdot 10^{14} g/cm^3$,	$\lambda = 2.61$						
A	0.494	1.505	0	0	12.87	0.088	197.84	0.0931	0.0934	9.38	$6.9{\cdot}10^{-4}$
B	0.796	4.543	0	0	11.95	0.102	48.49	0.1042	0.1047	3.17	$3.2{\cdot}10^{-3}$
C	2.222	4.631	2.74	0.020	10.75	0.087	53.78	0.0885	0.0887	1.94	$2.4{\cdot}10^{-3}$
F	79.506	9.180	10.39	1.408	11.00	1.439	11.36	1.4393	1.6209	73.28	$2.6{\cdot}10^{-1}$
G	325.926	23.019	10.11	1.809	10.47	1.826	10.67	1.8262	2.1348	89.24	$4.2{\cdot}10^{-1}$

Table 3: The basic integral and structural parameters of characteristic configurations for equations of state with $\lambda > 3/2$.

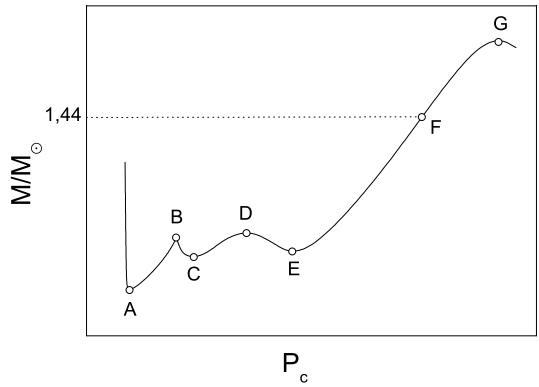

Figure 1. Schematic arrangement of characteristic configurations; their parameters are tabulated in Tables 2 and 3.

strange quark core, which may have interesting distinctive features. In particular, the configurations of this new additional stable branch have radii in excess of a thousand kilometer. In Table 3 besides the four mentioned critical configurations as above, for EoS $1a$, $2a$ and $3a$ the parameters of configurations C, D and E describing this new local maximum, and for EoS $3b$– configuration C describing the minimum after the kink attributable to the formation of quark phase, are given. The branch AB represents stable neutron stars without a quark core, and CD– stable configurations having small quark core. While in the case of EoS $1a$ and $2a$ the toothlike kink and the new local maximum are located in the low-mass range ($M \approx 0.08 M_\odot$), for the model $3a$ both the branch AB and the following additional stable branch CD move to the mass range of $\approx 0.6 M_\odot$. As it is seen from Fig. $2c$, in the density range $3.5 \cdot 10^{13}$ g/cm$^3 \leq \rho_c \leq 8.6 \cdot 10^{13}$ g/cm^3 the derivative $dM/d\rho_c$ is positive and corresponds to the stable white dwarfs of medium masses with a small central region (core), composed of neutron-rich atomic nuclei and degenerated neutrons and electrons. The critical (limiting) configuration of this stable branch (before the transition to the quark phase) has the following parameters: $M_{max} = 0.638 M_\odot$, $R_{max} = 2195$ km, the packing factor $\alpha = 9 \cdot 10^{-3}$, $M_{Aen} = 0.072 M_\odot$, $R_{Aen} = 14.6$ km.

In the case of EoS $3a$, unlike the other EoS with $\lambda > 3/2$, the values of M_{Aen}/M and R_{Aen}/R for configuration B are equal to 0.11 and $6.6 \cdot 10^{-3}$, respectively, i.e. these models are mainly composed of usual white dwarf matter. On the both branches AB and CD the packing factor α has the values typical for massive white dwarfs. While for EoS $1a$ $M_B > M_D$, in the case of EoS $2a$ and $3a$ the opposite is true, $M_D > M_B$. This fact makes it possible for the stars described by the latter two EoS a transition from configuration B to more dense configurations through two restructurings when there is an accre-

tion of matter on the star: first to a configuration of the branch CD, and then – to the main ascending branch of stable neutron stars with a strange quark core. As a result, there will be two successive energy releases [**?**, **?**].

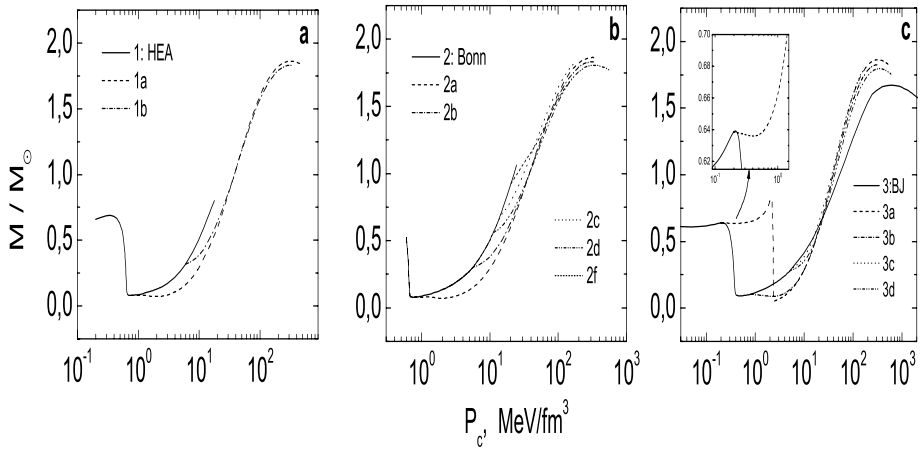

Figure 2. The dependences of gravitational mass M on central pressure P_c for the sets of EoS with variants $HEA(a)$, $Bonn(b)$ and $BJ-V(c)$. Solid lines correspond to the models of neutron stars without a quark core (the variant of nucleon component is indicated). On an enlarged scale the phase transition area is shown for EoS $3a$.

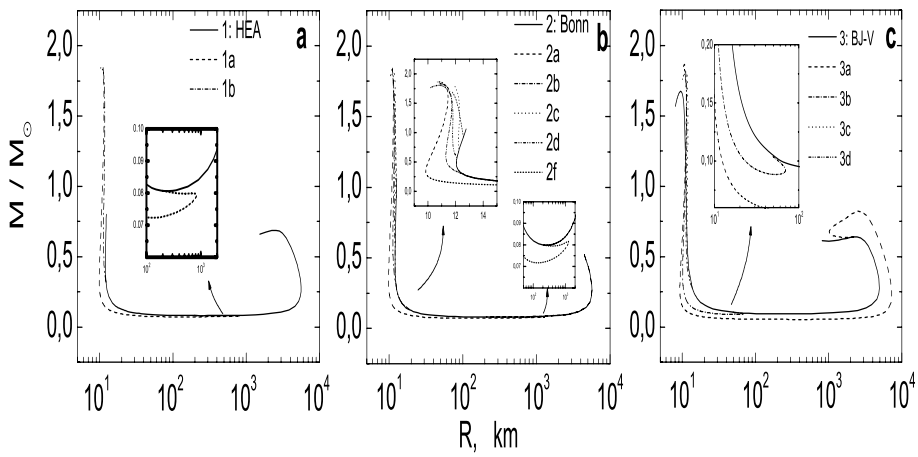

Figure 3. Mass M versus radius R. On an enlarged scale the new additional local mass maximum is shown for neutron stars with a strange quark core. In the upper left corner of Fig. 3b, the phase transition area is shown for the whole set of EoS.

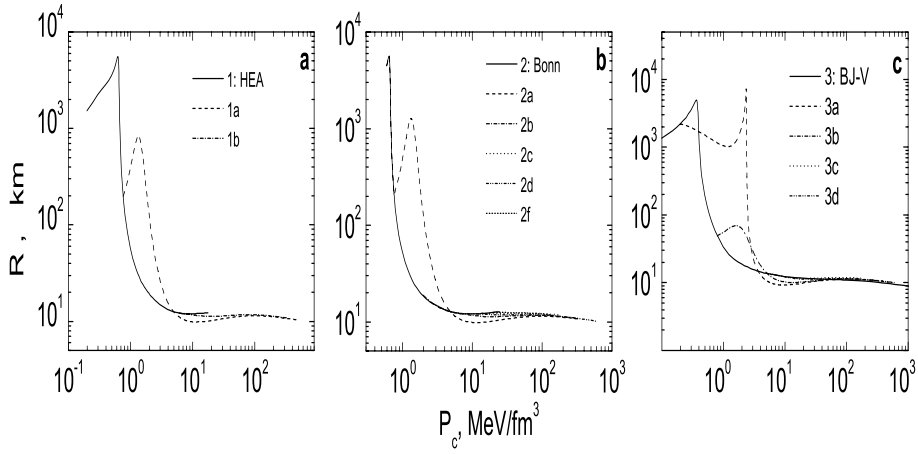

Figure 4. The dependences of the radius R on central pressure P_c (the EoS are denoted as in Fig.2,3).

The dependences of the gravitational mass M on the central pressure P_c, the mass M on the radius R, and the radius R on the central pressure P_c for the sets of EoS with nucleon variants HEA (a), $Bonn$ (b) and $BJ-V$ (c) are presented in Figs. 2, 3, and 4, respectively.

4. Summary

First-order phase transition from a nucleonic matter to the strange quark state with a transition parameter $\lambda > 3/2$ that occurs in superdense nuclear matter generally gives rise to a toothlike kink on the stable branch of the dependence of stellar mass on central pressure. Based on the extensive set of calculated realistic equations of state of superdense matter, we revealed a new stable branch of superdense configurations. The new branch emerges for some of our models with the transition parameter $\lambda > 3/2$ and a small quark core ($M_{core} \sim 0.004 \div 0.03 M_\odot$) on the $M(P_c)$ curve, with $M_{max} \sim 0.08 M_\odot$ and $M_{max} \sim 0.82 M_\odot$ for different equations of state. Stable equilibrium layered neutron stars, located in these additional ranges of stability, are characterized also by unusually large values of the stellar radius (from $R \sim 1300$ km to ~ 2700 km in different models). It should be noted that for such equations of state (if $M_D > M_B$), accretion onto a neutron star will lead to two successive jumplike transitions to a quark-core neutron star; as a result, there will be two successive energy releases.

Acknowledgments

This work was supported by the Armenian National Science and Education Foundation (ANSEF Grant No. PS 140) and the Ministry of Education and Science of the Republic of Armenia within the framework of the topic No. 0842.

References

[1] E. Witten, Phys. Rev. D. 30, 272 (1984).

[2] P. Haensel, J. L. Zdunik, R. Schaeffer,Astron. Astrophys. 160, 121 (1986).

[3] Yu. L. Vartanyan, A. R. Arutyunyan, A. K. Grigoryan, Astronomy Letters 21, 122 (1995).

[4] P. A. Carinhas, Astrophys. J. 412, 213 (1993).

[5] G. B. Alaverdian, A. R. Harutyunian, Yu. L. Vartanian, A. K. Grigorian, Rep. Nat. Acad. Sci. of Armenia, Physics 95, 98 (1995).

[6] G. B. Alaverdyan, A. R. Harutyunyan, Yu. L. Vartanyan, Astrophysics 44, 265 (2001).

[7] G. B. Alaverdyan, A. R. Harutyunyan, Yu. L. Vartanyan, Spacetime and Substance 2, No.3(8), 129 (2001).

[8] G. B. Alaverdyan, A. R. Arutyunyan, Yu. L. Vartanyan, Astronomy Letters 28, 24 (2002).

[9] A. R. Harutyunyan, Astrophysics 45, 248 (2002).

[10] H. Heiselberg, C. J. Pethick, E. F. Staubo, Phys. Rev. Lett. 70, 1355 (1993).

[11] C. P. Lorenz, D. G. Ravenhall, C. J. Pethick, Phys. Rev. Lett. 70, 379 (1993).

[12] N. K. Glendenning, astro-ph/9706236 (1997).

[13] H. Heiselberg, M. Hjorth-Jensen, Phys. Rep. 328, 237 (1999).

[14] D. Blaschke, N. K. Glendenning, A. Sedrakian (Eds.), Physics of Neutron Star Interiors. Springer, Berlin (2001).

[15] N. K. Glendenning, Phys. Rev. D. 46, 1274 (1992).

[16] D. N. Voskresensky, M. Yasuhira, T. Tatsumi, Nucl. Phys. A. 723, 291 (2003).

[17] A. Chodos, R. L. Jaffe, K. Johnson, C. B. Thorn, V. F. Weisskopf, Phys. Rev. D. 9, 3471 (1974).

[18] F. Weber, N. K. Glendenning, M. K. Weigel, Astrophys. J. 373, 579 (1991).

[19] R. Machleidt, K. Holinde, Ch. Elster, Phys. Rep. 149, 1 (1987).

[20] K. Holinde, K. Erkelenz, R. Alzetta, Nucl. Phys. A. 194, 161 (1972).

[21] K. Holinde, K. Erkelenz, R. Alzetta, Nucl. Phys. A. 198, 598 (1972).

[22] P. Poschenrieder, M. K. Weigel, Phys. Lett. B. 200, 231 (1988).

[23] P. Poschenrieder, M. K. Weigel, Phys. Rev. C. 38, 471 (1988).

[24] G. S. Bisnovatyi-Kogan, Physical Problems of the Theory of Stellar Evolution. Moscow (1989).

[25] R. C. Malone, M. B. Johnson, H. A. Bethe, Astrophys. J. 199, 741 (1975).

[26] Z. F. Seidov, Sov. Astron.Zh. 15, 347 (1971).

[27] J. H. Taylor, J. M. Weisberg, Astrophys.J. 345, 434 (1989).

[28] P. Haensel, M. Proszynski, Astrophys.J. 258, 306 (1982).

DIQUARK CONDENSATION EFFECTS ON HOT QUARK STAR CONFIGURATIONS

A. Ö ztas
Department of Physics, Hacettepe University, TR-06532 Ankara, Turkey
oztas@hacettepe.edu.tr

D. Blaschke
Fachbereich Physik, Universität Rostock, D-18051 Rostock, Germany
david.blaschke@physik.uni-rostock.de

S. Fredriksson
Department of Physics, Luleaa University of Technology, SE-97187 Luleaa, Sweden
sverker@mt.luth.se

H. Grigorian
Fachbereich Physik, Universität Rostock, D-18051 Rostock, Germany,
Department of Physics, Yerevan State University, 375025 Yerevan, Armenia
hovik@darss.mpg.uni-rostock.de

Abstract The equation of state for quark matter is derived for a nonlocal, chiral quark model within the mean field approximation. We investigate the effects of a variation of the form-factors of the interaction on the phase diagram of quark matter. Special emphasis is on the occurrence of a diquark condensate which signals a phase transition to color superconductivity and its effects on the equation of state under the condition of β- equilibrium and charge neutrality. We calculate the quark star configurations by solving the Tolman- Oppenheimer- Volkoff equations and obtain for the transition from a hot, normal quark matter core of a protoneutron star to a cool diquark condensed one a release of binding energy of the order of $\Delta Mc^2 \sim 10^{53}$ erg. We find that this energy could not serve as an engine for explosive phenomena since the phase transition is not first order. Contrary to naive expectations the mass defect increases when for a given temperature we neglect the possibility of diquark condensation.

Keywords: Relativistic stars - structure and stability, Quark-gluon plasma, Nuclear physics aspects of supernovae evolution

1. Introduction

Color superconductivity (CS) in quark matter [1] is one interesting aspect of the physics of compact star interiors [2]. Since calculations of the energy

D. Blaschke and D. Sedrakian (eds.), Superdense QCD Matter and Compact Stars, 341–351.

gap of quark pairing predict a value $\Delta \sim 100$ MeV and corresponding critical temperatures for the phase transition to the superconducting state are expected to follow the BCS relation $T_c = 0.57\ \Delta$, the question arises whether diquark condensation can lead to remarkable effects on the structure and evolution of compact objects. If positively answered, CS of quark matter could provide signatures for the detection of a deconfined phase in the interior of compact objects (pulsars, low-mass X-ray binaries) along the lines of previously suggested strategies

Diquarks gained popularity in astrophysics about a decade ago, when they were suggested to influence the supernova collapse and "bounce-off" [8–12], and to enhance the neutrino cooling of quark-stars. The latter effect is now subject to much research within improved scenarios Refs. [7, 9, 8].

Hong, Hsu and Sannino have conjectured [16] that the release of binding energy due to Cooper pairing of quarks in the course of proto-neutron star evolution could provide an explanation for the unknown source of energy in supernovae, hypernovae or gamma-ray bursts, see also [17]. which did not take into account the change in the gravitational binding energy due to the change in the structure of the stars quark core. In the present work we will reinvestigate the question of a possible binding energy release due to a CS transition by taking into account changes in the equation of state (EoS) and the configuration of the quark star selfconsistently.

As a first step in this direction we will discuss here the two flavor color superconducting (2SC) quark matter phase which occurs at lower baryon densities than the color-flavor-locking (CFL) one, see [18, 32]. Studies of three-flavor quark models have revealed a very rich phase structure (see [32] and references therein). However, for applications to compact stars the omission of the strange quark flavor within the class of nonlocal chiral quark models considered here may be justified by the fact that central chemical potentials in stable star configurations do barely reach the threshold value at which the mass gap for strange quarks breaks down and they appear in the system [20]. Therefore we will not discuss here first applications to calculate compact star configurations with color superconducting quark matter phases that have employed non-dynamical quark models

We will investigate the influence of the form-factor of the interaction on the phase diagram and the EoS of dense quark matter under the conditions of charge neutrality and isospin asymmetry due to β-equilibrium relevant for compact stars.

Finally we consider the question whether the effect of diquark condensation which occurs in the earlier stages of the compact star evolution ($t \simeq 100$ s) [8, 21, 22] at temperatures $T \sim T_c \sim 20 - 50$ MeV can be considered as an engine for explosive astrophysical phenomena like supernova explosions due

to the release of a binding energy of about $10^{52} \div 10^{53}$ erg [17], as has been suggested before [16, 17].

2. Thermodynamic potential for asymmetric 2SC quark matter

We consider a nonlocal chiral quark model described by the effective action which generalizes the approach of Ref. [23] by including the scalar diquark pairing interaction channel with a coupling strength G_2.

The order parameters the diquark gap Δ, which can be seen as the gain in energy due to diquark condensation, and the mass gaps ϕ_u, ϕ_d, which indicate chiral symmetry breaking.

The thermodynamic potential of asymmetric quark matter [27, 26, 29]

$$\begin{aligned}
&\Omega_q(\phi,\Delta;\mu_q,\mu_I,T) = \frac{\phi^2}{4\,G_1} + \frac{\Delta^2}{4\,G_2} - 2\int_0^\infty \frac{q^2\,dq}{2\pi^2}\Big\{2\,E_\phi \\
&+T\,\ln\left[1+\exp\left(-\frac{E_\phi-\mu_q-\mu_I}{T}\right)\right] + T\,\ln\left[1+\exp\left(-\frac{E_\phi-\mu_q+\mu_I}{T}\right)\right] \\
&+T\,\ln\left[1+\exp\left(-\frac{E_\phi+\mu_q-\mu_I}{T}\right)\right] + T\,\ln\left[1+\exp\left(-\frac{E_\phi+\mu_q+\mu_I}{T}\right)\right]\Big\} \\
&-4\int_0^\infty \frac{q^2\,dq}{2\pi^2}\Big\{E_+ + E_- \\
&+T\,\ln\left[1+\exp\left(-\frac{E_- -\mu_I}{T}\right)\right] + T\,\ln\left[1+\exp\left(-\frac{E_- +\mu_I}{T}\right)\right] \\
&+T\,\ln\left[1+\exp\left(-\frac{E_+ -\mu_I}{T}\right)\right] + T\,\ln\left[1+\exp\left(-\frac{E_+ +\mu_I}{T}\right)\right]\Big\} \\
&-\Omega_q^{\rm vac}\,.
\end{aligned} \tag{1}$$

The function $g(p)$ is the formfactor of the separable four-fermion interaction, depends only on the modulus of the three-momentum. We choice [24] $G_2 = 0.75\,G_1$ and $G_2 = G_1$.The dispersion relation $E_\phi = \sqrt{q^2 + (m + \phi\,g(q))^2}$ holds for unpaired quarks also in color-symmetry broken 2SC phase. The quarks with paired colors have a modified dispersion relation $E_\pm = (E_\phi \pm \mu_q)\sqrt{1 + \Delta^2\,g^2(q)/(E_\phi \pm \mu_q)^2}$.

For nonvanishing Δ in Eq. (1) the color symmetry is broken. Two of the three quark color degrees of freedom are coupled to bosonic Cooper pairs in the color antitriplet state which can form a Bose condensate.One can combine the chemical potentials μ_u, μ_d of u and d quarks by introducing $\mu_q = (\mu_u + \mu_d)/2$ and $\mu_I = (\mu_u - \mu_d)/2$ as the Lagrange multipliers related to, respectively, the quark number density n_q and the isospin asymmetry n_I. In thermal equilib-

rium characterized by a fixed set of thermodynamic variables $\{\mu_u, \mu_d, T\}$, the thermodynamic potential Ω_q shall attain a global minimum with respect to all its order parameters. Satisfying the gap equations is a necessary, but not a sufficient condition for the thermodynamic equilibrium state.

In Eq. (1), we subtract the term $\Omega_q^{\rm vac}$ in order to define the thermodynamic potential such that the vacuum pressure vanishes, $P_q(0,0,0) = 0$. On the mean-field level the present approach is analogous to a flavor- asymmetric generalization of the instanton-motivated model of Ref. [24] for two-flavor color superconductivity (2SC).

From BCS theory it is known, that in order to form Cooper pairs at $T = 0$ in a dense Fermi system, the difference in the chemical potentials of the Fermions to be paired should not exceed the size of the gap. As previous calculations within this type of models have shown [24], there is a critical chemical potential for the occurrence of quark matter $\mu_f \geq 300$ MeV and values of the gap in the region $\Delta \leq 150$ MeV have been found. Therefore it is natural to consider the problem of the color superconducting (2SC) phase with the assumption, that quark matter is symmetric or very close to being symmetric ($\mu_u \simeq \mu_d$).

We will apply this model for the construction of the EoS for stellar matter in β-equilibrium.

3. EoS for 2SC quark matter in β-equilibrium

We consider stellar matter in the quark core of compact stars consisting of electrons in chemical equilibrium with u and d quarks. Hence $\mu_d = \mu_u + \mu_e$, where μ_e is the electron chemical potential. The thermodynamic potential of such matter is

$$\Omega(\phi, \Delta; \mu_q, \mu_I, \mu_e, T) = \Omega_q(\phi, \Delta; \mu_q, \mu_I, T) + \Omega_e(\mu_e, T), \qquad (2)$$

with $\Omega_e(\mu_e, T)$ for ultrarelativistic electrons. The condition of local charge neutrality $2/3 n_u - 1/3 n_d - n_e = 0$, In our model we assume the neutrino chemical potential to be zero, which corresponds to a scenario where the neutrinos (and/or antineutrinos) leave the star as soon as they are created. The limits of such an approximation could be based on the calculations for the case of trapping of neutrinos in the hot stars interior [18].

In [25, 26] it is shown that at given μ_q the diquark gap is independent of the isospin chemical potential for $|\mu_{I(\mu_q)}| < \mu_{Ic}(\mu_q)$, otherwise vanishes. Increase of isospin asymmetry forces the system to pass a first order phase transition by tunneling through a barrier in the thermodynamic potential (2). Using this property we choose the absolute minimum of the thermodynamic potential (2) between two β-equilibrium states, one with and one without condensate for the given baryochemical potential $\mu_B = \mu_u + 2\mu_d$.

4. EoS of quark matter in 2SC phase for finite temperature

The gaps have been calculated by minimizing the thermodynamic potential Ω, Eq. (2), in the space of order parameters (ϕ, Δ) and the results are shown in Figs. 1 and 2.

In order to compare the effects of the quark interaction form-factors on the EoS, we study:
Gaussian (G) Lorentzian (L) cutoff (NJL) type
form-factors defined as

$$g_{\rm L}(q) = [1 + (q/\Lambda_{\rm L})^{2\alpha}]^{-1}, \quad \alpha > 1\,, \tag{3}$$

$$g_{\rm G}(q) = \exp(-q^2/\Lambda_{\rm G}^2)\,, \tag{4}$$

$$g_{\rm NJL}(q) = \theta(1 - q/\Lambda_{\rm NJL})\,. \tag{5}$$

We will employ parametrisations of the nonlocal quark model which reproduce pion properties: mass $m_\pi = 140$ MeV, decay constant $f_\pi = 93$ MeV and which have the same quark mass gap $\phi(T = 0, \mu = 0) = 330$ MeV in the vacuum. The results for the parameterization are taken from [23],

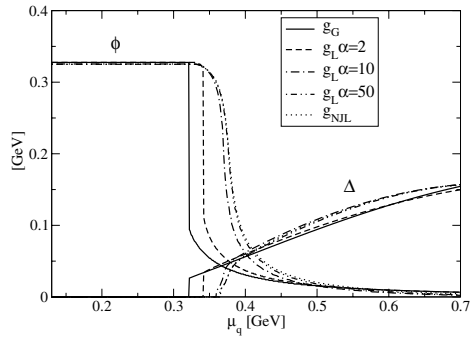

Figure 1. Solutions for the chiral gap ϕ and the diquark gap Δ for different form-factors at $T = 0$ in symmetric quark matter and $G_2 = 0.75\, G_1$.

Figure 1 displays the $T = 0$ solutions of the chiral gap ϕ and diquark gap Δ for different form-factors. For the densities relevant for stable star configurations, $\mu_q \leq 450$ MeV, the critical chemical potential μ_q^c for the chiral transition and for the onset of diquark condensation does depend on the type of the form-factor. The maximal value of the diquark gap $\Delta \simeq 150$ MeV, however, does not depend sensitively on it..

Figure 2 shows the solutions for the chiral gap ϕ and the diquark gap Δ for the Gaussian model form-factor at different temperatures $T = 0, 20, 40$ MeV.

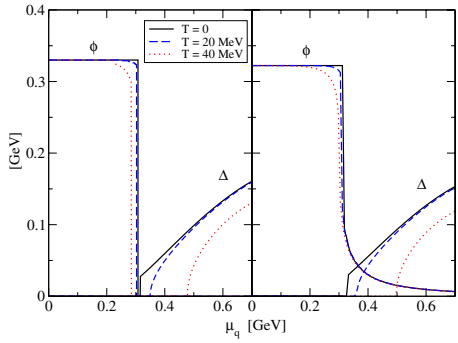

Figure 2. Solutions of the chiral gap ϕ and the diquark gap Δ for the Gaussian model form-factor in the chiral limit (left panel) and for finite current quark mass $m_0 = 2.41$ MeV (right panel) at different temperatures $T = 0, 20, 40$ MeV for symmetric quark matter and $G_2 = 0.75\, G_1$.

We compare results in the chiral limit ($m_0 = 0$) with those for finite current quark mass $m_0 = 2.41$ MeV and observe that the diquark gap is not sensitive to the presence of the current quark mass, which holds for all form-factors However, the choice of the form-factor influences the critical values of the phase transition as displayed in the quark matter phase diagram ($\mu_q - T$ plane) of Fig. 2, see also Fig. 1. A softer form-factor in momentum space gives lower critical values for T_c and μ_c at the borders of chiral symmetry restoration and diquark condensation.

The inset of Fig. 2 shows that the generalization of the BCS relation $T_c \simeq 0.57\ \Delta(T = 0, \mu_q)\ g(\mu_q)$, between the critical temperature T_c of the superconducting phase transition and the pairing gap Δ at $T = 0$ is satisfactorily fulfilled in the domain of the phase diagram relevant for compact stars.

At nonzero temperatures the mass gap decreases as a function of the chemical potential already in the phase with broken chiral symmetry. Hence the model here gives unphysical low-density excitations of quasi-free quarks. A systematic improvement of this situation should be obtained by including the phase transition construction to hadronic matter. However, in the present work we circumvent the confinement problem by considering the quark matter phase only for densities above the nuclear saturation density n_0, i.e. $n_B > 0.5\, n_0$.

5. Configurations of hot quark stars

Here we compare configurations with and without CS, in order to investigate the effect of diquark condensation on the total energy of a quark star and to

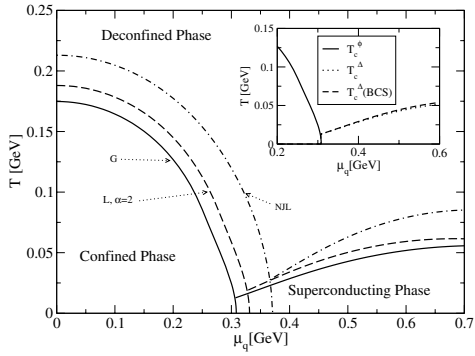

Figure 3. Phase diagrams for different form-factor models: Gaussian (solid lines), Lorentzian $\alpha = 2$ (dashed lines) and NJL (dash-dotted). In β-equilibrium, the color-superconducting phase does not exist for $G_2 \lesssim G_1$. In the inset we show for the Gaussian model the comparison of the numerical result with the modified BCS formula $T_c^{\Delta} = 0.57\ \Delta(T = 0, \mu_q)\ g(\mu_q)$ for the critical temperature of the superconducting phase transition.

decide whether the corresponding phase transition could serve as an engine for explosive phenomena like supernovae and gamma ray bursts. The CS transition can occur during the cooling evolution of a hot proto-neutron star [8, 21]. We suppose that the approximation of an isothermal temperature distribution [32] in the star interior is sufficient for the estimate of the mass defect [1]. In the present paper we consider selfbound configurations of pure quark matter as models for quark cores in hybrid stars which should be the general case to be discussed in a separate paper, see e.g. Ref. [28] for $T = 0$ configurations. The extrapolation from pure quark star configurations to hybrid ones, however, is strongly model dependent and cannot be done without a calculation. Quark matter effects are expected to be still valid in hybrid stars when rescaled with a monotonously rising function of the ratio of the quark core volume to the quark star volume.

The spherically symmetric, static star configurations are defined by the well known Tolman-Oppenheimer-Volkoff equations [30] for the mechanical equilibrium of self-gravitating matter (see also [14, 31])

$$\frac{dP(r)}{dr} = -\frac{[\varepsilon(r) + P(r)][m(r) + 4\pi r^3 P(r)]}{r[r - 2m(r)]}\ . \tag{6}$$

Here $\varepsilon(r)$ is the energy density and $P(r)$ the pressure at the distance r from the center of the star. The mass enclosed in a sphere with radius r is defined

[1] For a discussion of isentropic hot quark star configurations, see [14].

by $m(r) = 4\pi \int_0^r \varepsilon(r')r'^2 dr'$. These equations are solved with the boundary

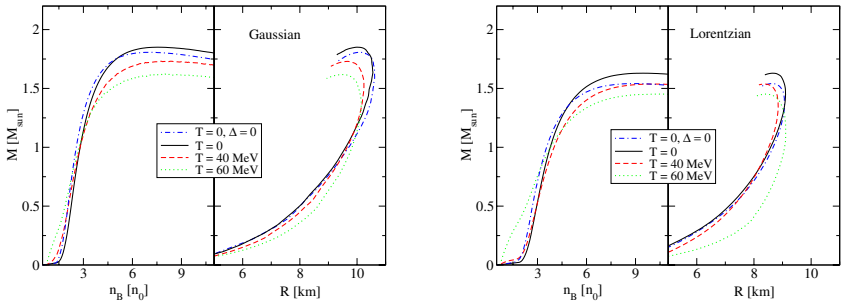

Figure 4. Stable configurations of quark stars for different temperatures $T = 0, 40, 60$ MeV. Mass as a function of central baryon density (left panels) and of the radius (right panels) for the Gaussian model (left graph) and for the Lorentzian model (right graph).

condition of a given central baryon number density $n_B(0)$ defining a configuration. In Fig. 3 we show the results for the dependence of the masses on the central energy density as well as on the radius of the configurations for different temperatures and two form-factor models: a Gaussian and a Lorentzian one. Stable configurations correspond to the rising branch on the mass-central density plane. Lorentzian form-factor, respectively. For comparison, we have included $T = 0$ configurations for small coupling constants $G_2 < G_1$, for which the diquark condensate does not occur. The comparison shows that the maximum mass decreases with increasing temperature due to a softening of the EoS. Also the disappearance of the diquark condensate (in our case due to lowering of the coupling G_2) softens the EoS and lowers the maximum mass. The Gaussian form-factor has the lowest critical baryochemical potential when compared with the Lorentzian and the NJL model. Therefore the Gaussian quark star configuration can extend to larger radii where the density is lower and can thus carry more mass than the Lorentzian model with the same central baryon density, see Fig.5.

Here we will discuss two scenarios for the proto-neutron star cooling which we denote by A and B, where A stands for cooling of a star configuration with SC whereas B is a scenario without SC. The initial states for both scenarios are chosen to have the same mass $M_i(A) = M_i(B)$ for a given initial temperature of $T = 60$ MeV. The final states at $T = 0$, however, have different masses $M_f(A) \neq M_f(B)$ while the total baryon number is conserved in the cooling evolution. The resulting mass differences are $\Delta M(A) = 0.06\ M_\odot$, $\Delta M(B) = 0.09\ M_\odot$ and $\Delta M(A) = 0.05\ M_\odot$, $\Delta M(B) = 0.07\ M_\odot$ for the Gaussian and Lorentzian models, respectively.

We make the observation that, contrary to naive expectations of the mass defect as a result of the binding energy from Cooper pairing [16], $\Delta M\ c^2 \sim$

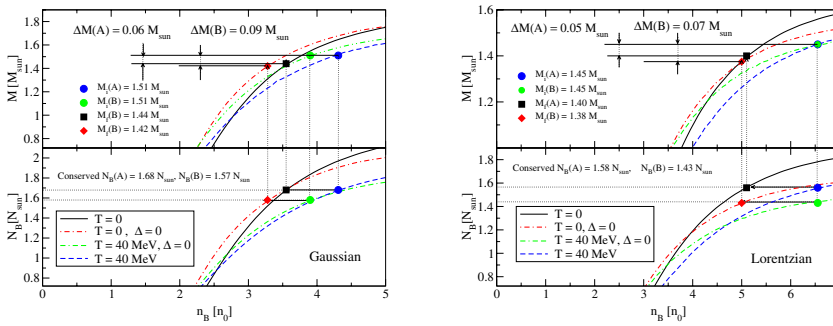

Figure 5. Hot ($T = 40$ MeV) versus cold ($T = 0$) quark star configurations for the Gaussian model(Left graphic)and Lorentzian(Right graphic); case A: with diquark condensation (dashed versus full lines) and case B: without diquark condensation (dash-dash-dotted versus dash-dotted lines). When a quark star with initial mass M_i cools down from $T = 40$ MeV to $T = 0$ at fixed baryon number N_B the mass defect ΔM occurs.

$(\Delta/\mu)^2 M_\odot\, c^2 \propto 10^{53}$ erg, the mass defect in the cooling evolution with diquark condensation (A) is about 40% smaller than in the scenario without SC (B), regardless of the choice of form-factor. The difference amounts to $\simeq 0.02 M_\odot$ for initial configurations with masses of about $1.4-1.5\ M_\odot$. Therefore, we conclude that general relativity effects play an important role in the estimate of the mass defect since the effects of diquark condensation on the mass of configurations via the change in the equation of state overcompensate effects due to the occurrence of the diquark gap in the one-particle energies.

6. Conclusion

We have investigated the influence of diquark condensation on the thermodynamics of quark matter under the conditions of β-equilibrium and charge neutrality relevant for the discussion of compact stars. The EoS has been derived for a nonlocal chiral quark model in the mean field approximation, and the influence of different form-factors of the nonlocal, separable interaction (Gaussian, Lorentzian, NJL) has been studied. The model parameters are chosen such that the same set of hadronic vacuum observable is described. We have shown that the critical temperatures and chemical potentials for the onset of the chiral and the superconducting phase transition are the lower the smoother the momentum dependence of the interaction form-factor is.

The phase transition to color superconducting quark matter from the lower density regions at small temperatures ($T < 5 \div 10$ MeV) is of first order, while the melting of the diquark condensate and the corresponding transition to normal quark matter at high temperatures is of second order. The presence

of flavor asymmetry due to β-equilibrium in quark matter does not destroy the diquark condensate since the electron fraction $n_e/n_{\rm total} < 0.01$ is too small for the cases when the coupling $G_2 \geq G_1$. The masses of the quark core configurations could be up to $1.8\ M_\odot$ for the Gaussian and up to $1.6\ M_\odot$ for the Lorentzian form-factor models. The quark core radii with Lorentzian form-factors are up to 9 km, while for Gaussian models could extend up to 11 km.

Diquark condensation makes the EoS harder, which leads to an increase in the maximum mass of the quark star configuration when compared to the case without diquark condensation. For finite temperatures the masses are smaller than at $T = 0$. For asymptotically high temperatures and densities the EoS behaves like a relativistic ideal gas, where the relation pressure versus energy density is temperature independent. In contrast to the bag model where this behavior occurs immediately after the deconfinement transition, our model EoS has a temperature dependent $P(\varepsilon)$ relation also beyond this point.

It has been shown for a hybrid star model which uses the quark matter EoS presented in this work that the possibility to obtain a stable star configuration with 2SC quark matter core depends on the form-factor of the quark interaction [34]. The Gaussian and Lorentzian form-factor models do allow a quark matter core, whereas the NJL form-factor model does not.

A mass defect of about $0.1\ M_\odot$ occurs in the cooling of a hot configuration to a cold one already without diquark condensation. It is mainly determined by the change of the configuration due to changes in the EoS. Cooling the star with diquark condensation results even in a lowering of the mass defect contrary to naive expectations.

References

[1] K. Rajagopal and F. Wilczek, In *Shifman, M. (ed.): At the frontier of particle physics, **3** (2000) 2061; [arXiv:hep-ph/0011333.]

[2] D. Blaschke, N. K. Glendenning and A. Sedrakian (Eds.), *Physics of Neutron Star Interiors*, Springer Lect. Notes Phys. **578** (2001).

[3] N. K. Glendenning, S. Pei and F. Weber, Phys. Rev. Lett. **79** (1997) 1603 [arXiv:astro-ph/9705235].

[4] N. K. Glendenning and F. Weber, in [2], p. 305 [arXiv:astro-ph/0106054].

[5] G. S. Poghosyan, H. Grigorian and D. Blaschke, Astrophys. J. **551** (2001) L73 [arXiv:astro-ph/0101002].

[6] M. Prakash, J. M. Lattimer, A. W. Steiner and D. Page, Nucl. Phys. A **715** 835c; [arXiv:astro-ph/0209122].

[7] H. Grigorian, D. Blaschke and G. Poghosyan, Nucl. Phys. A **715** (2003) 831c; [arXiv:nucl-th/0209068].

[8] S. Fredriksson, in *Workshop on Diquarks*, Eds. M. Anselmino and E. Predazzi (World Scientific, Singapore, 1989) 22.

[9] D. Kastor and J. Traschen, Phys. Rev. D **44** (1991) 3791.

[10] J. E. Horvath, O. G. Benvenuto and H. Vucetich, Phys. Rev. D **44** (1991) 3797.

[11] J. E. Horvath, J. A. de Freitas Pacheco and J. C. de Araujo, Phys. Rev. D **46** (1992) 4754.

[12] P. Sahu, Int. J. Mod. Phys. **E2**, 647 (1993).

[13] D. Blaschke, T. Klähn and D. N. Voskresensky, Astrophys. J. **533** (2000) 406; [arXiv:astro-ph/9908334].

[14] D. Page, M. Prakash, J. M. Lattimer and A. Steiner, Phys. Rev. Lett. **85** (2000) 2048; [arXiv:hep-ph/0005094].

[15] D. Blaschke, H. Grigorian and D. N. Voskresensky, Astron. Astrophys. **368** (2001) 561; [arXiv:astro-ph/0009120];
H. Grigorian, D. Blaschke and D. N. Voskresensky, in preparation.

[16] D. K. Hong, S. D. Hsu and F. Sannino, Phys. Lett. B **516** (2001) 362; [arXiv:hep-ph/0107017].

[17] R. Ouyed, eConf **C010815** (2002) 209.

[18] A. W. Steiner, S. Reddy and M. Prakash, Phys. Rev. D **66** (2002) 094007; [arXiv:hep-ph/0205201].

[19] F. Neumann, M. Buballa and M. Oertel, Nucl. Phys. A **714** (2003) 481 [arXiv:hep-ph/0210078].

[20] C. Gocke, D. Blaschke, A. Khalatyan and H. Grigorian, arXiv:hep-ph/0104183.

[21] G.W. Carter and S. Reddy, Phys. Rev. **D 62** (2000) 103002.

[22] P. Jaikumar and M. Prakash, Phys. Lett. B **516** (2001) 345.

[23] S. Schmidt, D. Blaschke and Yu. Kalinovsky, Phys. Rev. C **50** (1994) 435.

[24] J. Berges and K. Rajagopal, Nucl. Phys. B **538** (1999) 215.

[25] P. Bedaque, Nucl. Phys. A **697** (2002) 569.

[26] O. Kiriyama, S. Yasui and H. Toki, Int. J. Mod. Phys. E **10** (2002) 501.

[27] D. Blaschke, S. Fredriksson and A. M. Oztas, eConf **C010815** (2002) 167; [arXiv:astro-ph/0111587].

[28] M. Huang, P. F. Zhuang and W. Q. Chao, Phys. Rev. D **67** (2003) 065015; [arXiv:hep-ph/0207008].

[29] D. Blaschke, H. Grigorian, G. Poghosyan, C. D. Roberts and S. M. Schmidt, Phys. Lett. B **450** (1999) 207 [arXiv:nucl-th/9801060].

[30] J.R. Oppenheimer and G. Volkoff, Phys. Rev. **55**, (1939) 377.

[31] N.K. Glendenning, *Compact Stars* (Springer, New York & London, 2000).

[32] C. Kettner, F. Weber, M. K. Weigel and N. K. Glendenning, Phys. Rev. D **51** (1995) 1440.

[33] H. Grigorian, D. Blaschke and D. N. Aguilera, Phys.Rev.C69:065802 (2003).

[34] D. Blaschke, H. Grigorian, D. N. Aguilera, S. Yasui and H. Toki, in: *Hadron Physics*, AIP Conference Proceedings **660** (2003) 209; [arXiv:hep-ph/0301087].

GAMMA RAY BURSTS AND DELAYED QUARK-DECONFINEMENT

Ignazio Bombaci, Irene Parenti, and Isaac Vidaña

Dipartimento di Fisica "E. Fermi", Universita' di Pisa & INFN, Sezione di Pisa, via Buonarroti, 2, I-56127, Pisa, Italy

Abstract We describe a new model, proposed by Berezhiani et al. (2003), which is able to explain how a gamma-ray burst (GRB) can take place days or years after a supernova explosion. We show that above a threshold value of the gravitational mass a pure hadronic star ("neutron star") is metastable to the conversion into a quark star (hybrid star or strange star), *i.e.* a star made at least in part of deconfined quark matter. The stellar conversion process can be delayed if finite size effects at the interface between hadronic and deconfined quark matter phases are taken into account. A huge amount of energy, on the order of $10^{52} - 10^{53}$ ergs, is released during the conversion process and can produce a powerful gamma-ray burst. The delay between the supernova explosion generating the metastable neutron star and the new collapse can explain the delay inferred in GRB 990705 and in GRB 011211. Next, we explore the consequences of the metastability of "massive" neutron stars and of the existence of stable compact quark stars on the concept of limiting mass of compact stars. Finally, we discuss the implications of the present scenario on the interpretation of the stellar mass and radius extracted from the spectra of several X-ray compact sources.

Keywords: Gamma rays: Gamma Ray Burst. Stars: Neutron Stars, Strange Stars. Dense Matter: equation of state, quark matter.

1. Introduction

Gamma Ray Bursts (GRBs) are one of the most violent and mysterious phenomena in the universe which have challenged astrophysicists for decades (see *e.g.* (Piran 1999; Dermer 2001; Zhang & Meszaros 2003) for a general introduction on this subject). During the last ten years a large amount of new observational data, collected by a variety of instruments on board of various satellites, has revolutionized our understanding of GRBs. The Burst And Transient Source Experiment (BATSE) on board of the Compton Gamma Ray Observatory (CGRO) has demonstrated that GRBs originate at cosmological distances. The BeppoSAX satellite discovered the X-ray "afterglow". This has permitted

D. Blaschke and D. Sedrakian (eds.), Superdense QCD Matter and Compact Stars, 353–375.

to determine the position of some GRBs, to identify the host galaxy and, in a number of cases, to measure the red-shift. Accurate determination of the GRB distance from the measured red-shifts, permitted, for the first time, to derive the energy E_γ emitted by the GRB. The measured fluency of the bursts implies an energy of the order of 10^{53} erg in the case of isotropic emission. There is now, however, compelling evidence that the γ-ray emission is not isotropic, but displays a jet-like geometry. For these bursts, the geometrically corrected gamma-ray energy is about 10^{51} erg (Frayl et al. 2001).

The time duration T_γ of GRBs appears to have a bimodal distribution. Thus, according to their time duration, GRBs are classified as "short" GRBs when $T_\gamma < 2$ seconds, and "long" GRBs when $T_\gamma > 2$ s. Long GRBs represent about 75% of the total GRB population. It is believed that the two types of GRBs may have different progenitors.

Many cosmological models for the energy source (the so-called *central engine*) of GRBs have been proposed. Presently some of the most popular models are: the *collapsar* (*hypernova*) model, the merging of two neutron stars (or a neutron star and a black hole) in a binary system, the strong-magnetized millisecond pulsar model, the *supranova* model. Here, we will not discuss the various merits and drawbacks of the many theoretical models for the GRB central engine, and we refer the reader to recent review papers on this subject (*e.g.* Piran 1999; Dermer 2001; Zhang & Meszaros 2003)). In the following, we will report some recent research (Berezhiani et al. 2003; Bombaci et al. 2003) which try to make a connection between GRBs and quark-deconfinement phase transition.

1.1 The delayed Supernova–GRB connection

A mounting number of observational data suggest a clear connection between supernova (SN) explosions and GRBs (Bloom et al. 1999; Amati et al. 2000; Antonelli et al. 2000: Piro et al. 2000; Reeves et al. 2002; Hjorth et al. 2003; Butler et al. 2003). The detection of X-ray spectral features in the X-ray afterglow of several GRBs, has given evidence for a possible time delay between the SN explosion and the associated GRB. Particularly, in the case of the gamma ray burst of July 5, 1999 (GRB990705) and in the case of GRB011211, it has been possible to estimate the time delay between the two events. For GRB990705 the supernova explosion is evaluated to have occurred a few years before the GRB (Amati et al. 2000; Lazzati et al. 2001), while for GRB011211 about four days before the burst (Reeves et al. 2002).

The scenario which emerges from these findings is the following two-step scenario. The first event is the supernova explosion which forms a compact stellar remnant, *i.e.* a neutron star (NS); the second catastrophic event is associated with the NS and it is the energy source for the observed GRB. These

new observational data, and the two-step scenario outlined above, poses severe problems for most of the current theoretical models for the central energy source of GRBs. The main difficulty of all these models is to understand the origin of the second "explosion", and to explain the long time delay between the two events.

In the so-called *supranova* model (Vietri & Stella 1998) for GRBs the second catastrophic event is the collapse to a black hole of a *supramassive* neutron star, *i.e.* a fast rotating NS with a baryonic mass M_B above the maximum baryonic mass $M_{B,max}$ for non-rotating configurations. In this model, the time delay between the SN explosion and the GRB is equal to the time needed by the fast rotating newly formed neutron star to get rid of angular momentum and to reach the limit for instability against quasi-radial modes where the collapse to a black hole occurs (Datta et al. 1998). The supranova model needs a fine tuning in the initial spin period P_{in} and baryonic stellar mass $M_{B,in}$ to produce a supramassive neutron star that can be stabilized by rotation up to a few years. For example, if $P_{in} \geq 1.5$ ms, then the newborn supramassive neutron star must be formed within $\sim 0.03 M_\odot$ above $M_{B,max}$ (Datta et al. 1998).

1.2 The nature of Neutron Stars: Hadronic Stars or Quark Stars?

One of the most fascinating enigma in modern astrophysics concerns the true nature of the ultra-dense compact objects called *neutron stars*. Different models for the EOS of dense matter predict a neutron star maximum mass (M_{max}) in the range of 1.4 – 2.2 $M_\odot$, and a corresponding central density in range of 4 – 8 times the saturation density ($\rho_0 \sim 2.8 \times 10^{14}$g/cm^3) of nuclear matter (e.g. Shapiro & Teukolsky 1983; Haensel 2003). In the case of a star with $M \sim 1.4\ M_\odot$, different EOS models predict a radius in the range of 7 – 16 km (Shapiro & Teukolsky 1983; Haensel 2003; Dey et al. 1998).

In a simplistic and conservative picture the core of a neutron star is modeled as a uniform fluid of neutron rich nuclear matter in equilibrium with respect to the weak interaction (β-stable nuclear matter). However, due to the large value of the stellar central density and to the rapid increase of the nucleon chemical potentials with density, hyperons (Λ, Σ^-, Σ^0, Σ^+, Ξ^- and Ξ^0 particles) are expected to appear in the inner core of the star. Other *exotic* phases of hadronic matter such as a Bose-Einstein condensate of negative pion (π^-) or negative kaon (K^-) could be present in the inner part of the star.

According to Quantum Chromodynamics (QCD) a phase transition from hadronic matter to a deconfined quark phase should occur at a density of a few times nuclear matter saturation density. Consequently, the core of the more massive neutron stars is one of the best candidates in the Universe where such deconfined phase of quark matter (QM) could be found. Since β-stable hadronic matter posses two conserved "charges" (*i.e.,* electric charge and baryon

number) the quark-deconfinement phase transition proceeds through a mixed phase over a finite range of pressures and densities according to the Gibbs' criterion for phase equilibrium (Glendenning 1992). At the onset of the mixed phase, quark matter droplets form a Coulomb lattice embedded in a sea of hadrons and in a roughly uniform sea of electrons and muons. As the pressure increases various geometrical shapes (rods, plates) of the less abundant phase immersed in the dominant one are expected. Finally the system turns into uniform quark matter at the highest pressure of the mixed phase (Heiselberg et al. 1993; Voskresensky et al. 2003). Compact stars which possess a "quark matter core" either as a mixed phase of deconfined quarks and hadrons or as a pure quark matter phase are called *Hybrid Neutron Stars* or shortly *Hybrid Stars* (HyS) (Glendenning 1996). In the following of this paper, the more *conventional* neutron stars in which no fraction of quark matter is present, will be referred to as *pure Hadronic Stars* (HS).

Even more intriguing than the existence of a quark core in a neutron star, is the possible existence of a new family of compact stars consisting completely of a deconfined mixture of *up* (*u*), *down* (*d*) and *strange* (*s*) quarks (together with an appropriate number of electrons to guarantee electrical neutrality) satisfying the Bodmer–Witten hypothesis (Bodmer 1971; Witten 1984; see also Terazawa 1979). Such compact stars have been called *strange quark stars* or shortly *strange stars* (SS) (Alcock et al. 1986; Haensel et al. 1986) and their constituent matter as *strange quark matter* (SQM) (Farhi & Jaffe 1984; Madsen 1999). Presently there is no unambiguous proof about the existence of strange stars, however, a sizable amount of observational data collected by the new generations of X-ray satellites, is providing a growing body of evidence for their possible existence (Bombaci 1997; Cheng et al. 1998; Li et al. 1999a; Li et al. 1999b; Xu 2002; Drake et al. 2002).

Present accurate determinations of compact star masses in radio pulsar binaries (Thorsett & Chakrabarty 1999) permit to rule out only *extremely soft* EOS, *i.e.* those giving M_{max} less than about 1.45 $M_{\odot}$. However, in at least two accreting X-ray binaries it has been found evidence for compact stars with higher masses. The first of these star is Vela X-1, with a reported mass $1.88 \pm 0.13 M_{\odot}$ (Quaintrell et al. 2003), the second is Cygnus X-2, with a reported mass of $1.78 \pm 0.23 M_{\odot}$ (Orosz & Kuulkers 1999). Unfortunately, mass determinations in X-ray binaries are affected by large uncertainties (van Kerkwijk et al. 1995), therefore the previous quoted "high mass values" should always be handled with care. In addition to mass determination, existing observational data on the spin frequency of millisecond pulsars and on the thermal evolution of neutron stars do not put severe constraints on the EOS of dense matter. Fortunately, this situation is improving in the last few years. In fact, the extraordinary spectroscopic capabilities of the instruments on board Chandra X-ray and XMM-Newton satellites, are giving the unique possibility to perform accurate

measurements of the gravitational red-shift in the spectral lines of a few compact X-ray sources. This provide informations on the mass to radius ratio for compact stars and will help us to understand the true nature of these compact objects.

In this work (see Bombaci et al. 2003), we study the effects of the hadron-quark deconfinement phase transition in stellar compact objects. We show that when finite size effects at the interface between the quark- and the hadron-phase are taken into account, pure Hadronic Stars, above a threshold value of the central pressure (gravitational mass), are metastable to the *decay* (*conversion*) to hybrid neutron stars or to strange stars (depending on the properties of EOS for quark matter). The *mean-life time* of the metastable stellar configuration is related to the quantum nucleation time to form a drop of quark matter in the stellar center, and dramatically depends on the value of the stellar central pressure. The *delayed* stellar conversion liberates an enormous amount of energy, in the range of $0.5–1.7\times10^{53}$ erg, which could power a GRB. This model (Berezhiani et al. 2003) explains the SN–GRB association and in particular the long time delay inferred for GRB990705 and GRB011211. Also, we explore the consequences of the metastability of "massive" pure Hadronic Stars and the existence of stable compact "quark" stars (hybrid neutron stars or strange stars) on the concept of limiting mass of compact stars. Finally, we discuss the implications of our scenario in the interpretation of the mass-radius constraints extracted from the spectra of several X-ray compact sources.

2. Quantum nucleation of quark matter in hadronic stars

In the following, we assume that the compact star survives the early stages of its evolution as a pure hadronic star, and we study quark matter nucleation in cold (T = 0) neutrino-free hadronic matter. The thermal effects on quark matter nucleation in newly formed neutron stars (protoneutron stars) are discussed in Bombaci et al. (2003).

In bulk matter the quark-hadron mixed phase begins at the *static transition point* defined according to the Gibbs' criterion for phase equilibrium

$$\mu_H = \mu_Q \equiv \mu_0 \,, \qquad P_H(\mu_0) = P_Q(\mu_0) \equiv P_0 \tag{1}$$

where

$$\mu_H = \frac{\varepsilon_H + P_H}{n_{b,H}} \,, \qquad \mu_Q = \frac{\varepsilon_Q + P_Q}{n_{b,Q}} \tag{2}$$

are the chemical potentials for the hadron and quark phase respectively, ε_H (ε_Q), P_H (P_Q) and $n_{b,H}$ ($n_{b,Q}$) denote respectively the total (*i.e.,* including leptonic contributions) energy density, the total pressure and baryon number density for the hadron (quark) phase, in the case of cold matter.

Let us now consider the more realistic situation in which one takes into account the energy cost due to finite size effects in creating a drop of deconfined

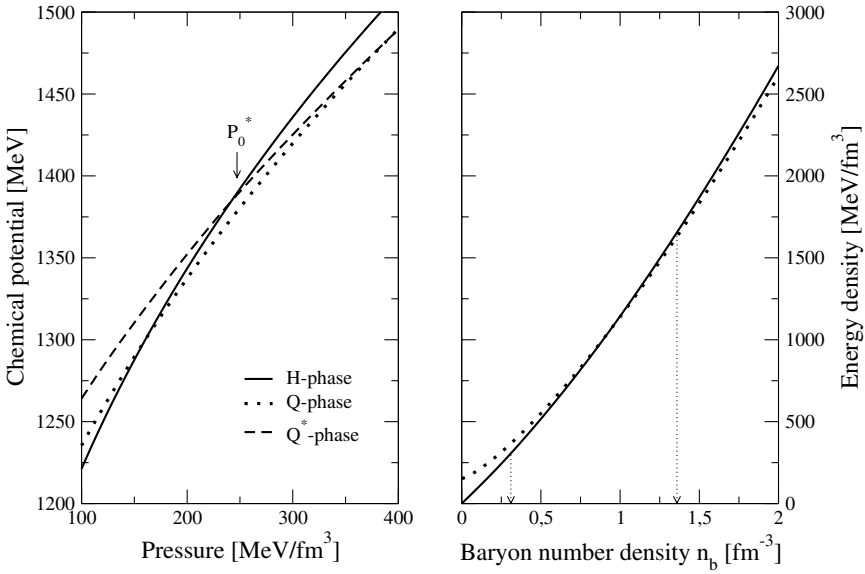

Figure 1. Chemical potentials of the three phases of matter (H, Q, and Q*), as defined by Eq. (2) as a function of the total pressure (left panel); and energy density of the H- and Q-phase as a function of the baryon number density (right panel). The hadronic phase is described with the GM3 model whereas for the Q and Q* phases is employed the MIT-like bag model with $m_s = 150$ MeV, $B = 152.45$ MeV/fm^3 and $\alpha_s = 0$. The vertical lines arrows on the right panel indicate the beginning and the end of the mixed hadron-quark phase defined according to the Gibbs criterion for phase equilibrium. On the left panel P_0^* denotes the static transition point.

quark matter in the hadronic environment. As a consequence of these effects, the formation of a critical-size drop of QM is not immediate and it is necessary to have an overpressure $\Delta P = P - P_0$ with respect to the static transition point. Thus, above P_0, hadronic matter is in a metastable state, and the formation of a real drop of quark matter occurs via a quantum nucleation mechanism. A sub-critical (virtual) droplet of deconfined quark matter moves back and forth in the potential energy well separating the two matter phases (see discussion below) on a time scale $\nu_0^{-1} \sim 10^{-23}$ seconds, which is set by the strong interactions. This time scale is many orders of magnitude shorter than the typical time scale for the weak interactions, therefore quark flavor must be conserved during the deconfinement transition. We will refer to this form of deconfined matter, in which the flavor content is equal to that of the β-stable hadronic system at the same pressure, as the Q*-phase. Soon afterwards a critical size drop of quark matter is formed the weak interactions will have enough time to act, changing the quark flavor fraction of the deconfined droplet to lower its energy, and a droplet of β-stable SQM is formed (hereafter the Q-phase).

We have adopted rather common models for describing both the hadronic and the quark phase of dense matter. For the hadronic phase we used models which are based on a relativistic Lagrangian of hadrons interacting via the exchange of sigma, rho and omega mesons. The parameters adopted are the standard ones (Glendenning & Moszkowski 1991). Hereafter we refer to this model as the GM equation of state (EOS). For the quark phase we have adopted a phenomenological EOS (Farhi & Jaffe 1984) which is based on the MIT bag model for hadrons. The parameters here are: the mass m_s of the strange quark, the so-called pressure of the vacuum B (bag constant) and the QCD structure constant α_s. For all the quark matter model used in the present work, we take $m_u = m_d = 0$, $m_s = 150$ MeV and $\alpha_s = 0$.

In the left panel of Fig. 1, we show the chemical potentials, defined according to Eq. (2), as a function of the total pressure for the three phases of matter (H, Q*, and Q) discussed above. In the right panel of the same figure, we plot the energy densities for the H- and Q*-phase as a function of the corresponding baryon number densities. Both panels in Fig. 1 are relative to the GM3 model for the EOS for the H-phase and to the MIT bag model EOS for the Q and Q* phases with $B = 152.45$ MeV/fm^3.

To calculate the nucleation rate of quark matter in the hadronic medium we use the Lifshitz–Kagan quantum nucleation theory (Lifshitz & Kagan 1972) in the relativistic form given by Iida & Sato (1997). The QM droplet is supposed to be a sphere of radius $\mathcal{R}$ and its quantum fluctuations are described by the Lagrangian

$$L(\mathcal{R}, \dot{\mathcal{R}}) = -\mathcal{M}(\mathcal{R})c^2\sqrt{1 - (\dot{\mathcal{R}}/c)^2} + \mathcal{M}(\mathcal{R})c^2 - U(\mathcal{R})\,, \qquad (3)$$

where $\mathcal{M}(\mathcal{R})$ is the effective mass of the QM droplet, and $U(\mathcal{R})$ its potential energy. Within the Lifshitz–Kagan quantum nucleation theory, one assumes that the phase boundary (*i.e.* the droplet surface) moves slowly compared to the high sound velocity of the medium ($\dot{\mathcal{R}} << v_s \sim c$). Thus the number density of each phase adjust adiabatically to the fluctuations of the droplet radius, and the system retains pressure equilibrium between the two phases. Thus, the droplet effective mass is given by (Lifshitz & Kagan 1972; Iida & Sato 1997)

$$\mathcal{M}(\mathcal{R}) = 4\pi\rho_H\Big(1 - \frac{n_{b,Q*}}{n_{b,H}}\Big)^2\mathcal{R}^3\,, \tag{4}$$

ρ_H being the hadronic mass density, $n_{b,H}$ and $n_{b,Q*}$ are the baryonic number densities at a same pressure in the hadronic and Q*-phase, respectively. The potential energy is given by (Lifshitz & Kagan 1972; Iida & Sato 1997)

$$U(\mathcal{R}) = \frac{4}{3}\pi\mathcal{R}^3 n_{b,Q*}(\mu_{Q*} - \mu_H) + 4\pi\sigma\mathcal{R}^2\,, \tag{5}$$

where μ_H and μ_{Q*} are the hadronic and quark chemical potentials at a fixed pressure P and σ is the surface tension for the surface separating the quark phase from the hadronic phase. The value of the surface tension σ is poorly known, and typical values used in the literature range within 10–50 MeV/fm^2 (Heiselberg et al. 1993; Iida & Sato 1997).

For sake of simplicity and to make our present discussion more transparent, in the previous expression (5) for the droplet potential energy, we neglected the terms connected with the electrostatic energy and with the so-called curvature energy. The inclusion of these terms will not modifies the conclusions of the present study (Iida & Sato 1997; Bombaci et al. 2003).

The process of formation of a bubble having a critical radius, can be computed using a semiclassical approximation. The procedure is rather straightforward. First one computes, using the well known Wentzel–Kramers–Brillouin (WKB) approximation, the ground state energy E_0 and the oscillation frequency ν_0 of the virtual QM drop in the potential well $U(\mathcal{R})$. Then it is possible to calculate in a relativistic framework the probability of tunneling as (Iida & Sato 1997)

$$p_0 = \exp\Big[-\frac{A(E_0)}{\hbar}\Big] \tag{6}$$

where A is the action under the potential barrier

$$A(E) = \frac{2}{c}\int_{\mathcal{R}_-}^{\mathcal{R}_+}\big\{[2\mathcal{M}(\mathcal{R})c^2 + E - U(\mathcal{R})] \times [U(\mathcal{R}) - E]\mathcal{R}\big\}^{1/2}\,d\mathcal{R}\,, \tag{7}$$

$\mathcal{R}_\pm$ being the classical turning points.

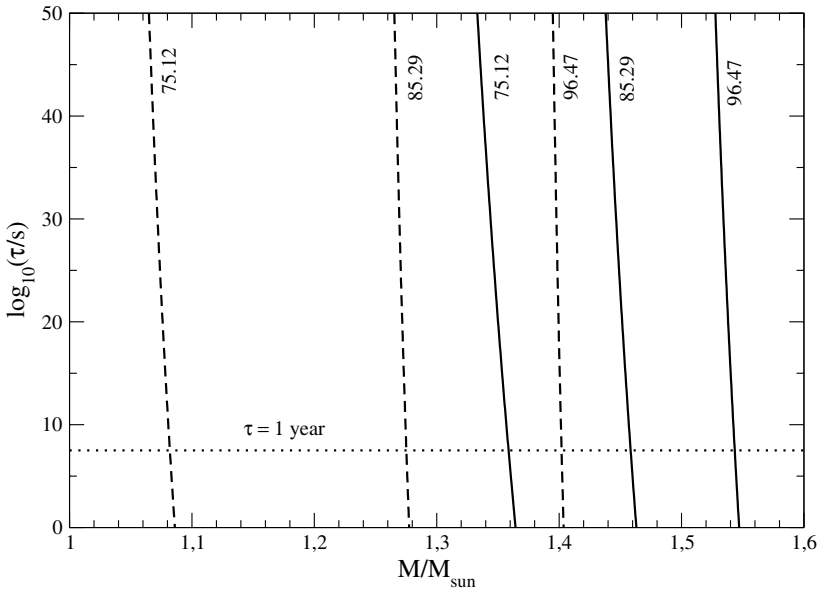

Figure 2. Nucleation time as a function of the maximum gravitational mass of the hadronic star. Solid lines correspond to a value of $\sigma = 30$ MeV/fm^2 whereas dashed ones are for $\sigma = 10$ MeV/fm^2. The nucleation time corresponding to one year is shown by the dotted horizontal line. The different values of the bag constant (in units of MeV/fm^3) are plotted next to each curve. The hadronic phase is described with the GM1 model.

The nucleation time is then equal to

$$\tau = (\nu_0 p_0 N_c)^{-1}\,, \tag{8}$$

where N_c is the number of virtual centers of droplet formation in the innermost region of the star. Following the simple estimate given in Iida & Sato (1997), we take $N_c = 10^{48}$. The uncertainty in the value of N_c is expected to be within one or two orders of magnitude. In any case, all the qualitative features of our scenario will be not affected by the uncertainty in the value of N_c.

3. Results

In our scenario, we consider a purely hadronic star whose central pressure is increasing due to spin-down or due to mass accretion, *e.g.,* from the material left by the supernova explosion (fallback disc), from a companion star or from the interstellar medium. As the central pressure exceeds the threshold value P_0^* at static transition point, a virtual drop of quark matter in the Q*-phase can be formed in the central region of the star. As soon as a real drop of Q*-matter is formed, it will grow very rapidly and the original Hadronic Star will be converted to and Hybrid Star or to a Strange Star, depending on the detail of

Table 1. The critical mass and energy released in the conversion process of an HS into a QS for several values of the Bag constant and the surface tension. Column labeled $M_{QS,max}$ denotes the maximum gravitational mass of the final QS sequence. The value of the critical gravitational mass of the initial HS is reported on column labeled M_{cr} whereas those of the mass of the final QS and the energy released in the stellar conversion process are shown on columns labeled M_{fin} and E_{conv} respectively. BH denotes those cases in which the baryonic mass of the critical mass configuration is larger than the maximum baryonic mass of the QS sequence ($M^b_{cr} > M^b_{QS,max}$). In these cases the stellar conversion process leads to the formation of a black hole. Units of B and σ are MeV/fm^3 and MeV/fm^2 respectively. All masses are given in solar mass units and the energy released is given in units of 10^{51} erg. The hadronic phase is described with the GM1 model, m_s and α_s are always taken equal to 150 MeV and 0 respectively. The GM1 model predicts a maximum mass for the pure HS of 1.807 $M_\odot$.

		$\sigma = 10$			$\sigma = 30$		
B	$M_{QS,max}$	M_{cr}	M_{fin}	E_{conv}	M_{cr}	M_{fin}	E_{conv}
208.24	1.769	1.798	BH		1.805	BH	
169.61	1.633	1.754	BH		1.778	BH	
136.63	1.415	1.668	BH		1.719	BH	
108.70	1.426	1.510	BH		1.615	BH	
106.17	1.433	1.490	BH		1.602	BH	
103.68	1.441	1.469	1.434	62.5	1.588	BH	
101.23	1.449	1.447	1.411	64.0	1.574	BH	
98.83	1.459	1.425	1.388	66.0	1.559	BH	
96.47	1.470	1.402	1.364	68.5	1.543	BH	
94.15	1.481	1.378	1.339	71.1	1.527	1.474	94.8
91.87	1.494	1.354	1.313	74.2	1.511	1.456	98.1
89.64	1.507	1.329	1.285	77.3	1.495	1.438	101.8
87.45	1.552	1.302	1.257	80.7	1.477	1.417	105.9
85.29	1.538	1.275	1.228	84.4	1.458	1.397	110.4
80.09	1.581	1.196	1.144	92.9	1.410	1.342	122.7
75.12	1.631	1.082	1.029	93.8	1.359	1.284	133.1
65.89	1.734	0.820	0.764	100.6	1.212	1.123	159.9
63.12	1.770	0.727	0.672	98.1	1.160	1.067	166.5
59.95	1.814	0.545	0.501	79.7	1.081	0.986	168.8

the EOS for quark matter employed to model the phase transition (particularly depending on the value of the parameter B within the model adopted in the present study).

The nucleation time τ, *i.e.,* the time needed to form a critical droplet of deconfined quark matter, can be calculated for different values of the stellar central pressure P_c which enters in the expression of the energy barrier in Eq. (5). The nucleation time can be plotted as a function of the gravitational mass

M_{HS} of the HS corresponding to the given value of the central pressure, as implied by the solution of the Tolmann-Oppeneimer-Volkov equations for the pure Hadronic Star sequences. The results of our calculations are reported in Fig. 2 which is relative to the GM1 EOS for the hadronic phase. Each curve refers to a different value of the bag constant and the surface tension.

As we can see, from the results in Fig. 2, a metastable hadronic star can have a mean-life time many orders of magnitude larger than the age of the universe $T_{univ} = (13.7 \pm 0.2) \times 10^9$ yr $= (4.32 \pm 0.06) \times 10^{17}$ s (Spergel et al. 2003). As the star accretes a small amount of mass (of the order of a few per cent of the mass of the sun), the consequential increase of the central pressure lead to a huge reduction of the nucleation time and, as a result, to a dramatic reduction of the HS *mean-life time*.

To summarize, in the present scenario pure hadronic stars having a central pressure larger than the static transition pressure for the formation of the Q*-phase are metastable to the "decay" (conversion) to a more compact stellar configuration in which deconfined quark matter is present (*i.e.,* HyS or SS). These metastable HS have a *mean-life time* which is related to the nucleation time to form the first critical-size drop of deconfined matter in their interior (the actual *mean-life time* of the HS will depend on the mass accretion or on the spin-down rate which modifies the nucleation time via an explicit time dependence of the stellar central pressure). We define as *critical mass* M_{cr} of the metastable HS, the value of the gravitational mass for which the nucleation time is equal to one year: $M_{cr} \equiv M_{HS}(\tau = 1\mathrm{yr})$. Pure hadronic stars with $M_H > M_{cr}$ are very unlikely to be observed. M_{cr} plays the role of an *effective maximum mass* for the hadronic branch of compact stars. While the Oppenheimer–Volkov maximum mass $M_{HS,max}$ (Oppenheimer & Volkov 1939) is determined by the overall stiffness of the EOS for hadronic matter, the value of M_{cr} will depend in addition on the bulk properties of the EOS for quark matter and on the properties at the interface between the confined and deconfined phases of matter (*e.g.,* the surface tension σ).

To explore how the outcome of our scenario depends on the details of the stellar matter EOS, we have considered two different parameterizations (GM1 and GM3) for the EOS of the hadronic phase, and we have varied the value of the bag constant B. Moreover, we have considered two different values for the surface tension: $\sigma = 10$ MeV/fm^2 and $\sigma = 30$ MeV/fm^2. These results, in the case of the GM1 EOS, are summarized in Tab. 1.

In Fig. 3, we show the MR curve for pure HS within the GM1 model for the EOS of the hadronic phase, and that for hybrid stars or strange stars for different values of the bag constant B. The configuration marked with an asterisk on the hadronic MR curves represents the hadronic star for which the central pressure is equal to P_0^*. The full circle on the hadronic star sequence represents the critical mass configuration, in the case $\sigma = 30$ MeV/fm^2. The full

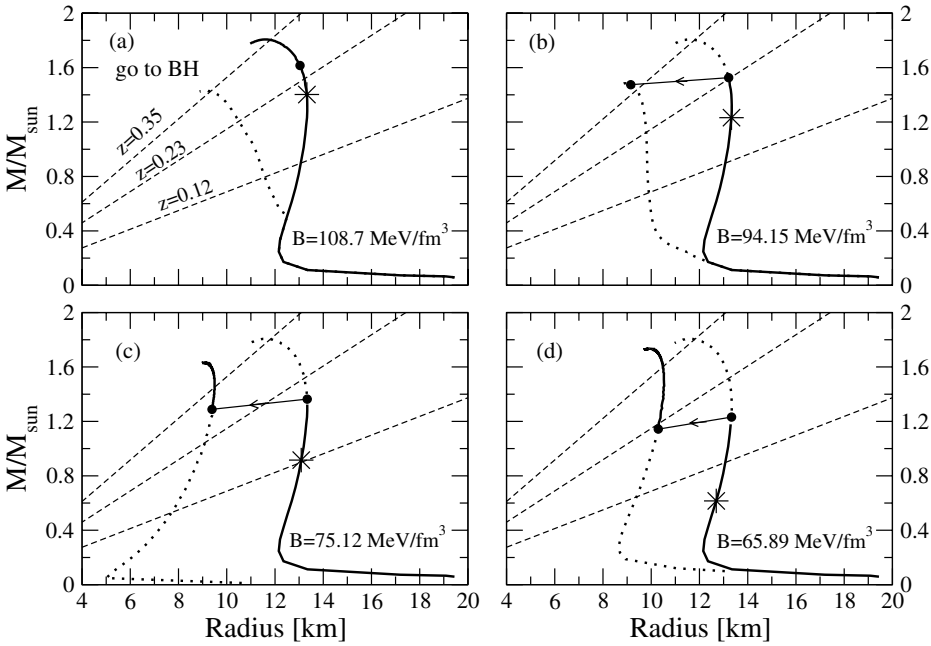

Figure 3. Mass-radius relation for a pure HS described within the GM1 model and that of the HyS or SS configurations for several values of the Bag constant and $m_s = 150$ MeV and $\alpha_s = 0$. The configuration marked with an asterisk represents in all cases the HS for which the central pressure is equal to P_0^*. The conversion process of the HS, with a gravitational mass equal to M_{cr}, into a final HyS or SS is denoted by the full circles connected by an arrow. In all the panels σ is taken equal to 30 MeV/fm^2. The dashed lines show the gravitational red shift deduced for the X-ray compact sources EXO 0748-676 ($z = 0.35$) and 1E 1207.4-5209 ($z = 0.12 - 0.23$).

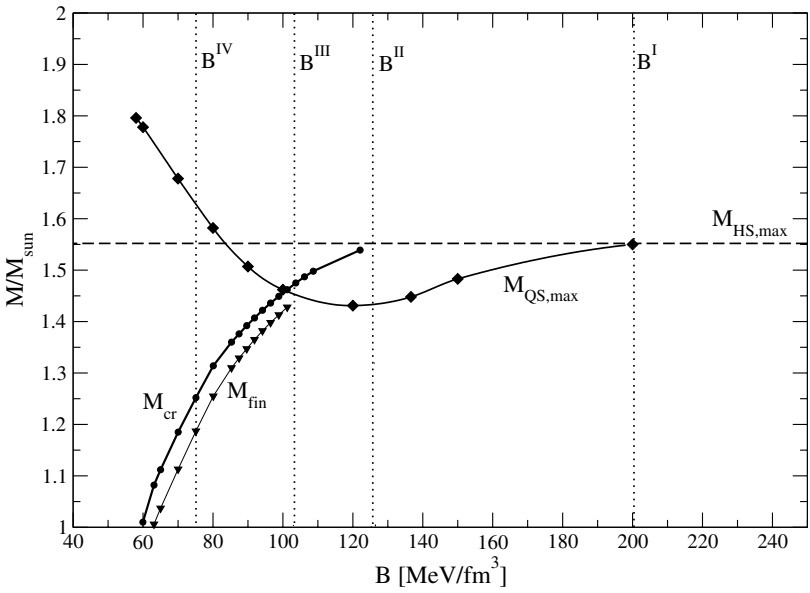

Figure 4. The maximum mass $M_{QS,max}$ for the quark star configurations (HS or SS), the critical mass M_{cr} and the mass M_{fin} of the stable QS to which it evolves are plotted as a function of the bag constant B. The vertical doted lines labeled B^I – B^{IV} mark the boundary of different ranges of the bag constant which give a different astrophysical output for our scenario, as discussed in the text. The dashed horizontal line gives the value of the maximum mass for the pure hadronic star sequence. All the results are relative to the GM3 model for the EOS for the hadronic phase, the surface tension σ is taken equal to 30 MeV/fm^2.

circle on the HyS (SS) mass-radius curve represents the hybrid (strange) star which is formed from the conversion of the hadronic star with $M_{HS} = M_{cr}$. We assume (Bombaci & Datta 2000) that during the stellar conversion process the total number of baryons in the star (or in other words the stellar baryonic mass) is conserved. Thus the total energy liberated in the stellar conversion is given by the difference between the gravitational mass of the initial hadronic star ($M_{in} \equiv M_{cr}$) and that of the final hybrid or strange stellar configuration with the same baryonic mass ($M_{fin} \equiv M_{QS}(M^b_{cr})$):

$$E_{conv} = (M_{in} - M_{fin})c^2 \,. \tag{9}$$

The stellar conversion process, described so far, will start to populate the new branch of quark stars (the part of the QS sequence plotted as a continuous curve in Fig. 3). Long term accretion on the QS can next produce stars with masses up to the limiting mass $M_{QS,max}$ for the quark star configurations.

As we can see from the results reported in Tab. 1, within the present model for the EOS, we can distinguish several ranges for the value of the bag constant, which gives a different astrophysical output for our scenario. To be more

specific, in Fig. 4 we plot the maximum mass of the QS sequence, the critical mass and the corresponding final mass M_{fin} as a function of B, in the particular case of the GM3 model for the EOS of the hadronic phase and taking $\sigma = 30\mathrm{MeV/fm}^2$. Let us start the following discussion from "high" values of B down to the minimum possible value B^V ($\sim 57.5\mathrm{MeV/fm}^3$ for $\alpha_s = 0$) for which atomic nuclei will be unstable to the decay to a drop of deconfined *u,d* quark matter (non-strange QM) (Farhi & Jaffe 1984).

(1) $B > B^I$. These "high" values of the bag constant do not allow the quark deconfinement to occur in the maximum mass hadronic star either. Here B^I denotes the value of the bag constant for which the central density of the maximum mass hadronic star is equal to the critical density for the beginning of the mixed quark-hadron phase. For these values of B, all compact stars are pure hadronic stars.

(2) $B^{II} < B < B^I$. Now, in addition to pure HS, there is a new branch of compact stars, the hybrid stars; but the nucleation time $\tau(M_{HS,max})$ to form a droplet of Q*-matter in the maximum mass hadronic star, is of the same order or much larger than the age of the Universe. Therefore, it is extremely unlikely to populate the hybrid star branch. Once again, the compact star we can observe are, in this case, pure HS.

(3) $B^{III} < B < B^{II}$. In this case, the critical mass for the pure hadronic star sequence is less than the maximum mass for the same stellar sequence, *i.e.,* $M_{cr} < M_{HS,max}$. Nevertheless (for the present EOS model), the baryonic mass $M^b(M_{cr})$ of the hadronic star with the critical mass is larger than the maximum baryonic mass $M^b_{QS,max}$ of the hybrid star sequence. In this case, the formation of a critical size droplet of deconfined matter in the core of the hadronic star with the critical mass, will trigger off a stellar conversion process which will produce, at the end, a black hole (see cases marked as "BH" in Tab. 1 and Tab. 2). As in the previous case, it is extremely unlikely to populate the hybrid star branch. The compact star predicted by these EOS models are pure HS. Hadronic stars with a gravitational mass in the range $M_{HS}(M^b_{QS,max}) < M_{HS} < M_{cr}$ (where $M^b_{QS,max}$ is the baryonic mass of the maximum mass configuration for the hybrid star sequence) are metastable with respect to a conversion to a black hole.

(4) $B^{IV} < B < B^{III}$. In this range for B one has $M_{cr} < M_{HS}(M^b_{QS,max})$. There are now two different branches of compact stars: pure hadronic stars with $M_{HS} < M_{cr}$, and hybrid stars with $M_{QS}(M^b_{cr}) < M_{QS} < M_{QS,max}$ (here $M_{QS}(M^b_{cr}) \equiv M_{fin}$ is the gravitational mass of the hybrid star with the same baryonic mass of the critical mass hadronic star).

(5) $B^V < B < B^{IV}$. Finally, as B falls below the value B^{IV}, the Bodmer-Witten hypothesis starts to be fulfilled. Now the stable quark stars formed in the stellar conversion process are strange stars.

3.1 The limiting mass of compact stars

The possibility to have metastable hadronic stars, together with the feasible existence of two distinct families of compact stars, demands an extension of the concept of maximum mass of a "neutron star" with respect to the *classical* one introduced by Oppenheimer & Volkoff (1939). Since metastable HS with a "short" *mean-life time* are very unlikely to be observed, the extended concept of maximum mass must be introduced in view of the comparison with the values of the mass of compact stars deduced from direct astrophysical observation. Having in mind this operational definition, we call *limiting mass* of a compact star, and denote it as M_{lim}, the physical quantity defined in the following way:
(a) if the nucleation time $\tau(M_{HS,max})$ associated to the maximum mass configuration for the hadronic star sequence is of the same order or much larger than the age of the universe T_{univ}, then

$$M_{lim} = M_{HS,max}\,, \tag{10}$$

in other words, the limiting mass in this case coincides with the Oppenheimer–Volkoff maximum mass for the hadronic star sequence.
(b) If the critical mass M_{cr} is smaller than $M_{HS,max}$ (*i.e.* $\tau(M_{HS,max}) <$ 1 yr), thus the limiting mass for compact stars is equal to the largest value between the critical mass for the HS and the maximum mass for the quark star (HyS or SS) sequence

$$M_{lim} = max\big[M_{cr}\,, M_{QS,max}\big]\,. \tag{11}$$

(c) Finally, one must consider an "intermediate" situation for which 1yr $<$ $\tau(M_{HS,max}) < T_{univ}$. As the reader can easily realize, now

$$M_{lim} = max\big[M_{HS,max}\,, M_{QS,max}\big]\,, \tag{12}$$

depending on the details of the EOS which could give $M_{HS,max} > M_{QS,max}$ or vice versa.

In Fig. 5, we show the limiting mass M_{lim} calculated in the case of the GM1+Bag model (dashed line) and in the case of the GM3+Bag model (continuous line) as a function of the bag constant B. In the same figure, we compare our theoretical determination for M_{lim} with some of the "measured" masses of compact stars in radio pulsar binaries (Thorsett & Chakrabarty 1999) and for the compact stars Vela X-1 (Quaintrell et al. 2003) and Cygnus X-2 (Orosz & Kuulkers 1999).

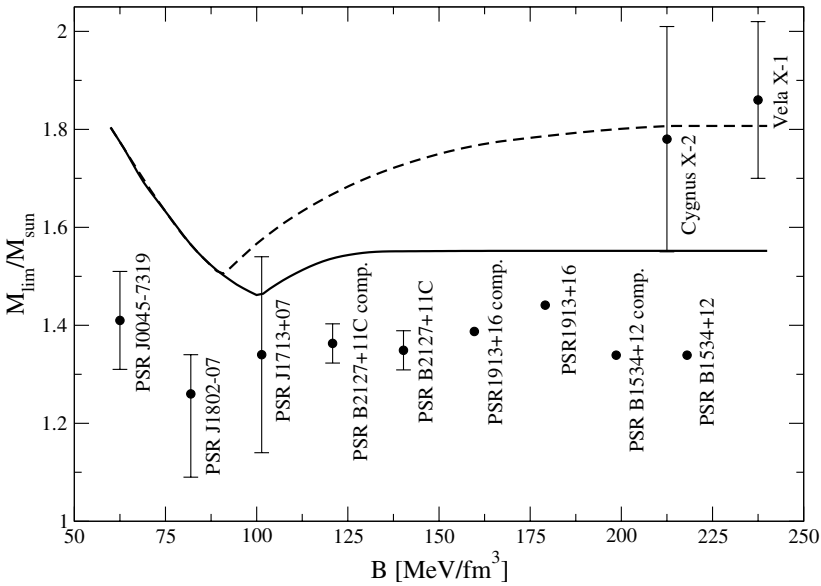

Figure 5. The limiting (gravitational) mass M_{lim}, according to generalized definition given in the present work, is plotted as a function of the Bag constant. Solid (dashed) lines show the results for the GM3+Bag (GM1+Bag) model. In both cases we take $\sigma = 30$ MeV/fm^2. The values of some "measured" masses of compact stars in radio pulsars and in Vela X-1 and Cygnus X-2 are also reported for comparison.

4. Mass-to-radius ratio and internal constitution of compact stars

An accurate measure of the radius and the mass of an individual "neutron star" will be of fundamental importance to discriminate between different models for the equation of state of dense hadronic matter. Unfortunately such a crucial information is still not available. A decisive step in such a direction has been done thanks to the instruments on board of the last generation of X-ray satellites. These are providing a large amount of fresh and accurate observational data, which are giving us the possibility to extract very tight constraints on the radius and the mass for some compact stars.

The analysis of different astrophysical phenomena associated with compact X-ray sources, seems to indicate in some case the existence of neutron stars with "large" radii in the range of 12 – 20 km and in some other cases the existence of compact stars with "small" radii in the range of 6 – 9 km (Bombaci 1997; Li et al. 1999a; Poutanen & Gierlinski 2003; Bombaci 2003). Clearly, this possibility is a natural outcome of our scenario, where two different families of compact stars, the pure hadronic stars and the quark stars (HyS or SS), may exist in the universe.

In the following of this section, we will consider some of the most recent constraints on the mass-to-radius ratio for compact stars extracted from the observational data for a few X-ray sources, and we will try make an interpretation of these results within our scenario.

In Fig. 6, we report the radius an the mass of the compact star RX J1856.5-3754 inferred by Walter & Lattimer (2002) (see also Kaplan et al. 2002) from the fit of the full spectral energy distribution for this isolated radio-quite "neutron star", after a revised parallax determination (Kaplan et al. 2002) which implies a distance to the source of 117 ± 12 pc. Comparing the mass-radius box for RX J1856.5-3754 reported in Fig. 6 with the theoretical determination of the MR relation for different equations of state, one concludes that RX J1856.5-3754 could be (see *e.g.* Fig. 2 in Walter & Lattimer, 2002) either an hadronic star or an hybrid or strange star (see also Drake et al. 2002).

Next we consider the compact star in the low mass X-ray binary 4U 1728-34. In a very recent paper Shaposhnikov et al. (2003) (hereafter STH) have analyzed a set of 26 Type-I X-ray bursts for this source. The data were collected by the Proportional Counter Array on board of the Rossi X-ray Timing Explorer (RXTE) satellite. For the interpretation of these observational data Shaposhnikov et al. 2003 used a model of the X-ray burst spectral formation developed by Titarchuk (1994) and Shaposhnikov & Titarchuk (2002). Within this model, STH were able to extract very stringent constrain on the radius and the mass of the compact star in this bursting source. The radius and mass for 4U 1728-34, extracted by STH for different best-fits of the burst data, are depicted in Fig. 6 by the filled squares. Each of the four MR points is relative to a different value of the distance to the source (d = 4.0, 4.25, 4.50, 4.75 kpc, for the fit which produces the smallest values of the mass, up to the one which gives the largest mass). The error bars on each point represent the error contour for 90% confidence level. It has been pointed out (Bombaci 2003) that the semi-empirical MR relation for the compact star in 4U 1728-34 obtained by STH is not compatible with models pure hadronic stars, while it is consistent with strange stars or hybrid stars.

Assuming RX J1856.5-3754 to be a pure hadronic star and 4U 1728-34 an hybrid or a strange star, we see from our results plotted in Fig. 6, that this possibility can be realized as a natural consequence of our scenario. Thus, we find that the existence of quark stars (with "small" radii) does not exclude the possible existence of pure hadronic stars (with "large" radii), and *vice versa*.

Decisive informations on the mass-to-radius ratio can be provided by measuring the gravitational redshift of lines in the spectrum emitted from the compact star atmosphere. Very recently, redshifted spectral lines features have been reported for two different X-ray sources (Cottam et al. 2002; Sanwal et al. 2002). The first of these sources is the compact star in the low mass X-ray binary EXO 0748-676 . Studying the spectra of 28 type-I X-ray bursts in

EXO 0748-676 , Cottam et al. (2002) have found absorption spectral line features, which they identify as signatures of Fe XXVI (25-time ionized hydrogen-like Fe) and Fe XXV from the $n = 2 \rightarrow 3$ atomic transition, and of O VIII ($n = 1 \rightarrow 2$ transition). All of these lines are redshifted, with a unique value of the redshift $z = 0.35$. Interpreting the measured redshift as due to the strong gravitational field at the surface of the compact star (thus neglecting general relativistic effects due to stellar rotation on the spectral lines (Öezel & Psaltis 2003)), one obtains a relation for the stellar mass-to-radius ratio:

$$M/M_{\odot} = \Big(1 - \frac{1}{(z+1)^2}\Big) R/R_{g\odot}\,, \tag{13}$$

($R_{g\odot} = 2GM_{\odot}/c^2 = 2.953$ km) which is reported in Fig. 3 as a dashed line labeled $z = 0.35$. Comparing with the theoretical MR relations for different EOS (see e.g. Fig. 3, and also Xu 2003) it is clear that all three possible families of compact stars discussed in the present paper are completely consistent with a redshift $z = 0.35$.

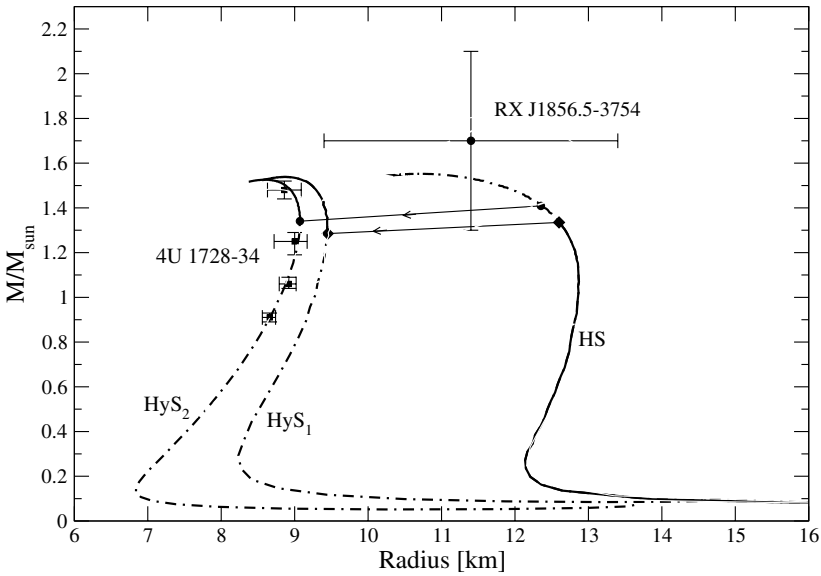

Figure 6. The radius and the mass for RX J1856.5-3754 (full circle with error bars labeled RX J1856.5-3754) obtained by Walter & Lattimer (2002) from fitting the multi-wave length spectral energy distribution. The radius and mass for 4U 1728-34, extracted by Shaposhnikov et al. (2003) for different best-fits of the X-ray burst data, is shown by the filled circles with error bars (error contour for 90% confidence level). The curves labeled HS represents the MR relation for pure hadronic star with the GM3 equation of state. The curves labeled $\mathrm{HyS_1}$ and $\mathrm{HyS_2}$ are the MR curves for hybrid stars with the GM3+Bag model EOS, for $B = 85.29\mathrm{MeV/fm}^3$ and $m_s = 150$ MeV ($\mathrm{HyS_1}$), and $B = 100\mathrm{MeV/fm}^3$ and $m_s = 0$ MeV ($\mathrm{HyS_2}$). The full circles and diamonds on the MR curves represent the critical mass configuration (symbols on the HS curve) and the corresponding hybrid star configurations after the stellar conversion process (symbols on the $\mathrm{HyS_1}$ and $\mathrm{HyS_2}$ curves).

The second source for which it has been claimed the detection of redshifted spectral lines is 1E 1207.4-5209, a radio-quite compact star located in the center of the supernova remnant PSK 1209-51/52. 1E 1207.4-5209 has been observed by the Chandra X-ray observatory. Two absorption features have been detected in the source spectrum and have been interpreted (Sanwal et al. 2002) as spectral lines associated with atomic transitions of once-ionized helium in the atmosphere of a strong magnetized ($B \sim 1.5 \times 10^{14}$ G) compact star. This interpretation gives for the gravitational redshift at the star surface $z = 0.12$ – 0.23 (Sanwal et al. 2002), which is reported in Fig. 3 and by the two dashed lines labeled $z = 0.12$ and $z = 0.23$.

A different interpretation of similar data, collected by the XMM-Newton satellite, has been recently given by Bignami et al. (2003), who interpreted the absorption features in the spectrum of 1E 1207.4-5209 as electron cyclotron lines in the stellar magnetic field. Within this interpretation and assuming the gravitational redshift of a "canonical neutron star" with $M = 1.4 M_{\odot}$ and $R =$ 10 km Bignami et al. (2003) derived a magnetic field strength $B = 8 \times 10^{10}$ G for the compact star in 1E 1207.4-5209 .

The two values of the stellar magnetic field inferred in the above quoted papers (Sanwal et al. 2002; Bignami et al. 2003) are in disagreement to each other and in disagreement with the B field deduced from the 1E 1207.4-5209 timing parameters (P and $\dot{P}$), which give $B = (2 - 3) \times 10^{12}$ G within the rotating magnetic dipole model. However, the latter value of the magnetic field strength presents serious problems since the current values of the timing parameters implies a characteristic pulsar age $\tau_c = P/(2\dot{P}) \sim 4.8 \times 10^5$ yr (Bignami et al. 2003) which is not compatible with the age $\tau_{SNR} = (3$–$20) \times 10^3$ yr (Roger et al. 1988). Clearly this source needs a more accurate study before any final and unambiguous interpretations of the observed spectral features can be drawn. Here, we will assume that the interpretation of the spectral feature given by Sanwal et al. (2002) and by Cottam et al. (2002) is correct. In that case, how it is possible to reconcile the gravitational redshift z =012–0.23 for 1E 1207.4-5209 with that ($z = 0.35$) deduced for EXO 0748-676? Within the commonly accepted view, in which there exist in nature only one family of compact stars (the "neutron stars"), different values of the gravitational redshift could be a consequence of a different mass of the two stars. In our scenario, we can give a different interpretation: 1E 1207.4-5209 is a pure hadronic star whereas EXO 0748-676 is an hybrid star or a strange star. This is illustrated in Fig. 3 by comparing our calculated MR relations with the redshifts deduced for the two compact X-ray sources.

5. Quark Deconfinement Nova and GRBs

The delayed stellar conversion process, described so far, represents the second "explosion" – the *Quark Deconfinement Nova (QDN)* (Bombaci et al. 2003) – in the two-step scenario proposed by Berezhiani et al. (2003) to explain the delayed SN-GRB connection.

As we can see from the results reported in Tab. 1, the total energy (E_{conv}) liberated during the stellar conversion process is in the range 0.5–1.7$\times 10^{53}$ erg. This huge amount of energy will be mainly carried out by the neutrinos produced during the stellar conversion process. It has been shown by Salmonson & Wilson (1999) that near the surface of a compact stellar object, due to general relativity effects, the efficiency of the neutrino-antineutrino annihilation into e^+e^- pairs is strongly enhanced with respect to the Newtonian case, and it could be as high as 10%. The total energy deposited into the electron-photon plasma can therefore be of the order of 10^{51}–10^{52} erg.

The strong magnetic field of the compact star will affect the motion of the electrons and positrons, and in turn could generate an anisotropic γ-ray emission along the stellar magnetic axis. This picture is strongly supported by the analysis of the early optical afterglow for GRB990123 and GRB021211 (Zhang et al. 2003), and by the recent discovery of an ultra-relativistic outflow from a "neutron star" in a binary stellar system (Fender et al. 2004). Moreover, it has been recently shown (Lugones et al. 2002) that the stellar magnetic field could influence the velocity of the "burning front" of hadronic matter into quark matter. This results in a strong geometrical asymmetry of the forming quark matter core along the direction of the stellar magnetic axis, thus providing a suitable mechanism to produce a collimated GRB (Lugones et al. 2002). Other anisotropies in the GRB could be generated by the rotation of the star.

6. Summary

In this report, we have investigated the consequences of the hadron-quark deconfinement phase transition in stellar compact objects when finite size effects between the deconfined quark phase and the hadronic phase are taken into account. We have found that above a threshold value of the gravitational mass a pure hadronic star is metastable to the decay (conversion) to a hybrid neutron star or to a strange star. We have calculated the *mean-life time* of these metastable stellar configurations, the critical mass for the hadronic star sequence, and have explored how these quantities depend on the details of the EOS for dense matter. We have introduced an extension of the concept of limiting mass of compact stars, with respect to the classical one given by Oppenheimer & Volkov (1939). We have demonstrated that, within the astrophysical scenario proposed in the present work, the existence of compact stars with "small" radii (quark stars) does not exclude the existence of compact stars with "large" radii (pure hadronic stars), and *vice versa*. We have shown that the present scenario implies, as a natural consequence a two step-process which is able to explain the inferred "delayed" connection between supernova explosions and GRBs, giving also the correct energy to power GRBs.

There are various specific features and predictions of the present model, which we briefly mention in the following. The second explosion (QDN) take place in a "baryon-clean" environment due to the previous SN explosion. Is is possible to have different time delays between the two events since the *mean-life time* of the metastable hadronic star depends on the value of the stellar central pressure. Thus the model of Berezhiani et al. (2003) is able to interpret a time delay of a few years (as observed in GRB990705 (Amati et al. 2000; Lazzati et al. 2001)), of a few months (as in the case of GRB020813 (Butler et al. 2003)), of a few days (as deduced for GRB011211 (Reeves et al. 2002)), or the nearly simultaneity of the two events (as in the case of SN2003dh and GRB030329 (Hjorth et al. 2003).

References

[1] Alcock, C., Farhi, E., & Olinto, A. 1986, ApJ 310, 261.

[2] Amati, L. et al., 2000, Science, 290, 953.

[3] Antonelli, L.A., et al., 2000, ApJ, 545, L39.

[4] Berezhiani, Z., Bombaci, I., Drago, A., Frontera, F., & Lavagno, A., 2003, ApJ, 586, 1250.

[5] Bignami, G.F., Carvero, P.A., De Luca, A., & Mereghetti, S., 2003, Nature, 423, 725.

[6] Bloom, J.S. et al., 1999, Nature, 401, 453.

[7] Bodmer, A.R., 1971, Phys. Rev. D, 4, 1601.

[8] Bombaci, I., 1997, Phys. Rev. C, 55, 1587.

[9] Bombaci, I., 2003, astro-ph/0307522.

[10] Bombaci, I., Parenti, I., & Vidaña, I. (2003) Astrophys.J.614:314-325.

[11] Bombaci, I., & Datta, B., 2000, ApJ, 530, L69.

[12] Butler N.R., et al., 2003, ApJ 597, 1010.

[13] Cheng, K.S., Dai, Z.G., Wai, D.M., & Lu, T., 1998, Science, 280, 407.

[14] Cottam, J., Paerels, F., & Mendez, M. 2002, Nature, 420, 51.

[15] Dey, M., Bombaci, I., Dey, J., Ray, S., & Samanta, B.C. 1998, Phys. Lett. B, 438, 123; erratum 1999, Phys. Lett. B, 467, 303.

[16] Datta, B., Thampan, A.V., & Bombaci, I. 1998, A& A, 334 (1998) 943.

[17] Dermer, C.D. 2001, Proceedings of the 27th International Cosmic Ray Conference, Hamburg, Germany (7-15 August 2001). astro-ph/0202254.

[18] Drake, J.J., et al., 2002, ApJ, 572, 996.

[19] Farhi, E., & Jaffe, R.L., 1984, Phys. Rev. D, 30, 2379.

[20] Fender, R., et al. 2004, Nature, 427, 222.

[21] Frayl, D.A. et al., 2001, ApJ 562, L55 .

[22] Glendenning, N.K 1992, Phys. Rev. D, 46, 1274.

[23] Glendenning, N.K., 1996, Compact Stars: Nuclear Physics, Particle Physics, and General Relativity, Springer Verlag.

[24] Glendenning, N.K., & Moszkowski, S.A. 1991, Phys. Rev. Lett., 67, 2414.

[25] Haensel, P., Zdunik, J.L. & Schaefer, R. 1986, A&A, 160, 121.

[26] Haensel, P. 2003, Equation of state of dense matter and maximum mass of neutron stars, in Final Stages of Stellar Evolution, Ed. C. Motch and J.-M. Hameury, EAS Publications Series 7, 249.

[27] Heiselberg, H., Pethick, C.J., & Staubo, E.F. 1993, Phys. Rev. Lett., 70, 1355.

[28] Hjorth, J. et al, 2003, Nature, 423, 847.

[29] Iida, K., & Sato, K. 1997, Prog. Theor. Phys., 1, 277: 1998, Phys. Rev. C, 58, 2538.

[30] Kaplan, D.L., van Kerkwijk, M.H, & Anderson, J. 2002, ApJ, 571, 447.

[31] Lazzati, D., Ghisellini, G., Amati, L., Frontera, F., Vietri, M., & Stella, L. 2001, ApJ, 556, 471.

[32] Li, X.–D., Bombaci, I., Dey, M., Dey J., & van den Heuvel, E.P.J. 1999a, Phys. Rev. Lett., 83, 3776.

[33] Li, X.–D., Ray, S., Dey, J., Dey, M., & Bombaci, I. 1999b, ApJ, 527, L51.

[34] Lifshitz, I. M., & Kagan, Y. 1972, Sov. Phys. JETP, 35, 206.

[35] Lipkin, Y.M. 2003, Astrophys.J.606:381-394.

[36] Lugones, G., Ghezzi, C.R., de Gouveia Dal Pino E.M., & Horvath, J.E., 2002, ApJ, 581, L101.

[37] Madsen, J. 1993, Phys. Rev. Lett., 70, 391.

[38] Madsen, J. 1999, Lectures Notes in Physics Vol. 500, Springer Verlag, 162.

[39] Oppenheimer, J.R., & Volkoff, G.M. 1939, Phys. Rev., 55, 374.

[40] Orosz, J.A., & Kuulkers, E. 1999, MNRAS, 305, 132.

[41] Özel, F. & Psaltis, D. 2003, ApJ, 582, L31.

[42] Piran, T. 1999, Phys. Rep. 314 575; 2000, Phys. Rep. 333, 529.

[43] Piro, L. et al. 2000, Science, 290, 955.

[44] Poutanen, J. & Gierliǹski, M. 2003, MNRAS, 343, 1301.

[45] Quaintrell, H., et al., 2003, A&A, 401, 313.

[46] Reeves, J.N. et al., 2002, Nature, 414, 512.

[47] Roger, R.S., Milne, D.K., Kesteven, M.J., Wellington, K.J., & Haynes, R.F. 1988, ApJ, 332, 940.

[48] Salmonson, J.D., & Wilson, J.R. 1999, ApJ, 517, 859.

[49] Sanwal, D., Pavlov, G.G., Zavlin, V.E., & Teter, M.A. 2002, ApJ, 574, L61.

[50] Shapiro, S.L. & Teukolsky, S.A. 1983, Black holes, white dwarfs and neutron stars, Ed. J. Wiley& Sons.

[51] Shaposhnikov, N. , & Titarchuk, L. 2002, ApJ, 570, L25.

[52] Shaposhnikov, N. , Titarchuk, L., & Haberl, F. 2003, ApJ, 593, L38 (STH).

[53] Spergel, D.N. 2003, ApJ Suppl., 148, 175.

[1979] Terazawa, H. 1979, INS-Report, 336 (INS, Univ. of Tokyo); 1989, J. Phys. Soc. Japan, 58, 3555; 1989, J. Phys. Soc. Japan, 58, 4388.

[54] Thorsett, S.E., & Chakrabarty D. 1999, ApJ, 512, 288.

[1994] Titarchuk, L. 1994, ApJ, 429, 330.

[55] van Kerkwijk, M.H. *et al.* 1995, A&A 303, 483.

[56] Vietri, M., & Stella, L. 1998, ApJ, 507, L45.

[57] Voskresensky, D.N., Yasuhira, M, & Tatsumi, T. 2003, Nucl. Phys. A, 723, 291.

[58] Walter, F.M., & Lattimer, J.M., 2002, ApJ, 576, L148.

[59] Witten, E., 1984, Phys. Rev. D, 30, 272.

[60] Xu, R.X,. 2002, ApJ, 570, L65.

[61] Xu, R.X. 2003, Chin. J. Astron. Astrophys., 3, 33.

[62] Zhang, B., Kobayashi, S., & Meszaros, P., 2003, ApJ, 595, 950.

[63] Zhang, B. & Meszaros, P., 2003, Int.J.Mod.Phys.A19:2385-2472.

COLOR SUPERCONDUCTING QUARK MATTER AND COMPACT STAR OBSERVABLES

D. N. Aguilera [1,2], J. Berdermann [1], D. B. Blaschke [1,3], H. A. Grigorian [1,4], A. Khalatyan [5], G. Poghosyan [6] and D. N. Voskresensky [7,8]

[1] *Fachbereich Physik, Universität Rostock, 18051 Rostock, Germany*

[2] *Institute of Physics Rosario, 2000 Rosario, Argentina*

[3] *Bogoliubov Laboratory of Theoretical Physics, JINR Dubna, 141980 Dubna, Russia*

[4] *Department of Physics, Yerevan State University, 375025 Yerevan, Armenia*

[5] *Astrophysikalisches Institut Potsdam, D-14482 Potsdam, Germany*

[6] *Departement für Physik und Astronomie der Universität Basel, CH-4056 Basel, Switzerland*

[7] *Moscow Physical Engineering Institute, 31, Kashirskoe shosse, 115409 Moscow, Russia*

[8] *Gesellschaft für Schwerionenforschung mbH, D-64291 Darmstadt, Germany*

Abstract We investigate a nonlocal chiral quark model with separable 4-fermion interaction for the case of $U(3)$ flavor symmetry and show that strange quark matter is unlikely to occur in a large enough volume of a compact star to entail remarkable observational consequences. The phase diagram in the two-flavor sector of such model has a critical end point of the line of first order chiral/deconfinement phase transitions on which a triple point marks the junction with the critical line for second order phase transitions to two-flavor color superconductivity (2SC) below $T \sim 80$ MeV. Stable hybrid star configurations with large quark matter core in a color superconducting phase can exist. We suggest that for accreting compact stars in Low-mass X-ray binary (LMXB) systems a *population gap* in the phase diagram (Ω-M plane) for rotating compact star configurations would be an observable indicator of such a quark matter core. A consistent cooling phenomenology for such hybrid stars requires that no direct Urca type fast cooling process in the hadronic shell occurs and that all quark species be gapped, with the minimum pairing gap being a decreasing function of the chemical potential in the range of 1 MeV to 10 keV. We discuss possible implications of a QCD phase transition for the early evolution of hot proto-neutron stars regarding delayed energy release by neutrinos and a possible gamma-ray burst (GRB) mechanism.

Keywords: dense matter equation of state, quark matter superconductivity, rotating neutron stars, cooling evolution, neutrino trapping, gamma ray bursts

D. Blaschke and D. Sedrakian (eds.), Superdense QCD Matter and Compact Stars, 377–377.

1. Introduction

The investigation of the QCD phase diagram has become a research topic of highest priority. Relativistic heavy ion collisions in the RHIC era have provided results which confirm previous information about the critical temperature $T_c \sim 170$ MeV of the hadronization transition in the approximately baryon-free regime [1], which parallels the situation a few microseconds after the big bang. This value is in agreement with the deconfinement transition temperature calculated in 2+1 flavor Lattice QCD [2]. These simulations are now extended into the region of (small) finite chemical potentials where one of the characteristic features is a critical endpoint of first order phase transitions (tricritical point). Future heavy-ion collision experiments planned at GSI Darmstadt (FAIR) will explore the phase diagram in the finite density domain and hope to find experimental signatures of the tricritical point. In dense quark matter at temperatures below ~ 50 MeV, due to attractive interaction channels, the Cooper pairing instability is expected to occur which should lead to a variety of possible quark pair condensates corresponding to color superconductivity (CSC) phases, see [3] for a review. Since it is difficult to provide low enough temperatures for CSC phases in heavy-ion collisions, only precursor phenomena [4, 5] are expected under these conditions. CSC phases may occur in neutron star interiors [6] and could manifest themselves, e.g., in the cooling behavior [7–10].

However, the domain of the QCD phase diagram where neutron star conditions are met is not yet accessible to Lattice QCD studies and theoretical approaches have to rely on nonperturbative QCD modeling. The class of models closest to QCD are Dyson-Schwinger equation (DSE) approaches which have been extended recently to finite temperatures and densities [11–13]. Within simple, infrared-dominant DSE models early studies of quark stars [14] and diquark condensation [15] have been performed.

The present contribution will be based on results which have been obtained within a nonlocal chiral quark model (NCQM) using a covariant, separable representation of the gluon propagator [16] with formfactors suitable for an extension to finite temperatures and chemical potentials [17–19]. Alternative approaches to separable chiral quark models are based on the instanton approach [20–22]. As a limiting case, the well-known Nambu–Jona-Lasinio (NJL) model is obtained for a cutoff formfactor. For recent applications of the NJL model to QCD at high density in compact stars, see [23] and references therein. A different class of QCD-models is of the bag-model type. These models do not describe the chiral phase transition in a self-consistent way and will not be considered here. We will consider within a NCQM the following questions: (i) Is strange quark matter relevant for structure and evolution of

compact stars? (ii) Are stable hybrid stars with quark matter interior possible? (iii) What can we learn about possible CSC phases from neutron star cooling?

2. Nonlocal chiral quark model (NCQM)

In order to answer the question whether strange quark matter phases should be expected in the neutron star interiors, we consider here a three-flavor generalization of a NCQM with the action

$$\begin{aligned} \mathcal{S}[q,\bar{q}] &= \int_k \big\{\bar{q}(k)(\not{k}-\hat{m})q(k) \\ &\quad +G_1\int_{k'}\sum_{\alpha=0}^{8}[j_s^\alpha(k)j_s^\alpha(k')+j_p^\alpha(k)j_p^\alpha(k')]\big\}, \end{aligned} \tag{1}$$

where $\int_k = \int \frac{d^4k}{(2\pi)^4}$ and G_1 the coupling constant in the scalar/pseudoscalar channel. We restrict us here to the scalar current $j_s^\alpha(k) = \bar{q}(k)\lambda_\alpha f(k)q(k)$ and the pseudoscalar current $j_p^\alpha(k) = \bar{q}(k)i\gamma_5\lambda_\alpha f(k)q(k)$ in Dirac space with $q(k)$ and $\bar{q}(k)$ being quark 4-spinors and the formfactor $f(k)$ accounts for the nonlocality of the interaction. For the applications to compact stars, the quark matter equation of state is needed and can be obtained from the partition function in Feynman's path integral representation

$$\mathcal{Z}[T,\hat{\mu}] = \int \mathcal{D}\bar{q}\mathcal{D}q \exp\left(\mathcal{S}[q,\bar{q}] - \int_k \hat{\mu}\gamma^0\bar{q}q\right), \tag{2}$$

where the constraint of baryon number conservation is realized by the diagonal matrix of chemical potentials $\hat{\mu}$ (Lagrange multipliers). Further details concerning the notation and the parametrization of this model can be found in Ref. [24].

In order to perform the functional integrations over the quark fields $\bar{q}$ and q we use the formalism of bosonisation which is based on the Hubbard-Stratonovich transformation of the four-fermion interaction. The resulting transformed partition function in terms of bosonic variables will be considered in the mean-field approximation

$$\mathcal{Z}[T,\hat{\mu}] = \mathrm{e}^{-2N_c\sum_f\left[\frac{\phi_f^2}{8D_0}+\int_k \ln(M_f^2-\tilde{k}_f^2)\right]}, \tag{3}$$

with the 4-vector $\tilde{k}_f = (k_0-\mu_f,\vec{k})$ and the effective quark masses $M_f = M_f(\tilde{k}) = m_f + \phi_f f(\tilde{k})$ containing the flavor dependent mass gaps ϕ_f. In the mean field approximation, the grand canonical thermodynamical potential is

$$\Omega(T,\{\mu\}) = \frac{T}{V}\ln\left\{\mathcal{Z}[T,\{\mu_f\}]/\mathcal{Z}[0,\{0\}]\right\}\ , \tag{4}$$

where fluctuations are neglected and the divergent vacuum contribution has been subtracted. The quark mass gaps ϕ_f are determined by solving the gap equations which correspond to the minimization conditions $\partial\Omega/\partial\phi_f = 0$ and read

$$\phi_f = 8G_1 N_c \int \frac{d^4k}{(2\pi)^4} \frac{2M_f f(\tilde{k})}{M_f^2 - \tilde{k}_f^2} \,. \tag{5}$$

As can be seen from (5), for the chiral $U(3)$ quark model the three gap equations for $\phi_u,\ \phi_d,\ \phi_s$ are decoupled and can be solved separately.

In the remainder of this section we consider the case $T = 0$ only. All thermodynamical quantities can now be derived from Eq. (4), for details see [24]. For instance, pressure, density and the chiral condensate are given by

$$p = -\Omega \ , \ n_f = -\frac{\partial\Omega}{\partial\mu_f} \ , \ <\bar{q}q>= -\frac{\partial\Omega}{\partial m_q} \ , \tag{6}$$

the energy density follows from $\varepsilon = -p + \sum_f \mu_f n_f$. For most of the numerical investigations within the NCQM described above we will employ a simple Gaussian formfactor $f(k) = \exp(k^2/\Lambda^2)$, which has been used previously for studies of meson and baryon properties in the vacuum [21] as well as quark deconfinement and mesons at finite temperature [17, 19]. A systematic extension to other choices of formfactors can be found in [22]. The Gaussian model has four free parameters to be defined: the coupling constant G_1, the interaction range Λ, and the current quark masses $m_u = m_d$, m_s. These are fixed by the pion mass $m_\pi = 140$ MeV, kaon mass $m_K = 494$ MeV, pion decay constant $f_\pi = 93$ MeV and the chiral condensate $-<\bar{q}q>= (240\ \mathrm{MeV})^4$. Fig. 1 shows the behavior of the thermodynamic potential as a function of the light quark mass gap $\phi_q = \phi_u = \phi_d$ for different values of the chemical potential μ. For $\mu < \mu_c = 330$ MeV the argument and the value of the global minimum is independent of μ which corresponds to a vanishing quark density (confinement). At $\mu = \mu_c$ a phase transition from the massive, confining phase to a deconfining phase with negligibly small mass gap occurs. In Fig. 2 we show that the quark pressure vanishes for $\mu < \mu_c$ (confinement) and can be well described by a two-flavor bag model with a bag constant $B = 81.3$ MeV/fm^3 in the region of chemical potentials 330 MeV $\leq \mu \leq$ 492 MeV where the third flavor is still confined. A three-flavor bag model adjusted to describe the same critical chemical potential for quark matter deconfinement as the NCQM does not give an acceptable description of the EoS, even above the onset of strangeness.

In Ref. [24] it has been investigated whether with the above three- flavor quark matter EoS of the NCQM strange quark matter can appear in the interior of compact stars. The constraints of β equilibrium and charge neutrality have been applied (see below) in order to constrain the partial densities of electrons and up-, down-, strange quarks, see Fig. 3. It can be seen that strange

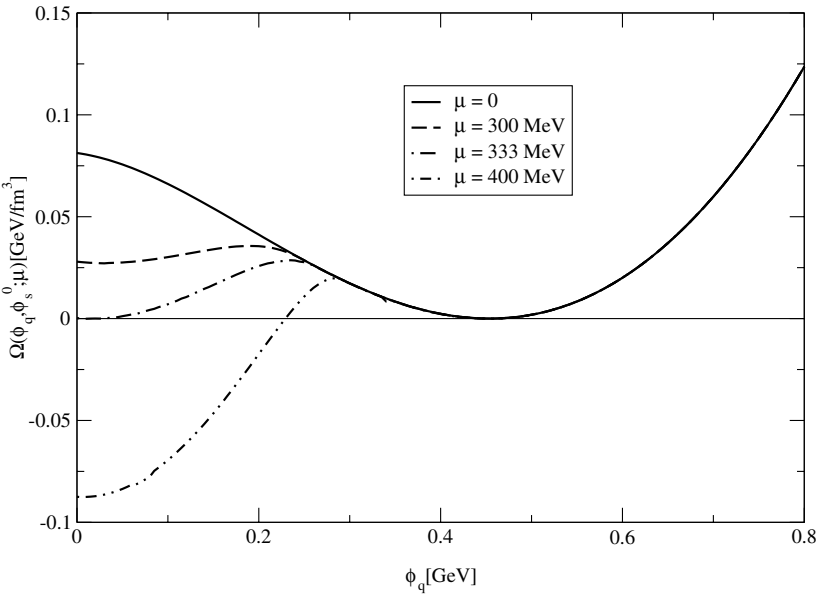

Figure 1. Dependence of the thermodynamic potential on the light flavor gap $\phi_q = \phi_u = \phi_d$ (order parameter) for different values of the chemical potential, $\phi_s = 682$ MeV.

quarks appear only above energy densities of about 1 GeV/fm^3 and the question arises whether they can play a significant role in the structure and composition of compact star interiors. To answer this question, solutions of the Tolman-Oppenheimer-Volkoff (TOV) equation has been performed and the resulting NCQM quark star solutions are shown in Fig. 4. A comparison of the $N_f = 3$ with $N_f = 2$ mass-radius relations for NCQM quark stars shows that the third flavor appears only for configurations very close to the maximum mass above which the solutions become unstable against gravitational collaps to black holes. Even at the maximum mass the volume of strange quark matter in the quark star is to small to produce significant observable effects. Therefore we conclude that for the discussion of quark matter in compact stars it is sufficient to discuss below the two-flavor case only.

3. EoS for nonstrange compact stars

Two-flavor color superconductivity. The quark-quark interaction in the color anti-triplet scalar diquark channel is attractive driving the pairing with a large zero-temperature pairing gap $\Delta \sim 100$ MeV for the quark chemical potential $\mu_q \sim 300 - 500$ MeV. Therefore, we consider now a NCQM

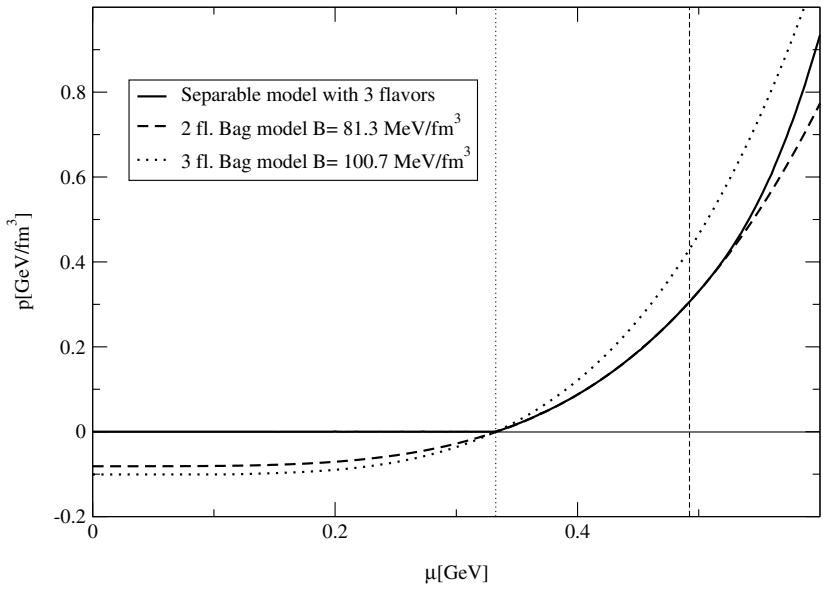

Figure 2. Pressure of the NCQM as a function of the chemical potential for the separable model (solid line) compared to a three-flavor (dotted line) and a two-flavor (dashed line) bag model. All models have the same critical chemical potential $\mu_c = 330$ MeV for (light) quark deconfinement.

described by the effective action

$$S_{2SC}[\bar{q},q] \;=\; S[\bar{q},q] + G_2 \int_{k,k'} j_d^\dagger(k) j_d(k'), \tag{7}$$

where $j_d(k) = q^T(k) C i\gamma_5 \tau_2 \lambda_2 f(k) q(k)$ is the scalar diquark current with the charge conjugation matrix $C = i\gamma_0\gamma_2$. After bosonization, the mean field approximation introduces a new order parameter: the diquark gap Δ, which can be seen as the gain in energy due to diquark condensation. The mass gaps ϕ_u, ϕ_d indicate dynamical chiral symmetry breaking. The grand canonical thermodynamic potential per volume can be obtained as

$$\begin{aligned}\Omega_q(\phi_u,\phi_d,\Delta;\mu_u,\mu_d,T) \;=\; & \frac{\phi_u^2+\phi_d^2}{8\,G_1} + \frac{|\Delta|^2}{4\,G_2} \\ & -\frac{T}{2}\sum_n \int \frac{d^3k}{(2\pi)^3} \mathrm{Tr}\ln\left[\frac{1}{T}G^{-1}(i\omega_n,\vec{k})\right],\end{aligned} \tag{8}$$

where $\omega_n = (2n+1)\pi T$ are the Matsubara frequencies for fermions and the inverse Nambu-Gorkov quark propagator is

$$G^{-1} = \begin{pmatrix} \not{k} - \hat{M} - \hat{\mu}\gamma_0 & \Delta\gamma_5\tau_2\lambda_2 f(k) \\ -\Delta^*\gamma_5\tau_2\lambda_2 f(k) & \not{k} - \hat{M} + \hat{\mu}\gamma_0 \end{pmatrix}. \tag{9}$$

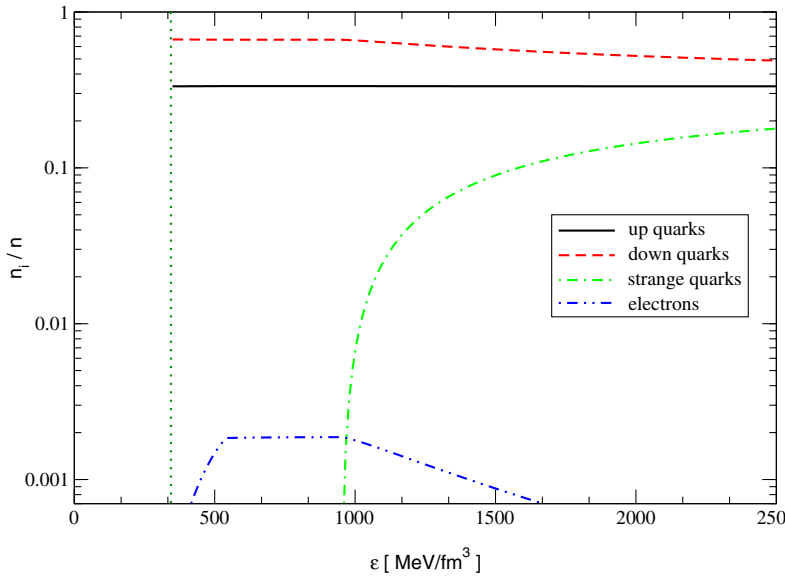

Figure 3. Composition of three-flavor quark matter in β equilibrium with electrons.

The resulting phase diagram is shown in Fig. 5. It includes a 2-flavor color superconductivity (2SC) phase for which quarks of one color, say blue, remain unpaired. The color-flavor locking (CFL) phase [25] requires approximate SU(3) flavor symmetry and can be excluded from our discussion since strange quarks remain confined up to the highest densities occuring in a compact star configuration [24].

Thermodynamic potential in the instantaneous approximation.

In the instantaneous approximation, see [26], the formfactor of the nonlocal interaction depends on the three-momentum only and the Matsubara summation in Eq. (7) can be performed analytically using standard methods.

The resulting grand canonical thermodynamic potential for 2SC quark matter within the instantaneous nonlocal chiral quark model (INCQM) [27, 28] in the mean field approximation is given by

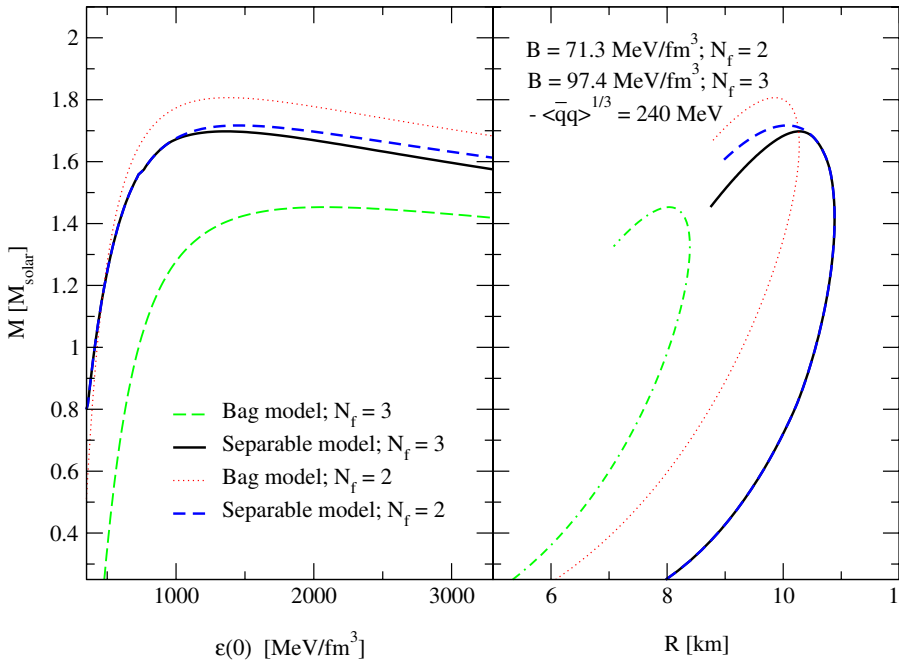

Figure 4. Stability for compact stars composed of three-flavor quark matter in the NCQM.

$$\Omega_q(\{\phi_f\},\Delta;\{\mu_{fc}\},T) = \sum_{c,f} \Omega^{c,f}(\phi_f,\Delta;\mu_{fc},T)\;, \tag{10}$$

where T is the temperature and μ_{fc} the chemical potential for the quark with flavor ($f \in \{u,d\}$) and color ($c \in \{r,b,g\}$).

The contribution of quarks with given color c and flavor f to the thermodynamic potential is

$$\Omega^{c,f}(\phi_f,\Delta;\mu_{fc},T) + \Omega^c_{vac} = \frac{\phi_f^2}{24\,G_1} + \frac{\Delta^2}{24\,G_2}$$
$$-\frac{1}{\pi^2}\int_0^\infty dq q^2 \{\omega\left[\epsilon_c(E_f(q)+\mu_{fc}),T\right] + \omega\left[\epsilon_c(E_f(q)-\mu_{fc}),T\right]\} \tag{11}$$

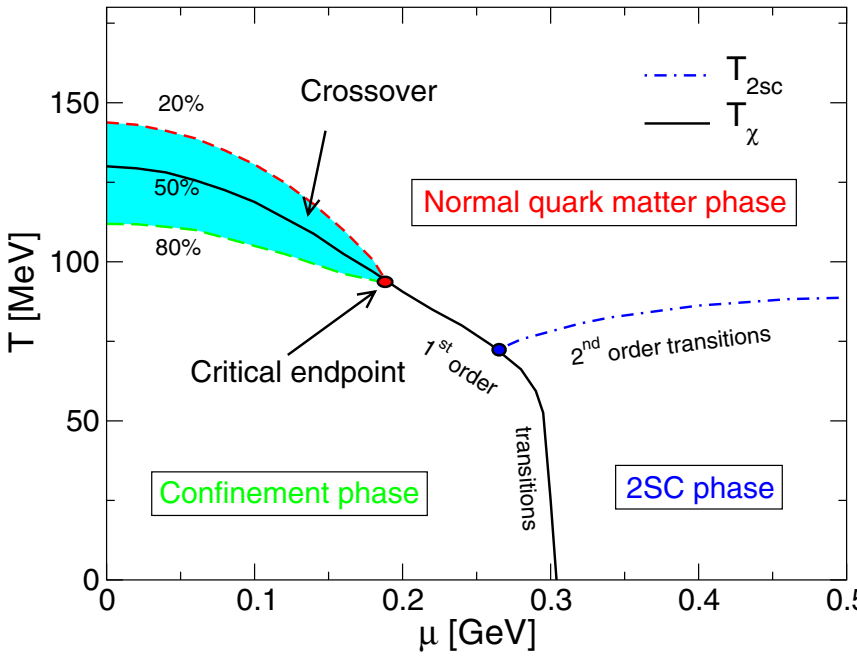

Figure 5. Phase diagram for $N_f = 2$ quark matter in the NCQM. The critical temperature for color superconductivity (2SC phase) can be high enough for this phase to reach close to the tricritical point which shall be explored in future heavy-ion collision experiments.

where the dispersion relation for unpaired quarks with dynamical mass function $m_f(q) = m_f + g(q)\phi_f$ is given by

$$E_f(q) = \sqrt{q^2 + m_f^2(q)}\,, \tag{12}$$

and we use the notation

$$\omega\left[\epsilon_c, T\right] = T \ln\left[1 + \exp\left(-\frac{\epsilon_c}{T}\right)\right] + \frac{\epsilon_c}{2}\,, \tag{13}$$

with the first argument given by

$$\epsilon_c(\xi) = \xi\sqrt{1 + \Delta_c^2/\xi^2}\,. \tag{14}$$

When we choose the green and blue colors to be paired and the red ones to remain unpaired, we have

$$\Delta_c = g(q)\Delta(\delta_{c,b} + \delta_{c,g}). \tag{15}$$

For a homogeneous system in equilibrium, the minimum of the thermodynamic potential Ω_q with respect to the order parameters $\{\phi_f\}$ and Δ corresponds to a negative pressure; therefore the constant $\Omega_{vac} = \sum_c \Omega^c_{vac}$ is chosen such that the pressure of the physical vacuum vanishes.

The nonlocality of the interaction between the quarks in both channels $q\bar{q}$ and qq is implemented via the same formfactor functions $g(q)$ in the momentum space. In our calculations we use the Gaussian (G), Lorentzian (L) and cutoff (NJL) type of formfactors defined as

$$g_{\rm G}(q) = \exp(-q^2/\Lambda_{\rm G}^2)\,, \tag{16}$$
$$g_{\rm L}(q) = [1+(q/\Lambda_{\rm L})^2]^{-1}, \tag{17}$$
$$g_{\rm NJL}(q) = \theta(1-q/\Lambda_{\rm NJL})\,. \tag{18}$$

Following Ref. [29] we introduce the quark chemical potential for the color c, μ_{qc} and the chemical potential of the isospin asymmetry, μ_I, defined as

$$\mu_{qc} = (\mu_{uc}+\mu_{dc})/2 \tag{19}$$
$$\mu_I = (\mu_{uc}-\mu_{dc})/2, \tag{20}$$

where the latter is color independent.

The diquark condensation in the 2SC phase induces a color asymmetry which is proportional to the chemical potential μ_8. Therefore we can write

$$\mu_{qc} = \mu_q + \frac{\mu_8}{3}(\delta_{c,b}+\delta_{c,g}-2\delta_{c,r})\,, \tag{21}$$

where μ_q and μ_8 are conjugate to the quark number density and the color charge density, respectively. As has been shown in [30] for the 2SC phase the relation $\phi_u = \phi_d = \phi$ holds so that the quark thermodynamic potential is [31]

$$\Omega_q(\phi,\Delta;\mu_q,\mu_I,\mu_8,T)+\Omega_{vac}=\frac{\phi^2}{4G_1}+\frac{\Delta^2}{4G_2}$$
$$-\frac{1}{\pi^2}\int_0^\infty dqq^2\{\omega\left[\epsilon_r(E(q)-\mu_q+\frac{2}{3}\mu_8-\mu_I),T\right]$$
$$+\omega\left[\epsilon_r(E(q)+\mu_q-\frac{2}{3}\mu_8-\mu_I),T\right]+\omega\left[\epsilon_r(E(q)-\mu_q+\frac{2}{3}\mu_8+\mu_I),T\right]$$
$$+\omega\left[\epsilon_r(E(q)+\mu_q-\frac{2}{3}\mu_8+\mu_I),T\right]\}$$
$$-\frac{2}{\pi^2}\int_0^\infty dqq^2\{\omega\left[\epsilon_b(E(q)-\mu_q-\frac{1}{3}\mu_8)-\mu_I,T\right]$$
$$+\omega\left[\epsilon_b(E(q)+\mu_q+\frac{1}{3}\mu_8)-\mu_I,T\right]+\omega\left[\epsilon_b(E(q)-\mu_q-\frac{1}{3}\mu_8)+\mu_I,T\right]$$
$$+\omega\left[\epsilon_b(E(q)+\mu_q+\frac{1}{3}\mu_8)+\mu_I,T\right]\}\,, \tag{22}$$

where the factor 2 in the last integral comes from the degeneracy of the blue and green colors ($\epsilon_b = \epsilon_g$). The total thermodynamic potential Ω contains besides the quark contribution Ω_q also that of the leptons Ω^{id}

$$\begin{aligned}\Omega(\phi,\Delta;\mu_q,\mu_I,\mu_8,\mu_l,T) &= \Omega_q(\phi,\Delta;\mu_q,\mu_I,\mu_8,T)\\ &+ \sum_{l=e,e^+,\bar\nu_e,\nu_e}\Omega^{id}(\mu_l,T)\,.\end{aligned} \tag{23}$$

where latter is assumed to be that of an ideal mixture of massless, noninteracting Fermi gas degrees of freedom with

$$\Omega^{id}(\mu,T)=-\frac{1}{12\pi^2}\mu^4-\frac{1}{6}\mu^2T^2-\frac{7}{180}\pi^2T^4\,. \tag{24}$$

At the present stage, we include only contributions of the first family of leptons in the thermodynamic potential. The conditions for the local extremum of Ω_q correspond to coupled gap equations for the two order parameters ϕ and Δ

$$\left.\frac{\partial\Omega}{\partial\phi}\right|_{\phi=\phi_0,\Delta=\Delta_0}=\left.\frac{\partial\Omega}{\partial\Delta}\right|_{\phi=\phi_0,\Delta=\Delta_0}=0\,. \tag{25}$$

The global minimum of Ω_q represents the state of thermodynamic equilibrium from which all equations of state can be obtained by derivation.

Beta equilibrium, neutrino trapping, charge and color neutrality. The stellar matter in equilibrium has to obey the constraints of β-equilibrium ($d\longrightarrow u+e^-+\bar\nu_e$,$u+e^-\longrightarrow d+\nu_e$), expressed as

$$\mu_{dc} = \mu_{uc} + \mu_e + \mu_{\bar{\nu}_e} \,, \tag{26}$$

color and electric charge neutrality and baryon number conservation. We use in the following the electric charge density

$$Q = \frac{2}{3}\sum_c n_{uc} - \frac{1}{3}\sum_c n_{dc} - n_e \,, \tag{27}$$

the baryon number density

$$n_B = \frac{1}{3}\sum_{f,c} n_{fc} \,, \tag{28}$$

and the color charge density

$$n_8 = \frac{1}{3}\sum_f (n_{fb} + n_{fg} - 2n_{fr}) \tag{29}$$

as conserved densities. During the regime of neutrino trapping in hot compact star configurations ($T \gtrsim 1$ MeV) also the lepton number density

$$n_L = n_e + n_{\nu_e} - n_{e^+} - n_{\bar{\nu}_e} \tag{30}$$

is conserved. The number densities n_j occuring on the right hand sides of the above Eqs. (27) - (29) are defined as derivatives of the thermodynamic potential (22) with respect to corresponding chemical potentials μ_j

$$n_j = -\left.\frac{\partial\Omega}{\partial\mu_j}\right|_{\phi_0,\Delta_0;T,\{\mu_j,j\neq i\}} \,, \tag{31}$$

Here the index j stands for the particle species.

In order to express the Gibbs free enthalpy density G in terms of those chemical potentials which are conjugate to the conserved densities and to implement the $\beta-$equilibrium condition (26) we make the following algebraic transformations

$$G = \sum_{f,c}\mu_{fc}n_{fc} + \sum_l \mu_l n_l = \mu_B\, n_B + \mu_Q\, Q + \mu_8\, n_8 + \mu_L\, n_L \,, \tag{32}$$

where we have defined the chemical potential $\mu_B = 3\mu_q - \mu_I$ conjugate to the baryon number density n_B in the same way as $\mu_Q = -\mu_e$ is the chemical potential conjugate to Q, μ_8 to n_8, and μ_L to n_L. Then, the electric and color charge neutrality conditions read,

$$Q = 0 \,, \tag{33}$$

$$n_8 = 0 \,, \tag{34}$$

at given n_B. In the neutrino untrapping transition, neutrinos leave the star and their chemical potential drops to zero $\mu_L = -\mu_{\bar{\nu}_e} \to 0$. The solution of the gap equations (25) can be performed under these constraints.

The solution of the color neutrality condition shows that μ_8 is about $5 \div 7$ MeV in the region of relevant densities ($\mu_q \simeq 300 \div 500$ MeV). Since μ_I is independent of μ_8 we consider $\mu_{qc} \simeq \mu_q$ ($\mu_8 \simeq 0$) in our following calculations.

To demonstrate how to define a charge neutral state of quark star matter including neutrino trapping and color superconductivity we plot in Fig. 6 the charge neutrality condition and the β- equilibrium condition as a function of μ_I and μ_e for different fixed values of μ_B, when the system is in the global minimum of the thermodynamic potential and $G_2 = G_1$. As has been shown before in Ref. [32] for the NJL model case, the pure phases ($\Delta > 0$: superconducting, $\Delta = 0$: normal) in general are charged. These branches end at critical values of μ_I where their pressure is equal and the corresponding states are degenerate

$$P = P_{\Delta=0}(\mu_B, \mu_I, \mu_e, T) = P_{\Delta>0}(\mu_B, \mu_I, \mu_e, T) \; . \tag{35}$$

In order to fulfill the charge neutrality condition one can construct a homogeneous mixed phase of these states using the Gibbs conditions [33].

The volume fraction that is occupied by the subphase with diquark condensation is defined by the charges in the subphases

$$\chi = Q_{\Delta>0}/(Q_{\Delta>0} - Q_{\Delta=0}) \tag{36}$$

and is plotted in Fig. 7 for the different formfactor functions as a function of μ_B.

In the same way, the number densities for the different particle species j and the energy density are given by

$$n_j = \chi n_{j\Delta>0} + (1-\chi) n_{j\Delta=0} \tag{37}$$

$$\varepsilon = \chi \varepsilon_{\Delta>0} + (1-\chi)\varepsilon_{\Delta=0} \; . \tag{38}$$

The formulas (35)-(38) define a complete set of thermodynamic relations and can be evaluated numerically. We display the results for the pressure in a form remniscent of a bag model

$$P^{(s)} = P_{id}(\mu_B) - B^{(s)}(\mu_B) \; , \tag{39}$$

where $P_{id}(\mu_B)$ is the ideal gas pressure of quarks and $B^{(s)}(\mu_B)$ a *density dependent* bag pressure, see Fig. 8. The occurrence of diquark condensation depends on the value of G_2 and the superscript $s \in \{S, N\}$ indicates whether we consider the matter in the superconducting mixed phase ($G_2 = G_1$) or in the normal phase ($G_2 = 0$), respectively.

Note that the mean-field EoS of the two-flavor INCQM in the normal phase can be described by a bag model with a small, and almost constant bag function whereas in the superconducting phase the bag function decreases with the density, see Fig. 8. Such a behavior has been parametrized in heuristic quark matter models, see e.g. [34].

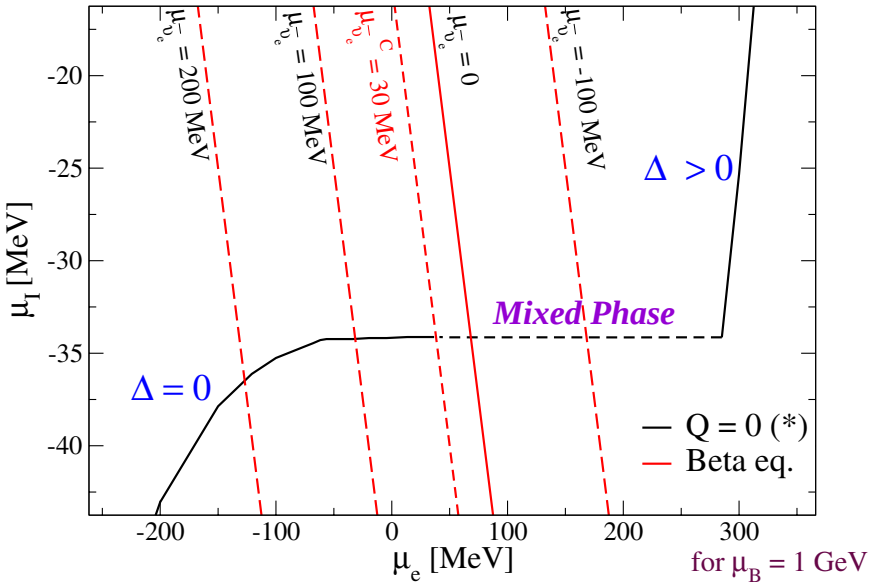

Figure 6. Solutions of the gap equations and the charge neutrality condition (solid black line) in the μ_I vs μ_e plane. Two branches are shown: states with diquark condensation on the upper right ($\Delta > 0$) and normal quark matter states ($\Delta = 0$) on the lower left. The plateau in between corresponds to a mixed phase. The lines for the β-equilibium condition are also shown (solid and dashed straight lines) for different values of the (anti-)neutrino chemical potential. Matter under stellar conditions should fulfill both conditions and therefore for $\mu_{\bar{\nu}_e} = 0$ a 2SC-normal quark matter mixed phase is preferable.

Hadronic EoS and phase transition. In describing the hadronic shell of a hybrid star we exploit a parametrized form [35] of the Argonne $V18+\delta v + UIX^*$ model of the EoS given in [36], which is based on the most recent models for the nucleon-nucleon interaction with the inclusion of a parameterized three-body force and relativistic boost corrections. All details concerning the EoS and the hadronic cooling processes are given in [37]. As we have seen in the previous section, it may be sufficient to discuss only two-flavor quark matter for applications to compact stars. We will focus on the model of the quark EoS developed in [27] as an instantaneous approximation to the covariant NCQM. In some density interval at the first order phase transition there may appear the region of the mixed phase, see [33]. Ref. [33] disregarded finite size

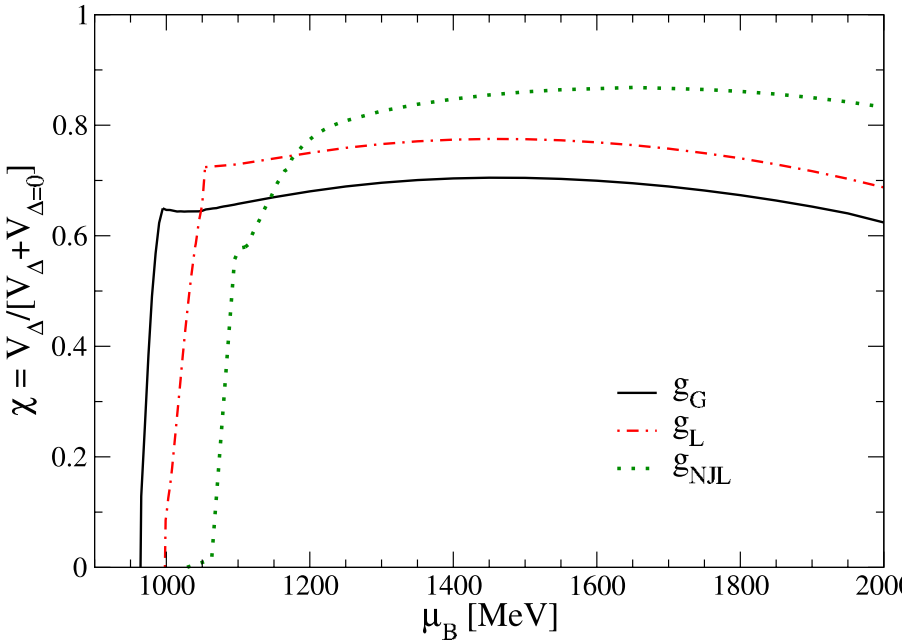

Figure 7. Volume fraction χ of the phase with nonvanishing diquark condensate obtained by a Glendenning construction of a charge-neutral mixed phase. Results are shown for three different formfactors introduced in the text.

effects, such as surface tension and charge screening. In Refs. [38] it has been demonstrated on the example of the hadron-quark mixed phase that finite size effects might play a crucial role by substantially narrowing the region of the mixed phase or even preventing its appearance. Therefore we omit the possibility of the hadron-quark mixed phase in our model where the quark phase arises by the Maxwell construction. For the case of the instantaneous Gaussian formfactor with 2SC phase the quark core appears for $M > 1.21\ M_\odot$. Without 2SC phase or for the Lorentzian or NJL formfactor no stable hybrid stars are obtained, see Fig. 9.

Phase diagram for rotating compact stars. We treat rotating compact stars in the framework of General Relativity theory for the axially symmetric case within a perturbative expansion with respect to the angular velocity Ω up to order Ω^2, see [39]. The account of the centrifugal forces due to the rotation of the star changes the stability curves for the configurations as shown in the Fig. 10. As a result, the maximum mass of a star rotating at the mass shedding limit is about 10 % larger than that of the nonrotating one. The

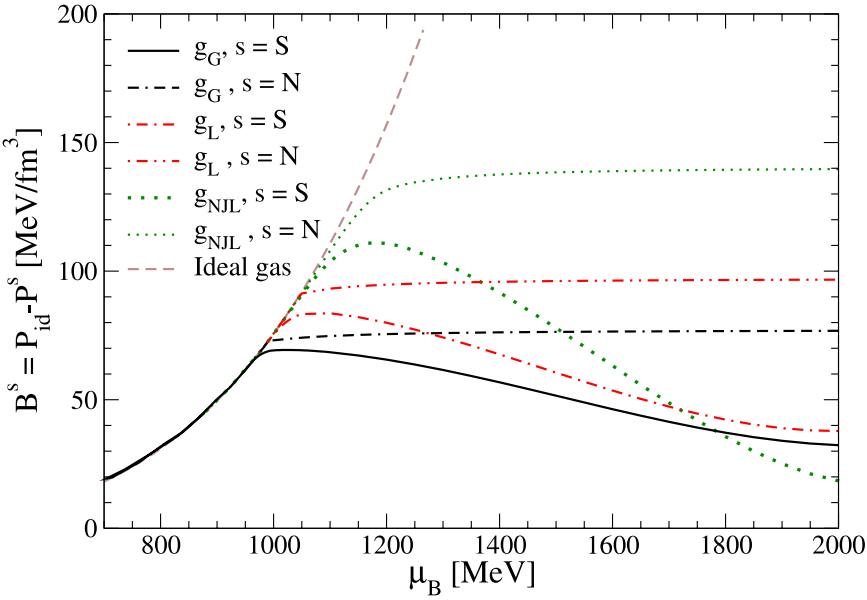

Figure 8. Bag pressure B^s for different formfactors of the quark interaction in dependence on the baryon chemical potential for normal ($s = N$) and superconducting ($s = S$, $G_2 = G_1$) quark matter under neutron star constraints.

radius of the rotating configurations can be larger than that of the static ones by approximately 2 to 3 km.

We have performed the calculation using the same EoS as in Fig. 9 and show the results in Fig. 10. From that Figure it can be seen that the stability state of the star depends uniquely on the value of the central density irrespective of the angular velocity.

The information about the structure of the compact star configurations as thermodynamical systems in dependence on their "thermodynamic variables", mass M and angular velocity Ω, is summarized in the phase diagram for rotating star configurations [40], which displays the situation for the three model EoS of Fig. 9, see Fig. 10.

These phase diagrams have four regions: (i) the region above the maximum frequency $\Omega > \Omega_{\rm K}(N)$ where no stationary rotating configurations are found, (ii) the region of black holes $N > N_{\rm max}(\Omega)$, and the region of stable compact stars which is subdivided by the critical line $N_{\rm crit}(\Omega)$ into (iii) the region of hybrid stars for $N > N_{\rm crit}(\Omega)$ where configurations contain a core with a quark matter phase and (iv) the region of hadronic stars without such a core.

The critical line $N_{\rm crit}(\Omega)$ may manifest itself in observations by a population clustering of compact objects in LMXBs [41]. A *population gap* in the

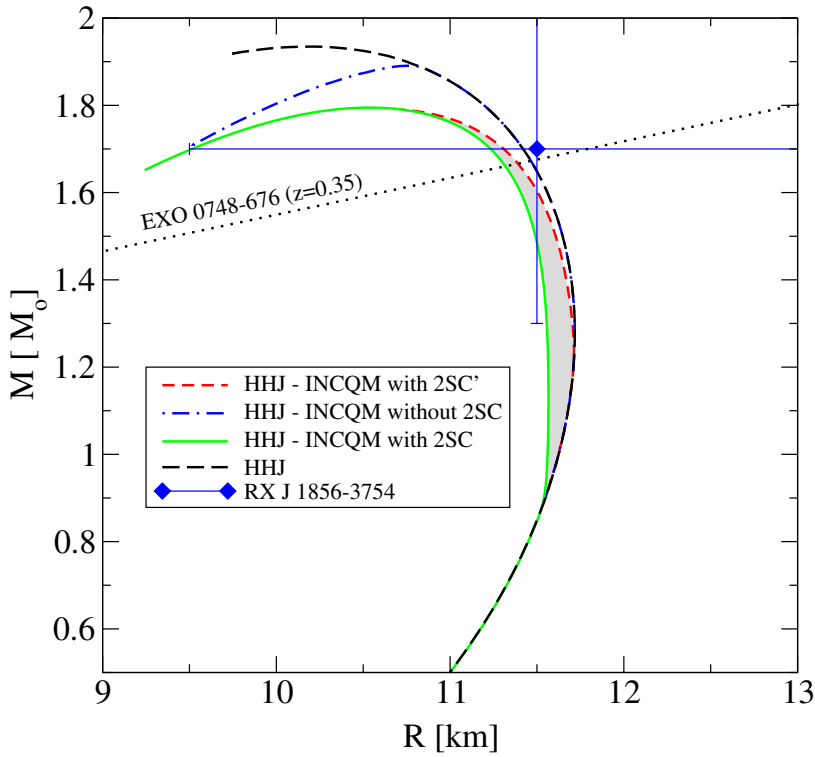

Figure 9. Mass - radius relations for compact star configurations with different EoS: purely hadronic star with HHJ EoS (long-dashed), stable hybrid stars for HHJ - INCQM EoS with 2SC (solid) and without 2SC phase (dash-dotted) for the Gaussian formfactor. We show the influence of a tiny variation of the coupling constant G_1 by the filled grey band. The difference between the models 2SC and 2SC' corresponds to a shift in the bag function (see Fig. 8) 3 MeV/fm^3. For comparison, observational constraints on the compactness are given from the "small" compact star RX J1856.5-3754 and from the high surface redshift object EXO 0748-676 which can both be obeyed by our hybrid star EoS.

phase diagram of compact stars appears as a detectable indicator for hybrid star configurations.

The EoS HHJ - INCQM with 2SC quark matter phase has a type of hard - soft - hard EoS [40]. Therefore critical line is mainly orthogonal to the mass axis and the expected population clustering seems to be not frequency but mass clustering. As already reported by M.C. Miller at this conference, there is observational evidence that the population of LMXB's is mainly homogeneous.

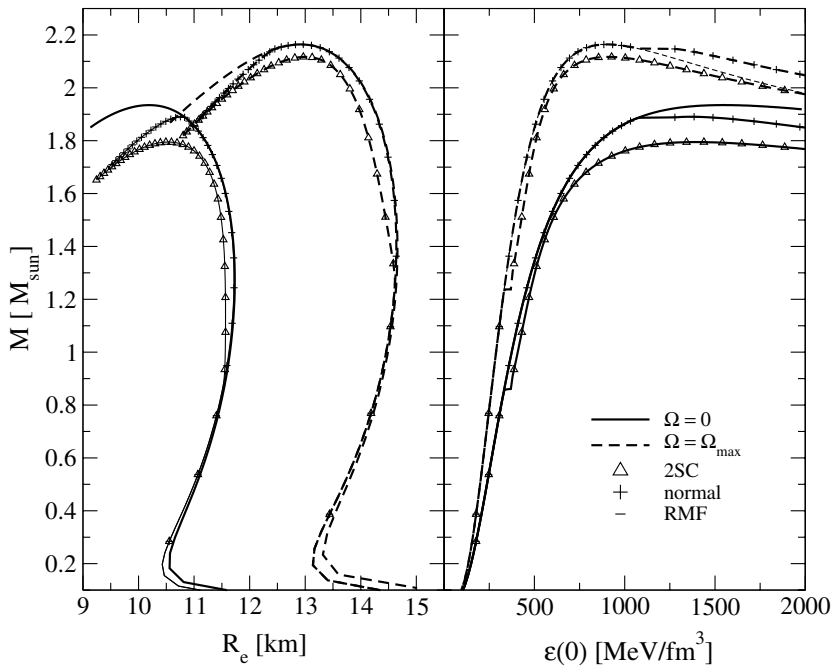

Figure 10. The Mass - radius relation and mass - central energy density dependencies for rotating (dashed lines) and nonrotating (solid lines) hybrid star configurations

In the following chapter we show the cooling behavior of hybrid stars very sensitive to the value of critical mass of phase transition. For our choice of EoS the critical mass is $M = 0.8M_{\odot}$ for non rotating configurations, which is smaller than that expected from the observations of pulsars, see next Section. From the critical line $M_{\rm crit}(\Omega)$ on the phase diagram in Fig. 11 one sees that the mass increases as a function of angular velocity and reaches $M = 1.2M_{\odot}$ at the mass shedding limit. This value is already comparable with the recently observed mass value $M = 1.25M_{\odot}$. As it has already been shown above in Fig. 9 the critical value may change in the band $M = 0.8 - 1.2M_{\odot}$ due to tiny changes in the model parameters. So to fix the critical mass we have one additional parameter Ω. Therefore, to make a robust conclusion about the constraints on the EoS from observational data one needs to make complex investigations of the rotational and cooling evolution.

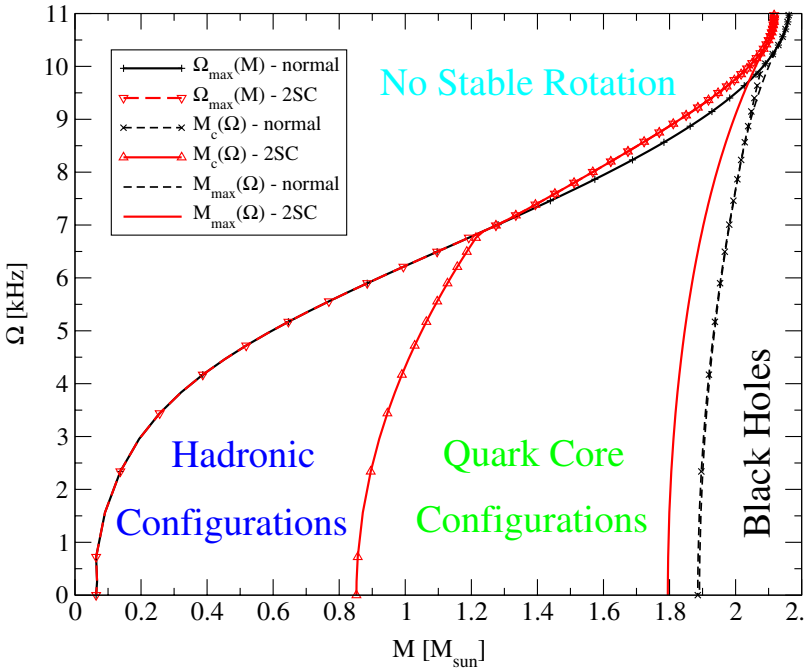

Figure 11. Phase diagrams for rotating star configurations of Fig. 10.

4. Cooling of compact stars

In order to describe the cooling of stable hybrid star configurations, we use the approach to the hadronic cooling developed recently in Ref. [37] and add the contribution due to the quark core, see [10]. Once in the quark matter core of a hybrid star unpaired quarks are present the dominant quark direct Urca (QDU) process is operative and cools the star too fast in disagreement with the observational data [10]. If one allows for a residual weak pairing channel as, e.g., the CSL one with typical gaps of $\Delta \sim 10$ keV - 10 MeV, see [42], the hybrid star configuration will not be affected but the QDU cooling process will be efficiently suppressed as is required for a successful description of compact star cooling. Since we don't know yet the exact pairing pattern for which also the residual (in 2SC unpaired) quarks are paired in the 2-flavor quark matter, we will call this hypothetical phase "2SC+X". In such a way all the quarks may get paired, either strongly in the 2SC channel or weakly in the X channel. If now the X-gap is of the order of 1 MeV, then the QDU process

will be effectively switched off and the cooling becomes too slow, again in disagreement with the data [10]. This seems to be a weak point and we would like to explore whether a density-dependent X-gap could allow a description of the cooling data within a larger interval of compact star masses. For such a density-dependent X-gap function we employ the ansatz

$$\Delta_X(\mu) = \Delta_c \, \exp[-\alpha(\mu - \mu_c)/\mu_c] \, . \tag{40}$$

In Fig. 12 we show the resulting cooling curves for the parameters $\Delta_c = 1.0$ MeV and $\alpha = 10$. We observe that the mass interval for compact stars which

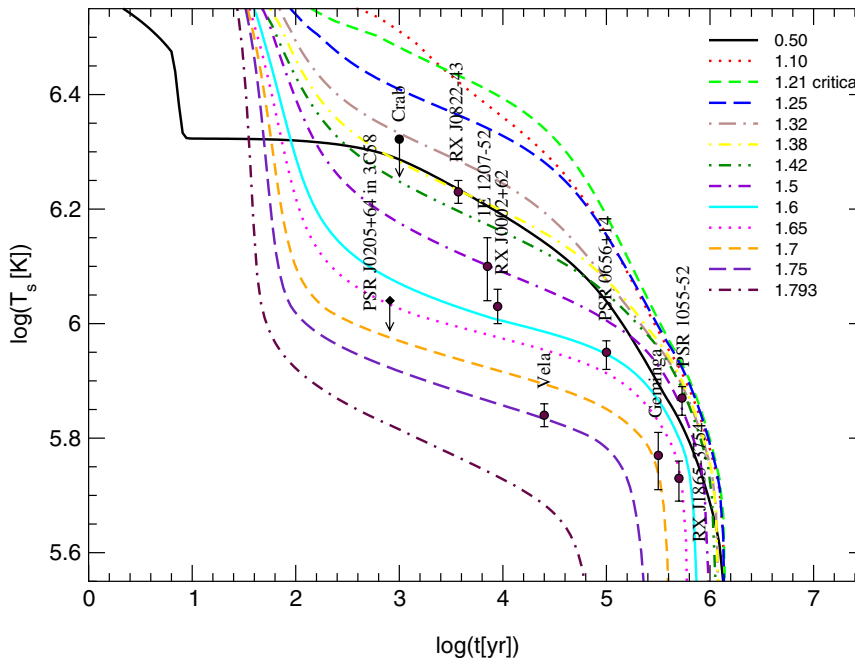

Figure 12. Cooling of hybrid star configurations of Fig. 9 with color superconducting quark matter core in 2SC+X phase. Different lines correspond to hybrid star masses in units of the solar mass.

obey the cooling data constraint ranges now from $M = 1.32 \, M_\odot$ for slow coolers up to $M = 1.75 \, M_\odot$ for fast coolers such as Vela.

5. Protoquark star evolution and Gamma Ray Bursts

Energy release due to (anti)neutrino untrapping. The configurations for the quark stars are obtained by solving the Tolman-Oppenheimer-Volkoff equations for a set of central quark number densities n_q for which the stars are stable. In Fig. 13 the configurations for different antineutrino chemical potentials are shown. The equations of state with trapped antineutrinos are softer and therefore this allows more compact configurations. The presence of antineutrinos tends to increase the mass for a given central density.

A reference configuration with total baryon number $N_B = 1.51\ N_\odot$ (where $N_\odot$ is the total baryon number of the sun) is chosen and the case with (configurations A and B in Fig. 13) and without antineutrinos (f in Fig. 13) are compared. A mass defect can be calculated between the configurations with trapped antineutrinos and without it at a constant total baryon number and the result is shown in Fig. 14). The mass defect could be interpreted as an energy release if the configurations A, B with antineutrinos are initial states and the configuration f without them is the final state of a protoneutron star evolution.

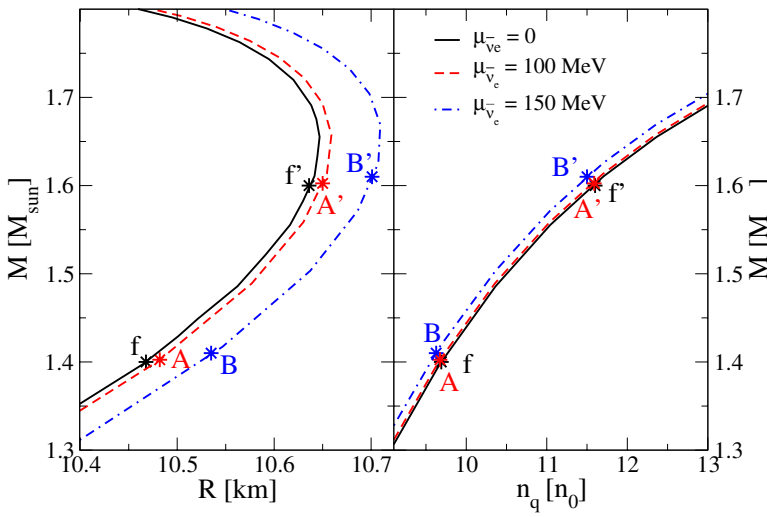

Figure 13. Quark star configurations for different antineutrino chemical potentials $\mu_{\bar{\nu}_e} = 0,\ 100,\ 150$ MeV. The total mass M in solar masses ($M_{\rm sun} \equiv M_\odot$ in the text) is shown as a function of the radius R (left panel) and of the central number density n_q in units of the nuclear saturation density n_0 (right panel). Asterisks denote two different sets of configurations (A,B,f) and (A',B',f') with a fixed total baryon number of the set.

After the collapse of a protoneutron star the star cools down by surface emission of photons and antineutrinos. Antineutrinos are trapped because they were generated by the direct β-process in the hot and dense matter and could

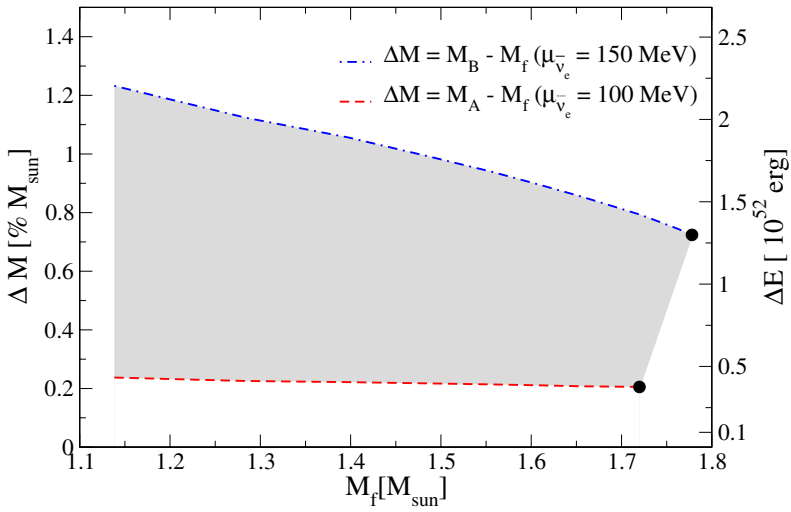

Figure 14. Mass defect ΔM and corresponding energy release ΔE due to antineutrino untrapping as a function of the mass of the final state M_f. The shaded region is defined by the estimates for the upper and lower limits of the antineutrino chemical potential in the initial state $\mu_{\bar{\nu}_e} = 150$ MeV (dashed-dotted line) and $\mu_{\bar{\nu}_e} = 100$ MeV (dashed line), respectively.

not escape due to their small mean free path. The region of the star where the temperature falls below the density dependent critical value for diquark condensation, will transform to the color superconducting state which is almost transparent to (anti)neutrinos. But nevertheless due to the trapped antineutrinos there is a dilute normal quark matter shell which prevents neutrino escape from the superconducting bulk of the star, see Fig. 15 and Fig. 16. The criterion for the neutrino untrapping transition is to cool the star below a temperature of about 1 MeV when the mean free path of neutrinos becomes larger than the shell radius [47]. If at this temperature the antineutrino chemical potential is still large then the neutrinos can escape in a sudden outburst. If it is small then there will be only a gradual increase in the luminosity. An estimate for the possible release of energy within the outburst scenario can be given via the mass defect defined in the previous subsection between an initial configuration with trapped neutrinos (state A or B) and a final configuration without neutrinos (state f).

Cooling delay due to neutrino trapping. Estimates of the time interval after which an explosive effect of energy release like a GRB could be observed, depend on the possible structure of a compact object after the

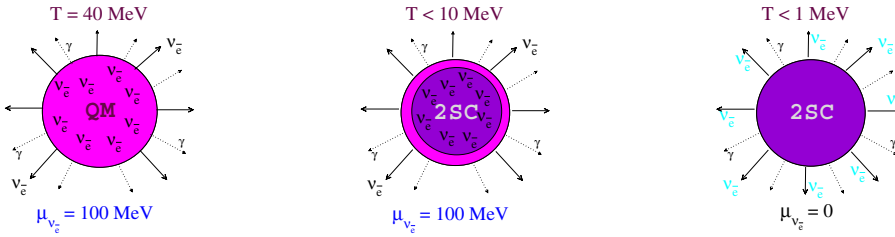

Figure 15. Left graph: Quark star cooling by antineutrino and photon emission from the surface. Middle graph: Two-phase structure developes due to the trapped antineutrinos: a normal quark matter shell and a superconducting interior. Right graph: Antineutrino untrapping and burst-type release of energy.

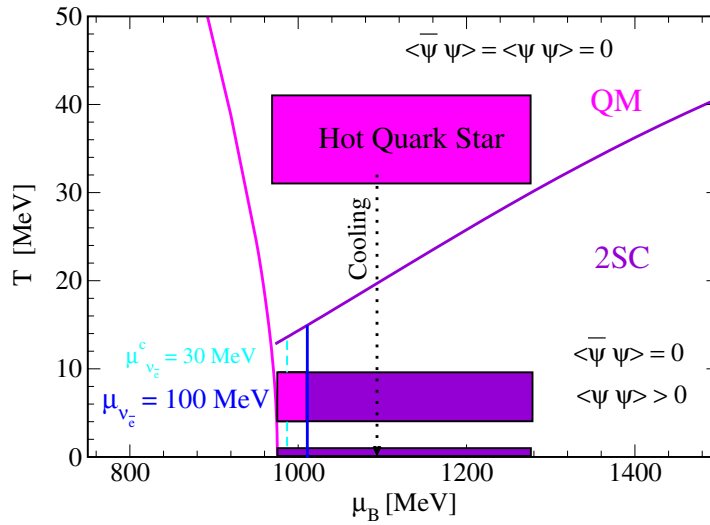

Figure 16. Schematic protoquark star evolution corresponding to Fig. 15 plotted in the phase diagram for 2-flavor quark matter

leptonization stage. As it has been discussed in the previous Section the compact star can be a quark or a hybrid one, where for $T < T_c$ the quark matter is expected to be in a color superconducting state. The possibility of pure quark stars has been extensively discussed in the literature, see [43] and references therein. We also can deal with a hybrid star instead of a pure quark star. However, in that case the experimental constraint of a low baryon loading of the GRB [44] with a mass $\lesssim 10^{-4} M_\odot$ should be obeyed. Therefore the hadronic shell and the crust should be rather thin or there is a special reason for a low baryon loading.

In the previous Section we noted that the typical temperature, above which the star becomes opaque to neutrinos is $T_{opac} \sim 0.4 \div 3$ MeV, where we ignore here the differences in the absorption/production properties of different neutrino flavors [45]. Saying neutrino we actually will not distinguish neutrino and antineutrino, although their absorption/production could be different. If we assume an initial temperature of $T_0 < T^{\nu}_{opac}$, the star radiates neutrinos directly from the interior region. For $T_0 > T^{\nu}_{opac}$, the neutrino transport to the surface is operative and leads to a delay of the cooling evolution.

Energy content. Let us estimate the energy content of different species. The total quark thermal energy is related to the temperature as [45]

$$E^q_T \sim 5 \cdot 10^{47} (n_B/n_0)^{2/3} (R/10\ \mathrm{km})^3 T_9^2\ \mathrm{erg}, \tag{41}$$

where n_B is the baryon density, T_9 is the temperature in units of 10^9 K.

For $\Delta \ll \mu_q$ the pairing does not significantly change this estimate. Thus, the superconducting quark matter phase contains a thermal energy of $E^q_T \lesssim 10^{53}$ erg for an initial temperature $T_0 \sim 30 \div 50$ MeV.

Neutrinos are degenerate within the first second, if $T \sim 10 \div 30$ MeV. Their energy content is

$$E^{\nu} \simeq \frac{\mu^4_{\nu}}{4\pi^2} \frac{N_B}{n_B}, \tag{42}$$

where μ_{ν} is the neutrino non-equilibrium chemical potential. This estimate yields $E^{\nu} \sim 10^{51} \div 10^{52}$ erg for relevant values of $\mu_{\nu} \sim 100 \div 200$ MeV.

Energy radiation for $T > T^{\nu}_{opac}$. The neutrino/antineutrino collisions produce $e^- e^+$ pairs outside the star, which efficiently convert to photons. We use the estimate of Ref. [45] for the $\nu\bar{\nu} \to e^- e^+$ conversion rate:

$$E_{e^- e^+} \sim 5 \cdot 10^{32} T^9_{s,9} (R/10\ \mathrm{km})(\Delta t/s)\ \mathrm{erg}, \tag{43}$$

where T_s is the surface temperature. For T_s of the order of several MeV we would get only $E_{e^- e^+} \lesssim 10^{46} \div 10^{48}$ erg for $\Delta t \sim 1 \div 100$ s in the range of our interest. However, for $T_s \sim 30 \div 50$ MeV most of the total thermal energy can be converted in $e^- e^+$ with an energy of $E_{e^- e^+} \sim$ several $\cdot\, 10^{53}$ erg within a short time interval $\Delta t \sim 10^{-3} \div 10^{-1}$ s.

In the case of the neutron star T_s is significantly smaller than the internal temperature. Then only a few percent of the $\nu\bar{\nu}$ energy is converted to photons, on a time scale appropriate for GRB. Ref. [46] demonstrated that the presence of a strong gravitational field near the star may increase this efficiently by an order of magnitude and $E_{\gamma}/E_{e^- e^+}$ becomes ~ 0.1. Moreover, in the presence

of baryons the $\nu/\bar{\nu}$ absorption on baryons is efficient, further decreasing the $\nu\bar{\nu} \to e^- e^+$ rate.

The advantage of the quark star model is that the quark star has a thin hadron shell and a tiny crust, if any. In this case we may assume that the surface temperature is of the same order of magnitude as the internal temperature. Thus for $T \sim 10 \div 50$ MeV the neutrino energy of the order of $E_\nu \sim 10^{53}$ erg can be converted to $e^- e^+$ during a short time $t \sim 10^{-3} \div 10^{-1}$ s. Then all the $e^- e^+$ energy is converted to photons. In the presence of beaming already $E_\gamma \sim 10^{51}$ erg produced on a time scale $\Delta t \sim 10^{-3} \div 100$ s would be sufficient to explain GRB.

Moreover, $e^- e^+$ pairs are accelerated in the strong magnetic field, which we assume to be present, increasing the hard component of the γ-ray spectrum, that is in coincidence with experimental findings.

Now let us discuss how efficiently the energy can be radiated from the quark star.

If the phase transition is somewhat stronger than we have discussed in the previous subsection, the initial temperature is higher, $T_0 \gtrsim 10$ MeV. Neutrinos are trapped for a while in the interior of the newly formed quark star. For lower densities, where the quark matter contains trapped neutrinos the direct Urca process is operative and neutrino cooling is a surface effect.

Only at smaller temperature $T \approx 1$ MeV when the emissivity of the direct Urca process has dropped according to the typical T^6 dependence, most of the neutrino energy will be released within a small time. Neutrinos in the diffusion regime can escape from the surface in the time

$$t_R \sim \frac{R^2}{\lambda\, c}\,, \tag{44}$$

where λ is the mean free path of neutrinos in matter. If λ is of the order of the star radius, then they can leave the star within $t_R \sim 3 \times 10^{-5}$ s. From the surface of the remaining trapped area neutrinos are released by blackbody radiation, with a time delay due to the heat transport. When the neutrinos reach the surface then they can be converted to electron - positron pairs by $\nu\bar{\nu} \leftrightarrow e^- e^+$ with the above described rate [45]. A quark star has, if at all, only a very thin hadronic shell and crust. Therefore the surface temperature should be of the order of the inner surface temperature. At a surface temperature of $T_s \sim 10 - 30$ MeV within only $10^{-3} - 10^{-1}$s the neutrino energy of up to 10^{52}erg can be transformed in $e^- e^+$ pairs, which can convert with nearly 100 % efficiency to photons. These photons have energies of several MeV and cover the energy range of gamma radiation in GRBs.

6. Conclusions

We have presented the QCD phase diagram obtained within the NCQM approach. We find that in the framework of our model for neutron star applications it is sufficient to consider only two quark flavors since the critical densities of strange quark deconfinement are not accessible in typical compact star interiors. We investigate the phase transition between superconducting quark matter and hadronic matter under neutron star constraints and find that stable hybrid stars are possible with large quark matter cores in the 2SC phase. We suggest that the population of compact stars in LMXBs should show a mass clustering rather than a frequency clustering with mass values around the critical mass for a deconfinement phase transition in the star interior. The solution of the cooling evolution equations for hybrid star configurations shows that the presence of ungapped quark species entails too fast cooling due to the QDU process in disagreement with modern neutron star cooling data. A successful description of hybrid star cooling requires that direct Urca-like processes be excluded in the hadronic shell and that a pairing pattern in the quark matter core occurs where all quarks are gapped and a weak pairing channel with a decreasing density dependence of the gap in the range of 1 MeV to 10 keV is present. A precise microscopic model for this conjectured "2SC+X" phase is still lacking. Possible candidate for a weak pairing channel is the color-spin-locking (CSL) phase. We have demonstrated on the example of hybrid star cooling how astrophysical observations could provide constraints for microscopic approaches to the QCD phase diagram in the domain of cold dense matter presently not accessible to heavy-ion collision experiments and lattice QCD simulations.

Acknowledgments

We like to thank our colleagues M. Buballa, S. Fredriksson, C. Gocke, Yu. Kalinovsky, A. Öztaş, F. Sandin, S. Schmidt, N. Scoccola and P.C. Tandy for their contributions to the formulation of the separable chiral quark model used in this work. The work of D.N.A. was supported by Landesgraduiertenförderung Mecklenburg-Vorpommern; D.B. thanks for partial support of the Department of Energy during the program INT-04-1 on *QCD and Dense Matter: From Lattices to Stars* at the University of Washington; D.N.V. was supported by DFG grant 436 RUS 113/558/0-2. We acknowledge the support of DAAD for scientist exchange between the Universities of Rostock and Yerevan. This research has been supported in part by the Virtual Institute *Dense hadronic matter and QCD phase transition* of the Helmholtz Association under grant number VH-VI-041.

References

[1] P. Braun-Munzinger, K. Redlich and J. Stachel, in: *Quark-Gluon Plasma III*, R. Hwa and X.-N. Wang (Eds.), World Scientific, Singapore (2004), p. 491.

[2] F. Karsch and E. Laermann, in: [1], p. 1.

[3] M. G. Alford, Ann. Rev. Nucl. Part. Sci. **51** (2001) 131.

[4] M. Kitazawa, T. Koide, T. Kunihiro and Y. Nemoto, Phys. Rev. D **65** (2002) 091504.

[5] D. N. Voskresensky, Phys. Rev. C **69** (2004) 065209.

[6] D. Blaschke, N.K. Glendenning, A. Sedrakian (Eds.), *Physics of Neutron Star Interiors*, Springer, Berlin (2001).

[7] D. Blaschke, T. Klahn and D. N. Voskresensky, Astrophys. J. **533** (2000) 406.

[8] D. Blaschke, H. Grigorian and D. N. Voskresensky, Astron. Astrophys. **368** (2001) 561.

[9] D. Page, M. Prakash, J. M. Lattimer and A. Steiner, Phys. Rev. Lett. **85** (2000) 2048.

[10] D. Blaschke, D. N. Voskresensky and H. Grigorian, arXiv:astro-ph/0403171.

[11] A. Bender, D. Blaschke, Y. Kalinovsky and C. D. Roberts, Phys. Rev. Lett. **77** (1996) 3724.

[12] D. Blaschke, C. D. Roberts and S. M. Schmidt, Phys. Lett. B **425** (1998) 232.

[13] C. D. Roberts and S. M. Schmidt, Prog. Part. Nucl. Phys. **45** (2000) S1.

[14] D. Blaschke, H. Grigorian, G. S. Poghosyan, C. D. Roberts and S. M. Schmidt, Phys. Lett. B **450** (1999) 207.

[15] J. C. R. Bloch, C. D. Roberts and S. M. Schmidt, Phys. Rev. C **60** (1999) 065208.

[16] C. J. Burden, L. Qian, C. D. Roberts, P. C. Tandy and M. J. Thomson, Phys. Rev. C **55** (1997) 2649.

[17] D. Blaschke, Yu.L. Kalinovsky, P.C. Tandy, in: *Problems of Quantum Field Theory*, Dubna, July 13-17, 1998, p. 454.

[18] D. Blaschke and P. C. Tandy, in: *Understanding Deconfinement in QCD*, Eds. D. Blaschke, F. Karsch, C.D. Roberts, World Scientific, Singapore (2000), p. 218.

[19] D. Blaschke, G. Burau, Y. L. Kalinovsky, P. Maris and P. C. Tandy, Int. J. Mod. Phys. A **16** (2001) 2267.

[20] H. Ito, W. Buck, F. Gross, Phys. Rev. **C 43** (1991) 2483; **C 45** (1992) 1918; M. Buballa, S. Krewald, Phys. Lett. **B 294** (1992) 19; D. Diakonov, H. Forkel, and M. Lutz, Phys. Lett. **B 373** (1996) 147; G.W. Carter, and D. Diakonov, Phys. Rev. **D 60** (1999) 016004; R. Rapp, T. Schäfer, E.V. Shuryak, and M. Velkovsky, Ann. Phys. **280** (2000) 35;

[21] R.S. Plant, M.C. Birse, Nucl. Phys. **A 628** (1998) 607; B. Golli, W. Broniowski, G. Ripka, Phys. Lett. **B437** (1998) 24.

[22] D. Gómez Dumm, N.N. Scoccola, Phys. Rev. **D 65** (2002) 074021.

[23] M. Buballa, Phys. Rep. **407** (2005) 205.

[24] C. Gocke, D. Blaschke, A. Khalatyan, and H. Grigorian, arXiv:hep-ph/0104183.

[25] M. Alford, K. Rajagopal, and F. Wilczek, Phys. Lett. **B 422** (1998) 247.

[26] S. M. Schmidt, D. Blaschke and Y. L. Kalinovsky, Phys. Rev. C **50** (1994) 435.

[27] D. Blaschke, S. Fredriksson, H. Grigorian and A. M. Oztas, Nucl. Phys. A **736** (2004) 203.

[28] H. Grigorian, D. Blaschke and D. N. Aguilera, Phys. Rev. C **69** (2004) 065802.

[29] M. Huang, P. f. Zhuang and W. q. Chao, Phys. Rev. D **67** (2003) 065015.

[30] M. Frank, M. Buballa and M. Oertel, Phys. Lett. B **562** (2003) 221.

[31] O. Kiriyama, S. Yasui and H. Toki, Int. J. Mod. Phys. E **10** (2001) 501.

[32] F. Neumann, M. Buballa and M. Oertel, Nucl. Phys. A **714** (2003) 481.

[33] N. K. Glendenning, Phys. Rev. D **46** (1992) 1274.

[34] M. Baldo, G. F. Burgio and H. J. Schulze, arXiv:astro-ph/0312446.

[35] H. Heiselberg, and M. Hjorth-Jensen, Astrophys. J. **525** (1999) L45.

[36] A. Akmal, V.R. Pandharipande, and D.G. Ravenhall, Phys. Rev. **C 58**, (1998) 1804.

[37] D. Blaschke, H. Grigorian and D. N. Voskresensky, Astron. Astrophys. **424** (2004) 979.

[38] D.N. Voskresensky, M. Yasuhira, and T. Tatsumi, Phys. Lett. **B 541** (2002) 93; Nucl. Phys. **A 723** (2002) 291.

[39] E. Chubarian, H. Grigorian, G. S. Poghosyan and D. Blaschke, Astron. Astrophys. **357** (2000) 968.

[40] H. Grigorian, D. Blaschke and G. S. Poghosyan, Nucl. Phys. A **715** (2003) 831.

[41] G. S. Poghosyan, H. Grigorian and D. Blaschke, Astrophys. J. **551** (2001) L73.

[42] A. Schmitt, arXiv:nucl-th/0405076.

[43] J. E. Horvath and G. Lugones, arXiv:astro-ph/0311449.

[44] M. A. Ruderman, L. Tao and W. Kluzniak, arXiv:astro-ph/0003462.

[45] P. Haensel, B. Paczynski and P. Amsterdamski, Astrophys. J. **375** (1991) 209.

[46] J. D. Salmonson and J. R. Wilson, Astrophys. J. **517** (1999) 859.

[47] M. Prakash, J. M. Lattimer, R. F. Sawyer and R. R. Volkas, Ann. Rev. Nucl. Part. Sci. **51** (2001) 295.

LOOKING INSIDE THE EARTH WITH SOLAR AND SUPERNOVA NEUTRINOS: AN ANALYTIC APPROACH

A. N. Ioannisian
Yerevan Physics Institute, Alikhanian Brothers 2, 375036 Yerevan, Armenia
Institute for Theoretical Physics and Modeling, 375036 Yerevan, Armenia
ICTP, Strada Costeria 11, 34014 Trieste, Italy

A. Yu. Smirnov
ICTP, Strada Costeria 11, 34014 Trieste, Italy

Abstract For the case of small matter effects: $V \ll \Delta m^2/2E$, where V is the matter potential, we develop the perturbation theory using $\epsilon \equiv 2VE/\Delta m^2$ as the expansion parameter. We derive simple and physically transparent formulas for the oscillation probabilities in the lowest order in ϵ which are valid for an arbitrary density profile. They can be applied for the solar and supernova neutrinos propagating in matter of the Earth. Using these formulas we study features of averaging of the oscillation effects over the neutrino energy. Sensitivity of these effects to remote (from a detector), $d > l_\nu E/\Delta E$, structures of the density profile is suppressed.

1. Introduction

For the LMA parameters the oscillations of solar and supernova (low energy) neutrinos inside the Earth occur in the vacuum (kinetic) energy dominating regime. This means that the matter potential V is much smaller than the kinetic energy of the neutrino system:

$$V \ll \frac{\Delta m^2}{2E}, \tag{1}$$

where

$$V(x) = \sqrt{2} G_F N_e(x), \tag{2}$$

G_F is the Fermi constant, $N_e(x)$ is the number density of the electrons, $\Delta m^2 = m_2^2 - m_1^2$ is the mass squared difference.

D. Blaschke and D. Sedrakian (eds.), Superdense QCD Matter and Compact Stars, 405–413.

In this case we can introduce a small parameter [1]:

$$\epsilon(x) = \frac{2EV(x)}{\Delta m^2} \ll 1 \tag{3}$$

and develop the corresponding perturbation theory.

Neutrino oscillations in the weak matter effect regime have been discussed extensively before [1-13], in particular, for the solar and supernovae neutrinos propagating in the matter of the Earth. The previous work has been done mainly in the approximation of constant density profile which consists of several layers with constant density.

Here we derive general formula which is valid for arbitrary density profile provided that the condition (1) is satisfied.

2. ϵ- perturbation theory and oscillation probabilities

We will consider two active neutrino mixing

$$\nu_f = U(\theta)\nu_{mass}, \tag{4}$$

where $\nu_f \equiv (\nu_e, \nu_a)^T$, $\nu_{mass} \equiv (\nu_1, \nu_2)^T$, and

$$U = \begin{pmatrix} \cos\theta & \sin\theta \\ \text{-}\sin\theta & \cos\theta \end{pmatrix}. \tag{5}$$

ν_a is in general a combination of ν_μ and ν_τ.

We will first find the evolution matrix for the mass eigenstates and then make projection onto the flavor states. In the mass eigenstate basis the Hamiltonian has the following form

$$H(x) = \begin{pmatrix} 0 & 0 \\ 0 & \frac{\Delta m^2}{2E} \end{pmatrix} + U^\dagger \begin{pmatrix} V(x) & 0 \\ 0 & 0 \end{pmatrix} U \tag{6}$$

It can be rewritten as

$$H(x) = U'(x) \begin{pmatrix} 0 & 0 \\ 0 & \frac{\Delta m^2_m(x)}{2E} \end{pmatrix} U'^\dagger(x), \tag{7}$$

where

$$\Delta m^2_m(x) \equiv \Delta m^2 \sqrt{(\cos 2\theta - \epsilon(x))^2 + \sin^2 2\theta}$$

is the energy split in matter and U' is the unitary matrix which diagonalizes the Hamiltonian (6). U' is the mixing matrix of the mass states in matter, so that $\nu_{mass} = U'\nu_m$, where $\nu_m \equiv (\nu_{1m}, \nu_{2m})^T$ are the eigenstates in matter. The matrix U' has the form of (5) with the angle determined by

$$\sin 2\theta'(x) = \frac{\epsilon(x)\ \sin 2\theta}{\sqrt{(\cos 2\theta - \epsilon(x))^2}}. \tag{8}$$

Mixing of the flavor states in mater is defined by $\nu_f = U_m \nu_m$, where $U_m = U(\theta_m)$ is the usual mixing matrix in matter with the angle θ_m

$$\sin 2\theta_m(x) = \frac{\sin 2\theta}{\sqrt{(\cos 2\theta - \epsilon(x))^2 + \sin^2 2\theta}} \,. \tag{9}$$

From definitions of the flavor states, mass states and eigenstates in matter we find $\nu_f = U_m (U')^\dagger \nu_{mass}$, so that $U = U_m U'$, and therefore

$$\theta' = \theta_m - \theta. \tag{10}$$

Evolution of the mass states is given by the equation $id\nu_{mass}/dx = H(x)\nu_{mass}$ with the Hamiltonian given in (6). Its formal solution - the evolution matrix from the initial point x_0 to the final point x_f - can be written as

$$S(x_0 \to x_f) = T e^{-i \int_{x_0}^{x_f} H(x)\, dx}, \tag{11}$$

where T means chronological ordering.

Let us divide a trajectory of neutrinos into n equal parts (layers) of the size, Δx, so that $n = (x_f - x_0)/\Delta x$, and assume constant density inside each layer. Then for the evolution matrix we obtain

$$S(x_0 \to x_f) = e^{-iH(x_n)\,\Delta x} \cdot e^{-iH(x_{n-1})\,\Delta x} \cdots e^{-iH(x_i)\,\Delta x} \cdots e^{-iH(x_1)\,\Delta x} \tag{12}$$

$$= U'_n D_n U'^\dagger_n \cdot U'_{n-1} D_{n-1} U'^\dagger_{n-1} \cdots U'_i D_i U'^\dagger_i \cdots U'_1 D_1 U'^\dagger_1, \tag{13}$$

where $x_n \equiv x_f$,

$$D_i = \begin{pmatrix} 1 & 0 \\ 0 & e^{i\phi^m_{x_{i-1} \to x_i}} \end{pmatrix} \tag{14}$$

is the evolution matrix of the matter eigenstates in ith layer with constant density; $\phi^m_{x_{i-1} \to x_i}$ is the relative phase between the matter eigenstates acquired in the layer i, and the phase between points a and b is determined by integral

$$\phi^m_{a \to b} = \frac{\Delta m^2}{2E} \int_a^b dy \sqrt{\left(\cos 2\theta - \frac{2V(y)E}{\Delta m^2}\right)^2 + \sin^2 2\theta} \tag{15}$$

The matix U'_i relates the mass states with the matter eigenstates in the layer i:

$$U'_i = \begin{pmatrix} \cos\theta'(x_i) & \sin\theta'(x_i) \\ -\sin\theta'(x_i) & \cos\theta'(x_i) \end{pmatrix} \,. \tag{16}$$

Structure of the expression (13) is rather transparent: it is given by the product of the blocks $(U'_i D_i U'^\dagger_i)$ for all the layers. In each layer we first project the

mass states onto the matter eigenstates, then evolve the eigenstates and then project back to mass states.

We expand each block ($U_i' D_i U'^{\dagger}$) in a power series of Δx and keep it to the first order in Δx. As a result, we obtain

$$S(x_0 \to x_n) = (D_n + i\,\Delta x\,\Upsilon_n)(D_{n-1} + i\,\Delta x\,\Upsilon_{n-1}) \cdots (D_1 + i\,\Delta x\,\Upsilon_1), \tag{17}$$

where

$$\Upsilon(x) = \frac{\Delta m_m^2(x)}{2E} \begin{pmatrix} \sin^2\theta'(x) & \frac{1}{2}\sin 2\theta'(x) \\ \frac{1}{2}\sin 2\theta'(x) & -\sin^2\theta'(x) \end{pmatrix} \tag{18}$$

$$= \frac{\Delta m^2}{2E}\frac{1}{2}\sin 2\theta\,\epsilon(x) \begin{pmatrix} \frac{1}{2}\sin 2\theta\,\epsilon(x) & 1 \\ 1 & -\frac{1}{2}\sin 2\theta\,\epsilon(x) \end{pmatrix} + O(\epsilon^3) \tag{19}$$

(In the lowest order in $\epsilon(x)$ the diagonal terms of this matrix are zeros.)

The evolution matrix (17) can be rewritten in the following form

$$\begin{aligned} S_(x_0 \to x_f) &= D_n D_{n-1} \cdots D_1 \\ &+ i\,\Delta x \sum_{i=1}^{n} D_n \cdots D_{i+1} \Upsilon_i D_{i-1} \cdots D_1 \\ &- (\Delta x)^2 \sum_{i=1}^{n} \sum_{j=1}^{i-1} D_n \cdots D_{i+1} \Upsilon_i D_{i-1} \cdots D_{j+1} \Upsilon_j D_{j-1} \cdots D_1 \\ &+ \cdots \end{aligned} \tag{20}$$

In the limit $n \to \infty$ we can replace $\sum$'s by $\int$'s in this expression. Then taking into account definition of D_i (14) we find

$$\begin{aligned} S(x_0 \to x_f) &= \begin{pmatrix} 1 & 0 \\ 0 & e^{i\phi^m_{x_0 \to x_f}} \end{pmatrix} + i \int_{x_0}^{x_f} dx \begin{pmatrix} 1 & 0 \\ 0 & e^{i\phi^m_{x \to x_f}} \end{pmatrix} \Upsilon(x) \begin{pmatrix} 1 & 0 \\ 0 & e^{i\phi^m_{x_0 \to x}} \end{pmatrix} \\ &- \int_{x_0}^{x_f} dx \int_{x_0}^{x} dy \begin{pmatrix} 1 & 0 \\ 0 & e^{i\phi^m_{x \to x_f}} \end{pmatrix} \Upsilon(x) \begin{pmatrix} 1 & 0 \\ 0 & e^{i\phi^m_{y \to x}} \end{pmatrix} \Upsilon(x) \begin{pmatrix} 1 & 0 \\ 0 & e^{i\phi^m_{x_0 \to y}} \end{pmatrix} \\ &+ \cdots \end{aligned} \tag{21}$$

Finally, making use of eqs. (18) and (20) the evolution matrix can be expanded in a power series of small parameter ϵ:

$$\begin{aligned} S(x_0 \to x_f) &= S(x_0 \to x_f)^{(0)} + S(x_0 \to x_f)^{(1)} + S(x_0 \to x_f)^{(2)} + \cdots \\ &\simeq S(x_0 \to x_f)^{(0)} + S(x_0 \to x_f)^{(1)} \\ &- \begin{pmatrix} 1 & 0 \\ 0 & e^{i\phi^m_{x_0 \to x_f}} \end{pmatrix} + i\frac{\sin(2\theta)}{2} \int_{x_0}^{x_f} dx\, V(x) \begin{pmatrix} 0 & e^{i\phi^m_{x_0 \to x}} \\ e^{i\phi^m_{x \to x_f}} & 0 \end{pmatrix}, \end{aligned} \tag{22}$$

where in the last expression we have taken the zero and the first order terms in ϵ only.

Using the evolution matrix in mass states basis (21) we can calculate the amplitudes and probabilities for different transitions. Notice that the evolution matrix in the flavor basis, S_f, can be obtained immediately:

$$S_f = USU^{\dagger}. \tag{23}$$

The evolution matrix from the mass states to the flavor states S_{fm} is then

$$S_{fm} = US, \tag{24}$$

and U is the vacuum mixing matrix (5).

Let us consider the most important examples. The amplitude of mass to flavor transition, $\nu_i \to \nu_\alpha$, on the way from x_0 to x_f is given by

$$A_{\nu_i \to \nu_\alpha} = U_{\alpha j} S_{ji}. \tag{25}$$

In particular, inserting the matrix (21) in this expression we find the amplitude of the $\nu_1 \to \nu_e$ oscillations in the first order in V:

$$ginequation A_{\nu_1 \to \nu_e} = \cos\theta + \frac{i}{2}\sin 2\theta \, \sin\theta \int_{x_0}^{x_f} dx \, V e^{i\phi^m_{x \to x_f}}. \tag{26}$$

Probability of the $\nu_1 \to \nu_e$ oscillations equals

$$P_{\nu_1 \to \nu_e} = \cos^2\theta - \frac{1}{2}\sin^2 2\theta \int_{x_0}^{x_f} dx \, V \sin\phi^m_{x \to x_f} \, . \tag{27}$$

Inserting the expression for phase (15) up to the first order in V we obtain

$$P_{\nu_1 \to \nu_e} \approx \cos^2\theta - \frac{1}{2}\sin^2 2\theta \int_{x_0}^{x_f} dx \, V \sin\left(\frac{\Delta m^2}{2E}(x_f - x) - \cos 2\theta \int_x^{x_f} V dy\right) \tag{28}$$

The probability of $\nu_2 \to \nu_e$ transition relevant for the solar neutrino oscillations in the Earth can be obtained immediately from the unitarily condition:

$$P_{\nu_2 \to \nu_e} = \sin^2\theta + \frac{1}{2}\sin^2 2\theta \int_{x_0}^{x_f} dx \, V \sin\phi^m_{x \to x_f}. \tag{29}$$

Then the regeneration parameter ($f_{reg} \equiv P_{\nu_2 \to \nu_e} - \sin^2\theta$) equals

$$f_{reg} = \frac{1}{2}\sin^2 2\theta \int_{x_0}^{x_f} dx \, V \sin\phi^m_{x \to x_f}. \tag{30}$$

and $\phi^m_{x \to x_f}$ is given in eq.(15)

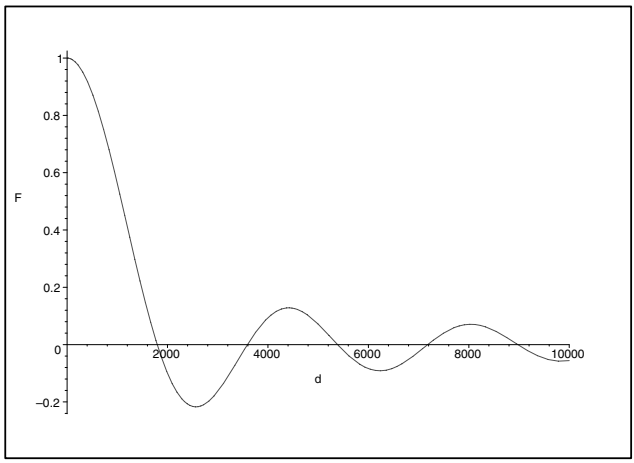

Figure 1. The averaging factor F as function of $d \equiv x_f - x$ for E=10 MeV, $\Delta E = 2$ MeV, and $\Delta m^2 = 7\ 10^{-5}$ eV^2.

3. Effect of averaging over neutrino energy

The formulas obtained in section 2 can be used to estimate a sensitivity of oscillation experiments to different structures in the density profile. Apparently, an integration over the neutrino energy leads to averaging of oscillations and therefore to lost of the sensitivity. To estimate this effect we introduce the energy resolution function $f(E', E)$ and perform averaging of the probability:

$$\overline{P}_{\nu_1 \to \nu_e} = \int dE' f(E', E)\, P_{\nu_1 \to \nu_e} = \cos^2\theta - \frac{1}{2}\sin^2 2\theta \int_{x_0}^{x_f} dx\, V\, F \sin\phi_{x \to x_f}\,. \tag{31}$$

Here we have parameterized the effect of averaging by the averaging factor $F(d)$, so that in the absence of averaging $F = 1$. The factor is a function of distance from the "detection" point x_f: $d \equiv x_f - x$.

Let us take for simplicity the box like resolution function $f(E', E)$, so that

$$\overline{P}_{\nu_1 \to \nu_e} = \frac{1}{\Delta E} \int_{E - \frac{\Delta E}{2}}^{E + \frac{\Delta E}{2}} dE P_{\nu_1 \to \nu_e}. \tag{32}$$

Then assuming that $\Delta E \ll E$ and making use of the approximation $\Delta m^2_m \simeq \Delta m^2[1 - \cos(2\theta)\epsilon]$ we find

$$F = \frac{1}{\pi}\frac{l_\nu}{d}\frac{E}{\Delta E}\sin\frac{\pi d \Delta E}{l_\nu E}\ , \tag{33}$$

where $l_\nu \approx l_m$ is the oscillation length (see Fig. 1).

As follows from the Fig. 1, $F(d)$ is a decreasing function of the distance from the detector. The decrease of F means that contributions from the large distances to the integral (31) are suppressed. According to Fig.1 which corresponds to $\Delta E/E = 0.2$, the contributions from distances above 1500 km are attenuated by F at least by factor 5 in comparison with those from structures situated near the detector. Correspondingly, the sensitivity to remote structures is much weaker.

The larger ΔE, the smaller the width of the first peak which produces main effect. As follows from (33), the width of the peak and therefore the region of unsuppressed contributions due averaging is given by

$$d < l_\nu \frac{E}{\Delta E}. \tag{34}$$

4. Conclusions

We have derived expressions for the oscillation probabilities in matter with *arbitrary* density profile for the vacuum dominated case: $V \ll \Delta m^2/2E$. An accuracy of the expressions is determined by the parameter ϵ and does not depend on the length of neutrino trajectory.

The results can be applied for the solar and supernova (low energy) neutrinos crossing the Earth.

The obtained formulas reproduce the known probabilities for particular density distributions (one layer with constant density, several layers, *etc.*).

The formulas have very simple structure which allows us to use them efficiently for analysis of various phenomena. In particular, the effect of averaging over the neutrino energy can be easily traced. Averaging reduces sensitivity of the oscillation effects observed at the detector to remote structures of density profile.

Appendix: Effect of higher order corrections

Let us show that the $S^{(2)}$ term of the evolution matrix in eq. (21) is not proportional to the full length of the neutrino trajectory in matter, $x_f - x_0$, as it happens in the ordinary perturbation theory. So that $S^{(2)}$ can be neglected for any value of the length provided that $\epsilon \ll 1$.

According to (20) the correction $S^{(2)}$ can be written as

$$S(x_0 \to x_f)^{(2)} \quad - \quad i\frac{\sin^2 2\theta}{4}\frac{2E}{\Delta m^2}\int_{x_0}^{x_f} dx \cdot V^2 \begin{pmatrix} 1 & 0 \\ 0 & -e^{i\phi^m_{x_0\to x_f}} \end{pmatrix} -$$
$$- \quad \frac{\sin^2 2\theta}{4}\int_{x_0}^{x_f} dx \int_{x_0}^{x} dy \cdot V(x)V(y) \begin{pmatrix} e^{i\phi^m_{x\to y}} & 0 \\ 0 & e^{i\phi^m_{x_0\to x_f}} e^{-i\phi^m_{x\to y}} \end{pmatrix} . \tag{35}$$

The (11) term of the first term in rhs of the eq. (34) produces large effect:

$$\frac{2E}{\Delta m^2}\int_{x_0}^{x_f} dx \cdot V^2 \;\propto\; (x_f - x_0) \tag{36}$$

Let us calculate the (11) term in the second term of rhs of eq. (34):

$$\int_{x_0}^{x_f} dx \int_{x_0}^{x} dy \cdot V(x)V(y)(\cos\phi^m_{x\to y} + i\sin\phi^m_{x\to x}) \,. \tag{37}$$

Changing the variables of the integration as $x \to x + (x_f + x_0)/2$ and $y \to y + (x_f + x_0)/2$, we find the real part of the integral:

$$\int_{-a}^{a} dx \int_{-a}^{x} dy \cdot V(x)V(y)\cos\phi^m_{x\to y} = \frac{1}{2}\left(\int_{-a}^{a} dx\, V(x)\, \cos\phi^m_{0\to a}\right)^2 . \tag{38}$$

Here $a \equiv (x_f - x_0)/2$ and we make use of the symmetry $V(x) = V(-x)$ which appears in new variables. The imaginary part of the integral (37) equals

$$\int_{-a}^{a} dx \int_{-a}^{x} dy \cdot V(x)V(y)\sin\phi^m_{x\to y} =$$
$$\int_{-a}^{a} dx \int_{-a}^{x} dy \cdot \frac{d\epsilon'(x)}{dx}\frac{d\epsilon'(y)}{dy}\sin\phi^m_{x\to y}$$
$$+\epsilon'(a)^2 \sin 2\phi^m_{0\to a} - 2\epsilon'(a)\cos\phi^m_{0\to a}\int_{-a}^{a} dx\, V(x)\, \cos\phi^m_{0\to x}$$
$$+\int_{-a}^{a} dx\, \epsilon'(x)\, V(x),$$

where

$$\epsilon'(x) = \frac{\epsilon(x)}{\sqrt{(\cos 2\theta - \epsilon(x))^2 + \sin^2 2\theta}} = \epsilon(x) + O(\epsilon^2).$$

In this integral only the last term is proportional to $(x_f - x_0)$ and it cancels precisely the contribution of eq. (36).

References

[1] Ara N. Ioannisian, Alexei Yu. Smirnov, hep-ph/0201012.

[2] L. Wolfenstein, Phys. Rev. **D 17**, 2369 (1978); L. Wolfenstein, in "Neutrino-78", Purdue Univ. C3 - C6, (1978).

[3] S. P. Mikheyev and A. Yu. Smirnov, *'86 Massive Neutrinos in Astrophysics and in Particle Physics*, proceedings of the Sixth Moriond Workshop, edited by O. Fackler and J. Trân Thanh Vân (Editions Frontières, Gif-sur-Yvette, 1986), pp. 355.

[4] J. Bouchez *et. al.*, Z. Phys. **C32**, 499 (1986); M. Cribier *et. al.*, Phys. Lett. B **182**, 89 (1986); E. D. Carlson, Phys. Rev. **D34**, 1454 (1986) .

[5] A.J. Baltz and J. Weneser, Phys. Rev. **D35**, 528 (1987); C. Lunardini, A.Yu. Smirnov, Nucl.Phys.B616:307-348,2001.

[6] Amol S. Dighe, Mathias T. Keil, Georg G. Raffelt JCAP 0306:006,2003

[7] M.C. Gonzalez-Garcia, Carlos Pena-Garay, Alexei Yu. Smirnov. Phys.Rev.D63:113004,2001

[8] Lian-You Shan, Xin-Min Zhang. Phys.Rev.D65:113011,2002

[9] Vernon D. Barger, D. Marfatia, K. Whisnant, B.P. Wood. Phys.Rev.D64:073009,2001

[10] A. Dar *et. al.*, Phys. Rev. **D 35** (1987) 3607; S. P. Mikheyev and A. Yu. Smirnov, Sov. Phys. Usp. 30 (1987) 759-790; L. Cherry and K. Lande, Phys. Rev D **36** 3571 (1987); S. Hiroi, H. Sakuma, T. Yanagida, M. Yoshimura, Phys. Lett. B**198** 403, (1987) and Prog. Theor. Phys. **78** 1428, (1987); A. J. Baltz and J. Weneser, Phys. Rev. **D37**, 3364 (1988). M. Spiro and D. Vignaud, Phys. Lett. B **242** 297 (1990).

[11] E.K. Akhmedov, Nucl. Phys. B**538**(1999)25.

[12] E. Lisi and D. Montanino, Phys. Rev. D**56**(1997)1792.

[13] G. L. Fogli, E. Lisi, A. Marrone, D. Montanino and A. Palazzo, Phys. Rev. D **66**, 053010 (2002).

DECONFINEMENT PHASE TRANSITION IN RELATIVISTIC NEUTRON STAR MERGERS

G. Poghosyan*
Departement für Physik und Astromonie der Universität Basel, 4056 Basel, Switzerland

R. Oechslin
Max-Planck Institut für Astrophysik, D-85741 Garching, Germany

K. Uryū
Astrohysical Sector, SISSA, Trieste 34013, Italy

F. K. Thielemann
Departement für Physik und Astromonie der Universität Basel, 4056 Basel, Switzerland

Abstract We consider the influence of the deconfinement phase transition on gravitational waves (GW) emitted in a binary neutron star merger. We perform 3D hydrodynamic simulations based on the conformally flat approximation to general relativity and the GW signal extracted up to quadrupole order. We vary the initial constituent masses of the binary by use of physically-motivated equations of state (EoS) at zero temperature in two ways - allowing stellar matter to undergo or not the hadron-quark phase transition. It has been shown, that for a binary system close to the innermost stable circular orbit (ISCO) with constituent gravitational masses larger than $M_\infty \simeq 1.5\ M_\odot$ the EoS dependent effects in GW signals begin to play a role. The difference in the gravitational wave frequency at the ISCO is to up to $\simeq 10\%$ for the maximal allowed mass given by the used model EsoS - $M_\infty \simeq 1.75\ M_\odot$. We determine the characteristic GW frequencies of the merger remnants, where the pronounced implications of quark matter show up as a phase difference in the post-merger GW signal, for stellar matter undergoing or not the deconfinement phase transition and collapse does not take place immediately after merger.

Keywords: hydrodynamics, gravitational waves, equation of state, neutron stars, quark stars

*Partially supported by Department of Physics, Yerevan State University, Armenia

D. Blaschke and D. Sedrakian (eds.), Superdense QCD Matter and Compact Stars, 415–425.

1. Introduction

Since the discovery of the parton substructure of nucleons and its interpretation within the constituent quark model, much effort has been spent to explain the properties of these particles and the structure of high density phases of matter is under current experimental investigation in heavy-ion collisions [17]. While the diagnostics of a phase transition in experiments with heavy-ion beams faces the problems of strong non-equilibrium and finite size, the dense matter in a compact star forms a macroscopic system in thermal and chemical equilibrium for which effects signalling a phase transition shall be most pronounced [8].

The influence of the appearance of such exotic states like quarks in stellar matter is topic of the study of quasi-stationary simulations of the evolution of isolated compact stars [15, 12, 7, 23] and accreting systems, where one companion is a superdense compact object [9, 27]. In this work we investigate the observability of the hadron-quark deconfinement phase transition in the dynamical evolution of a neutron star merger.

Binary neutron star mergers are considered to be among the strongest sources of GW signals for interferometer-type gravitational wave observatories as LIGO [1], VIRGO [10], GEO600 [21] and TAMA [2]. After a long inspiral process which lasts millions of years, the final merger phase takes place on a millisecond timescale. The onset of the merger phase occurs when the two companions become dynamically unstable near the innermost stable circular orbit (ISCO) and mass transfer starts. Combining lower-frequency narrow-band detectors with broadband LIGO measurements appears extremely feasible, and may be the technique which allows to learn about high density stellar matter from GW signals. This will require networks of broadband detectors combined with narrowband detectors that have good sensitivity at high frequencies, as suggested in [18].

It has been pointed out that the gravitational wave frequency f_{GW} relates to the compactness $(M/R)_\infty$ of a neutron star as $f_{\rm GW} \sim (M/R)_\infty^{3/2}$ near the ISCO, meaning that the gravitational wave frequency just before merger carries information on the radius of the neutron star ([28]). Especially, deconfinement hadron-quark phase transition being one of the most dramatic phenomena, which changs the compactness of neutron stars ([27]), could result to clearly observed signals in the GW spectrum of both inspiralling and merged binary systems.

The neutron star formed after the merger may be supported by rapid and differential rotation even if its mass exceeds 60% of the maximum mass of a single non-rotating neutron star, and the GWs are emitted due to non-axisymmetric and quasiradial oscillations of the remnant for longer than the dynamical timescale [30]. If these oscillations persist for a longer time, the integrated GW may be

detectable. Our investigation shows, that this type of GW is carrying most pronounced information on the high density matter.

Due to the complexity of taking into account many aspects of the binary neutron star merger problem [26], such as general relativistic gravity, the microscopic physics as a physically motivated EoS including neutrino physics [29] and magnetic fields, the present investigations have been concentrated either on the relativistic aspects of the problem using a simple EoS [22, 25, 13, 30], or on the microphysical aspects while treating gravity in a Newtonian framework [3, 14]. For a review on the topic, see [28]. We constrain the constituent stars of binary system by physically motivated EoS allowing or not stellar matter to undergo a hadron-quark deconfinement phase transition [12]. We assume the binary to be symmetric, initially irrotational, in a quasi-equilibrium state, at slightly wide initial orbits, and need about half an orbit to begin with the inspiral. The merger problem is then solved in the conformally flat approximation.

2. Equation of State

For the simulations of astrophysical systems with the goal to find extraordinary changes in macroscopic parameters of the system, due to processes in stellar matter at microscopic levels, the Equation of State (EoS) plays not the last role, if not say the main. Ideally for description of stellar matter, one would like to have a single theory that describes both phases: the confined hadronic phase and locally deconfined quark matter phase. We construct an EoS connecting the hadronic EoS based on Relativistic Mean Field (RMF) approximation [34] and the quark EoS given by the MIT BaG model [11] via variable pressure phase transition construction [16] and neglect the influence of strangeness - hyperons in the hadronic and strange quarks in the quark phase.

The generalized Lagrangian density of the non-linear σ-ω-model in the RMF approximation used for modeling the phase of uniform nuclear matter containing interacting neutrons, protons, muons and electrons can be written as

$$\begin{aligned}\mathcal{L} &= \sum_{B=\{n,p\}} \bar{\psi}_B \left[i\gamma_\mu \partial^\mu - (m_B - g_{\sigma B}\sigma) - (g_{\omega B}\omega + g_{\rho B}\tau_3\rho)\,\gamma^0 \right] \psi_B \\ &+ \frac{1}{2}m_\omega^2\omega^2 + \frac{a}{4}\omega^4 - \frac{1}{2}m_\sigma^2\sigma^2 - \frac{b}{3}\sigma^3 - \frac{c}{4}\sigma^4 + \frac{1}{2}m_\rho^2\rho^2 \\ &+ \sum_{l=\{e^-,\mu^-\}} \bar{\psi}_l \left(i\gamma_\mu \partial^\mu - m_l \right) \psi_l \,,\end{aligned}$$

σ scalar and ω,ρ vector mean fields and related coupling constants $g_{(\sigma,\omega,\rho)B}$ must be defined to fit finite nuclear properties. We use the TM1 parameter set, which is motivated by a least-square fit to experimental results including stable

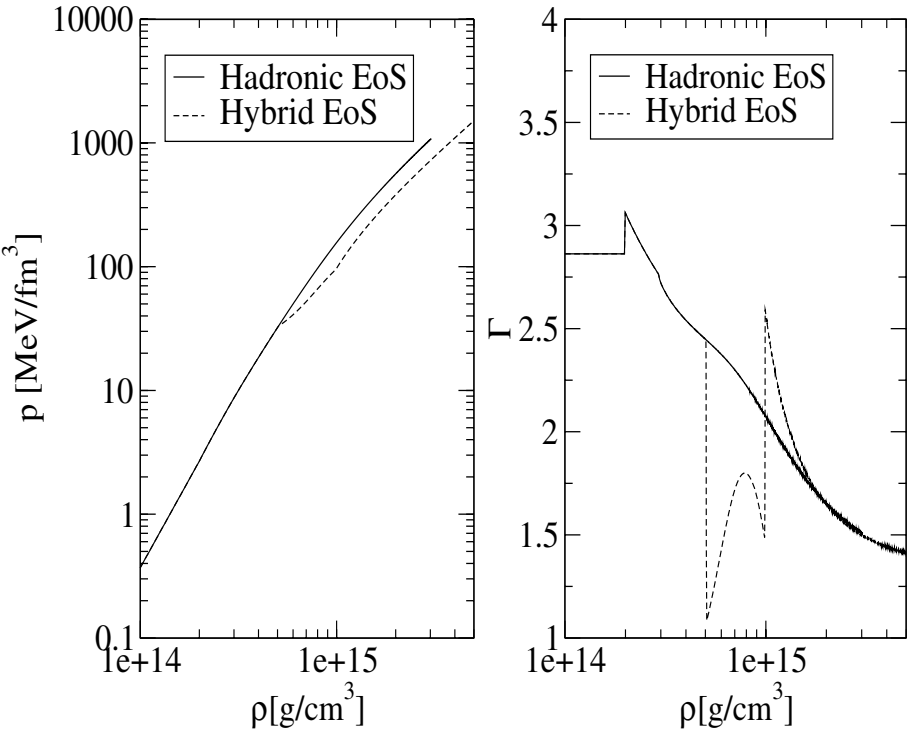

Figure 1. Comparison of the considered nuclear EoS. The hybrid EoS (dashed curve) has a phase transition region ($1.8\rho_0 < \rho < 3.5\rho_0$) where adiabatic indices are substantially lower, followed by a quark phase which is has a similar stiffness as the nuclear matter at those densities.

and unstable nuclei [31]. For densities above $\rho \gtrsim 10^{14}$ g/cm^3 this is a good approximation.

Using the MIT BaG model with massless up and down quarks and a Bag constant $B = 90$ MeV/fm^3, we describe an exotic phase of nuclear matter at high - supranuclear densities. The resulting EoS describing stellar matter undergoing a phase transition to quark matter at very high densities we call *hybrid EoS* and *hadronic EoS* is same model excluding appearance of quarks. The resulting hybrid EoS (see fig.1) describes three physical phases

- A pure hadronic phase below $\approx 5 \times 10^{14}$g/cm^3 $\approx 1.8\rho_0$ where the EoS coincides with the hadronic matter. The stiffness in this region varies between $\Gamma \approx 3$ and $\Gamma \approx 2.5$.
- A quark-hadron mixed phase between $\approx 5{\times}10^{14}$g/cm^3 and $\approx 10^{15}$g/cm^3 $\approx 3.5\rho_0$ where both quark and hadrons are present. In this phase transition region, the EoS substantially softens with $\Gamma \approx 1 - 1.5$.
- A pure quark phase above $\approx 10^{15}$g/cm^3 where the MIT-bag-model EoS applied.$\Gamma \approx 4/3$

Here, ρ_0 is the nuclear saturation density 2.8×10^{14}g/cm^3 $\Leftrightarrow$ 0.16 fm^{-3}. We neglect temperature effects considering cold T=0 matter in any phase, which is a good approximation in the high-density regime where thermal effects to the pressure are rather small. For densities below 0.5 ρ_0, we use the approach of polytropic EoS [32] $P = K\rho^{\Gamma}$ where κ and Γ are adjusted to fulfill smoothness of pressure and internal energy for transition between uniform and non-uniform nuclear matter as well as fit common physically motivated EoSs used for this density regime. This limits our investigation of realistic microscopical-physical effects to low densities, that could be found in merger event, in particular at outflowing matter, in the disk around the merger remnant and in the crust of neutron stars, where everywhere also the thermal component is certainly not negligible.

3. Summary

To investigate the different consequences of the EoSs in details, we split the discussion on whole merger event in a pre-merger evolution, where the binary still consists of two tidally stretched objects and in a following post-merger evolution where a merger remnant, a NS or BH is forming. We use the waveless approximation to general relativity proposed by [20], where the conformally flat condition for the spatial geometry suggested. This bring to a considerable simplification of the Einstein equations, allowing to solve the system of hydrodynamic equations using the Smoothed Particle Hydrodynamics method (SPH; [6, 24, 25, 13]).

To model the pre-merger evolution, we apply the method of Uryū & Eriguchi (2000) to construct an initial configuration varying the EoS and the gravitational mass M_∞ - the mass of a single NS in isolation. The lowest value we use $1.2M_\odot$ is at the lower limit of the observational range and $M_\infty = 1.75M_\odot$ is the maximal gravitational mass of hybrid star. We observe a pronounced

Table 1. Here are summarized the used models. The letter (A-E) indicates the mass and number part indicates the 1-hadronic and 2-hybrid Equations of State (EsoS). M_∞ denotes the gravitational mass of one NS in isolation, C is the compactness, P the orbital period, $f_{GW,0}$ the corresponding GW frequency, d_0 the initial orbital separation and R_∞ the radius of one single isolated NS measured in Schwarzschild coordinates.

Model	$M_\infty[M_\odot]$	$C = (M/R)_\infty$	$P[ms]$	$f_{GW,0} = 2/P$	$d_0[km]$	$R_\infty[km]$
A1	1.2	0.1276	2.92	685	38.00	13.88
B1,B2	1.35	0.1424	2.72	737	36.93	13.99
C1,C2	1.4	0.1475	2.65	756	36.71	14.01
D1	1.5	0.1577	2.57	777	36.19	14.03
D2	1.5	0.1579	2.57	777	36.19	14.02
E1	1.75	0.1853	2.20	909	33.40	13.93
E2	1.75	0.1959	1.97	1058	31.14	13.07

EoS impact on pre-merger evolution of the quasi-equilibrium binary only for the most massive cases D and E. The orbital frequency and the gravitational wave frequency of a binary system depends on the compactness of its components [33], as it could be seen in Fig. 2 the GW frequency of the hybrid EoS binary is up to 10% larger than that of the hadronic EoS binary. Such a change of tendency for increasing gravitational wave frequency may suggest the existence of a drastic change of EoS, for our EoS it is a deconfinement phase transition. For lower stellar masses, the stellar matter does not reach even the phase transition density necessary to form a "mixed" hadron-quark matter $1.8\rho_0$ in our model EoS (see Fig. 3) and drastic changes in compactness and therefore in the GW frequencies are not expected.

Following the evolution of the maximum density of merger - maximum of a statistical average over the particles densities, that results to values with a small numerical noise, one could see a slow decrease during the pre-merger phase, when the two stars become tidally stretched and reaches its minimum during the actual merger. This is the case when the GW luminosity either approaches

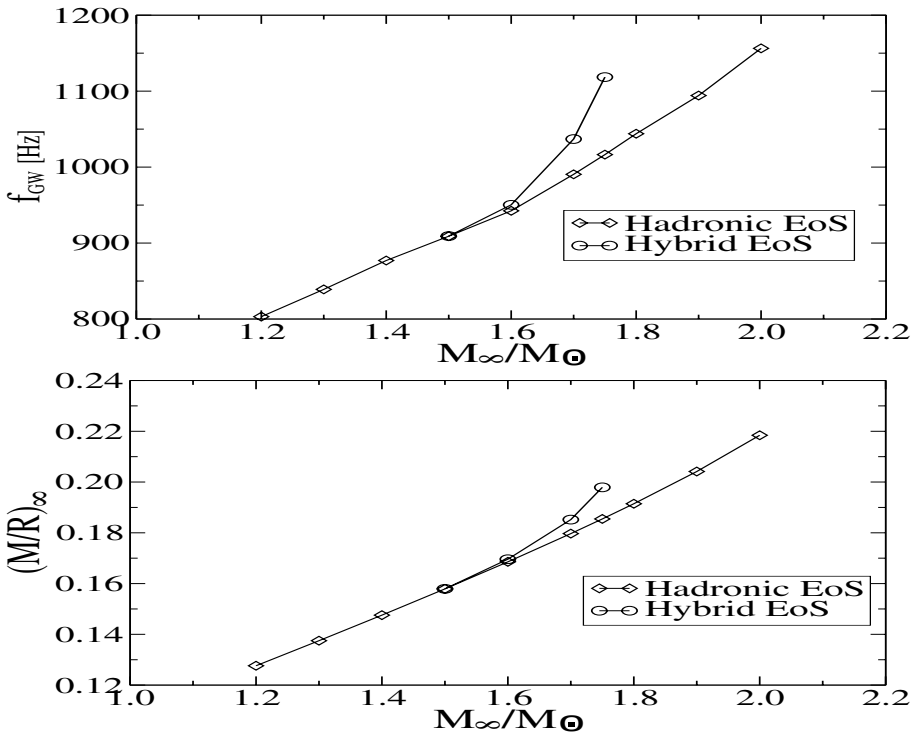

Figure 2. Left: GW frequencies depending on the gravitational mass in isolation at the ISCO. Right: compactness of an isolated neutron star with respect to the gravitational mass.

its maximum and the constituent stars are maximally tidally stretched. Later when a new merger remnant has already formed, but a twin-core structure is still present, three possible evolutionary scenarios of ρ_{max} could be distinguished: the remnant can be stabilized by pressure and centrifugal forces - ρ_{max} slowly increases, becoming approximately constant (A1,B1,B2,C1,D1); or the delayed collapse is possible - ρ_{max} slowly increases on several dynamical timescales, then this fragile equilibrium is concluded by a final collapse, which is visible as a steep rise of ρ_{max} in C2 and D2 models. The last scenario is the immediate collapse just after the merger - ρ_{max} increases without delay on a dynamical timescale E1 and E2. We consider that the second scenario of delayed collaps caused by the EoS, as of appearing when ρ_{max} crosses the mixedphase - pure quark phase transition density $3.5\rho_0$ in C2 and D2 models, this could be seen also for B2 most realistic model with $1.4M_{\odot}$ constituent stars, if the numerical simulation of collapsing remnant could be followed at more time steps.

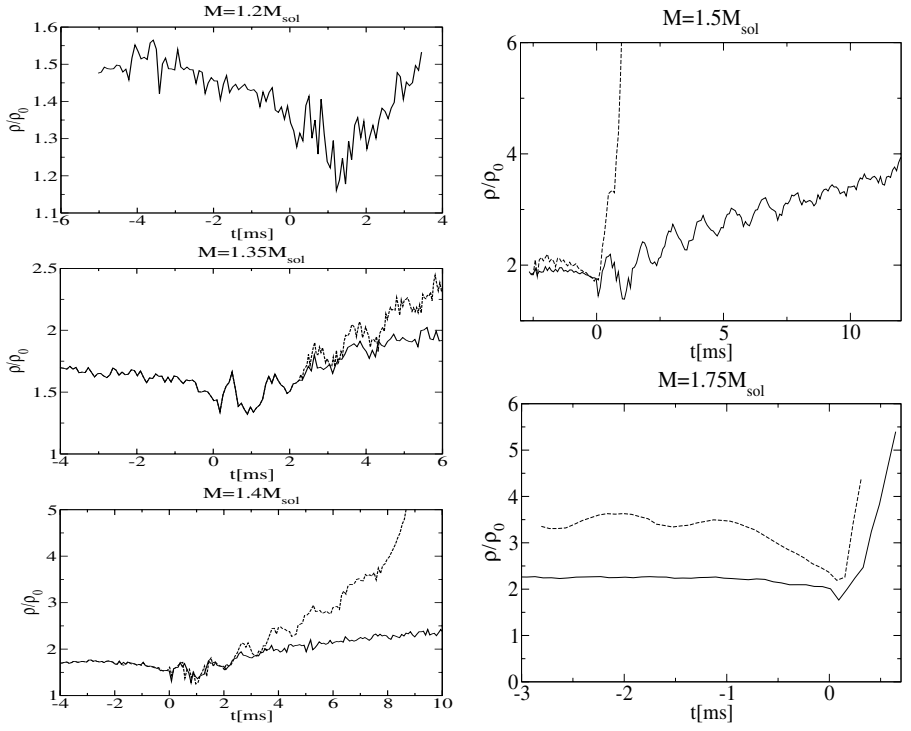

Figure 3. Evolution of the maximal density in units of the nuclear saturation density. The origin of negaive timesteps is pre-merger evolution with two objects and after 0 it is post-merger with one object. Solid lines correspond to hadronic models, dashed lines to hybrid models.

Since the waveform of GW is sensitive to dynamical mass motions we expect that all mentioned maximal density differences are reflected in the GW signal mainly in the form of different frequencies, that could help to constrain an observable scenario of EoS effects based on possible GW signals from mergers. For that, like the Newtonian and the first-order post-Newtonian (1PN) approximation, the CF approximation does not include gravitational radiation and its reaction by construction. We therefore have to add an additional gravitational wave (GW) extraction scheme and a radiation reaction force which accounts for the angular momentum and energy carried away by GW. The waveform in transverse-traceless gauge is extracted in the slow-motion limit and up to quadrupole order [25].

In Fig. 4 we plot the waveforms of all models sorted according to the initial mass. Model E1/E2, the most massive one is the only one where a significant pre-merger EoS difference in the waveform are most pronounced. D1/D2, does not show any EoS differences in the GW frequency at pre-merger phase, may be for larger binary distances and therefore smaller tidal interaction, GW frequency differences could be seen already in that phase. The more interesting

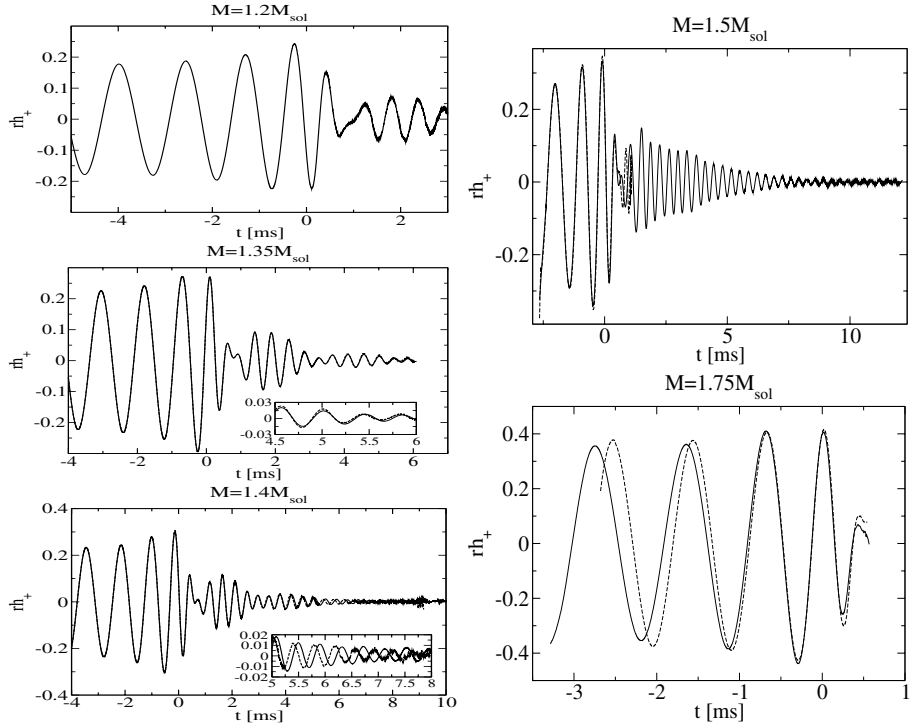

Figure 4. Gravitational waveforms of all models sorted according to their initial mass. The origin of the time axis has been shifted to the GW luminosity maximum. Solid lines correspond to hadronic models, dashed lines to hybrid models.

part of this model is the different collapse behaviour and therefore the totally different waveform. While the hybrid model D2 only produces a short, high-frequent burst before the collapse, the hadronic model emits a long wavetrain which decreases slowly in amplitude. Models C1/C2 and B1/B2 emit both a quasi-periodic (QP) GW-signal which is characteristic for the rotation and oscillation mode in the merger remnant. EoS-differences in the waveform do not appear until a considerable mixed matter core has formed in the hybrid case. As a consequence, the first part of the post-merger GW signal, which is the strongest in our simulations, will not be affected by any EoS difference. However, when the mixed matter core becomes large enough, an accumulating phase shift in the waveform becomes clearly visible. In the C1/C2-model the shift adds up to more than half a period before the collapse of the hybrid remnant happens, in the B1/B2 model, the shift is only very small, but visible.

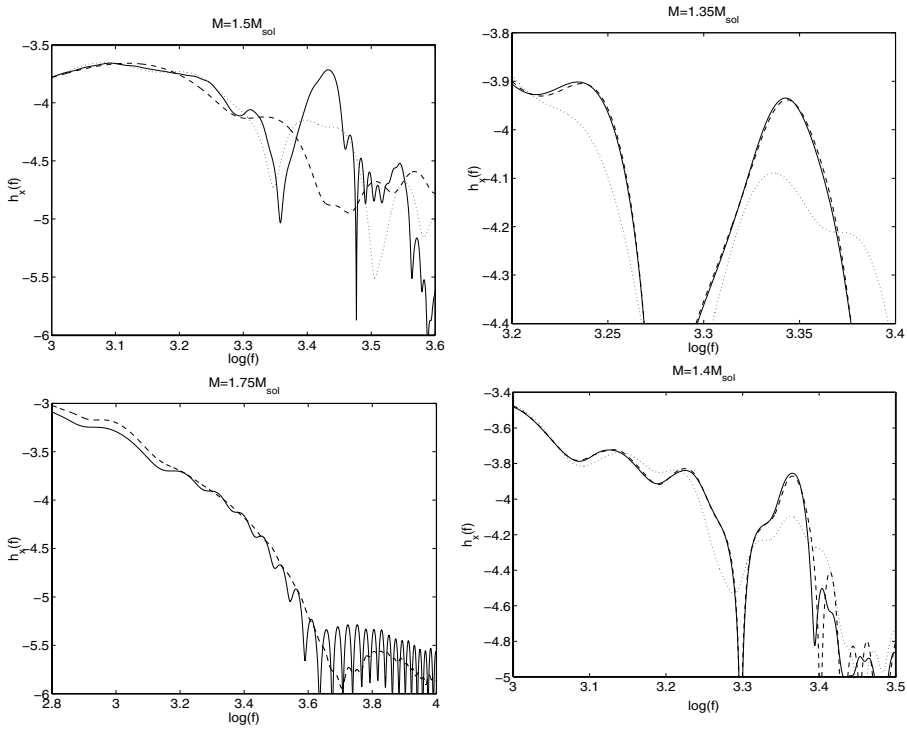

Figure 5. Fourier spectrum of the waveform h_+ for models B1/B2 to E1/E2 sorted according to their initial mass. The frequency is in units of kHz. Solid lines correspond to hadronic models, dotted lines to the spectra of the corresponding truncated waveforms and the dashed lines correspond to hybrid models.

Fourier spectrum of the GW waveform - the truncated wavesignals, which only contain the first few oscillations of the post-merger signals, plotted in Fig.5, shows EoS-differences via different frequency peaks of different models. The difference is most obvious in the D1/D2-model. For the hadronic EoS model D1, a distinct Fourier peak is clearly visible, whereas the hybrid EoS model D2 leads only to a much weaker and very broad Fourier peak since the remnant is collapsing very soon after merging producing a much shorter post-merger GW signal. In the C1/C2-model, both the hadronic and the hybrid models have strong QP peaks where the one of the C2-model is slightly shifted to higher frequencies due to the more compact remnant. The same can be seen for the model B1/B2. However, effects here are smaller and a measurement may be difficult. The EoS-effects are this tiny because the spectrum is dominated by the first GW burst after merging which is insensible to EoS-differences.

Whether there will be observered the gravitational wave signal form a binary system merger, the exact constituent masses of which will be determined, it will allow to constrain mass and radius of the system and then simulate the merger with a different EoS trying to fit the maximum time of existence of gravitational wave signal, that connected to type of stellar matter, as shown above.

Acknowledgments

R.O., G.P. and F.K.T. are funded by the Schweizerischer Nationalfonds under grant No. 2000-061822.00.

References

[1] Abramovici A. et al., 1996, Phys. Lett. **A 218**, 157

[2] Ando M. et al., the TAMA collaboration, 2001, Phys. Rev. Lett.,**86**, 3950

[3] Ayal S., Piran T., Oechslin R., Davies M., Rosswog R., 2001, ApJ, 550, 846

[4] Baumgarte T. W., Shapiro S. L., 2003, Phys. Rept. **376**, 41

[5] Baumgarte T. W., Cook G. B., Scheel M. A., Shapiro S. L., Teukolsky S. A., 1998, Phys. Rev. D 57, 7299

[6] Benz W., 1990, in Buchler, J. R., ed., The Numerical Modeling of Nonlinear Stellar Pulsations: Problems and Prospects, Kluwer, Dordrecht, p. 269

[7] Blaschke D.,Grigorian H., Poghosyan G., Roberts C. D., Schmidt S., 1999, Phys.Let.**B 450**, 207

[8] Blaschke D.,Grigorian H.,Poghosyan G., 2001, *Physics of Neutron Star Interiors*, Lecture Notes in Physics **578**, p.285, Springer-Verlag.

[9] Blaschke D.,Bombaci I.,Grigorian H.,Poghosyan G., 2002, New Astronomy **7**, 107.

[10] Bradaschia C. et al., 1990, Nucl. Instrum. Methods **A 289**, 518

[11] Chodos A., Jaffe R. L., Johnson K., Thorn C. B. and Weisskopf V. F., Phys. Rev. D **9**, 3471.

[12] Chubarian E., Grigorian H., Poghosyan G., Blaschke D., 2000, Astron. & Astrophys. **357**, 968

[13] Faber J. A., Grandclément P., Rasio F. A., gr-qc/0312097, submitted to Phys. Rev. D

[14] Faber J. A., Rasio F. A., 2002, Phys. Rev. D., 65, 084042

[15] Glendenning N. K., Pei S., Weber F., 1997, Phys. Rev. Lett. **79**, 1603.

[16] N. K. Glendenning, 1992, Phys. Rev. **D 46**, 1274.

[17] Hallmann T. J. et. al. (eds.), 2002, *Quark Matter 2001: Proceedings*, Nucl. Phys. 698.

[18] Hughes S. A., 2002, Phys. Rev. **D 66**, 102001.

[19] Hockney R. W., Eastwood J. W., 1994, Computer Simulation Using Particles, IoP, London

[20] J. Isenberg and J. Nester, in *General Relativity and Gravitation* Vol.1, edited by A. Held, (Plenum Press, New York 1980).

[21] Lück H., 1997,Class. Quant. Grav. **14**, 1471

[22] Mathews G. R., Wilson J. R., 2000, Phys. Rev. **D 61**, 127304

[23] Mishustin I.N., Hanauske M., Bhattacharyya A., Satarov L.M., Stker H., Greiner W., 2003, Phys. Lett. **B 552**, 1.

[24] Monaghan J, Gingold R, 1983, J. Comp. Phys.,**52**, 374

[25] Oechslin R., Rosswog S., Thielemann F. K., 2002, Phys. Rev. **D 65**, 103005

[26] Oohara K., Nakamura, T., 1999, Prog. Theor. Phys. Suppl.,**136**, 270

[27] Poghosyan G., Grigorian H., Blaschke D., 2001,The Astrophysical Journal **551**:L73.

[28] Rasio F. A. & Shapiro S. L., 1999, Class. Quant. Grav., **16**, R1-R29

[29] Rosswog S, Liebendörfer M., 2003,astro-ph/0302301, submitted to MNRAS

[30] Shibata M, Taniguchi K, Uryū K, 2003, Phys. Rev. D, in press

[31] Sugahara, Y, Toki, H, 1994, Nucl. Phys. **A 579**, 557

[32] Tooper R. F., 1965, ApJ Lett., **405**, L29.

[33] Uryū K., Eriguchi Y., 2000, Phys. Rev. D, 61, 124023

[34] J. D. Walecka, 1975, Phys. Lett. B **59**, 109

Index

Accretion disk, 26, 313
  corotating, 27
Angular momentum, 10

BCS relation, 193
Beta-equilibrium
  2-flavor quark matter, 387
  3-flavor quark matter, 128, 196
  nuclear matter, 120
Binary mergers, 318, 416
  BH-NS, 325
  magnetic mechanism, 322
  Neutrino annihilation, 319
  NS-NS, 319
Black hole, 3, 313, 419
Bound states,α-particles, 77
Brueckner equation, 122

Charge neutrality
  2-flavor quark matter, 344
  3-flavor quark matter, 129, 196
  global, 234
  nuclear matter, 120
Clusters,α-particles, 77, 89
Collapsars, 314
Condensates
  2SC, 188
  2SC+X, 395
  CFL, 268
  CSL, 395
  diquark, 157, 346
  nuclear matter, 88
    pairing, 88
    quartetting, 89
  specific heat, 193
  spin-1, 189
Correlations, 77
Critical point, 9

Deconfinement, 17, 359, 371, 416
Density oscillations, 7
Doppler shift, 31
Dual chiral density wave, 254

Effective Lagrangians, 147
  $SU_c(2)$ Glueball, 159
  2SC, 157
  CFL-Solitons, 155
  Goldstone bosons, 151
  high density effective theory, 170, 178
  NJL, 190, 195, 219, 226, 254
  quantum fluctuations, 359
  vector mesons, 153
Einstein equations
  conformally flat, 419
  fifth dimension, 299, 302
EoS, 93, 113, 135, 201, 332, 359
  constraints, 109
  hadronic matter, 114
    Brueckner-Hartree-Fock, 114
    three body forces, 118
  interacting particles, 6
  medium modifications
    clusters, 86
    two particle correlations, 82
  mixed phase, 129
  neutron gas, 5
  nuclear matter, 75
    Hyperons, 122
  polytropic, 10, 419
  quark matter, 127
    2SC, 344
    MIT bag model, 127, 142, 418
  quasiparticle models, 136
    HTL, 138
    non-zero chemical potential, 140
    phenomenological, 139
  relativistic mean field, 80, 417
  variable adiabatic index, 11
EXO 0748-676, 369, 393

Fermi surfaces, 212, 252
  deformed, 217
Ferromagnetism in quark matter, 243
Fifth dimension, 298
  field equations, 298
    general solution, 301
    special solution, 300

Fluctuations, 279
density, 289
magnetic susceptibility, 289
temperature, 289
Fock exchange interaction, 243
Formfactor, 283, 343

Gamma ray bursts, 353, 371, 398
central engine, 313
fireball model, 312
long-soft bursts, 314
observations, 309
origin, 19, 311
short-hard bursts, 318
Gap, 228, 278, 344
CFL, 182
Cooper pair, 174
fluctuations, 281
heavy ion collisions, 290
hybrid stars, 291
specific heat above T_c, 288
specific heat below T_c, 283
Gap equation, 173, 176, 192, 211, 219, 248
Ginzburg number, 286
Ginzburg-Landau equations, 267, 271
Ginzburg-Levanyuk criterion, 286
Glitches, 43
Vela pulsar, 48
Goldstone bosons, 151, 161, 194
Gould Belt, 66
Gravitational waves, 416

Heavy ion collisions, 278
High density effective theory, 166, 177
Hot spot, 28
Hybrid stars, 17, 130, 201, 278, 347, 356
configurations, 363, 393
cooling, 395
gap fluctuations, 291
maximum mass, 419
rotating, 393
Hydrodynamic stability, 7
Hypernova, 314

Kepler periods, 131

Lattice simulations, 179
LMXB, 392
Low energy effective theory, 178

Magnetars, 63, 242
Magnetic braking, 28
Magnetization, 247
Magnetosphere, 26
Mass accretion, 361
Maxwell's relation, 140
Mixed phase, 196, 234, 332, 357
Gibbs conditions, 129, 236, 357
Glendenning construction, 129, 417
Maxwell construction, 391

Nambu-Gorkov formalism, 248, 382
Neutrino mixing, 406
Neutrino oscillation, 406
Neutrino trapping, 399
Neutron stars, 130, 278, 337, 355
bimodality, 65
binaries, 25
configurations, 333
constitution, 367
constraints, 109
cooling, 395
finite size effects, 357
history, 5
isentropic, 11
isolated, 55
accretion, 66
magnetic field, 62
spectral features, 61
kick mechanisms, 65
magnetic field, 25, 269
components, 273
mass limits, 367
nucleation time, 361
observations, 53, 57
quantum nucleation, 357
rotation, 269, 391
structure, 44, 120
velocity distribution, 65
x-ray binaries, 25
Nova, 371

OGE-type action, 248
Oppenheimer-Volkoff equation, 5, 121, 347
oscillation probabilities, 409

Partition function, 379
Pauli blocking, 82
Pauli-Lubanski vector, 244
Phase diagram
rotating compact stars, 392
two-flavor quark matter, 385
Phase transitions, 203, 391, 416
Phi-4 theory, 136
Postglitch relaxation, 44, 46
Proto-neutron star cooling, 348
Pulsars, 43
bimodality, 65
kick mechanisms, 65
magnetic field, 242
observations, 57
pulsations, 28
velocity distribution, 65

QCD partition function, 179

Quark matter drop, 357
Quark stars, 175, 355
configurations, 346
history, 16
structure, 143

Regularization, 257
Rotation
arbitrary, 9
CFL condensate, 268
energy, 15, 323
symmetry, 246
RX J1856.5-3754, 369, 393
spectrum, 64

Schwarzschild
coordinates, 419
formula, 36
radius, 242
Self-energy, 137
Solar neutrino oscillations, 409
Spontaneous spin polarization, 243
Strange stars, 17, 356
configurations, 364
Superconductivity, 142, 187, 209, 225, 341
asymmetric, 210
DFS phase, 215
LOFF phase, 213
quark matter, 160, 172, 264, 277
2SC, 156, 159, 194, 219, 383
2SC phases, 197
CFL, 149, 180, 194, 265
color magnetic, 248
free energy, 266
g2SC, 230
magnetic field, 264
pairing fluctuations, 279
Superfluidity, 44, 269
Supernova-GRB connection, 354
Supranova, 317
Symmetry energy, 94, 119
Brueckner-Hartree-Fock, 96
decomposition, 96
Dirac-Brueckner-Hartree-Fock, 100
effective field theory, 101
Green function method, 98
heavy-ion reactions, 108
Landau-Migdal, 104
N-N interaction, 97
neutron skin, 103
neutron skin experimental constrains, 106
relativistic mean field, 101

Thermodynamic potential, 136, 256, 382
2-flavor quark matter, 191, 219, 227, 343
3-flavor quark matter, 127, 280, 380
Three body force, 99, 115
microscopic, 116
phenomenologic, 117
Trapping, 344
Tunneling probability, 360

Vacuum polarization tensor, 171
Variational principle,energetic method, 11
Vela pulsar, 44, 356, 396
Vortices, 44
corotating, 45
pinning, 46
structure, 269

Wess-Zumino effective action, 152
White dwarf, 10

X-ray binaries
accretion, 25
companions, 33
energy release, 25
high mass, 29
light curve, 37
low-mass, 27
magnetic field, 25, 30
mass function, 31
orbital frequencies, 37
radial velocity, 31
Roche lobe overflow, 25, 27
spectral lines, 35, 369
Vela X-1, 33
X-ray bursts, 29

Yamaguchi interaction, 85